PHOTOGRAPH THIS SHEET

AD A995050

DTIC ACCESSION NUMBER

LEVEL

INVENTORY

AEC

Rpt. No. WT-525

DOCUMENT IDENTIFICATION

Date: Feb. 1953

DISTRIBUTION STATEMENT A

Approved for public release;
Distribution Unlimited

DISTRIBUTION STATEMENT

ACCESSION FOR

NTIS GRA&I [X]

DTIC TAB [ ]

UNANNOUNCED [ ]

JUSTIFICATION

(Feb. 1953)

BY

DISTRIBUTION /

AVAILABILITY CODES

DIST	AVAIL AND/OR SPECIAL	
A		

DISTRIBUTION STAMP

Released

DTIC
ELECTE
S NOV 17 1980 D
D

DATE ACCESSIONED

UNANNOUNCED

80 11 12 122

DATE RECEIVED IN DTIC

PHOTOGRAPH THIS SHEET AND RETURN TO DTIC-DDA-2

DTIC FORM OCT 79 70A

DOCUMENT PROCESSING SHEET

AD A995050

Copy No. A

Operation SNAPPER

NEVADA PROVING GROUNDS

April - June, 1952

Project 3.1

VULNERABILITY OF PARKED AIRCRAFT TO ATOMIC BOMBS

RESTRICTED DATA

SECRET

80 11 12 122

SECRET
CONFIDENTIAL
WT-525

This document consists of 493 pages
No. of 283 copies, Series A

OPERATION SNAPPER

Project 3.1

VULNERABILITY OF PARKED AIRCRAFT TO ATOMIC BOMBS

REPORT TO THE TEST DIRECTOR

by

K. C. Schraut
and
Staff
Division of Research
University of Dayton

and

L. J. Breidenbach
Project Officer
Wright Air Development Center

February 1953

Statement A
Approved for public release;
Distribution unlimited.

Classification (Cancelled) ([redacted])
By Authority of TT Rev ONR/DOE
By [redacted] Date 24 Sept 0

Aircraft Laboratory
Wright Air Development Center
Dayton, Ohio

CONFIDENTIAL
SECRET
RESTRICTED DATA
ATOMIC ENERGY ACT 1946

Reproduced Direct from Manuscript Copy by
AEC Technical Information Service
Oak Ridge, Tennessee

Inquiries relative to this report may be made to

Chief, Armed Forces Special Weapons Project
P. O. Box 2610
Washington, D. C.

If this report is no longer needed, return to

AEC Technical Information Service
P. O. Box 401
Oak Ridge, Tennessee

[redacted]

ABSTRACT

This report is a presentation of the data obtained on Operation SNAPPER relating to the parked aircraft vulnerability problem. To determine the vulnerability of parked aircraft to atomic detonations, 28 aircraft (16 F-47's, 2 F-86's, 1 F-90, 7 B-17's, 1 B-29, and 1 B-45) were subjected to three different detonations, while deployed at various ranges and orientations with respect to ground zero, such that they experienced overpressures ranging from less than 1 psi to 35 psi and thermal energies of from 1 cal/cm^2 to 235 cal/cm^2. These inputs covered the range from no damage to complete destruction. For purposes of discussion, aircraft damage has been divided into arbitrary categories designated as light, moderate, heavy, beyond economical repair, and destroyed, depending on the ratios of man-hours to repair to maximum man-hours considered economical for each aircraft type. Aircraft damaged beyond economical repair may retain a number of usable components and be able to support substantial structural loads, whereas destroyed aircraft may be expected to have only negligible airframe salvage value due to failure of main structural members. Aircraft responses, including wing and fin bending moments, aircraft accelerations, and skin temperature changes were measured by oscillographic instrumentation. A presentation and detailed discussion of these data are included. A peak skin temperature survey using a maximum temperature indicating device was also conducted.

Damage was correlated as a function of overpressure using the aircraft headings relative to ground zero as parameters. Aircraft oriented side-in were found to be the most vulnerable while aircraft oriented nose-in were the least vulnerable. General results, therefore, must be based on the nose-in orientation to be conservative. An estimate of the overpressures required to initiate damage and to cause damage beyond economical repair is tabulated below for each of the six types of aircraft tested.

Aircraft Type	Damage Threshold (psi)	Damage Beyond Economical Repair (psi)
F-47	2½	9
F-86	2½	10
F-90	3	11
B-17	1	4
B-29	1	6
B-45	1½	8

Additional protection afforded by certain passive defense measures must be compensated for by increased overpressures. Degree of damage is a strong function of aircraft configuration, with aircraft of the

[redacted]

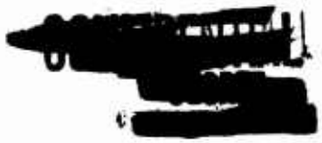

B-17 type being much more vulnerable than aircraft of the F-90 type. Obtaining of additional data on modern aircraft types and a thorough analysis of the coupling effect of thermal and blast inputs in producing aircraft damage is recommended.

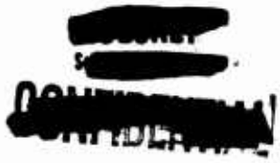

[redacted]

PREFACE

The purpose of this report is to set forth the data acquired on Operation TUMBLER-SNAPPER relating to the aircraft vulnerability problem with particular emphasis on parked aircraft.

The reader is reminded that the data obtained are specific only for the type of aircraft exposed to definite phenomena and that the damage resulting from a second exposure cannot always be completely isolated from the cumulative effects, since previous damage may have resulted in permanent structural weaknesses. Also, extrapolation to modern types of American and foreign aircraft and to various orientations may introduce gross errors. The availability of modern aircraft was extremely limited for destructive tests of this nature, and therefore most of the information on present day aircraft is an extension of singular data. The conclusions presented are intended as a general guide based on the available data.

A detailed prognosis of the effects of nuclear weapons on foreign aircraft must include a reasonable consideration of their structural variations as compared to the types actually tested. Very scant information of this nature is available at this writing.

The satisfactory completion of the work undertaken as Project 3.1 was made possible by the cooperation and support of a number of agencies and individuals. It is the desire of the authors to acknowledge the efforts of all contributing elements, including the Los Alamos Scientific Laboratory, Test Command of the Armed Forces Special Weapons Project, and the U. S. Naval Radiological Defense Laboratory.

The authors also specifically wish to acknowledge the direct support furnished by the Boeing Airplane Company, the Lockheed Aircraft Corporation, North American Aviation, Inc., and the Republic Aviation Corporation. In addition, acknowledgment is gratefully extended the Aeronautical Ice Research Laboratories, the David Taylor Model Basin, the Maintenance Division of the Air Materiel Command, the Technical Photographic Services Section, Flight Test Division, Electronics Sub-Division, Equipment Laboratory, Propeller Laboratory, Power Plant Laboratory, and the Armament Laboratory of the Wright Air Development Center whose contributions were responsible for the results obtained and presented herein.

Finally, the authors desire to acknowledge the support of Mr. Ralph C. Lenz, Jr. and of Alan D. Sapowith, Captain, USAF. Mr. Lenz planned and directed the entire instrumentation effort reported as Appendix A. Captain Sapowith directed the peak skin temperature effort and prepared the material which is included herein as Appendix B.

[redacted]

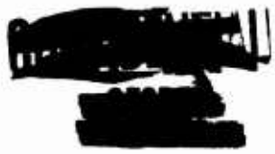

CONTENTS

ABSTRACT 3

PREFACE 5

CHAPTER 1 INTRODUCTION 39

1.1 General 39
1.2 Objective 39
1.3 Background 39
1.4 General Test Program 39

CHAPTER 2 PROCEDURE 41

2.1 General 41
2.2 Selection of Test Articles 41
2.2.1 Parked Aircraft 41
2.2.2 Aircraft Components 41
2.2.3 Passive Defense Structures 42
2.3 Selection and Location of Test Sites 42
2.3.1 Close-in Station 43
2.3.2 Intermediate Stations 43
2.3.3 Remote Station 43
2.4 Selection of Instrumentation 44
2.4.1 Photographic Records 44
2.4.2 General Input Measurements 44
2.4.3 Specific Input Measurements 45
2.4.4 Aircraft Response Measurements . . . 45
2.5 General Layout of Test Array 45
2.5.1 Shot 1 45
2.5.2 Shot 2 46
2.5.3 Shot 3 46
2.5.4 Shot 4 47
2.5.5 Revetments 47

CHAPTER 3 TEST RESULTS 53

3.1 General, Including Shot 1 53
3.2 Shot 2 54
3.2.1 Station 2200 55
3.2.1.1 Aircraft F-47 (9232) 55
3.2.1.2 Aircraft F-47 (9114) 56
3.2.1.3 Aircraft F-47 (8785) 56
3.2.1.4 Aircraft F-90 (6688) 57
3.2.2 Station 4000 57
3.2.3 Station 8000 57

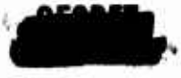

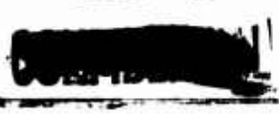

[redacted]

CONTENTS (Cont.)

	3.2.4	Station 10,500	58
	3.2.5	General Observations	58
3.3	Shot 3		58
	3.3.1	Station 1000	58
		3.3.1.1 Aircraft F-47 (9114)	70
	3.3.2	Station 1384	70
		3.3.2.1 Aircraft F-47 (9232)	71
	3.3.3	Station 2200	71
		3.3.3.1 Aircraft F-47 (9082)	72
		3.3.3.2 Aircraft F-47 (9931)	72
		3.3.3.3 Aircraft F-47 (9851)	74
		3.3.3.4 Aircraft F-47 (8785)	74
		3.3.3.5 Aircraft F-90 (6688)	76
	3.3.4	Station 4000	77
		3.3.4.1 Aircraft F-47 (9075)	77
		3.3.4.2 Aircraft F-47 (9110)	78
		3.3.4.3 Aircraft F-47 (9186)	79
	3.3.5	Station 4500	80
	3.3.6	Station 8000	80
		3.3.6.1 Aircraft F-47 (9074)	80
		3.3.6.2 Aircraft F-47 (9785)	81
		3.3.6.3 Aircraft F-47 (9072)	82
		3.3.6.4 Aircraft F-47 (0065)	83
		3.3.6.5 Aircraft F-47 (9719)	84
		3.3.6.6 Aircraft F-86 (8209)	84
		3.3.6.7 Aircraft F-86 (9597)	85
		3.3.6.8 Aircraft B-17 (3722)	86
		3.3.6.9 Aircraft B-17 (7746)	87
		3.3.6.10 Aircraft B-17 (5715)	88
		3.3.6.11 Aircraft B-45 (9481)	89
	3.3.7	Station 10,500	90
		3.3.7.1 Aircraft F-47 (3828)	90
		3.3.7.2 Aircraft F-47 (0297)	90
		3.3.7.3 Aircraft B-17 (3769)	91
		3.3.7.4 Aircraft B-17 (3730)	92
		3.3.7.5 Aircraft B-17 (3575)	93
		3.3.7.6 Aircraft B-29 (7349)	94
	3.3.8	General Observations	95
3.4	Shot 4		96
	3.4.1	Station 1000	96
	3.4.2	Station 1350	96
	3.4.3	Station 1384	181
	3.4.4	Station 1500	181
	3.4.5	Station 2200	181
	3.4.6	Station 2500	181

[redacted]

CONTENTS (Cont.)

3.4.6.1 Aircraft F-47 (9931) 182
3.4.6.2 Aircraft F-47 (9719) 182
3.4.6.3 Aircraft F-86 (8209) 183
3.4.6.4 Aircraft F-90 (6688) 183
3.4.7 Station 3320 184
3.4.7.1 Aircraft F-47 (9072) 184
3.4.8 Station 3450 185
3.4.8.1 Aircraft F-47 (3828) 185
3.4.8.2 Aircraft B-45 (9481) 186
3.4.9 Station 4000 187
3.4.9.1 Aircraft F-47 (3828) 187
3.4.9.2 Aircraft F-47 (0065) 188
3.4.9.3 Aircraft F-47 (9074) 189
3.4.9.4 Aircraft F-47 (9110) 189
3.4.9.5 Aircraft F-47 (9186) 190
3.4.9.6 Aircraft F-86 (9597) 190
3.4.9.7 Aircraft B-17 (5715) 191
3.4.10 Station 5000 192
3.4.10.1 Aircraft B-29 (7349) 192
3.4.11 Station 8000 193
3.4.11.1 Aircraft B-17 (3575) 193
3.4.12 General Observations 194
3.5 Test Panels 194
3.5.1 Panel A, Station 8000, Shot 3 268
3.5.2 Panel B, Station 2200, Shot 3 268
3.5.3 Panel C, Station 1000, Shot 4 268
3.6 General Input Functions 268
3.6.1 Peak Overpressure, Shots 2, 3, and 4 . 269
3.6.2 Total Thermal Energy, Shots 2, 3, and 4 269
3.6.3 Radiation Dosage, Shots 2, 3, and 4 . . 269
3.6.4 Pressure Measurements at Aircraft Parking Stations 269
3.7 General Test Data 270
3.8 Photographic Results 270
3.8.1 Motion Pictures 270
3.8.2 Sequencing Still Shots 271
3.8.3 Still Photography 271
3.8.4 Problems of Test Phase Photography . . 271

CHAPTER 4 DISCUSSION 287

4.1 General 287
4.2 Aircraft Damage Analysis 288
4.2.1 F-47 Aircraft 289
4.2.2 B-17 Aircraft 290

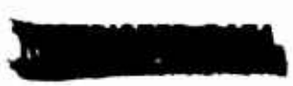

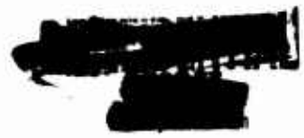

CONTENTS (Cont.)

4.2.3 B-29 and B-45 Aircraft 291
4.2.4 F-86 and F-90 Aircraft 292
4.2.5 Equipment and Systems 293
4.2.6 General Observations 295
4.3 Passive Defense Structures 297
4.4 Thermal Damage 298
4.5 Instrumentation Results 298
4.5.1 Total Thermal Energy 299
4.5.2 Overpressure 299
4.5.3 Temperature Rise 299
4.5.4 Wing and Fin Bending Moment Measurements 300
4.5.5 Acceleration 300
4.5.6 Measurement of Overpressure on Aircraft Wings 301

CHAPTER 5 CONCLUSIONS AND RECOMMENDATIONS 317

5.1 Conclusions 317
5.2 Recommendations 319

APPENDIX A OSCILLOGRAPHIC INSTRUMENTATION 321

A.1 Introduction 321
A.1.1 General 321
A.1.2 Objective 321
A.2 Procedure 321
A.2.1 Selection of Instrumentation 321
A.2.1.1 General Input Measurements . . 321
A.2.1.2 Specific Input Measurements . 325
A.2.1.3 Response Measurements . . . 326
A.2.2 Calibration 330
A.2.2.1 Introduction 330
A.2.2.2 General Procedure 330
A.2.2.3 General and Specific Input Functions 331
A.2.2.4 Response Functions 332
A.2.3 Operations 334
A.3 Test Results 335
A.3.1 General 335
A.3.2 Presentation of Shot 2 Data 372
A.3.2.1 Station 2200 372
A.3.2.2 Station 4000 372
A.3.2.3 Station 8000 373
A.3.2.4 Station 10,500 375
A.3.3 Presentation of Shot 3 Data 375

CONTENTS (Cont.)

A.3.3.1 Station 2200 375
A.3.3.2 Station 4000 392
A.3.3.3 Station 8000 392
A.3.3.4 Station 10,500 395
A.3.4 Presentation of Shot 4 Data 396
A.3.4.1 Station 2200 396
A.3.4.2 Station 4000 396
A.3.4.3 Station 8000 418
A.3.4.4 Station 10,500 418
A.4 Discussion 418
A.4.1 Total Thermal Energy Measurements . . 418
A.4.1.1 Particle Attenuation 418
A.4.1.2 Specific Attenuation 431
A.4.1.3 Variation in Rise Time . . . 432
A.4.2 Blast Phenomena 432
A.4.2.1 Overpressure Measurements . . 432
A.4.2.2 Angle-of-Blast Incidence Measurements 433
A.4.3 Temperature Rise Measurements 433
A.4.3.1 Comparison of Polished and Unpolished Surfaces 434
A.4.3.2 Comparison of Skin and Stringer Temperature Rise 434
A.4.3.3 Propeller Cuff Failure . . . 434
A.4.3.4 Copper Insert vs Standard Thermocouple Installation . . . 435
A.4.3.5 Effects of Shock Wave . . . 435
A.4.3.6 Computed Absorptivities . . . 436
A.4.4 Wing Bending Moment Measurements . . . 437
A.4.4.1 World War II Bomber 437
A.4.4.2 World War II Fighter 438
A.4.4.3 World War II Fighter vs Modern Fighter 438
A.4.4.4 Fin Bending on World War II Fighter 439
A.4.5 Acceleration Measurements 440
A.4.5.1 Normal Acceleration Measurements 440
A.4.5.2 Lateral Acceleration Measurements 441
A.4.6 Overpressure Measurements on Aircraft Surfaces 441
A.4.6.1 F-47 Wing 442
A.4.6.2 F-47 Wing vs F-86 Wing . . . 442

[redacted]

CONTENTS (Cont.)

A.4.6.3 Wing Surface With Obtuse Angle-of-Incidence 443

APPENDIX B SURVEY OF MAXIMUM SKIN TEMPERATURES 457

B.1 General 457
B.2 Temp Tape Instrumentation 457
B.2.1 Temp Tape Configuration 457
B.2.2 Mounting Procedure 457
B.2.3 Organic Pigment Tapes 458
B.3 Calibration 459
B.3.1 Accuracy of Maximum Temperature Indicator Tapes 459
B.3.1.1 Eutectic Alloy Tapes 459
B.3.1.2 Organic Pigment Tapes . . . 460
B.4 Correlating Measurements 460
B.4.1 Skin Material 460
B.4.2 Skin Thickness 460
B.4.3 Incidence Angles at Surfaces 461
B.4.4 Absorptivities of Skin Surfaces . . . 461
B.5 Results 461
B.5.1 Maximum Skin Temperatures 461
B.5.2 Thermal Input Comparisons 461
B.5.3 Critical Thermal Energies For Various Aircraft Skin Surfaces 462
B.6 Discussion 462
B.6.1 Correlation of Data 462
B.6.2 Discarded Data 463
B.6.3 Computed Incident Thermal Energies . . 463
B.6.4 Critical Thermal Energies 464
B.6.5 Residual Effect on Material Properties . 465
B.6.6 Calibration 465
B.6.7 Passive Defense 465

[redacted]

[redacted]

ILLUSTRATIONS

CHAPTER 2 PROCEDURE

2.1 Relative Locations of Aircraft Parking Stations and Revetments for Shots 2, 3, and 4 48

2.2 Location and Orientation of Aircraft for Shot 2 49

2.3 Location and Orientation of Aircraft for Shot 3 50

2.4 Location and Orientation of Aircraft for Shot 4 51

2.5 Orientations and Structural Configurations of Aircraft Revetments 52

CHAPTER 3 TEST RESULTS

3.1 Aircraft Damage Summary, Shot 2 59

3.2 Aerial View of Aircraft and Stabilized Area at Station 2200 Prior to Shot 2, Looking Away From Ground Zero 60

3.3 Aerial View of Aircraft and Stabilized Area at Station 8000 Prior to Shot 2, Looking Away From Ground Zero 61

3.4 Aerial View of Aircraft and Stabilized Area at Station 10,500, Prior to Shot 2, Looking Away From Ground Zero 62

3.5 F-47 (9232), Left Side-in, Station 2200 (4.7 psi), Shot 2, Showing Damage to Left Side of Fuselage, Rudder, and Tail Wheel Door . . . 63

3.6 F-47 (9232), Left Side-in, Station 2200 (4.7 psi), Shot 2, Close-up View of Crushing Effect of Positive Pressure Phase on Fuselage . . . 64

3.7 F-47 (9114), Tail-in, Station 2200 (4.7 psi), Shot 2, Showing Damage to Right Aileron, Flap, and Elevator 65

3.8 F-47 (9114), Tail-in, Station 2200 (4.7 psi), Shot 2, Close-up View of Damaged Right Flap and Broken Hinge Fittings 66

[redacted]

[redacted]

ILLUSTRATIONS (Cont.)

3.9 F-47 (8785), Nose-in, Station 2200 (4.7 psi), Shot 2, Showing Light Buckling Damage to Fuselage Skin Just Aft of Cowl Flaps 67

3.10 F-90 (6688), Nose-in, Station 2200 (4.7 psi), Shot 2, Showing General Post-shot Condition of Aircraft 68

3.11 F-90 (6688), Nose-in, Station 2200 (4.7 psi), Shot 2, Close-up View of Fuselage 69

3.12 Aircraft Damage Summary, Shot 3 97

3.13 F-47 (9114), Nose-in, Station 1000 (10.6 psi, 70 cal/cm^2), Shot 3, Showing General Burned and Buckled Areas Over Entire Aircraft 98

3.14 F-47 (9114), Nose-in, Station 1000 (10.6 psi), Shot 3, Close-up View Showing Damaged Right Flap and Aileron 99

3.15 F-47 (9114), Nose-in, Station 1000 (10.6 psi), Shot 3, Close-up View of Cockpit Showing Destroyed Canopy and Thermal Effects 100

3.16 F-47 (9232), Nose-in, Station 1384 (9.9 psi), Shot 3, Showing Burned and Buckled Left Side of Aircraft 101

3.17 F-47 (9232), Nose-in, Station 1384 (9.9 psi), Shot 3, Showing Burned and Buckled Right Side of Aircraft 102

3.18 F-47 (9232), Nose-in, Station 1384 (9.9 psi), Shot 3, Full Rear View, Emphasizing Burned Areas On Wing and Horizontal Stabilizer . . . 103

3.19 F-47 (9082), Right Side-in, Station 2200 (8.4 psi), Shot 3, Showing Buckled Skin Panels, Damaged Rudder, and Thermal Damage to Control Surfaces and Horizontal Stabilizer 104

3.20 F-47 (9082), Side-in, Station 2200 (8.4 psi), Shot 3, Showing Degree of Aircraft Rotation During Blast Phase By Comparing With Ground

[redacted]

ILLUSTRATIONS (Cont.)

Shadow of Aircraft Caused By Thermal Phase . . 105

3.21 F-47 (9931), Right Front Quarter-in, Station 2200 (8.4 psi), Shot 3, Showing Damage to Left Side of Fuselage and Rudder (Downward Side) . 106

3.22 F-47 (9931), Right Front Quarter-in, Station 2200 (8.4 psi), Shot 3, Showing Torsion and Bending Failure in Right Horizontal Stabilizer 107

3.23 F-47 (9931), Right Front Quarter-in, Station 2200 (8.4 psi), Shot 3, Close-up View of Aft Section of Fuselage, Showing Charred and Buckled Right Side and Horizontal Stabilizer Failure 108

3.24 F-47 (9931), Right Front Quarter-in, Station 2200 (8.4 psi), Shot 3, Close-up View of Left Main Landing Gear 109

3.25 F-47 (9851), Tail-in, Station 2200 (8.4 psi), Shot 3, Showing Damage to Right Side of Fuselage, Empennage, and Wing 110

3.26 F-47 (9851), Tail-in, Station 2200 (8.4 psi), Shot 3, Close-up View of Buckled Carburetor Air Duct After the Caved-in Radio Access Door Was Removed 111

3.27 F-47 (9851), Tail-in, Station 2200 (8.4 psi), Shot 3, Close-up View of Skin Damage on Left Horizontal Stabilizer 112

3.28 F-47 (8785), Nose-in, Station 2200 (8.4 psi), Shot 3, Showing Buckled Areas Over Entire Aircraft 113

3.29 F-47 (8785), Nose-in, Station 2200 (8.4 psi), Shot 3, Showing Bent Right Horizontal Stabilizer and Holes in Horizontal Stabilizers Where "No Lift" Was Lettered in Black 114

3.30 F-90 (6688), Nose-in, Station 2200 (8.4 psi), Shot 3, Showing Damage to Right Side Radio Access Door, Tail Cone, and Fin 115

[redacted]

ILLUSTRATIONS (Cont.)

3.31 F-90 (6688), Nose-in, Station 2200 (8.4 psi), Shot 3, Close-up View of Buckled Radio Access Door and Charred Radome 116

3.32 F-90 (6688), Nose-in, Station 2200 (8.4 psi), Shot 3, Showing General Thermal Effects . . . 117

3.33 F-90 (6688), Nose-in, Station 2200 (8.4 psi), Shot 3, Close-up of Canopy, Showing Cracks . . 118

3.34 F-90 (6688), Nose-in, Station 2200 (8.4 psi), Shot 3, Close-up View, Showing Ripples on Aileron and Buckles in Upper Aft Section of Fuselage 119

3.35 F-90 (6688), Nose-in, Station 2200 (8.4 psi), Shot 3, Close-up View of Damage to Inboard Section of Right Aileron 120

3.36 F-90 (6688), Nose-in, Station 2200 (8.4 psi), Shot 3, Close-up View of Damaged Stainless Steel Tail Cone 121

3.37 F-90 (6688), Nose-in, Station 2200 (8.4 psi), Shot 3, Close-up View of Left Main Landing Gear 122

3.38 F-47 (9075), Side-in, Station 4000 (6.4 psi), Shot 3, Showing General Scorched and Buckled Regions on Right Side of Fuselage 123

3.39 F-47 (9110), Side-in in Pit Revetment, Station 4000 (6.4 psi), Shot 3, Showing Scorched and Buckled Right Side and Scorched Areas of Skin on Vertical Tail 124

3.40 F-47 (9186), Side-in Behind Wall Revetment, Station 4000 (6.4 psi), Shot 3, Close-up View of Damaged and Burned Fuselage Surface . . . 125

3.41 F-47 (9186), Side-in Behind Wall Revetment, Station 4000 (6.4 psi), Shot 3, Close-up View of Scorched Vertical Stabilizer and Rudder Paint 126

[redacted]

[redacted]

ILLUSTRATIONS (Cont.)

3.42 F-47 (9186), Side-in Behind Wall Revetment, Station 4000 (6.4 psi), Shot 3, Close-up View of Outboard Section of Left Wing, Showing Buckling and Overheating Effect 127

3.43 B-17 (3699), Nose-in, Station 4500 (5.8 psi), Shot 3, Close-up of Crushed Lower Left Wing of BUSTER-JANGLE Aircraft, Showing Protruding Rib 128

3.44 F-47 (9074), Right Side-in in G-Type Revetment, Station 8000 (3.6 psi), Shot 3, Showing Buckling of Fuselage Skin Panels 129

3.45 F-47 (9074), Right Side-in in G-Type Revetment, Station 8000 (3.6 psi), Shot 3, Close-up View of Forward Section of Fuselage and Inboard Section of Right Wing and Cracked Canopy . . 130

3.46 F-47 (9074), Right Side-in in G-Type Revetment, Station 8000 (3.6 psi), Shot 3, Close-up View of Cracks in Canopy 131

3.47 F-47 (9785), Left Side-in, Station 8000 (3.6 psi), Shot 3, Showing General Blast Damage to Left Side of Fuselage 132

3.48 F-47 (9785), Side-in, Station 8000 (3.6 psi), Shot 3, Close-up View of Bending Failure and Buckles of Rudder 133

3.49 F-47 (9072), Tail-in, Station 8000 (3.6 psi), Shot 3, Showing Bending Failures and Buckles of Ailerons and Flaps 134

3.50 F-47 (9072), Tail-in, Station 8000 (3.6 psi), Shot 3, Close-up View of Damaged Right Flap and Aileron 135

3.51 F-47 (9072), Tail-in, Station 8000 (3.6 psi), Shot 3, Showing Buckled Area on Left Aft Section of Fuselage 136

3.52 F-47 (0065), Nose-in, Station 8000 (3.6 psi), Shot 3, Showing General Post-shot Condition . 137

[redacted]

[redacted]

ILLUSTRATIONS (Cont.)

3.53 F-47 (0065), Nose-in, Station 8000 (3.6 psi), Shot 3, Close-up View of Cracked Canopy . . . 138

3.54 F-47 (9719), Nose-in in G-Type Revetment, Station 8000 (3.6 psi), Shot 3, Close-up View of Cracked Canopy 139

3.55 F-86 (8209), Right Side-in, Station 8000 (3.6 psi), Shot 3, Showing Damage to Aft Fuselage Section 140

3.56 F-86 (8209), Right Side-in, Station 8000 (3.6 psi), Shot 3, Close-up View of Buckled and Torn Skin Aft of Fuselage Disconnect Joint . . 141

3.57 F-86 (8209), Right Side-in, Station 8000 (3.6 psi), Shot 3, Access Doors With Messerschmidt Fasteners Popped Open Due to Blast 142

3.58 F-86 (8209), Right Side-in, Station 8000 (3.6 psi), Shot 3, Showing Charred Plastic Nose on Right Side 143

3.59 F-68 (8209), Right Side-in, Station 8000 (3.6 psi), Shot 3, Close-up View of Charred Antenna Housing and Wrinkled Skin on Rudder 144

3.60 F-86 (9597), Nose-in, Station 8000 (3.6 psi), Shot 3, Showing General Post-shot Condition of Aircraft 145

3.61 F-86 (9597), Nose-in, Station 8000 (3.6 psi), Shot 3, Close-up View of Scorched Rubber Coating on Nose, Slight Buckles in Area Below Cockpit, and Smoked Canopy 146

3.62 B-17 (3722), Left Side-in, Station 8000 (3.6 psi), Shot 3, Showing Fuselage Failure Aft of Wing Trailing Edge, Generally Buckled Fuselage Skin, and Severely Buckled Vertical Stabilizer and Dorsal Fin 147

3.63 B-17 (3722), Left Side-in, Station 8000 (3.6 psi), Shot 3, Showing Failure of Fuselage Aft of Wing Trailing Edge, and the Burned Rudder,

[redacted]

[redacted]

ILLUSTRATIONS (Cont.)

Right Aileron and Left Elevator 148

3.64 B-17 (7746), Tail-in, Station 8000 (3.6 psi), Shot 3, Showing Total Damage to Wing Structure Aft of Rear Spars, Crushed Fuselage and Dorsal Fin, and Burned Elevator and Upper Surface of Aileron 149

3.65 B-17 (7746), Tail-in, Station 8000 (3.6 psi), Shot 3, Showing Wing Damage and Distortion of Fuselage Skin 150

3.66 B-17 (5715), Nose-in, Station 8000 (3.6 psi), Shot 3, Close-up View of Nose and Forward Section, Showing Damage to Radar Housing and Fuselage Forward of Wing Leading Edge . . . 151

3.67 B-17 (5715), Nose-in, Station 8000 (3.6 psi), Shot 3, Showing Buckled Bomb-bay Doors . . . 152

3.68 B-17 (5715), Nose-in, Station 8000 (3.6 psi), Shot 3, Showing Pressure Damage to Vertical Stabilizer Surface and Dorsal Fin 153

3.69 B-17 (5715), Nose-in, Station 8000 (3.6 psi), Shot 3, Showing Buckled Under Surface of Right Wing Outboard Section 154

3.70 B-17 (5715), Nose-in, Station 8000 (3.6 psi), Shot 3, Showing Thermal and Blast Damage to Cockpit 155

3.71 B-17 (5715), Nose-in, Station 8000 (3.6 psi), Shot 3, External View of Top of Cabin Showing Charred Interior 156

3.72 B-17 (5715), Nose-in, Station 8000 (3.6 psi), Shot 3, Interior View, Showing Failed Fuselage Frames and Buckled Skin 157

3.73 B-45 (9481), Nose-in, Station 8000 (3.6 psi), Shot 3, Close-up View of Right Hand Engine Nacelle, Showing Dished Upper and Lower Nose Fairing 158

[redacted]

[redacted]

ILLUSTRATIONS (Cont.)

3.74 B-45 (9481), Nose-in, Station 8000 (3.6 psi), Shot 3, Close-up View of Blown-in Bomb-bay Doors 159

3.75 B-45 (9481), Nose-in, Station 8000 (3.6 psi), Shot 3, Close-up View of Empennage, Showing Buckled Tail-gunner's Cone and Fairing Between Dorsal Fin and Vertical Stabilizer 160

3.76 B-45 (9481), Nose-in, Station 8000 (3.6 psi), Shot 3, Showing Broken Support Member of Bomb-bay Door Actuating Mechanism 161

3.77 B-45 (9481), Nose-in, Station 8000 (3.6 psi), Shot 3, Showing Broken Linkage of Bomb-bay Door Actuating Mechanism 162

3.78 B-45 (9481), Nose-in, Station 8000 (3.6 psi), Shot 3, Close-up View of Right Main Landing Gear, Showing Thermal Damage to Exposed Portion of Tire 163

3.79 F-47 (3828), Right Side-in, Station 10,500 (2.4 psi), Shot 3, Showing Buckled Area Below Aft Section of Cockpit 164

3.80 F-47 (0297), Tail-in, Station 10,500 (2.4 psi), Shot 3, Close-up View of Cracked Canopy . 165

3.81 B-17 (3769), Right Side-in, Station 10,500 (2.4 psi), Shot 3, Showing Burned Rudder, and Buckled Vertical Stabilizer and Dorsal Fin . . 166

3.82 B-17 (3769), Right Side-in, Station 10,500 (2.4 psi), Shot 3, Showing Pressure Damage to Nose Section of Fuselage 167

3.83 B-17 (3769), Right Side-in, Station 10,500 (2.4 psi), Shot 3, Interior View, Showing Bent Fuselage Frames and Buckled Skin 168

3.84 B-17 (3769), Right Side-in, Station 10,500 (2.4 psi), Shot 3, Interior View, Showing Bent and Buckled Condition of Skin and Fuselage Frames 169

[redacted]

[redacted]

ILLUSTRATIONS (Cont.)

3.85 B-17 (3730), Tail-in, Station 10,500 (2.4 psi), Shot 3, Showing Burned Elevators and Generally Dished-in Skin on Vertical Stabilizer, Dorsal Fin, and Wing Area Above Flap . . 170

3.86 B-17 (3575), Nose-in, Station 10,500 (2.4 psi), Shot 3, Showing Wrinkles in Vertical Stabilizer 171

3.87 B-17 (3575), Nose-in, Station 10,500 (2.4 psi), Shot 3, Close-up View of Right Wing, Showing Upper and Lower Buckled Surfaces . . 172

3.88 B-29 (7349), Nose-in, Station 10,500 (2.4 psi), Shot 3, Close-up View From Left Side of Totally Wrecked Forward Bomb-bay Doors . . . 173

3.89 B-29 (7349), Nose-in, Station 10,500 (2.4 psi), Shot 3, Showing Totally Wrecked Right Hand Forward Bomb-bay Door 174

3.90 B-29 (7349), Nose-in, Station 10,500 (2.4 psi), Shot 3, Showing Buckled Skin on Right Hand Aft Bomb-bay Door 175

3.91 B-29 (7349), Nose-in, Station 10,500 (2.4 psi), Shot 3, Interior View of Totally Wrecked Forward Bomb-bay Doors 176

3.92 B-29 (7349), Nose-in, Station 10,500 (2.4 psi), Shot 3, Showing Crew Tunnel Perforated by Bomb Rack Quick-release Pin 177

3.93 B-29 (7349), Nose-in, Station 10,500 (2.4 psi), Shot 3, Showing Slight Skin Buckles on Lower Surface of Right Wing Outer Panel . . 178

3.94 B-29 (7349), Nose-in, Station 10,500 (2.4 psi), Shot 3, Close-up View of Left Inboard Nacelle, Showing Buckled Tail Fairing . . . 179

3.95 B-29 (7349), Nose-in, Station 10,500 (2.4 psi), Shot 3, Showing Buckles on Vertical Stabilizer 180

[redacted]

[redacted]

ILLUSTRATIONS (Cont.)

3.96 Aircraft Damage Summary, Shot 4 195

3.97 F-47 (9114), Nose-in, Station 1000 (36 psi), Shot 4, Showing Burned Wreckage of Fuselage and Power Plant 196

3.98 Debris Near Station 1350, Looking West, Following Shot 4 197

3.99 F-47 (9851), Tail-in, Station 1350 (22 psi), Shot 4, Showing Remains of Totally Wrecked Aircraft 198

3.100 F-47 (9851), Tail-in, Station 1350 (22 psi), Shot 4, Close-up View of Wrecked Fuselage . . 199

3.101 F-47 (9232), Nose-in, Station 1384 (21 psi), Shot 4, Showing Destroyed Forward Section of Fuselage and Miscellaneous Wreckage After Fire Was Extinguished 200

3.102 B-17 (3699), Nose-in, Station 1500 (18 psi), Shot 4, Showing General View of Wreckage . . 201

3.103 B-17 (3699), Nose-in, Station 1500 (18 psi), Shot 4, Close-up View of Wrecked Engine . . . 202

3.104 B-17 (3699), Nose-in, Station 1500 (18 psi), Shot 4, Close-up View of Engine Remains and Test Propeller 203

3.105 B-17 (3699), Nose-in, Station 1500 (18 psi), Shot 4, Close-up View of Destroyed Engine Showing Miscellaneous Wreckage in Background . 204

3.106 B-17 (3699), Nose-in, Station 1500 (18 psi), Shot 4, Close-up View Engine Wreckage . . . 205

3.107 F-47 (8785), Nose-in, Station 2200 (9.4 psi), Shot 4, General View of Demolished Aircraft Showing Failure of Fuselage at Turbo Station . 206

3.108 F-47 (8785), Nose-in, Station 2200 (9.4 psi), Shot 4, Showing Collapsed Right Landing Gear and Missing Right Wing Outboard of Outboard

[redacted]

[redacted]

ILLUSTRATIONS (Cont.)

[illegible] Rear Fin

[illegible] Side-On, Station [illegible] General View of Wreckage, [illegible] Rear Fairing Outboard of Wing [illegible]

[illegible] Side-On, Station [illegible] Showing Right and Left Wing [illegible] Raised Right Landing Gear

[illegible] Left Side-On, [illegible] Shot [illegible] Showing Fuselage Broken Behind Cockpit

[illegible] Left Side-On at [illegible] Shot [illegible] Showing Buffed Area Between Fuselage and Broken Wing Tips

[illegible] Side-On, Station [illegible] Shot [illegible] Showing Absence of Vertical Stabilizer and Damaged Empennage

[illegible] Side-On, Station [illegible] Shot [illegible] Showing Bent Propellers [illegible] Ground with Ground

[illegible] (3719), Close-On, Station [illegible] Shot [illegible] Close-Up View of Windshield and Canopy Damage

3.116 F-86 (3209), Close-On, Station [illegible] Shot [illegible] Showing General Condition of Aircraft [illegible]

3.117 F-86 (3209), Close-On, Station [illegible] Shot [illegible] Close-Up View From Left Side of Severely Buckled and Torn Fuselage Section [illegible]

3.118 F-86 (3209), Close-On, Station 2500 (8.4 psi), Shot 4, Close-Up View From Left Side of Severely Buckled and Torn Fuselage Section Just Forward of Dorsal Fin [illegible]

3.119 F-80 (6688), Left Side-On, Station 2500 (8.9 psi), Shot 4, General View of Wreckage,

[redacted]

[redacted]

ILLUSTRATIONS (Cont.)

Showing Position of Rear Section After Being Torn Off at Removable Joint 218

3.120 F-90 (6688), Left Side-in, Station 2500 (8.9 psi), Shot 4, Showing Shredded Nose Compartment, Collapsed Landing Gear, and Destroyed Canopy 219

3.121 F-90 (6688), Left Side-in, Station 2500 (8.9 psi), Shot 4, Close-up View of Destroyed Cockpit 220

3.122 F-90 (6688), Left Side-in, Station 2500 (8.9 psi), Shot 4, Close-up View of Punctured Top Left Wing Surface Near Wing Root Caused By Landing Gear 221

3.123 F-90 (6688), Left Side-in, Station 2500 (8.9 psi), Shot 4, Showing Aft Fuselage and Tail Assembly Wreckage 222

3.124 F-90 (6688), Left Side-in, Station 2500 (8.9 psi), Shot 4, Showing Aft Fuselage and Tail Assembly Wreckage 223

3.125 F-90 (6688), Left Side-in, Station 2500 (8.9 psi), Shot 4, Close-up View of Wrecked Empennage, Showing Broken Right Stabilizer . . 224

3.126 F-47 (9072), Nose-in, Station 3320 (6.9 psi), Shot 4, Showing General Post-shot Condition of Aircraft 225

3.127 F-47 (3828), Tail-in, Station 3450 (6.5 psi), Shot 4, Showing Buckled, Bent, and Torn-off Control Surfaces 226

3.128 F-47 (3828), Tail-in, Station 3450 (6.5 psi), Shot 4, Close-up View of Buckled Skin Panels on Fuselage, and Inboard Section of Right Wing With Dismembered Flap 227

3.129 B-45 (9481), Nose-in, Station 3450 (6.5 psi), Shot 4, General View of Aircraft, Showing Forward Bomb-bay Doors Hanging Loose and Main

[redacted]

[redacted]

ILLUSTRATIONS (Cont.)

Landing Gear Doors Broken Open 228

3.130 B-45 (9481), Nose-in, Station 3450 (6.5 psi), Shot 4, Close-up View of Nose, Showing Pushed-in Radome, and Smoked Interior of Bombardier's Enclosure 229

3.131 B-45 (9481), Nose-in, Station 3450 (6.5 psi), Shot 4, Close-up View of Empennage, Showing Tail Cone Failure and Buckled Skin on Fuselage Just Below Serial Number 230

3.132 B-45 (9481), Nose-in, Station 3450 (6.5 psi), Shot 4, Close-up View of Empennage, Showing Increased Caving-in of Fairing Between Dorsal and Vertical Fin 231

3.133 B-45 (9481), Nose-in, Station 3450 (6.5 psi), Shot 4, Interior View of Cockpit, Showing Charred Upholstery 232

3.134 B-45 (9481), Nose-in, Station 3450 (6.5 psi), Shot 4, Interior View, Showing Opened Bomb-bay Doors and Damaged Bulkhead Door Aft of Bomb Bay 233

3.135 B-45 (9481), Nose-in, Station 3450 (6.5 psi), Shot 4, Close-up View (Looking Aft) of Twisted Bulkhead Door and Bent Bulkhead Vertical Stiffeners 234

3.136 B-45 (9481), Nose-in, Station 3450 (6.5 psi), Shot 4, Close-up View (Looking Forward) of Damaged Bulkhead Door Just Aft of Bomb Bays . 235

3.137 B-45 (9481), Nose-in, Station 3450 (6.5 psi), Shot 4, Interior View of Bent Fuselage Frames and Pushed-in Skin 236

3.138 F-47 (9785), Left Side-in, Station 4000 (5.8 psi), Shot 4, Showing Severely Buckled Left Side of Fuselage and Empennage 237

3.139 F-47 (9785), Left Side-in, Station 4000 (5.8 psi), Shot 4, Showing Buckled Rudder and

[redacted]

ILLUSTRATIONS (Cont.)

Failed Vertical Stabilizer 238

3.140 F-47 (9785), Left Side-in, Station 4000 (5.8 psi), Shot 4, Close-up View of Destroyed Canopy 239

3.141 F-47 (0065), Tail-in, Station 4000 (5.8 psi), Shot 4, Showing General Post-shot Condition of Aircraft 240

3.142 F-47 (9074), Tail-in, Station 4000 (5.8 psi), Shot 4, Showing General Post-shot Condition of Aircraft 241

3.143 F-47 (9074), Tail-in, Station 4000 (5.8 psi), Shot 4, Close-up View of Buckles in Fuselage and Damaged Aileron 242

3.144 F-47 (9074), Tail-in, Station 4000 (5.8 psi), Shot 4, Close-up View of Buckled and Torn-off Left Wing Flap 243

3.145 F-47 (9074), Tail-in, Station 4000 (5.8 psi), Shot 4, Close-up View of Empennage, Showing Failed Rudder and Elevator Hinge Brackets . . 244

3.146 F-47 (9110), Tail-in, in Pit Revetment, Station 4000 (5.8 psi), Shot 4, Showing Broken Wing Flaps and Fuselage Skin Buckles 245

3.147 F-47 (9110), Tail-in, in Pit Revetment, Station 4000 (5.8 psi), Shot 4, Close-up View of Buckled Left Aileron and Left Flap . . . 246

3.148 F-47 (9186), Tail-in, Behind Wall Revetment, Station 4000 (5.8 psi), Shot 4, Showing Tail-up Position Assumed During Shot 4 247

3.149 F-47 (9186), Tail-in, Behind Wall Revetment, Station 4000 (5.8 psi), Shot 4, Showing Position Assumed and Resulting Propeller Damage . 248

3.150 F-86 (9597), Tail-in, Station 4000 (5.8 psi), Shot 4, Showing General Post-shot Condition of Aircraft 249

[redacted]

ILLUSTRATIONS (Cont.)

3.151 F-86 (9597), Tail-in, Station 4000 (5.8 psi), Shot 4, Close-up View of Instrument Panel . . 250

3.152 F-86 (9597), Tail-in, Station 4000 (5.8 psi), Shot 4, Close-up View of Rudder, Showing Damage at Hinges Due to Rudder Encountering Travel Stops 251

3.153 B-17 (5715), Tail-in, Station 4000 (5.8 psi), Shot 4, Showing General Post-shot Condition of Aircraft 252

3.154 B-17 (5715), Tail-in, Station 4000 (5.8 psi), Shot 4, Close-up View of Wreckage of Left Wing Torn Off Aft of Rear Spar 253

3.155 B-17 (5715), Tail-in, Station 4000 (5.8 psi), Shot 4, Close-up View of Completely Buckled Fuselage and Wreckage of Right Wing Torn Off Aft of Rear Spar 254

3.156 B-29 (7349), Nose-in, Station 5000 (4.0 psi), Shot 4, Showing General Post-shot Condition of Aircraft 255

3.157 B-29 (7349), Nose-in, Station 5000 (4.0 psi), Shot 4, Close-up View of Lower Surface of Left Wing, Showing Buckled Skin on Wing Outer Panels 256

3.158 B-29 (7349), Nose-in, Station 5000 (4.0 psi), Shot 4, Close-up View of Right Wing Lower Surface, Showing Buckled Skin on Outboard Section 257

3.159 B-29 (7349), Nose-in, Station 5000 (4.0 psi), Shot 4, Close-up View of Buckles on the Left Wing Aft Section in Vicinity of Inboard Nacelle 258

3.160 B-29 (7349), Nose-in, Station 5000 (4.0 psi), Shot 4, Showing Evidence of Buckled Ribs in Left Wing Outer Panels 259

3.161 B-29 (7349), Nose-in, Station 5000 (4.0 psi),

[redacted]

[redacted]

ILLUSTRATIONS (Cont.)

Shot 4, Close-up View of Empennage, Showing Buckled Vertical Tail and Dorsal Fin 260

3.162 B-17 (3575), Left Side-in, Station 8000 (1.9 psi), Shot 4, Showing General Post-shot Condition of Aircraft 261

3.163 B-17 (3575), Left Side-in, Station 8000 (1.9 psi), Shot 4, Close-up View of Torque Failure of Fuselage in Area Above Wing Trailing Section 262

3.164 B-17 (3575), Left Side-in, Station 8000 (1.9 psi), Shot 4, Close-up View of Lower Surface of Left Wing, Showing Pressure Damage to Skin in Outer Panels 263

3.165 B-17 (3575), Left Side-in, Station 8000 (1.9 psi), Shot 4, Showing Buckled Dorsal Fin and Vertical Stabilizer and Burned Rudder . . . 264

3.166 B-17 (3575), Left Side-in, Station 8000 (1.9 psi), Shot 4, Interior View of Torque Failure of Right Side of Fuselage, Showing Bent Fuselage Frames and Buckled Skin 265

3.167 B-17 (3575), Left Side-in, Station 8000 (1.9 psi), Shot 4, Interior View of Left Side Fuselage in Area of Wing Trailing Edge Showing Damaged Fuselage Frames 266

3.168 B-17 (3575), Left Side-in, Station 8000 (1.9 psi), Shot 4, Interior View of Damaged Dorsal Fin Bulkhead 267

3.169 Special Component Test Panel Array at Station 8000 After Shot 3 273

3.170 Seat Cushion Panel Array at Station 8000 After Shot 3 274

3.171 Bearing Panel Array at Station 8000 After Shot 3 275

3.172 Integral Fuel Cell Model Array at Station

[redacted]

ILLUSTRATIONS (Cont.)

8000 After Shot 3 276

3.173 Variation of Peak Overpressure at Ground Level With Ground Range for Shots 2, 3, and 4 (Composite Data) 277

3.174 Variation of Total Thermal Energy With Ground Range for Shots 2, 3, and 4 278

3.175 Variation of Gamma Radiation With Ground Range for Shots 2, 3, and 4, Based on Film Badge Data 279

3.176 Comparison of Overpressure-time Measurements Made Behind the Wall Revetment and in the Open at Station 4000, Shot 4 (Project 1.13 Data) 280

3.177 Station Elevations and Horizontal Distances From Target Ground Zero Showing Bomb Burst Points 284

3.178 B-17 (3722), Left Side-in, Station 8000 (11 cal/cm^2), Shot 3, Showing Condition of Aircraft During Thermal Phase Approximately One Second After Time Zero 285

3.179 B-17 (3730), Tail-in, Station 10,500 (6.7 cal/cm^2), Shot 3, Showing Condition of Aircraft During Thermal Phase Approximately One Second After Detonation 286

CHAPTER 4 DISCUSSION

4.1 Pictorial Representation of Aircraft Exposed During Shot 3, Showing Extent and Severity of Damage 303

4.2 Vulnerability of F-47 Aircraft Parked Side-in as a Function of Peak Overpressure 305

4.3 Vulnerability of F-47 Aircraft Parked Tail-in as a Function of Peak Overpressure 306

4.4 Vulnerability of F-47 Aircraft Parked Nose-in

[redacted]

ILLUSTRATIONS (Cont.)

as a Function of Peak Overpressure 307

4.5 Vulnerability of B-17 Aircraft Parked Side-in as a Function of Peak Overpressure 308

4.6 Vulnerability of B-17 Aircraft Parked Tail-in as a Function of Peak Overpressure 309

4.7 Vulnerability of B-17 Aircraft Parked Nose-in as a Function of Peak Overpressure 310

4.8 Vulnerability of B-29 Aircraft Parked Nose-in as a Function of Peak Overpressure 311

4.9 Vulnerability of B-45 Aircraft Parked Nose-in as a Function of Peak Overpressure 312

4.10 Section Views of the Aircraft Revetments Utilized During Shots 3 and 4, Showing the Areas Exposed to Direct Thermal Radiation 314

4.11 Skin Thicknesses (Inches) of F-47 Aircraft Wing and Horizontal Stabilizer, Top Surfaces . . . 315

4.12 Skin Thickness (Inches) of F-47 Aircraft Fuselage and Vertical Tail 316

APPENDIX A OSCILLOGRAPHIC INSTRUMENTATION

A.1 Location of the Instrumented Airplane, Instrument Pit, and Concrete Base With Respect to the Survey Control Point at Station 2200 336

A.2 Location of the Instrumented Airplanes, Instrument Pits, and Concrete Bases With Respect to the Survey Control Point at Station 4000 . . 337

A.3 Location of the Instrumented Airplanes, Instrument Pits, and Concrete Bases With Respect to the Survey Control Point at Station 8000 . . 338

A.4 Location of the Instrumented Airplanes, Instrument Pit, and Concrete Base With Respect to the Survey Control Point at Station 10,500 . . . 339

[redacted]

[redacted]

ILLUSTRATIONS (Cont.)

A.5 Typical Installation of the Recording and Amplifying Equipment in the Instrument Pits at Stations 4000 and 8000 340

A.6 Typical Installation of the Recording and Amplifying Equipment in the Instrument Pit at Station 2200 341

A.7 Schematic Wiring Diagram of Calorimeter Circuit and a Typical Mounting Installation of the Calorimeter 342

A.8 Schematic Wiring Diagram of Pressure Transmitter Circuit and a Typical Mounting Installation of the Pressure Transmitter 343

A.9 Typical Installation of Pressure Transmitter for Ground Overpressure Measurement 344

A.10 Vane-type Angle-of-blast Incidence Indicator . 345

A.11 Typical Installation of Angle-of-blast Incidence Indicator, Calorimeter and Site Pressure Transmitter 346

A.12 Installation of Calorimeter in the Co-pilot's Seat of B-17 (5715) 347

A.13a Location of Instrumentation Inside the Fuselage of B-17 (5715) 348

A.13b Location of Instrumentation on the Wing of B-17 (5715) 349

A.14 Installation of the Pressure Transmitters on the Vertical Stabilizer of F-47 (9785) . . . 350

A.15a Location of Instrumentation on F-47 (9785) . . 351

A.15b Location of Instrumentation on F-47 (9785) . . 352

A.16 Installation of the Pressure Transmitters on the Wing of F-86 (9597) 353

A.17a Location of Instrumentation Inside the Fuselage

ILLUSTRATIONS (Cont.)

of F-47 (0065) 354

A.17b Location of Instrumentation on F-47 (0065) . 355

A.17c Location of Instrumentation on Left Wing Gun-bay Door on F-47 (0065) 356

A.18a Location of Instrumentation Inside Fuselage of F-86 (9597) 357

A.18b Location of Instrumentation on F-86 (9597) . 358

A.19a Location of Instrumentation on F-47 (8785) . 359

A.19b Location of Instrumentation on F-47 (8785) . 360

A.20 Installation of the Thermocouple on the Propeller Cuff of F-47 (8785) 361

A.21 Standard and Copper Insert Type Thermocouple Installations and Schematic Wiring Diagram of the Thermocouple Circuit 362

A.22a Instrumentation Schematic for Station 2200, Shot 3 363

A.22b Instrumentation Schematic for Station 2200, Shot 4 364

A.23a Instrumentation Schematic for Station 8000, Left Side, Shots 2 and 3 365

A.23b Instrumentation Schematic for Station 8000, Right Side, Shot 2 366

A.23c Instrumentation Schematic for Station 8000, Right Side, Shot 3 367

A.24a Instrumentation Schematic for Station 10,500, Shots 2 and 3 368

A.24b Instrumentation Schematic for Station 8000, Shot 4 369

A.25a Instrumentation Schematic for Station 4000,

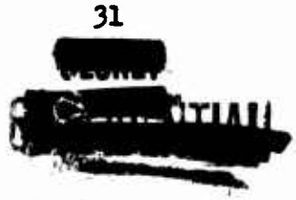

ILLUSTRATIONS (Cont.)

	Left Side, Shot 4	370
A.25b	Instrumentation Schematic for Station 4000, Right Side, Shot 4	371
A.26	Comparison of the Variation of Corrected Total Thermal Energy With Time at Various Heights, Station 8000, Shot 2	382
A.27	Comparison of the Variation of Overpressure With Time, at Two Points on the Ground, 148 Ft Apart, Station 8000, Shot 2	383
A.28	Comparison of the Variation of Corrected Total Thermal Energy With Time, at Various Heights, Station 8000, Shot 2	384
A.29	Comparison of the Variation of Overpressure With Time on the Wing of F-47 (0065) and a Point on the Ground, Station 8000, Shot 2 . .	385
A.30	Comparison of the Variation of Overpressure With Time on Wings of F-47 (0065) and F-86 (9597) at Different Stations and Shots . . .	386
A.31	Comparison of the Variation of Total Thermal Energy 5 Ft Above Ground With B-17 (5715) Wing Temperature Rise, Station 8000, Shot 2 .	387
A.32	Comparison of the Variation of Normal Acceleration and Wing Bending Moment With Time, Station 8000, Shot 2, B-17 (5715)	388
A.33	Comparison of the Variation of Fin Bending Moment on F-47 (9785), Wing Bending Moment on B-17 (5715), and Overpressure at a Point on the Ground, Station 8000, Shot 2	389
A.34	Comparison of the Variation of Corrected Total Thermal Energy With Time at Various Heights, Station 10,500, Shot 2	390
A.35	Comparison of the Variation of Overpressure With Time at a Point on the Ground, Station 10,500, Shot 2	391

[redacted]

ILLUSTRATIONS (Cont.)

A.36 Comparison of the Variation of Corrected Total Thermal Energy With Time at Various Heights, Station 2200, Shot 3 397

A.37 Comparison of the Variation of Normal Acceleration With Time on F-47 (8785) During Shots 3 and 4, Station 2200 398

A.38 Comparison of the Variation of Corrected Total Thermal Energy With Time at Various Heights, Station 8000, Shot 3 399

A.39 Comparison of the Variation of Angle-of-blast Incidence With Time, 3½ Ft Above Ground, Station 8000, Shot 3 400

A.40 Comparison of the Variation of Corrected Total Thermal Energy With Time at Various Heights, Station 8000, Shot 3 401

A.41 Comparison of the Variation of Corrected Total Thermal Energy, 5 Ft Above Ground With F-86 (9597) Wing Temperature Rise, Station 8000, Shot 3 402

A.42 Comparison of the Variation of Temperature Rise With Time, Station 8000, Shot 3 403

A.43 Comparison of the Variation of Corrected Total Thermal Energy and Temperature Rise of F-47 (0065) Wing With Time, Station 8000, Shot 3 . 404

A.44 Comparison of the Variation of Corrected Total Thermal Energy 5 Ft Above Ground and Temperature Rise of B-17 (5715) Wing, Polished and Unpolished Surface, With Time, Station 8000, Shot 3 405

A.45 Comparison of the Variation of Lateral Acceleration With Time on F-47 (9785), Station 8000, Shot 3, and Station 4000, Shot 4 . . . 406

A.46 Comparison of the Variation of Wing Bending Moment and Normal Acceleration With Time on B-17 (5715), Station 8000, Shot 3 407

[redacted]

[redacted]

ILLUSTRATIONS (Cont.)

A.47 Comparison of the Variation of Wing Bending Moment With Time on F-47 (0065) at Different Stations and Shots 408

A.48 Variation of Wing Bending Moment With Time at Station 8000, Shot 3, B-17 (5715) 409

A.49 Comparison of the Variation of Wing Bending Moment With Time on B-17 (5715), Station 8000, Shots 2 and 3, Station 4000, Shot 4 410

A.50 Comparison of the Variation of Fin Bending Moment With Time on F-47 (9785), Station 8000, Shots 2 and 3, Station 4000, Shot 4 411

A.51 Comparison of the Variation of Lateral Acceleration and Fin Bending Moment With Time on F-47 (9785), Station 8000, Shot 3 412

A.52 Comparison of the Variation of Corrected Total Thermal Energy With Time at Various Heights, Station 10,500, Shot 3 413

A.53 Comparison of the Variation of Ground Overpressure Measurements at Station 10,500, Shots 2 and 3 414

A.54 Comparison of the Variation of Corrected Total Thermal Energy 4 Ft Above Ground and Temperature Rise on Propeller Cuff of F-47 (8785), Station 2200, Shot 4 419

A.55 Comparison of the Variation of Corrected Total Thermal Energy With Time at Various Heights, Station 4000, Shot 4 420

A.56 Comparison of the Variation of the Angle-of-blast Incidence With Time, 3½ Ft Above Ground, at Different Stations and Shots 421

A.57 Comparison of the Variation of Corrected Total Thermal Energy With Time at Various Heights, Station 4000, Shot 4 422

A.58 Variation of Overpressure With Time at Station

[redacted]

ILLUSTRATIONS (Cont.)

4000, Shot 4, on Wing of F-86 (9597) 423

A.59 Comparison of the Variation of Corrected Total Thermal Energy 5 Ft Above Ground and Temperature Rise on F-86 (9597) With Time, Station 4000, Shot 4 424

A.60 Comparison of the Variation of Wing Temperature Rise With Time on F-47 (0065), Station 4000, Shot 4 425

A.61 Comparison of the Variation of Corrected Total Thermal Energy With Temperature Rise of B-17 (5715) Wing, Station 4000, Shot 4 426

A.62 Comparison of the Variation of Lateral Acceleration and Fin Bending Moment With Time on F-47 (9785), Station 4000, Shot 4 427

A.63 Comparison of the Variation of Corrected Total Thermal Energy With Time at Various Heights, Station 8000, Shot 4 428

A.64 Comparison of the Variation of Overpressure With Time at a Point on the Ground, Station 8000, Shots 2 and 4 429

A.65 Comparison of the Variation of the Particle Attenuation Factor With Corrected Ground Range for Different Shots and Burst Altitudes . . . 444

A.66 Comparison of the Variation of Corrected Total Thermal Energy With Time at Different Stations Shot 2 445

A.67 Comparison of the Variation of Corrected Total Thermal Energy With Time at Different Stations, Shot 3 446

A.68 Comparison of the Variation of Corrected Total Thermal Energy With Time at Different Stations, Shot 4 447

A.69 Comparison of the Variation of Corrected Total Thermal Energy With Time at Station 2200,

ILLUSTRATIONS (Cont.)

Shots 3 and 4 448

A.70 Comparison of the Variation of Corrected Total Thermal Energy With Time for Different Shots, Station 8000 449

A.71 Comparison of the Variation of Peak Total Thermal Energy With Corrected Ground Range at Different Shots 450

A.72 Comparison of the Variation of Peak Total Thermal Energy With Corrected Slant Range at Different Shots 451

A.73 Comparison of the Variation of Peak Overpressure With Corrected Ground Range for Different Shots 452

A.74 Variation of Overpressure With Time at a Point on the Ground, Station 8000, Shot 4 453

A.75 Comparison of the Variation of Corrected Total Thermal Energy With Wing Temperature Rise of F-47 (0065), Station 4000, Shot 4 454

A.76 Variation of the Tensile Strength of an F-47 Propeller Cuff With Time, Station 2200, Shot 4 455

A.77 F-47 Propeller Cuff Showing Damage Caused by Thermal Radiation and Blast, Station 2200. Shot 3 456

APPENDIX B SURVEY OF MAXIMUM SKIN TEMPERATURES

B.1 Comparison of Computed Thermal Energies From Temp Tape Data With Oscillographic Measurements by NRDL and by Project 3.1 For Shots 2 and 3 466

B.2 Comparison of Computed Thermal Energies From Temp Tape Data With Oscillographic Measurements by NRDL and by Project 3.1 For Shot 4 . 467

B.3 Trend of Critical Incident Thermal Energies for Various Skin Surfaces of Parked Aircraft Exposed to Atomic Detonations 468

[redacted]

TABLES

CHAPTER 3 TEST RESULTS

3.1 TUMBLER-SNAPPER Test Conditions 281

3.2 TUMBLER-SNAPPER Geometric Data 282

3.3 TUMBLER-SNAPPER Preliminary Forcing Functions . 283

CHAPTER 4 DISCUSSION

4.1 Aircraft Instrument Damage 313

APPENDIX A OSCILLOGRAPHIC INSTRUMENTATION

A.1 Presentation, Comparison, and Composite Curves for All Measured Quantities 376

A.2 Presentation, Comparison, and Composite Curves for Temperature Rise 377

A.3 Presentation, Comparison, and Composite Curves for Overpressure and Angle-of-Blast Incidence . 378

A.4 Presentation, Comparison, and Composite Curves for Bending Moment and Acceleration 379

A.5 Measured Quantity vs Quality of Data Obtained . 380

A.6 Computed Absorptivities 437

APPENDIX B SURVEY OF MAXIMUM SKIN TEMPERATURES

B.1 Maximum Skin Temperatures 469

B.1.1 Shot 2, Station 2200 469

B.1.2 Shot 3, Station 1000 471

B.1.3 Shot 3, Station 1384 472

B.1.4 Shot 3, Station 2200 472

B.1.5 Shot 3, Station 4000 474

B.1.6 Shot 3, Station 8000 476

[redacted]

TABLES (Cont.)

B.1.7 Shot 3, Station 10,500 479

B.1.8 Shot 4, Station 2200 480

B.1.9 Shot 4, Station 2500 480

B.1.10 Shot 4, Station 3320 482

B.1.11 Shot 4, Station 4000 483

B.1.12 Shot 4, Station 8000 484

[redacted]

CHAPTER 1

INTRODUCTION

1.1 GENERAL

The efficient application of nuclear weapons against various types of targets requires adequate information as to the response of the individual target components as related to the phenomena produced by the detonation of the weapon. One type of target complex which might be effectively reduced by a nuclear strike is an airdrome, specifically with reference to the aircraft which may be parked thereon, in addition to the other structural facilities. The subject treated in this report deals with aircraft parked on the ground and exposed to a nuclear device detonated in the air.

1.2 OBJECTIVE

The objective of this project was to determine the effects of an atomic bomb detonated above an airfield and particularly the effects upon the aircraft parked on the field or dispersed in the surrounding area.

1.3 BACKGROUND

Prior to Operation BUSTER-JANGLE very little information was available on the effects on parked aircraft. On Operation CROSSROADS and Operation GREENHOUSE various components were exposed. These components consisted of wing panels, fuselage sections, control surfaces, and various experimental test articles. On Operation BUSTER-JANGLE, one fighter and one bomber were exposed to provide the first information on complete aircraft parked on the ground and to serve as reference points on which future tests could be based. Flying aircraft had been exposed on previous operations; however, even the drone aircraft were at relatively low overpressures (less than 2 psi), and the dynamic conditions produced damage that would not be expected to affect aircraft at zero velocity.

1.4 GENERAL TEST PROGRAM

The test program for Operation SNAPPER was established to provide the maximum information from the limited quantity of aircraft allotted for ground testing. Aside from types of aircraft, range from target ground zero and aircraft orientation were considered to be the most important variables. A compromise of these two prime variables resulted in the initial test program being based on three parking areas

[redacted]

[redacted]

at different ground ranges, with one G-type revetment at each range. High estimated construction costs placed this revetment program beyond the limitations of the budget, and the plans were altered to provide for one revetment at the intermediate range. Later, two additional passive defense structures were added at a closer range. All passive defense structures were for fighter aircraft. Instrumentation utilized to obtain information during the actual exposure consisted of automatic photography of the complete aircraft or portions thereof and oscillographic records of the input functions and of the aircraft response. The instrumentation was limited by the availability of equipment, personnel, and time to prepare for the test.

[redacted]

[redacted]

CHAPTER 2

PROCEDURE

2.1 GENERAL

General plans were based on the assumption that three basic categories of damage produced by the nuclear experiment would offer the best compromise between the number of aircraft available and the effect of the range parameter. The primary effort was directed toward Shot 3, the predicted yield determining the ground ranges. Consequently, three ranges were selected for the primary effort based on peak overpressures in the region of 8, 4, and 2 psi, with a small station being added at 6 psi at a later date. One passive defense structure was to be erected at each range; however, limitations on the availability of aircraft and project funds were realized and plans were modified accordingly, resulting in a final program encompassing 28 aircraft and three protective structures.

2.2 SELECTION OF TEST ARTICLES

The selection of the test articles was based primarily on the availability of the various test items. In view of the destructive nature of the test, a majority of the test aircraft allocated were obsolete and did not include any foreign types.

2.2.1 Parked Aircraft

The aircraft were selected to provide "statistical" information on the vulnerability of fighter and bomber types exposed at various orientations and at different ranges from target ground zero. Aircraft were also required for exposure in conjunction with passive defense structures, although budget limitations did not permit a statistical study of revetments. Economy efforts in locating the aircraft made it advisable to construct the revetments at the same ranges at which unprotected aircraft were parked in order to provide a direct measure of the degree of protection achieved. The following aircraft types and quantities were employed: 16 F-47's, 2 F-86's, 1 F-90, 7 B-17's (including BUSTER-JANGLE B-17), 1 B-29, and 1 B-45.

2.2.2 Aircraft Components

Certain aircraft components which were not organic parts of the obsolete aircraft utilized in the test were exposed on panels mounted beside aircraft at the test stations or inside the test aircraft. Included were such items as ejection seat catapults complete

[redacted]

with cartridge, canopy remover squibs, scale-model integral fuel tanks with fuel enclosed, and transparent acrylic specimens, all mounted on racks beside test aircraft. Within the aircraft were placed electronic parts such as cathode ray tubes, electron tubes, and various small electrical resistors, condensors, and similar items.

2.2.3 Passive Defense Structures

Initial investigations indicated that the G-type revetment would be the type to investigate according to information then available from the Directorate of Intelligence, Target Analysis Branch. Plans were then made to include three G-type revetments in the test program. However, while this type is known to be used for fighter protection, there was no evidence to indicate that this same type structure was being used for larger aircraft; consequently, with little or no damage expected to occur to fighters at the 10,500 ft station, it did not appear worthwhile to erect a structure of this magnitude at that range. When it was learned that the projected budget would be required to cover construction costs at the site, an estimate based on previous construction costs at the Nevada Proving Grounds indicated that one G-type revetment might cost up to one-third of the total project budget. It was therefore decided to limit revetment construction to one item at the 8000 ft station.

The requirement for investigating additional passive defense measures resulted in the later inclusion of a fourth aircraft exposure station at a ground range of 4000 ft. Here, one wall-type and one pit-type revetment were constructed for fighter aircraft. An F-47 aircraft was placed in each revetment and a third F-47 was exposed without protection between these two revetments for comparative purposes. Lack of time and funds prevented soil stabilization at the 4000 ft station.

2.3 SELECTION AND LOCATION OF TEST SITES

The selection of the number, size, and location of the aircraft test sites was limited primarily by the number of aircraft of the various types which were allotted to the project. Budget restrictions limited the amount of station preparation such as clearing, grading, and soil stabilization which could be accomplished. An attempt was made to select the minimum number of stations which would be so located relative to ground zero that the range of damage produced would vary from definite destruction to light damage to permit maximum employment of the data. This approach really required that two separate bands of damage be determined, one for fighters designed to high load factors and one for bomber aircraft designed to a lower load factor.

The effect of the orientation parameter was considered to be very important for both aircraft classes.

For "statistical" purposes the F-47 and the B-17 aircraft were utilized as the test program framework. The individual (two F-86's included) modern aircraft were then positioned within the statistical framework for comparative purposes. Obviously the effect of the orientation parameter on these modern aircraft would not be obtained except by extrapolation.

Estimated overpressures were employed as the basis for all damage prognoses. All ranges selected were based on Shot 3, although the positioning of the aircraft was changed for each specific shot.

2.3.1 Close-in Station

After considering the various factors mentioned above, it was decided that the threshold of fighter destruction required substantially greater energy input than any of the available bomber aircraft could sustain; therefore, only fighter aircraft would be included at the close-in station. It was estimated that 8 psi would produce substantial damage to fighter aircraft, and the close-in station was located at 2200 ft to realize this overpressure on Shot 3.

2.3.2 Intermediate Stations

The original test program consisted of three stations because of aircraft availability limitations. An attempt was made to locate the middle station at such a range that bomber aircraft would sustain substantial damage, while fighter aircraft would be just inside the damage envelope. A peak overpressure somewhat over 3 psi but less than 5 psi was chosen. The station was located 8000 ft from ground zero so that it would be in the 4 psi overpressure region on Shot 3.

At a later date a second intermediate station was added, when funds were made available, to construct two additional revetments. These were placed in the 6 psi overpressure region at 4000 ft.

2.3.3 Remote Station

The outer limit of the damage envelope related to bomber aircraft, as represented by the B-17 structure, is probably slightly less than 1 psi overpressure. However, damage produced at this limit is confined to the very light structural components and would not be expected to reduce seriously the capabilities of the aircraft on operational missions. Consequently, the remote station was located at 10,500 ft, where an overpressure of 2 psi was anticipated. This station was primarily a bomber exposure station, although two fighter aircraft were available for exposure on Shot 3.

2.4 SELECTION OF INSTRUMENTATION

Project instrumentation was limited by time, equipment, and availability of trained personnel. Tremendous efforts are involved in planning, installing, calibrating, and operating instrumentation to investigate the great variety of functions associated with damage of complex aircraft structures. The problems are further complicated by the requirements for automatic operation of the entire instrumentation system. The time factor made it essential to utilize equipment on hand and gave little opportunity to select new components based on satisfactory performance experiences. Details of the instrumentation procedure and results are included as Appendix A.

2.4.1 Photographic Records

The photographic records include still photographs of various sizes and 16mm motion pictures. An attempt was made to secure photographs of the aircraft response to the thermal and blast energy; however, pre-shock dust and smoke were sufficiently dense to compromise a large portion of the photographic results during the actual bomb detonation. Still photographs and motion pictures, taken before and after each test, indicate more clearly the degree of damage than verbal description. Since the primary purpose of this project was to determine effects of A-bombs on aircraft, the post-shot photographs are analogous to instrumentation records, and a number of the representative still photographs are included in this report. The motion pictures have been edited and printed as a separate presentation.

2.4.2 General Input Measurements

General input measurements were made at all aircraft test stations except the 4000 ft station, where measurements were attempted only on Shot 4 (utilizing instrumentation from the 8000 ft station). The general input functions included overpressure, thermal energy, and total gamma radiation (film badges). Whereas gamma radiation was not expected to affect structural properties of the aircraft, dosages of serious magnitude from a physiological viewpoint are applicable to an airfield target complex insofar as the retaliation potential of the target organization would be reduced by attrition of trained flight crew and maintenance personnel.

The David Taylor Model Basin, operating as Project 1.13, measured ground level overpressure versus time at the aircraft test stations. A combination of interferometer (Buck) gages and capacitance gages were employed at the various stations. These results are included in the final report of Project 1.13.

From ground zero to a range of 9000 ft, thermal and blast input functions were measured by other agencies. Data from Operation

BUSTER-JANGLE indicate that the shock wave is quite symmetrical. The thermal energy may also be assumed to be uniformly distributed, although local attenuation variations due to dust and smoke could play an important effect near the ground. In general, the information measured on the blast line can be expected to apply to equivalent positions along other radial lines.

2.4.3 Specific Input Measurements

The specific input measurements include those of overpressure on aircraft surfaces, thermal flux in the cockpit, and total gamma radiation in the crew stations.

Overpressure measurements were attempted on B-17, F-86, and F-47 wing surfaces with the aircraft positioned nose-in at the 8000 ft station on Shots 2 and 3 and tail-in at the 4000 ft station on Shot 4. Overpressure was also measured on the vertical stabilizer of one F-47 orientated side-in on all three shots, though this aircraft was also moved from the 8000 ft to the 4000 ft station prior to Shot 4.

Thermal flux was measured in the cockpit of the nose-in B-17 at the 8000 ft station on Shots 2 and 3 and in the cockpit of a side-in F-47 on Shot 4.

2.4.4 Aircraft Response Measurements

Aircraft response measurements included strain in B-17, F-47, and F-86 wings and one F-47 vertical tail, variation of skin temperature with time, and aircraft center of gravity accelerations. In addition to these response functions measured on a time basis, the maximum skin temperatures of various aircraft components were measured with eutectic alloys and temperature sensitive organic pigment papers. Details of this procedure and the results are presented in Appendix B.

2.5 GENERAL LAYOUT OF TEST ARRAY

The relative location of the aircraft test stations and ground zero are shown in Fig. 2.1. The extent of the stabilized areas is indicated as homogeneous, whereas a variation did exist. The close-in station was located on the large stabilized circle which provided a very good hard-stand. The extreme rear portion of the 10,500 ft station was also a road mix stabilization but with less bearing strength than the 2200 ft station. The remaining stabilization was effected by rolling the test site and spraying oil on the sand.

2.5.1 Shot 1

No aircraft were involved in this shot. The objective of participation was to establish limitations of certain photographic

techniques. Twelve gun cameras were mounted in a temporary emplacement shielded by lead bricks and sandbags. Both color and black and white film were employed. Neutral density filters ranging from 4.0 to 1.5 were utilized on six of the cameras. A seventh camera was fitted with a "minus blue" (light yellow) filter. All cameras were set to run at 64 frames per second.

The object target consisted of a 55 gal drum to which an external skin of aluminum alloy had been attached to simulate aircraft reflectivity. An area of 100 sq ft was oil stabilized between the cameras and the 55 gal drum to determine the extent and density of smoke produced, which might compromise the photographic effort on subsequent shots.

The bank of cameras was located at 2200 ft from target ground zero facing away from the blast. The 55 gal drum was placed in the center of the field of view approximately 60 ft away from the cameras.

All cameras were to start at minus 5 sec. Running time at 64 frames per second is about 30 sec.

2.5.2 Shot 2

The positioning of aircraft for Shot 2 involved primarily the four fighters at the 2200 ft station since pressures at 4000 ft and beyond were expected to be non-critical (less than 2 psi). The aircraft at these intermediate and remote stations were positioned prior to Shot 2 because of the limited time available between shots to reposition aircraft. At the 8000 ft station the B-45 was placed side-in for this shot in order to photograph the response of the vertical tail to side-on blast loading of low amplitude. The locations and orientations of all aircraft for Shot 2 are shown in Fig. 2.2.

2.5.3 Shot 3

The entire program was keyed to this shot. Figure 2.3 portrays the aircraft array as positioned for Shot 3. The repositioning from the Shot 2 array included replacement of seriously damaged aircraft at the 2200 ft station with aircraft from the 10,500 ft station and the addition of one F-47, 45° nose-in at the close station. This aircraft also was taken from the 10,500 ft station. Evaluation of the damage inflicted on Shot 2 resulted in a decision to orient all three aircraft at the 4000 ft station side-in. The B-45 was placed nose-in and the one F-47 equipped with dropable fuel tanks was moved from the 8000 ft to the 10,500 ft station and again oriented side-in.

[redacted]

2.5.4 Shot 4

Although many of the aircraft had sustained damage on previous exposures, additional investigations of the overpressure, thermal, and orientation parameters were attempted in order to take advantage of this shot. The lower burst height was expected to produce substantially higher thermal energies than resulted from Shot 3 in the vicinity of the 2200 ft station, whereas the overpressure was expected to be only slightly higher than previously experienced. The lower predicted yield required a considerable repositioning of aircraft in order to investigate the desired pressure regions. No aircraft were exposed at ranges greater than 8000 ft. At the 8000 ft station, one B-17 was placed side-in. Figure 2.4 shows the relative positions of all aircraft exposed on Shot 4. The seven remaining aircraft not required for this shot were towed back to the vicinity of the Yucca Lake strip for storage or salvage.

2.5.5 Revetments

The three revetments employed were fixed structures built primarily with the local soil. Timber shoring was employed for the near vertical walls. The configuration and orientation of the revetments are shown in Fig. 2.5. The G-type had the soil surfaces stabilized. The wall type and the pit type were not stabilized.

[redacted]

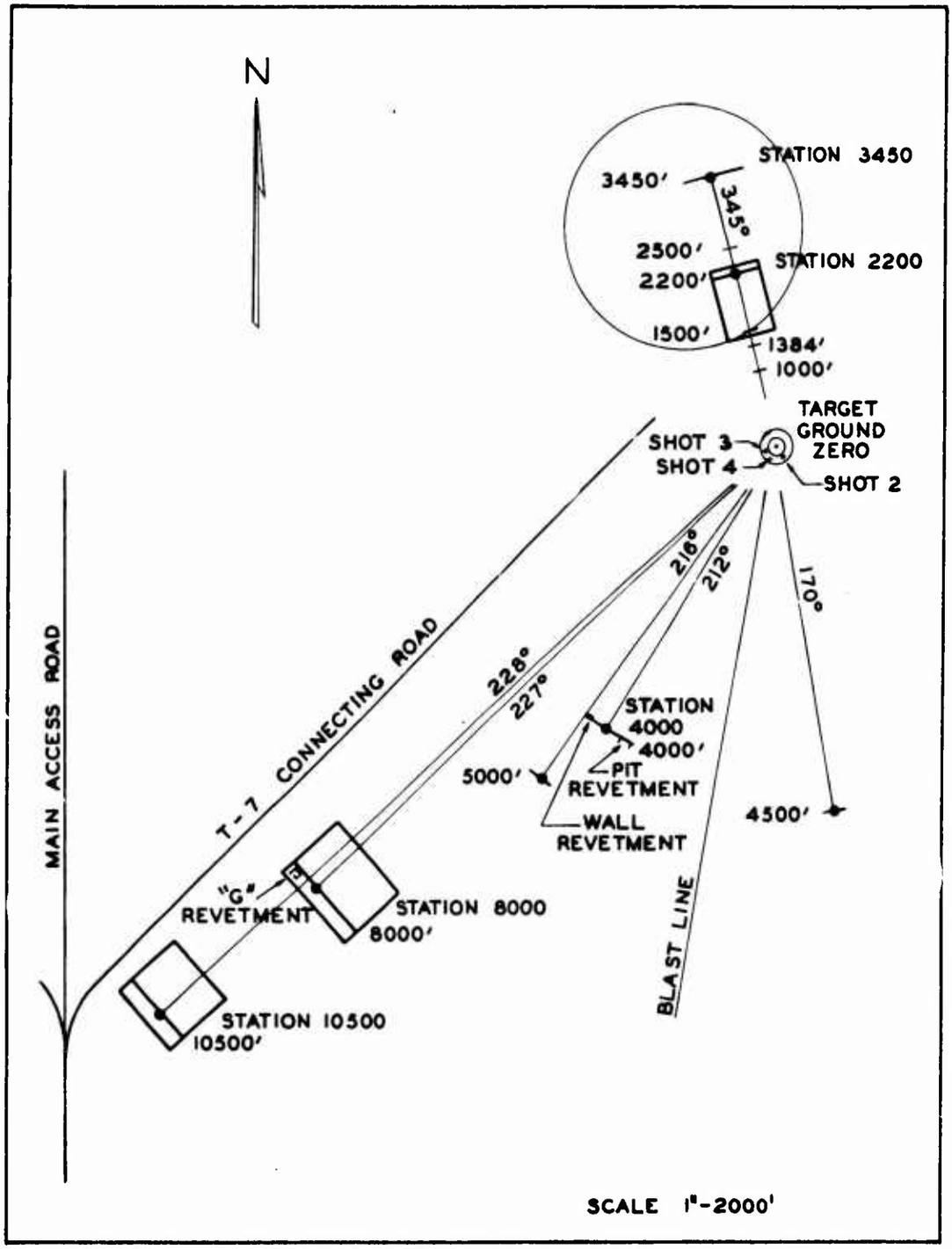

Fig. 2.1 Relative Locations of Aircraft Parking Stations and Revetments for Shots 2, 3, and 4

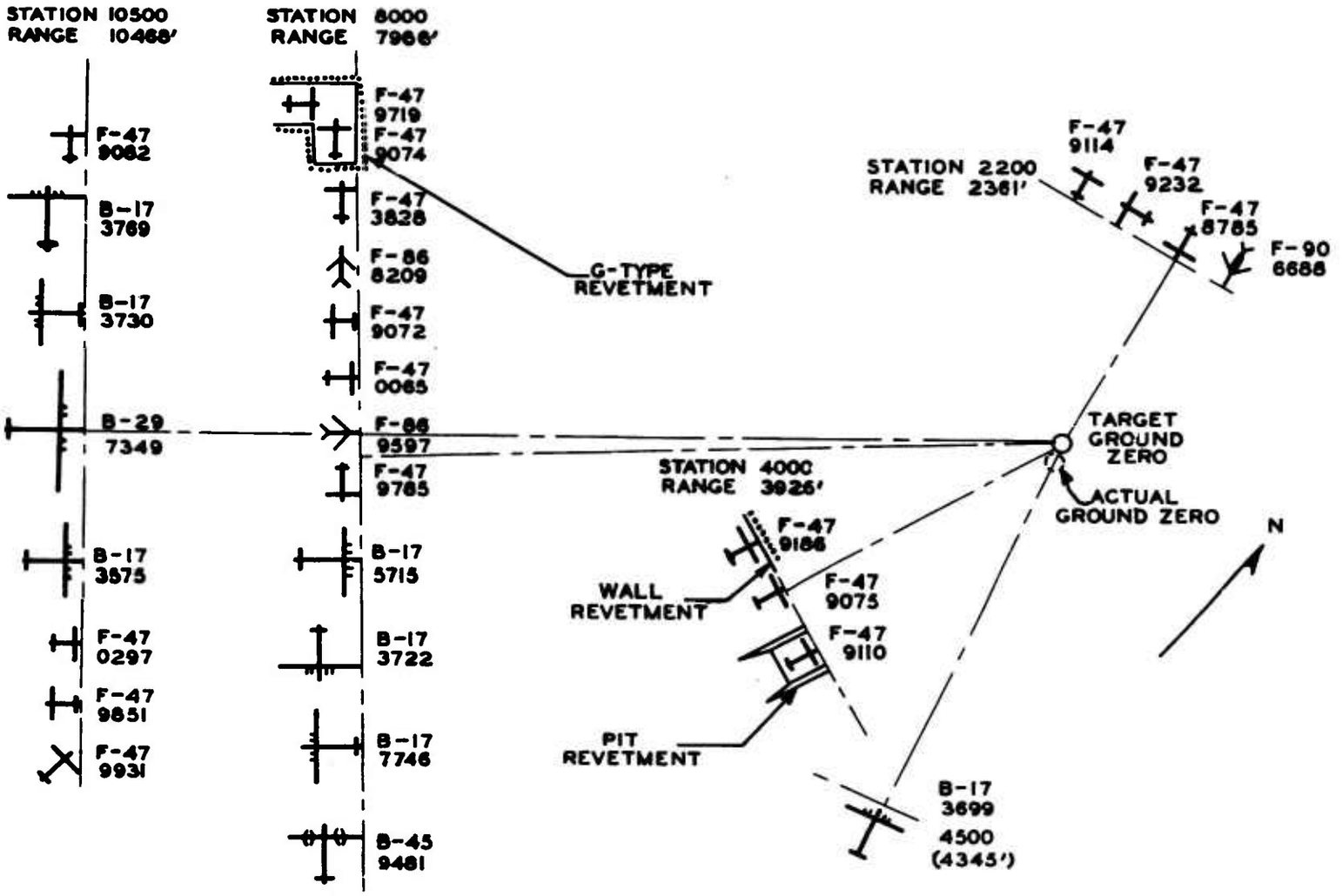

Fig. 2.2 Location and Orientation of Aircraft for Shot 2

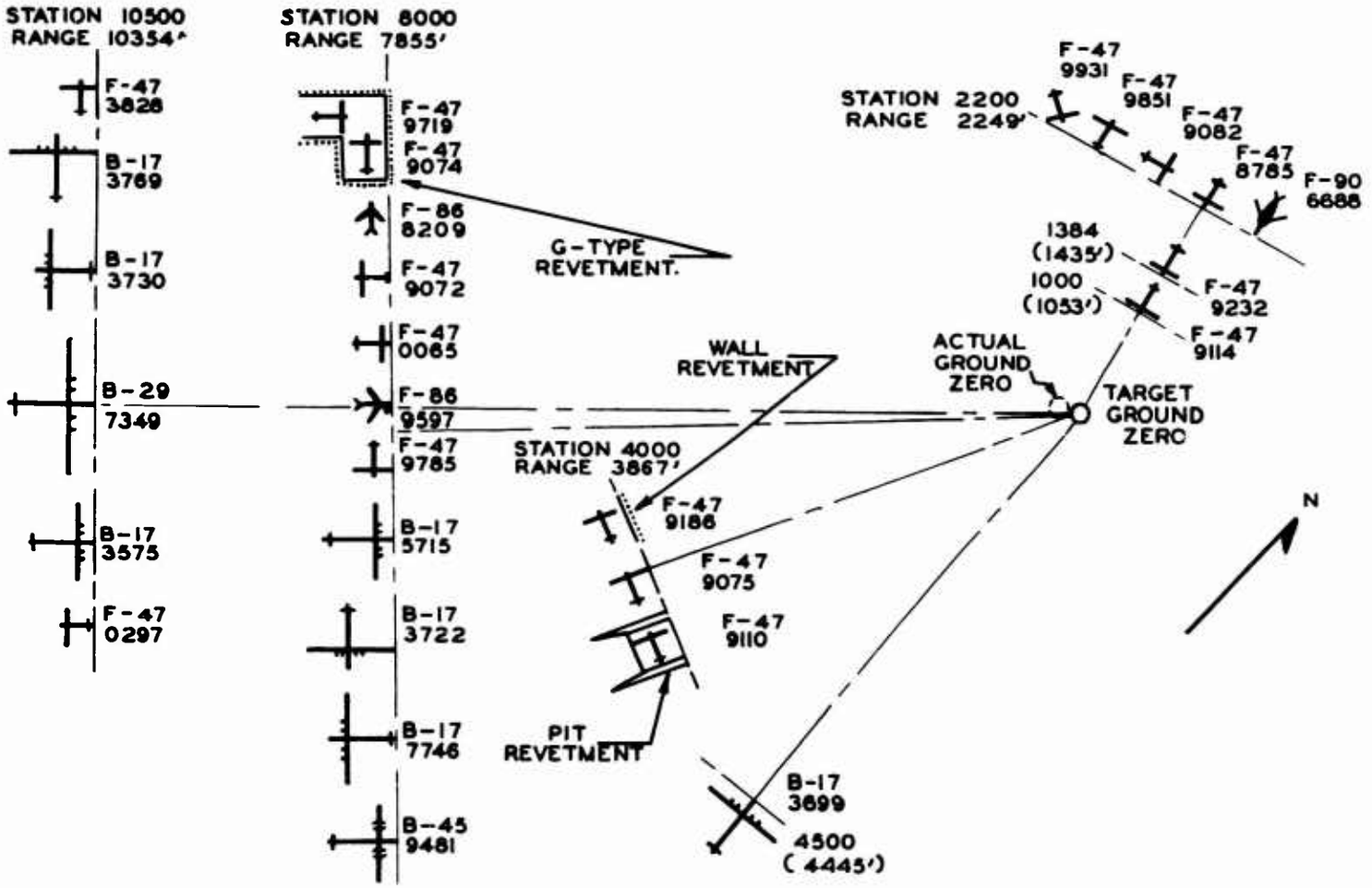

Fig. 2.3 Location and Orientation of Aircraft for Shot 3

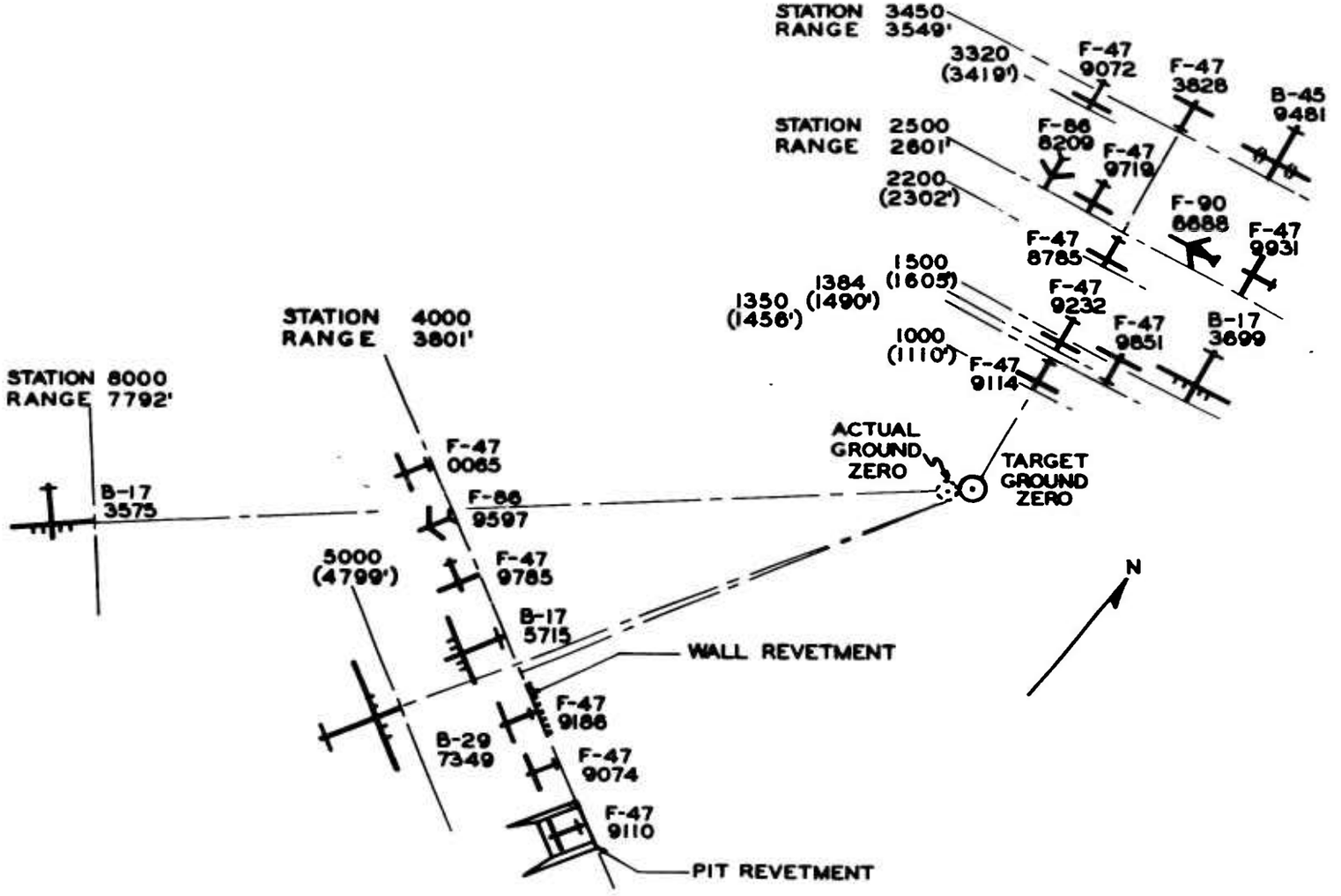

Fig. 2.4 Location and Orientation of Aircraft for Shot 4

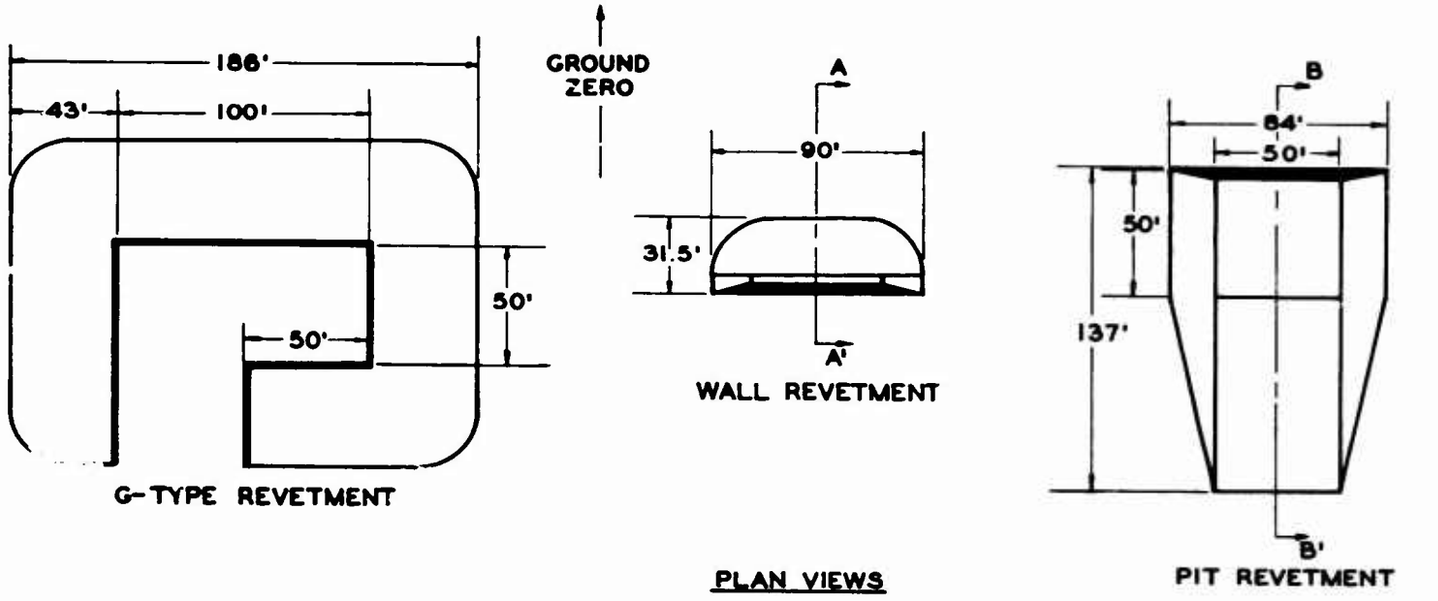

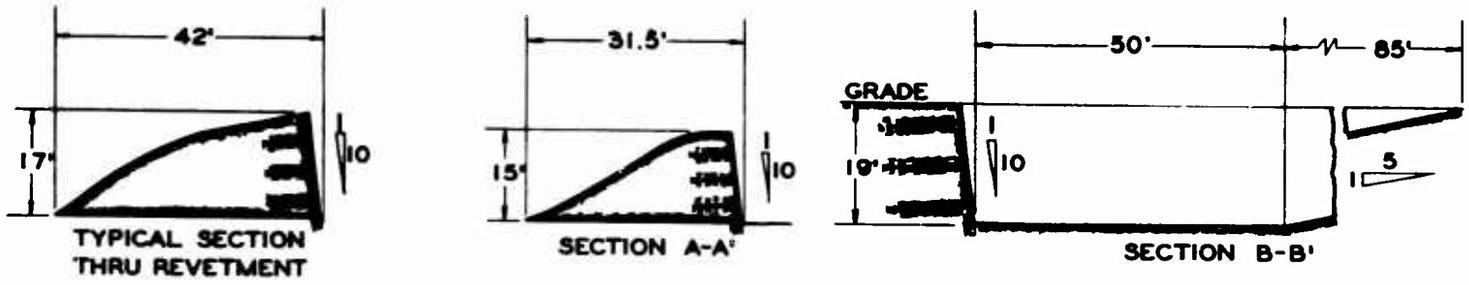

Fig. 2.5 Orientations and Structural Configurations of Aircraft Revetments

CONFIDENTIAL

CHAPTER 3

TEST RESULTS

3.1 GENERAL, INCLUDING SHOT 1

Participation in Operation TUMBLER-SNAPPER by Project 3.1 was limited to Shots 1, 2, 3, and 4. The effort in connection with Shot 1 was confined to obtaining basic photographic exposure data for use in the three succeeding test shots during which experimental data applicable to the parked aircraft vulnerability problem were obtained. The damage resulting from exposure of the 28 parked aircraft, deployed as described in Paragraph 2.5, to the thermal and blast inputs produced by the Shot 2, 3, and 4 bombs is summarized in this chapter. The damage sustained by individual aircraft as a result of each shot, including an estimate of the man-hours required to return the aircraft to pre-shot condition, was obtained from visual observations made during post-shot inspections. Photographs showing damage to the aircraft and components are included to supplement the verbal description. The results are presented in chronological order by shots, with the individual aircraft participating in the shot presented in order of increasing station number. The station number corresponds to the distance in feet from target ground zero to the particular station. The total aircraft damage is reported according to the following classifications: wing, fuselage, empennage, and miscellaneous. The miscellaneous classification includes canopies, instruments, landing gear, actuating systems, electronic equipment, armament, etc.

In evaluating the data presented in this chapter, certain factors pertaining to the method by which the data were obtained should be borne in mind. The test, having been conducted under field conditions which allowed limited time and facilities for inspection of aircraft, necessitated a damage survey procedure based largely upon visual examination of apparent damage. In several cases panels were cut away to obtain a more accurate survey of sub-structure damage. Also, damage assessment of aircraft which suffered significant damage in previous tests made analysis difficult and somewhat questionable because of insufficient knowledge of the effects of previous shots on structural integrity.

In addition to the damage summary covering each aircraft exposure station, values are given for peak overpressure and total thermal energy, distance from actual ground zero to station, and orientation of the aircraft during the exposure. The above variables represent only the more influential factors causing damage to aircraft; a more complete list of variables believed to affect aircraft damage is given

UNCLASSIFIED

UNCLASSIFIED

below.

1. Peak overpressure of the blast wave
2. Incident thermal energy
3. Aircraft structural configuration
4. Aircraft orientation with respect to burst point
5. Angle of blast incidence
6. Aircraft surface absorptivity
7. Aircraft attitude
8. Parking area surface
9. Aircraft restraint (tie-downs, etc.)
10. Pre-shot condition of aircraft

The tabulation of damage sustained by each aircraft includes, in addition to airframe damage, a listing of damage to miscellaneous equipment, components, and systems. A description of damage to articles displayed on test panels is also included.

TUMBLER-SNAPPER Shot 1 was detonated at an altitude of 793 ft and with a yield of 1.05 KT. Participation in this test by Project 3.1 was limited to one photographic installation at Station 2200, set up to determine basic exposure data for application in the photographic effort on Shots 2, 3, and 4, and also to determine the volatility of oil-stabilized surfaces when subjected to high intensity thermal radiation. Both objectives were achieved. First, 11 rolls of both color and black and white film were exposed with various density filters and camera diaphragm settings, and as a result it was possible to determine the camera settings required to record photographically specific phases of subsequent shots. Second, it was found that the oil-stabilized area sent up a dense, persistent, low-hanging, fog-like smoke as a result of volatilization of certain oil constituents during the thermal phase.

3.2 SHOT 2

The second bomb was detonated at an altitude of 1109 ft. The yield was reported to be 1.15 KT. All 28 test aircraft were parked in the T-7 area for Shot 2 as shown in Fig. 2.2; however, since deployment was chosen primarily for the succeeding shot, the damage area of interest included only the four fighters parked at Station 2200. Figure 3.1 shows the ranges and orientation of all aircraft deployed for Shot 2 and in addition indicates the degree of damage inflicted upon each aircraft. All aircraft at Station 2200 sustained sufficient damage to prevent their use for immediate retaliatory action. The degree of damage varied with orientation. The nose-in F-47 could have been made operational with a canopy replacement. Summarizing for all three stations, three aircraft were significantly damaged, one aircraft lightly damaged, and 24 aircraft were available for immediate retaliatory action.

UNCLASSIFIED

[redacted]

For a better appreciation of the physical arrangement of the test aircraft, an aerial view of Stations 2200, 8000, and 10,500 are presented in Figs. 3.2, 3.3, and 3.4, respectively. The pictures were taken prior to Shot 2, and show the approximate location of the aircraft during the shot.

3.2.1 Station 2200

Four aircraft, including three F-47's and an F-90, were parked at Station 2200 and oriented as shown in Fig. 3.1. At this station, 2361 ft from actual ground zero, they were subjected to a peak overpressure of 4.7 psi and total thermal energy of 5.7 cal/cm^2. All aircraft here were damaged. The F-47 aircraft and orientations in order of damage sensitivity are, F-47 (9232) side-in, F-47 (9114) tail-in, and F-47 (8785) nose-in. The total man-hour damage to the F-90 was approximately equivalent to the tail-in F-47 total.

3.2.1.1 Aircraft F-47 (9232)

The damage sustained by aircraft F-47 (9232), parked left side-in, is itemized below:

Wing

No damage.

Fuselage

1. Left side of fuselage badly buckled from engine accessory section to empennage,
2. Accessory section cowling bent in both sections,
3. Left side of plane seriously scorched,

Empennage

1. Vertical stabilizer surface buckled,
2. Right elevator dented at inboard end,
3. Rudder surfaces buckled and lower hinge attaching bracket pulled loose,

Miscellaneous

1. Left tail wheel door badly buckled,
2. Canopy badly shattered,
3. Rudder balance cable attaching bracket on left rudder pedal broken,
4. Directional gyro damaged - caging mechanism jammed,
5. Forward shock mounts of SCR-522 VHF radio set misaligned,

Repair Estimate

Estimated man-hours required for complete repair, 1154,

Figure Reference

1. Figure 3.5, general view showing damage to left side of fuselage, rudder, and tail wheel door,
2. Figure 3.6, close-up of aft section of fuselage.

[redacted]

[redacted]

3.2.1.2 Aircraft F-47 (9114)

The damage sustained by aircraft F-47 (9114), parked tail-in, is itemized below:

Wing
1. Minor sheet metal damage to trailing edge of right wing,
2. Skin of left wing buckled and gun access door dished in,
3. Left and right landing flap damaged beyond repair,
4. Left and right ailerons damaged beyond repair,

Fuselage
1. Fuselage skin caved in on top on left and right hand side just aft of cowl flaps,
2. Left and right upper cowling buckled,
3. Supercharger shroud dented and bent, right and left side,

Empennage
1. Left hand elevator buckled and scorched,
2. Right hand elevator scorched on top side and skin buckled on bottom side,
3. Horizontal stabilizer skin dished near tip, right hand side,

Miscellaneous
1. Internal control surface mechanism broken at bottom of stick in cockpit,
2. Left flap - center bearing housing broken, inboard and outboard lines broken, flap inoperative,
3. Right flap - all bearing housings broken, seals dished, lubricant blown out,
4. Ailerons - left and right hinge points broken; center bearing seats torn out,

Repair Estimate
1. Estimated man-hours required for complete repair, 157,
2. Estimated man-hours required for minimum repair, 132,

Figure Reference
1. Figure 3.7, over-all view showing damage to left elevator, flap, and aileron,
2. Figure 3.8, close-up view of damaged right flap.

3.2.1.3 Aircraft F-47 (8785)

The damage sustained by aircraft F-47 (8785), parked nose-in, is itemized below:

Wing
Undamaged,

Fuselage
1. Skin badly buckled on bottom left hand and right hand sides immediately aft of cowl flaps,
2. Shroud buckled along entire length,

[redacted]

Empennage
Undamaged,
Miscellaneous
1. Canopy cracked on both sides, replacement required,
2. Air-speed indicator and rate-of-climb indicator damaged,
Repair Estimate
1. Estimated man-hours required for complete repair, 8,
2. Estimated man-hours required for minimum repair, 4,
Figure Reference
Figure 3.9, general view of right side.

3.2.1.4 Aircraft F-90 (6688)

The damage sustained by aircraft F-90 (6688), parked nose-in, is itemized below:

Wing
Undamaged,
Fuselage
1. Stainless steel panels of the aft fuselage section buckled on the left and right bottom sides,
2. Skin slightly buckled above fire door left side of fuselage aft of wing trailing edge,
3. Fire door right side of fuselage warped and buckled,
Empennage
Small dent in leading edge of vertical stabilizer,
Miscellaneous
1. Few crazing cracks along front and top of canopy,
2. Paint on front of pilot's headrest scorched black,
Repair Estimate
1. Estimated man-hours required for complete repair, 106,
2. Estimated man-hours required for minimum repair, 20,
Figure Reference
1. Figure 3.10, general view, showing damage to left aft section of fuselage,
2. Figure 3.11, close-up of right side, showing buckled fire door.

3.2.2 Station 4000

Aircraft at this station were 3926 ft from actual ground zero. The incident thermal energy of 2.2 cal/cm^2 was coupled with a blast peak overpressure of 2.1 psi. These inputs were too low to inflict any noticeable damage on the three nose-in F-47 aircraft parked at this range. Two of the three aircraft were protected by revetments.

3.2.3 Station 8000

Moving pictures of Station 8000 aircraft, taken during

the thermal and blast phase, show fairly heavy loading of the bomber, especially the side-in B-17, although no permanent damage was discernible. The input functions at this station were: overpressure, 0.8 psi; thermal energy, 0.6 cal/cm^2.

3.2.4 Station 10,500

No damage was inflicted upon the Station 10,500 aircraft as a result of the 0.5 psi overpressure and 0.3 cal/cm^2 thermal energy.

3.2.5 General Observations

Power plants and power plant accessories of the aircraft participating in the Shot 2 test experienced no detectable damage. Examination of the wheels, lines and tubes, landing gear struts and components, hydraulic and pneumatic systems, and mechanical actuators revealed no damage that would impair operation. No damage to propellers was evident. Electronic equipment installed in the aircraft was likewise undamaged. The 50 cal machine guns and associated armament equipment of the aircraft F-47 (8785), which was the only aircraft having installed armament, suffered no ill effects from the explosion.

3.3 SHOT 3

The TUMBLER-SNAPPER Shot 3 bomb was detonated at an altitude of 3447 ft. The energy equivalent of the bomb was reported to be 30.0 KT. The range and orientations of the 28 test aircraft as arrayed for Shot 3 are given in Fig. 2.3. A symbolic summary of the degree of damage sustained by each aircraft, along with the values for associated overpressure and thermal energy input functions are presented in Fig. 3.12. This summary shows that all F-47 aircraft at Station 2200 and closer were damaged beyond economical repair regardless of orientation. All three B-17 aircraft at Station 8000 were damaged beyond economical repair. None of the aircraft were sufficiently intact following the test to be available for immediate retaliatory action. Two F-47 aircraft were operable except for damaged canopies (4 man-hours each). Another could have been made serviceable with the repair of the rudder control mechanism (6 man-hours). A detailed summary of the damage sustained by each aircraft is given below in order of increasing distance from target ground zero.

3.3.1 Station 1000

The F-47 aircraft parked nose-in at Station 1000 was 1053 ft from actual ground zero. At this range the peak overpressure was 10.6 psi and the incident total thermal energy was 70 cal/cm^2. The combined effects of the thermal and blast forcing functions were sufficient to damage the aircraft to the point where no major components were salvable.

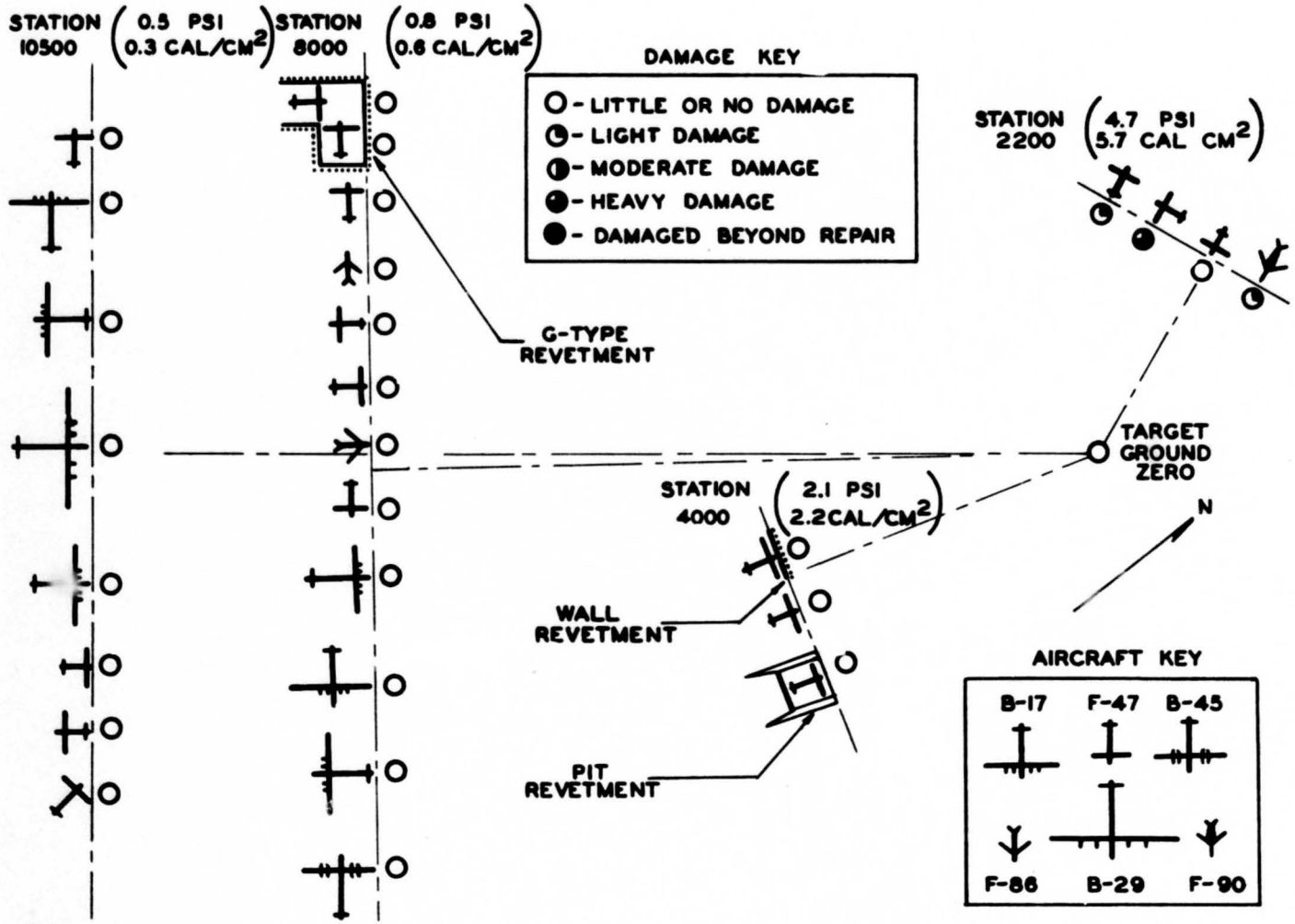

Fig. 3.1 Aircraft Damage Summary, Shot 2

UNCLASSIFIED

Fig. 3.2 Aerial View of Aircraft and Stabilized Area at Station 2200 Prior to Shot 2, Looking Away From Ground Zero

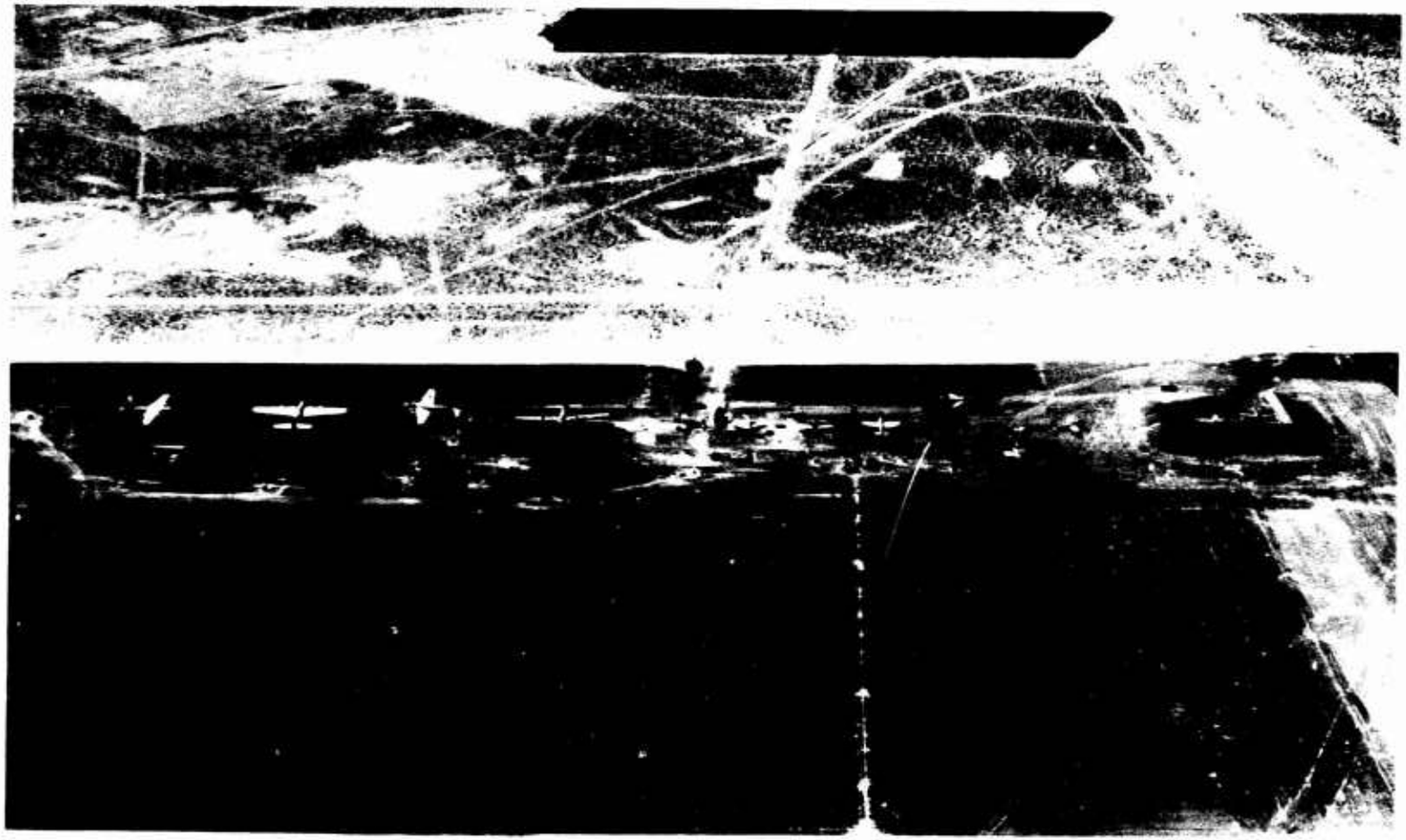

Fig. 3.3 Aerial View of Aircraft and Stabilized Area at Station 8000 Prior to Shot 2, Looking Away From Ground Zero. Note Station 10,500 in Background.

Fig. 3.4 Aerial View of Aircraft and Stabilized Area at Station 10,500, Prior to Shot 2, Looking Away From Ground Zero. The Two F-47 Aircraft Parked in the Background Were Moved to the Left End of This Line of Aircraft Prior to the Shot.

Fig. 3.5 F-47 (9232), Left Side-in, Station 2200 (4.7 psi), Shot 2, Showing Damage to Left Side of Fuselage, Rudder, and Tail Wheel Door

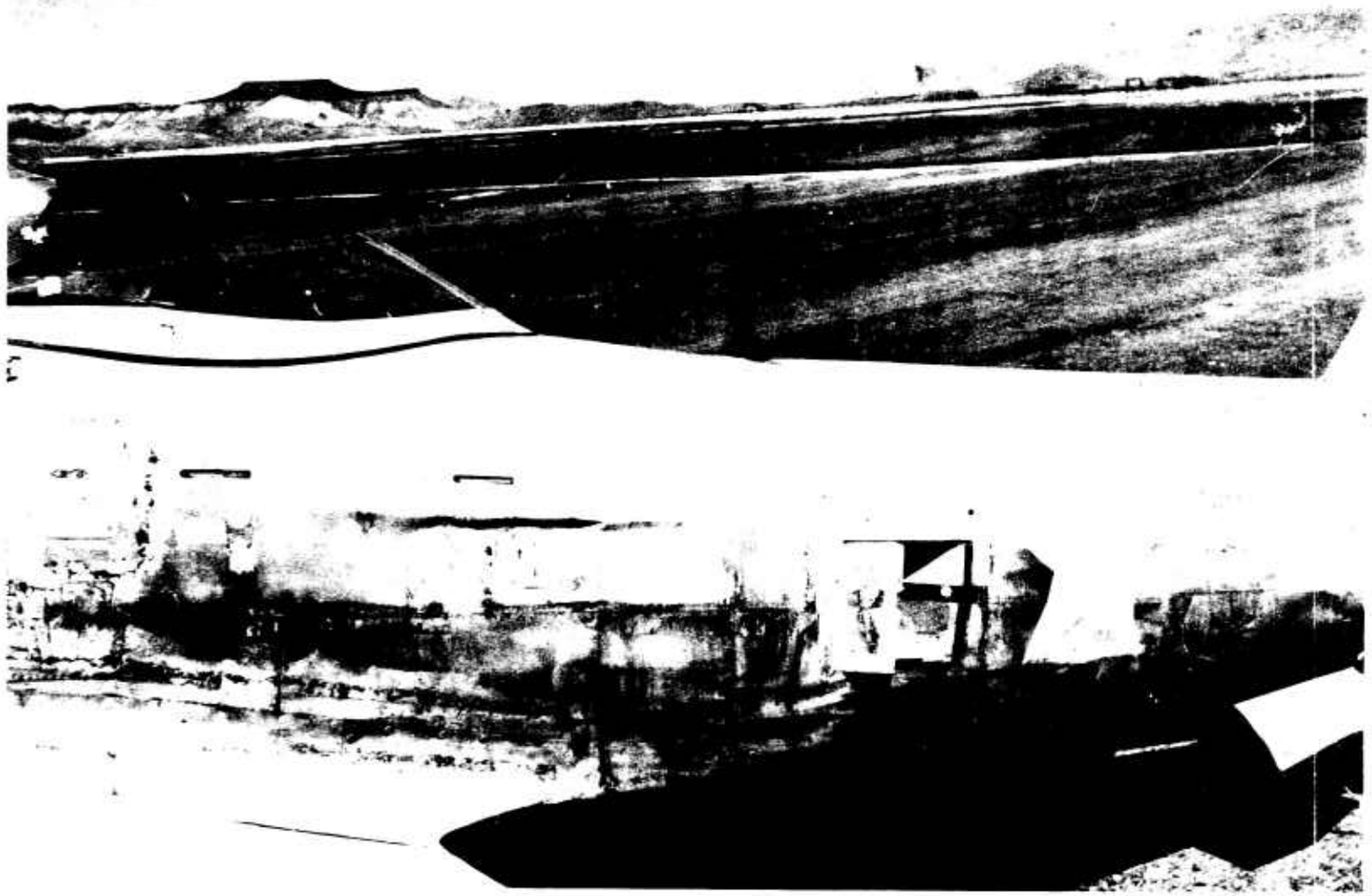

Fig. 3.6 F-47 (9232), Left Side-in, Station 2200 (4.7 psi), Shot 2, Close-up View of Crushing Effect of Positive Pressure Phase on Fuselage

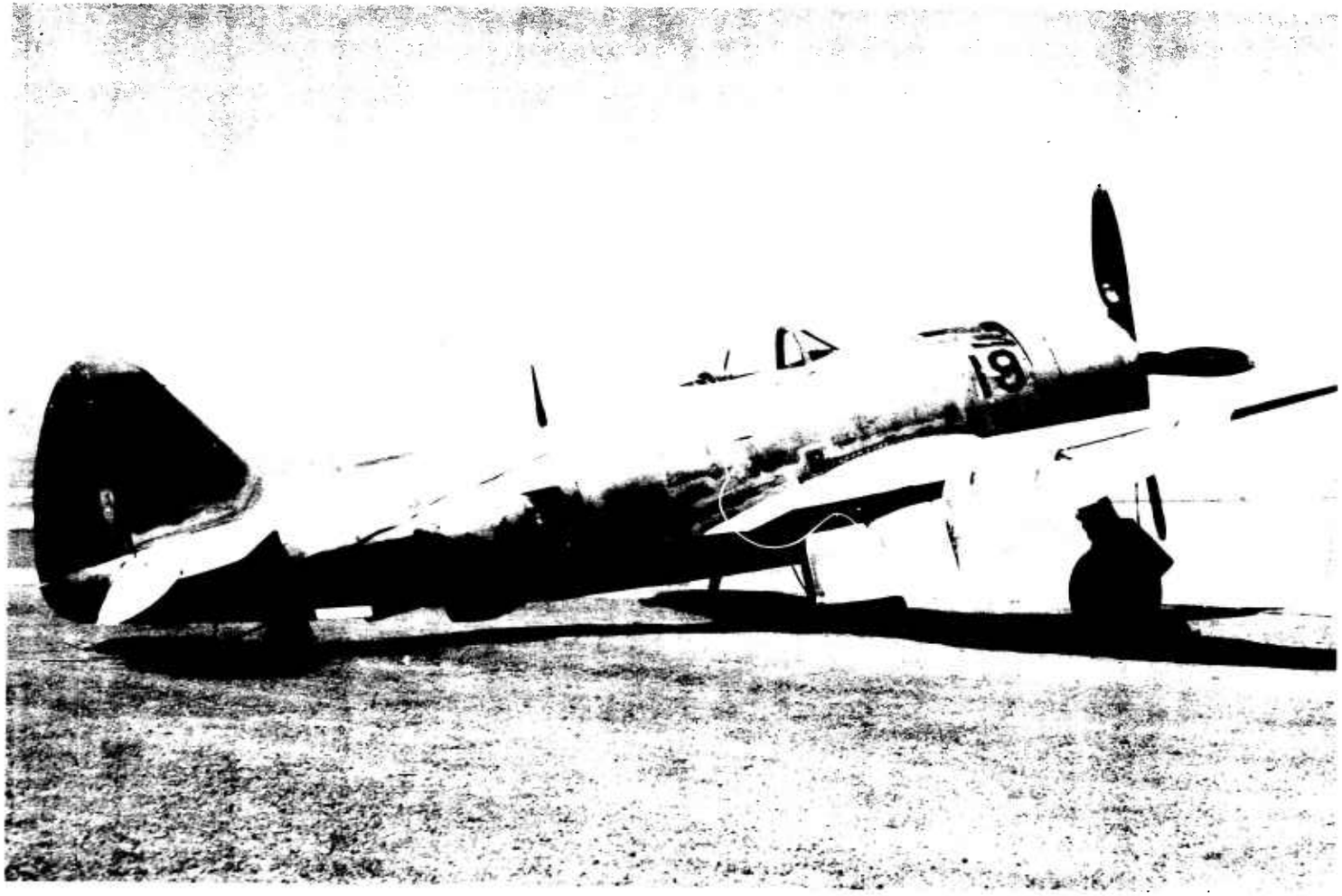

Fig. 3.7 F-47 (9114), Tail-in, Station 2200 (4.7 psi), Shot 2, Showing Damage to Right Aileron, Flap, and Elevator

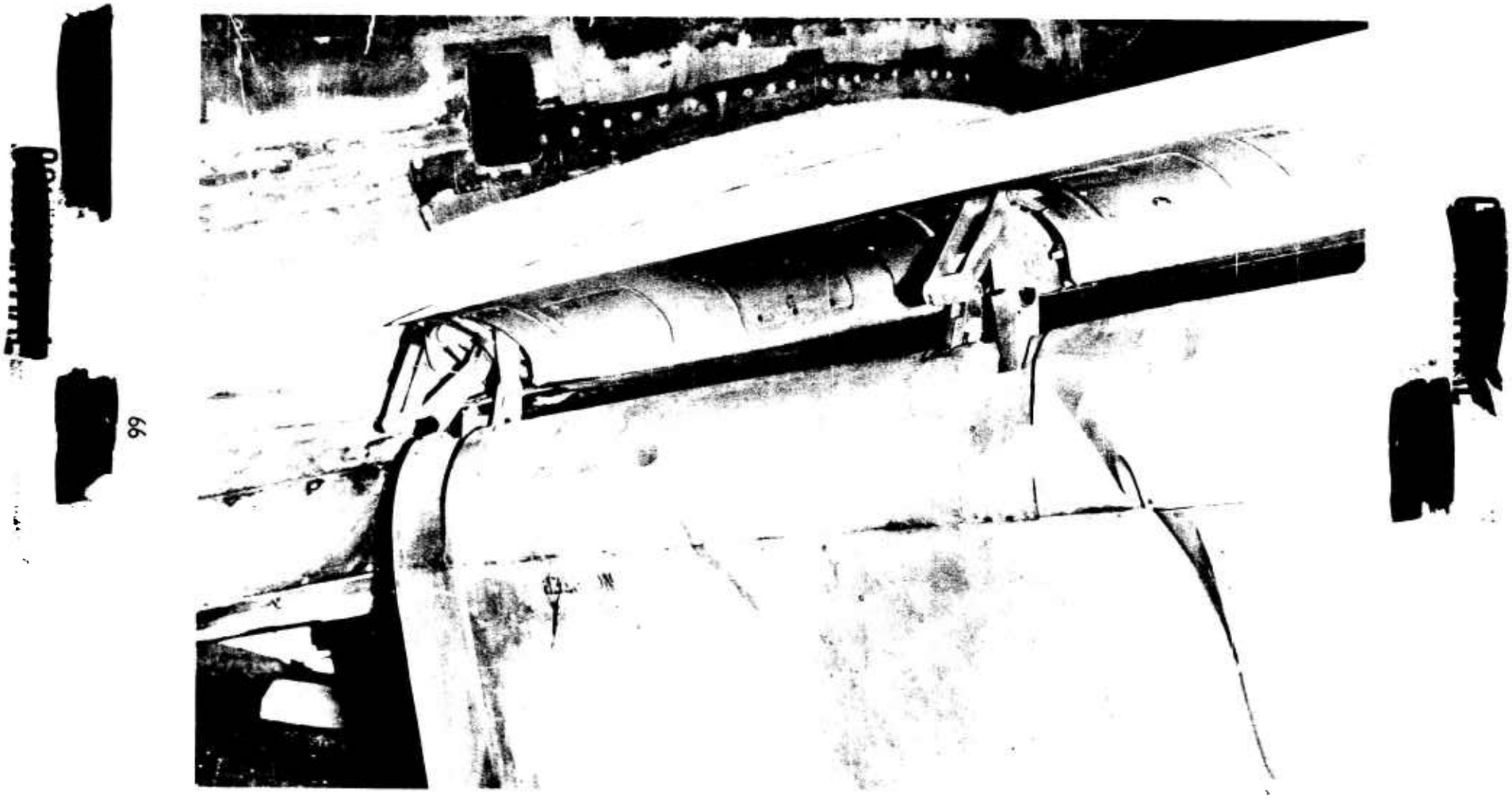

Fig. 3.8 F-47 (9114), Tail-in, Station 2200 (4.7 psi), Shot 2, Close-up View of Damaged Right Flap and Broken Hinge Fittings

Fig. 3.9 F-47 (8785), Nose-in, Station 2200 (4.7 psi), Shot 2, Showing Light Buckling Damage to Fuselage Skin Just Aft of Cowl Flaps

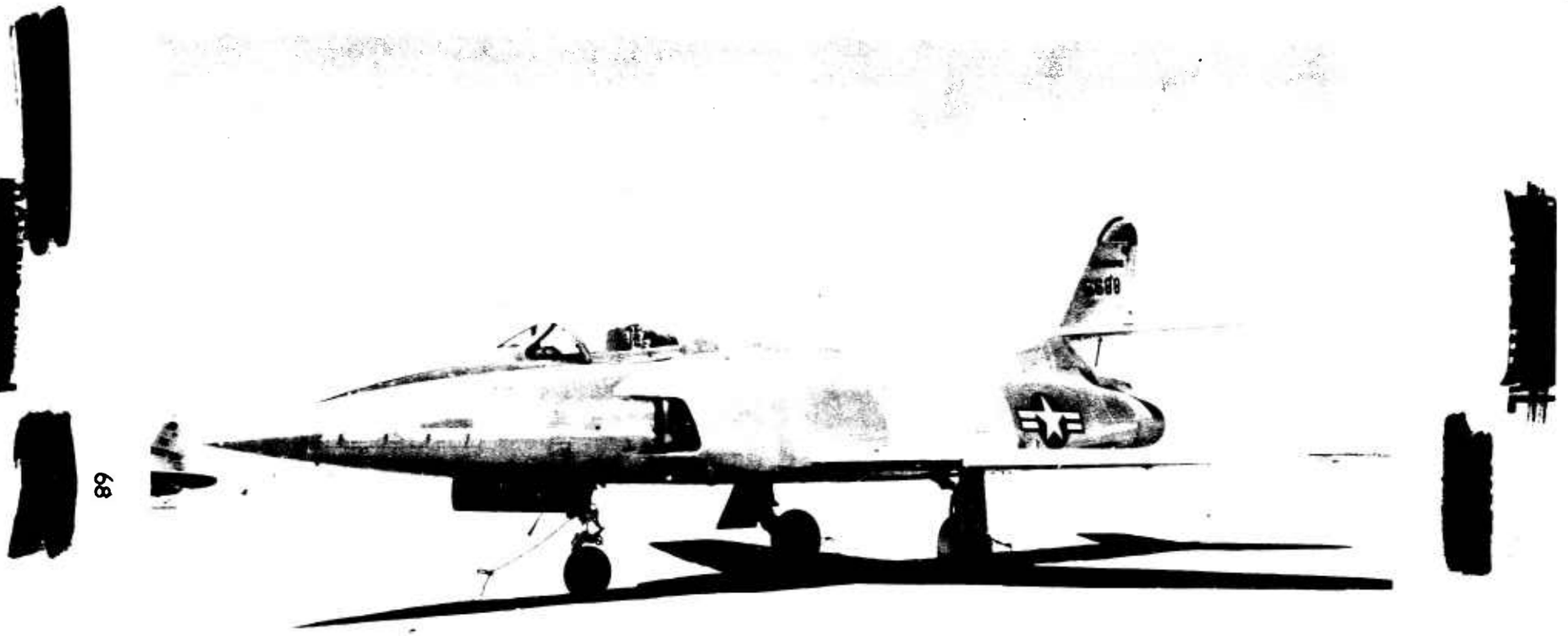

Fig. 3.10 F-90 (6688), Nose-in, Station 2200 (4.7 psi), Shot 2, Showing General Post-shot Condition of Aircraft

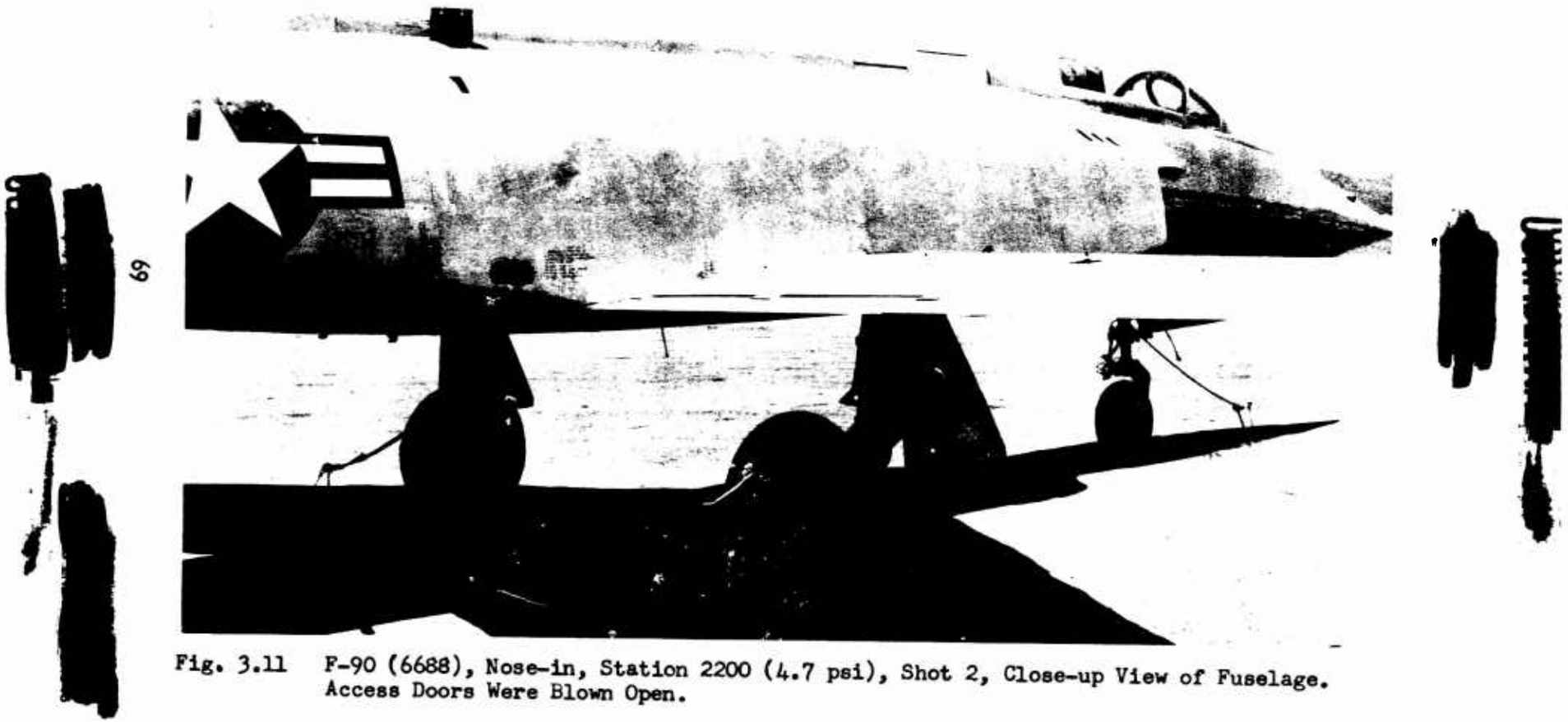

Fig. 3.11 F-90 (6688), Nose-in, Station 2200 (4.7 psi), Shot 2, Close-up View of Fuselage. Access Doors Were Blown Open.

[redacted]

3.3.1.1 Aircraft F-47 (9114)

The damage sustained by aircraft F-47 (9114), parked nose-in, is itemized below:

Wing
1. Internal structure of the wing suffered major damage,
2. Left and right ailerons badly burned and buckled, inoperable,
3. Left and right landing flaps badly burned and buckled, inoperable,

Fuselage
Entire airframe burned and buckled,

Empennage
Internal structure of the empennage suffered major damage,

Miscellaneous
1. Canopy shattered,
2. All thin skin directly exposed to thermal radiation vanished at unsupported places due to the action of the thermal and/or blast energy,
3. Rivets popped off by structural failure in elevators, ailerons, and flaps,
4. All paint, preservative, and zinc chromate burnt and scorched,
5. Bullet-proof windshield cracked,
6. Organic materials inside cockpit burnt and charred (headrest, shoulder harness, etc.),
7. Rear portion of main oil tank caved in about 4 to 6 in. with a 6 in. long tear along weld in upper left hand corner,
8. Propeller blades badly warped, cuffs burnt,
9. Air-speed indicator and rate-of-climb instrument damaged,
10. Broken left wing tip light,

Repair Estimate
Aircraft beyond economical repair,

Figure Reference
1. Figure 3.13, 3/4 rear view showing general damage,
2. Figure 3.14, close-up of right wing, showing damage to flap and aileron,
3. Figure 3.15, close-up view of damaged cockpit.

3.3.2 Station 1384

As with the aircraft at Station 1000, the F-47 aircraft parked nose-in at Station 1384 was damaged beyond economical repair. The aircraft was 1435 ft from actual ground zero and experienced a peak overpressure of 9.9 psi, coupled with a thermal energy of 64 cal/cm^2.

[redacted]

[redacted]

3.3.2.1 Aircraft F-47 (9232)

The damage sustained by aircraft F-47 (9232), parked nose-in, is itemized below:

Wing

Seriously damaged: holes burnt in thin skin, sub-structure damaged,

Fuselage

1. Entire airframe badly burned and buckled,
2. Fuselage damaged internally,

Empennage

1. Fin and rudder scorched,
2. All thin skin burned through and holes blasted in trailing edge of empennage,

Miscellaneous

1. Canopy destroyed,
2. Holes burnt and/or blasted in thin skin surfaces directly exposed to thermal radiation,
3. All paint scorched and burned,
4. Pilot's harness and headrest charred,
5. Rear section of main oil tank caved in sufficiently to cause tearing of the metal tank to about 3/4 of its height, permitting most of the oil to leak out,
6. Holes torn in cuffs on two blades; all blades dented and scorched,

Repair Estimate

Aircraft beyond economical repair,

Figure Reference

1. Figure 3.16, left side view, showing damage to fuselage, empennage, and wing,
2. Figure 3.17, right side view, showing damage to fuselage, empennage, and wing,
3. Figure 3.18, rear view, emphasizing burned areas on wing and horizontal stabilizer.

3.3.3 Station 2200

Five fighter aircraft, four F-47's and one F-90, at various orientations, were parked at Station 2200, a distance of 2249 ft from actual ground zero, where they were subjected to a blast peak overpressure of 8.4 psi and a total thermal energy input of 53 cal/cm^2. Four of the five aircraft were damaged beyond economical repair and none were available for immediate retaliatory action. The aircraft suffering the least damage was the F-90, parked nose-in. The F-90 sustained only light damage, whereas the neighboring F-47, similarly oriented, was damaged beyond economical repair.

[redacted]

[redacted]

3.3.3.1 Aircraft F-47 (9082)

The damage sustained by aircraft F-47 (9082), parked right side-in, is itemized below:

Wing
1. Wing panels buckled all over, left and right,
2. Left and right ailerons buckled and upper skin burned out aft of the aileron spar,
3. Top skin burned out and leading edges buckled on left and right flaps,

Fuselage
1. Left hand side of fuselage buckled aft of Station 180; there appear to be several ring and stringer failures in this area,
2. One severe isolated buckle in Frame 339½ one bay below the horizontal centerline,
3. Right hand side of fuselage from nose to tail burned and buckled,
4. Belly cowl panels pushed in,
5. Left hand lower secondary cowl panel pushed in,
6. Fuselage buckled in on left side at windshield attachment,
7. Two large dents in leading edge of left hand primary cowl at horizontal centerline,

Empennage
1. Dorsal fin burned out on right hand side, buckled in on left hand side,
2. Right hand stabilizer leading edge scorched and buckled,
3. Right hand elevator top skin burned out aft of spar,
4. Fin badly buckled on both sides (both skin and ribs),

Miscellaneous
1. Canopy glass shattered and canopy frame failed,
2. Thin skin remained where protected from direct thermal radiation but was severely buckled,
3. Headrest burnt
4. Left hand windshield frosted; right hand and main windshield smoked,
5. Structural damage grounded battery bus, discharging battery,

Repair Estimate
Aircraft beyond economical repair,

Figure Reference
1. Figure 3.19, left side view showing general damage,
2. Figure 3.20, front view with ground shadow in foreground.

3.3.3.2 Aircraft F-47 (9931)

The damage sustained by aircraft F-47 (9931),

[redacted]

[redacted]

parked right front quarter-in, is itemized below:

Wing
1. Flap and ailerons on both sides completely buckled; several holes in these surfaces,
2. Both wing panels completely buckled; right hand panel has bottom surface scorched and buckled,
3. Three small holes in top of wing near tip where black serial number was painted,

Fuselage
1. Complete fuselage buckled and scorched on right hand side,
2. Fuselage buckled aft of cockpit on left hand side,
3. Several fuselage ring and stringer failures,
4. Secondary cowling severely buckled, left and right,
5. Large dent near leading edge of primary cowling at horizontal centerline on right hand side,

Empennage
1. Right hand stabilizer and elevator failed completely in bending and torsion,
2. Left hand stabilizer and elevator severely buckled, top and bottom,
3. Rudder buckled,
4. Top hinge bracket torn out of fin,
5. Fin buckled on left hand side,

Miscellaneous
1. Canopy failed,
2. Tail wheel torn off,
3. Airplane rotated approximately 90° by the blast,
4. Headrest badly burned; seat back scorched,
5. Windshield frosted,
6. Cockpit littered with canopy fragments,
7. Main oil tank caved in about 4 in. on the aft side,
8. Air-speed indicator damaged,
9. Pitot-static tube cover installed prior to shot, burned or blown off,
10. Propeller blade bent when aircraft rotated under shock loading (touched ground),

Repair Estimate
Aircraft beyond economical repair,

Figure Reference
1. Figure 3.21, left side view showing damage to fuselage and rudder,
2. Figure 3.22, rear view, showing failure of right horizontal stabilizer,
3. Figure 3.23, close-up of right aft section of fuselage,
4. Figure 3.24, close-up view of left main landing gear.

[redacted]

[redacted]

3.3.3.3 Aircraft F-47 (9851)

The damage sustained by aircraft F-47 (9851), parked tail-in, is itemized below:

Wing
1. Both wing panels severely buckled all over,
2. Top skin panels outboard of ammunition-bay doors between spars burned out,
3. Flaps and ailerons blown off, both left and right, including portions of wing trailing edge; pieces scattered as far as fifty feet from aircraft,

Fuselage
1. Fuselage completely buckled aft of cockpit on both sides,
2. Several fuselage ring and stringer failures,
3. All belly cowl panels buckled in,
4. All secondary cowl panels pushed in,

Empennage
1. Leading edges of both left and right stabilizers buckled,
2. All top stabilizer skin panels (left and right) burned out between spars,
3. Top skins of both elevators burned out,
4. Bending failure in rudder between center and top hinges,
5. Fin skin buckled (not too severely),

Miscellaneous
1. Carburetor air ducts buckled at face of intercooler,
2. Canopy failed,
3. Tail gear assembly forced up into fuselage,
4. Main oil tank caved in about 4 in. on aft side,
5. Air-speed indicator and gyro horizon caging bar damaged,
6. Left flap linkages torn, inner race ring fractured on outboard bearings,
7. Shattered outer race ring of right aileron inboard airframe control bearing,
8. Rivet heads in control surfaces shorn off, torn out,

Repair Estimate
Aircraft beyond economical repair,

Figure Reference
1. Figure 3.25, a full view, showing damage to left side of fuselage, empennage, and wing,
2. Figure 3.26, close-up view of carburetor air duct damage (radio access door removed),
3. Figure 3.27, close-up view of skin damage on left horizontal stabilizer.

3.3.3.4 Aircraft F-47 (8785) ✓

The damage sustained by aircraft F-47 (8785), parked nose-in, is itemized below:

[redacted]

[redacted]

Wing

1. Complete left and right wing panels including flaps and ailerons buckled severely,
2. Panels outboard of ammunition-bay door between spars severely buckled, both top and bottom,

Fuselage

1. Fuselage buckled and scorched on top forward of windshield,
2. Secondary cowl panels buckled left and right hand sides,
3. Fuselage badly buckled on left and right hand sides aft of cockpit,
4. Several fuselage ring and stringer failures,
5. All belly cowl panels buckled in,

Empennage

1. Complete stabilizer surface buckled on left and right sides,
2. Right hand stabilizer suffered a bending and torsion failure,
3. Fin and rudder severely buckled in on both sides,

Miscellaneous

1. Stick base casting broken by stick lock,
2. Canopy shattered,
3. Essentially all thin skin on the airplane was buckled,
4. Elevators and flaps not operable,
5. Fasteners and latches corroded,
6. Seat back scorched, shoulder harness scorched, headrest ripped, windshield cracked,
7. Main oil tank caved in about 4 to 6 in. with 2 in. tear in a weld,
8. Structural damage shorted battery bus completely discharging battery,
9. Rate-of-climb instrument damaged,
10. The gun-sight head-support casting was broken and the reflecting glass destroyed,
11. Light bulb and spare were destroyed,
12. Machine gun ports in the leading edge of the wing were damaged by the blast and some of the muzzle covers were driven into the gun barrels; the guns seemed to have been loosened in their mounts and probably were well out of line,
13. Small amount of hydraulic fluid lost through loose fitting; leakage stopped by tightening fitting,

Repair Estimate

Aircraft beyond economical repair,

Figure Reference

1. Figure 3.28, a view of right side, showing general buckled areas,
2. Figure 3.29, rear view, showing torn spots and bent right horizontal stabilizer.

[redacted]

[redacted]

3.3.3.5 Aircraft F-90 (6688)

The damage sustained by aircraft F-90 (6688), parked nose-in, is itemized below:

Wing

1. Skin on left and right gun access doors, bottom of fuselage, forward of wing leading edge, buckled,
2. Left and right aileron assemblies warped and burnt beyond repair,
3. Top skin of left wing discolored by smoke,
4. Left wing tip upper skin slightly buckled,
5. Wing upper surface aft of rear spar has permanent buckling which appears to have occurred as a result of combined thermal and pressure effects,
6. Upper surface of ailerons buckled in light ripples,
7. Trailing edge of aileron skin has been burnt and many holes produced,

Fuselage

1. Aft stainless steel tail cone badly buckled,
2. Some canning of intake ducts and area above the left and right intake ducts,
3. Radio access doors right and left side of nose section badly buckled and burned beyond repair,
4. Slight buckling above fire door on right side,
5. All fuselage frames apparently undamaged,

Empennage

1. Small dent in leading edge of vertical stabilizer at junction of vertical and horizontal stabilizers,
2. Trailing portion of rudder buckled below horizontal stabilizer,

Miscellaneous

1. Canopy badly cracked,
2. Paint was scorched and burnt on nose and top of tail fin,
3. Windshield cracked; canopy smoked from cockpit fire,
4. Seat belt scorched; light green cushion charred,
5. All radio and radar plastic enclosures scorched,
6. Needle nose radome charred,
7. Flush antennas charred,
8. Gun sight shaken loose,

Repair Estimate

Estimated man-hours required for complete repair, 306,

Figure Reference

1. Figure 3.30, right side view, showing damage to rudder and fuselage,
2. Figure 3.31, close-up view of buckled radio access door,
3. Figure 3.32, close-up view of left side of aircraft,
4. Figure 3.33, close-up view of canopy,
5. Figure 3.34, close-up view, showing ripples on aileron

[redacted]

and buckles in upper aft section of fuselage,
6. Figure 3.35, close-up view of inboard section of right aileron,
7. Figure 3.36, close-up view of damaged stainless steel tail cone,
8. Figure 3.37, close-up view of left main landing gear.

3.3.4 Station 4000

The three F-47 aircraft parked right side-in at Station 4000 were 3867 ft from ground zero. One aircraft was protected by a wall revetment, another by a pit revetment, and the third was unprotected. Under the conditions prevailing, the revetments afforded limited protection. All three aircraft suffered major damage. The peak overpressure at this range was reported to be 6.4 psi with a thermal energy input of 32 cal/cm^2.

3.3.4.1 Aircraft F-47 (9075)

The damage sustained by aircraft F-47 (9075), parked right side-in, is itemized below:

Wing
1. Left and right wing panels scorched and buckled,
2. Left and right ailerons and landing flaps buckled and showed evidence of excessive heating,
3. Outboard ends and trailing edges of both wings showed excessive heating,
4. General panel buckling outboard of Station 202,

Fuselage
1. Right hand side of fuselage scorched and generally buckled; holes in several places,
2. Failure on both sides of fuselage at Station 339½ by moving tail wheel several feet through sand sideways,
3. Belly cowls pushed in,
4. Stick base casting failed by control lock load,

Empennage
1. Left and right stabilizer and elevator skins severely buckled,
2. Under side of right hand stabilizer between spars pushed in because of rib failure,
3. Elevator skins aft of spar burned through on top except in protected area,
4. Fin and rudder scorched badly on right hand side,
5. Rudder skin aft of spar burned through in several places on right hand side,
6. Holes burned in fin where aircraft serial number was painted,

Miscellaneous

[redacted]

1. Canopy destroyed, windshield smoked slightly, shoulder harness and top of seat burnt,
2. Rudder attachment bracket pulled out; rivets sheared,
3. Rudder balance cable failed by failure of lug on right hand rudder pedal,
4. Main landing gear slightly bowed,

Repair Estimate

Estimated man-hours required for complete repair, 1704,

Figure Reference

Figure 3.38, three-quarter rear view, showing scorched and buckled right fuselage.

3.3.4.2 Aircraft F-47 (9110)

The damage sustained by aircraft F-47 (9110), parked right side-in is itemized below:

Wing

1. Ammunition and gun-bay doors buckled left and right,
2. Panel outboard of Station 202 between spars buckled on both sides (top and bottom),
3. Left hand aileron flap and skin buckled,
4. Right hand aileron appears to have spar failure between center and outboard hinges; trailing edge badly buckled,

Fuselage

1. Fuselage skins, including several ring and stringer failures, buckled from Station 164 aft on right hand side,
2. Belly cowls pushed in,
3. Right hand side of primary cowl panels buckled and scorched,
4. Upper and lower right hand secondary cowl panels buckled in,
5. Area between Station 197 and 250 buckled on fuselage left side,
6. Ring failure at Station 339½ on left side below horizontal centerline,
7. Lower left hand secondary cowl panel pushed in,

Empennage

1. Right hand stabilizer skin pushed in around structure on top; bottom skin pushed in between spars; ribs failed,
2. Right hand elevator scorched and buckled,
3. Left hand elevator inboard trailing edge damaged by overtravel of rudder,
4. Left hand elevator buckled from center hinge outboard,
5. Skins on both sides of fin and rudder buckled; right hand side also scorched,

Miscellaneous

1. Right and left rudder balance cable attaching brackets failed,

[redacted]

[redacted]

2. Canopy blown completely off airplane; left hand roller still in canopy track,
3. Control lock loads broke stick base casting,
4. Seat back burnt; shoulder harness scorched,
5. Leading edge of cuff of one propeller blade slightly dented,

Repair Estimate

Estimated man-hours required for complete repair, 1410,

Figure Reference

Figure 3.39, general view of aircraft.

3.3.4.3 Aircraft F-47 (9186)

The damage sustained by aircraft F-47 (9186), parked right side-in behind the wall revetment, is itemized below:

Wing

1. Wing panels left and right buckled in outboard of Station 202 between spars,
2. Ammunition and gun-bay doors buckled left and right,
3. Left hand aileron failed between center and inboard hinges,
4. Right hand aileron had failure in spar between center and outboard hinges,
5. Right hand flap scorched and buckled in exposed area,
6. Left hand flap scorched and buckled where blanketed by fuselage from radiation,

Fuselage

1. Tail-wheel door hinge rivets sheared,
2. Belly cowls pushed in,
3. Right hand side of fuselage scorched and buckled,
4. Fuselage panel on right side below windshield side panel buckled,
5. Right side primary cowl scorched and buckled,
6. Right side upper and lower secondary cowl panel buckled and scorched,

Empennage

1. Right hand elevator skin aft of spar scorched and buckled,
2. Right hand stabilizer skin between spars scorched and buckled,
3. Left hand stabilizer skin buckled outboard of center hinge,
4. Buckle in left hand stabilizer just outboard of outboard hinge,
5. Skin on right side of rudder aft of trailing edge scorched and several holes apparent,
6. Rudder leading edge skin scorched on right hand side,
7. Fin skin between spars scorched on right side,

Miscellaneous

[redacted]

[redacted]

1. Canopy destroyed and seat b k burnt,
2. Right rudder balance cable attaching bracket broken,
3. Flight control lock broken on control stick,
4. AN/ARC-3 antenna scorched,
5. Air-speed indicator damaged,

Repair Estimate

Estimated man-hours required for complete repair, 1575,

Figure Reference

1. Figure 3.40, close-up view of scorched and buckled fuselage,
2. Figure 3.41, close-up view of severely scorched vertical stabilizer,
3. Figure 3.42, close-up view of scorched left wing tip.

3.3.5 Station 4500

The previously damaged BUSTER-JANGLE B-17 was the only aircraft exposed at Station 4500, where it was subjected to an overpressure of 5.8 psi and a thermal flux of 27 cal/cm^2. It was parked facing ground zero at a ground range of 4445 ft. The effects of Shot 3 caused a general increase in damage to the fuselage. The lower section of the nose just aft of the radome was caved in and the bombardier's nose glass blown out completely. Outer wing panels were caved in considerably more aft of the rear spar. A rib was protruding through the lower skin surface as shown in Fig. 3.43. The trailing edge of the wing aft of the rear spar was pushed in considerably more as a result of the exposure. The tail surfaces were pushed in and many ribs had failed.

3.3.6 Station 8000

The 11 aircraft at Station 8000 received a total thermal energy of 11 cal/cm^2 and an overpressure of 3.6 psi. Of the four bombers at this range, 7855 ft from ground zero, the three variously oriented B-17's were damaged beyond repair, while the nose-in B-45 sustained relatively light damage. None of the seven fighters were damaged beyond economical repair; however, all received sufficient damage to render them unavailable for immediate retaliatory action. The side-in F-47 protected by the G-type revetment was less damaged than the unprotected F-47 similarly oriented.

3.3.6.1 Aircraft F-47 (9074)

The damage sustained by aircraft F-47 (9074), parked right side-in in G-type revetment, is itemized below:

Wing

1. Left hand gun-bay and ammunition-bay doors dished in,
2. Left wing between spars dished in outboard of ammunition

[redacted]

[redacted]

door on top; two ribs apparently failed; lower surface buckled badly in same region between ribs and stringers,
3. Navigation light covers wrecked,
4. Aileron and flap trailing edges buckled slightly,

Fuselage
1. Frame 339½ buckled below horizontal centerline,
2. Radio access door buckled in,
3. Belly cowls dented in aft of wing trailing edge, lower panel of left hand secondary cowl dented in; sub-structure probably failed,
4. Upper panel of right hand secondary cowl dished in,

Empennage
Undamaged,

Miscellaneous
1. Left hand side of canopy cracked,
2. Right hand side of canopy cracked along frame from front to rear; headrest scorched and windshield scorched slightly,
3. Flaps inoperable because of hydraulic leak in cockpit; rudder balance cable broke lug on right hand rudder pedal,
4. Brush back wire housing slightly scorched,

Repair Estimate
1. Estimated man-hours required for complete repair, 92,
2. Estimated man-hours required for minimum repairs, 92,

Figure Reference
1. Figure 3.44, close-up view of right side of fuselage, showing damage on and aft of radio access door,
2. Figure 3.45, close-up view of forward section of fuselage and inboard section of right wing,
3. Figure 3.46, close-up view of cracked canopy.

3.3.6.2 Aircraft F-47 (9785)

The damage sustained by aircraft F-47 (9785), parked left side-in is itemized below:

Wing
1. Left hand flap buckled inboard of hinge,
2. Left and right panels outboard of ammunition-bay door between spars buckled on top; right hand also buckled on bottom,
3. Ammunition and gun-bay doors dished in right and left,

Fuselage
1. Severe blast damage on left side of fuselage from cockpit to tail; several wing failures apparent,
2. Left hand primary cowl panel dished in approximately at horizontal centerline,
3. Left hand secondary cowl panels severely buckled,

[redacted]

[redacted]

4. Left hand belly cowl panels dished in,
5. Frame 339½ buckled below horizontal centerline,
6. Windshield frame and adjacent fuselage structure on left hand side slightly dented,

Empennage

1. Dorsal fin dished in along entire length,
2. Rudder failed by bending between center and upper hinges,
3. Left side skin of fin buckled between spars; general bending including ribs except one rib supporting center rudder hinge bracket,
4. Slight buckle in dorsal fin near leading edge of vertical fin,
5. Root of right hand elevator trailing edge hit by rudder,
6. Left hand stabilizer dished in between spars on top; less severe dishing between spars on bottom,

Miscellaneous

1. Left hand main wheel fairing buckled,
2. Left hand tail wheel door actuating rod driven through door,
3. Bottom rudder hinge bracket rivets sheared,
4. Canopy cracked on left hand bottom edge; aluminum frame on bottom edge burned black,
5. Main landing gear bowed in slightly,

Repair Estimate

Estimated man-hours required for complete repair, 1053,

Figure Reference

1. Figure 3.47, left side view, showing fuselage damage,
2. Figure 3.48, close-up view of rudder, showing bending failure and buckles,

3.3.6.3 Aircraft F-47 (9072)

The damage sustained by aircraft F-47 (9072), parked tail-in, is itemized below:

Wing

1. Gun-bay doors dished in around sub-structure, left and right sides,
2. Wing structure outboard of ammunition-bay door dished in on top surface left and right,
3. Wing trailing edge structure dished in,
4. Left and right navigation light covers ruined,
5. Aileron center hinge pulled out of aileron spar left and right; both ailerons failed in bending,
6. Flaps failed in bending between inboard and center hinges,

Fuselage

1. Lower left hand secondary cowl dished in,
2. Belly cowls required replacement,
3. Radio door buckled,

[redacted]

[redacted]

4. Slight canning of fuselage in vicinity of radio access door,

Empennage

1. Skins aft of spar on both elevators scorched,
2. Elevator torque tube connector failed,
3. Elevator stops caused failure of fin spar flanges,
4. Elevator travel displaced from neutral,
5. Skin around upper rudder hinge bent on right hand side,

Miscellaneous

1. Evidence of hydraulic fluid leakage in left main landing gear wheel well,
2. Supercharger fairing dented left and right side,
3. Canopy cracked and broken; back of headrest burned,
4. VHF antenna charred,

Repair Estimate

Estimated man-hours required for complete repair, 202,

Figure Reference

1. Figure 3.49, rear view, showing bent and buckled ailerons and flaps,
2. Figure 3.50, close-up view of damaged right flap and aileron,
3. Figure 3.51, close-up view of buckled aft section of fuselage.

3.3.6.4 Aircraft F-47 (0065)

The damage sustained by aircraft F-47 (0065), parked nose-in is itemized below:

Wing

No damage,

Fuselage

1. Skin buckled at intersection of fuselage horizontal centerline stringer and frame at aft edge of radio access door,
2. Radio access door buckled,
3. Secondary cowl panels failed, upper and lower, left and right sides,
4. Belly cowls and lower surface wing fillets badly buckled from wing trailing edge aft,

Empennage

No damage,

Miscellaneous

1. Tail wheel moved and castered causing failure of internal fairing around tail wheel strut on left hand side (tail wheel lock may have failed),
2. Canopy cracked on both sides along bottom edges; right hand windshield crazed,

Repair Estimate

[redacted]

[redacted]

1. Estimated man-hours required for complete repair, 24,
2. Estimated man-hours required for minimum repairs, 20,

Figure Reference

1. Figure 3.52, three-quarter front view from right side,
2. Figure 3.53, close-up view of cracked canopy.

3.3.6.5 Aircraft F-47 (9719)

The damage sustained by aircraft F-47 (9719), parked nose-in in G-type revetment, is itemized below:

Wing

Rubber fairing strip around leading edge of tank adapter burned left and right sides,

Fuselage

1. Fuselage belly cowls bent in aft of wing trailing edge,
2. Radio access door dished in,

Empennage

No damage,

Miscellaneous

1. Canopy cracked on left hand side,
2. Headrest burned and charred at top,
3. Shoulder harness scorched,

Repair Estimate

1. Estimated man-hours required for complete repair, 24,
2. Estimated man-hours required for minimum repairs, 4,

Figure Reference

Figure 3.54, close-up view of cracked canopy.

3.3.6.6 Aircraft F-86 (8209)

The damage sustained by aircraft F-86 (8209), parked right side-in, is itemized below:

Wing

Wings and components apparently undamaged; slight evidence of heating on edge of right tip,

Fuselage

1. The second, third, and fourth right hand side frames, aft of the fuselage disconnect joint failed in bending, tearing the side skin (this failure was apparently due to positive dynamic pressure combined with shears produced by vertical tail load),
2. Permanent shear buckles in the upper portion of the fuselage just forward of the dorsal and above the side panel failure,
3. Cabin cooling access door pushed in,
4. Ammunition door on right hand side badly damaged,
5. Lower intercostal at right hand ammunition door

[redacted]

[redacted]

apparently failed in bending,
6. Area on right hand fuselage just forward of ammunition door had high positive pressures; frames and stringers are apparently intact,
7. Plastic nose charred on right hand side,

Empennage
1. Tip of vertical stabilizer surface charred - operable,
2. Minor wrinkles and buckles on right hand side of rudder,

Miscellaneous
1. Canopy and windshield smoked slightly,
2. Main landing gear doors blew open,
3. Messerschmidt fasteners released,

Repair Estimate
Estimated man-hours required for complete repair, 460,

Figure Reference
1. Figure 3.55, right side view, showing skin damage to fuselage,
2. Figure 3.56, close-up view of buckled and torn skin aft of fuselage disconnect joint,
3. Figure 3.57, close-up view of forward left fuselage, showing doors popped open,
4. Figure 3.58, close-up view of fuselage nose, showing charred plastic nose,
5. Figure 3.59, close-up view of charred vertical stabilizer and wrinkled rudder.

3.3.6.7 Aircraft F-86 (9597)

The damage sustained by aircraft F-86 (9597), parked nose-in is itemized below:

Wing
1. Wing tips slightly charred at leading edge but not noticeably damaged,
2. Slight positive pressure damage on upper surface of aileron tips,

Fuselage
1. Evidence of positive pressure loading on the right hand side of fuselage in the three bays forward of the ammunition door,
2. Slight buckles at lower edge of the ammunition door on the right hand side,
3. Very slight buckles in left hand side of fuselage in area just forward and below the left hand ammunition door,

Empennage
Leading edge of stabilizer charred,

Miscellaneous
1. Lower operating link broke on nose gear door

[redacted]

[redacted]

2. Headrest and wood block in pilot's seat burned partially and smoked up cabin,
3. Rubber coating on nose blistered and scorched,

Repair Estimate

Estimated man-hours required for complete repair, 283,

Figure Reference

1. Figure 3.60, over-all view from left side, showing general post-shot condition,
2. Figure 3.61, close-up view of fuselage and canopy damage.

3.3.6.8 Aircraft B-17 (3722)

The damage sustained by aircraft B-17 (3722), parked left side-in, is itemized below:

Wing

1. Right outboard wing panel trailing edge badly buckled,
2. Left outboard wing panel and tip buckled and warped beyond repair,
3. All engine accessory cowling badly buckled,
4. Right wing tip top skin buckled and warped,
5. Center wing section trailing edge badly buckled and oil-canned,
6. Right hand aileron fabric burned and ribs possibly damaged,

Fuselage

Complete loss; failed by bending and torsion at the wing root trailing edge,

Empennage

1. Rudder completely burned,
2. Right hand horizontal stabilizer badly buckled and warped,
3. Right hand elevator buckled; left hand elevator burned,
4. Vertical stabilizer and dorsal fin buckled and twisted beyond repair,

Miscellaneous

1. All windows broken except the following: window in main entry door, pilot and co-pilot's windshield, upper forward plexiglas, nose enclosure (crazed but not broken),
2. All Messerschmidt fasteners unlatched,
3. Airframe control cables not operable,
4. Radio operator's top hatch blown out of aircraft,
5. De-icer boots on vertical stabilizer ripped,
6. Bomb-bay doors slightly damaged,
7. Static dischargers burned off; electronic equipment torn from mounts,

Repair Estimate

Aircraft damaged beyond repair,

Figure Reference

[redacted]

[redacted]

1. Figure 3.62, general view of aircraft condition from left side,
2. Figure 3.63, general view of aircraft condition from right side.

3.3.6.9 Aircraft B-17 (7746)

The damage sustained by aircraft B-17 (7746), parked tail-in, is itemized below:

Wing

1. All wing structure aft of rear spars totally damaged,
2. Right and left aileron burned and bent,
3. Both wing tips pressure damaged,
4. Outer skin panels, corrugations and ribs between spars may have been damaged,
5. Accessory cowl panels dished in,

Fuselage

1. Fuselage suffered extensive bending and crushing of frames, formers, and ribs, and general distortion of skin panels by pressure loads; considered a complete loss,
2. Only areas of fuselage showing no appreciable damage are body skins and frames between the front and rear spar bulkheads and above the wing upper surface.

Empennage

1. Right and left elevators burned and buckled,
2. All fabric on both elevators burned,
3. Rudder fabric unburned,
4. Rudder surface lock torn loose from mounting structure; rudder spar bending failures general over upper two-thirds of rudder spar,
5. Stabilizer upper and lower surfaces, left and right, squeezed together by as much as 1 in. per surface,
6. Dorsal and vertical fin damaged by crushing and bending of frames and ribs,

Miscellaneous

1. Airframe controls not operable,
2. Radome areas facing ground zero charred and split; all windows broken except the following: pilot and co-pilot's windshield and upper forward panes, astrodome, nose enclosure, all windows on left side of navigator's compartment, small forward pane on right hand side of navigator's compartment, and rear gunner's aft and emergency hatch panes,
3. Rivet heads, Philip heads, and bolt heads in flaps shorn off,
4. Mechanical release to discharge carbon dioxide fire extinguishing system damaged beyond repair,
5. Wooden bracket holding radio equipment on right hand

[redacted]

[redacted]
CLASSIFIED

side of radio room broken,

Repair Estimate

Aircraft beyond economical repair,

Figure Reference

1. Figure 3.64, three-quarter rear view, showing general condition of the left side of aircraft,
2. Figure 3.65, close-up view of left wing, showing total damage aft of rear spar,

3.3.6.10 Aircraft B-17 (5715)

The damage sustained by aircraft B-17 (5715), parked nose-in, is itemized below:

Wing

1. Lower surface of outer panel pushed in inboard of mooring ring in area forward of rear spar,
2. Wing lower surface aft of rear spar pushed in,
3. Wing tip ribs apparently crippled,
4. Wing upper surface aft of rear spar pushed in, failing trusses,

Fuselage

1. Entire fuselage damaged with exception of lower surface of fuselage from wing rear spar aft,
2. Bomb-bay doors pushed in approximately 10 in.,

Empennage

1. Vertical stabilizer surfaces pushed in, causing rib failures,
2. Small buckles at top of rudder,
3. Bottom of elevator and tab surfaces pushed in,

Miscellaneous

1. Left and right wing clear plastic light cover cracked,
2. Radome charred and cracked; nose enclosure cracked at top,
3. Following windows are only windows that remained undamaged: astrodome, pilot and co-pilot's glass windshields, co-pilot's aft window, main entry door window,
4. ART-13 transmitter blown off mounts; BC-966A #27628 torn out of rack and fell to floor,
5. Carbon dioxide fire extinguishing system discharged,
6. Bombardier's altimeter and air-speed indicator ruptured (shorter lines than pilot's), and fuel pressure transmitters inoperable,

Repair Estimate

Aircraft damaged beyond economical repair,

Figure Reference

1. Figure 3.66, close-up view of damage to right side forward section,
2. Figure 3.67, close-up view of bomb-bay doors,

CLASSIFIED

[redacted]

3. Figure 3.68, right side view of aft section of fuselage, showing pressure damage to dorsal fin and vertical stabilizer,
4. Figure 3.69, close-up view of buckled under surface of right wing,
5. Figure 3.70, interior view of charred cockpit,
6. Figure 3.71, external view of damaged top of cabin,
7. Figure 3.72, interior view of damaged skin and fuselage frames.

3.3.6.11 Aircraft B-45 (9481)

The damage sustained by aircraft B-45 (9481), parked nose-in, is itemized below:

Wing
1. General wing structure shows no damage,
2. Upper and lower nose fairing of engine nacelles was dished in and lower surface of tail cone buckled,

Fuselage
1. Crew entrance door blown in,
2. Bomb-bay doors blown in,
3. Tail-gunner's tail cone fairing buckled left and right side,
4. Life-raft door on left hand side buckled along lower edge,

Empennage
Fairing between dorsal fin and vertical stabilizer buckled,

Miscellaneous
1. Main landing gear doors buckled along trailing edge,
2. All Messerschmidt fasteners unlocked,
3. Light radiation burn at forward area of both radome and nose enclosure,
4. Low-pressure oxygen-system door, below and aft of life-raft hatch, blown off,
5. Electric wiring to cabin-pressure regulator scorched,
6. Exciter regulator in variable frequency system inoperable,
7. Bombardier's altimeter and pilot's accelerometer damaged,

Repair Estimate
Estimated man-hours required for complete repair, 300,

Figure Reference
1. Figure 3.73, close-up front view of right hand engine nacelle,
2. Figure 3.74, close-up view of forward bomb-bay doors,
3. Figure 3.75, close-up view of tail assembly,
4. Figure 3.76, internal view of damage to forward bomb-bay door mechanism,
5. Figure 3.77, internal view of damage to aft bomb-bay

CLASSIFIED

door mechanism,
6. Figure 3.78, close-up view of thermal damage to right main landing gear tire.

3.3.7 Station 10,500

Six aircraft, two fighters and four bombers, were parked at Station 10,500 for Shot 3. At this range, 10,354 ft from ground zero, the peak overpressure was 2.4 psi, and the total thermal energy was 6.7 cal/cm^2. The two F-47 aircraft received only minor damage. The three B-17's all suffered moderate damage, whereas damage to the nose-in B-29 was relatively light.

3.3.7.1 Aircraft F-47 (3828)

The damage sustained by aircraft F-47 (3828), parked right side-in, is itemized below:

Wing
No damage,
Fuselage
1. Buckle in fuselage panel below and aft of radio access door,
2. Radio access door buckled,
3. Right hand secondary cowl panels buckled in,
4. Right hand belly cowl panels dished,
Empennage
Right hand fin skin slightly dished,
Miscellaneous
1. Internal rudder lock inoperative,
2. Rudder balance cable lug on right hand rudder pedal broken,
Repair Estimate
1. Estimated man-hours required for complete repair, 45,
2. Estimated man-hours required for minimum repairs, 6,
Figure Reference
Figure 3.79, close-up view of buckled areas in vicinity of radio access door.

3.3.7.2 Aircraft F-47 (0297)

The damage sustained by aircraft F-47 (0297), parked tail-in, is itemized below:

Wing
1. Right hand flap down because of bolt failure,
2. Aileron trailing edge buckled, left and right,
3. Wing gun access covers lightly dished in between stiffeners,

UNCLASSIFIED

[redacted]

UNCLASSIFIED

Fuselage
1. Belly cowls pushed in from wing trailing edge aft,
2. Louver in right hand secondary cowl bent in,

Empennage
No damage,

Miscellaneous
Canopy cracked in right and left side (crack approximately 18 in. long),

Repair Estimate
1. Estimated man-hours required for complete repair, 8,
2. Estimated man-hours required for minimum repairs, 4,

Figure Reference
Figure 3.80, close-up view of cracked canopy.

3.3.7.3 Aircraft B-17 (3769)

The damage sustained by aircraft B-17 (3769), parked right side-in, is itemized below:

Wing
1. Pressure loading is evident on wing outer panel, forward of rear spar,
2. Aft of rear spar surfaces pushed in, with damage to rib structure,
3. Wing tips pushed in by positive pressure, causing probable rib damage,
4. Access covers of engine nacelles pushed in,
5. Right hand landing light broken,
6. Right hand wing-root fillet ripped (vertically) from wing at aft-most screws and torn at top by relative movement, between wing trailing edge and fuselage structure,
7. Left hand wing-root fillet buckled and similarly torn,

Fuselage
1. Complete loss,
2. Body frames bent and sides torn at radio supporting station,
3. Both bomb doors damaged,
4. Torsion and side bending failure of body at wing-root trailing edge,
5. Torsion shear wrinkles, left rear side of body, immediately forward of fin front spar bulkhead,
6. Left hand and right hand aileron trailing edge warped, and fabric somewhat loosened,
7. Fuselage skin stringers and frame dished in throughout entire right side, except over center wing,

Empennage
1. Rudder vertical stabilizer and dorsal wrecked,
2. Horizontal stabilizer surfaces pushed in because of pressure,

UNCLASSIFIED

[redacted]

[redacted]

3. Elevators only slightly damaged,
4. Dorsal fin buckled and dished in; dorsal fin bulkheads buckled and torn,
5. Vertical stabilizer spar apparently buckled,
6. Vertical stabilizer to dorsal fin fairing pulled loose,
7. Rudder control surface fabric burned off,

Miscellaneous

1. Vertical stabilizer de-icer boot torn approximately 24 in.,
2. Pilot's side window broken; right and left waist-gunner's window broken out; fuselage top windows broken; co-pilot's side window broken; radar operator's window broken,
3. Radar modulator cover punctured; wave guide between modulator and RF unit damaged,
4. Tail-gunner's exit door dished in,
5. Rudder lock plunger mounting bracket broken loose,
6. Altimeter, in radio compartment, damaged and panel shock mount broken; No. 2 fuel-pressure transmitter damaged,

Repair Estimate

Estimated man-hours required for complete repair, 5704,

Figure Reference

1. Figure 3.81, three-quarter rear view, from right side, showing general aircraft condition,
2. Figure 3.82, close-up view of pressure damage to nose section of fuselage,
3. Figure 3.83, interior view of bent fuselage frames and the buckled and torn skin,
4. Figure 3.84, interior view of buckled and bent fuselage frames and skin.

3.3.7.4 Aircraft B-17 (3730)

The damage sustained by aircraft B-17 (3730), parked tail-in, is itemized below:

Wing

1. Right and left inboard wing skin dished above flaps,
2. Skin on outboard section of both wings buckled aft of rear spar,
3. All access covers in lower surface of wing unsecured,
4. Right and left aileron control surface fabric burned off,
5. Both wing tips damaged by pressure,

Fuselage

1. Fuselage skin and frame buckled in area of upper forward turret,
2. Fuselage skin and frame buckled at right and left sides, below cockpit windows,
3. Bomb-bay doors buckled throughout,

Empennage

UNCLASSIFIED

[redacted]

[redacted]

1. Elevator control surface fabric burned off,
2. Right elevator torque-tube rivets sheared,
3. Vertical stabilizer skin dished in,
4. Vertical stabilizer bulkheads buckled,
5. Dorsal fin skin dished in and bulkheads buckled,
6. Horizontal stabilizer skin dished in,

Miscellaneous

1. Side window in cockpit cracked, navigator's right hand window blown in, bombardier's right hand window blown in, and left hand waist window broken,
2. Horizontal stabilizer boot torn at left side,
3. Carbon dioxide extinguishing system discharged,

Repair Estimate

Estimated man-hours required for complete repair, 3936,

Figure Reference

Figure 3.85, three-quarter rear view from left side, showing general condition of aircraft.

3.3.7.5 Aircraft B-17 (3575)

The damage sustained by aircraft B-17 (3575), parked nose-in, is itemized below:

Wing

1. Lower surface of left wing outer panel buckled just aft of front spar,
2. Left hand wing tip pushed in, top and bottom,
3. Upper and lower surface of left wing outer panel, aft of rear spar, pushed in,
4. Condition of right hand wing approximately same as for left,

Fuselage

1. Fuselage frames and skins buckled in area above and below navigator's window on left hand side,
2. Four frames and six pieces of skin buckled on right hand side of fuselage in area just below navigator's windows,
3. At least two frames and four pieces of skin buckled on left hand side of nose fuselage in area below navigator's windows,
4. Skin and frames buckled below and three bays aft of escape door on left hand side of nose,
5. Eighteen frames buckled on right hand side of pilot's cabin,
6. Approximately four frames buckled on left hand side of pilot's cabin,
7. Skin and frames buckled in area forward of pilot's windshield on right hand side,
8. Frames and skin generally buckled on both bomb-bay doors,

Empennage

[redacted]

[redacted]

1. Loose skin and possible rib damage of vertical stabilizer and rudder,
2. Left elevator skin slack at trailing edge,
3. Slight positive pressure damage on upper and lower surfaces of horizontal stabilizer,

Miscellaneous

1. Plexiglas from navigator's large right hand window driven through left hand body skin,
2. Radio operator's hatch blown in,
3. Following windows cracked: pilot and co-pilot's side windows, pilot's windshield, navigator's left and right hand windows, and waist window,
4. Canopy fairing caved in on left and right hand sides,
5. Bombardier's air-speed indicator damaged by flying debris; fuel-pressure transmitters damaged,
6. Carbon dioxide fire extinguishing system discharged,
7. Shock mounts on compass indicator, (NAB) AN/ARN-7, slightly damaged,

Repair Estimate

Estimated man-hours required for complete repair, 4006,

Figure Reference

1. Figure 3.86, rear view of aircraft, showing loosened vertical stabilizer skin,
2. Figure 3.87, close-up view of outer panel of right wing, showing buckled upper and lower surfaces.

3.3.7.6 Aircraft B-29 (7349)

The damage sustained by aircraft B-29 (7349), parked nose-in, is itemized below:

Wing

1. Inconsequential loose-skin-type cans in the outer panels,
2. Wing tips slightly canned,
3. Nacelle access doors buckled; several buckles in tail fairing of inboard nacelles,

Fuselage

1. Skin and frames of aft bomb-bay doors buckled and generally failed,
2. Forward bomb-bay doors completely wrecked, including hinges,

Empennage

1. Loose-skin-type buckles of minor nature,
2. Left hand elevator trailing edge warped,
3. Some evidence of heat on fabric,
4. Light damage to elevator trailing edge, just outboard of tabs,

Miscellaneous

1. Buckle at forward end of left hand nose-gear door,

[redacted]

[redacted]

2. Astrodome blown in,
3. Crew tunnel perforated by missile (probably a bomb rack quick release pin) thrown upward when the forward bomb-bay doors received the pressure load,
4. Left rear emergency escape hatch blown in approximately one-half inch,
5. Vertical tail de-icer boot scorched,
6. Both life-raft doors lightly buckled,

Repair Estimate

Estimated man-hours required for complete repair, 488,

Figure Reference

1. Figure 3.88, close-up view from left side of wrecked forward bomb-bay doors,
2. Figure 3.89, close-up view of wrecked right hand forward bomb-bay door,
3. Figure 3.90, close-up view of buckled right hand aft bomb-bay door,
4. Figure 3.91, interior view of totally wrecked forward bomb-bay doors,
5. Figure 3.92, close-up view of perforated crew tunnel,
6. Figure 3.93, close-up view of loose-skin-type cans on lower surface of right wing outer panel,
7. Figure 3.94, close-up view of buckled left inboard nacelle fairing,
8. Figure 3.95, close-up view of empennage, showing warped trailing edge of left elevator and buckles on vertical stabilizer.

3.3.8 General Observations

Both jet and reciprocating type power plant and power plant accessories were undamaged, except for caving in of main oil tanks on the F-47 aircraft parked at Station 2200 or closer. Main landing gear of all aircraft were undamaged, except for slight bowing of the landing gear in the F-47 aircraft parked side-in at Stations 4000 and 8000. The electrical system and components were found to suffer little or no damage up to the point where aircraft were damaged beyond repair. The hydraulic system was unaffected, except for a few cases of loosening of fittings. Wheels and brakes of all aircraft were considered serviceable. Charring of tires was noted at all ranges. Depth of charring appeared to be approximately one-sixteenth inch on tires at ranges from 2000 to 8000 ft. De-icer boots smoked during thermal phase but were found to be operable following the test; however, their useful life may have been shortened. Fire detecting and extinguishing systems, cooling equipment, and pressurization equipment were in general undamaged. Electronic equipment received adequate protection from the aircraft fuselage to prevent damage, except when located in a position to receive direct thermal radiation. Antenna components and radomes were quite vulnerable to charring at the closer

[redacted]

[redacted]

ranges. Relative to the airframe, propellers were found to be insensitive to the thermal and blast inputs experienced; occasional scuffing of cuffs was noted. Thirteen aircraft instruments were damaged in the test. The damage area was widespread, including aircraft at Station 10,500. Installation of pitot-tube covers served to minimize instrument damage in all except the extreme forward areas.

Any armament equipment installed on aircraft parked at stations up to and including 4000 would have been destroyed or damaged sufficiently to require replacement. At Station 8000 the armament directly exposed to thermal and blast shock would be damaged to varying degrees, whereas armament on the side facing away from the blast would probably be serviceable after check-out and re-alignment. Armament equipment at 10,500 ft from ground zero, would probably need only check-out and minor maintenance.

3.4 SHOT 4

Shot 4 of the TUMBLER series was detonated at an altitude of 1040 ft. The energy equivalent was reported to be 19.6 KT. Twenty-one aircraft, parked at ground ranges of 1000 ft to 8000 ft from target ground zero, participated in the test. The location and orientation of these aircraft are shown in Fig. 2.4. A complete summary of the degree of damage sustained by each aircraft, along with the thermal and overpressure inputs, is presented in Fig. 3.96. All aircraft parked at Station 2500 and closer were either destroyed or damaged beyond economical repair. The tail-in B-17 at Station 4000 was damaged beyond repair, and the fuselage of the B-29, nose-in at Station 5000, was destroyed by fire. The two tail-in F-47 aircraft protected by the wall and pit revetments at Station 4000 received considerably less damage than the openly exposed aircraft parked between them. A complete summary of the damage sustained by the 21 aircraft participating in Shot 4 is given below in order of increasing distance from ground zero.

3.4.1 Station 1000

Aircraft F-47 (9114) was the only aircraft exposed at Station 1000. The overpressure at this distance of 1110 ft from ground zero was 36 psi with a thermal input of 235 cal/cm^2. The combined effect of the thermal and blast forcing functions on the nose-in F-47 and the resulting fire were sufficient to damage the aircraft to the extent that only the power plant and bare skeleton of the fuselage remained. Figure 3.97 shows the burned wreckage of the fuselage and power plant.

3.4.2 Station 1350

The overpressure and thermal energy inputs at Station 1350 for Shot 4 were 22 psi and 170 cal/cm^2, respectively. Aircraft F-47 (9851), parked tail-in at a ground range of 1456 ft from ground

[redacted]

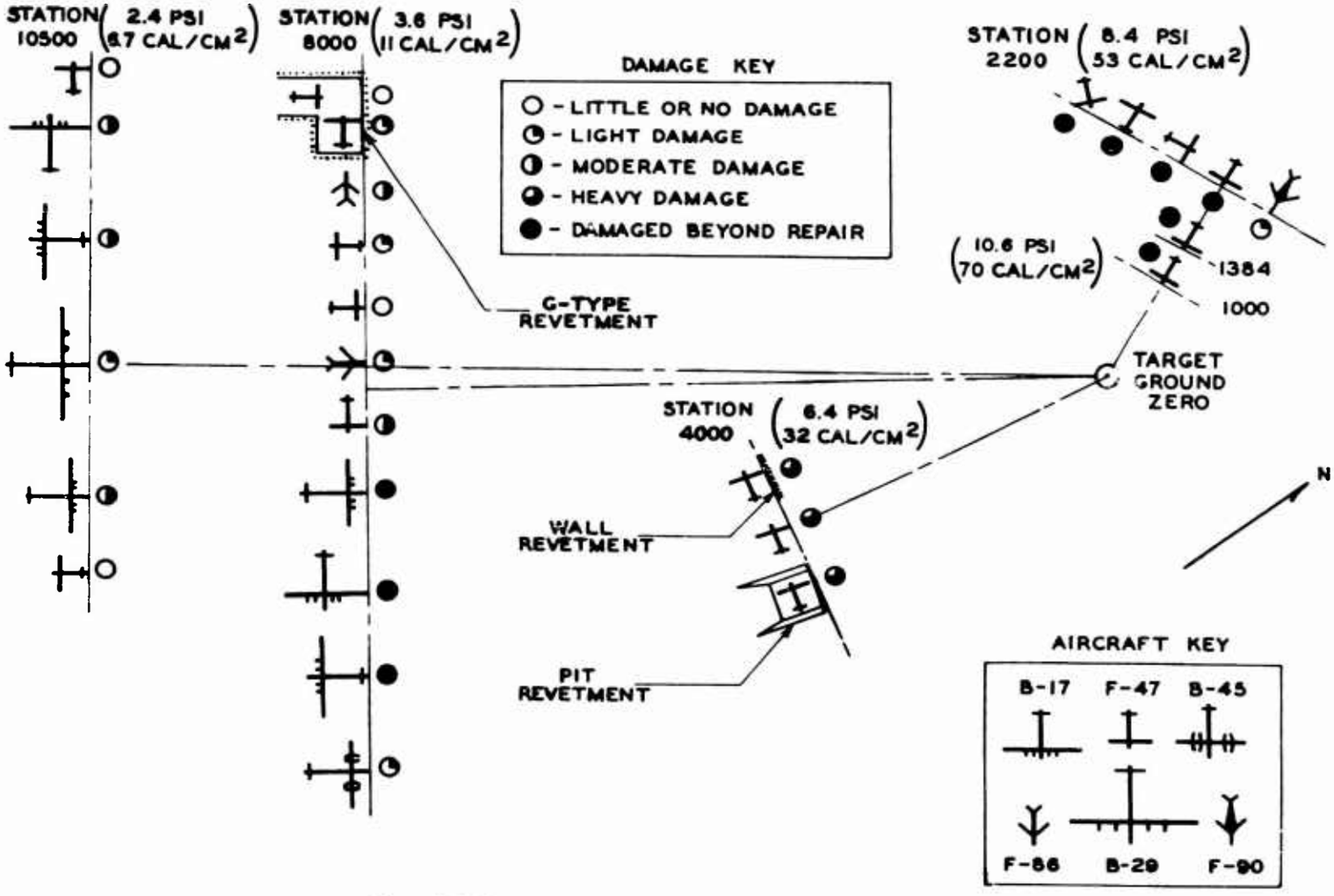

Fig. 3.12 Aircraft Damage Summary, Shot 3

Fig. 3.13 F-47 (9114), Nose-in, Station 1000 (10.6 psi, 70 cal/cm^2), Shot 3, Showing General Burned and Buckled Areas Over Entire Aircraft

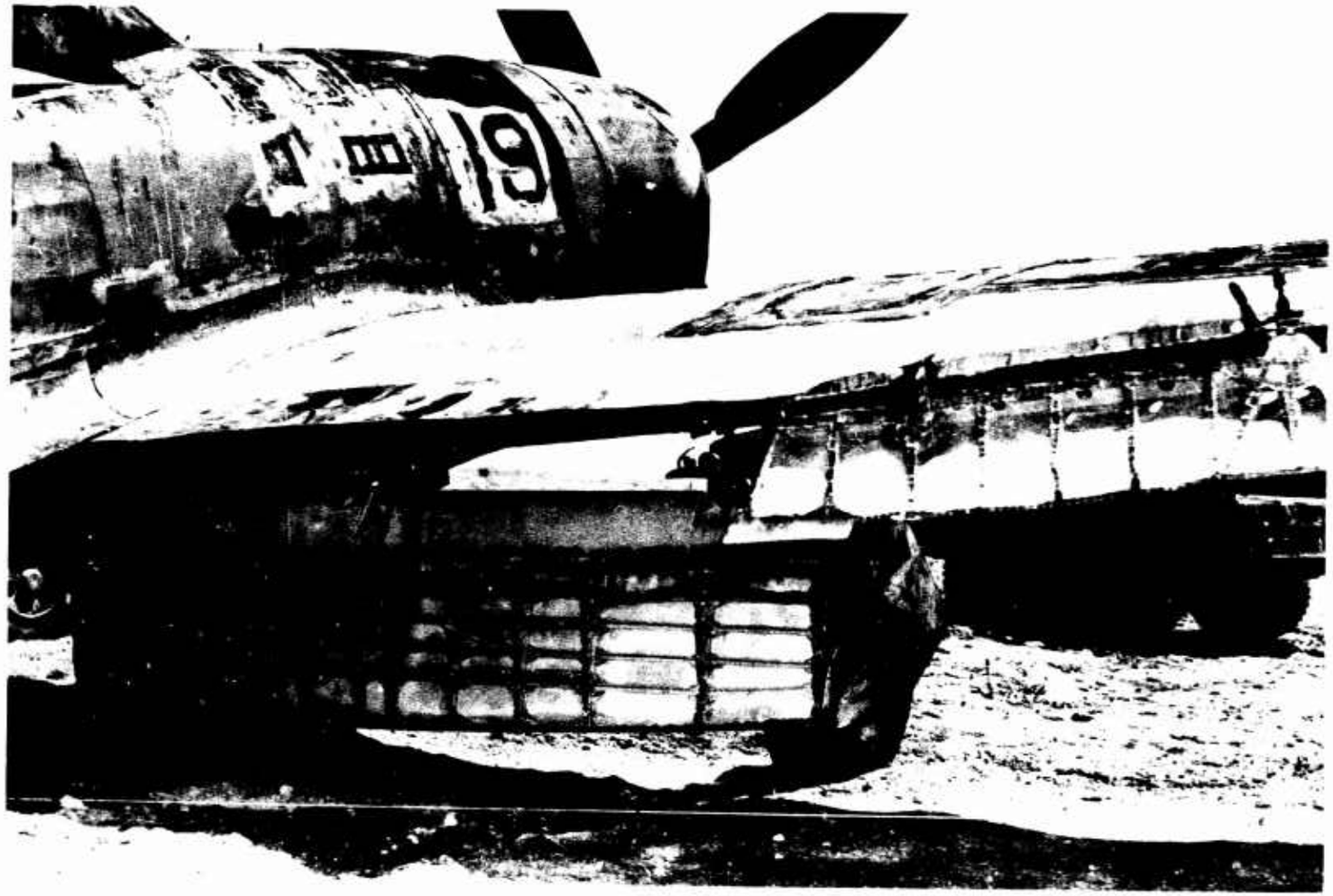

Fig. 3.14 F-47 (9114), Nose-in, Station 1000 (10.6 psi), Shot 3, Close-up View Showing Damaged Right Flap and Aileron. Compare with Figures 3.7 and 3.8.

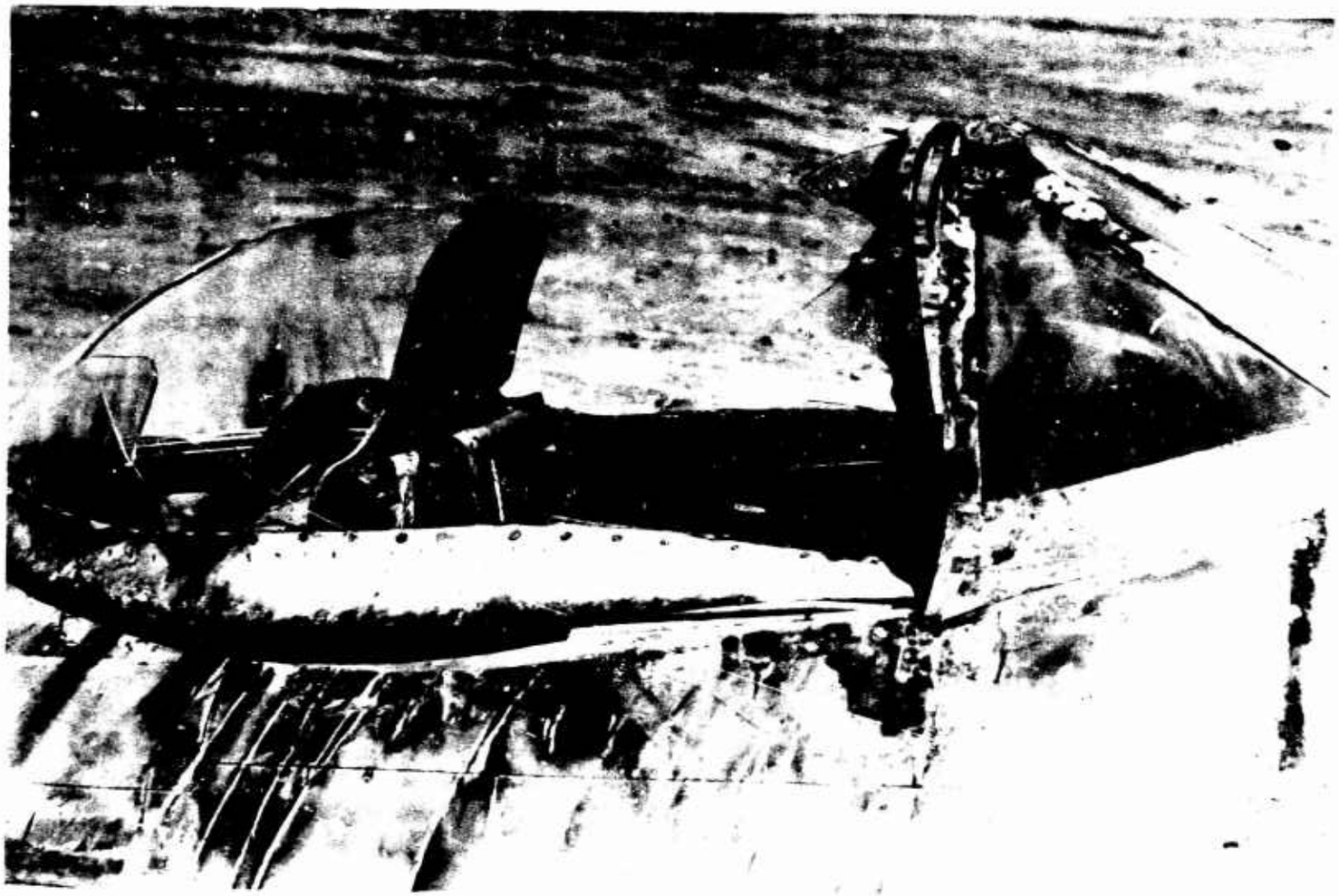

Fig. 3.15 F-47 (9114), Nose-in, Station 1000 (10.6 psi), Shot 3, Close-up View of Cockpit Showing Destroyed Canopy and Thermal Effects

Fig. 3.16 F-47 (9232), Nose-in, Station 1384 (9.9 psi), Shot 3, Showing Burned and Buckled Left Side of Aircraft. Compare with Figure 3.5.

Fig. 3.17 F-47 (9232), Nose-in, Station 1384 (9.9 psi), Shot 3, Showing Burned and Buckled Right Side of Aircraft. Compare with Figure 3.6.

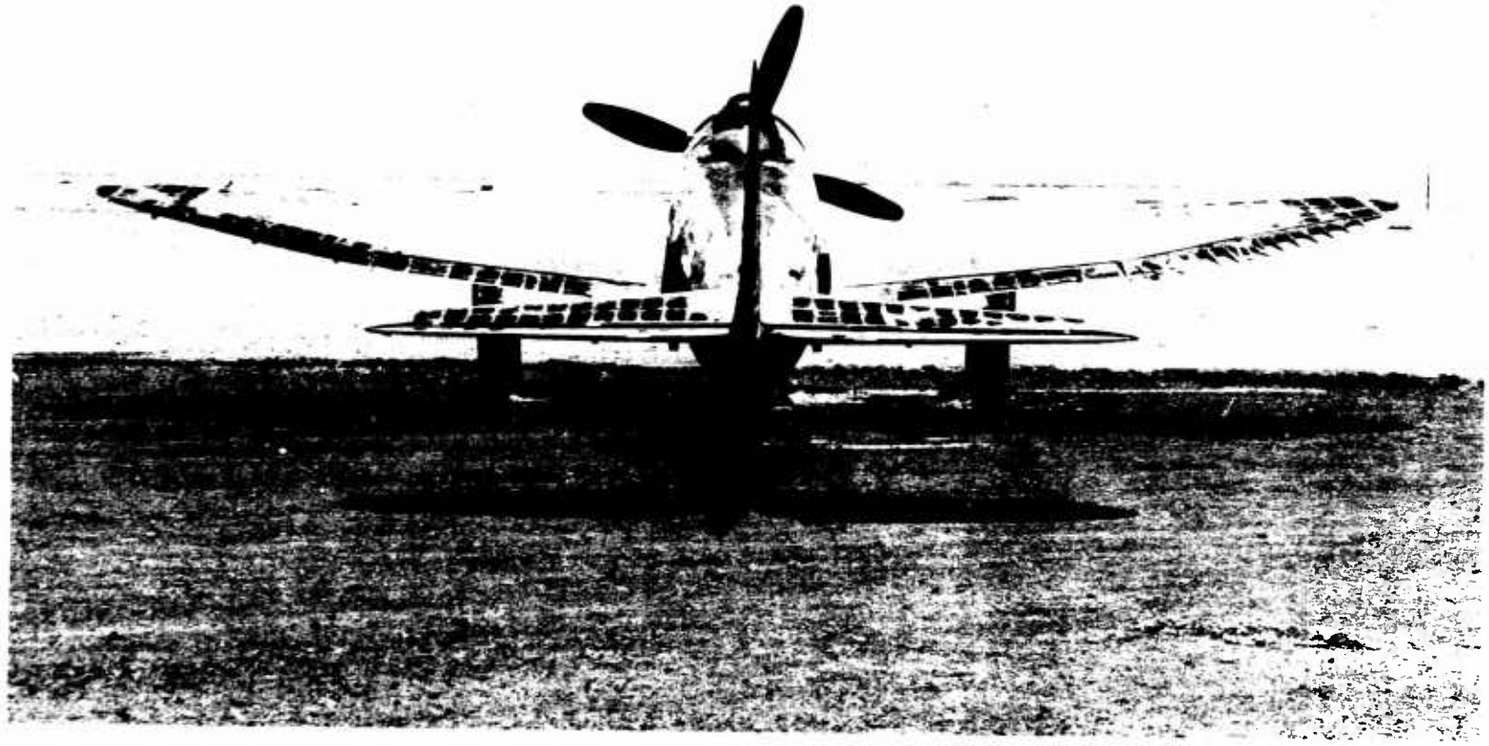

Fig. 3.18 F-47 (9232), Nose-in, Station 1384 (9.9 psi), Shot 3, Full Rear View, Emphasizing Burned Areas On Wing and Horizontal Stabilizer

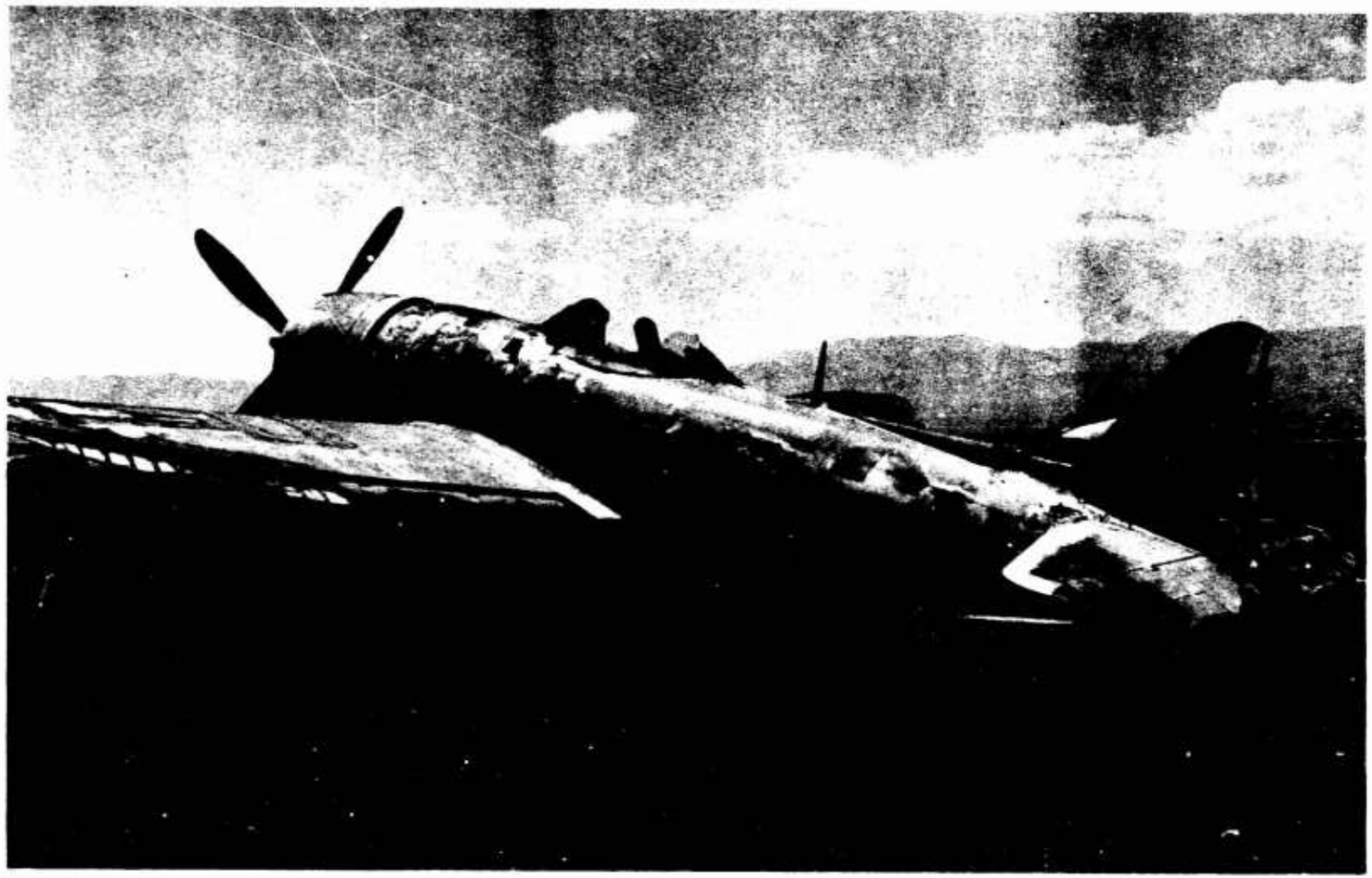

Fig. 3.19 F-47 (9082), Right Side-in, Station 2200 (8.4 psi), Shot 3, Showing Buckled Skin Panels, Damaged Rudder, and Thermal Damage to Control Surfaces and Horizontal Stabilizer. Note Protection Afforded Horizontal Tail By Vertical Fin.

Fig. 3.20 F-47 (9082), Side-in, Station 2200 (8.4 psi), Shot 3, Showing Degree of Aircraft Rotation During Blast Phase By Comparing With Ground Shadow of Aircraft Caused By Thermal Phase

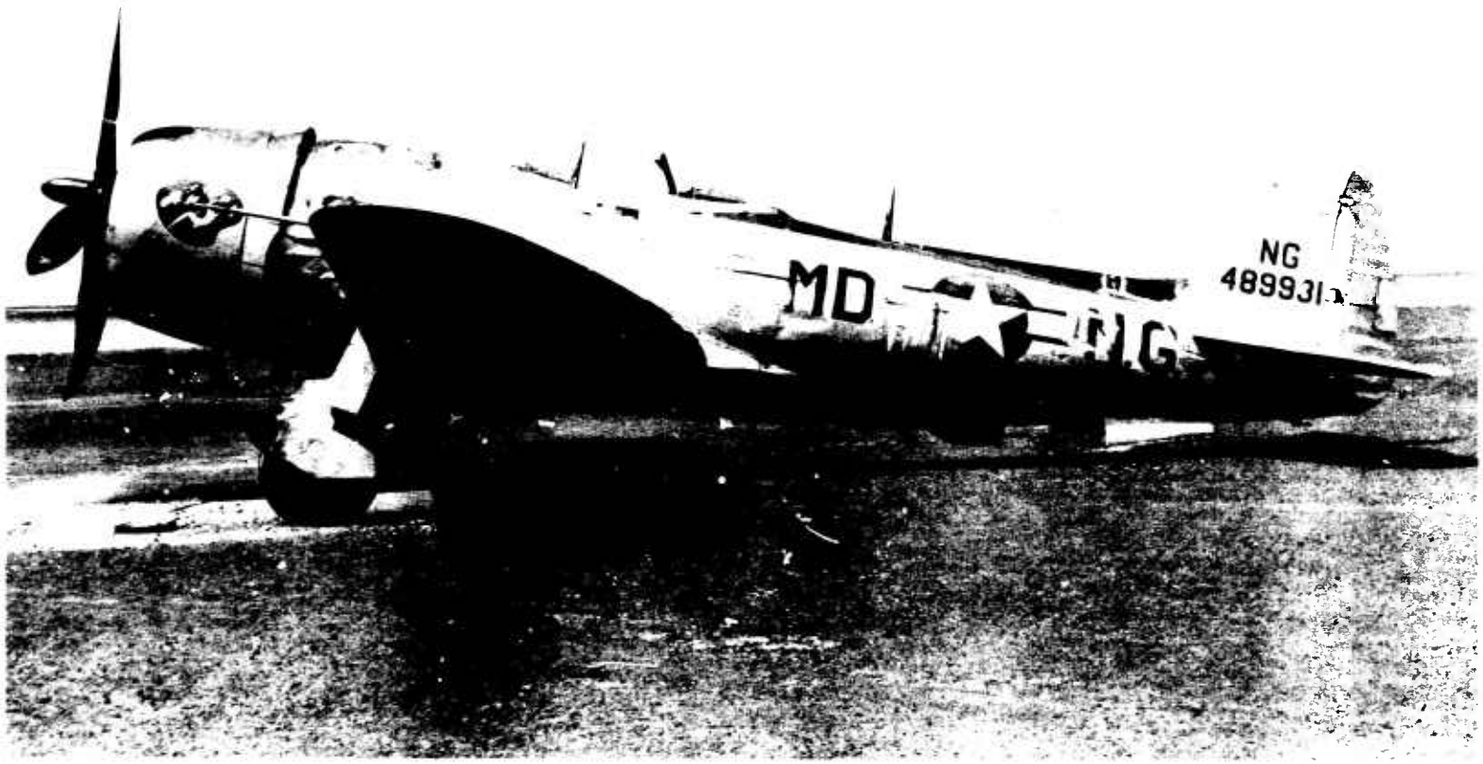

Fig. 3.21 F-47 (9931), Right Front Quarter-in, Station 2200 (8.4 psi), Shot 3, Showing Damage to Left Side of Fuselage and Rudder (Downward Side)

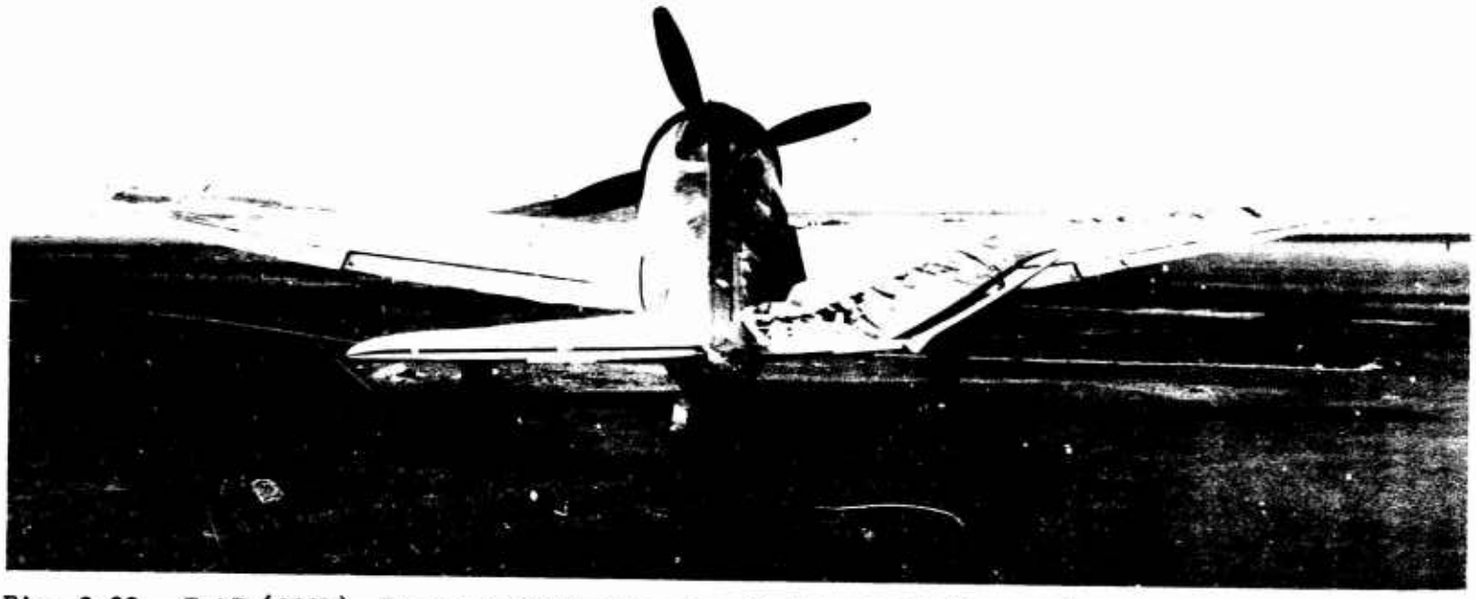

Fig. 3.22 F-47 (9931), Right Front Quarter-in, Station 2200 (8.4 psi), Shot 3, Showing Torsion and Bending Failure in Right Horizontal Stabilizer

Fig. 3.23 F-47 (9931), Right Front Quarter-in, Station 2200 (8.4 psi), Shot 3, Close-up View of Aft Section of Fuselage, Showing Charred and Buckled Right Side and Horizontal Stabilizer Failure

Fig. 3.24 F-47 (9931), Right Front Quarter-in, Station 2200 (8.4 psi), Shot 3, Close-up View of Left Main Landing Gear

Fig. 3.25 F-47 (9851), Tail-in, Station 2200 (8.4 psi), Shot 3, Showing Damage to Right Side of Fuselage, Empennage, and Wing

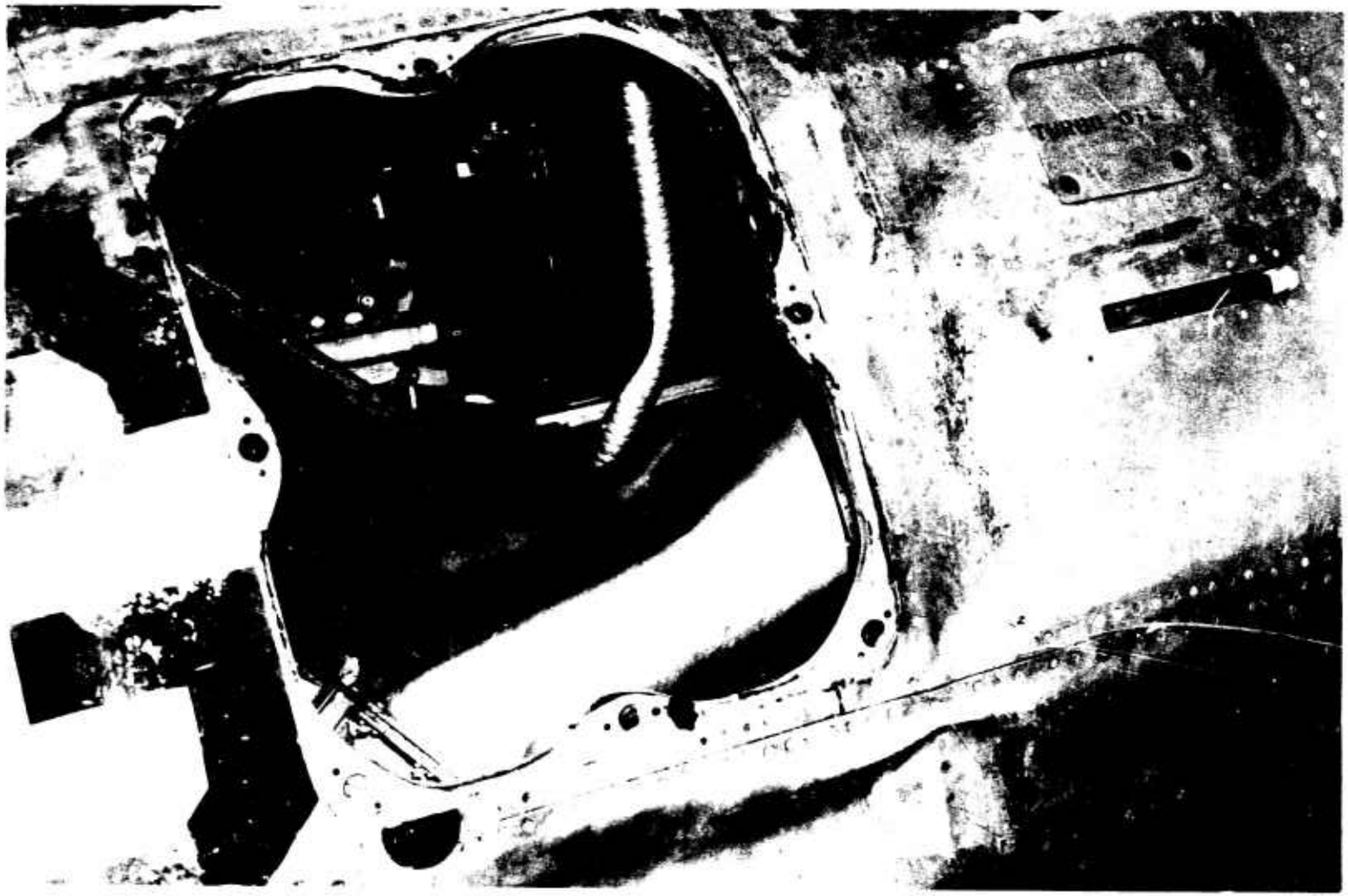

Fig. 3.26 F-47 (9851), Tail-in, Station 2200 (8.4 psi), Shot 3, Close-up View of Buckled Carburetor Air Duct After the Caved-in Radio Access Door Was Removed

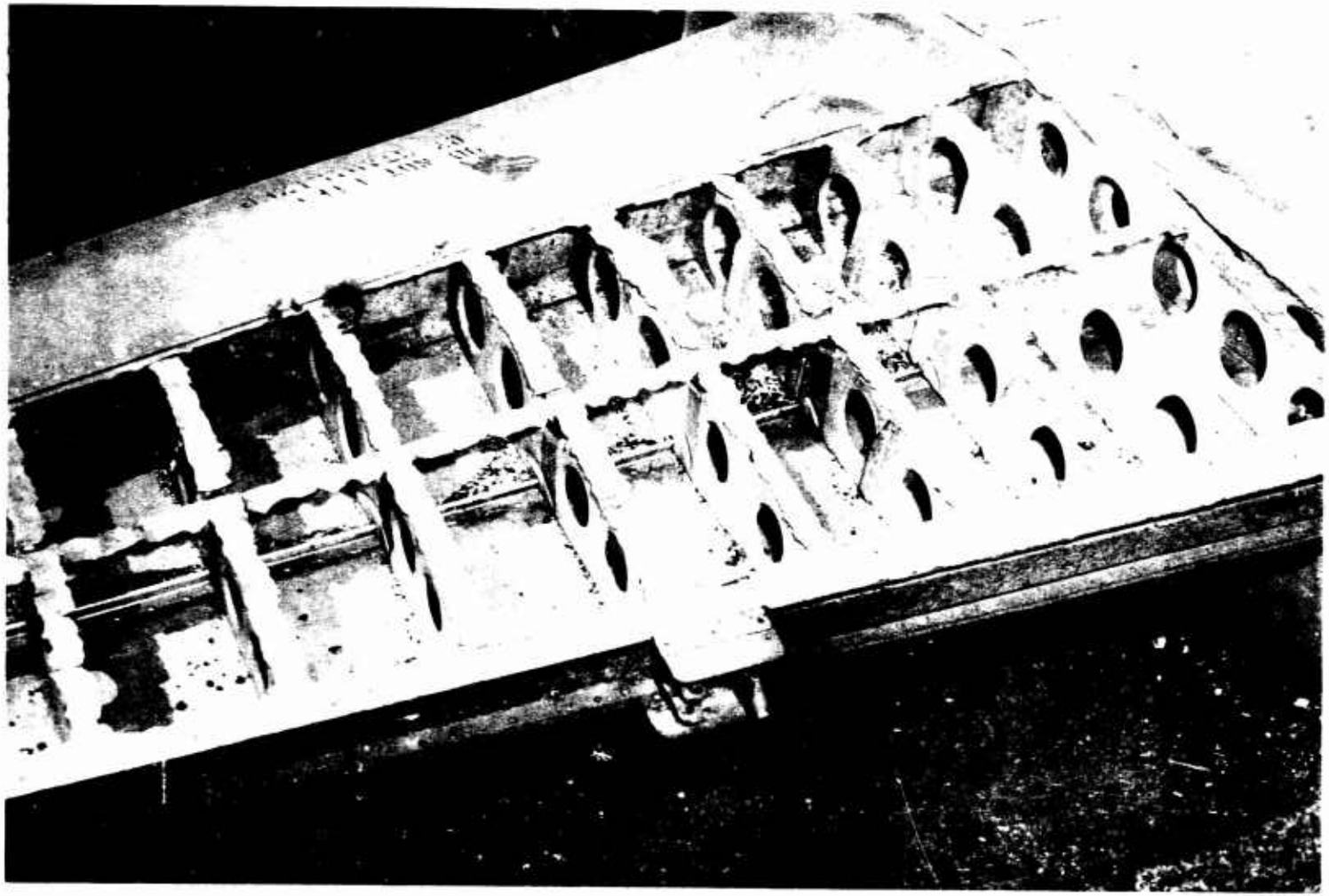

Fig. 3.27 F-47 (9851), Tail-in, Station 2200 (8.4 psi), Shot 3, Close-up View of Skin Damage on Left Horizontal Stabilizer

Fig. 3.28 F-47 (8785), Nose-in, Station 2200 (8.4 psi), Shot 3, Showing Buckled Areas Over Entire Aircraft. Note Wrinkled Area on Right Horizontal Stabilizer. Compare with Figure 3.9.

Fig. 3.29 F-47 (8785), Nose-in, Station 2200 (8.4 psi), Shot 3, Showing Bent Right Horizontal Stabilizer and Holes in Horizontal Stabilizers Where "No Lift" Was Lettered in Black. Permanent Skin Buckles Are Also Evident.

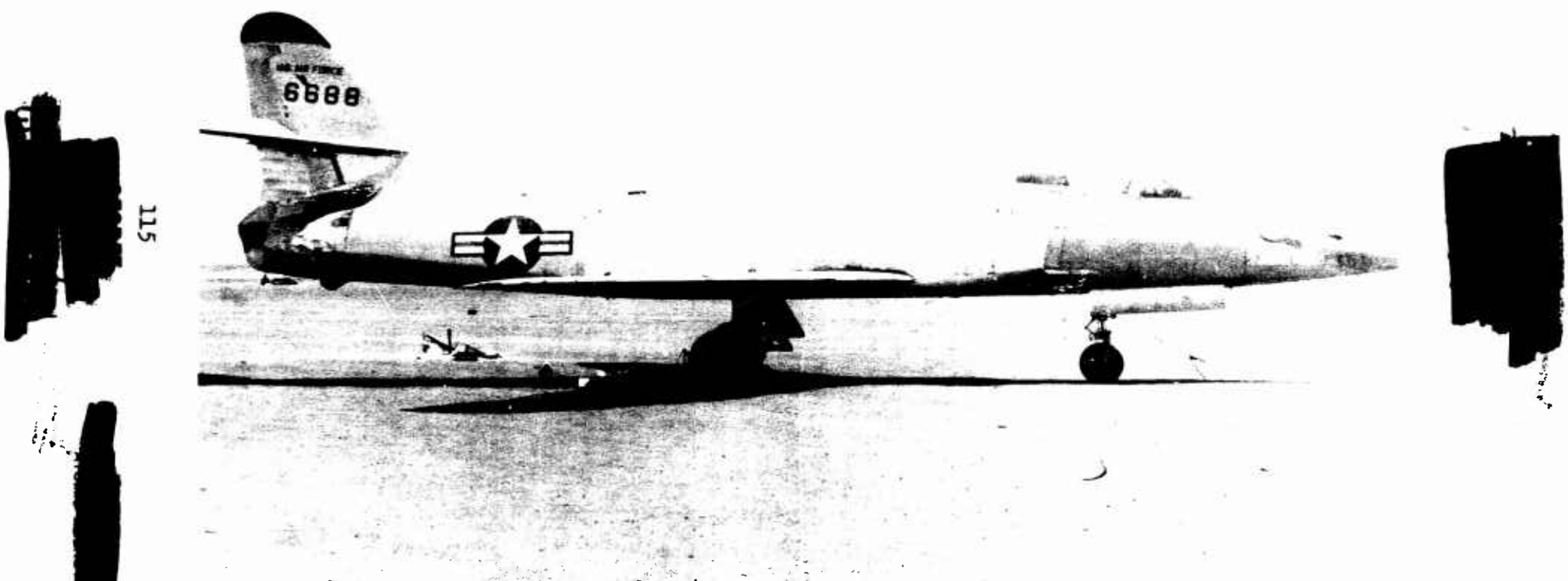

Fig. 3.30 F-90 (6688), Nose-in, Station 2200 (8.4 psi), Shot 3, Showing Damage to Right Side Radio Access Door, Tail Cone, and Fin. Compare with Figure 3.4.

Fig. 3.31 F-90 (6688), Nose-in, Station 2200 (8.4 psi), Shot 3, Close-up View of Buckled Radio Access Door and Charred Radome

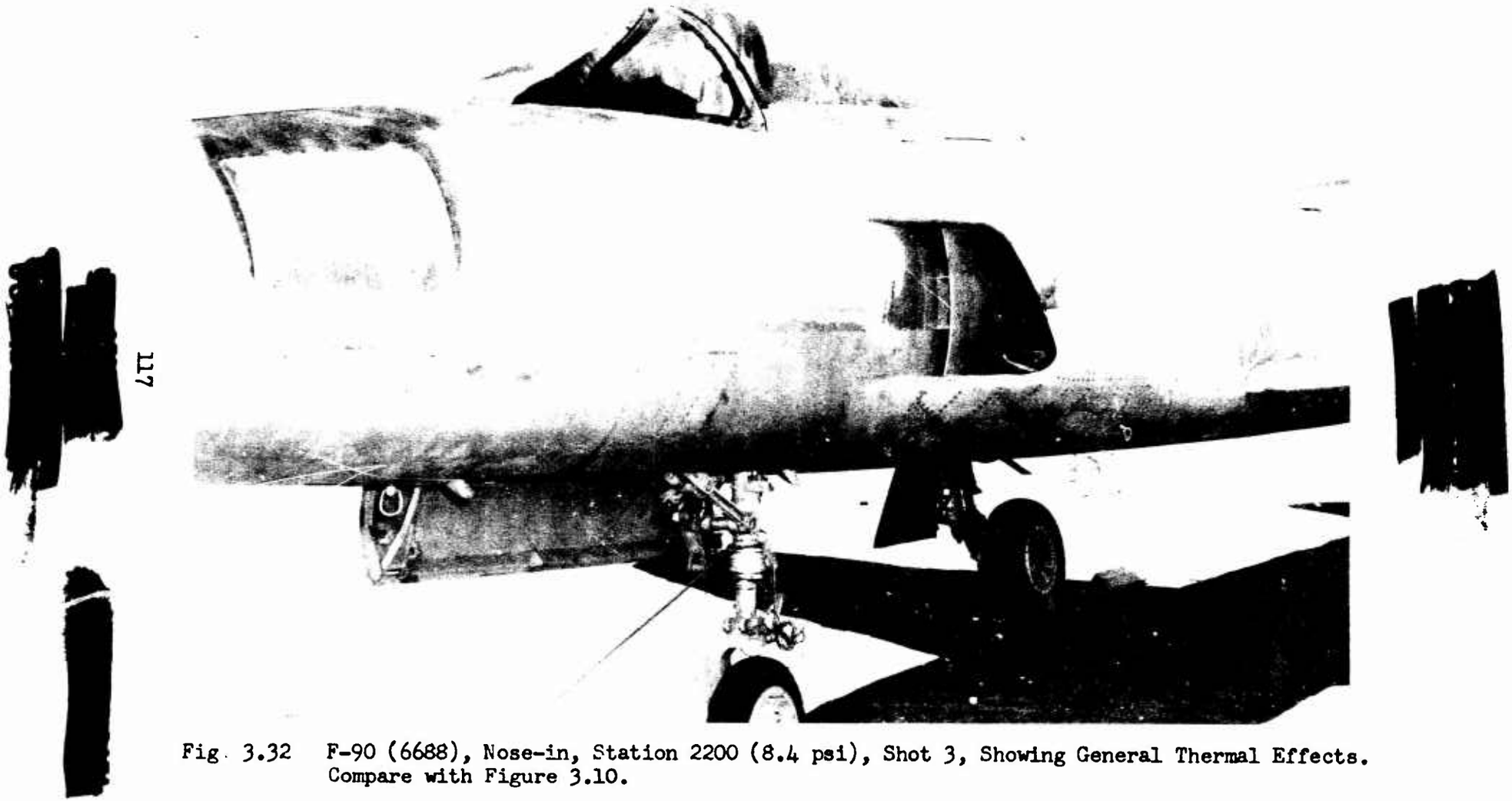

Fig. 3.32 F-90 (6688), Nose-in, Station 2200 (8.4 psi), Shot 3, Showing General Thermal Effects. Compare with Figure 3.10.

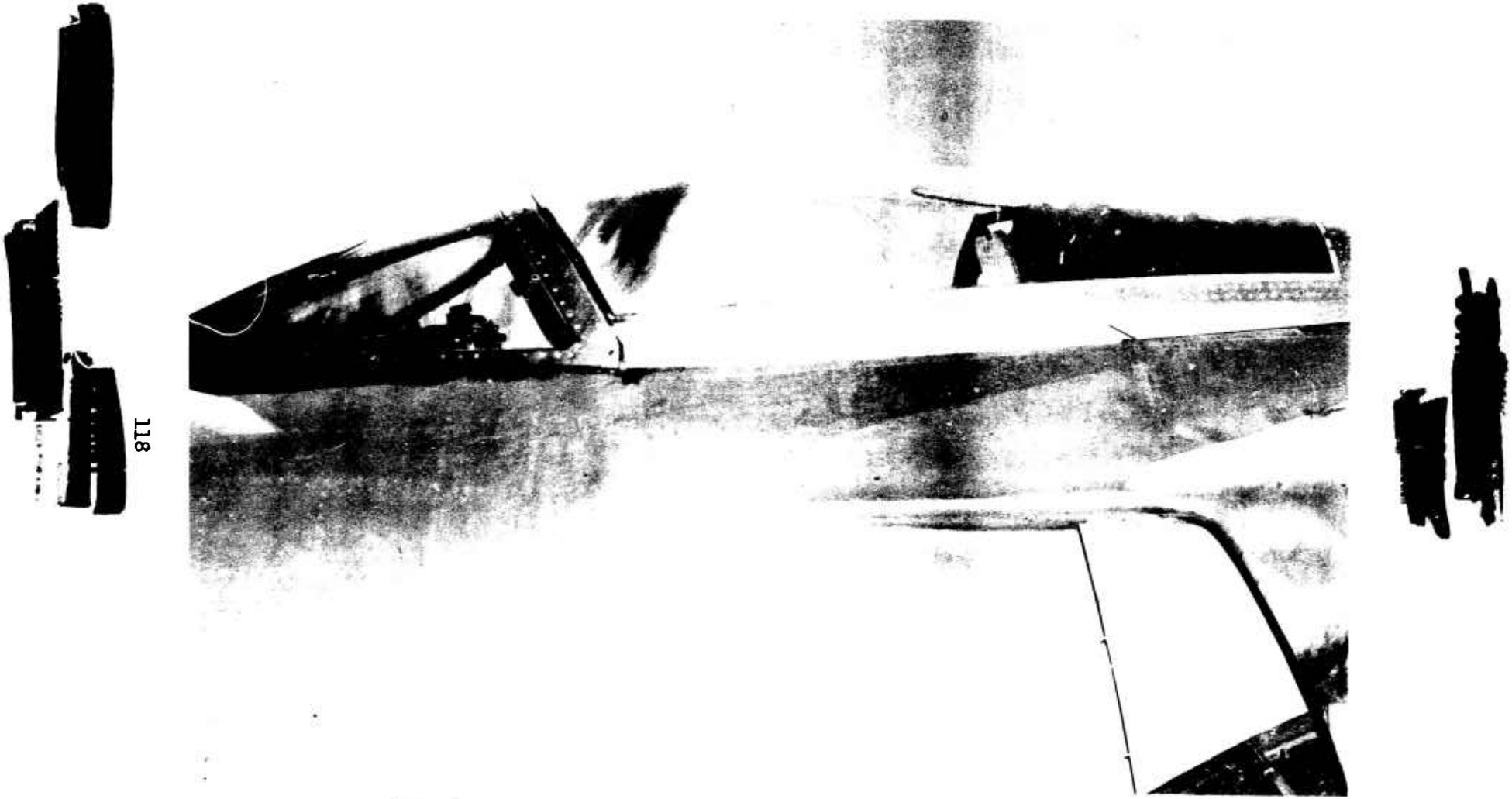

Fig. 3.33 F-90 (6688), Nose-in, Station 220 (8.4 psi), Shot 3, Close-up of Canopy, Showing Cracks. Note Smoked Canopy Caused By Thermal Effects on Organic Material in Cockpit.

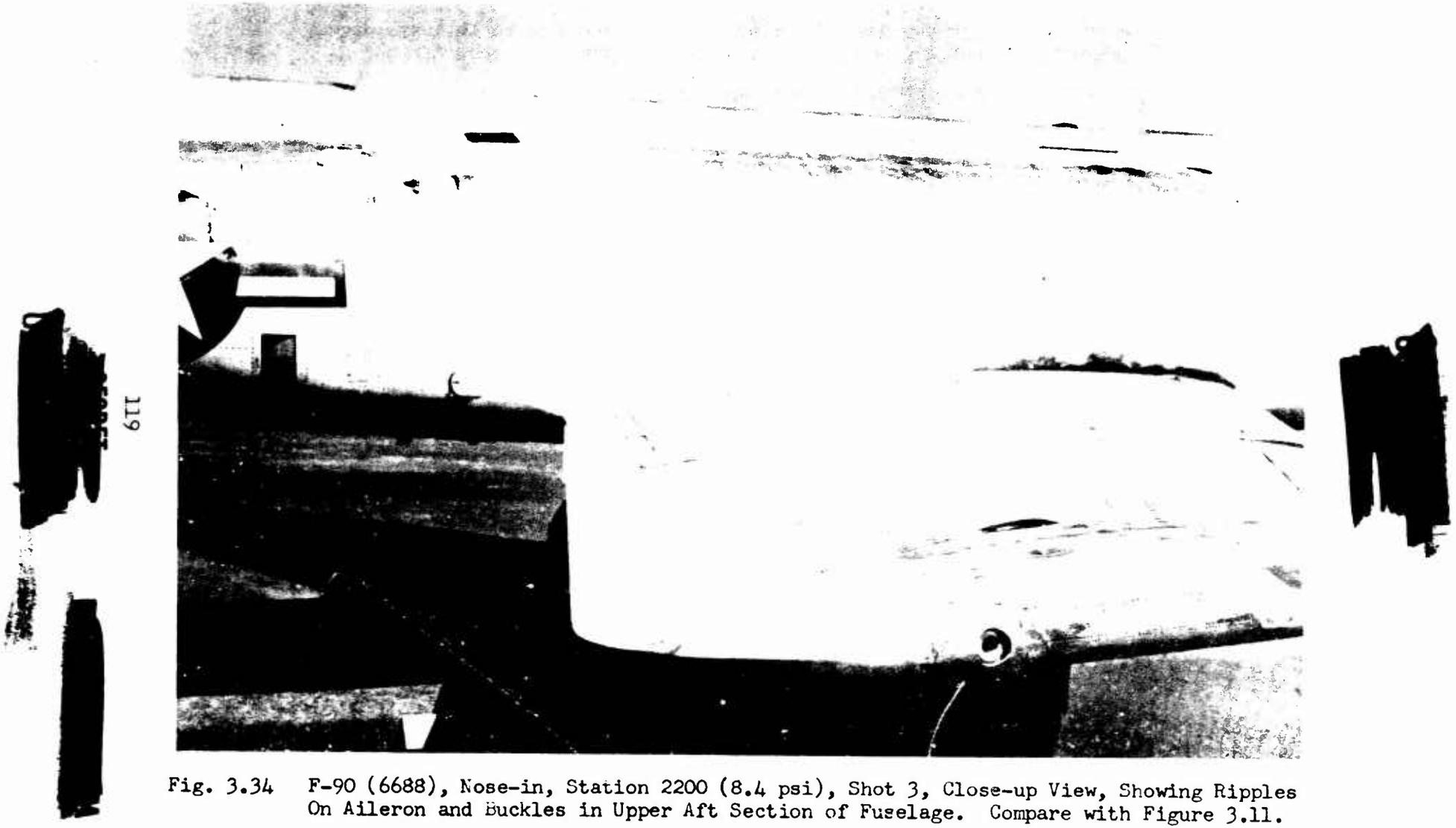

Fig. 3.34 F-90 (6688), Nose-in, Station 2200 (8.4 psi), Shot 3, Close-up View, Showing Ripples On Aileron and Buckles in Upper Aft Section of Fuselage. Compare with Figure 3.11.

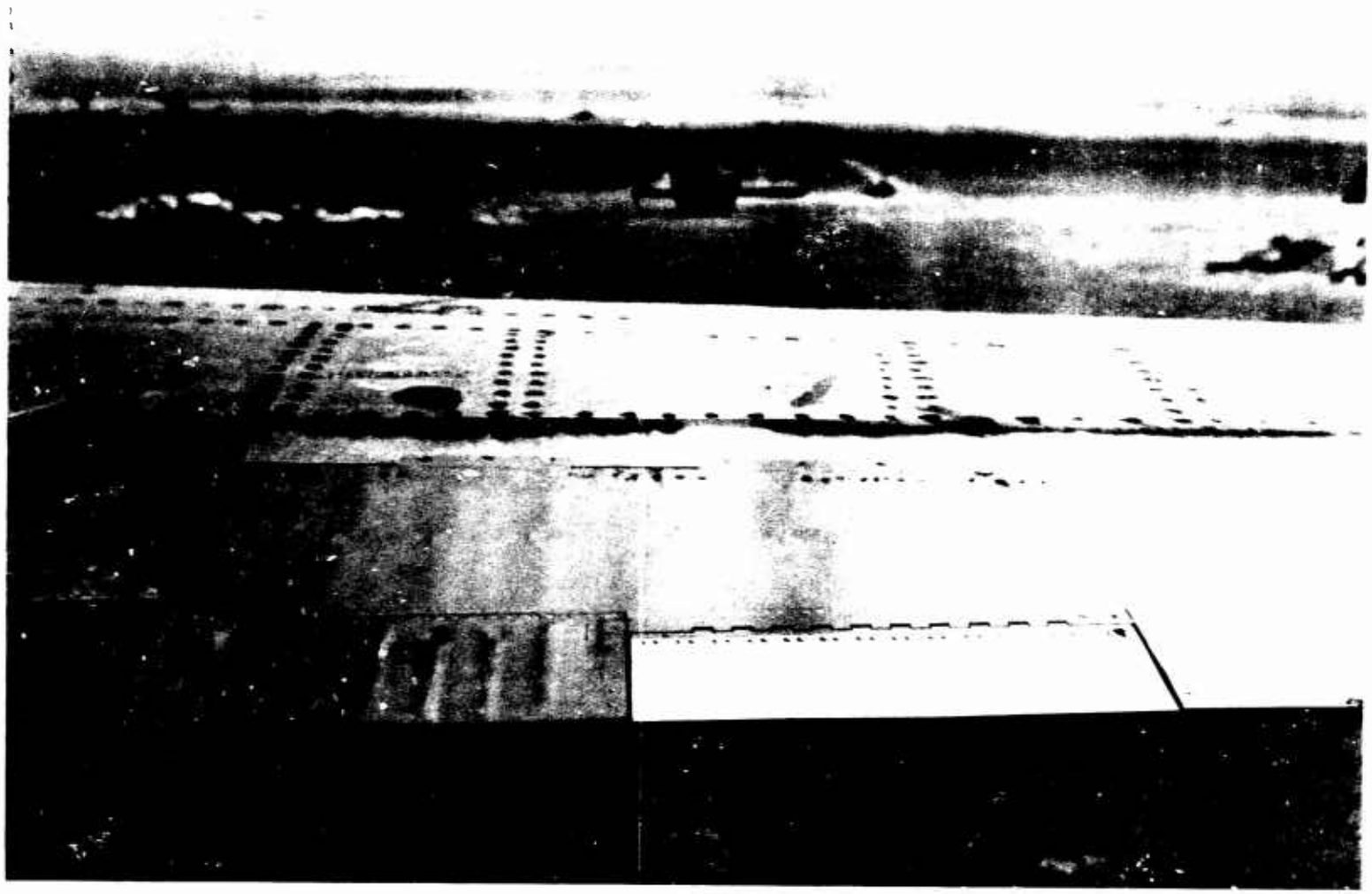

Fig. 3.35 F-90 (6688), Nose-in, Station 2200 (8.4 psi), Shot 3, Close-up View of Damage to Inboard Section of Right Aileron. Hole at Inboard End of Aileron is in Magnesium Skin.

Fig. 3.36 F-90 (6688), Nose-in, Station 2200 (8.4 psi), Shot 3, Close-up View of Damaged Stainless Steel Tail Cone. Note Results of Thermal Effects on Strain Gages on Lower Spar Cap of Left Stabilizer.

[redacted]

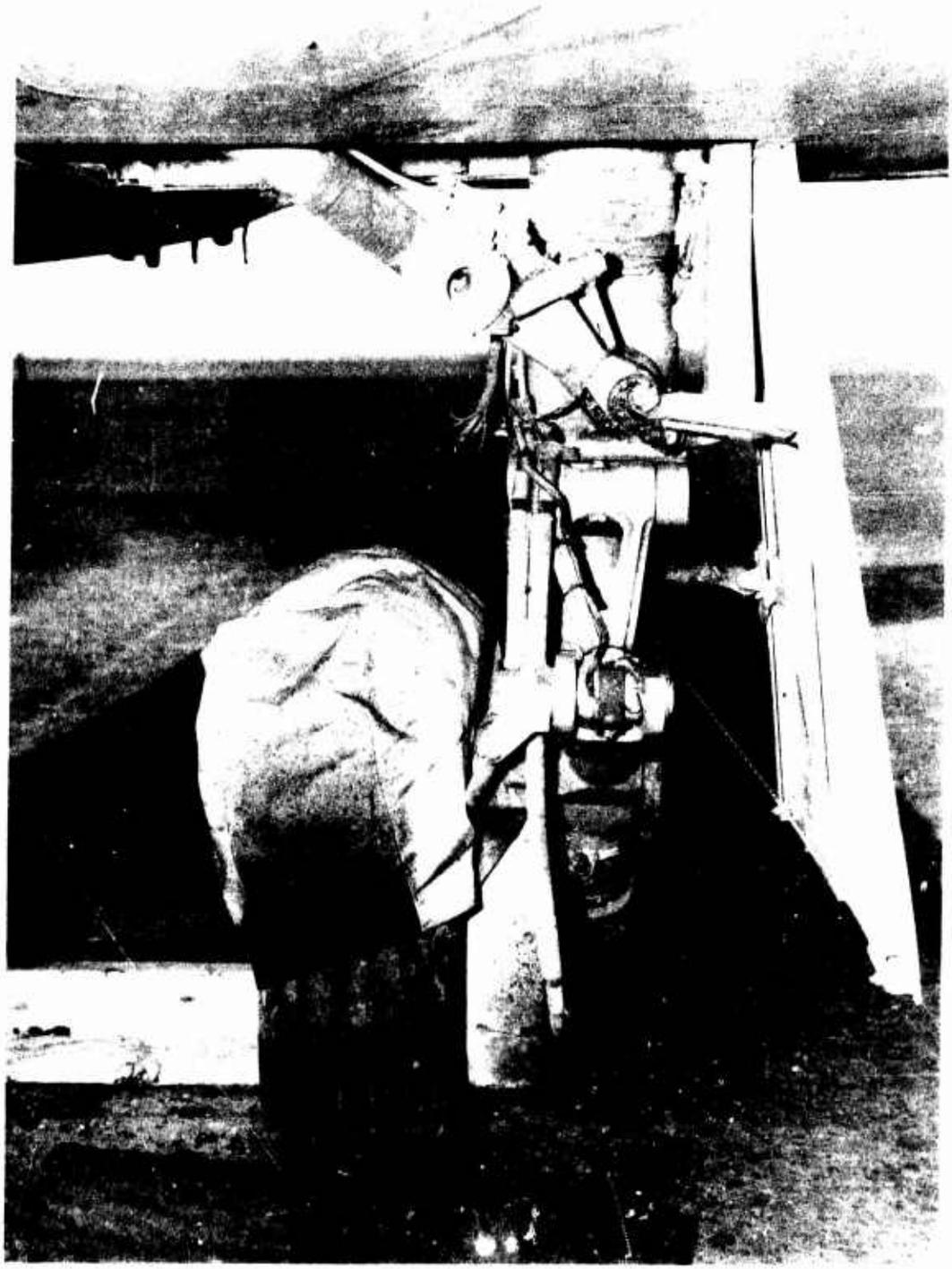

Fig. 3.37 F-90 (6688), Nose-in, Station 2200 (8.4 psi), Shot 3, Close-up View of Left Main Landing Gear. Note Thermal Effect on Tire.

[redacted]

Fig. 3.38 F-47 (9075), Side-in Station 4000 (6.4 psi), Shot 3, Showing General Scorched and Buckled Regions on Right Side of Fuselage

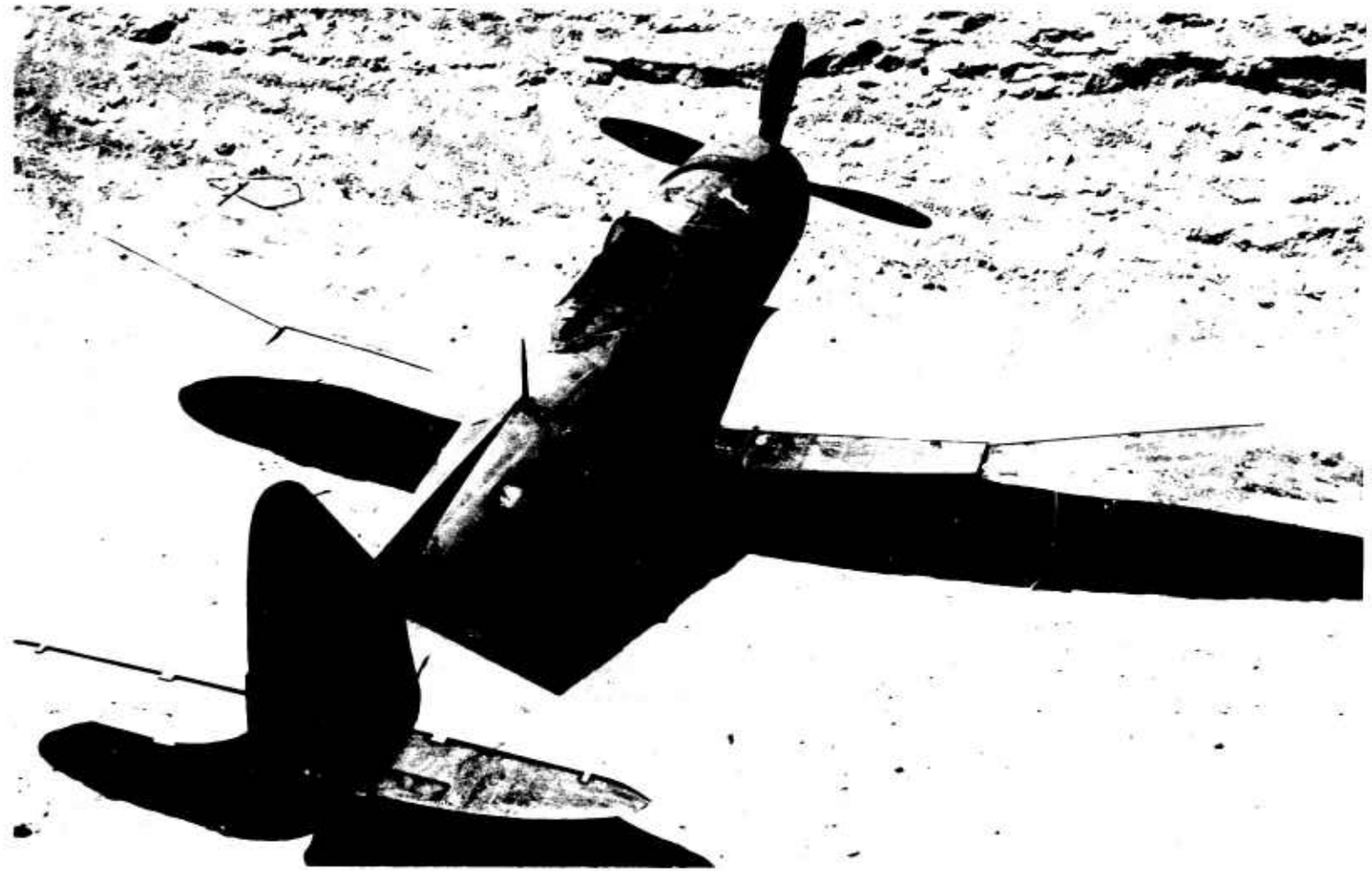

Fig. 3.39 F-47 (9110), Side-in in Pit Revetment, Station 4000 (6.4 psi), Shot 3, Showing Scorched and Buckled Right Side and Scorched Areas of Skin on Vertical Tail. Note Buckled Left Aileron and Flap.

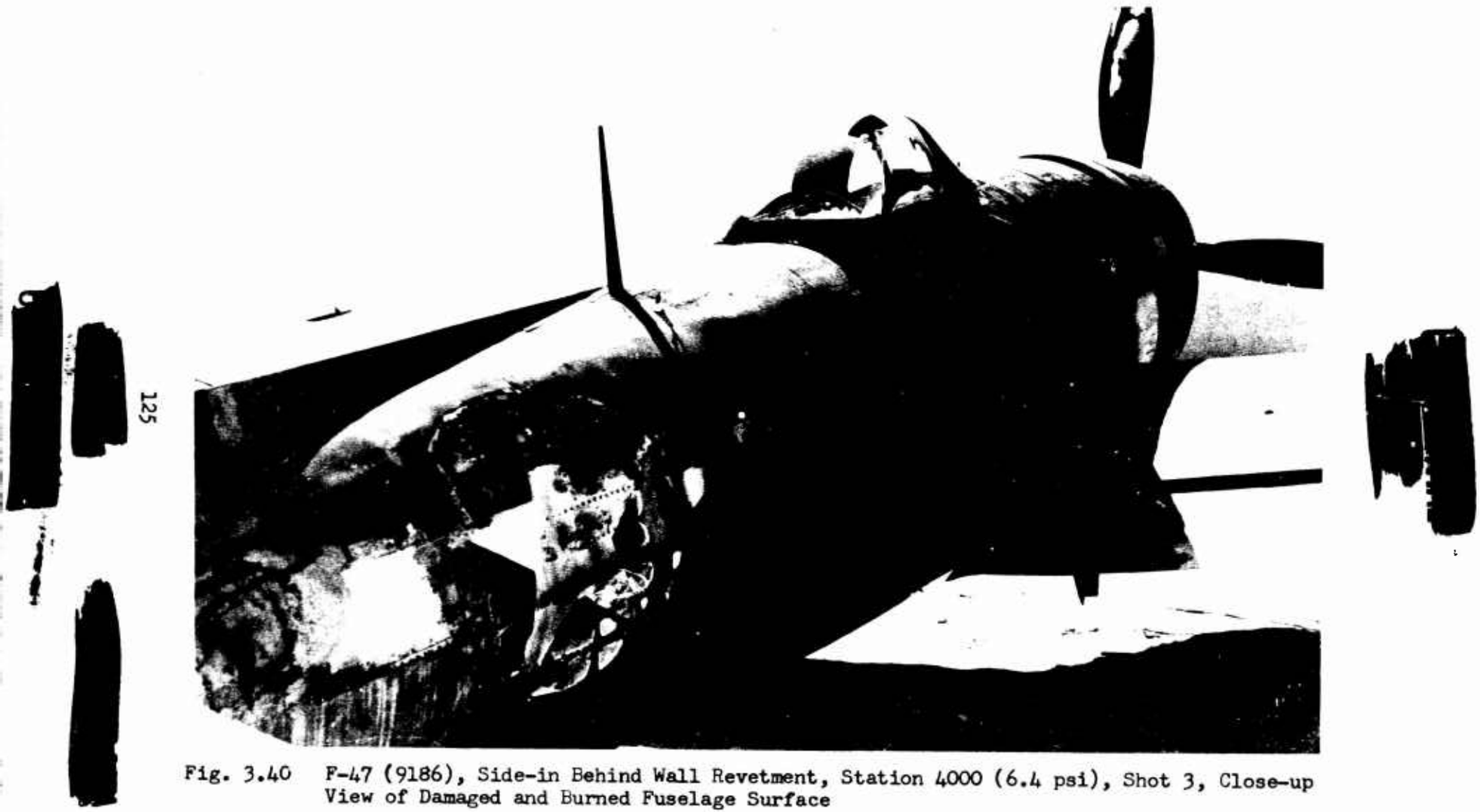

Fig. 3.40 F-47 (9186), Side-in Behind Wall Revetment, Station 4000 (6.4 psi), Shot 3, Close-up View of Damaged and Burned Fuselage Surface

Fig. 3.41 F-47 (9186), Side-in Behind Wall Revetment, Station 4000 (6.4 psi), Shot 3, Close-up View of Scorched Vertical Stabilizer and Rudder Paint

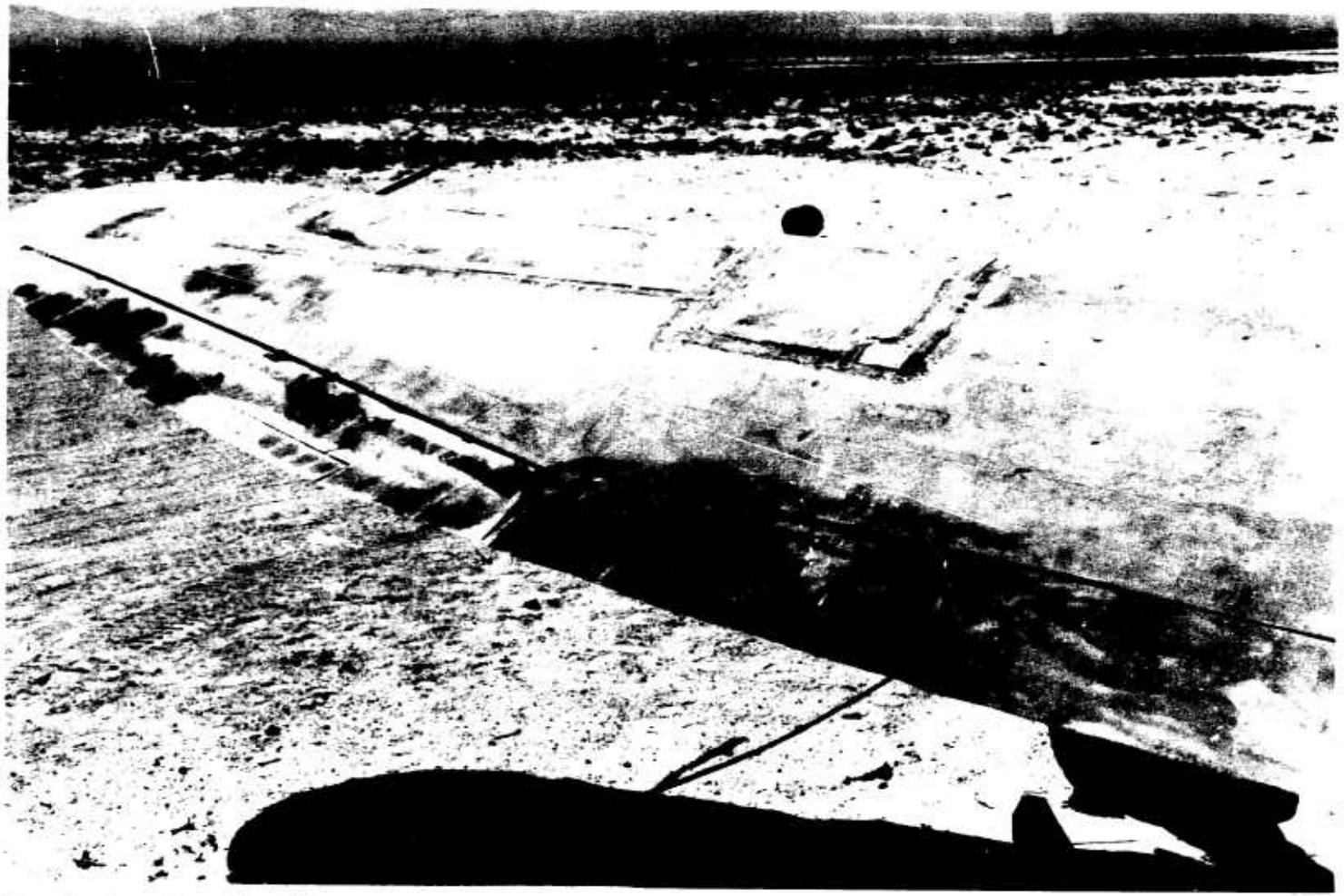

Fig. 3.42 F-47 (9186), Side-in Behind Wall Revetment, Station 4000 (6.4 psi), Shot 3, Close-up View of Outboard Section of Left Wing, Showing Buckling and Overheating Effect

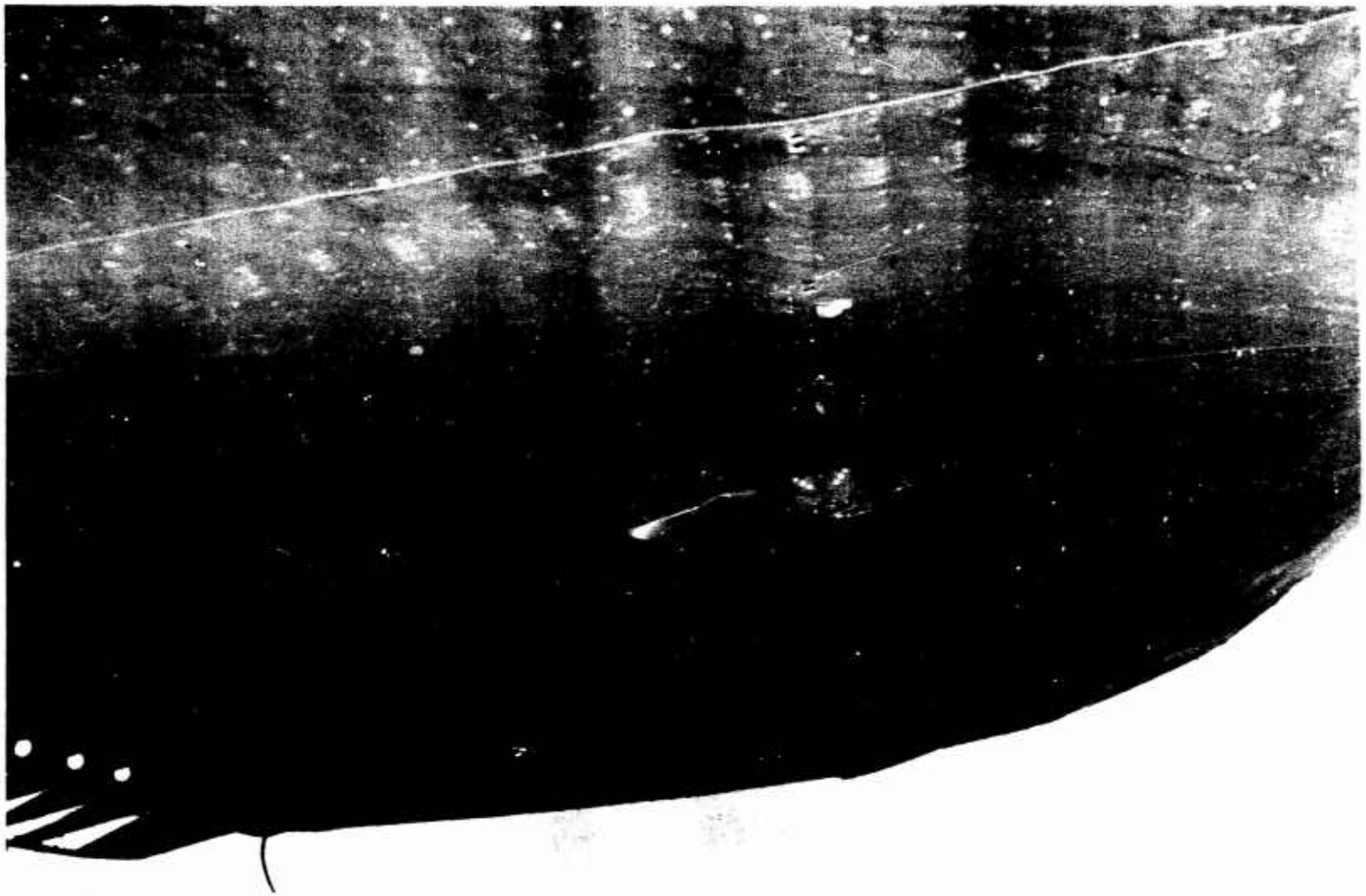

Fig. 3.43 B-17 (3699), Nose-in, Station 4500 (5.8 psi), Shot 3, Close-up of Crushed Lower Left Wing of BUSTER-JANGLE Aircraft Showing Protruding Rib

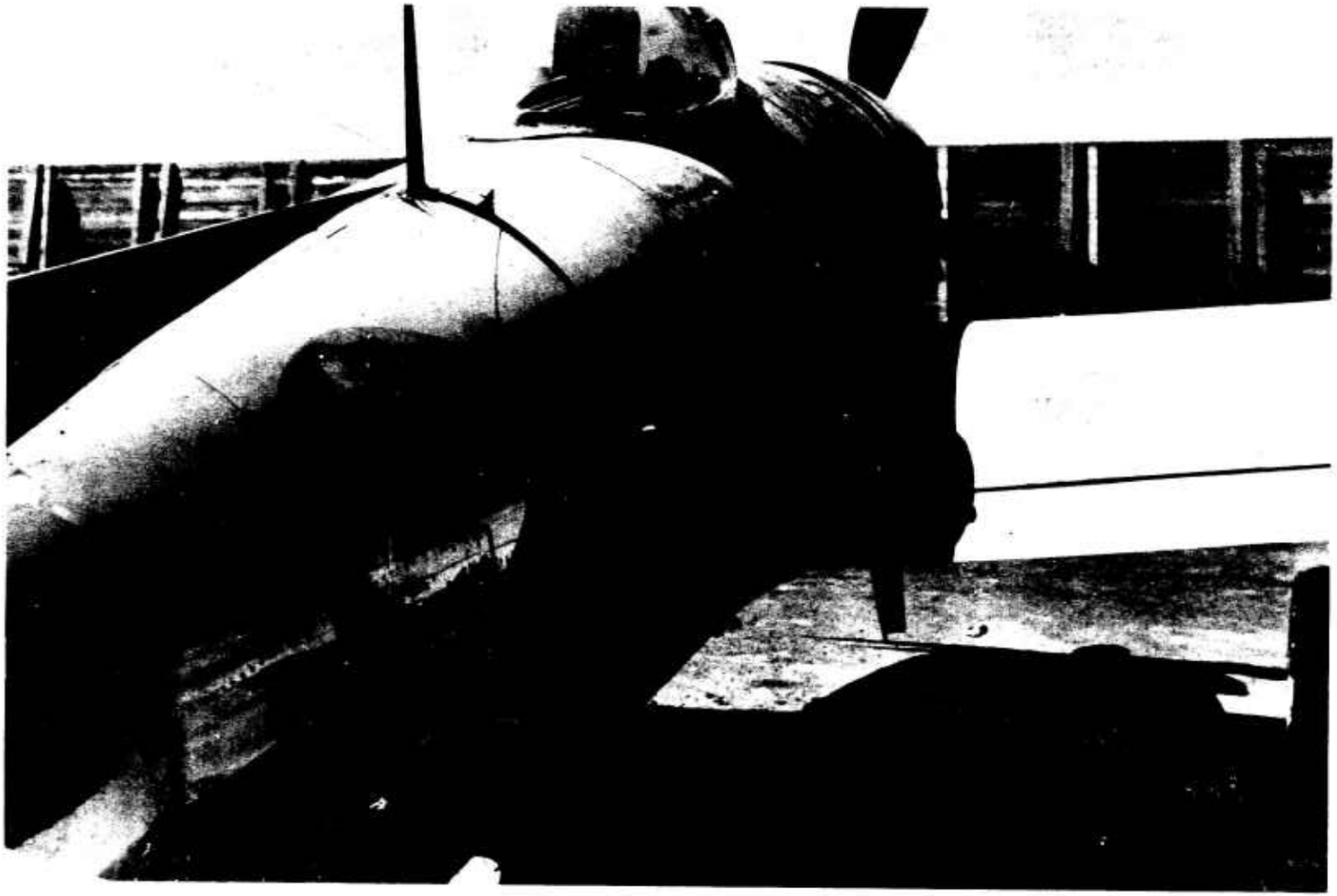

Fig. 3.44 F-47 (9074), Right Side-in in G-Type Revetment, Station 8000 (3.6 psi), Shot 3, Showing Buckling of Fuselage Skin Panels

Fig. 3.45 F-47 (9074), Right Side-in in G-Type Revetment, Station 8000 (3.6 psi), Shot 3, Close-up View of Forward Section of Fuselage and Inboard Section of Right Wing and Cracked Canopy

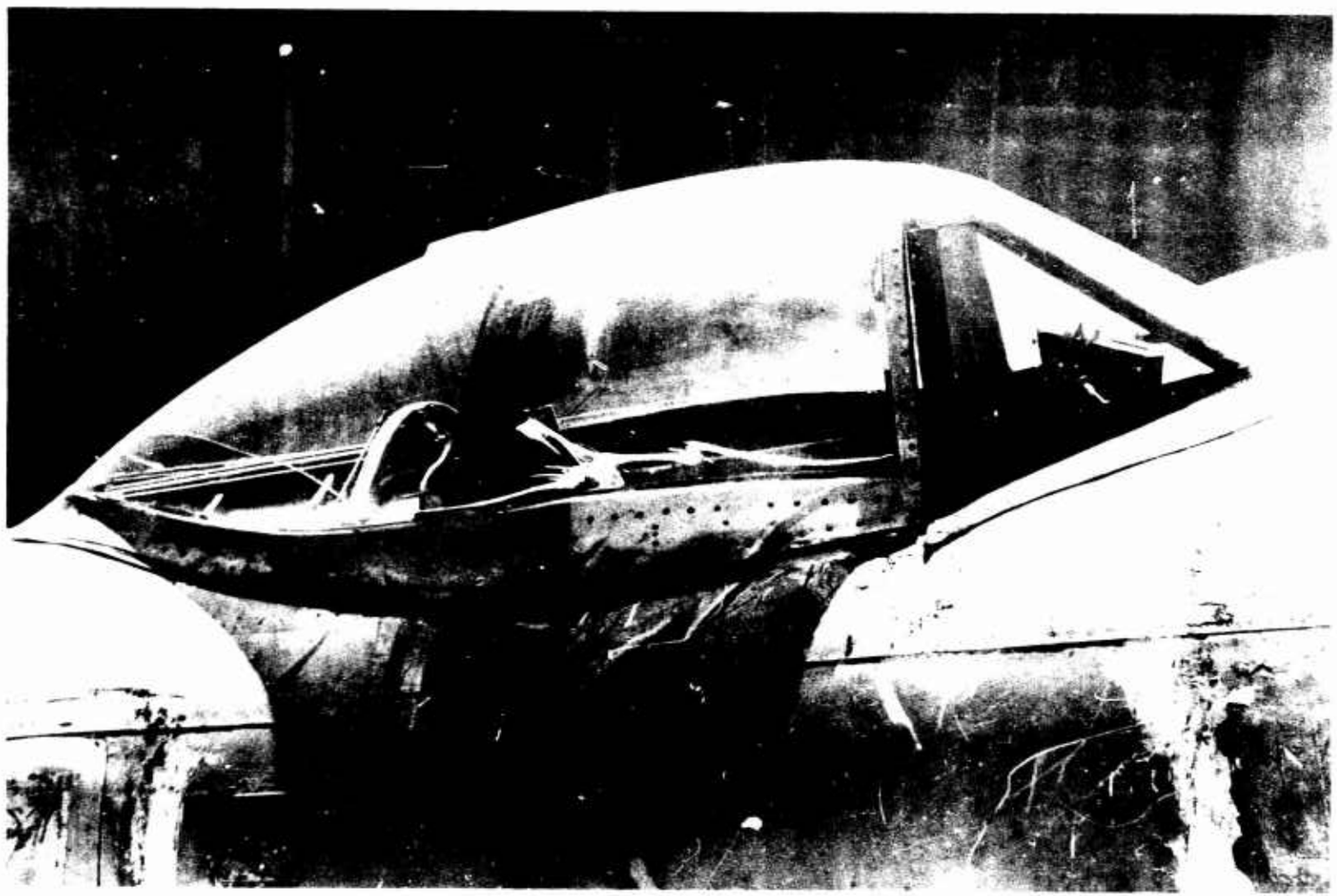

Fig. 3.46 F-47 (9074), Right Side-in in G-Type Revetment, Station 8000 (3.6 psi), Shot 3, Close-up View of Cracks in Canopy

Fig. 3.47 F-47 (9785), Left Side-in, Station 8000 (3.6 psi), Shot 3, Showing General Blast Damage to Left Side of Fuselage

Fig. 3.48 F-47 (9785), Side-in, Station 8000 (3.6 psi), Shot 3, Close-up View of Bending Failure and Buckles of Rudder

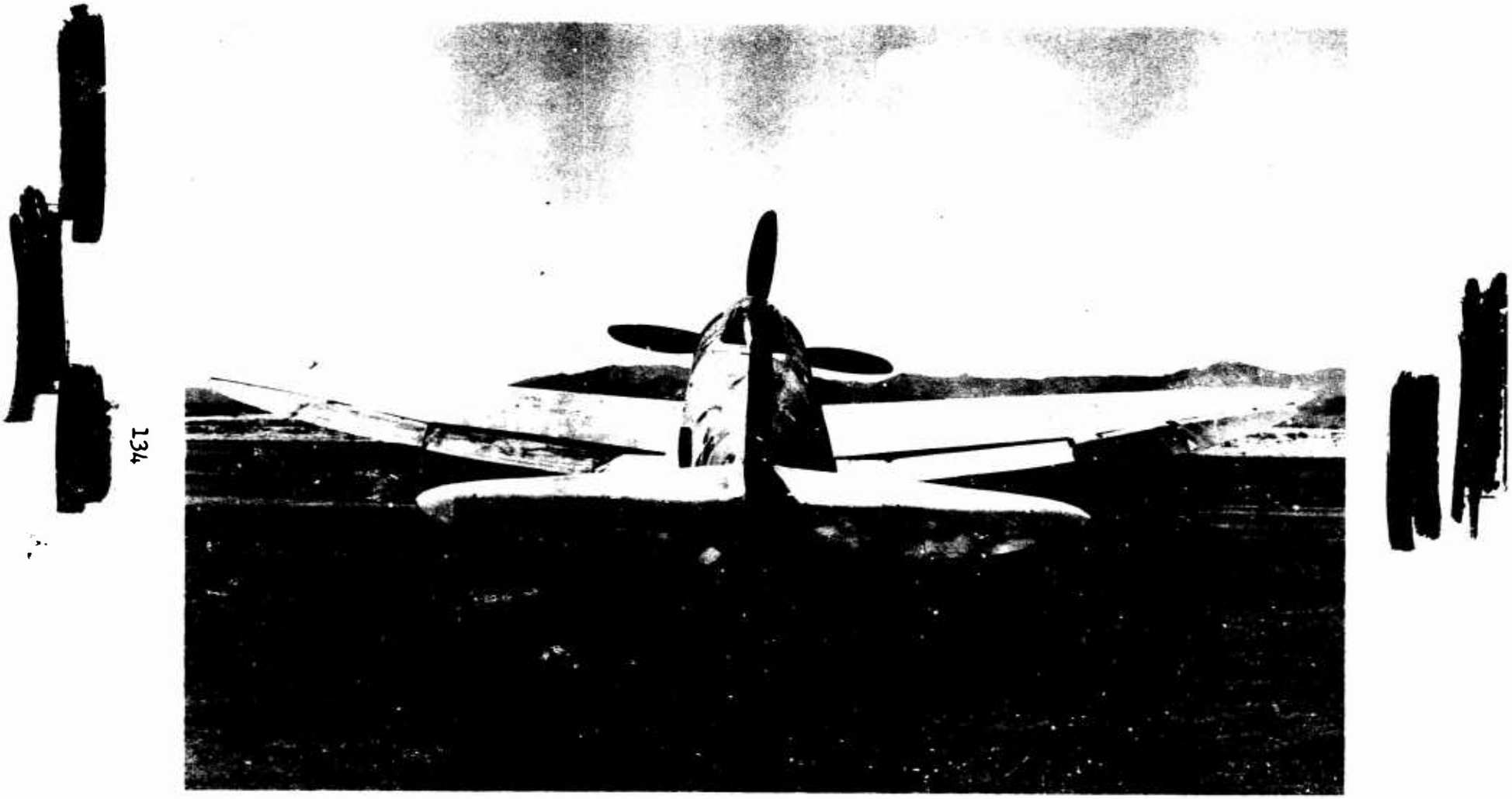

Fig. 3.49 F-47 (9072), Tail-in, Station 8000 (3.6 psi), Shot 3, Showing Bending Failures and Buckles of Ailerons and Flaps. Note Slightly Scorched Elevators.

Fig. 3.50 F-47 (9072), Tail-in, Station 8000 (3.6 psi), Shot 3, Close-up View of Damaged Right Flap and Aileron

Fig. 3.51 F-47 (9072), Tail-in, Station 8000 (3.6 psi), Shot 3, Showing Buckled Area on Left Aft Section of Fuselage

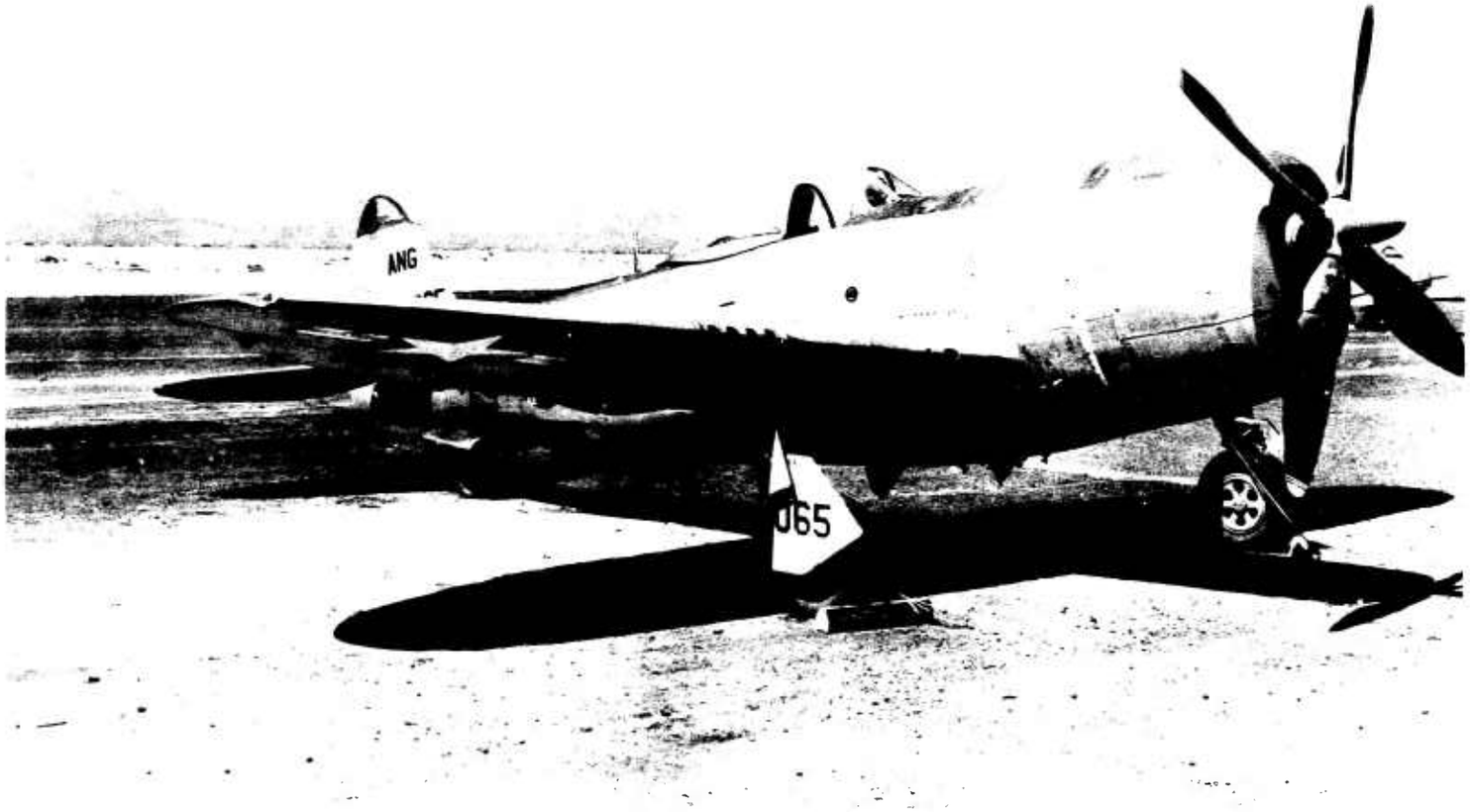

Fig. 3.52 F-47 (0065), Nose-in, Station 8000 (3.6 psi), Shot 3, Showing General Post-shot Condition. Compare with Figure 3.44.

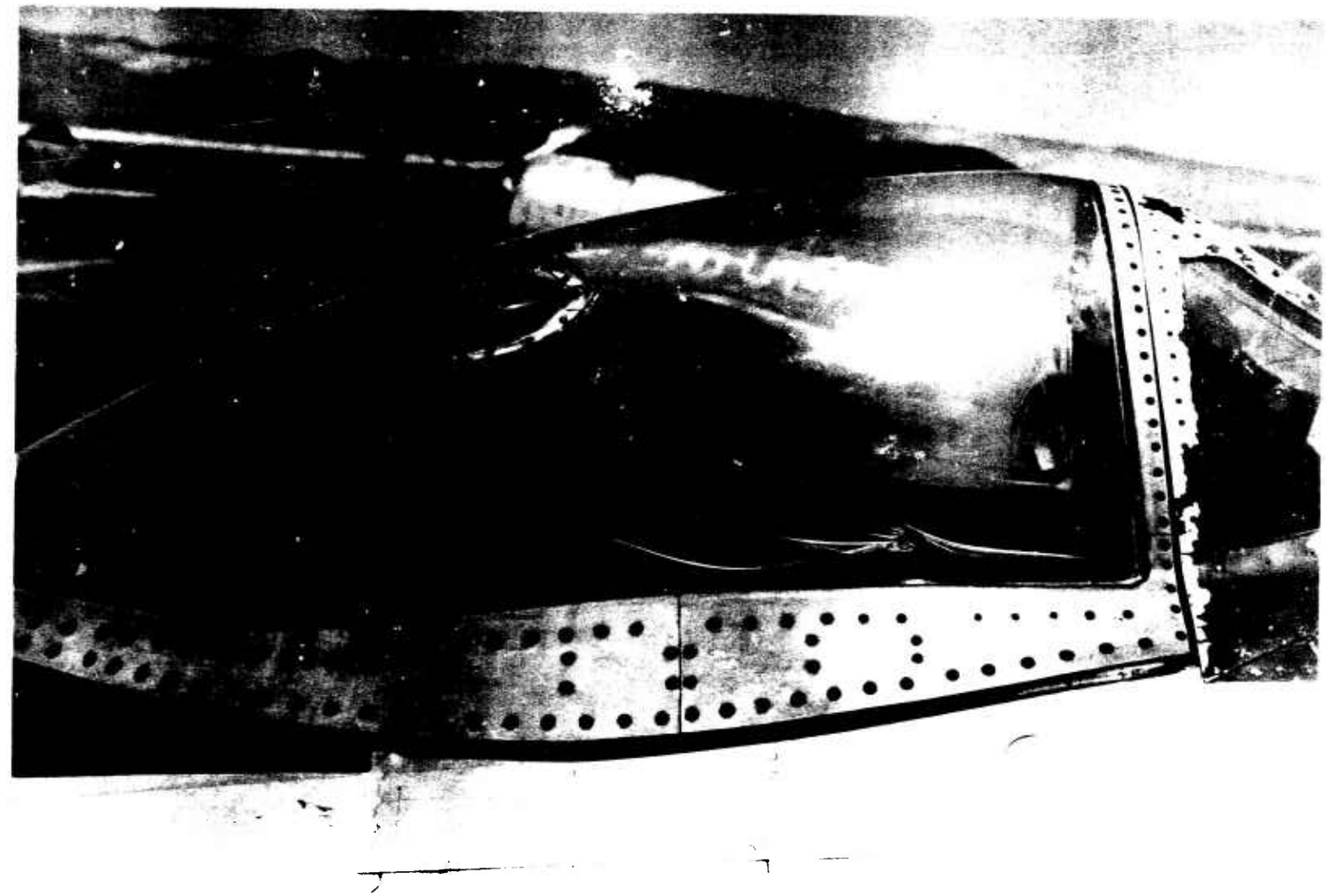

Fig. 3.53 F-47 (0065), Nose-in, Station 8000 (3.6 psi), Shot 3, Close-up View of Cracked Canopy

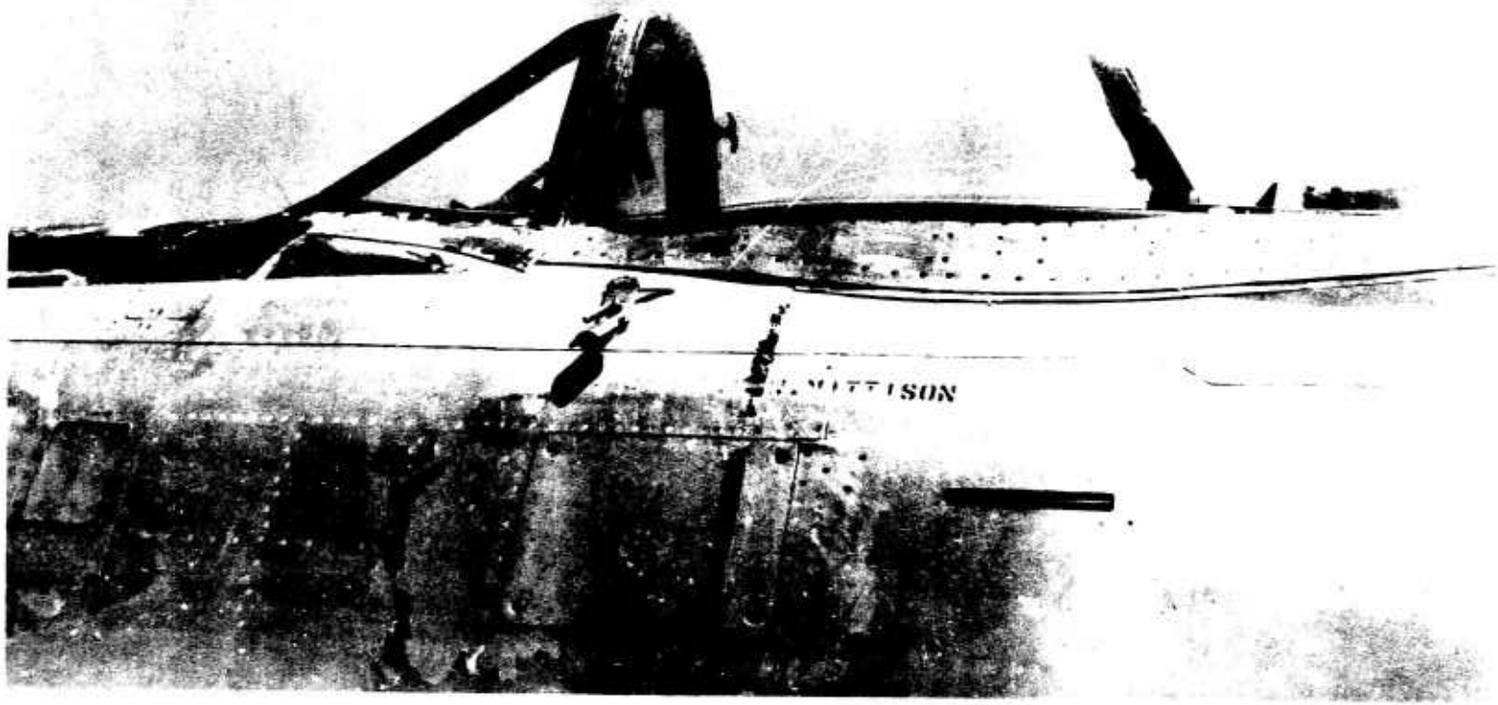

Fig. 3.54 F-47 (9719), Nose-in in G-Type Revetment, Station 8000 (3.6 psi), Shot 3, Close-up View of Cracked Canopy

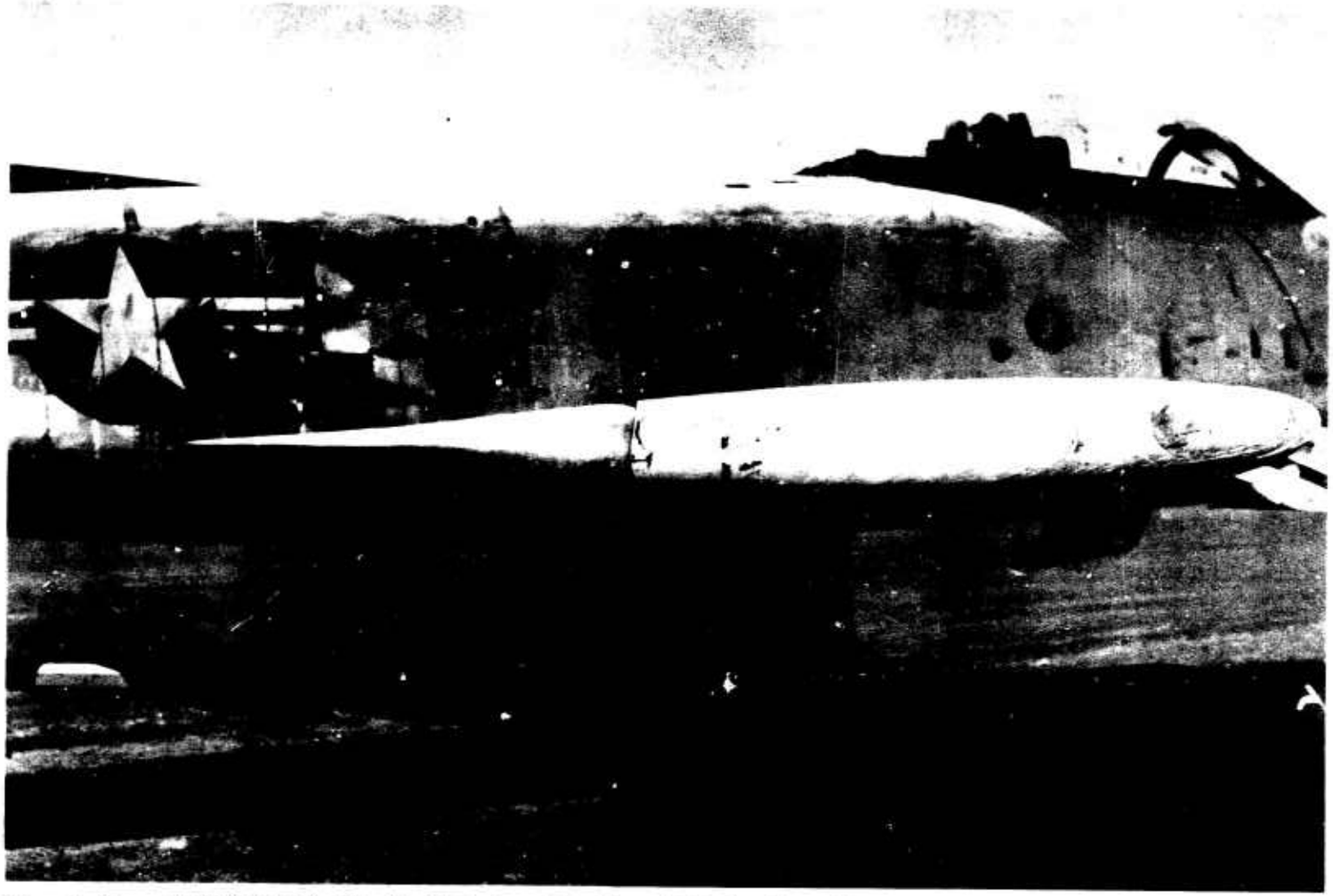

Fig. 3.55 F-86 (8209), Right Side-in, Station 8000 (3.6 psi), Shot 3, Showing Damage to Aft Fuselage Section

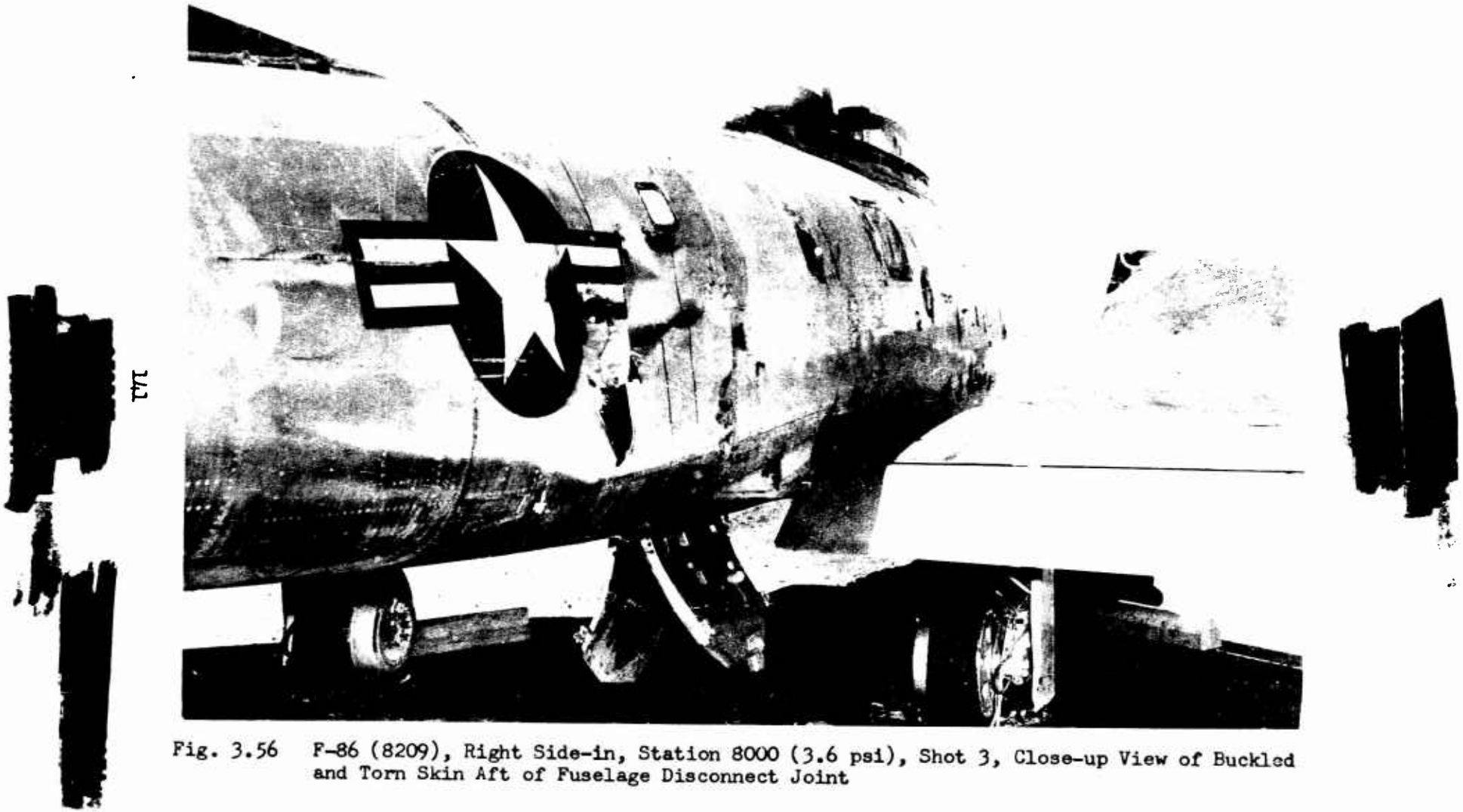

Fig. 3.56 F-86 (8209), Right Side-in, Station 8000 (3.6 psi), Shot 3, Close-up View of Buckled and Torn Skin Aft of Fuselage Disconnect Joint

Fig. 3.57 F-86 (8209), Right Side-in, Station 8000 (3.6 psi), Shot 3, Access Doors with Messerschmidt Fasteners Popped Open Due to Blast. Note Permanent Skin Buckles Produced by Torsional Loading on Vertical Tail.

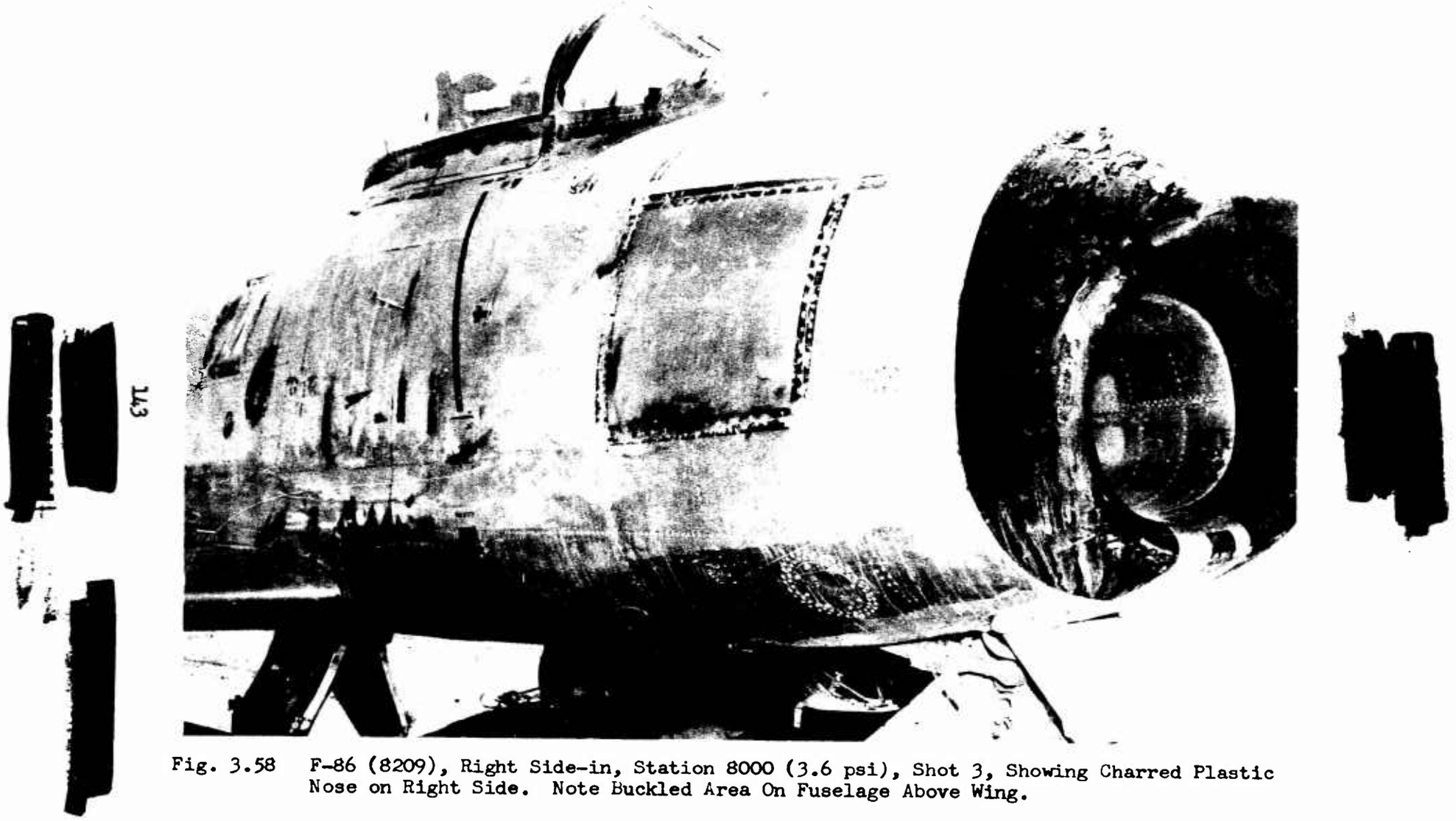

Fig. 3.58 F-86 (8209), Right Side-in, Station 8000 (3.6 psi), Shot 3, Showing Charred Plastic Nose on Right Side. Note Buckled Area On Fuselage Above Wing.

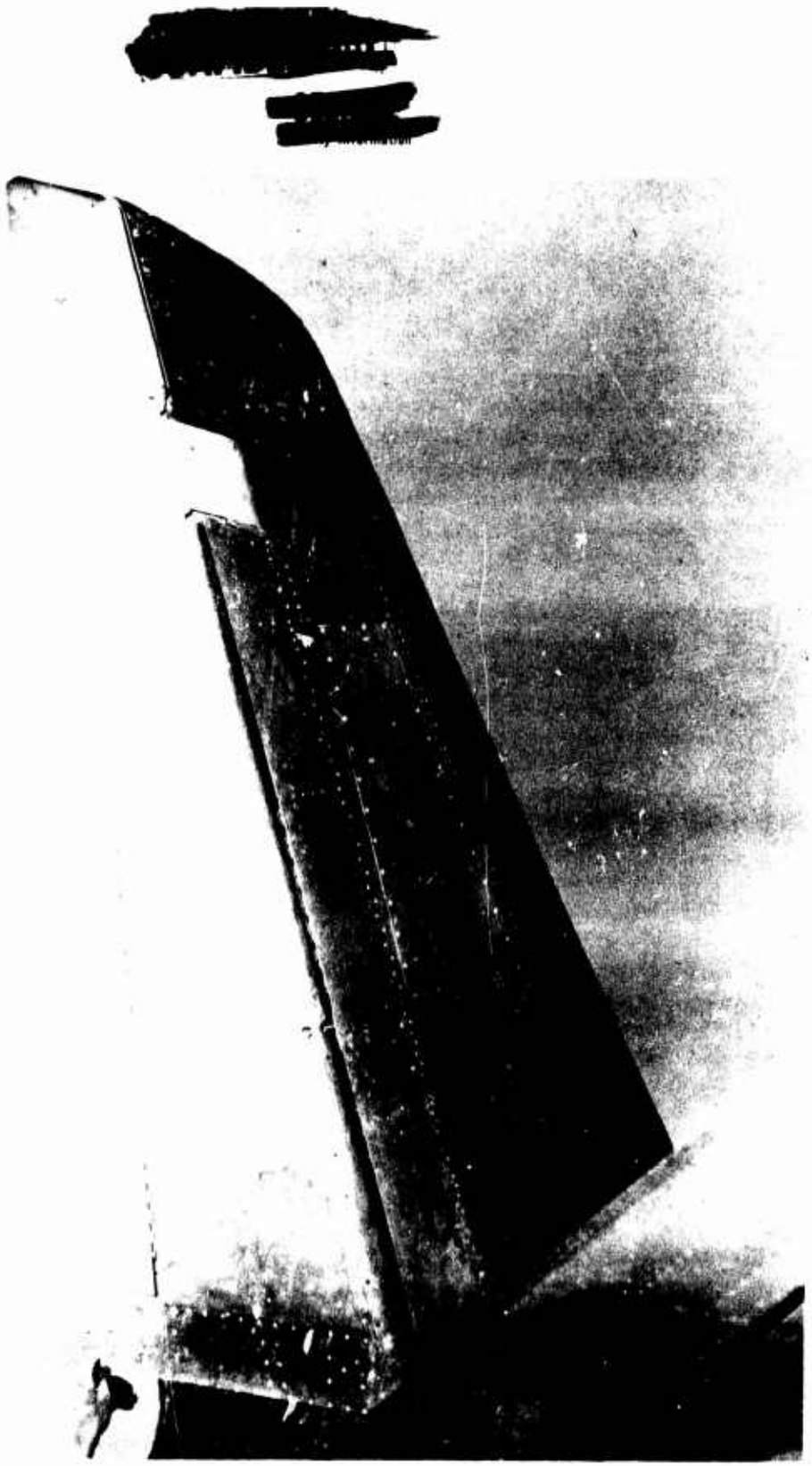

Fig. 3.59 F-86 (8209), Right Side-in, Station 8000 (3.6 psi), Shot 3, Close-up View of Charred Antenna Housing and Wrinkled Skin on Rudder

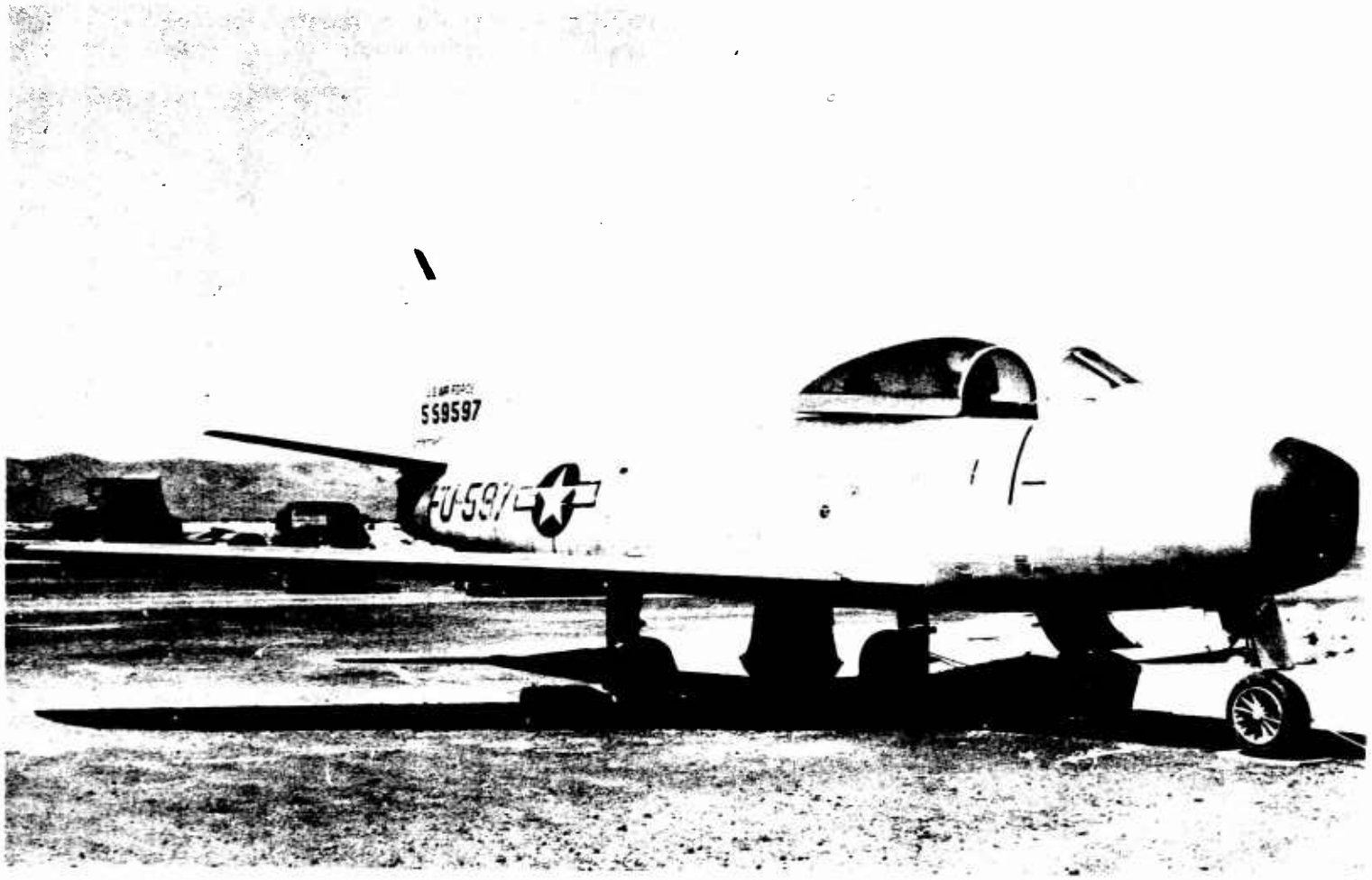

Fig. 3.60 F-86 (9597), Nose-in, Station 8000 (3.6 psi), Shot 3, Showing General Post-shot Condition of Aircraft. There Would be 283 Man-hours Repair Required to Return This Aircraft to Flight Condition.

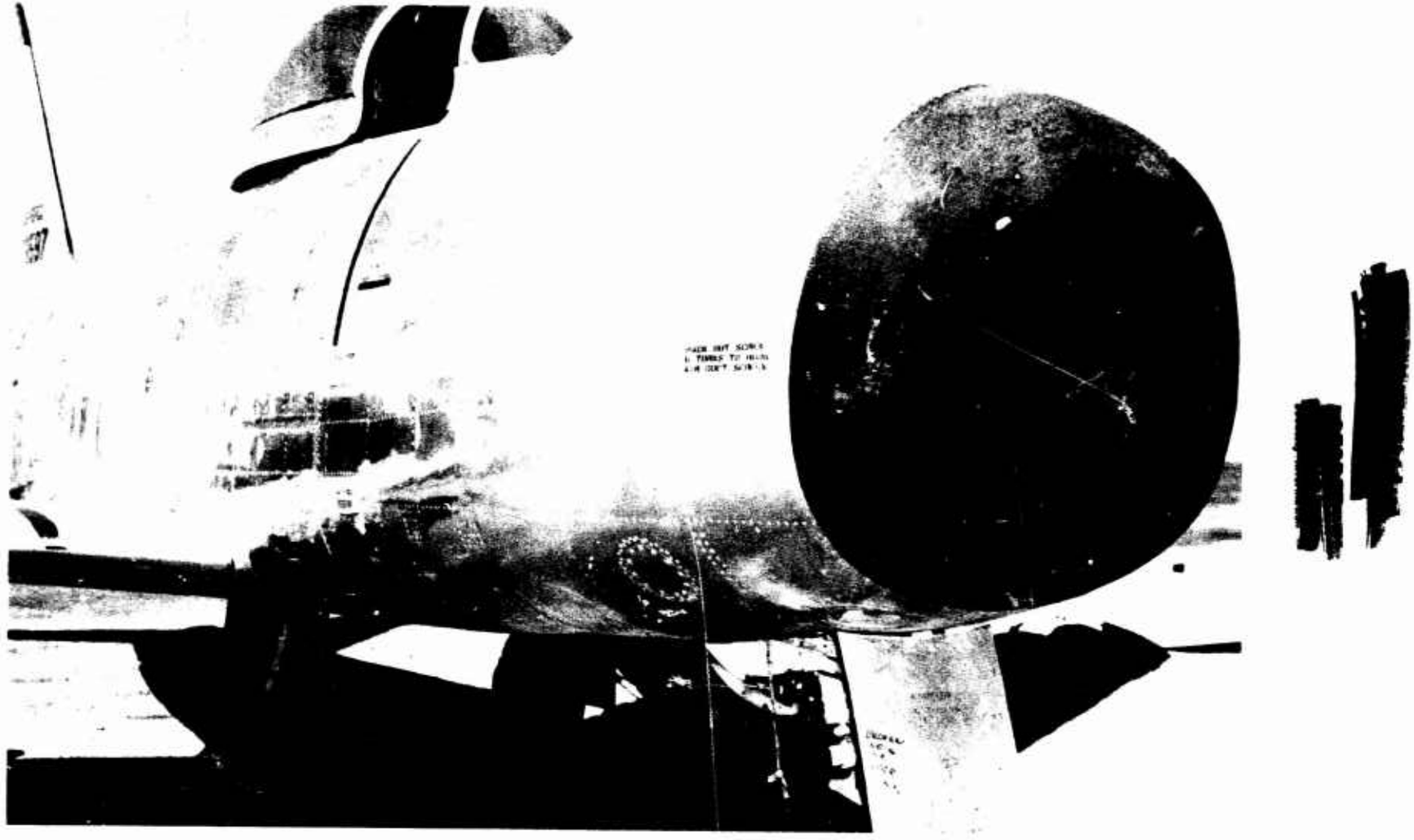

Fig. 3.61 F-86 (9597), Nose-in, Station 8000 (3.6 psi), Shot 3, Close-up View of Scorched Rubber Coating on Nose, Slight Buckles in Area Below Cockpit, and Smoked Canopy

Fig. 3.62 B-17 (3722), Left Side-in, Station 8000 (3.6 psi), Shot 3, Showing Fuselage Failure Aft of Wing Trailing Edge, Generally Buckled Fuselage Skin, and Severely Buckled Vertical Stabilizer and Dorsal Fin

Fig. 3.63 B-17 (3722), Left Side-in, Station 8000 (3.6 psi), Shot 3, Showing Failure of Fuselage Aft of Wing Trailing Edge, and the Burned Rudder, Right Aileron and Left Elevator

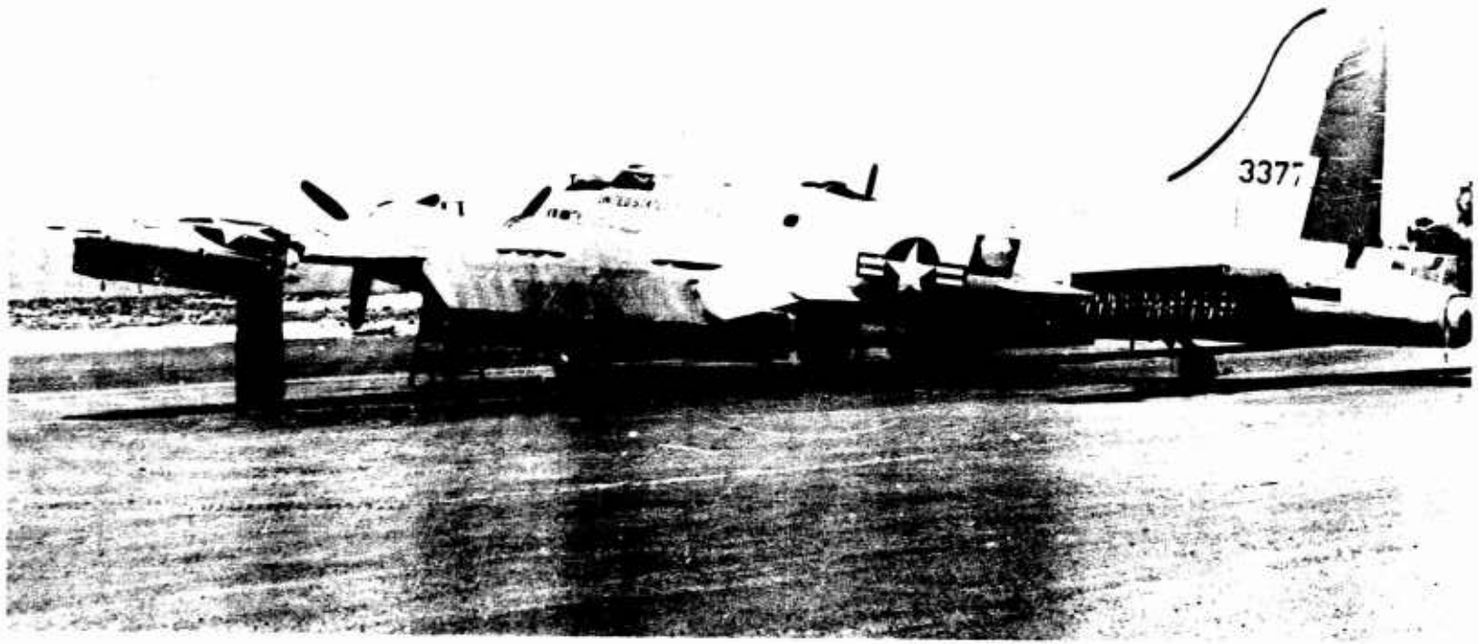

Fig. 3.64 B-17 (7746), Tail-in, Station 8000 (3.6 psi), Shot 3, Showing Total Damage to Wing Structure Aft of Rear Spars, Crushed Fuselage and Dorsal Fin, and Burned Elevator and Upper Surface of Aileron

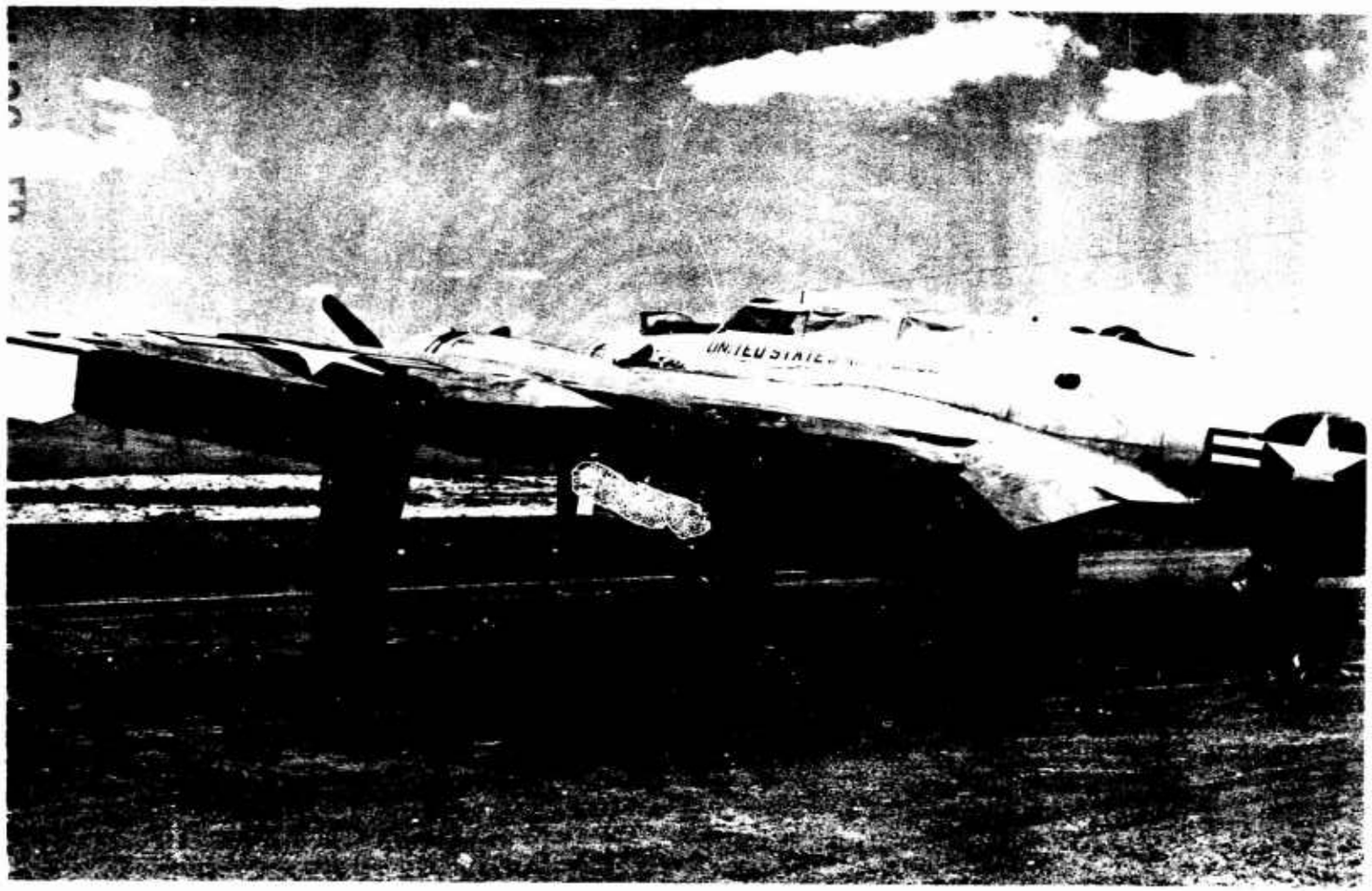

Fig. 3.65 B-17 (7746), Tail-in, Station 8000 (3.6 psi), Shot 3, Showing Wing Damage and Distortion of Fuselage Skin. Note Wing Structure Aft of Rear Spars Totally Damaged and Ailerons Burned and Bent.

Fig. 3.66 B-17 (5715), Nose-in, Station 8000 (3.6 psi), Shot 3, Close-up View of Nose and Forward Section, Showing Damage to Radar Housing and Fuselage Forward of Wing Leading Edge

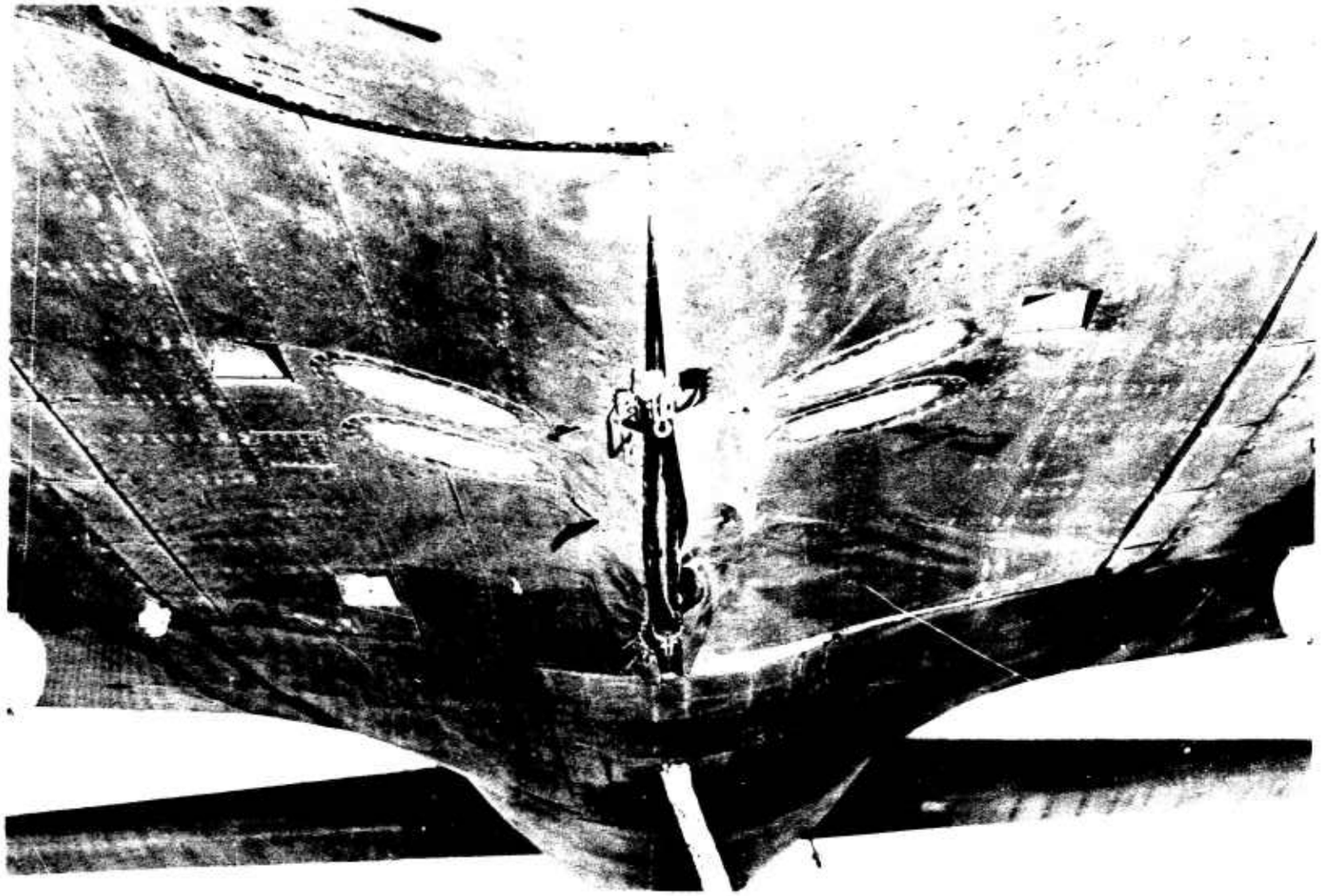

Fig. 3.67 B-17 (5715), Nose-in, Station 8000 (3.6 psi), Shot 3, Showing Buckled Bomb-bay Doors

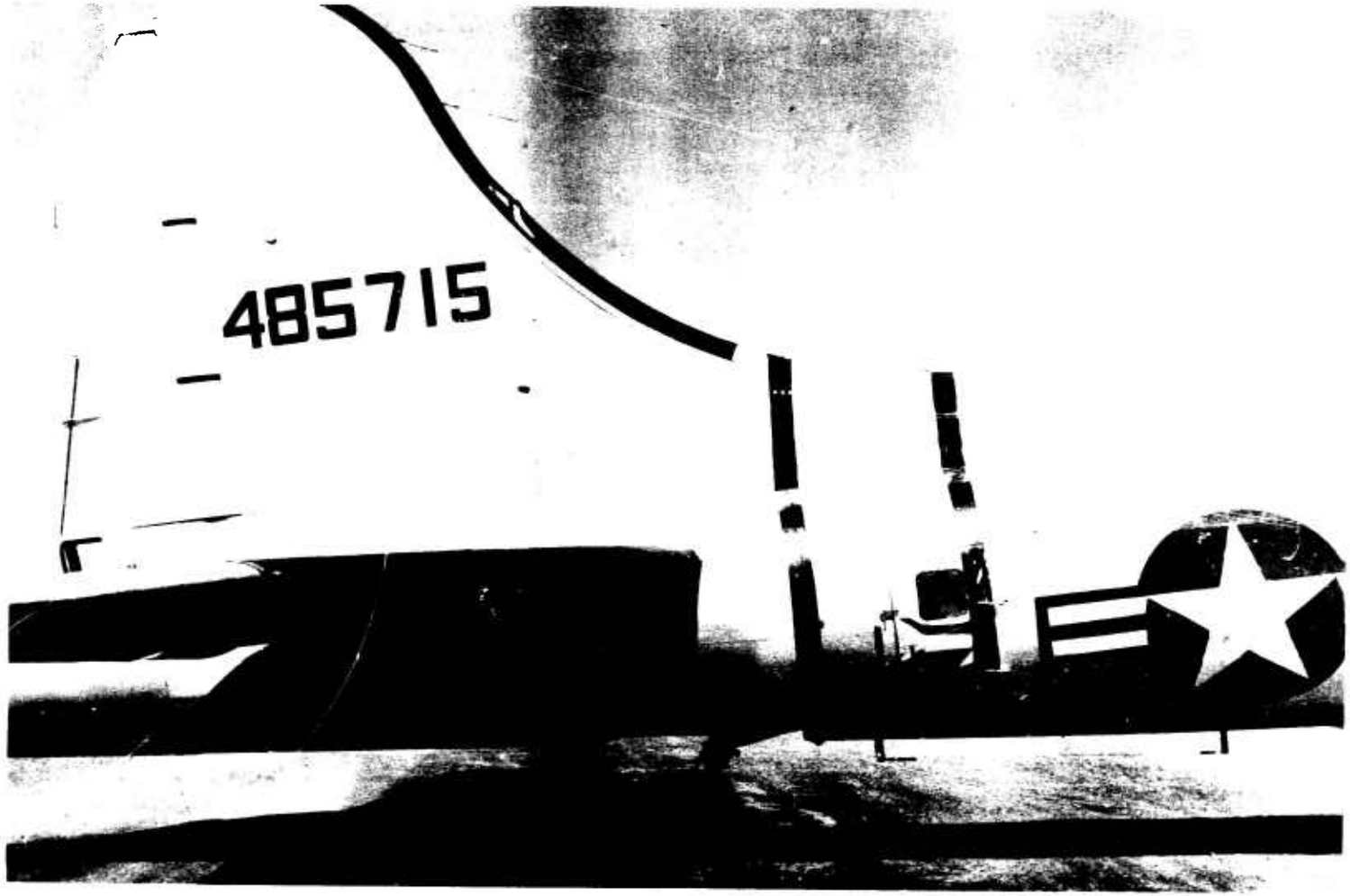

Fig. 3.68 B-17 (5715), Nose-in, Station 8000 (3.6 psi), Shot 3, Showing Pressure Damage to Vertical Stabilizer Surface and Dorsal Fin

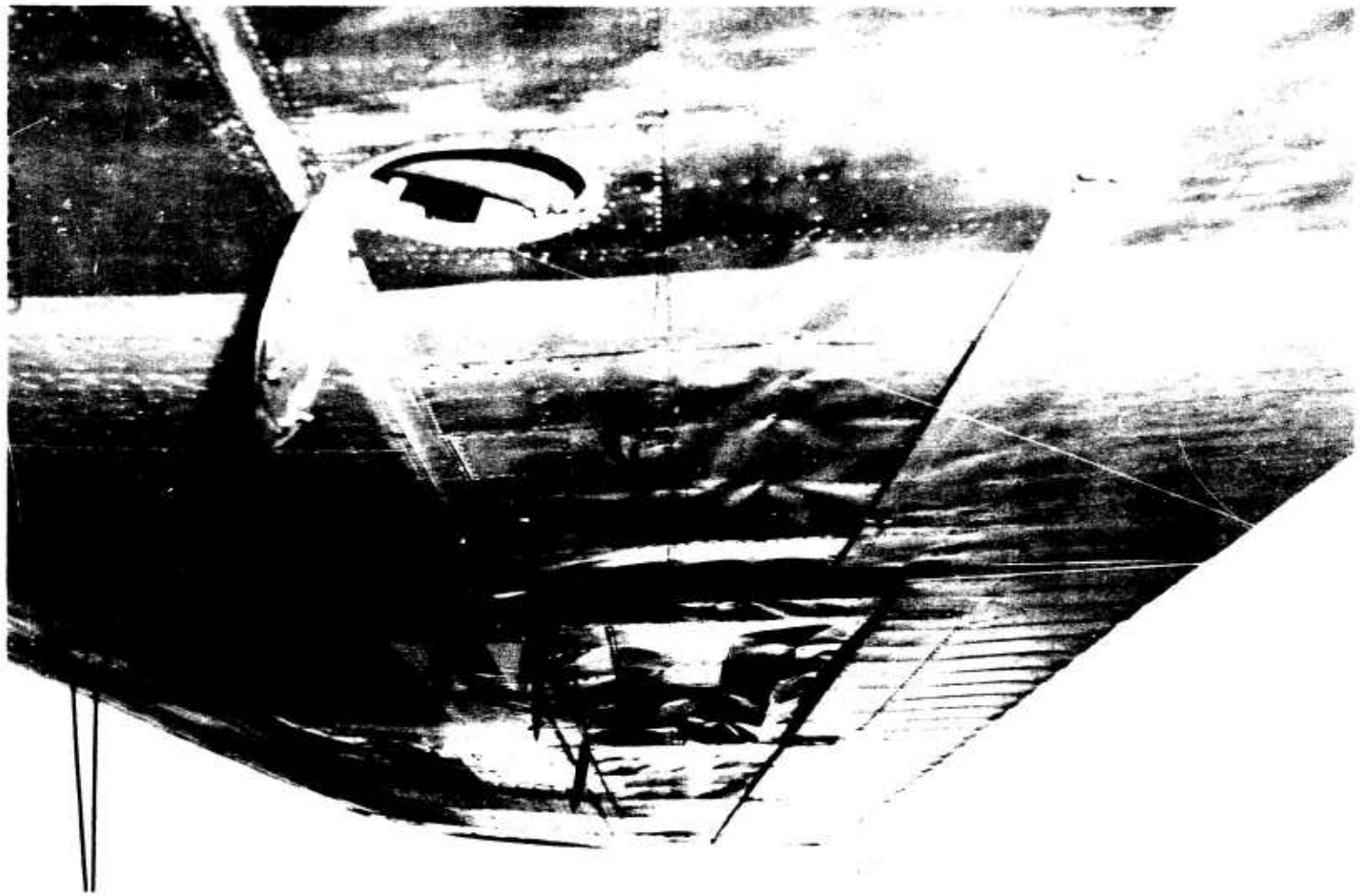

Fig. 3.69 B-17 (5715), Nose-in, Station 8000 (3.6 psi), Shot 3, Showing Buckled Under Surface of Right Wing Outboard Section

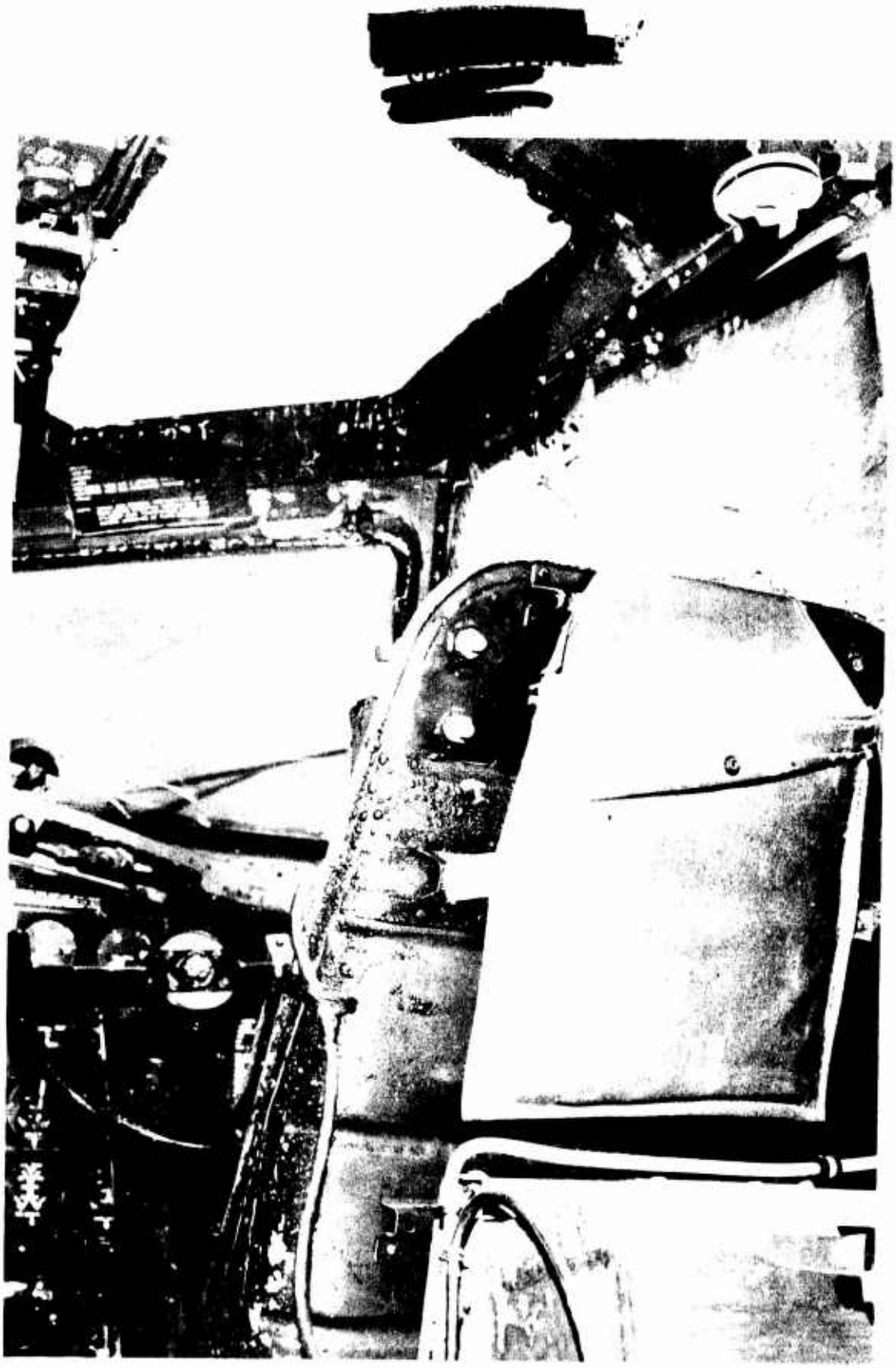

Fig. 3.70 B-17 (5715), Nose-in, Station 8000 (3.6 psi), Shot 3, Showing Thermal and Blast Damage to Cockpit

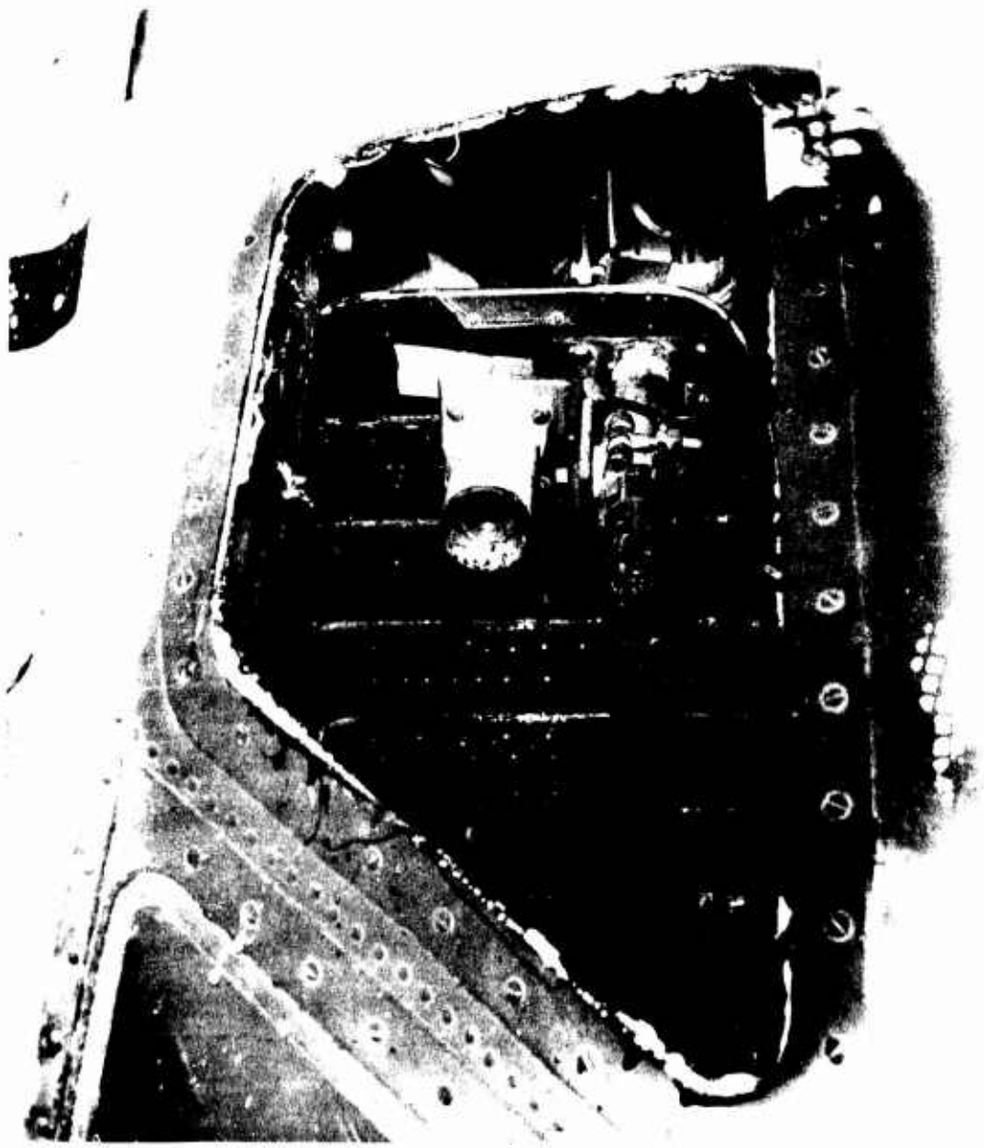

Fig. 3.71 B-17 (5715), Nose-in, Station 8000 (3.6 psi), Shot 3, External View of Top of Cabin Showing Charred Interior. Note Molten Plexiglas on Co-pilot's Seat Back and Calorimeter Fastened Thereto.

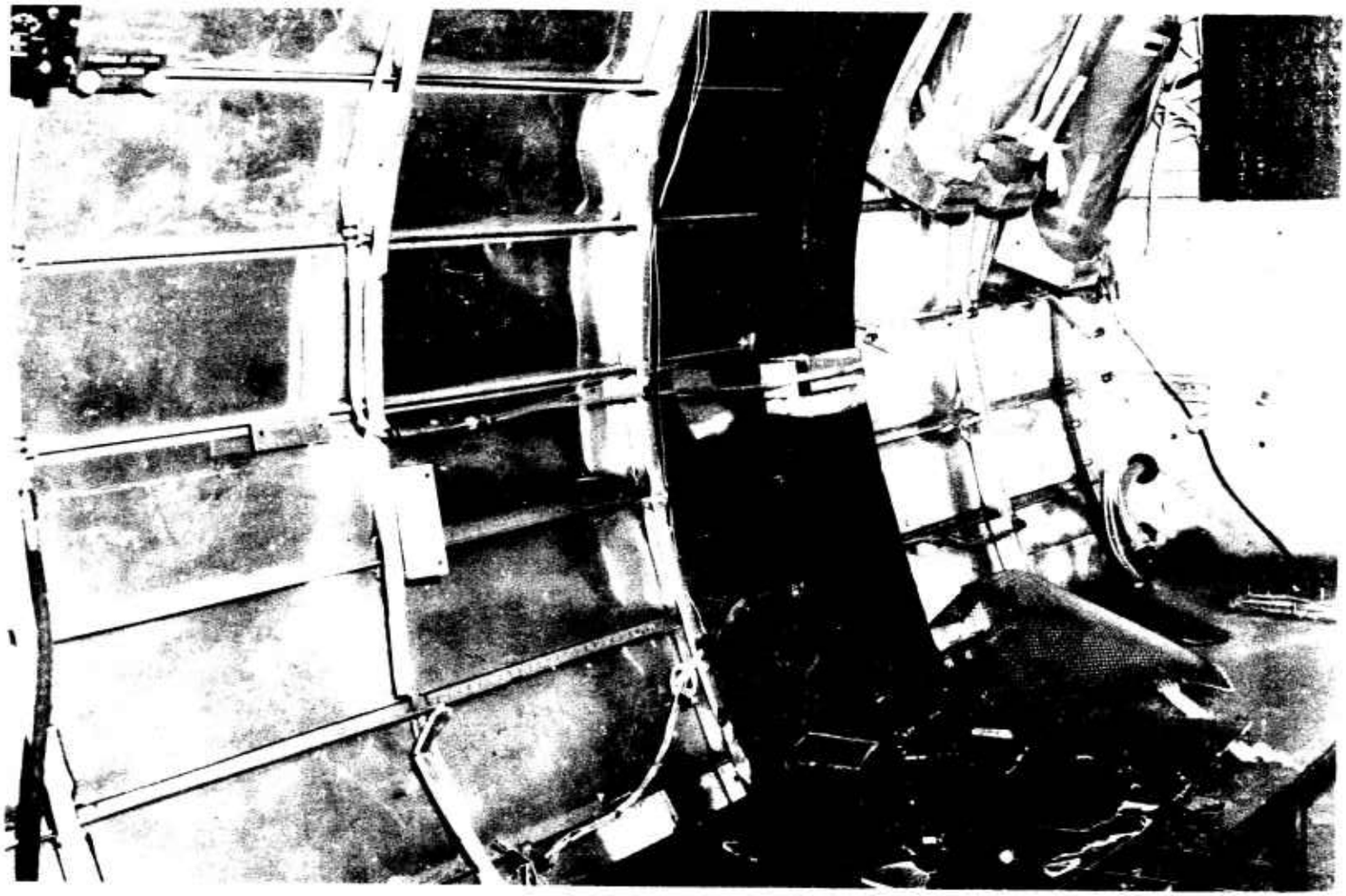

Fig. 3.72 B-17 (5715), Nose-in, Station 8000 (3.6 psi), Shot 3, Interior View, Showing Failed Fuselage Frames and Buckled Skin

Fig. 3.73 B-45 (9481), Nose-in, Station 8000 (3.6 psi), Shot 3, Close-up View of Right Hand Engine Nacelle, Showing Dished Upper and Lower Nose Fairing

UNCLASSIFIED

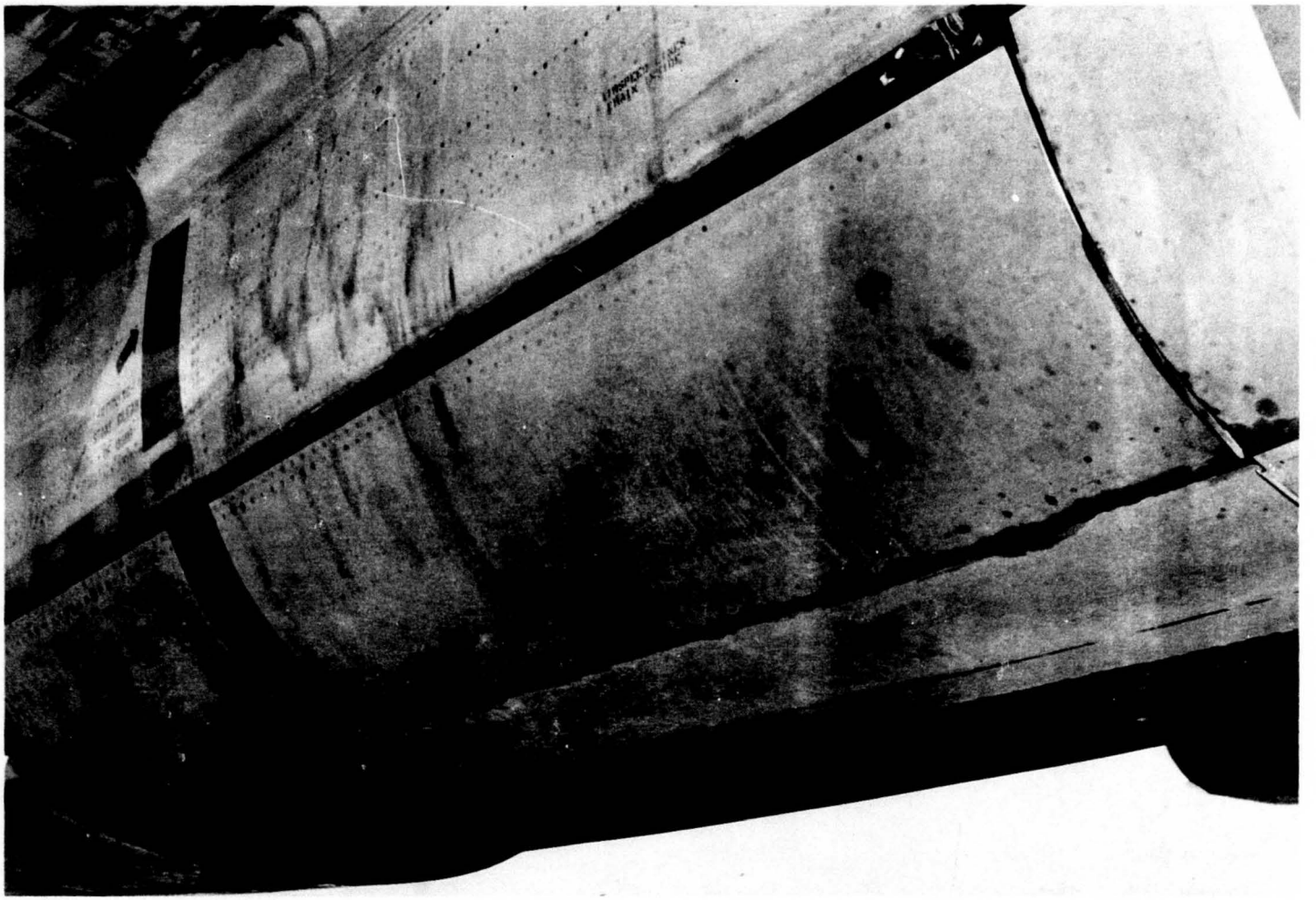

Fig. 3.74 B-45 (9481), Nose-in, Station 8000 (3.6 psi), Shot 3, Close-up View of Blown-in Bomb-bay Doors

UNCLASSIFIED

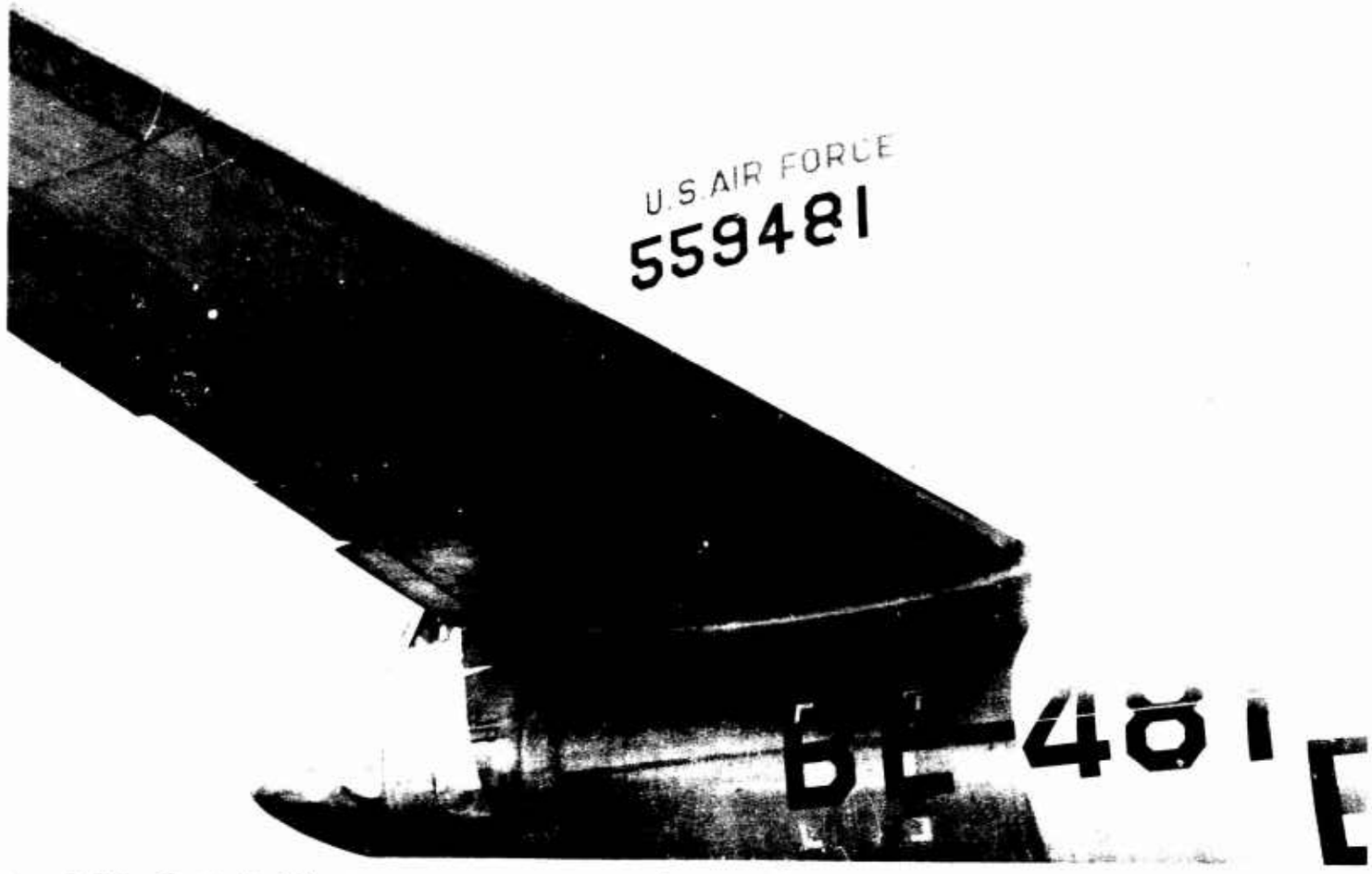

Fig. 3.75 B-45 (9481), Nose-in, Station 8000 (3.6 psi), Shot 3, Close-up View of Empennage, Showing Buckled Tail-gunner's Cone and Fairing Between Dorsal Fin and Vertical Stabilizer

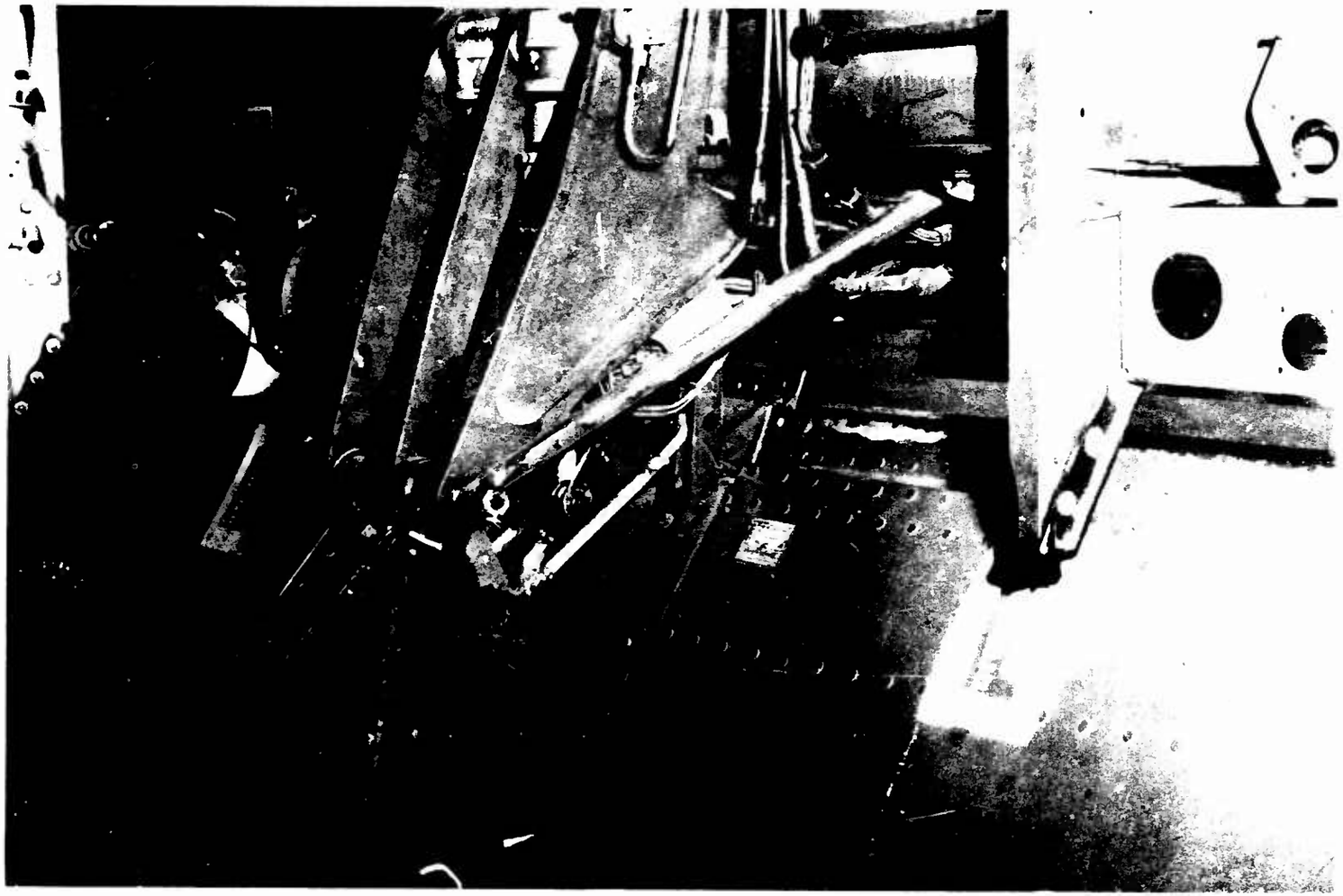

Fig. 3.76 B-45 (9481), Nose-in, Station 8000 (3.6 psi), Shot 3, Showing Broken Support Member of Bomb-bay Door Actuating Mechanism

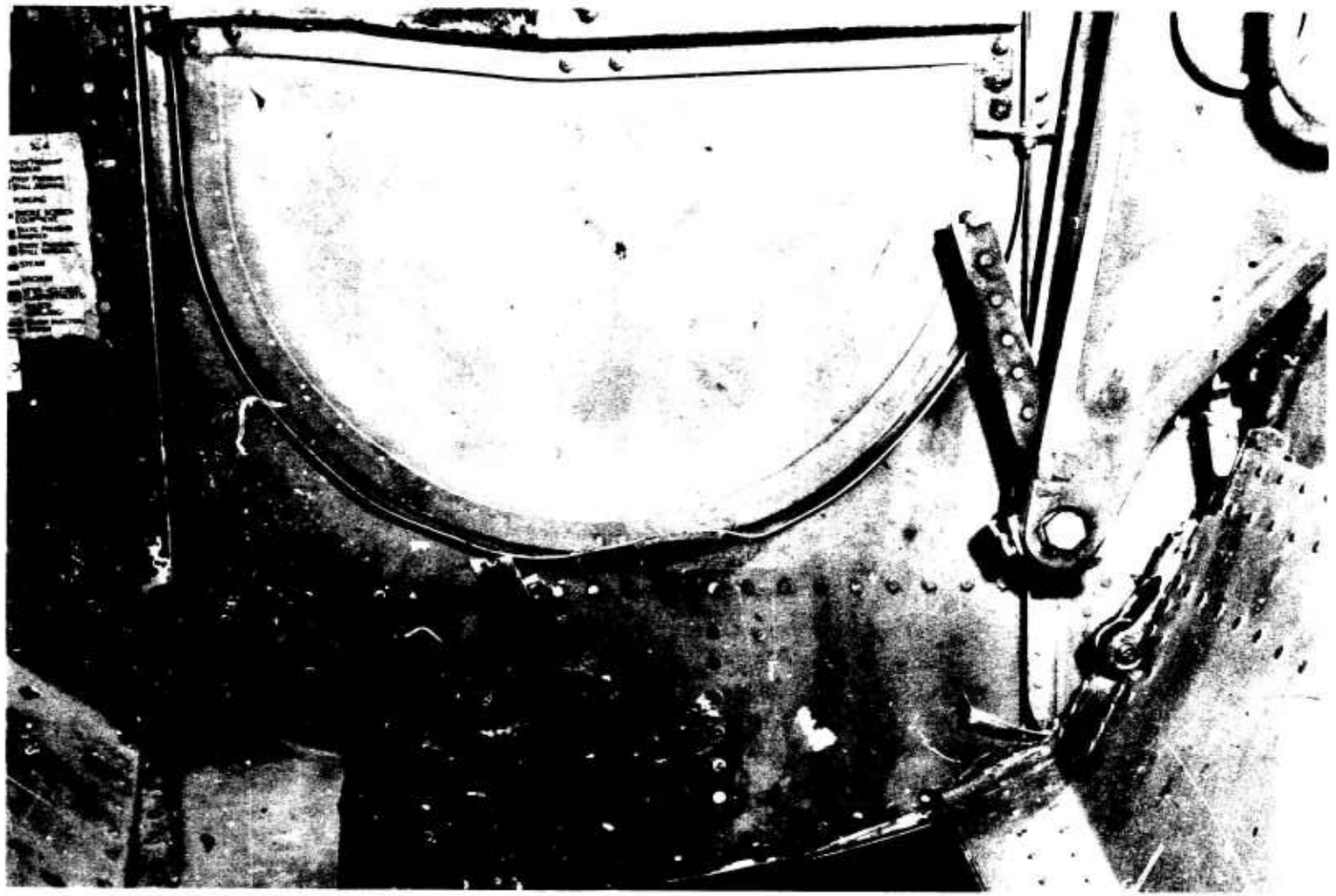

Fig. 3.77 B-45 (9481), Nose-in, Station 8000 (3.6 psi), Shot 3, Showing Broken Linkage of Bomb-bay Door Actuating Mechanism

Fig. 3.78 B-45 (9481), Nose-in, Station 8000 (3.6 psi), Shot 3, Close-up View of Right Main Landing Gear, Showing Thermal Damage to Exposed Portion of Tire

Fig. 3.79 F-47 (3828), Right Side-in, Station 10,500 (2.4 psi), Shot 3, Showing Buckled Area Below Aft Section of Cockpit

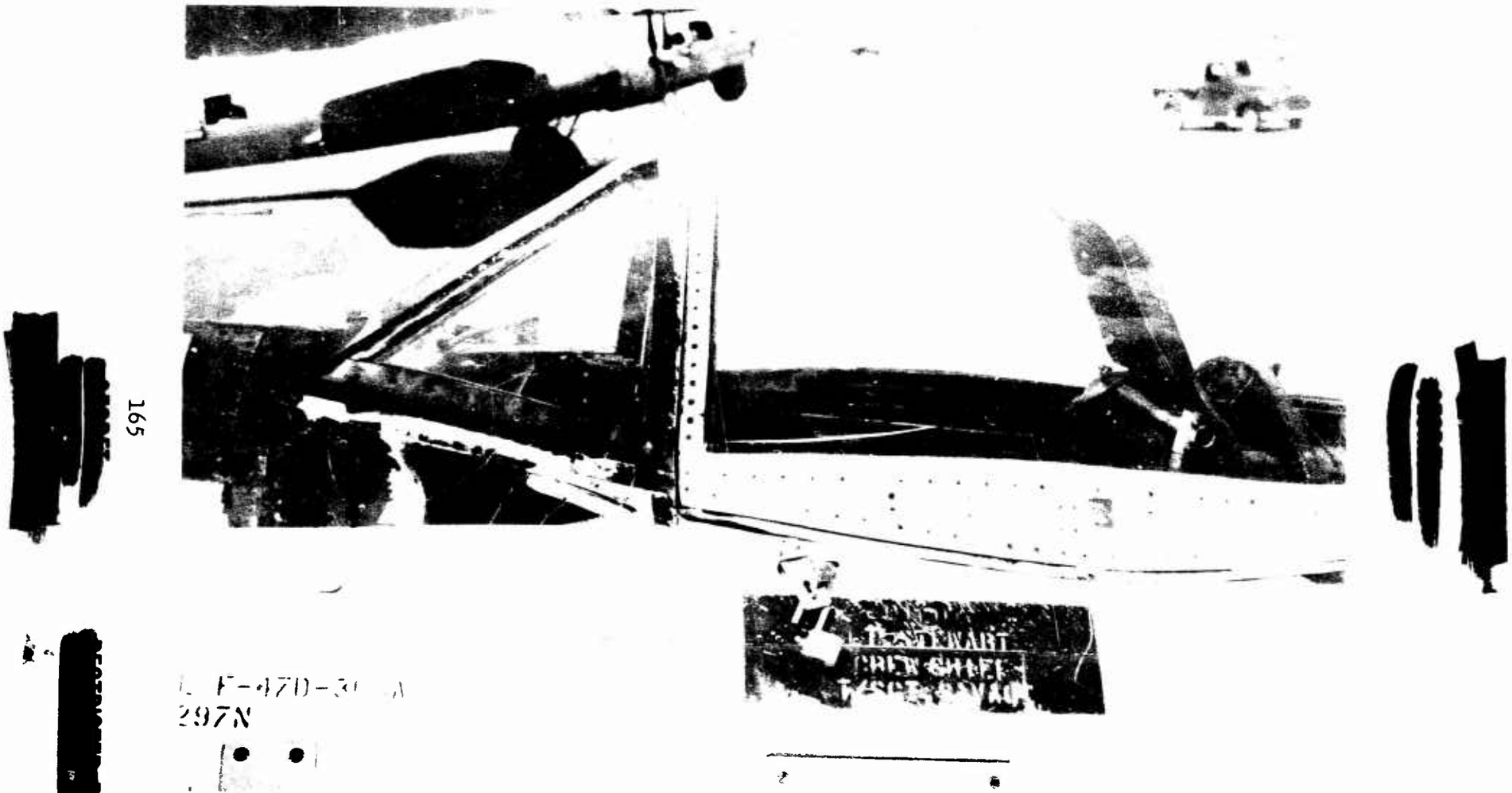

Fig. 3.80 F-47 (0297), Tail-in, Station 10,500 (2.4 psi), Shot 3, Close-up View of Cracked Canopy

Fig. 3.81 B-17 (3769), Right Side-in, Station 10,500 (2.4 psi), Shot 3, Showing Burned Rudder, and Buckled Vertical Stabilizer and Dorsal Fin

Fig. 3.82 B-17 (3769), Right Side-in, Station 10,500 (2.4 psi), Shot 3, Showing Pressure Damage to Nose Section of Fuselage

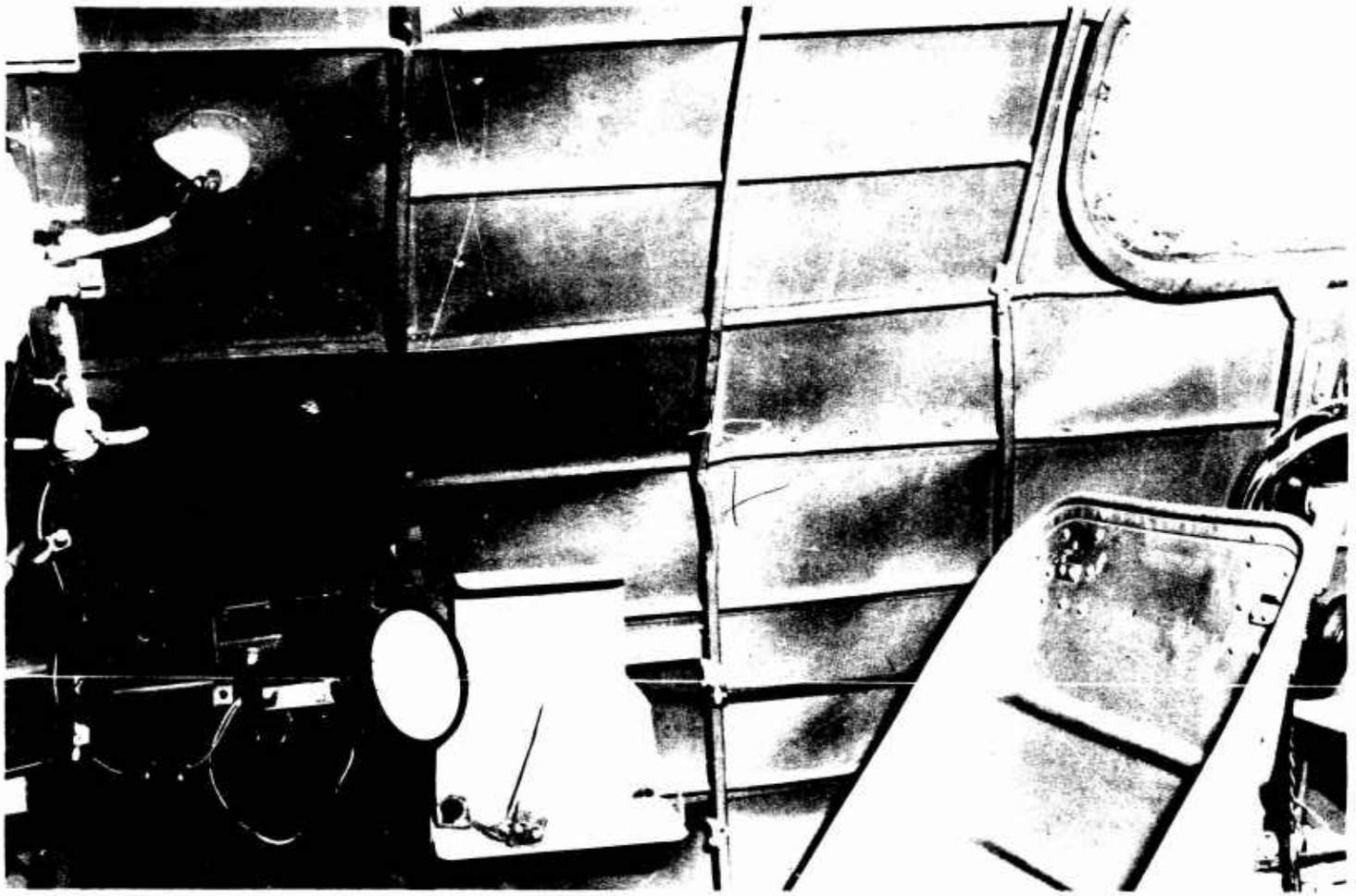

Fig. 3.83 B-17 (3769), Right Side-in, Station 10,500 (2.4 psi), Shot 3, Interior View, Showing Bent Fuselage Frames and Buckled Skin

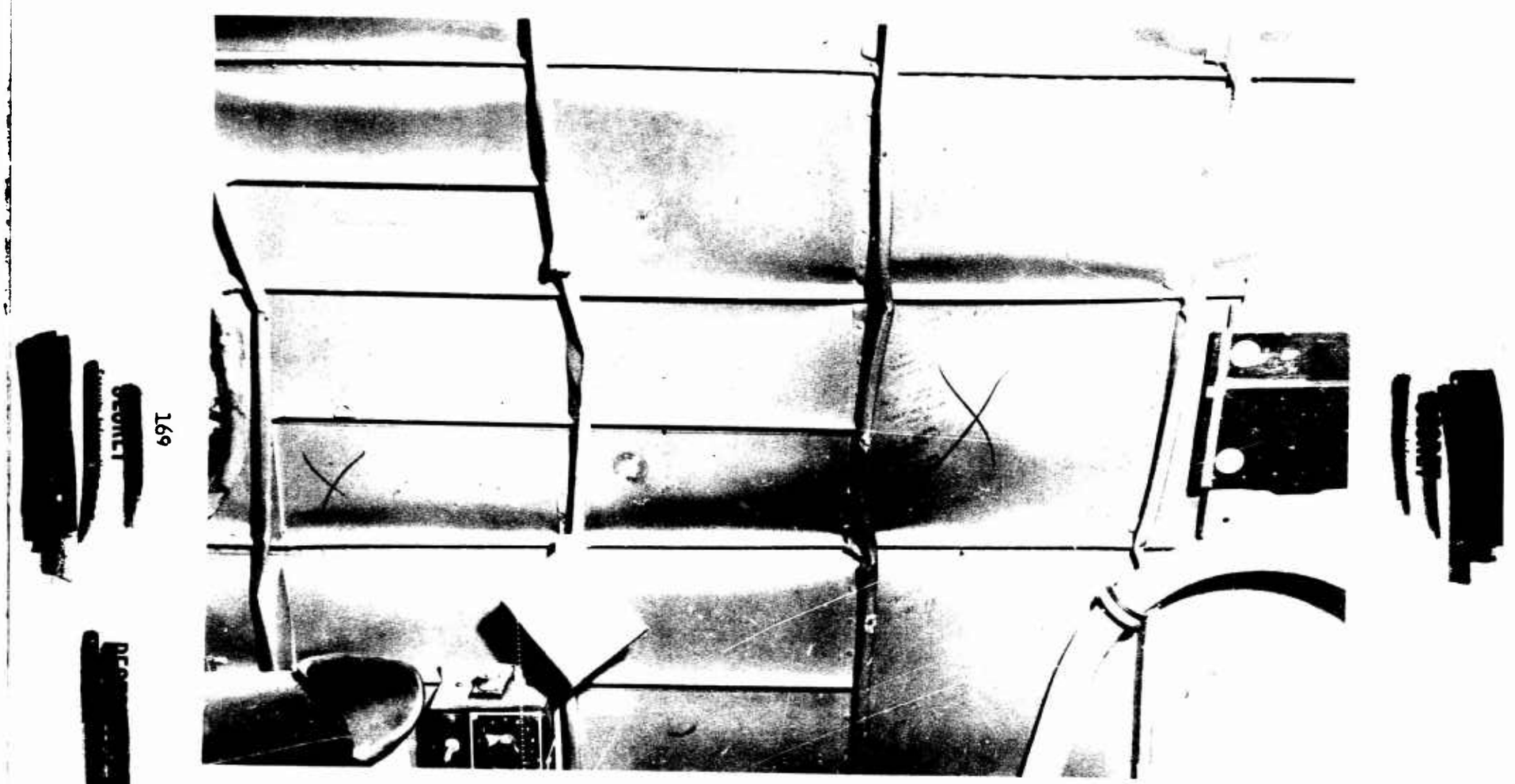

Fig. 3.84 B-17 (3769), Right Side-in, Station 10,500 (2.4 psi), Shot 3, Interior View, Showing Bent and Buckled Condition of Skin and Fuselage Frames

Fig. 3.85 B-17 (3730), Tail-in, Station 10,500 (2.4 psi), Shot 3, Showing Burned Elevators and Generally Dished-in Skin on Vertical Stabilizer, Dorsal Fin, and Wing Area Above Flap

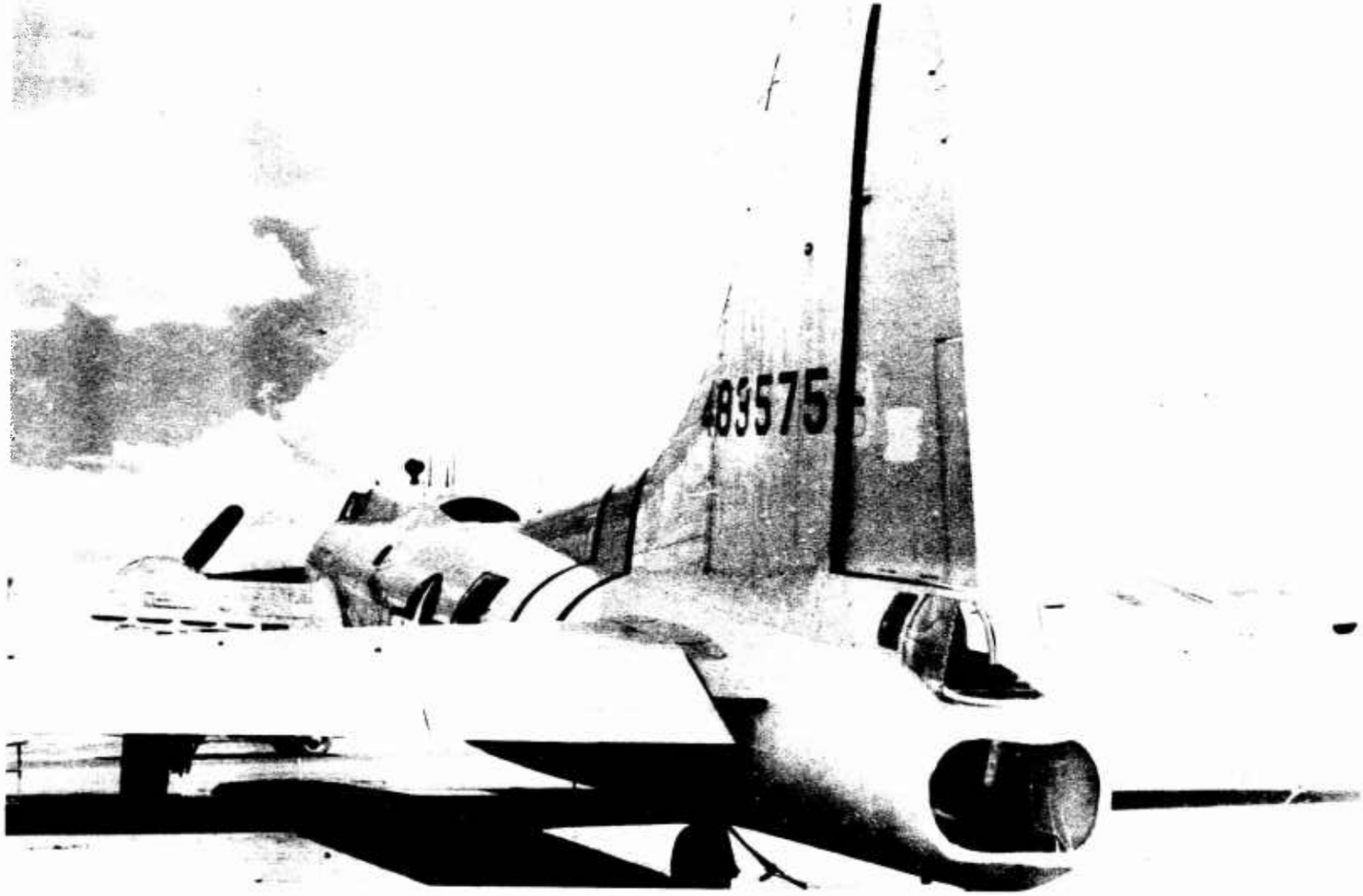

Fig. 3.86 B-17 (3575), Nose-in, Station 10,500 (2.4 psi), Shot 3, Showing Wrinkles in Vertical Stabilizer. Note Slack Skin on Left Elevator Trailing Edge.

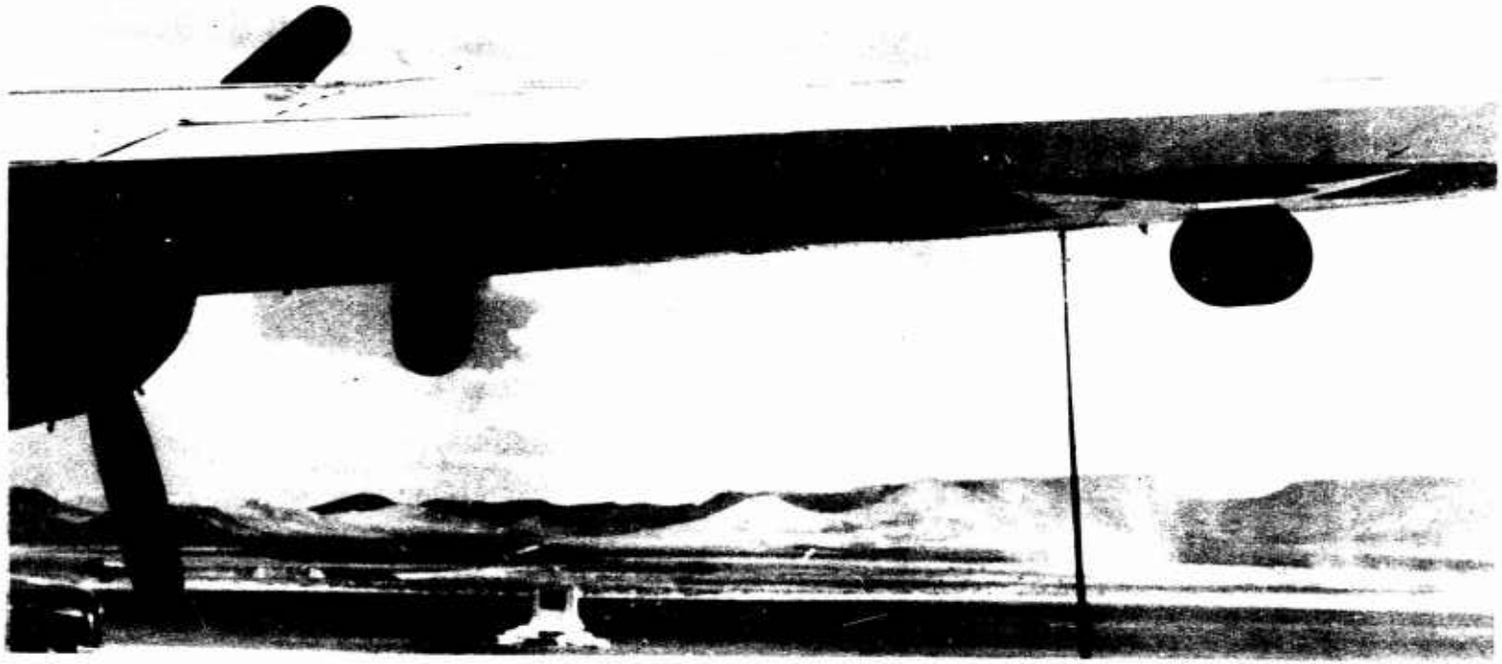

Fig. 3.87 B-17 (3575), Nose-in, Station 10,500 (2.4 psi), Shot 3, Close-up View of Right Wing, Showing Upper and Lower Buckled Surfaces

Fig. 3.88 B-29 (7349), Nose-in, Station 10,500 (2.4 psi), Shot 3, Close-up View from Left Side of Totally Wrecked Forward Bomb-bay Doors

Fig. 3.89 B-29 (7349), Nose-in, Station 10,500 (2.4 psi), Shot 3, Showing Totally Wrecked Right Hand Forward Bomb-bay Door

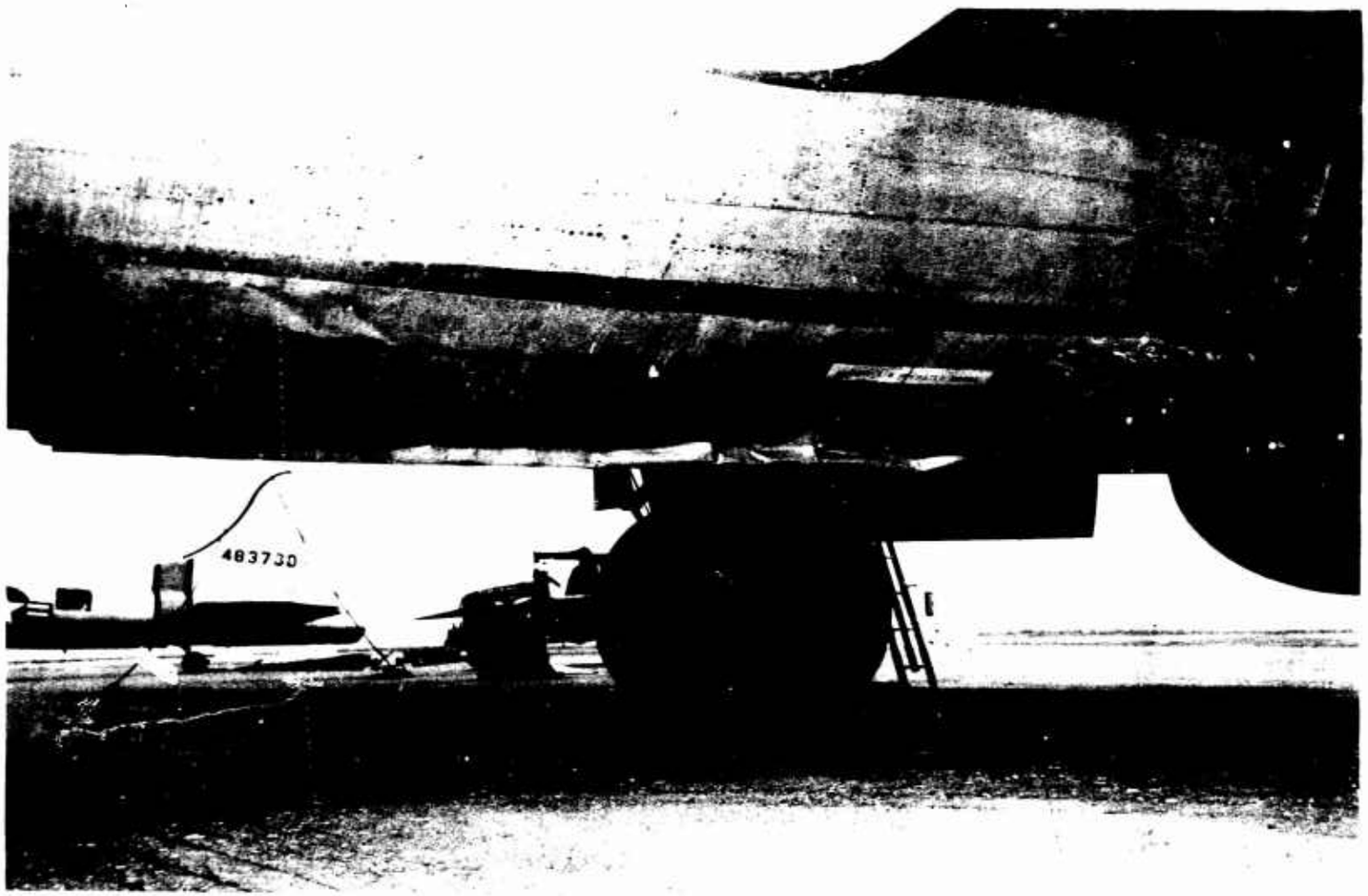

Fig. 3.90 B-29 (7349), Nose-in, Station 10,500 (2.4 psi), Shot 3, Showing Buckled Skin on Right Hand Aft Bomb-bay Door

Fig. 3.91 B-29 (7349), Nose-in, Station 10,500 (2.4 psi), Shot 3, Interior View of Totally Wrecked Forward Bomb-bay Doors

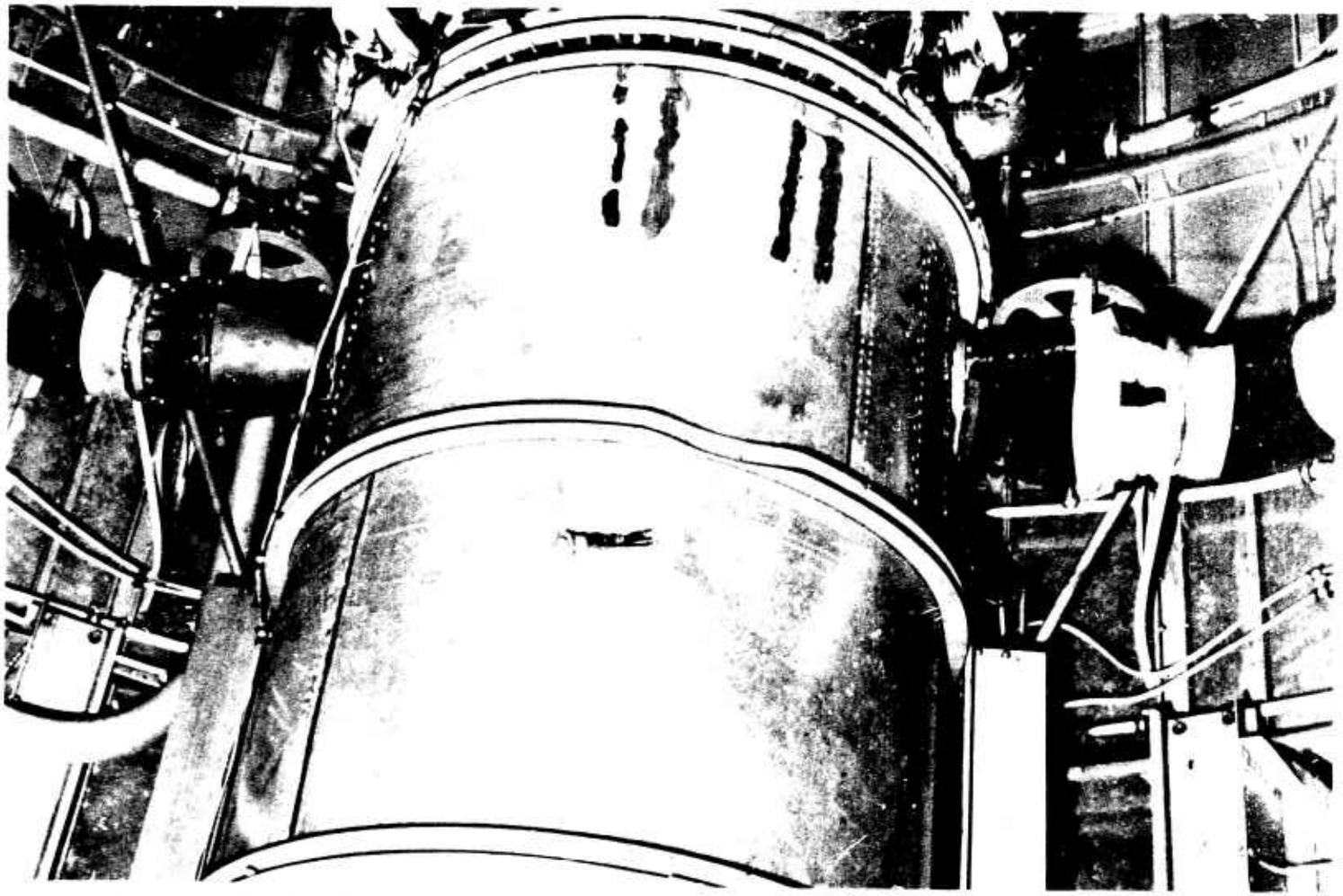

Fig. 3.92 B-29 (7349), Nose-in, Station 10,500 (2.4 psi), Shot 3, Showing Crew Tunnel Perforated by Bomb Rack Quick-release Pin

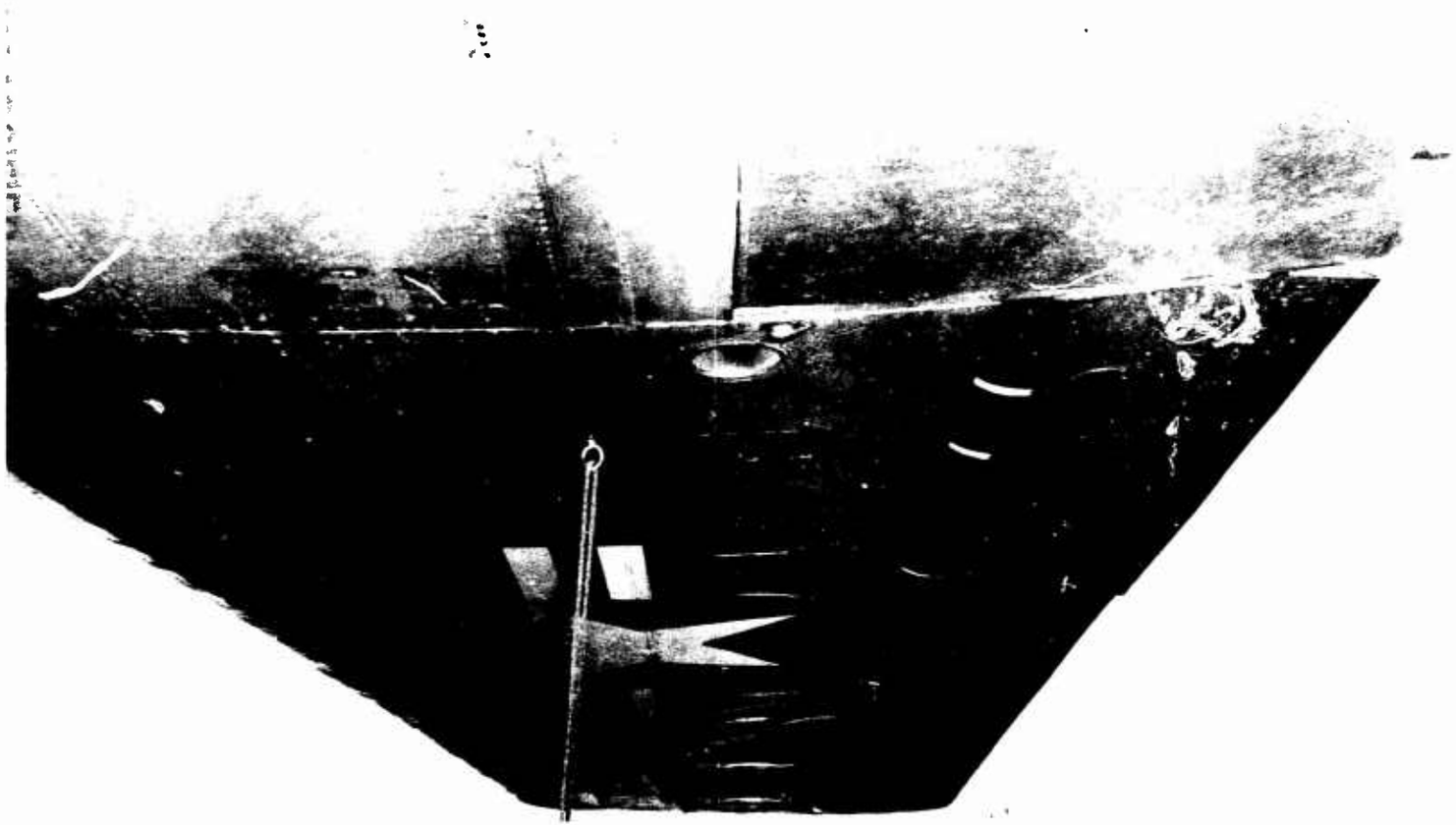

Fig. 3.93 B-29 (7349), Nose-in, Station 10,500 (2.4 psi), Shot 3, Showing Slight Skin Buckles on Lower Surface of Right Wing Outer Panel

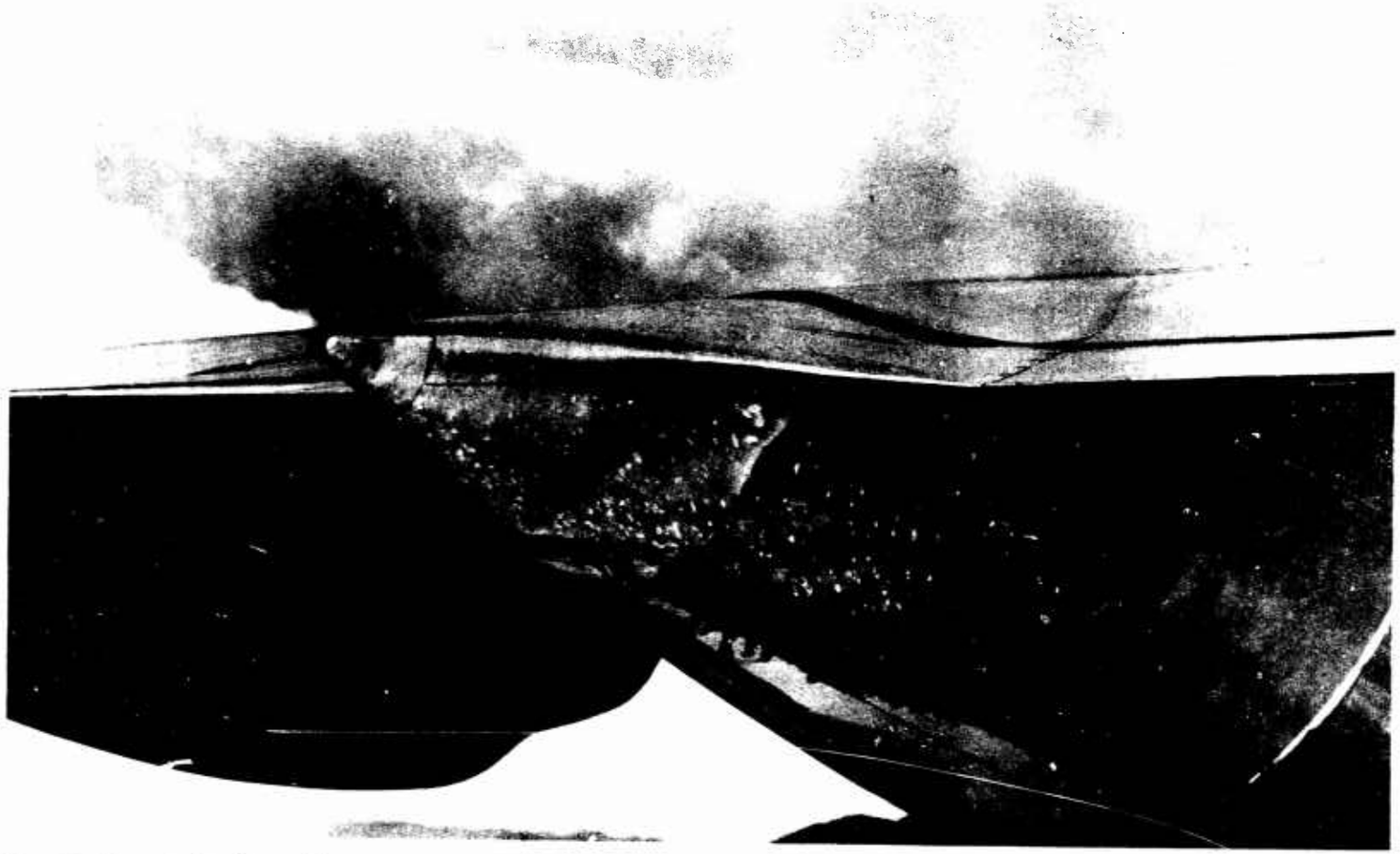

Fig. 3.94 B-29 (7349), Nose-in, Station 10,500 (2.4 psi), Shot 3, Close-up View of Left Inboard Nacelle, Showing Buckled Tail Fairing

Fig. 3.95 B-29 (7349), Nose-in, Station 10,500 (2.4 psi), Shot 3, Showing Buckles on Vertical Stabilizer. Note Warped Trailing Edge of Left Hand Elevator Near Tab.

zero, was dismembered and sandblasted to the point where only a partial skeleton of the fuselage remained. A view of the debris at Station 1350 is shown in Fig. 3.98. Figure 3.99 and 3.100 show, respectively, the remains of this totally wrecked aircraft and a close-up view of the cockpit area.

3.4.3 Station 1384

Aircraft F-47 (9232), parked nose-in at Station 1384, was completely destroyed by blast and thermal effects and the resulting fire. Figures 3.98 and 3.101 show the remains of this aircraft. Located 1490 ft from ground zero, this aircraft was subjected to a peak overpressure of 21 psi and a thermal energy of 164 cal/cm^2.

3.4.4 Station 1500

The B-17 (3699) aircraft, previously damaged in BUSTER-JANGLE and Shot 3, was parked nose-in at Station 1500 for use as a propeller stand in the propeller evaluation program. As a result of the 18 psi overpressure and 148 cal/cm^2 thermal energy, this aircraft was demolished to the extent of being no longer recognizable as an aircraft. The exposure was at a ground range of 1605 ft from ground zero. Figures 3.102, 3.103, 3.104, 3.105, and 3.106 show engines and debris from this aircraft.

3.4.5 Station 2200

One aircraft, F-47 (8785), was exposed at Station 2200, a distance of 2302 ft from ground zero. This aircraft, although oriented nose-in, was very heavily damaged leaving no major components salvable. The overpressure at this range was 9.4 psi and the incident thermal energy was 83 cal/cm^2. The damage produced appears to be inordinately high for these input levels. The explanation may lie in the fact that debris from aircraft forward of F-47 (8785) was picked up by the blast wave and hurled against the craft. The dented appearance of the leading edges of the aircraft lends support to this hypothesis. In addition to the dented and sandblasted leading edges, there was a complete failure of the fuselage at the turbo station, the left and right wings were missing outboard of the outboard landing gear rib, and the right hand landing gear and wing spars had failed. Figures 3.107, 3.108, 3.109, and 3.110 show the general condition of this aircraft after Shot 4.

3.4.6 Station 2500

Four fighter aircraft were exposed at Station 2500, 2601 ft from actual ground zero. The blast overpressure of 8.9 psi and thermal energy of 68 cal/cm^2 damaged the four aircraft beyond economical repair.

[redacted]

3.4.6.1 Aircraft F-47 (9931)

The damage sustained by aircraft F-47 (9931), parked left side-in, is itemized below:

Wing
1. Both wing tips shredded,
2. Right and left aileron burned, torn, and buckled,
3. Right and left wing flap badly burned, torn, and buckled,

Fuselage
1. Fuselage broke off behind wing,
2. Fuselage bauly burned, buckled, and torn,

Empennage
Damaged beyond recognition,

Miscellaneous
1. All four blades of propeller bent to varying degrees,
2. Tail wheel main bracket broken,

Repair Estimate
Beyond economical repair,

Figure Reference
1. Figure 3.111, three-quarter front view of right side of wreckage,
2. Figure 3.112, three-quarter front view of left side of wreckage.

3.4.6.2 Aircraft F-47 (9719)

The damage sustained by aircraft F-47 (9719), parked nose-in, is itemized below:

Wing
1. Leading edges failed by thermal shock and sandblasting,
2. Wing tips burned beyond repair,

Fuselage
1. Complete fuselage failure in region of intercooler exit,
2. Holes burned and sandblasted through leading edge of primary cowl,

Empennage
Empennage virtually disintegrated; only a few stray pieces remained,

Miscellaneous
1. Canopy destroyed,
2. Propeller blades damaged from contact with ground,
3. Aircraft shows evidence of extensive heating and sandblasting,

Repair Estimate
Aircraft is beyond economical repair,

Figure Reference
1. Figure 3.113, left side view, showing demolished

[redacted]

[redacted]

empennage and fuselage failure,
2. Figure 3.114, front view of aircraft, showing propeller and cowling damage,
3. Figure 3.115, close-up view of destroyed canopy.

3.4.6.3 Aircraft F-86 (8209)

The damage sustained by aircraft F-86 (8209), parked tail-in, is itemized below:

Wing
1. Right wing and aileron buckled,
2. Left wing and aileron severely buckled,
3. Leading edge of both wings heavily sandblasted,

Fuselage
Dented from flying objects and severely buckled all over,

Empennage
1. Left hand horizontal stabilizer broken 18 in. from the tip,
2. Entire empennage well dented and sandblasted,

Miscellaneous
All flush antennas charred and sandblasted; compass antenna destroyed with canopy,

Repair Estimate
Aircraft beyond economical repair,

Figure Reference
1. Figure 3.116, left side view, showing general condition of aircraft after Shot 4,
2. Figure 3.117, close-up view of right side of severely buckled fuselage,
3. Figure 3.118, close-up view of left side of severely buckled fuselage.

3.4.6.4 Aircraft F-90 (6688)

The damage sustained by aircraft F-90 (6688), parked left side-in, is itemized below:

Wing
1. General damage by thermal, pressure, and sandblasting effects; main wing structure remained intact,
2. Panel torn by collapsing of landing gear,

Fuselage
1. Aft fuselage torn off at the removable joint; lower attaching bolt failed in tension,
2. All skin panels caved in on left hand side of fuselage except those between main rings of wing attachment,
3. Nose compartment shredded,
4. Tail cone blown off.

[redacted]

[redacted]

Empennage
1. Fin wrecked by thermal shock and sandblasting,
2. Right hand stabilizer broken off, probably by ground contact,
3. Sustained general damage from thermal, pressure, and sandblasting effects,

Miscellaneous
1. Left and right landing gear torn out of wings,
2. Aircraft rotated about 90° and thrown backward 60 ft by blast,
3. Gun-sight head destroyed,

Repair Estimate
Aircraft beyond economical repair,

Figure Reference
1. Figure 3.119, general view of aircraft condition after Shot 4,
2. Figure 3.120, left side view of damaged forward section of the fuselage
3. Figure 3.121, close-up view of destroyed cockpit,
4. Figure 3.122, close-up view of punctured top left wing surface near wing root,
5. Figure 3.123, left side view of torn off aft section of fuselage,
6. Figure 3.124, close-up view of right side of aft section of fuselage and empennage,
7. Figure 3.125, close-up view of empennage, showing broken right stabilizer.

3.4.7 Station 3320

Aircraft F-47 (9072) was parked nose-in at a distance of 3419 ft from ground zero. It was the only aircraft at Station 3320 and sustained moderate damage as a result of the 6.9 psi peak overpressure and 41 cal/cm^2 thermal energy.

3.4.7.1 Aircraft F-47 (9072)

The damage sustained by aircraft F-47 (9072), parked nose-in, is itemized below:

Wing
1. Left wing panel leading edges cracked and badly burned at tip,
2. Left and right wing panel top skin badly buckled and oil-canned,
3. Left and right wing tip top skin badly buckled,

Fuselage
Right and left side engine cowling badly buckled,

Empennage

[redacted]

[redacted]

Left hand elevator scorched,

Miscellaneous

1. Propeller blade bent from ground contact,
2. Tail wheel, tire, and strut damaged beyond repair (blown off crib),

Repair Estimate

Estimated man-hours required for complete repair, 350,

Figure Reference

Figure 3.126, three-quarter rear view of right side, showing general post-shot condition of aircraft.

3.4.8 Station 3450

Two aircraft, F-47 (3828), tail-in, and B-45 (9481), nose-in, were exposed at Station 3450. The F-47 aircraft was heavily damaged and the B-45 aircraft moderately damaged. These aircraft, located 3549 ft from ground zero, were subjected to a blast overpressure of 6.5 psi and a thermal flux of 38 cal/cm^2.

3.4.8.1 Aircraft F-47 (3828)

The damage sustained by aircraft F-47 (3828), parked tail-in, is itemized below:

Wing

1. Right and left wing top skin buckled near outboard end of wing panel,
2. Trailing edge of right and left wing panels slightly damaged,
3. Left and right wing gun access doors and ammunition doors buckled,
4. Left wing panel top skin badly burned,
5. Left and right aileron and landing flap torn completely from aircraft and damaged beyond repair.

Fuselage

1. Left engine accessory cowling badly buckled,
2. Right and left sides of fuselage slightly buckled,
3. Right and left side supercharger fairing badly dented and buckled,

Empennage

1. Rudder and horizontal stabilizer buckled and warped beyond repair,
2. Vertical stabilizer damaged beyond repair,
3. Left elevator torn completely from aircraft and blown forward,
4. Right elevator badly buckled and torn loose, except from inboard end,

Miscellaneous

1. Right main landing gear door, outboard section, damaged

[redacted]

[redacted]

beyond repair,
2. Left drop fuel tank has two large dents in trailing end; right drop fuel tank similarly damaged,
3. Top rudder hinge pulled out of fin spar,
4. Cribbed aircraft fell off stand and moved forward approximately 6 ft,
5. Rear section of main oil tank dented,
6. Air-speed indicator and fuel-quantity gage damaged,

Repair Estimate

Estimated man-hours required for complete repair, 1488,

Figure Reference

1. Figure 3.127, three-quarter rear view of right side, showing general post-shot condition of aircraft,
2. Figure 3.128, close-up view showing damage to right wing flap and fuselage.

3.4.8.2 Aircraft B-45 (9481)

The damage sustained by aircraft B-45 (9481), parked nose-in, is itemized below:

Wing

No apparent damage,

Fuselage

1. Vertical stiffeners on bulkhead at aft end of bomb bay have failed in bending due to pressures on the bulkhead; door in bulkhead is twisted and damaged,
2. Bomb-bay door broken and hanging loose,
3. Fuselage pushed in on both sides from aft end of life raft door to forward edge of vertical stabilizer frame; failure was principally by bending of frames,
4. Tail cone failed completely aft of tail-gunner's compartment,
5. Life-raft door pushed in,

Empennage

No significant damage,

Miscellaneous

1. Bombardier's enclosure smoked and sandblasted,
2. Radome pushed in,
3. Extensive crushing of nacelle skins and internal structure of nose and tail of each nacelle,
4. Main landing gear doors broken open; linkage broken on right hand door,
5. Charring of upholstery at bombardier's, pilot's, co-pilot's, and tail-gunner's stations; no evidence of actual fires,
6. Radio equipment not operative, possibly due to small fire in wing,
7. Pilot's air-speed indicator, cabin-pressure altimeter,

[redacted]

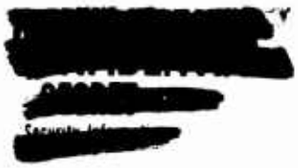

and pilot's altimeter all ruptured,
8. Gyro horizon failed to erect,

Repair Estimate

Estimated man-hours required for complete repair, 2838,

Figure Reference

1. Figure 3.129, three-quarter front view of right side showing general post-shot condition of aircraft,
2. Figure 3.130, close-up view of pushed in radome,
3. Figure 3.131, close-up view of empennage, showing fuselage buckles and tail cone failure,
4. Figure 3.132, close-up view of empennage, showing damage to dorsal fairing,
5. Figure 3.133, interior view of cockpit, showing charred upholstery,
6. Figure 3.134, interior view of damaged aft bomb-bay doors and bulkhead door,
7. Figure 3.135, close-up view of forward side of damaged bulkhead door,
8. Figure 3.136, close-up view aft side of damaged bulkhead door,
9. Figure 3.137, interior view of bent fuselage frames and pushed-in skin.

3.4.9 Station 4000

Seven aircraft were exposed at Station 4000; six were fighters and one was a medium bomber. These aircraft were 3801 ft from actual ground zero. Measurements showed that directly exposed aircraft were subjected to an overpressure of 5.8 psi and a thermal energy of 33 cal/cm^2. Two of the F-47 fighters were protected by revetments; one in a pit revetment and the other behind a wall revetment. A third F-47 fighter, located in the open between the aircraft which were protected by the revetments, suffered considerably more damage than the protected aircraft. All three aircraft were oriented tail-in toward ground zero. The tail-in F-86 (the only F-86 aircraft exposed at this station) was less severely damaged than the similarly oriented F-47 aircraft. The B-17 bomber, parked tail-in, suffered extensive damage to all major components and was considered beyond repair.

3.4.9.1 Aircraft F-47 (9785)

The damage sustained by aircraft F-47 (9785), parked left side-in, is itemized below:

Wing

1. Left hand wing skin outboard of ammunition door buckled in,
2. Left hand flap buckled,

Fuselage

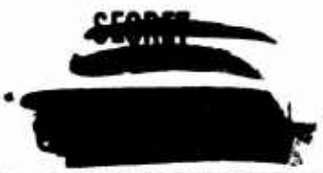

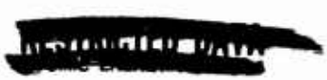

[redacted]

1. Severe blast damage on left hand side; several ring and stringer failures,
2. Left hand side scorched in all painted areas,
3. Frame at station 339½ buckled on right hand side,
4. Left hand side secondary cowls severely buckled,

Empennage

1. Fin and rudder badly buckled on left hand side; failure on right side of fin,
2. Left hand stabilizer badly buckled between spars,
3. Root of elevator trailing edge hit by rudder,

Miscellaneous

1. Canopy failed; frame badly bent,
2. Tail wheel door burned; tail wheel supports may have failed (wheel buried in sand),
3. Left main landing gear wheel and strut fairing burned,

Repair Estimate

No estimate given, aircraft sustained heavy damage from Shot 3,

Figure Reference

1. Figure 3.138, left side view of blast-damaged fuselage,
2. Figure 3.139, right side view of empennage and fuselage aft section,
3. Figure 3.140, close-up view of destroyed canopy.

3.4.9.2 Aircraft F-47 (0065)

The damage sustained by aircraft F-47 (0065), parked tail-in, is itemized below:

Wing

1. Flaps and ailerons blown off both sides,
2. Wing gun and ammunition doors dished in,
3. Wing panels outboard of gun and ammunition doors between spars buckled in,
4. Aileron hinges pulled out of wing spar,
5. Several flap links failed,

Fuselage

1. Both sides of fuselage slightly buckled,
2. Belly cowls dented,
3. Secondary cowl panels dished in,

Empennage

1. Rudder failed several places in bending,
2. Both elevators blown off; all hinge brackets failed,
3. Elevator interconnect tube failed both sides,
4. Right and left horizontal stabilizer buckled,
5. Fin skin dished on both sides,

Miscellaneous

1. Hole in left hand wheel fairing,
2. Canopy failed completely in area over seat,

DECLASSIFIED DATA

[redacted]

[redacted]

3. Rear view mirror cracked, smoked, and blown down out of position,

Repair Estimate

Estimated man-hours required for complete repair, 1660,

Figure Reference

Figure 3.141, right side view, showing general post-shot condition of aircraft.

3.4.9.3 Aircraft F-47 (9074)

The damage sustained by aircraft F-47 (9074), parked tail-in, is itemized below:

Wing

1. Both flaps and ailerons blown off,
2. Wing panels outboard of ammunition door buckled in,
3. Wing skin torn where flap hinge brackets broke loose,
4. Gun-bay and ammunition door buckled in,

Fuselage

1. Right and left sides of fuselage buckled,
2. Secondary cowl panels buckled,

Empennage

1. Hinge brackets of both elevators failed,
2. Rudder failed,
3. Several scorched spots on horizontal stabilizer (reskinning required),

Miscellaneous

1. Tail-wheel doors damaged,
2. Canopy shattered,
3. Left and right hand wheel and strut fairing bent at trailing edge, probably struck by flap,

Repair Estimate

Estimated man-hours required for complete repair, 2020,

Figure Reference

1. Figure 3.142, rear view, showing general post-shot condition of aircraft,
2. Figure 3.143, close-up view of forward right side of fuselage and blown-off wing control surfaces,
3. Figure 3.144, close-up view of blown-off left wing flap,
4. Figure 3.145, close-up view of empennage.

3.4.9.4 Aircraft F-47 (9110)

The damage sustained by aircraft F-47 (9110), parked tail-in in a pit-type revetment, is itemized below:

Wing

1. Linkage to both flaps broken,
2. Right aileron torn off,

[redacted]

[redacted]

3. Wing panels outboard of ammunition doors buckled top and bottom,

Fuselage

No additional damage as result of Shot 4,

Empennage

No additional damage as result of Shot 4,

Miscellaneous

Air-speed indicator damaged,

Repair Estimate

Estimated man-hours required for complete repair, 388,

Figure Reference

1. Figure 3.146, right side view of aircraft from top of pit revetment,
2. Figure 3.147, close-up view of left wing control surfaces and forward section of fuselage.

3.4.9.5 Aircraft F-47 (9186)

The damage sustained by aircraft F-47 (9186), parked tail-in behind a wall-type revetment, is itemized below:

Wing

1. Wing trailing edge damaged in flap region,
2. Flaps failed probably because of flap links,
3. Both ailerons blown off,

Fuselage

No additional damage,

Empennage

1. Right hand elevator buckled,
2. Rear spar of fin damaged,

Miscellaneous

1. Aircraft came to rest on propeller blade in a tail-up attitude, resulting in bent propeller blade,
2. Canopy failed,

Repair Estimate

Estimated man-hours required for complete repair, 481,

Figure Reference

1. Figure 3.148, right side view, showing control surface damage,
2. Figure 3.149, three-quarter front view of left side, showing position of aircraft following shot.

3.4.9.6 Aircraft F-86 (9597)

The damage sustained by aircraft F-86 (9597), parked tail-in, is itemized below:

Wing

1. Slight canning in wing fairing in area between aileron

[redacted]

[redacted]

and rear spar,
2. Wing tips charred on upper surface,
3. Ailerons ripped off; except for failure of outboard hinge bracket on right wing, cause was aileron hinge failures,

Fuselage
1. Cabin cooling access door, right side, badly buckled,
2. Moderate buckling of body skin panels from pressure loading, especially forward of the wing,

Empennage
1. Rudder and elevator surfaces buckled slightly,
2. Rudder and fin damaged at the hinges when the rudder encountered its travel stop,

Miscellaneous
1. Canopy broken and right hand windshield wrecked,
2. Tachometer damaged by flying debris,

Repair Estimate
Estimated man-hours required for complete repair, 148,

Figure Reference
1. Figure 3.150, three-quarter rear view of left side, showing general post-shot condition of aircraft,
2. Figure 3.151, close-up view of instrument panel,
3. Figure 3.152, close-up view of right side rudder.

3.4.9.7 Aircraft B-17 (5715)

The damage sustained by aircraft B-17 (5715), parked tail-in, is itemized below:

Wing
1. Wings torn off aft of rear spar,
2. Flaps and ailerons completely ripped off,
3. Wing outer panels and tips severely buckled,

Fuselage
Complete fuselage buckled and pushed in, failing many frames and stringers,

Empennage
1. Vertical stabilizer and dorsal completely wrecked,
2. Rudder fabric burned off and ribs buckled,
3. Elevator ribs buckled and fabric burned off,
4. Horizontal stabilizer and tips badly buckled with many rib failures,

Miscellaneous
1. Additional damage to bomb-bay doors,
2. ART-13 completely off racks, hanging by wiring, radio operator's desk smashed, radio control panel in cockpit blown off, and indicator I-152C blown off,
3. Pilot's air-speed indicator damaged,

Repair Estimate
Aircraft damaged beyond repair,

[redacted]

RESTRICTED DATA

[redacted]

Figure Reference

1. Figure 3.153, three-quarter rear view of right side, showing general post-shot condition of aircraft,
2. Figure 3.154, close-up view of left wing wreckage and forward section of fuselage,
3. Figure 3.155, close-up view of right side of fuselage and remains of right wing.

3.4.10 Station 5000

The B-29 aircraft, only slightly damaged by Shots 2 and 3, was parked nose-in at Station 5000. At this range of 4799 ft from actual ground zero the total thermal energy input was 21 cal/cm^2, and the peak overpressure of the blast wave was 4.0 psi. The aircraft, the only aircraft parked at Station 8000, was not too severely damaged by the blast phase; however, because of fire, which apparently originated in the forward nose compartment as a result of direct thermal radiation, the plane was seriously damaged and considered a total loss.

3.4.10.1 Aircraft B-29 (7349)

The damage sustained by aircraft B-29 (7349), parked nose-in, is itemized below:

Wing

1. Ribs buckled in wing outer panels,
2. Wing tips must be rebuilt because of ribs buckling from positive pressure,

Fuselage

Fuselage completely destroyed by fire,

Empennage

1. Buckled in lower rudder,
2. Elevators warped and damaged beyond flyable condition,
3. Horizontal stabilizer skin stretched and ribs crippled; vertical tail and dorsal similarly damaged,

Miscellaneous

1. Fuselage nose section completely burned,
2. Fuselage aft section completely burned from forward bulkhead of aft pressure compartment, to and including, aft fuselage entrance door,
3. Nose landing gear and door completely destroyed by fire,
4. Forward bomb-bay doors suffered further buckling,
5. All equipment in fuselage completely burned,

Repair Estimate

Aircraft was destroyed by fire,

Figure Reference

1. Figure 3.156, right side view, showing general post-shot condition of aircraft,
2. Figure 3.157, close-up view of lower surface of left wing

[redacted]

outboard section,
3. Figure 3.158, close-up view of lower surface of left wing outboard section,
4. Figure 3.159, close-up view of buckles on top of left wing near inboard nacelle,
5. Figure 3.160, top view of outboard section of left wing,
6. Figure 3.161, close-up view of empennage and aft section of burned fuselage.

3.4.11 Station 8000

Only one aircraft, B-17 (3575), previously damaged in Shot 3 (See Figs. 3.86 and 3.87), was parked at Station 8000, an actual distance of 7792 ft from ground zero. This aircraft, parked left side-in, was significantly damaged as a result of the 1.9 psi overpressure and 8.0 cal/cm^2 thermal flux.

3.4.11.1 Aircraft B-17 (3575)

The damage sustained by aircraft B-17 (3575), parked left side-in, is itemized below:

Wing
1. Pressure damage in area aft of rear spar,
2. Wing outer panels must be rebuilt because of pressure damage to skin and ribs,
3. Moderate damage to left and right flaps,

Fuselage
1. Torque failure of fuselage in section above wing trailing section,
2. Cabin area and forward failed by positive pressures,
3. Badly damaged from rear spar bulkhead aft,

Empennage
1. Ribs and skin of vertical tail badly deformed,
2. Rudder fabric burned off and ribs buckled,
3. Light positive pressure damage to horizontal stabilizer,
4. Fabric loose on left hand elevator,
5. Dorsal heavily damaged,

Miscellaneous
1. Bomb doors heavily damaged,
2. Radomes charred and cracked on ground zero side,
3. All removable accessory cowling dished in,
4. Pilot's speed indicator damaged,

Repair Estimate
Estimated man-hours required for complete repair, 5724,

Figure Reference
1. Figure 3.162, left side view, showing general post-shot condition of aircraft,
2. Figure 3.163, close-up view of right side fuselage where

[redacted]

torque failure occurred,
3. Figure 3.164, close-up view of left wing lower surface, showing pressure damaged outer panel skin,
4. Figure 3.165, left side view of burned and buckled empennage,
5. Figure 3.166, interior view of fuselage section where torque failure occurred,
6. Figure 3.167, interior view of left side fuselage, showing damaged fuselage frames,
7. Figure 3.168, interior view of damaged dorsal fin bulkhead.

3.4.12 General Observations

No significant damage to power plants or power plant equipment of aircraft parked at Station 3320 or farther was noted. Aircraft parked closer than Station 3320 were damaged beyond repair, and a complete investigation of power plants and accessory equipment was not made. Damage to electronic equipment and aircraft instruments was similar to Shot 3, described in Paragraph 3.3.8. Electronic equipment in aircraft located at Station 2500 or closer would be suitable for return to operational status only as individual components. Except for conditions where wires to external lights and lights themselves were broken through major structural damage, the electrical system and components were unaffected by Shot 4. With one exception, landing gear on all aircraft not completely destroyed by fire or blast were found to be serviceable. The one exception was the collapsing of the right main landing gear of the nose-in F-86 at Station 2500, caused by failure of the side brace. Wheels seemed unaffected by the heating but in some cases suffered sufficient sandblast damage to warrant check-out prior to being returned to service. The hydraulic systems of aircraft retaining their general airframe configuration were not damaged. No loosening of fittings as in Shot 3 was noticed. Propellers represent a rather insensitive part of the aircraft and should remain essentially undamaged up to the point where the aircraft is damaged beyond economical repair. In no event should propeller damage be the cause for grounding. The component of F-47 aircraft most likely to cause grounding is the canopy.

3.5 TEST PANELS

Various test articles were displayed on test panels to determine the effects of direct thermal radiation and/or blast pressure. These articles include integral fuel cell models, ejection seat catapults with firing cartridge, canopy removing squibs, sealed bearings, pressure seals, and fabric and acrylic specimens. Given below is a description of the damage sustained by the articles displayed on three test panels.

[redacted]

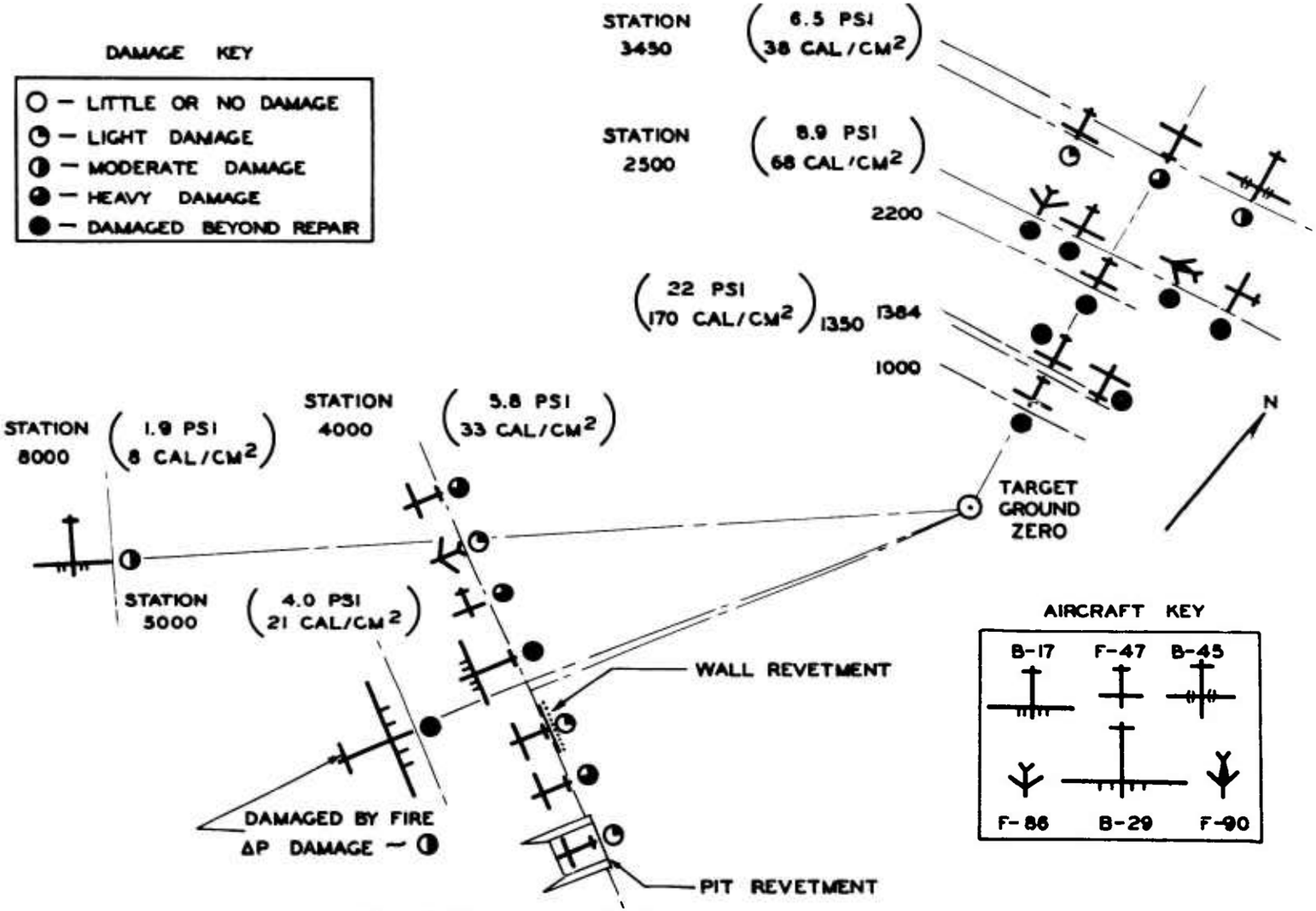

Fig. 3.96 Aircraft Damage Summary, Shot 4

Fig. 3.97 F-47 (9114), Nose-in, Station 1000 (36 psi), Shot 4, Showing Burned Wreckage of Fuselage and Power Plant

Fig. 3.98 Debris Near Station 1350, Looking West, Following Shot 4. Note Remains of Aircraft F-47 (9232) Near Truck in Right Background. Aircraft F-47 (9232) Was Parked Nose-in at Station 1384 (21 psi).

Fig. 3.99 F-47 (9851), Tail-in, Station 1350 (22 psi), Shot 4, Showing Remains of Totally Wrecked Aircraft

Fig. 3.100 F-47 (9851), Tail-in, Station 135C (22 psi), Shot 4, Close-up View of Wrecked Fuselage. Note Thermal Effects on Skin.

Fig. 3.101 F-47 (9232), Nose-in, Station 1384 (21 psi), Shot 4, Showing Destroyed Forward Section of Fuselage and Miscellaneous Wreckage After Fire Was Extinguished

Fig. 3.102 B-17 (3699), Nose-in, Station 1500 (18 psi), Shot 4, Showing General View of Wreckage. Note Engine Remains in Background.

Fig. 3.103 B-17 (3699), Nose-in, Station 1500 (18 psi), Shot 4, Close-up View of Wrecked Engine. Note Wreckage Scattered in Background and Landing Gear Remains to Left of Engine.

Fig. 3.104 B-17 (3699), Nose-in, Station 1500 (18 psi), Shot 4, Close-up View of Engine Remains and Test Propeller. Note Wreckage in Background.

Fig. 3.105 B-17 (3699), Nose-in, Station 1500 (18 psi), Shot 4, Close-up View of Destroyed Engine, Showing Miscellaneous Wreckage in Background

Fig. 3.106 B-17 (3699), Nose-in, Station 1500 (18 psi), Shot 4, Close-up View Engine Wreckage

Fig. 3.107 F-47 (8785), Nose-in, Station 2200 (9.4 psi), Shot 4, General View of Demolished Aircraft, Showing Failure of Fuselage at Turbo Station. Note Failed Right Hand Landing Gear, Missing Outboard Wing and Wrecked Empennage.

Fig. 3.108 F-47 (8785), Nose-in, Station 2200 (9.4 psi), Shot 4, Showing Collapsed Right Landing Gear and Missing Right Wing Outboard of Outboard Landing Gear Rib. Note Fuselage Failure at Turbo Station and Empennage Wreckage.

Fig. 3.109 F-47 (8785), Nose-in, Station 2200 (9.4 psi), Shot 4, General View of Wreckage, Showing Left Wing Spar Failure Outboard of Landing Gear. Note Fuselage Failure at Turbo Station and Wrecked Empennage.

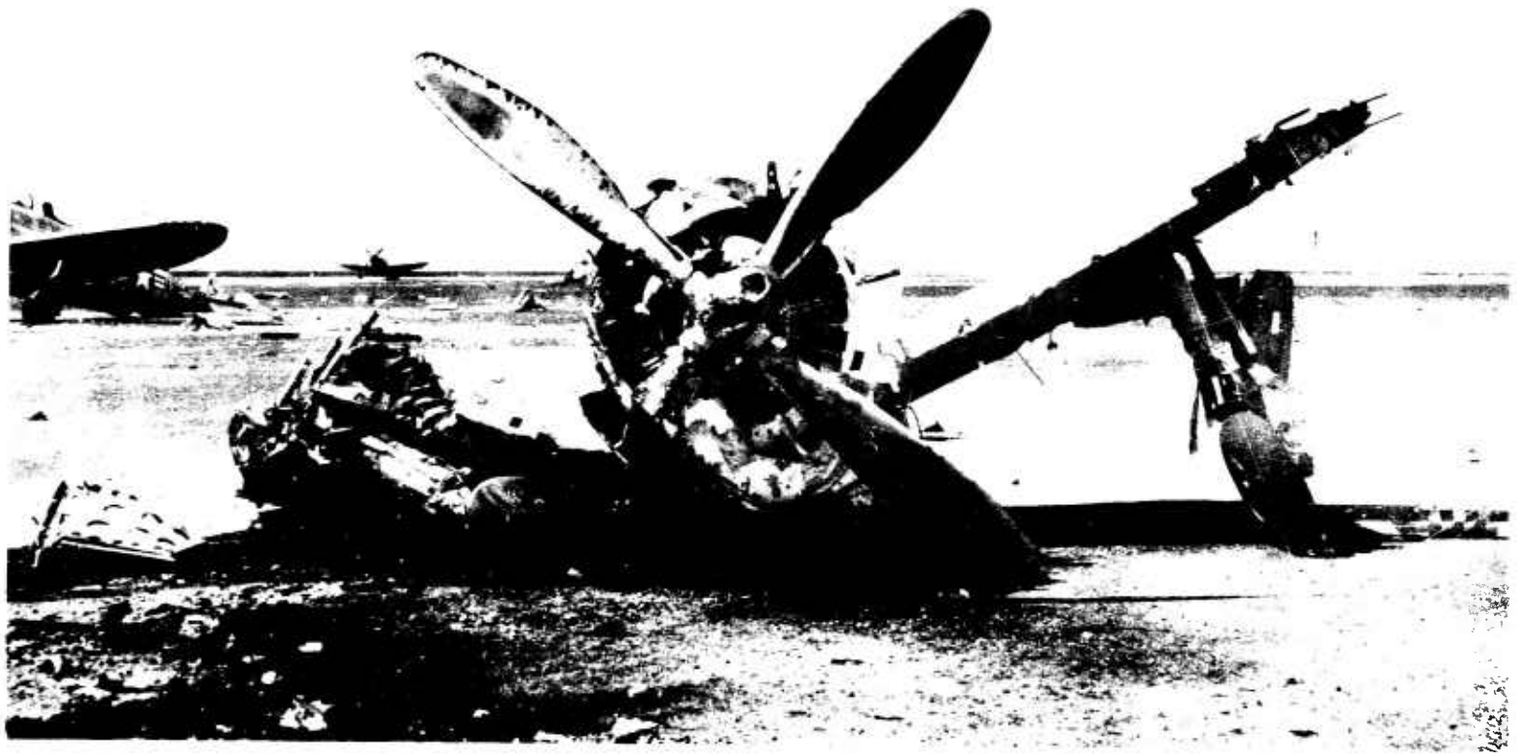

Fig. 3.110 F-47 (8785), Nose-in, Station 2200 (9.4 psi), Shot 4, Showing Right and Left Wing Failure and Collapsed Right Landing Gear

Fig. 3.111 F-47 (9931), Left Side-in, Station 2500 (8.9 psi), Shot 4, Showing Fuselage Broken Off Behind Cockpit. Note Shredded Wing Tips and Collapsed Right Hand Main Landing Gear.

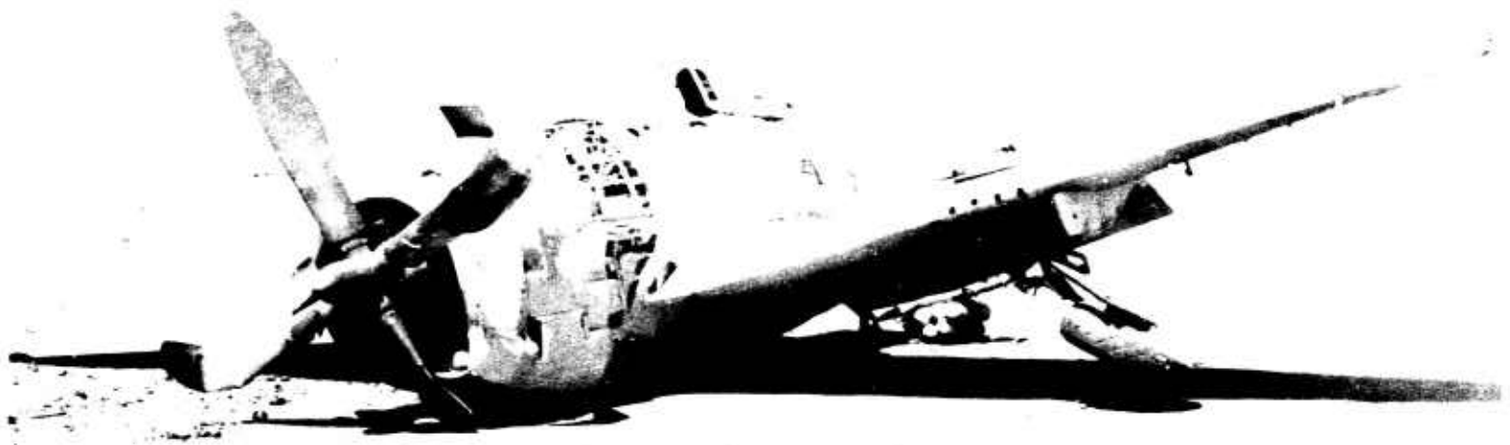

Fig. 3.112 F-47 (9931), Left Side-in at Station 2500 (8.9 psi), Shot 4, Showing Burned and Buckled Fuselage and Broken Wing Tips. Note Collapsed Right Landing Gear and Badly Bent Left Landing Gear.

Fig. 3.113 F-47 (9719), Nose-in, Station 2500 (8.9 psi), Shot 4, Showing Absence of Virtually Disintegrated Empennage. Note Fuselage Failure Near Intercooler Exit.

Fig. 3.114 F-47 (9719), Nose-in, Station 2500 (8.9 psi), Shot 4, Showing Bent Propellers Due to Contact With Ground. Note Holes Burned and Sandblasted in Leading Edge of Cowl.

Fig. 3.115 F-47 (9719), Nose-in, Station 2500 (8.9 psi), Shot 4, Close-up View of Windshield and Canopy Damage

Fig. 3.116 F-86 (8209), Nose-in, Station 2500 (8.9 psi), Shot 4, Showing General Condition of Aircraft. Note Broken Tip of Left Wing Due to Contact With Ground.

Fig. 3.117 F-86 (8209), Nose-in, Station 2500 (8.9 psi), Shot 4, Close-up View from Left Side of Severely Buckled and Torn Fuselage Section

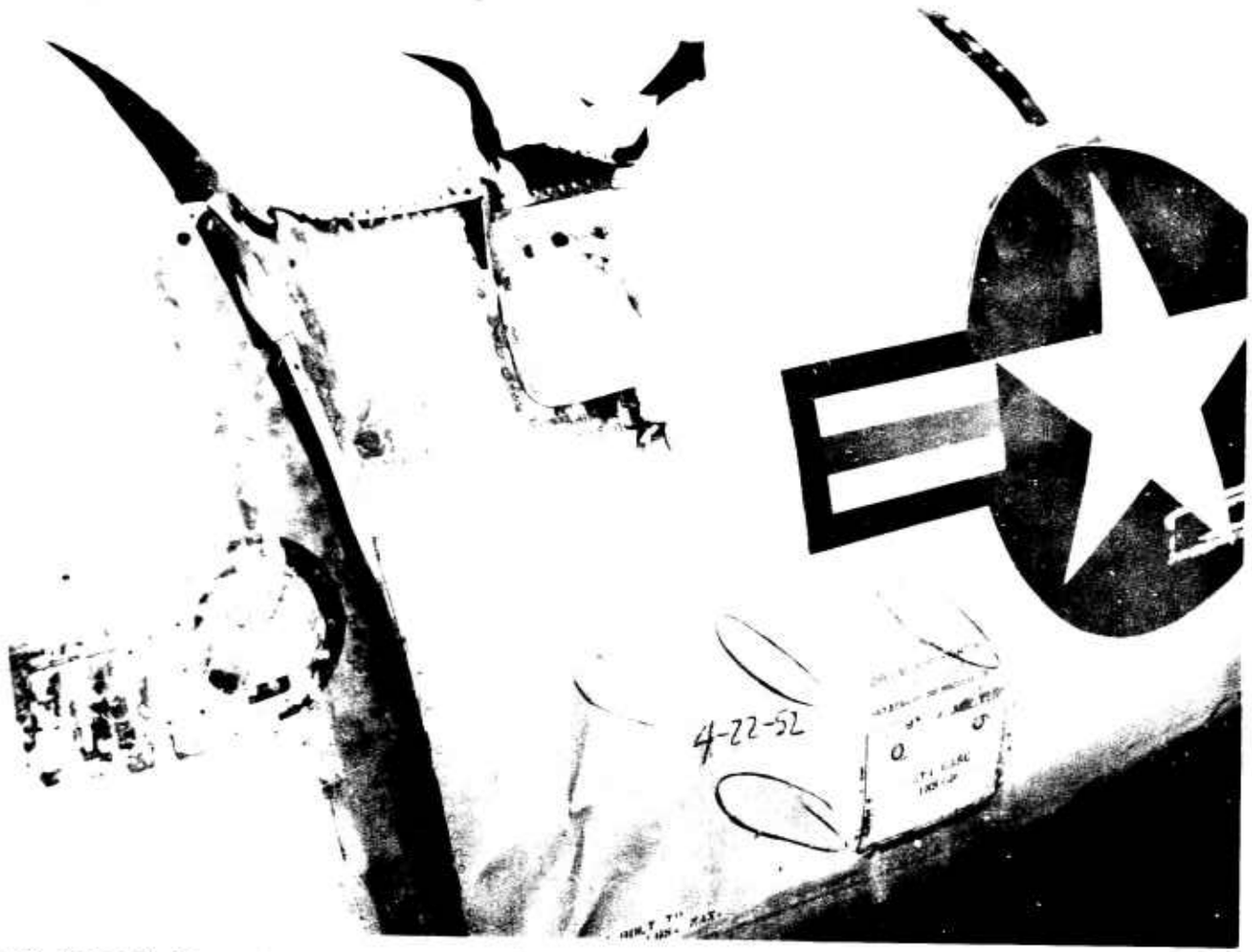

Fig. 3.118 F-86 (8209), Nose-in, Station 2500 (8.9 psi), Shot 4, Close-up View from Left Side of Severely Buckled and Torn Fuselage Section Just Forward of Dorsal Fin

Fig. 3.119 F-90 (6688), Left Side-in, Station 2500 (8.9 psi), Shot 4, General View of Wreckage, Showing Position of Rear Section After Being Torn Off at Removable Joint. The Severed Aft Section Initially Restrained By the Control Cables Swung on an Arc and Came to Rest Aligned With the Nose of the Aircraft.

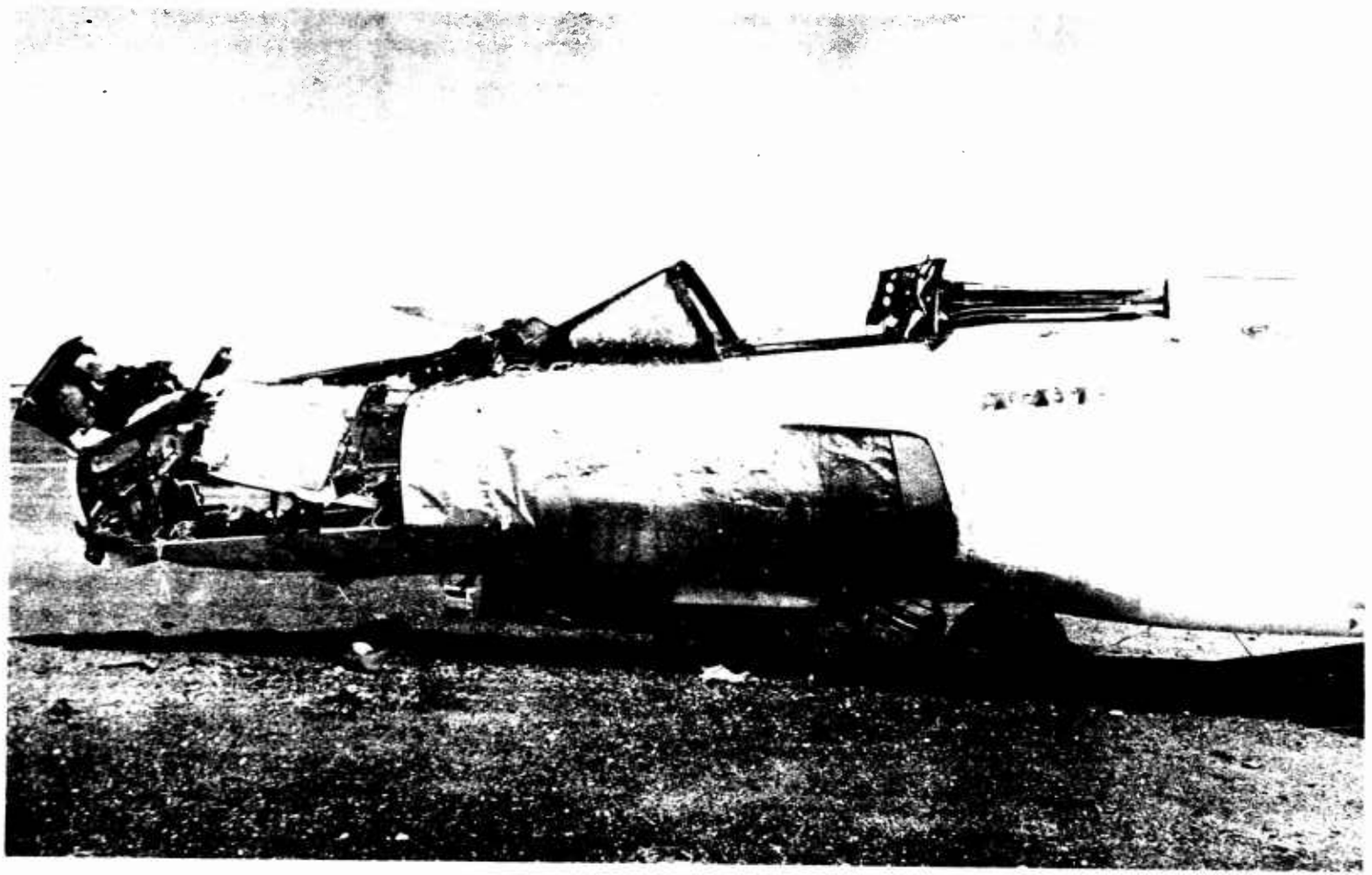

Fig. 3.120 F-90 (6688), Left Side-in, Station 2500 (8.9 psi), Shot 4, Showing Shredded Nose Compartment, Collapsed Landing Gear, and Destroyed Canopy. Note Caved-in and Sand-blasted Skin.

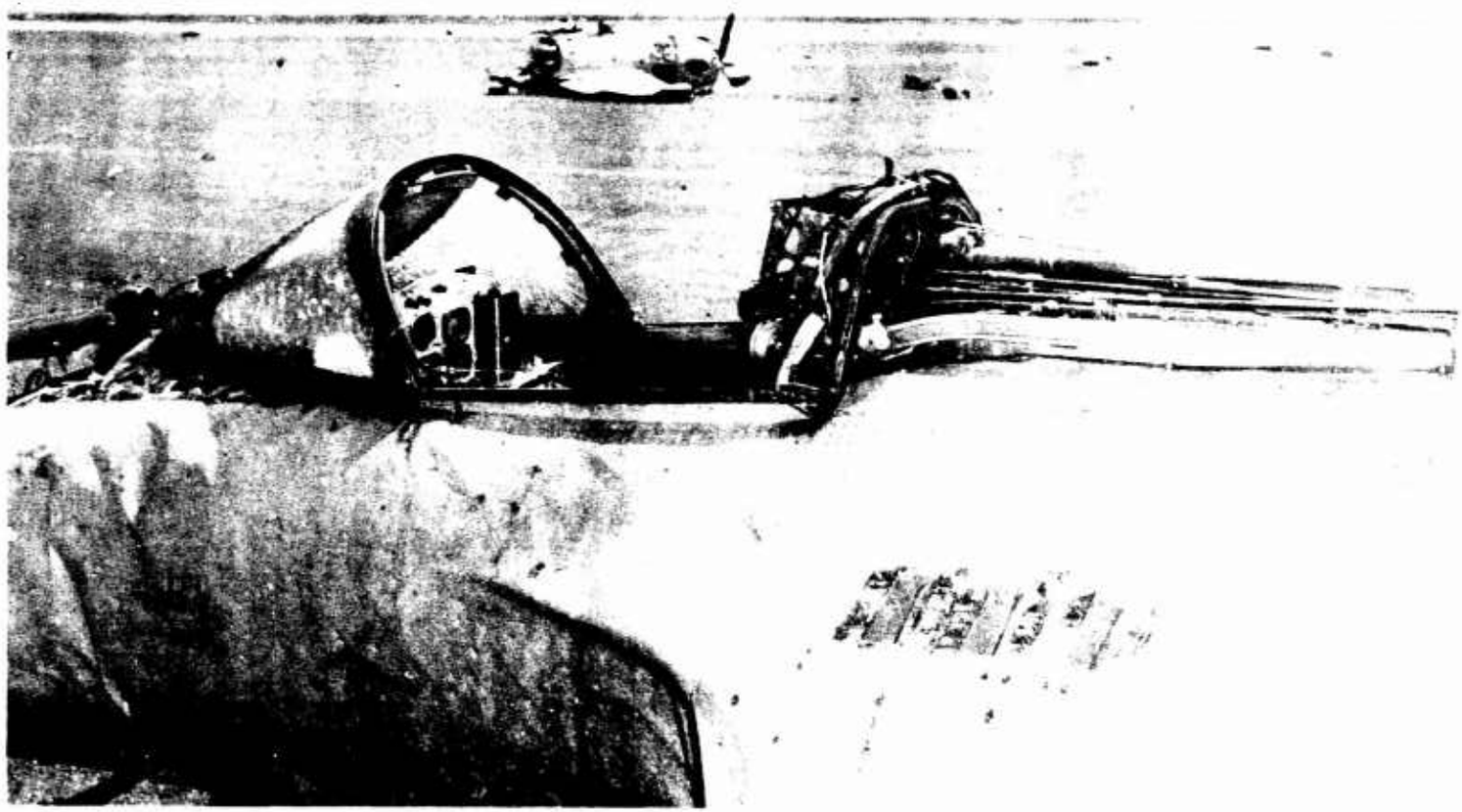

Fig. 3.121 F-90 (6688), Left Side-in, Station 2500 (8.9 psi), Shot 4, Close-up View of Destroyed Cockpit. Note Caved-in and Sandblasted Skin.

[redacted]

Fig. 3.122 B-00 (6688) Left sideing Station 2500 (R) pair Shot 1, Close-up Turned 90 deg. Nine cameras

[redacted]

Fig. 3.123 F-90 (6688), Left Side-in, Station 2500 (8.9 psi), Shot 4, Showing Aft Fuselage and Tail Assembly Wreckage. Note Missing Tail Cone and Severe Sandblasting and Thermal Effects.

Fig. 3.124 F-90 (6688), Left Side-in, Station 2500 (8.9 psi), Shot 4, Showing Aft Fuselage and Tail Assembly Wreckage.

Fig. 3.125 F-90 (6688), Left Side-in, Station 2500 (8.9 psi), Shot 4, Close-up View of Wrecked Empennage, Showing Broken Right Stabilizer

Fig. 3.126 F-47 (9072), Nose-in, Station 3320 (6.9 psi), Shot 4, Showing General Post-shot Condition of Aircraft. Note Collapsed Tail Wheel. Compare with Figure 3.50.

Fig. 3.127 F-47 (3828), Tail-in, Station 3450 (6.5 psi), Shot 4, Showing Buckled, Bent, and Torn-off Control Surfaces

Fig. 3.128 F-47 (3828), Tail-in, Station 3450 (6.5 psi), Shot 4, Close-up View of Buckled Skin Panels on Fuselage, and Inboard Section of Right Wing with Dismembered Flap. Compare with Figure 3.79.

Fig. 3.129 B-45 (9481), Nose-in, Station 3450 (6.5 psi), Shot 4, General View of Aircraft, Showing Forward Bomb-bay Doors Hanging Loose and Main Landing Gear Doors Broken Open

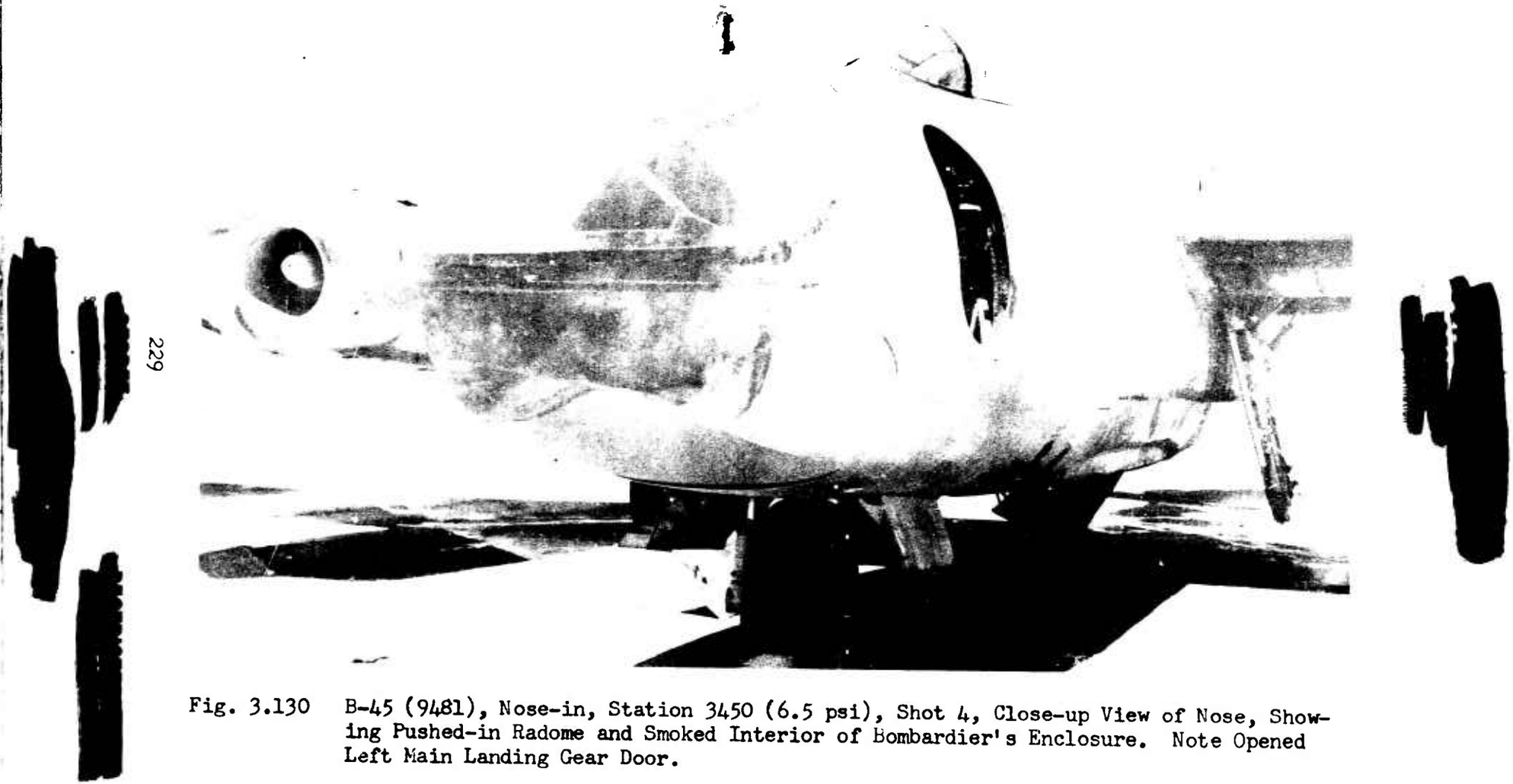

Fig. 3.130 B-45 (9481), Nose-in, Station 3450 (6.5 psi), Shot 4, Close-up View of Nose, Showing Pushed-in Radome and Smoked Interior of Bombardier's Enclosure. Note Opened Left Main Landing Gear Door.

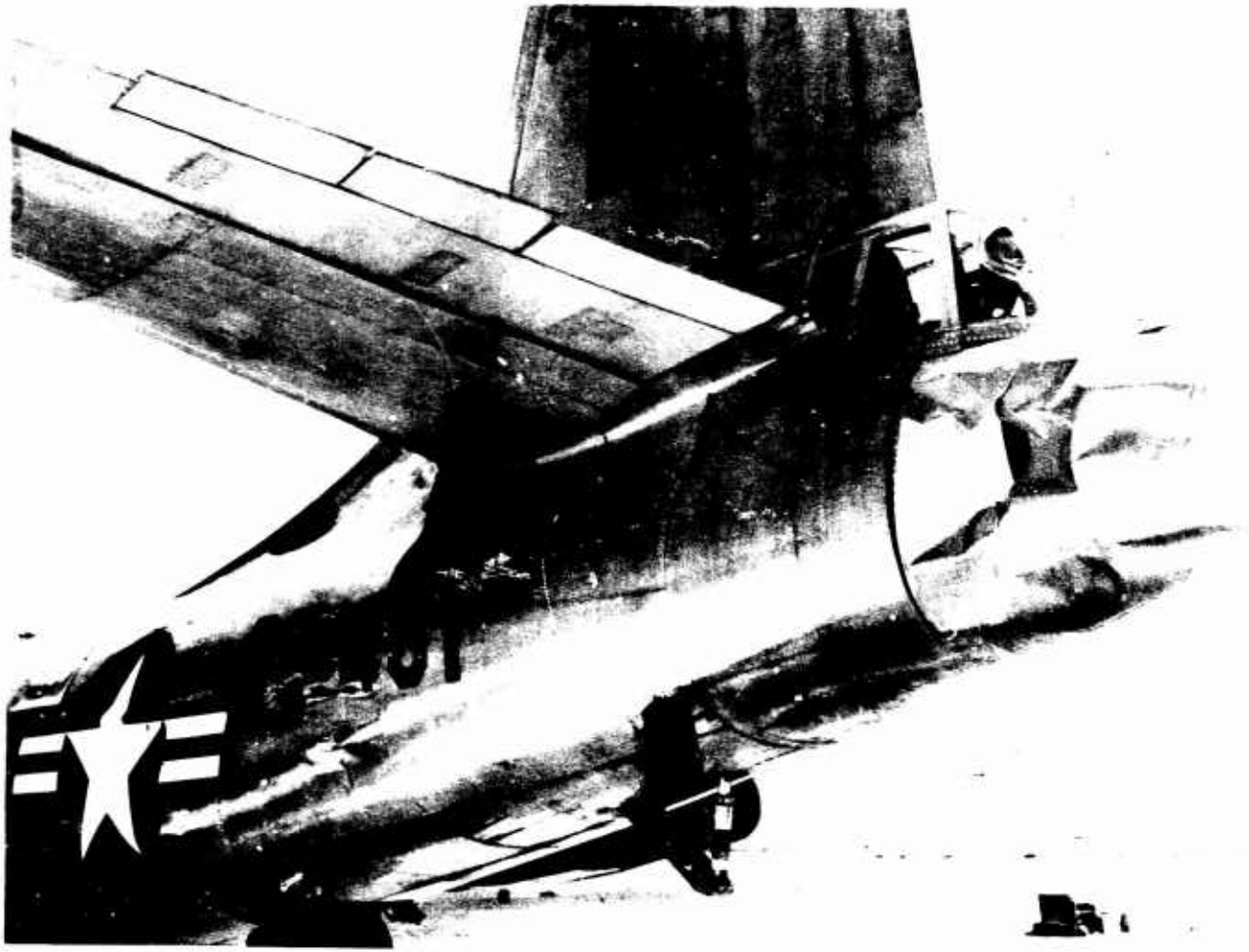

Fig. 3.131 B-45 (9481), Nose-in, Station 3450 (6.5 psi), Shot 4, Close-up View of Empennage, Showing Tail Cone Failure and Buckled Skin on Fuselage Just Below Serial Number. Fuselage Frames Were Failed Along Buckles.

U.S. AIR FORCE
559481

Fig. 3.132 B-45 (9481), Nose-in, Station 3450 (6.5 psi), Shot 4, Close-up View of Empennage, Showing Increased Caving-in of Fairing Between Dorsal and Vertical Fin. Compare with Figure 3.75.

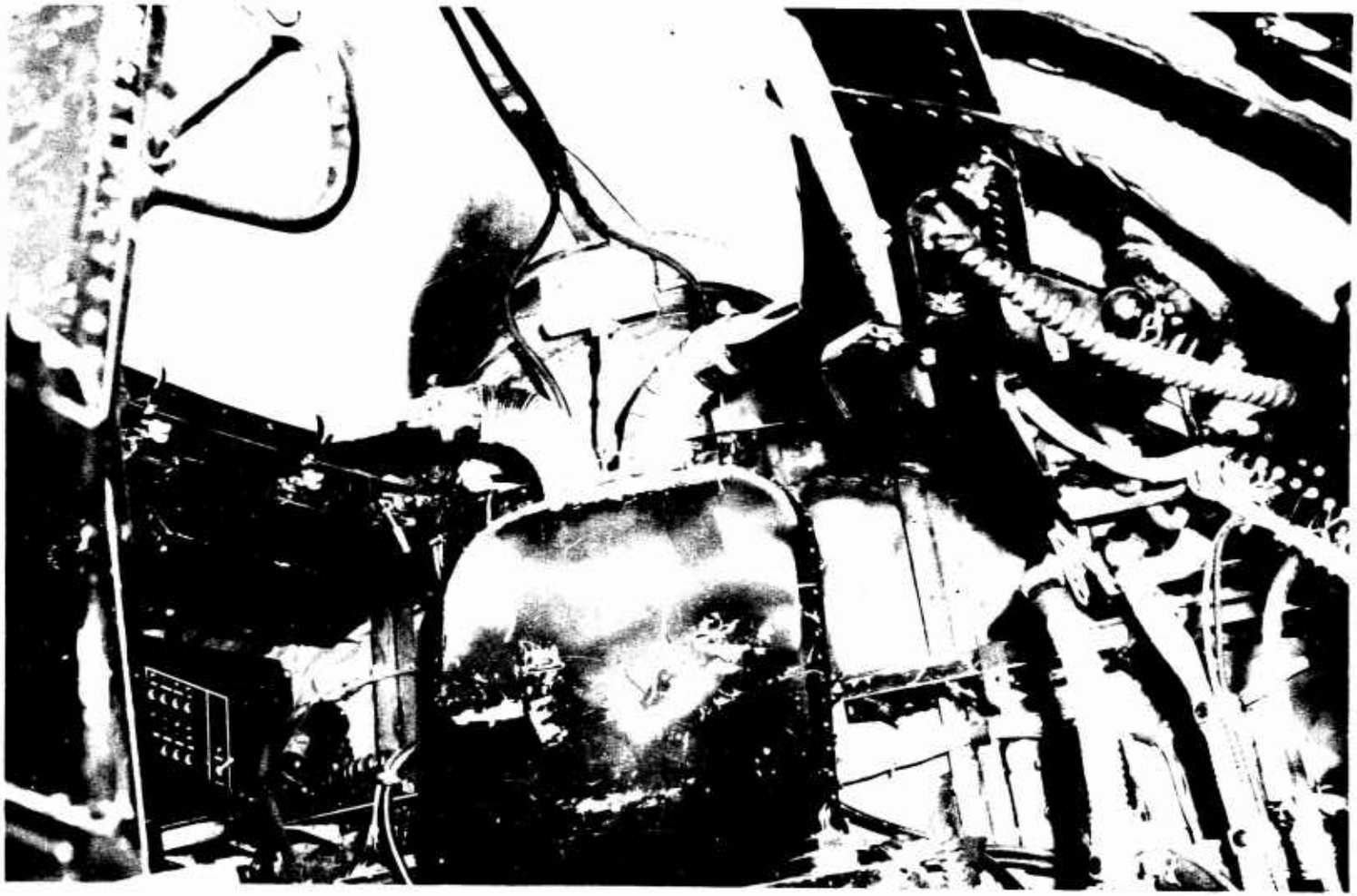

Fig. 3.133 B-45 (9481), Nose-in, Station 3450 (6.5 psi), Shot 4, Interior View of Cockpit, Showing Charred Upholstery

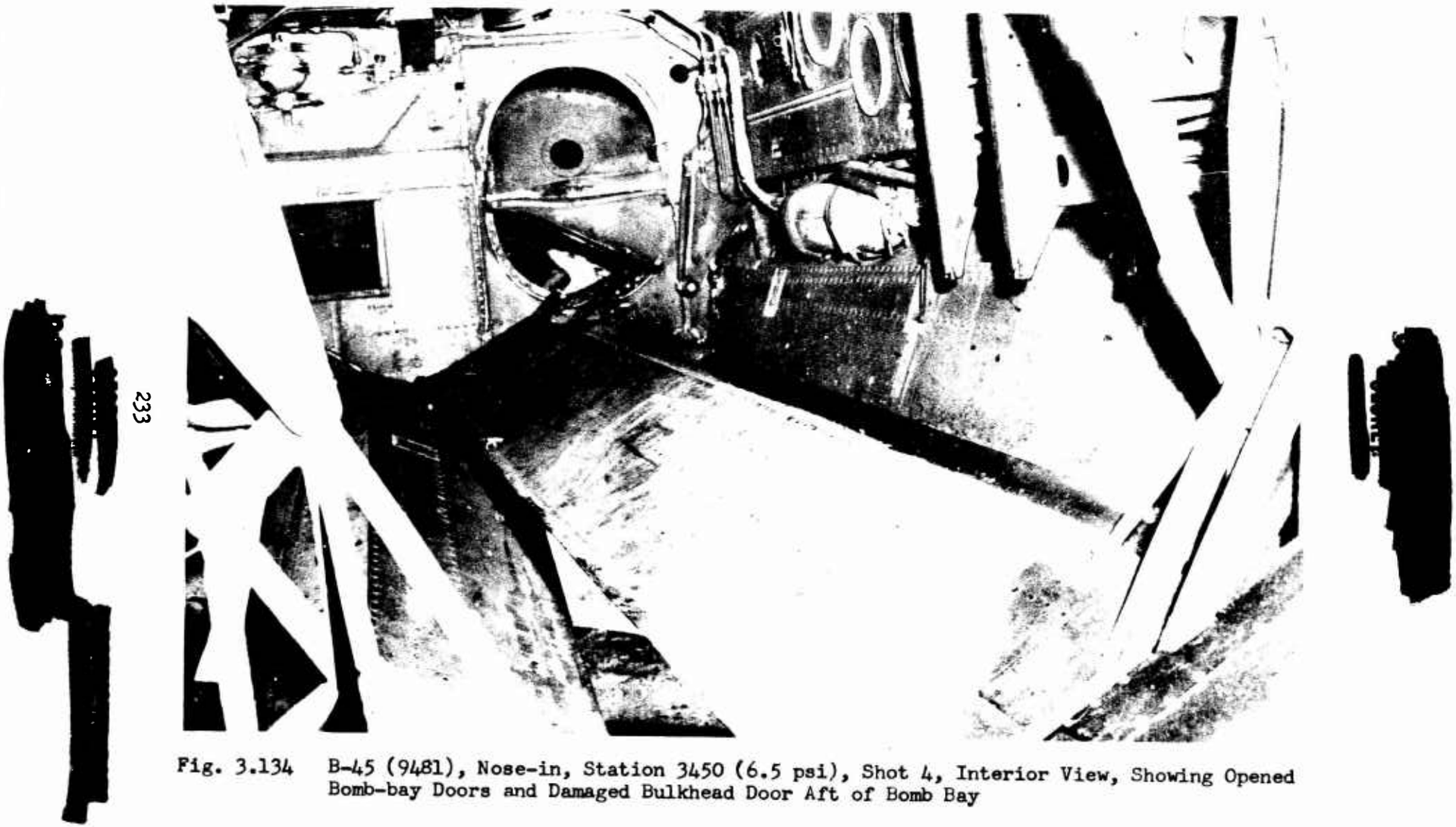

Fig. 3.134 B-45 (9481), Nose-in, Station 3450 (6.5 psi), Shot 4, Interior View, Showing Opened Bomb-bay Doors and Damaged Bulkhead Door Aft of Bomb Bay

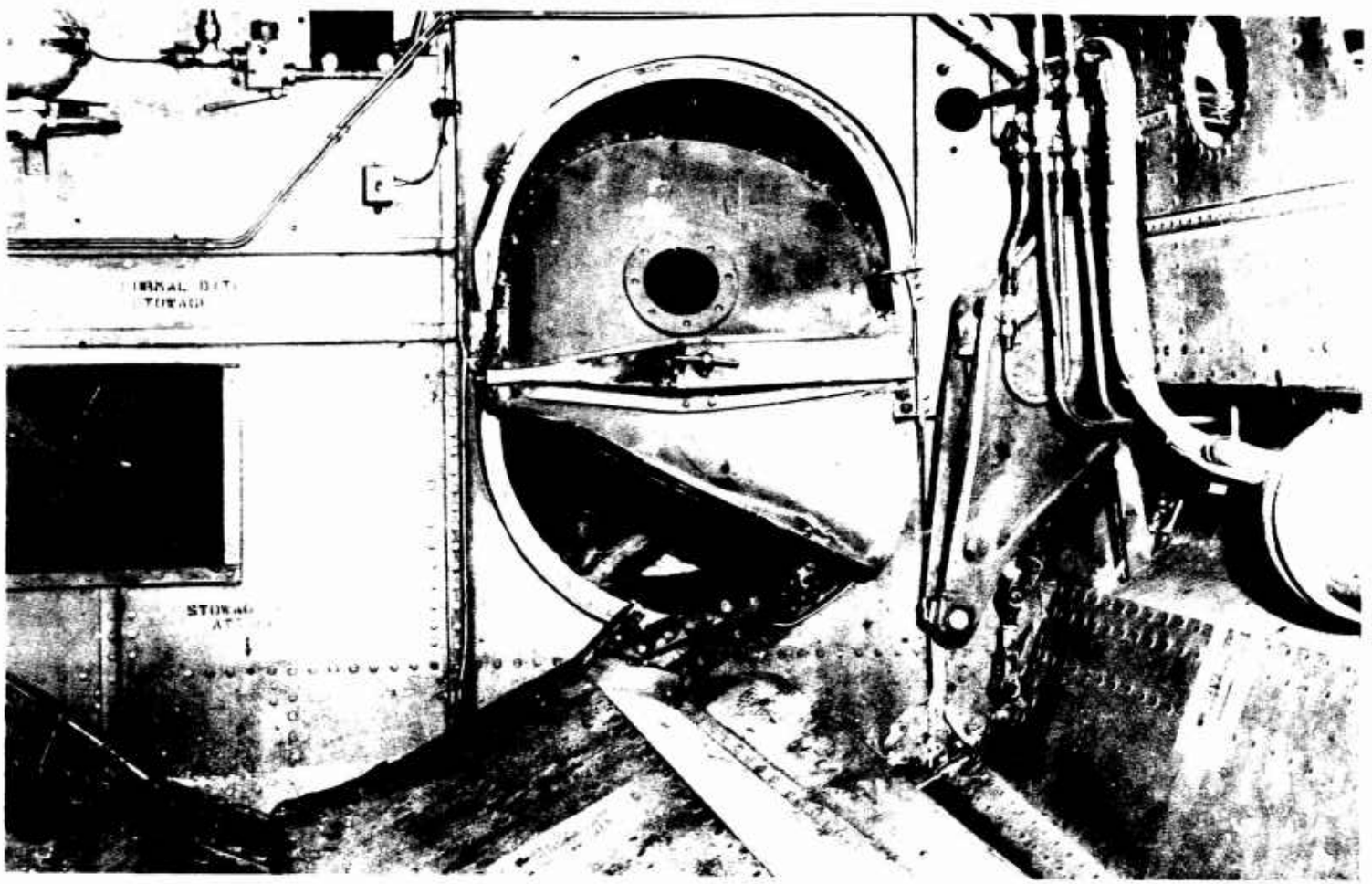

Fig. 3.135 B-45 (9481), Nose-in, Station 3450 (6.5 psi), Shot 4, Close-up View (Looking Aft) of Twisted Bulkhead Door and Bent Bulkhead Vertical Stiffeners. Note Broken Bomb-bay Door Actuating Mechanism Beneath Bulkhead Door.

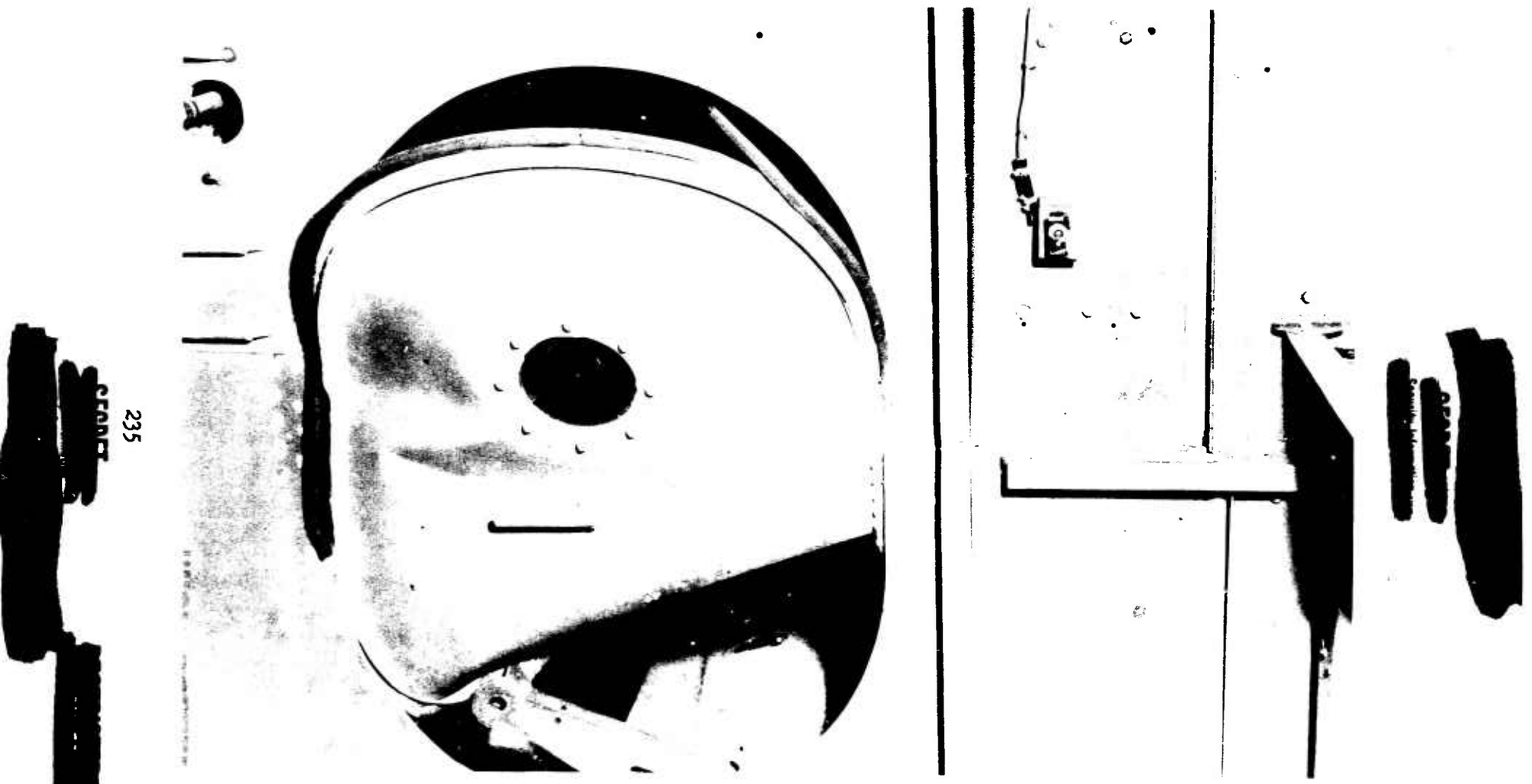

Fig. 3.136 B-45 (9481), Nose-in, Station 3450 (6.5 psi), Shot 4, Close-up View (Looking Forward) of Damaged Bulkhead Door Just Aft of Bomb Bays

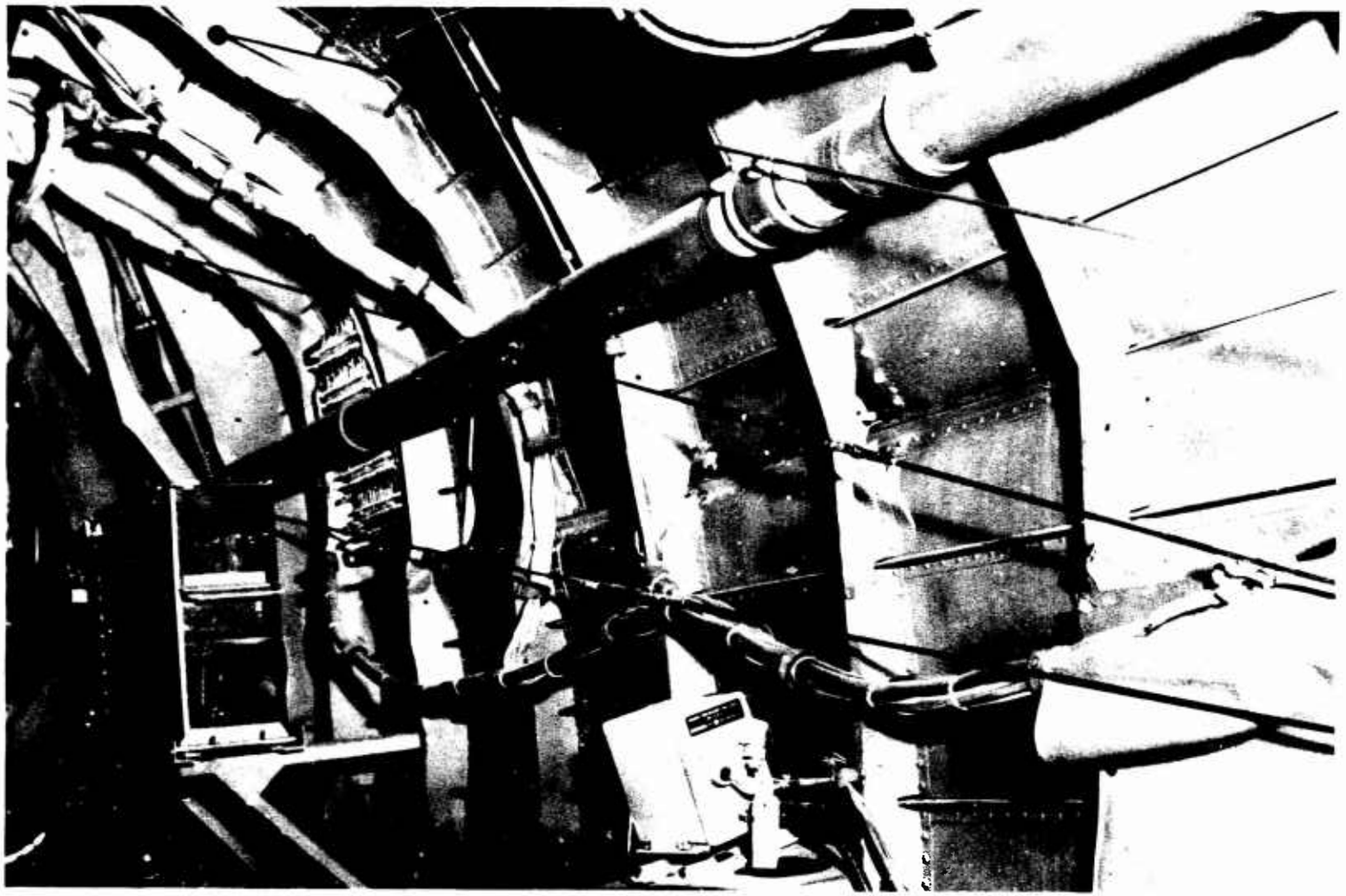

Fig. 3.137 B-45 (9481), Nose-in, Station 3450 (6.5 psi), Shot 4, Interior View of Bent Fuselage Frames and Pushed-in Skin

Fig. 3.138 F-47 (9785), Left Side-in, Station 4000 (5.8 psi), Shot 4, Showing Severely Buckled Left Side of Fuselage and Empennage. Note Buckle in Left Flap and Scorched Areas.

RESTRICTED DATA
SECRET

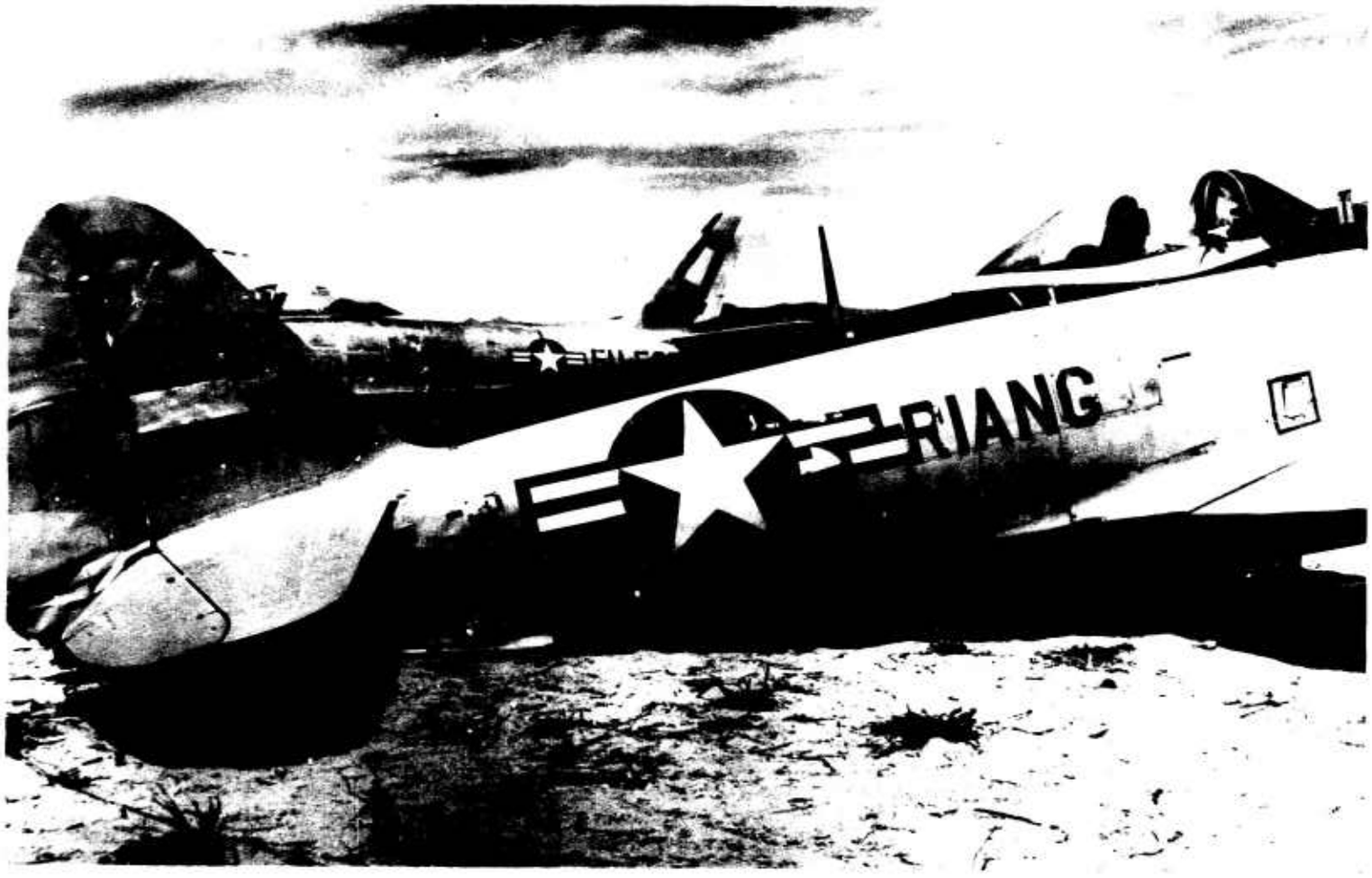

Fig. 3.139 F-47 (9785), Left Side-in, Station 4000 (5.8 psi), Shot 4, Showing Buckled Rudder and Failed Vertical Stabilizer. Note Buckled Fuselage Frame Just Forward of Horizontal Stabilizer.

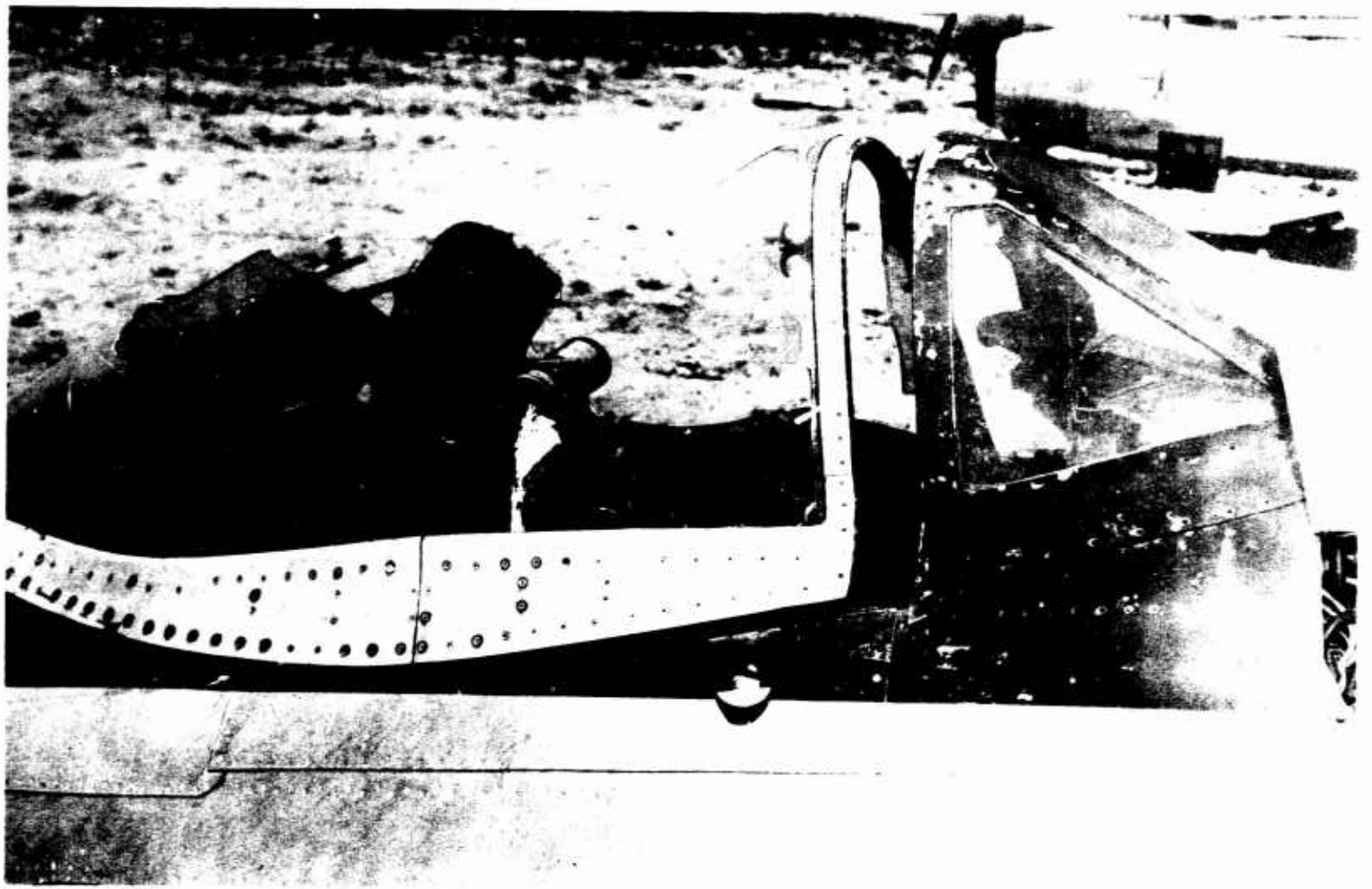

Fig. 3.140 F-47 (9785), Left Side-in, Station 4000 (5.8 psi), Shot 4, Close-up View of Destroyed Canopy

Fig. 3.141 F-47 (0065), Tail-in, Station 4000 (5.8 psi), Shot 4, Showing General Post-shot Condition of Aircraft. Note Absence of Elevator, Flap, and Aileron.

Fig. 3.142 F-47 (9074), Tail-in, Station 4000 (5.8 psi), Shot 4, Showing General Post-shot Condition of Aircraft. Note Absence of Flaps and Ailerons, and Thermal Damage to Skin of Right Elevator Outboard of Trim Tab.

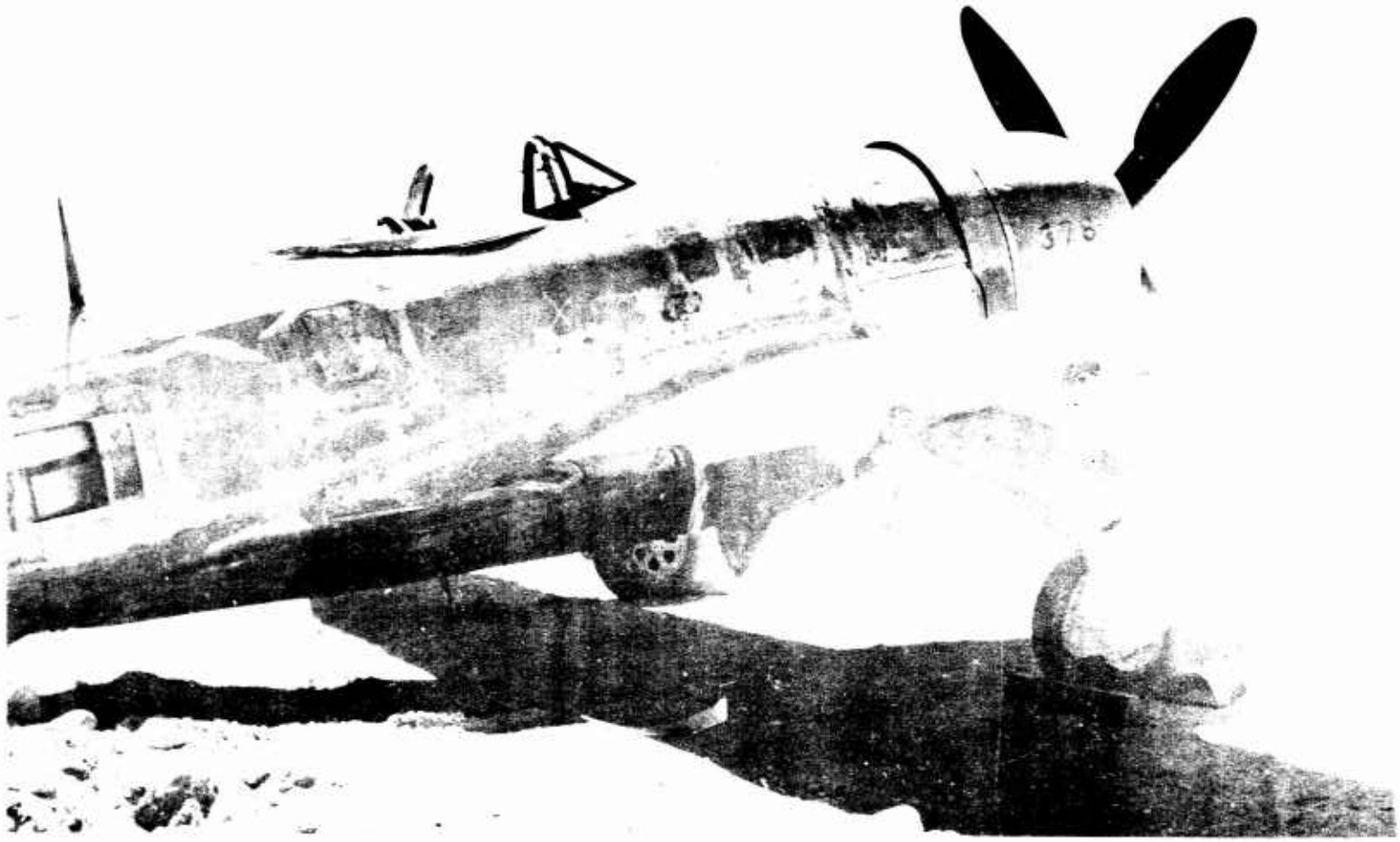

Fig. 3.143 F-47 (9074), Tail-in, Station 4000 (5.8 psi), Shot 4, Close-up View of Buckles in Fuselage and Damaged Aileron

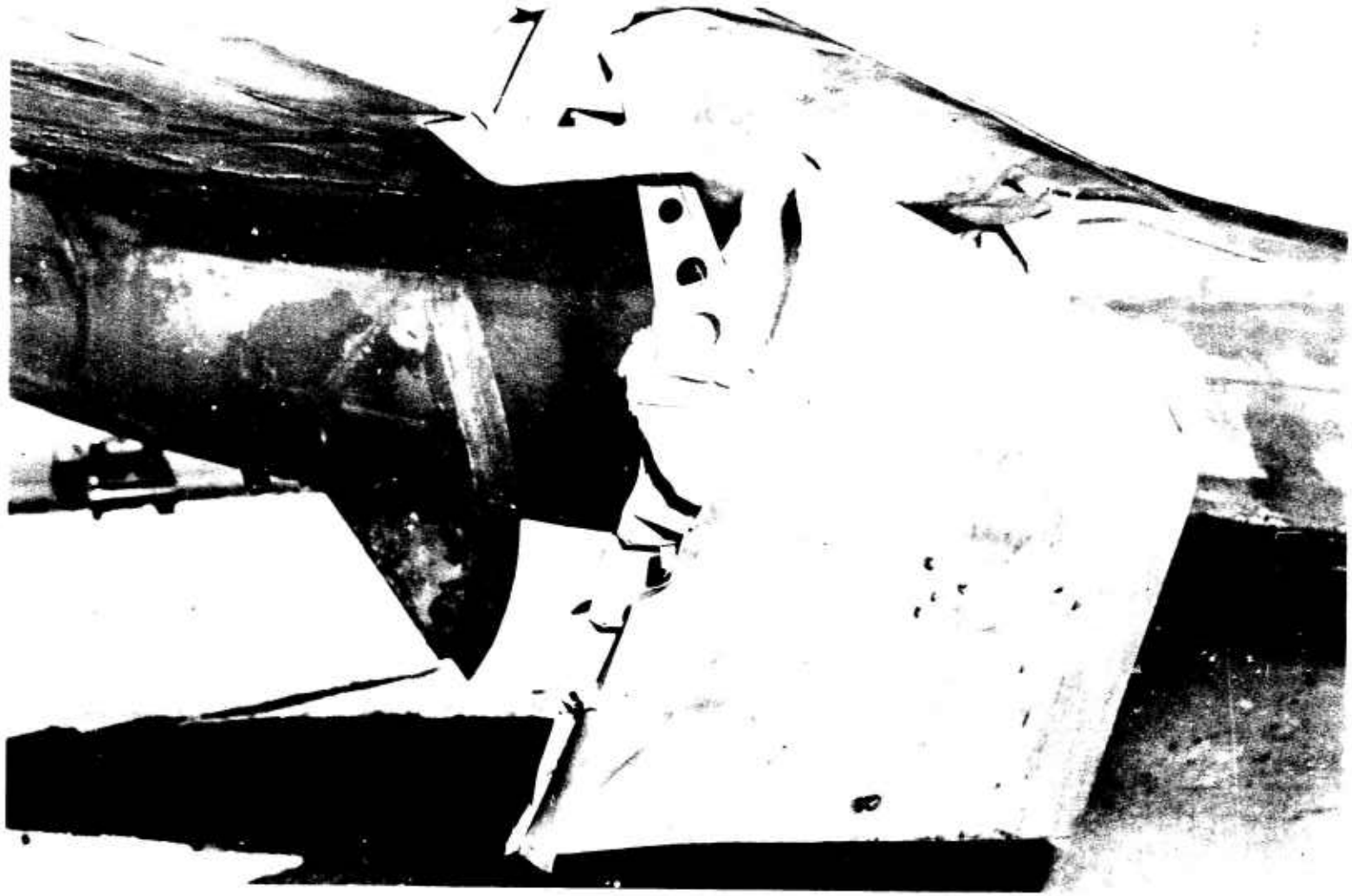

Fig. 3.144 F-47 (9074), Tail-in, Station 4000 (5.8 psi), Shot 4, Close-up View of Buckled and Torn-off Left Wing Flap. Note That Only Inboard Half of Flap Remains.

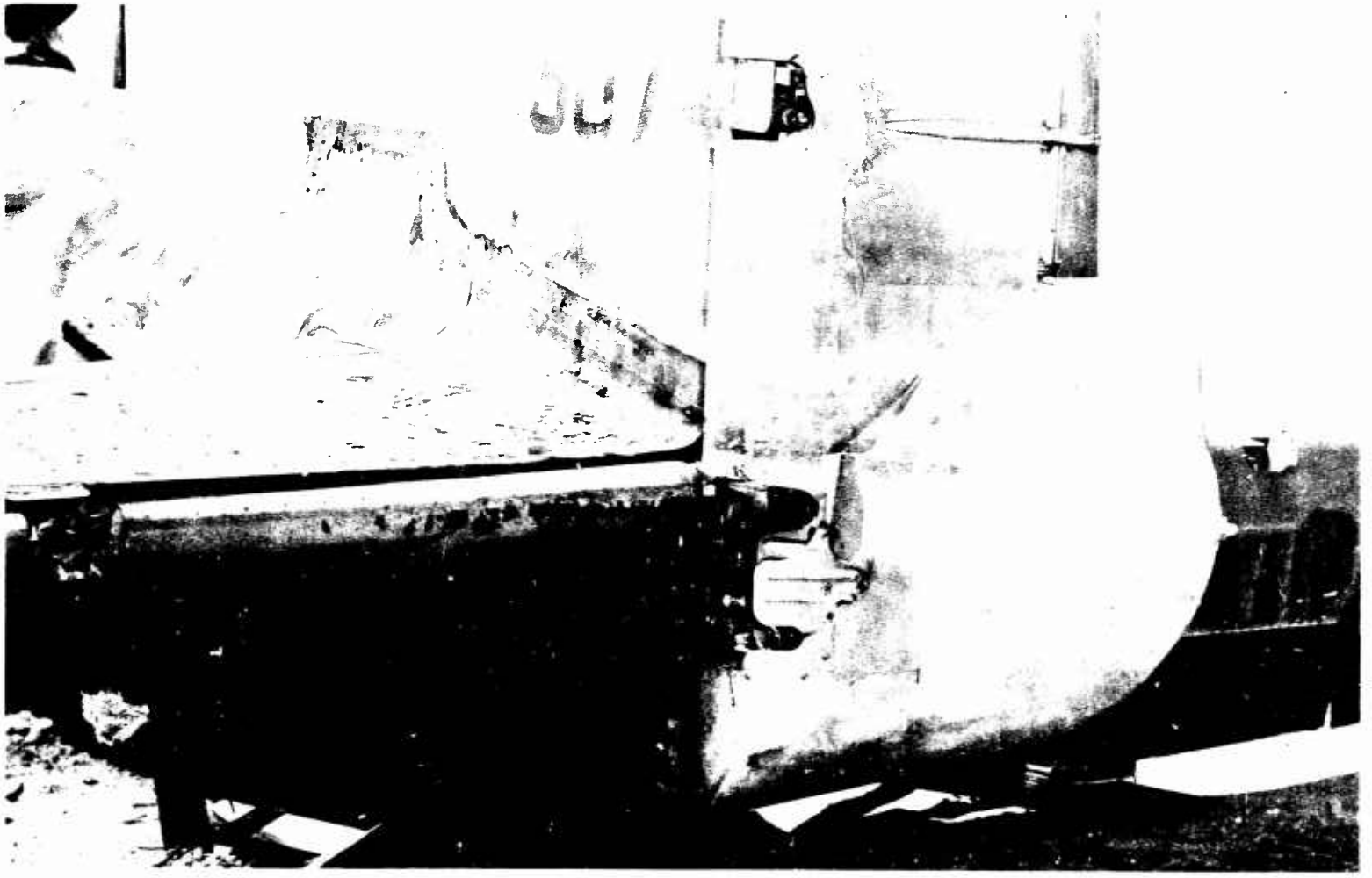

Fig. 3.145 F-47 (9074), Tail-in, Station 4,000 (5.8 psi), Shot 4, Close-up View of Empennage, Showing Failed Rudder and Elevator Hinge Brackets. Note Scorched Elevator and Horizontal Stabilizer Skin.

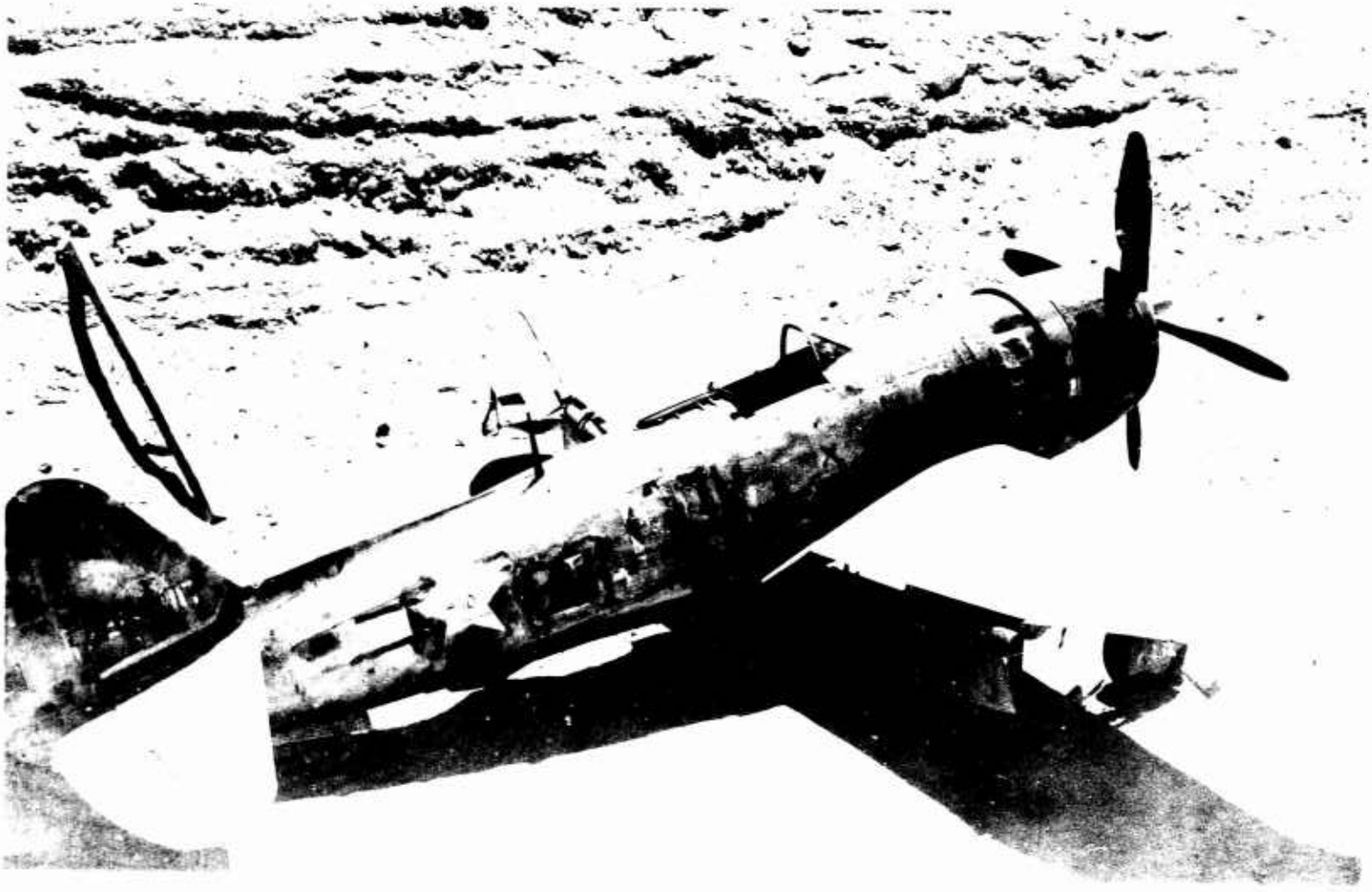

Fig. 3.146 F-47 (9110), Tail-in, in Pit Revetment, Station 4000 (5.8 psi), Shot 4, Showing Broken Wing Flaps and Fuselage Skin Buckles. Note That Right Hand Aileron Has Been Blown Off. Compare with Figure 3.39.

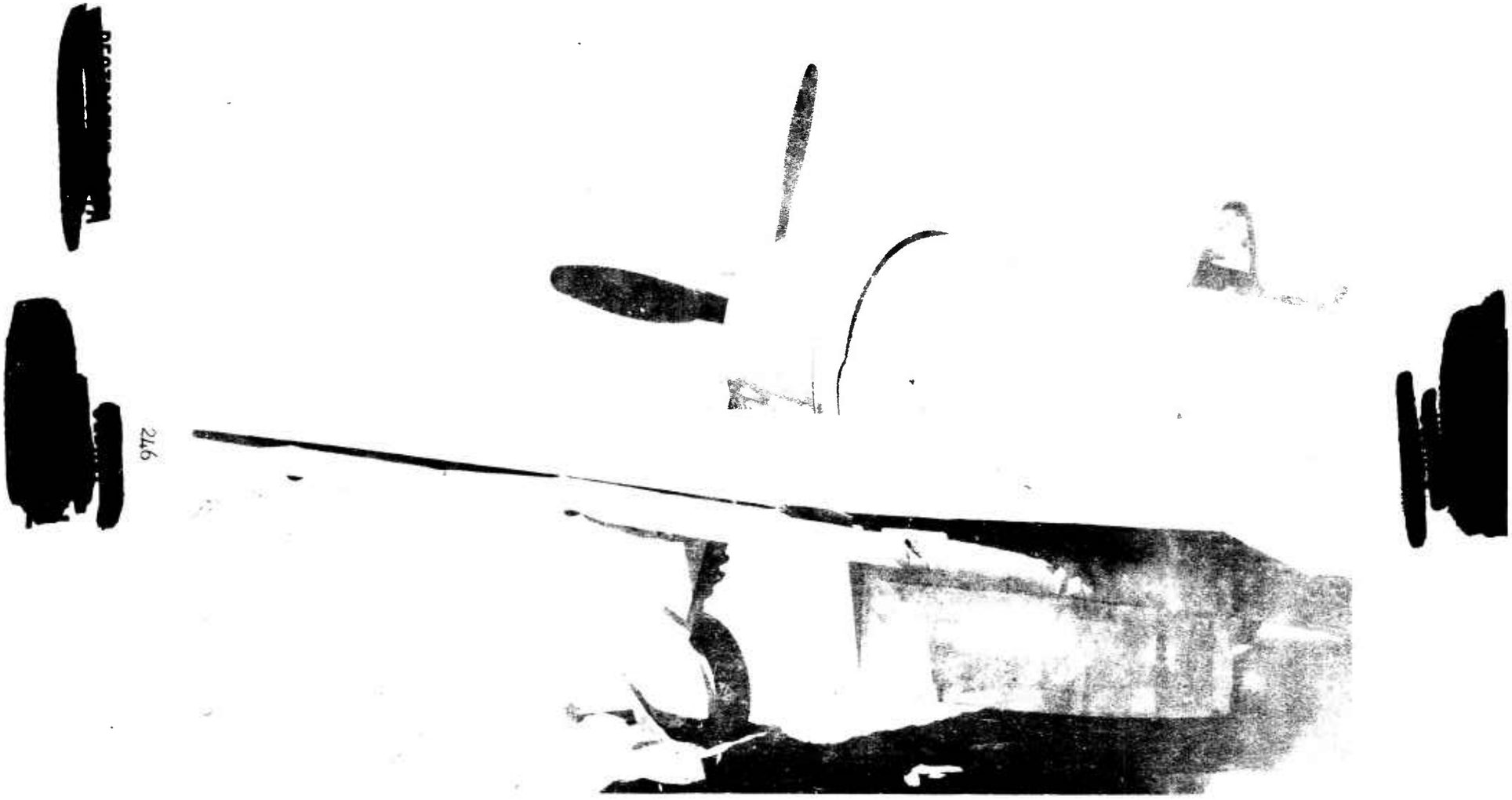

Fig. 3.147 F-47 (9110), Tail-in, in Pit Revetment, Station 4000 (5.8 psi), Shot 4, Close-up View of Buckled Left Aileron and Left Flap. Note Broken Flap Links.

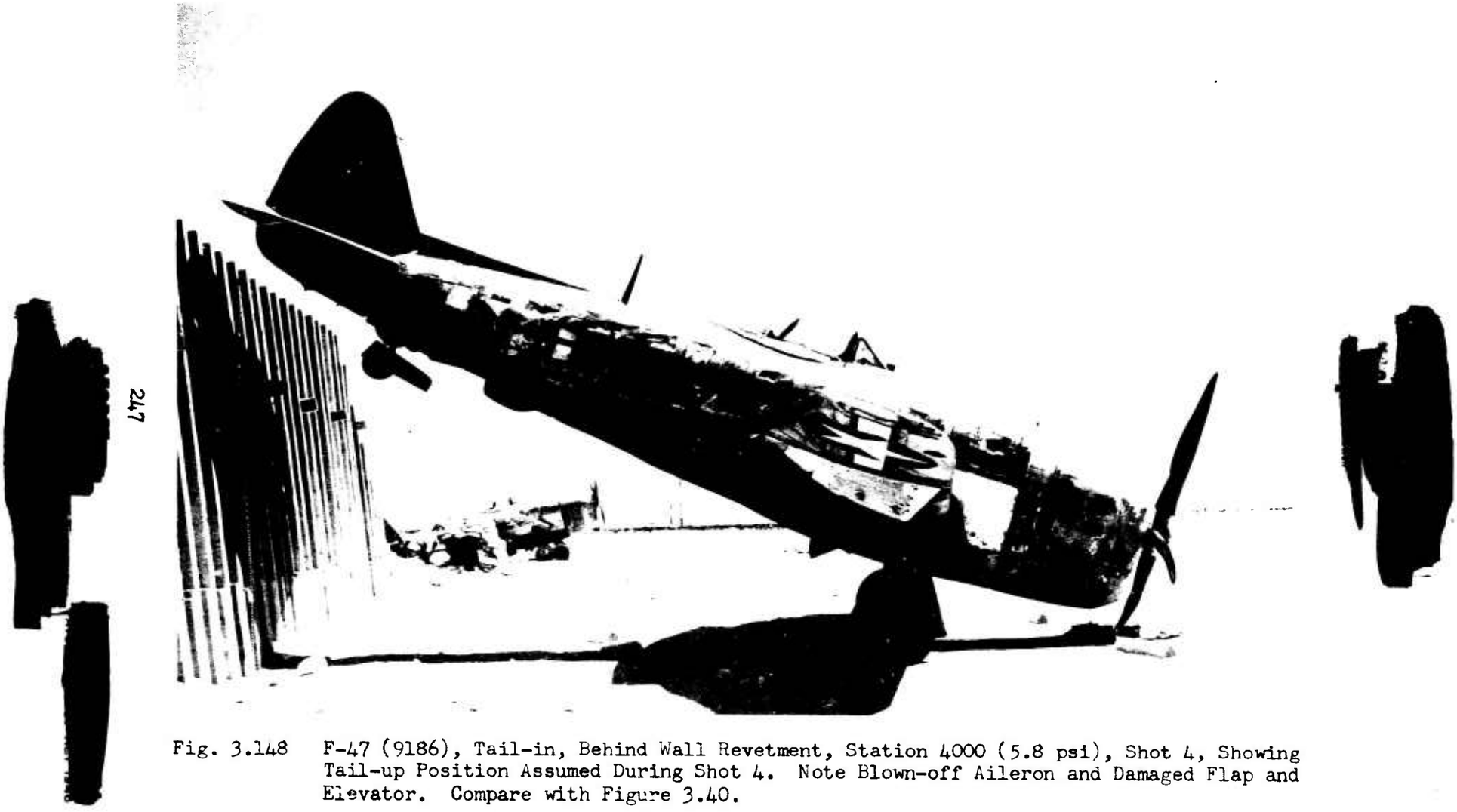

Fig. 3.148 F-47 (9186), Tail-in, Behind Wall Revetment, Station 4000 (5.8 psi), Shot 4, Showing Tail-up Position Assumed During Shot 4. Note Blown-off Aileron and Damaged Flap and Elevator. Compare with Figure 3.40.

Fig. 3.149 F-47 (9186), Tail-in, Behind Wall Revetment, Station 4000 (5.8 psi), Shot 4, Showing Position Assumed and Resulting Propeller Damage. Note Destroyed Canopy.

Fig. 3.150 F-86 (9597), Tail-in, Station 4000 (5.8 psi), Shot 4, Showing General Post-shot Condition of Aircraft. Note Blown-off Ailerons and Broken Canopy.

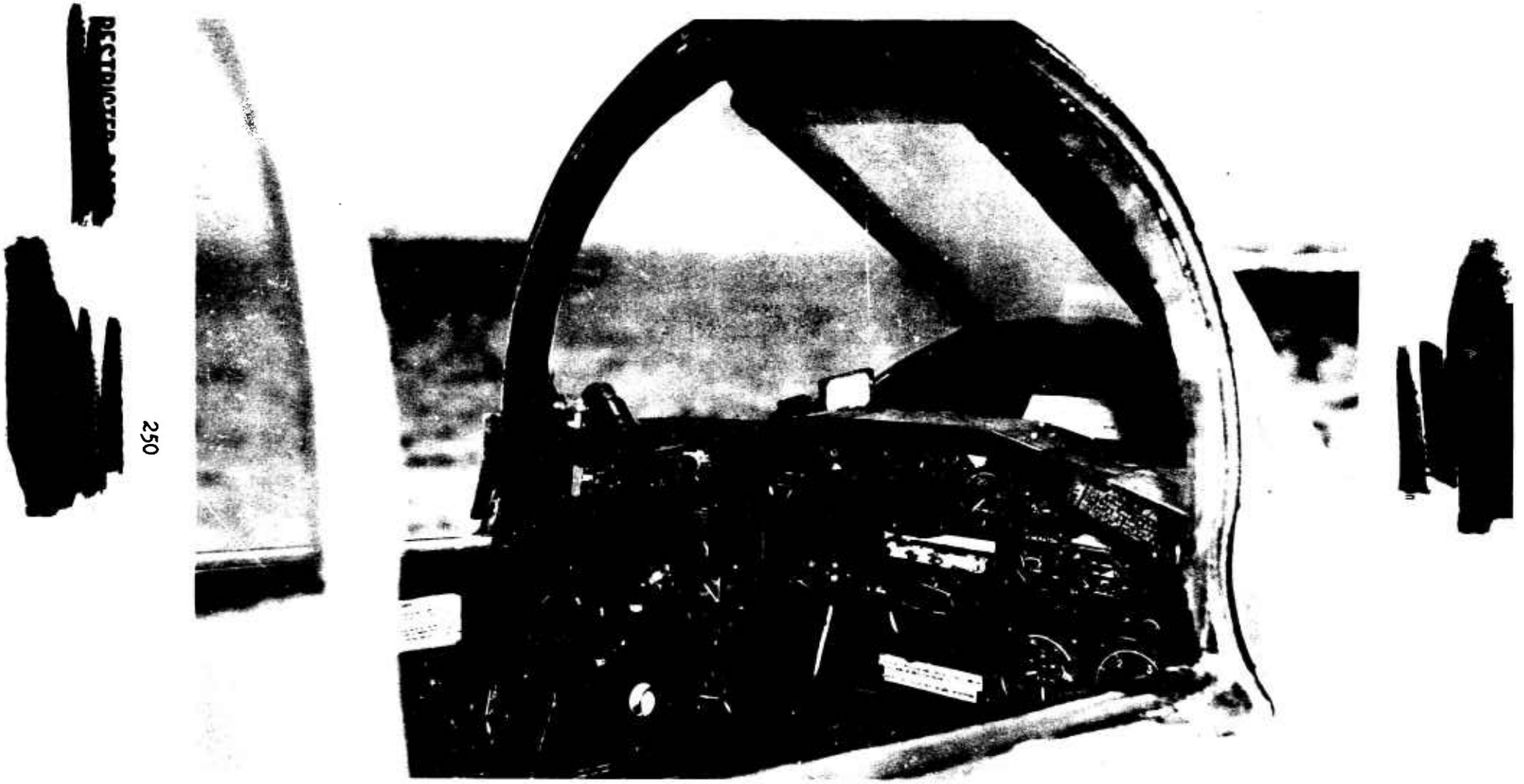

Fig. 3.151 F-86 (9597), Tail-in, Station 4000 (5.8 psi), Shot 4, Close-up View of Instrument Panel. Note Damaged Tachometer.

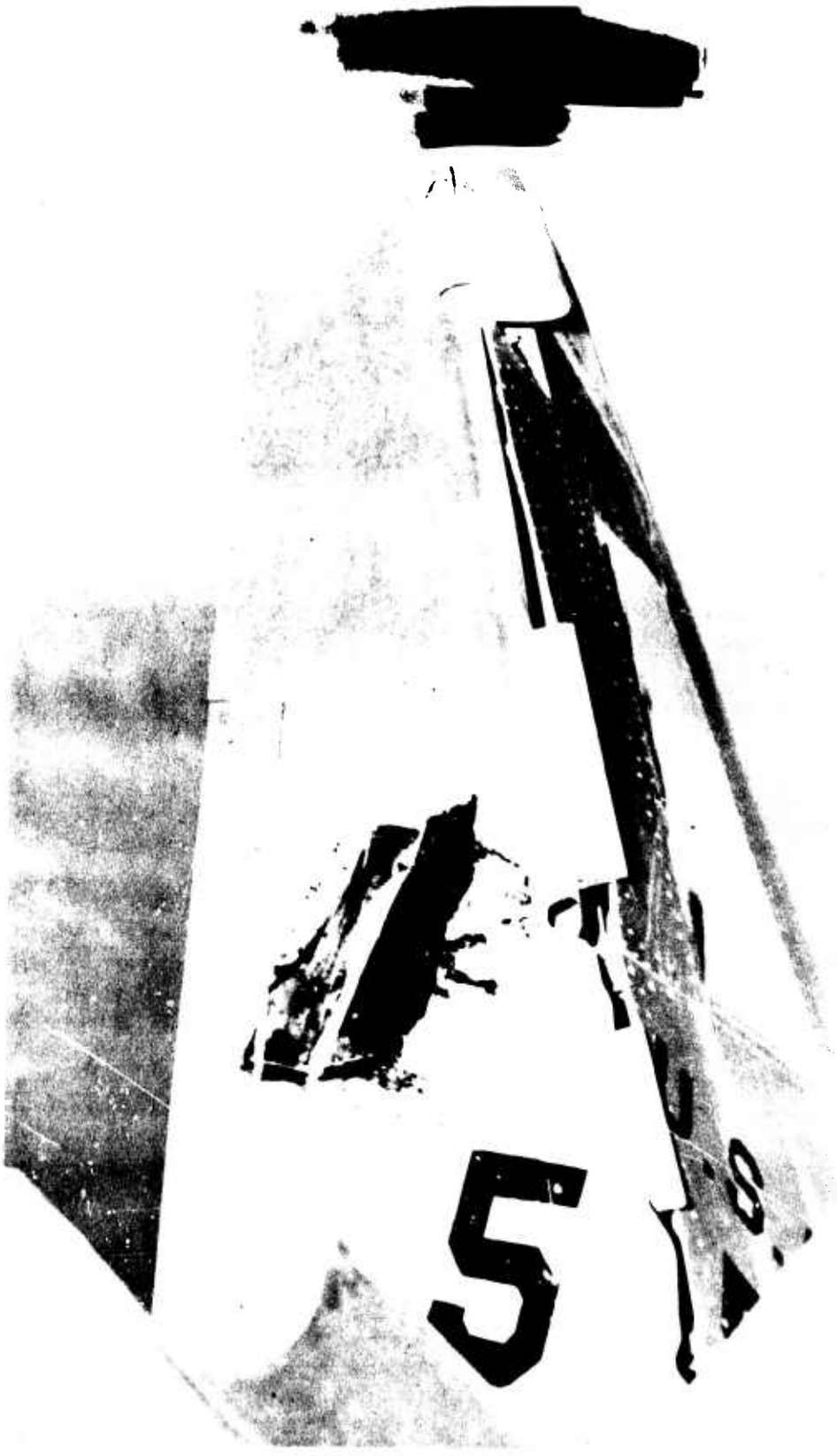

Fig. 3.152 F-86 (9597), Tail-in, Station 4000 (5.8 psi), Shot 4, Close-up View of Rudder, Showing Damage at Hinges Due to Rudder Encountering Travel Stops

Fig. 3.153 B-17 (5715), Tail-in, Station 4000 (5.8 psi), Shot 4, Showing General Post-shot Condition of Aircraft. Note Burned Empennage Control Surfaces.

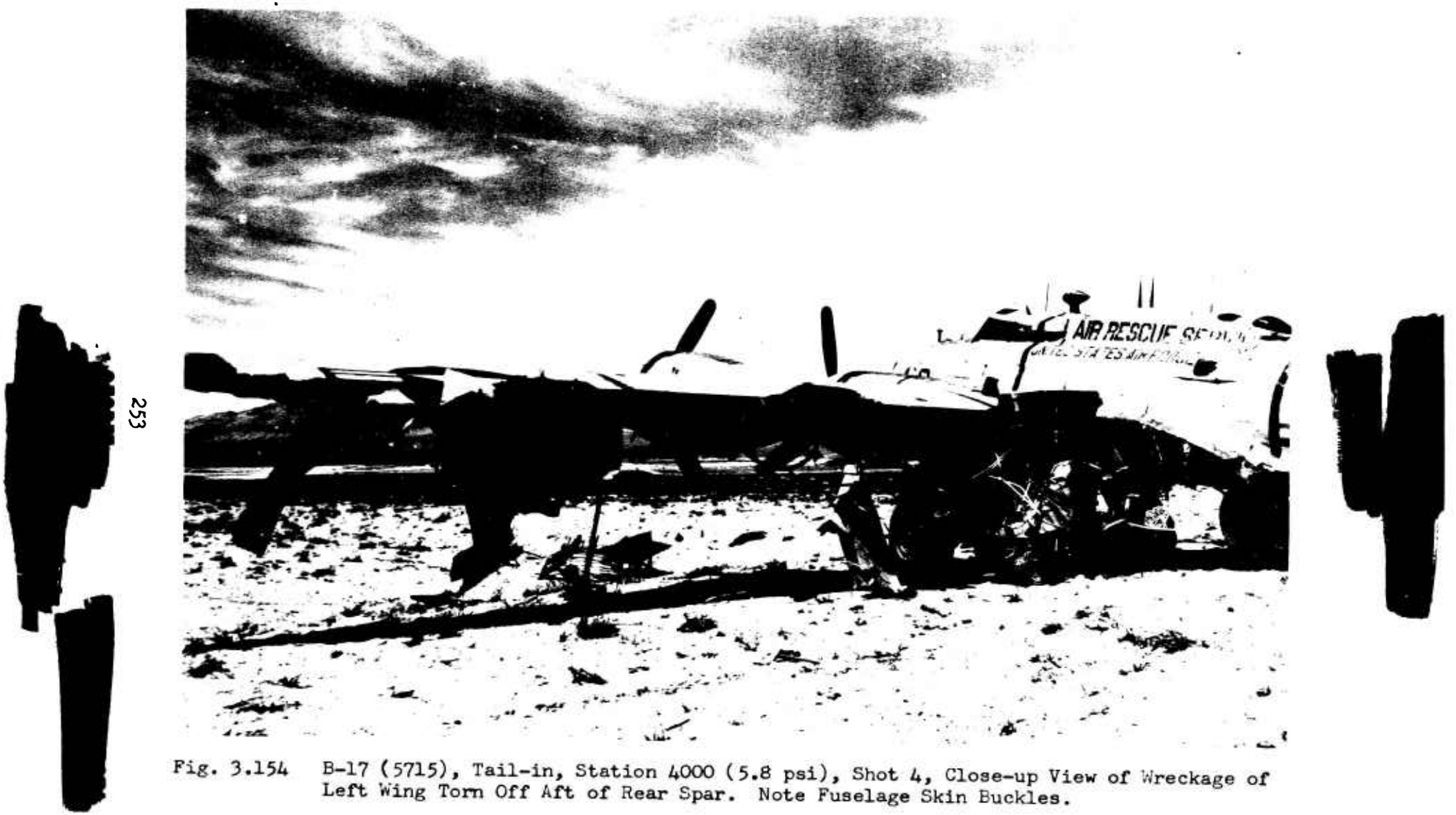

Fig. 3.154 B-17 (5715), Tail-in, Station 4000 (5.8 psi), Shot 4, Close-up View of Wreckage of Left Wing Torn Off Aft of Rear Spar. Note Fuselage Skin Buckles.

Fig. 3.155 B-17 (5715), Tail-in, Station 4000 (5.8 psi), Shot 4, Close-up View of Completely Buckled Fuselage and Wreckage of Right Wing Torn Off Aft of Rear Spar

Fig. 3.156 B-29 (7349), Nose-in, Station 5000 (4.0 psi), Shot 4, Showing General Post-shot Condition of Aircraft. Note Nose Section and Nose Landing Gear Completely Destroyed By Fire.

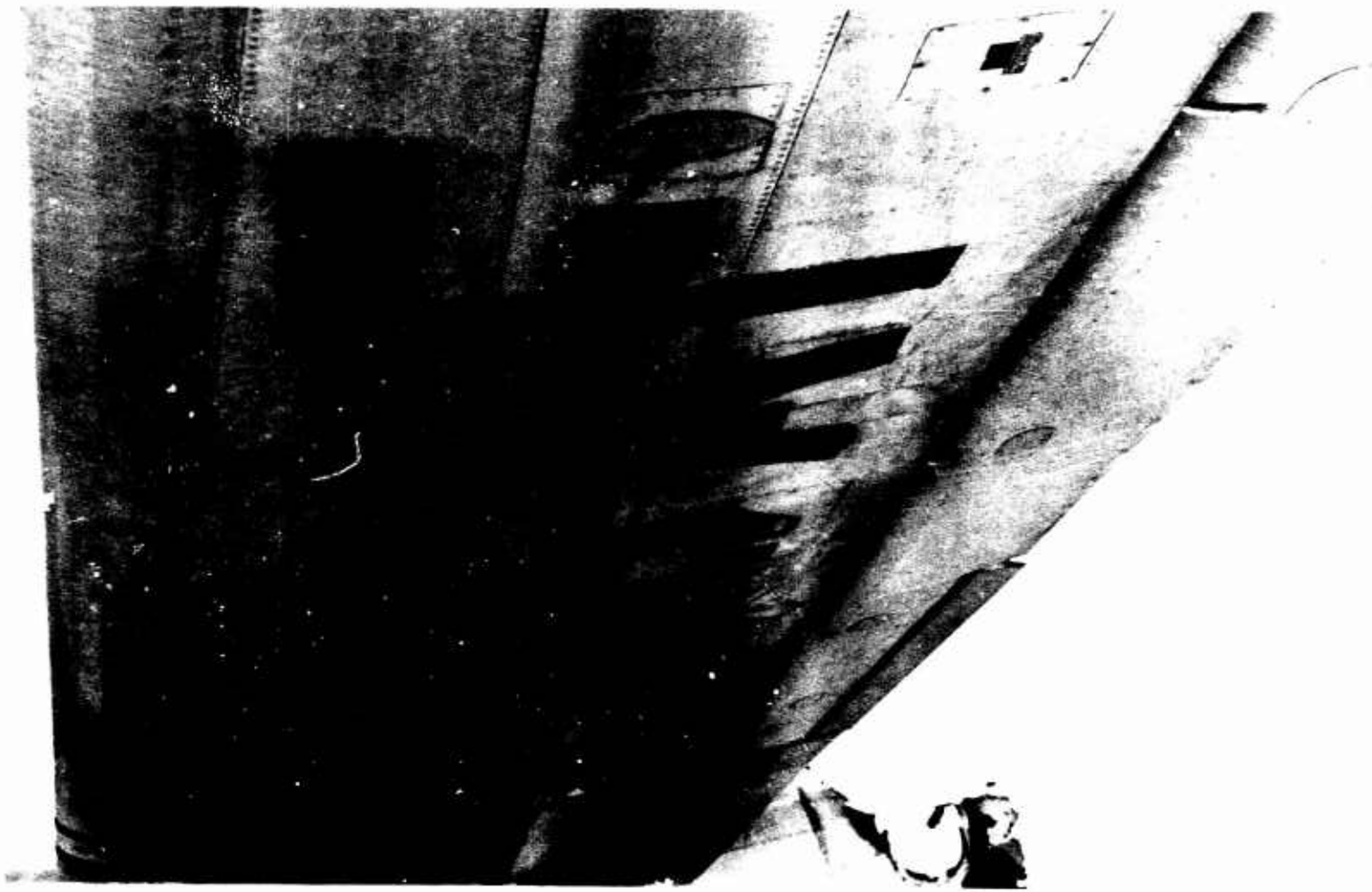

Fig. 3.157 B-29 (7349), Nose-in, Station 5000 (4.0 psi), Shot 4, Close-up View of Lower Surface of Left Wing, Showing Buckled Skin on Wing Outer Panels. Note Heating Effect on Black Paint.

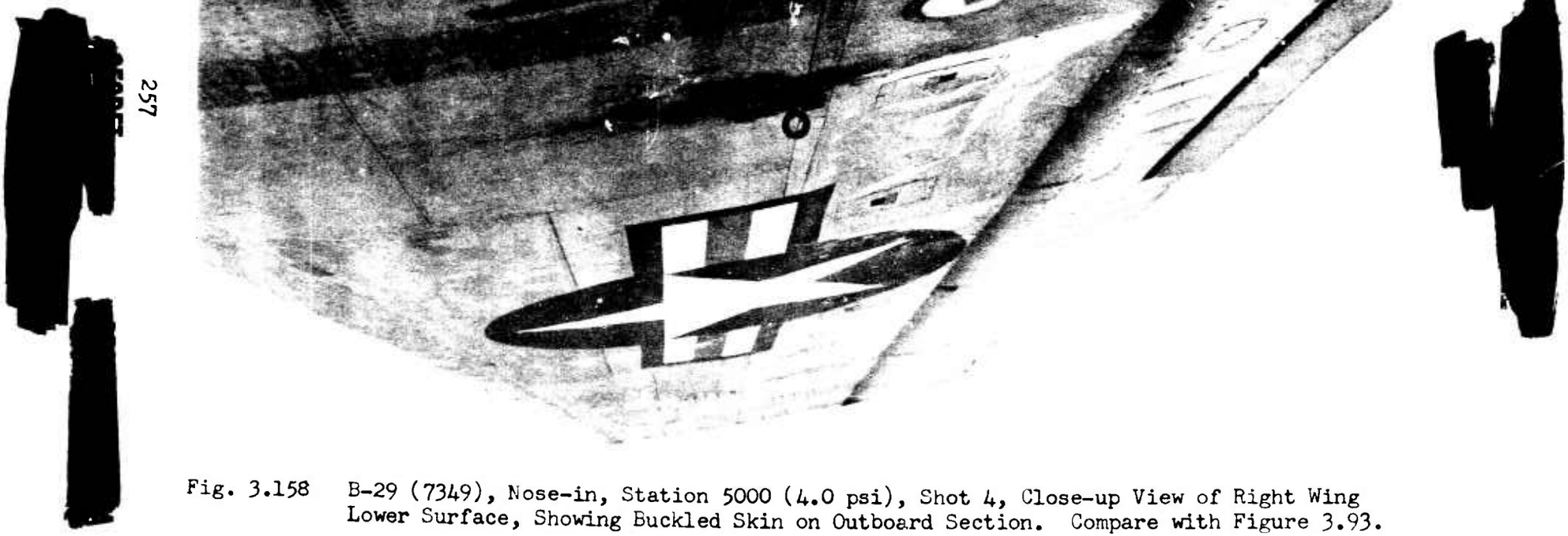

Fig. 3.158 B-29 (7349), Nose-in, Station 5000 (4.0 psi), Shot 4, Close-up View of Right Wing Lower Surface, Showing Buckled Skin on Outboard Section. Compare with Figure 3.93.

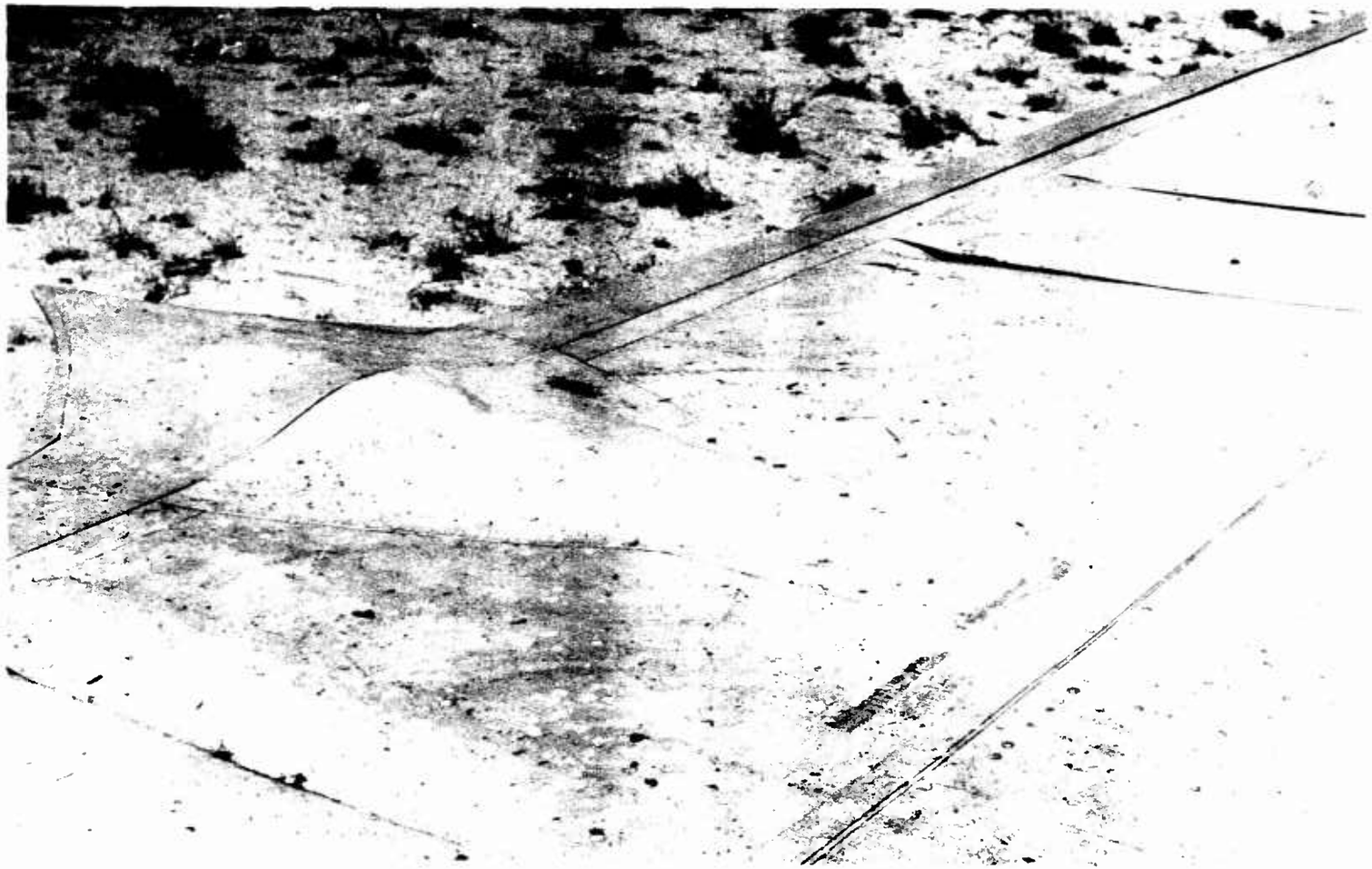

Fig. 3.159 B-29 (7349), Nose-in, Station 5000 (4.0 psi), Shot 4, Close-up View of Buckles on the Left Wing Aft Section in Vicinity of Inboard Nacelle. Note Failures Along Rivet Lines. Compare with Figure 3.94.

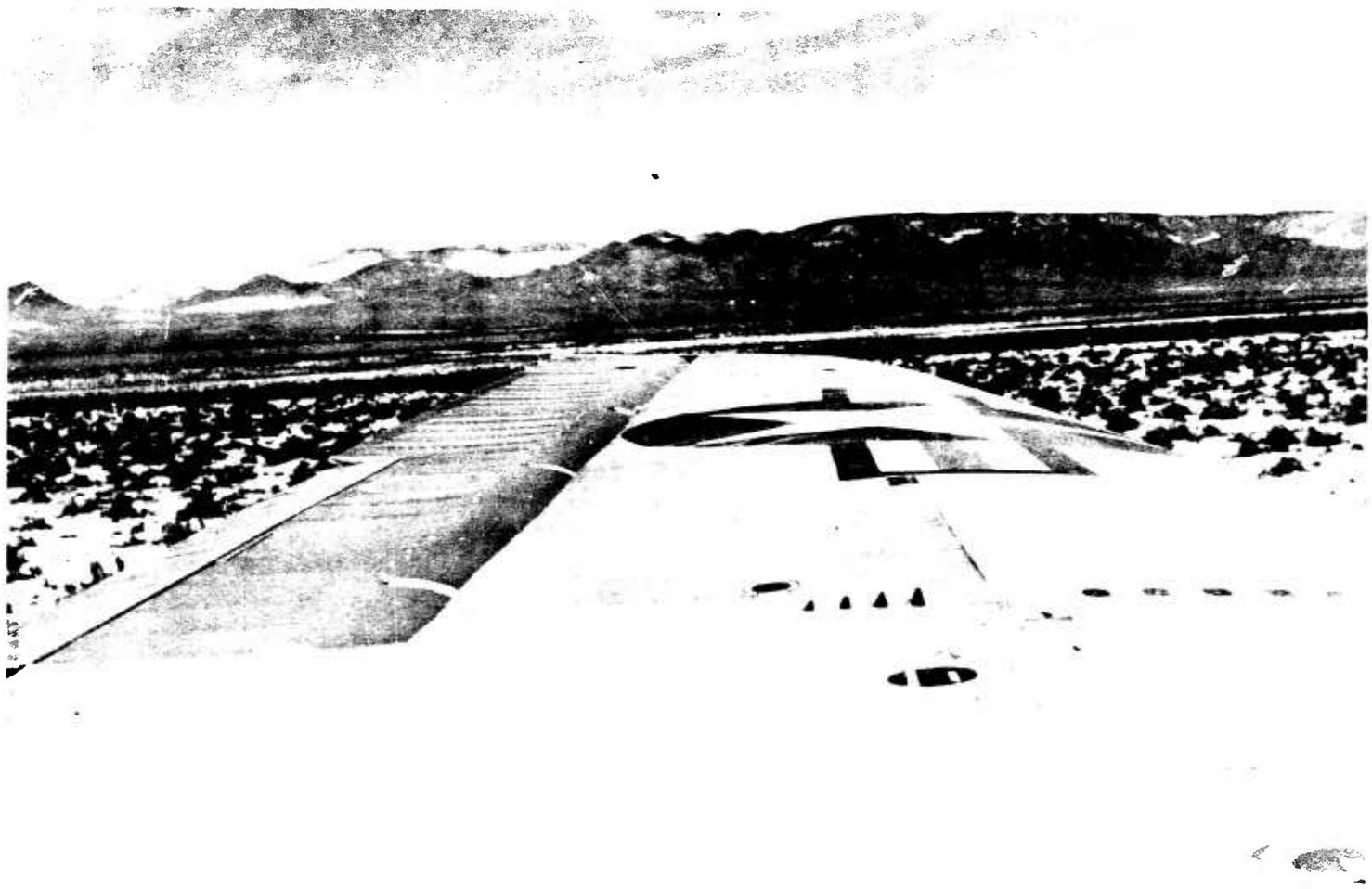

Fig. 3.160 B-29 (7349), Nose-in, Station 5000 (4.0 psi), Shot 4, Showing Evidence of Buckled Ribs in Left Wing Outer Panels

Fig. 3.161 B-29 (7349), Nose-in, Station 5000 (4.0 psi), Shot 4, Close-up View of Empennage, Showing Buckled Vertical Tail and Dorsal Fin. Note Buckles in Lower Rudder and Results of Fire in Aft Fuselage Section.

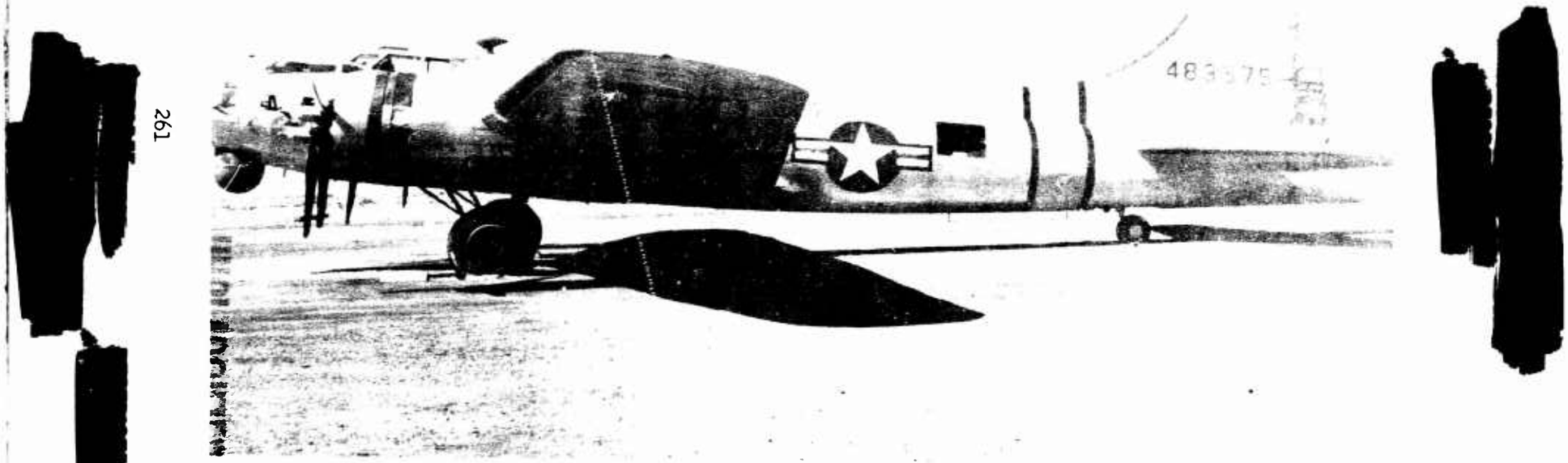

Fig. 3.162 B-17 (3575), Left Side-in, Station 8000 (1.9 psi), Shot 4, Showing General Post-shot Condition of Aircraft. Note Crushed Wing Tip and Caved-in Fuselage in Vicinity of Cabin.

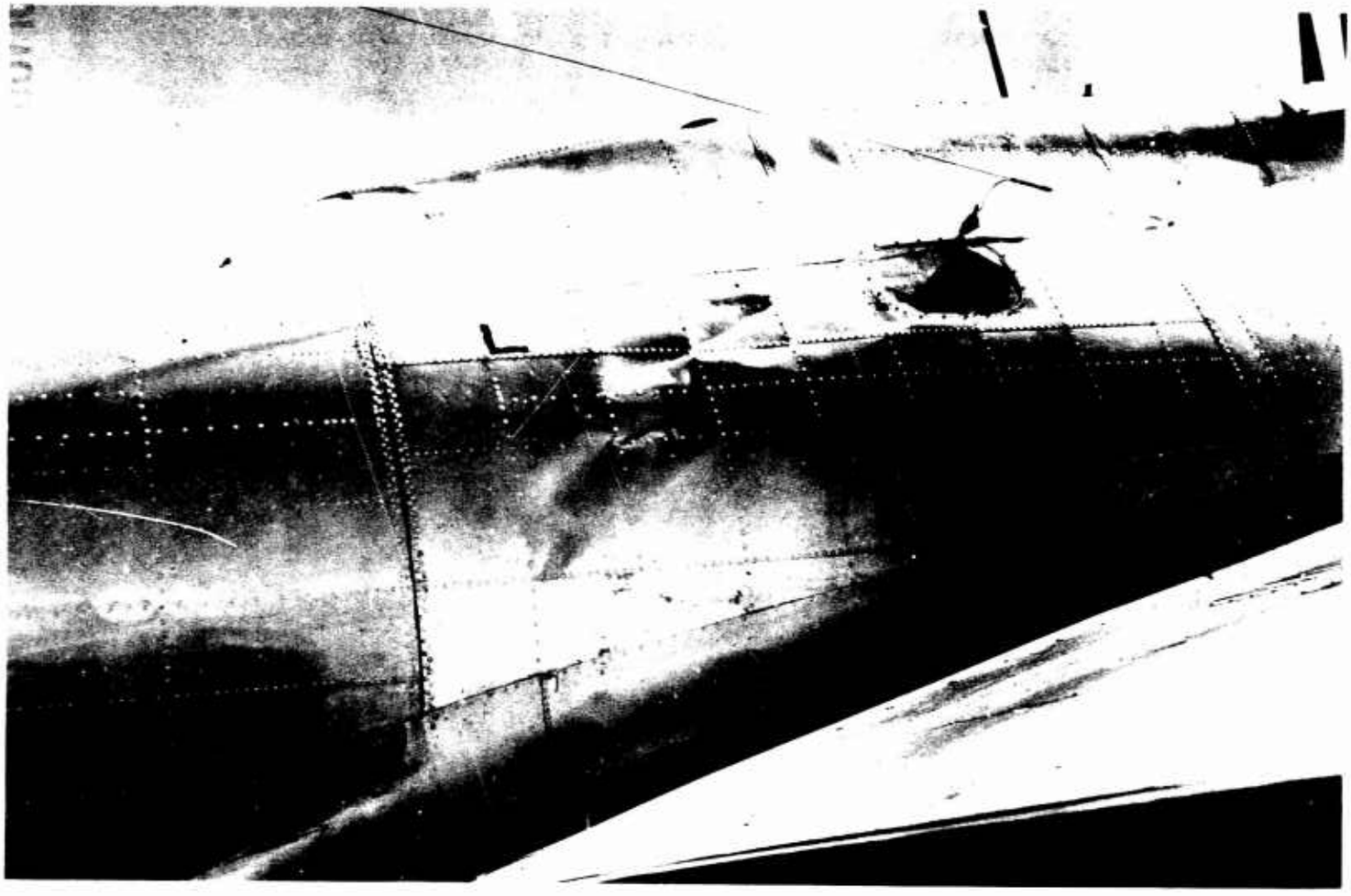

Fig. 3.163 B-17 (3575), Left Side-in, Station 8000 (1.9 psi), Shot 4, Close-up View of Torque Failure of Fuselage in Area Above Wing Trailing Section

Fig. 3.164 B-17 (3575), Left Side-in, Station 8000 (1.9 psi), Shot 4, Close-up View of Lower Surface of Left Wing, Showing Pressure Damage to Skin in Outer Panels

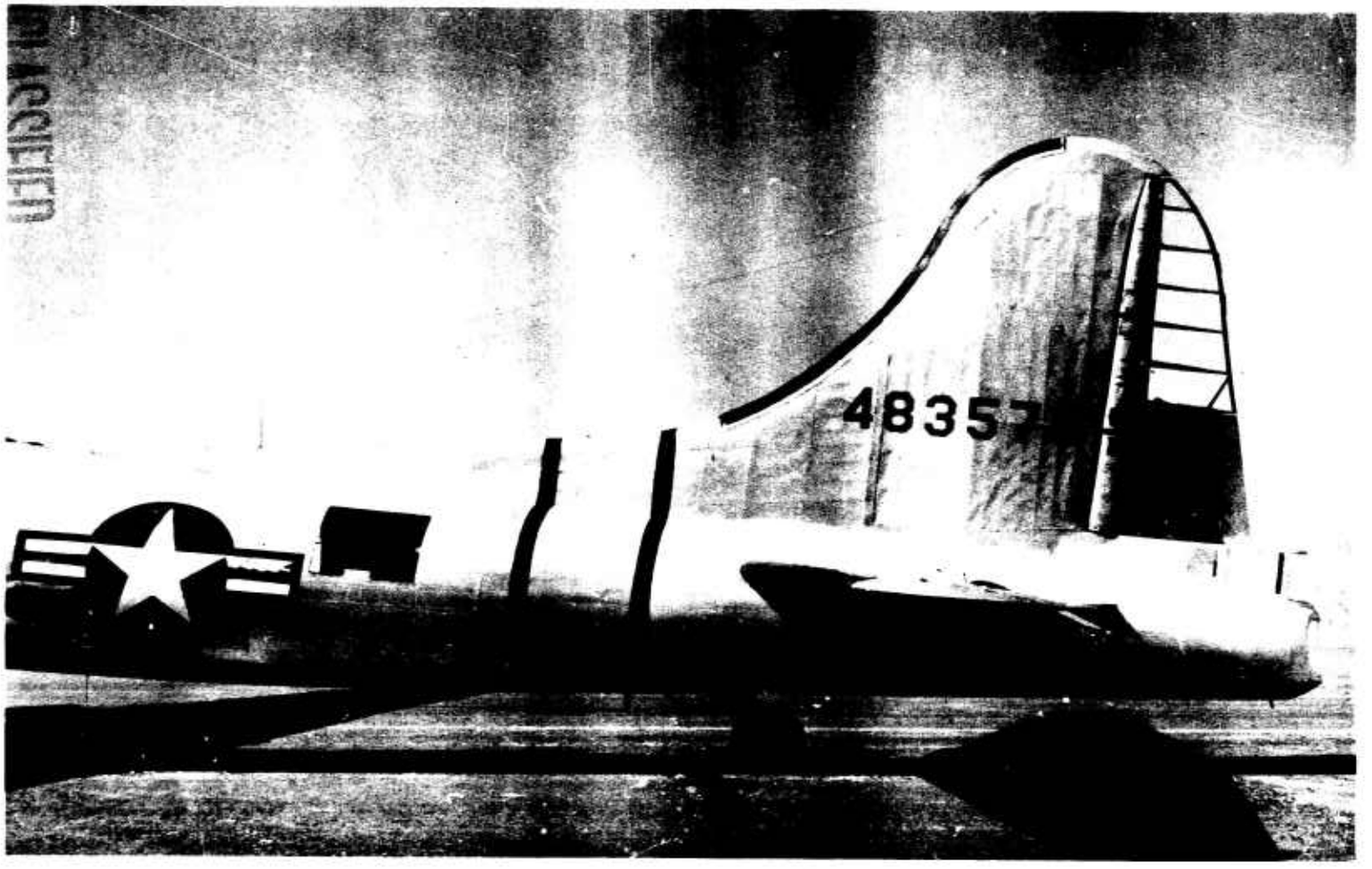

Fig. 3.165 B-17 (3575), Left Side-in, Station 8000 (1.9 psi), Shot 4, Showing Buckled Dorsal Fin and Vertical Stabilizer and Burned Rudder

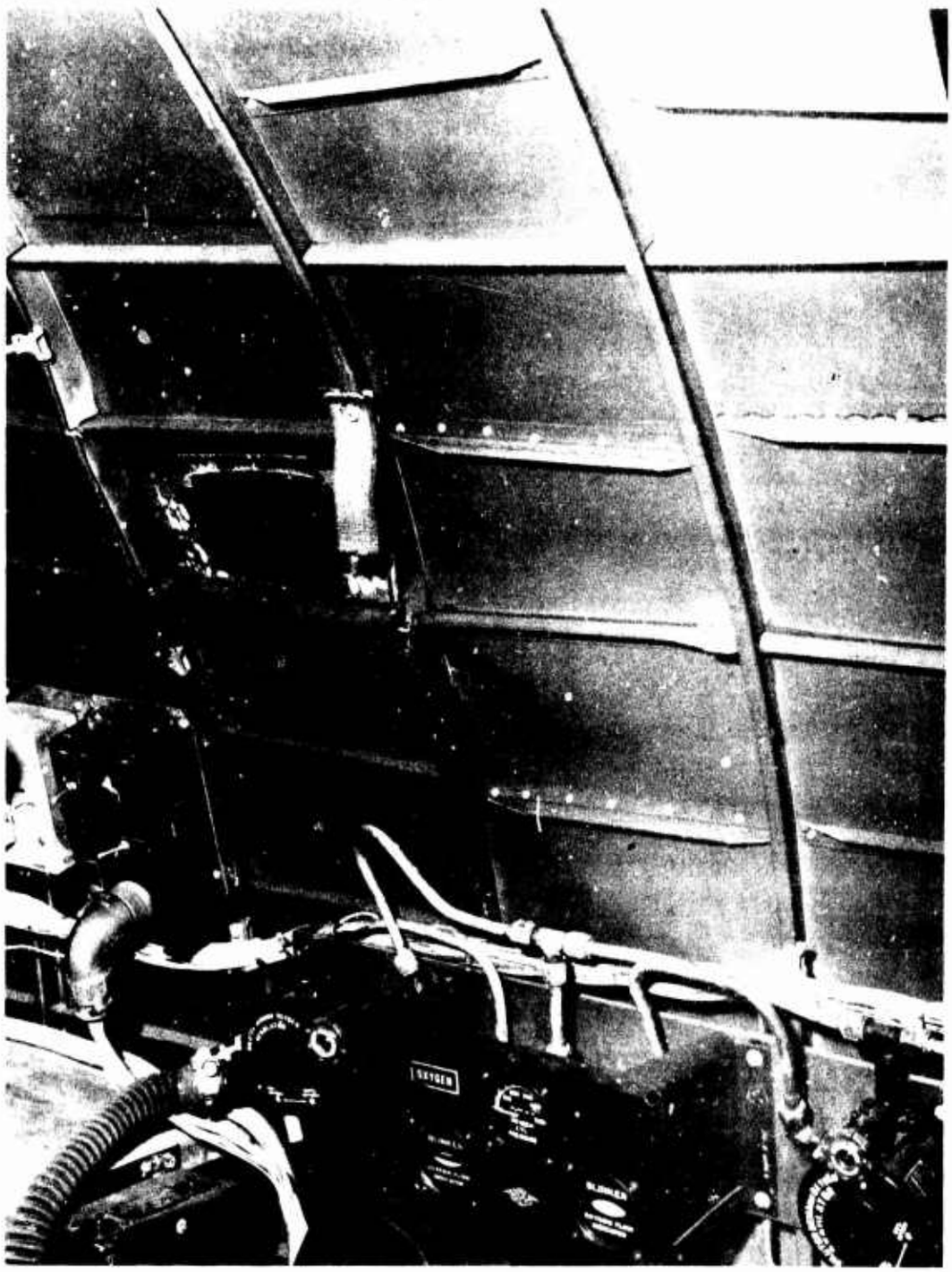

Fig. 3.166 B-17 (3575), Left Side-in, Station 8000 (1.9 psi), Shot 4, Interior View of Torque Failure of Right Side of Fuselage, Showing Bent Fuselage Frames and Buckled Skin. Compare with Figure 3.163.

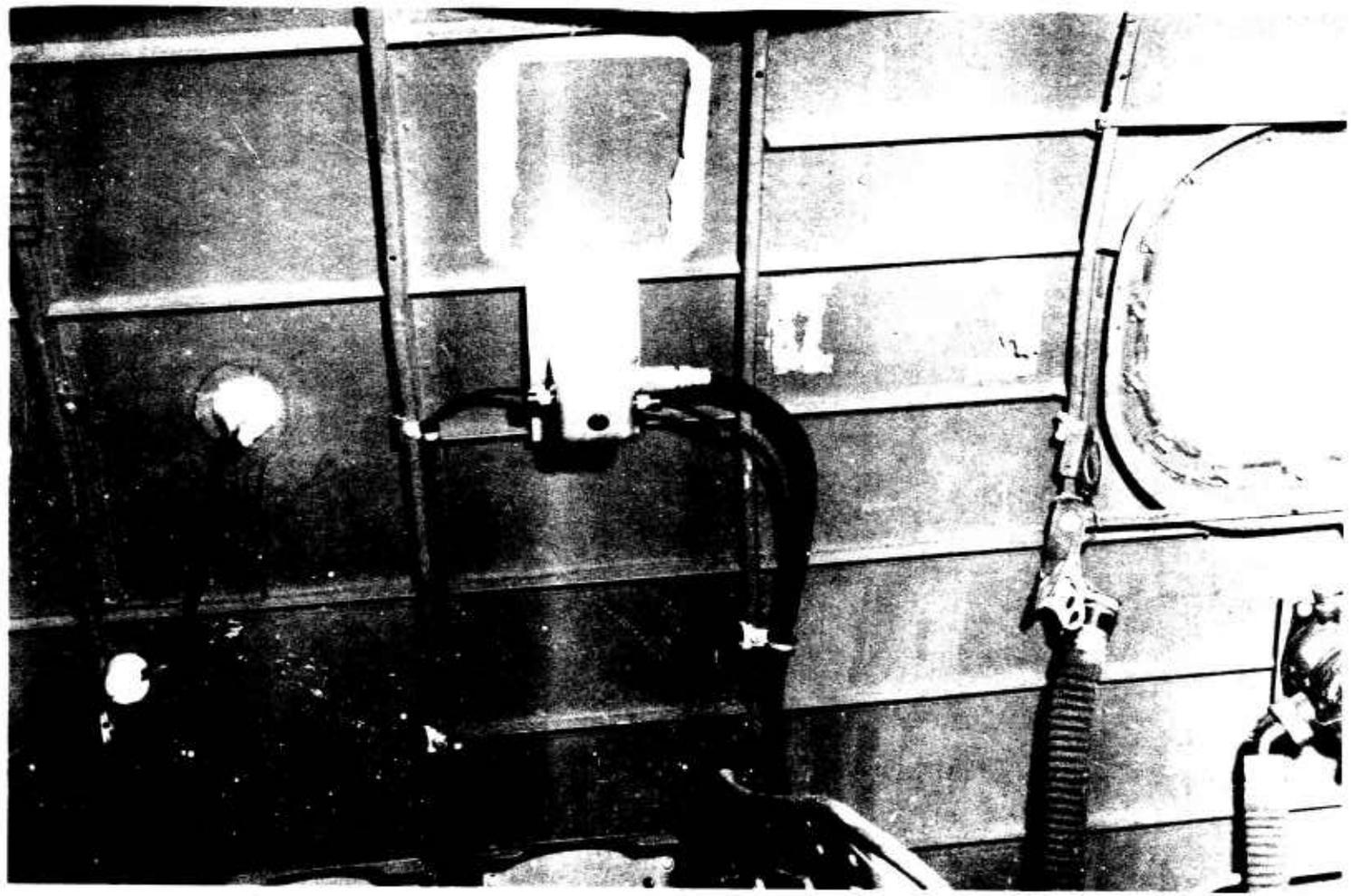

Fig. 3.167 B-17 (3575), Left Side-in, Station 8000 (1.9 psi), Shot 4, Interior View of Left Side Fuselage in Area of Wing Trailing Edge, Showing Damaged Fuselage Frames

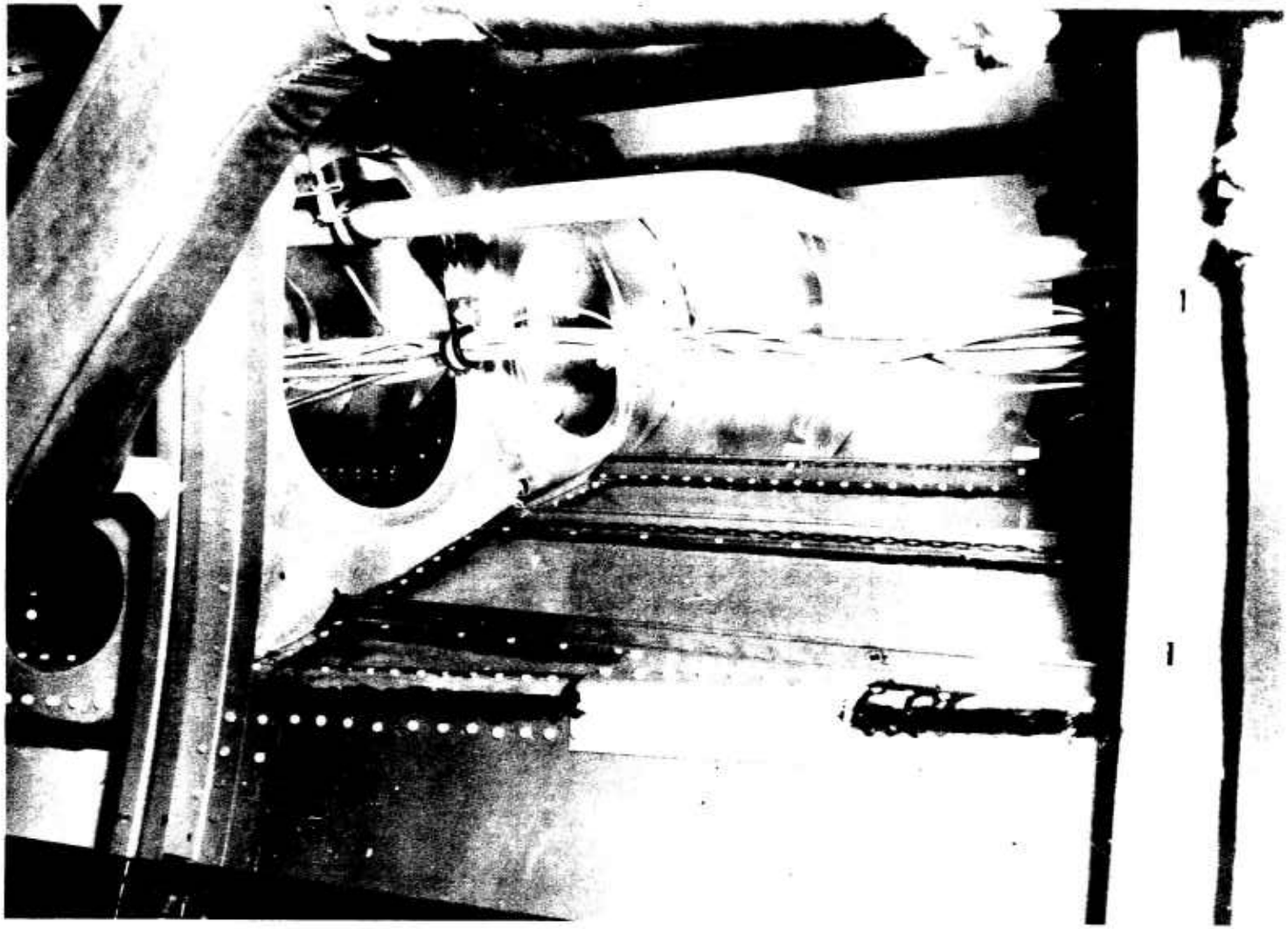

Fig. 3.168 B-17 (3575), Left Side-in, Station 8000 (1.9 psi), Shot 4, Interior View of Damaged Dorsal Fin Bulkhead

[redacted]

3.5.1 Panel A, Station 8000, Shot 3

Panel A, which is typical of all test panels exposed, is shown, as it appeared after Shot 3, in Figs. 3.169, 3.170, 3.171, and 3.172. The articles on this test panel were subjected to a peak overpressure of 3.6 psi and a total thermal energy of 11 cal/cm^2. These inputs were too low to cause damage to the integral fuel cell models, various types of bearings (open, sealed, and shielded), plastics, and grease samples. Seat cushion samples were generally well scorched and burnt. Pressure seals suffered thermal damage. The seat catapult did not detonate. The plastic was unaffected except for the burning through of painted numbers.

3.5.2 Panel B, Station 2200, Shot 3

Panel B was subjected to an overpressure of 8.4 psi and a thermal energy of 53 cal/cm^2. These inputs were still not sufficiently high to damage the integral fuel cell models significantly but did produce some scorching. Open bearings were locked; sealed and shielded bearings remained operable. All bearing and pressure seals were scorched and burnt. Plastic samples were scorched and sandblasted but retained general configuration. The seat catapult was sandblasted and scorched but did not fire.

3.5.3 Panel C, Station 1000, Shot 4

The peak overpressure of the blast wave at Station 1000 was 36 psi with an attendant thermal energy input of 235 cal/cm^2. Because of arrival of blast wave during thermal phase, the incident thermal energies realized by the test articles were probably considerably less than 235 cal/cm^2; nevertheless, test articles were severely damaged and in many cases separated from the panel and not recovered. Several integral fuel cell model walls, facing ground zero, burst, and the gasoline exploded or burned. Bearings recovered were for the most part broken or inoperative. Grease samples were completely consumed and plastic components destroyed. Pressure and bearing seals also were destroyed. The plug of one catapult tube was removed prior to the test to facilitate detonation of the charge. The other catapult tube was also armed, but the safety plug was left in. Even though the tubes were blown as far as 200 ft from the panel location and suffered damage from ground contact and sandblasting, they did not fire.

3.6 GENERAL INPUT FUNCTIONS

A list of ten variables believed to affect damage to parked aircraft is given in the introduction to this chapter. Of these ten, only two are primary causes of aircraft damage: namely, the thermal and blast inputs. Thus, in evaluating the effects of atomic bombs on parked aircraft, it is of utmost importance to know the value of these

[redacted]

[redacted]

two input functions at each particular exposure station.

Measurement of the overpressure of the blast phase as a function of time at various distances from ground zero along a given azimuth (blast line) was undertaken by various organizations. In addition to these blast line measurements of overpressure, the David Taylor Model Basin, operating as Project 1.13, measured the overpressures experienced at several of the aircraft parking stations used in this project. These measurements were all made at ground level.

3.6.1 Peak Overpressure, Shots 2, 3, and 4

The values of peak overpressure, reported by the agencies of Program 1 responsible for overpressure measurements, were plotted against ground range as a log log presentation. The best smooth curve was drawn through the data points. The curves based on these composite data for Shots 2, 3, and 4 are presented in Fig. 3.173. The overpressure forcing functions quoted in Paragraphs 3.2, 3.3, and 3.4 were obtained from the above plot.

3.6.2 Total Thermal Energy, Shots 2, 3, and 4

The total thermal energy received at various elevations and distances from the burst point was measured calorimetrically by NRDL. These data, corrected to zero atmospheric attenuation, were plotted on a log log scale and are presented in Fig. 3.174 for Shots 2, 3, and 4. The thermal measurements made by Project 3.1 at the aircraft parking stations are shown on the same plot. These measurements were not corrected for atmospheric attenuation nor for the attenuation introduced by preshock dust and smoke. Because of this attenuation these values are lower than those reported by NRDL, except for the value measured at the most distant station (Station 8000) in Shot 4. There is no reason to suspect the accuracy of this measurement. Smoke emitted from the oil stabilization of the close-in stations may have been the major factor contributing to the increased attenuation. A more detailed presentation of Project 3.1 thermal measurements may be found in Appendix A.

3.6.3 Radiation Dosage, Shots 2, 3, and 4

The variation of gamma radiation with ground range is shown in Fig. 3.175 for Shots 2, 3, and 4 of Operation TUMBLER-SNAPPER. These curves are based upon data obtained from exposure of film badges. The results were not considered in the aircraft damage analysis; however, they are presented for use in evaluation of the physiological effect on maintenance and crew personnel.

3.6.4 Pressure Measurements at Aircraft Parking Stations

The Project 3.1 instrumentation group and the David

[redacted]

[redacted]

Taylor Model Basin determined overpressures experienced at several of the aircraft parking stations. The measurements made by Project 3.1 are discussed in Appendix A. All pressure sensing elements employed by the DTMB were mounted at grade level. Interferometer and capacitance type gages were used. The capacitance gage was considered a more sensitive instrument than those generally employed by pressure measuring agencies on the blast line. To compare the capacitance gages with the blast line gages, a capacitance gage was installed on the blast line at 3000 ft from target ground zero. A comparison of the readings at various aircraft stations with blast line measurements shows the DTMB values to run consistently higher. The DTMB blast line value, although slightly higher than the average of the other gage data, was well within the experimental scatter.

Measurement of overpressure in the open and behind the wall revetment during Shot 4 indicated that slightly higher pressure was obtained behind the revetment, although the pressure rise was faster in the open. Figure 3.176 shows the pressure-time curves for the two measuring stations.

3.7 GENERAL TEST DATA

Table 3.1 gives a summary of test conditions, such as meteorlogical data, bombing error, yield of weapon, burst height, etc., for Shots 1, 2, 3, and 4. The ranges from the aircraft parking stations to ground zero and burst point for Shots 2, 3, and 4 are given in Table 3.2. The elevations of ground zero and the aircraft parking stations are also given. Overpressure, as well as thermal and nuclear radiation inputs, experienced at the various stations employed in Shots 2, 3, and 4 are summarized in Table 3.3.

The aircraft parking station elevations, ranges from target ground zero, and angle of incidence of direct radiation for Shots 2, 3, and 4 are given in Fig. 3.177. Bomb burst points are shown in relation to station locations.

3.8 PHOTOGRAPHIC RESULTS

The photographic effort included still and motion picture photography with both color and black and white film. Still photography was confined largely to pre-shot and post-shot work, whereas motion picture photography was concerned more with recording the reaction of the parked aircraft to the thermal and blast effects of the bombs.

3.8.1 Motion Pictures

All motion picture film taken before, during, and after the tests were edited and combined into a continuous production entitled

[redacted]

[redacted]

"Operation SNAPPER, Project 3.1". Much of the film taken during the tests was discarded because of obscuration of the subject by smoke and dust produced during the thermal and blast phases. This problem, along with the problem of nuclear radiation, is discussed in Paragraph 3.8.4.

3.8.2 Sequencing Still Shots

Sequenced still shots were obtained during the test phase by operating K-24 cameras at a speed of approximately three frames per second. The problem of dust and smoke interference also affected these results. Two photographs taken during the thermal phase but prior to shock arrival on Shot 3 show the effect of the thermal inputs of 6.7 and 11 cal/cm^2 on B-17 aircraft. These photographs, taken approximately one second after time zero, are shown in Figs. 3.178 and 3.179.

3.8.3 Still Photography

A total of 784 still shots were taken of construction work, test equipment, pre-shot and post-shot condition of aircraft, passive defense structures, and miscellaneous items. Aerial views of aircraft parking stations were also obtained. A portion of these photographs were selected for presentation in this report. A complete set of the photographs and a cross-referenced index is being forwarded to AFSWP.

3.8.4 Problems of Test Phase Photography

The two main problems involved in the operation of photographic equipment during a nuclear test are the obliteration of the subject by smoke and dust and the fogging of the film by nuclear radiation. In order to minimize the dust problem and at the same time more nearly simulate conventional aircraft parking surfaces, most of the parking areas were graded and sandy surfaces stabilized by using either oil and water or road mix. The exceptions were Stations 1000, 1350, 1384, 1500, and 4000, where the sand surfaces remained ungraded and unstabilized. From the photographic standpoint, the stabilization did not represent a satisfactory solution to the dust problem, because during the thermal phase the high intensity thermal radiation was strongly absorbed by the black surface, causing volatilization of certain of the constituents which produced a dense, persistent, and low-hanging cloud, thus obscuring the intended subject during a major period of the exposure. Additional density was added to the cloud, as dust kicked up by the blast wave continued to hide the subject.

In order to reduce or eliminate fogging of photographic film by nuclear radiation, the cameras operating during the test had to be shielded sufficiently to keep the total radiation dosage received within the tolerance for the film being utilized. The shielding requirements for the camera installations at the various ranges were

[redacted]

based on predicted values of radiation dosage for Shot .

The installations in which the cameras were placed consisted of concrete pedestals, which were open in front and back. Further shielding was afforded by placing two-inch by three-inch by six-inch lead bricks around the inside of the pedestals. Around the outside lead bricks and sandbags were employed where they were required. On the exit pupil face, which is referred to as the front, the shielding consisted of steel plates and lead bricks wherever they did not interfere with the field of view of the cameras. At the openings for the exit pupils the shielding was limited to a piece of optical glass. The rear of each of the pedestals was enclosed with varying thicknesses of steel plate.

In order to measure the radiation dosage received by the photographic film, Rad-Safe Personnel Badges were located at various points on the cameras and on the inside and outside walls of the pedestals. The results obtained from these badges are given below:

Shot No.	Station	Dosage (Roentgens)	
		Interior	Exterior
2	2200	2.6	280
2	8000	0	0.26
2	10500	0	0.05
3	2200	4.2	2200
3	8000	0.3	7.7
3	10500	0.1	1.0

By comparing the badges located near the exit pupils with the badges located at other points interior to the pedestals and also by comparing the apparent and calculated attenuation factor, there is indication that a large percentage of the radiation received inside the pedestals was from back-scatter radiation entering through the exit pupils.

A correlation of film density as a function of measured radiation will be attempted; however, data on film densities are not available at this writing.

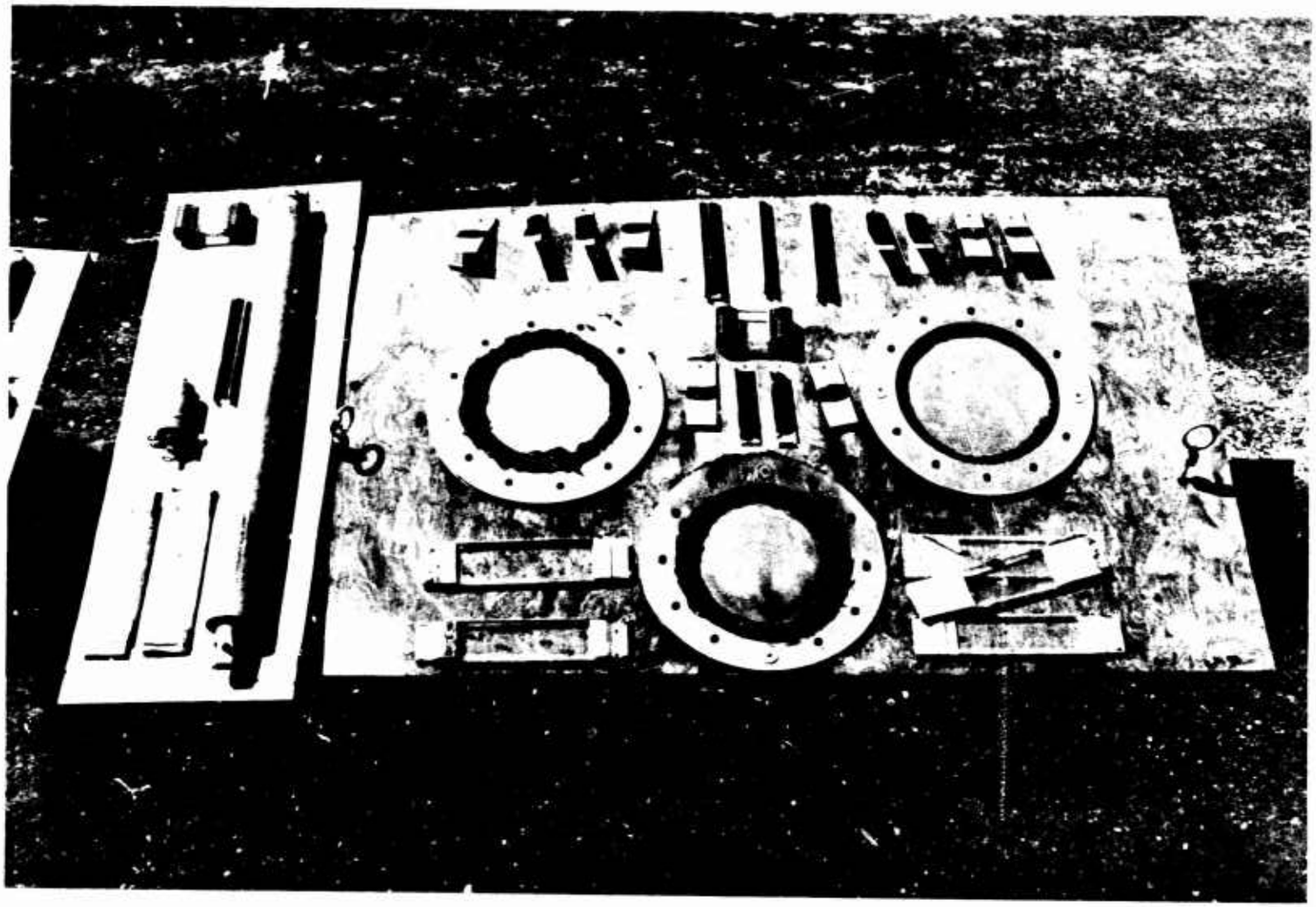

Fig. 3.169 Special Component Test Panel Array at Station 8000 After Shot 3

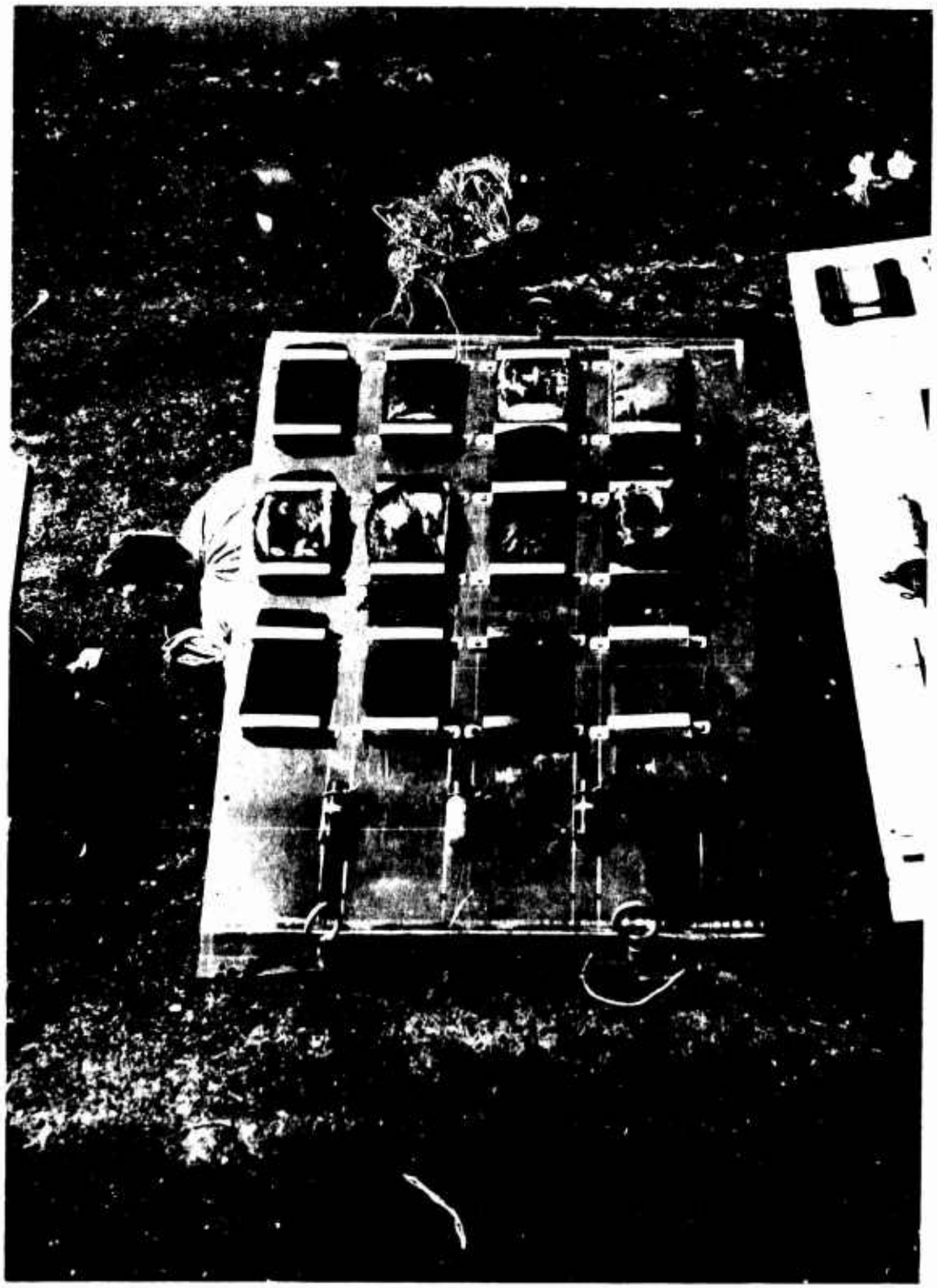

Fig. 3.170 Seat Cushion Panel Array at Station 8000 After Shot 3

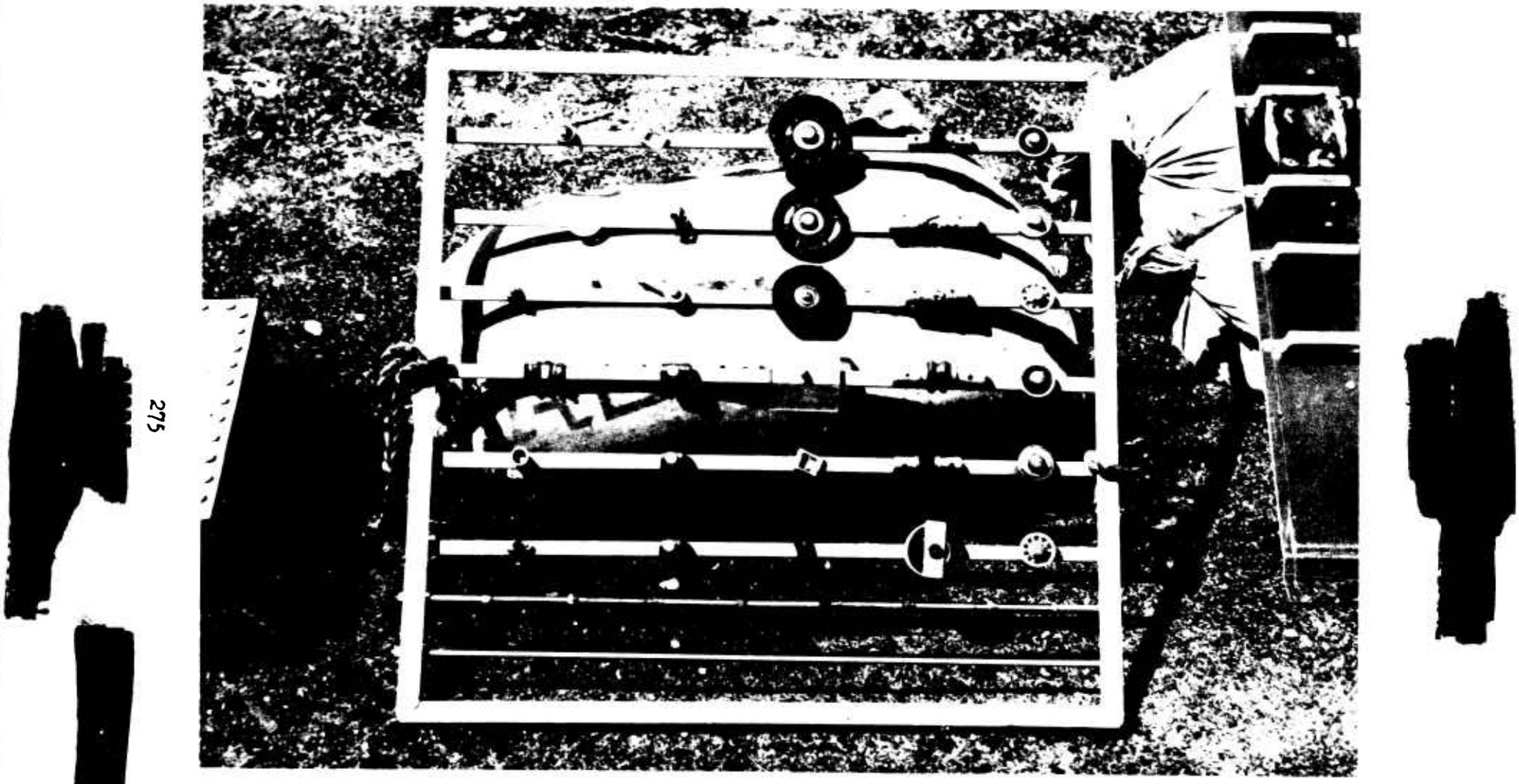

Fig. 3.171 Bearing Panel Array at Station 8000 After Shot 3

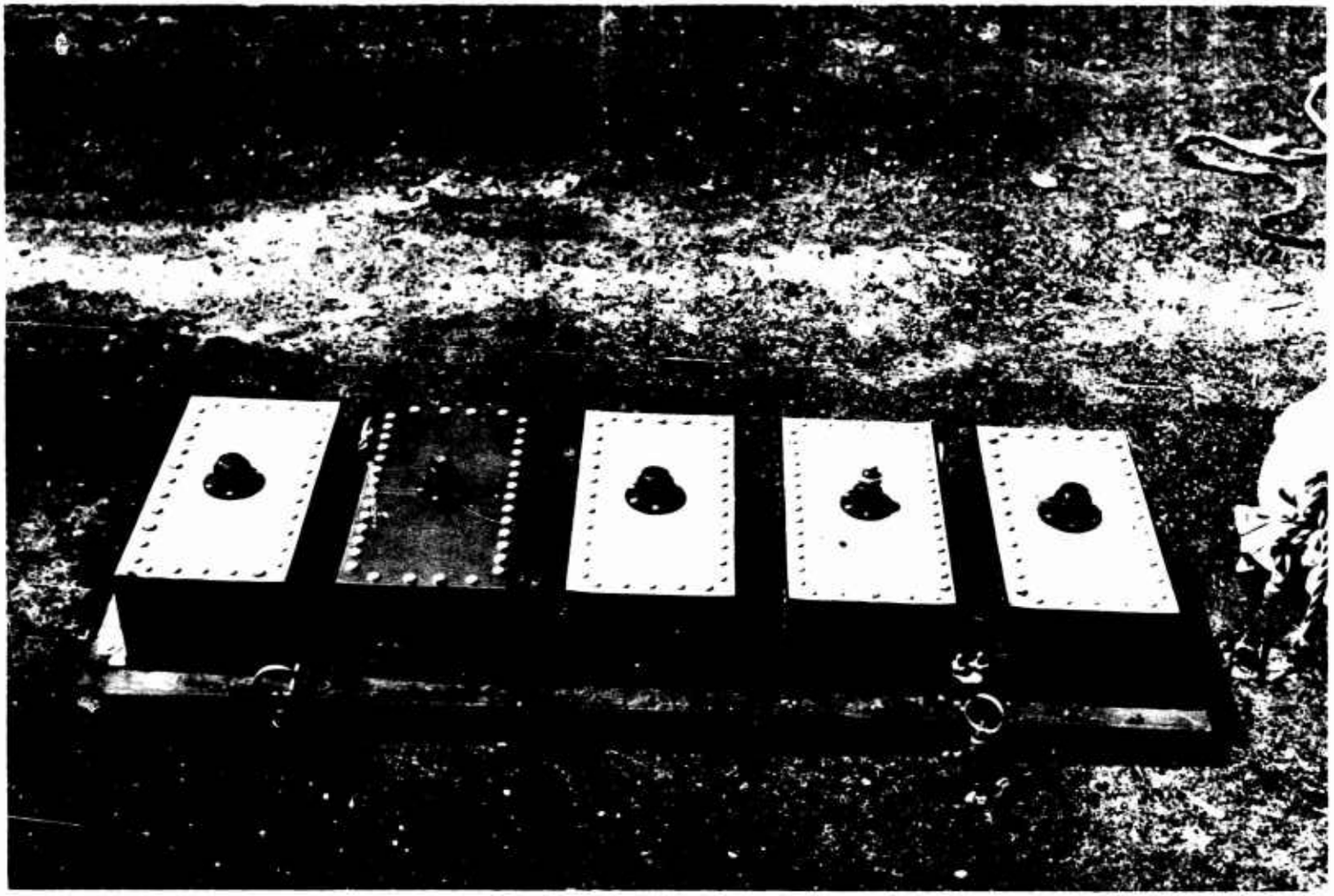

Fig. 3.172 Integral Fuel Cell Model Array at Station 8000 After Shot 3

[redacted]

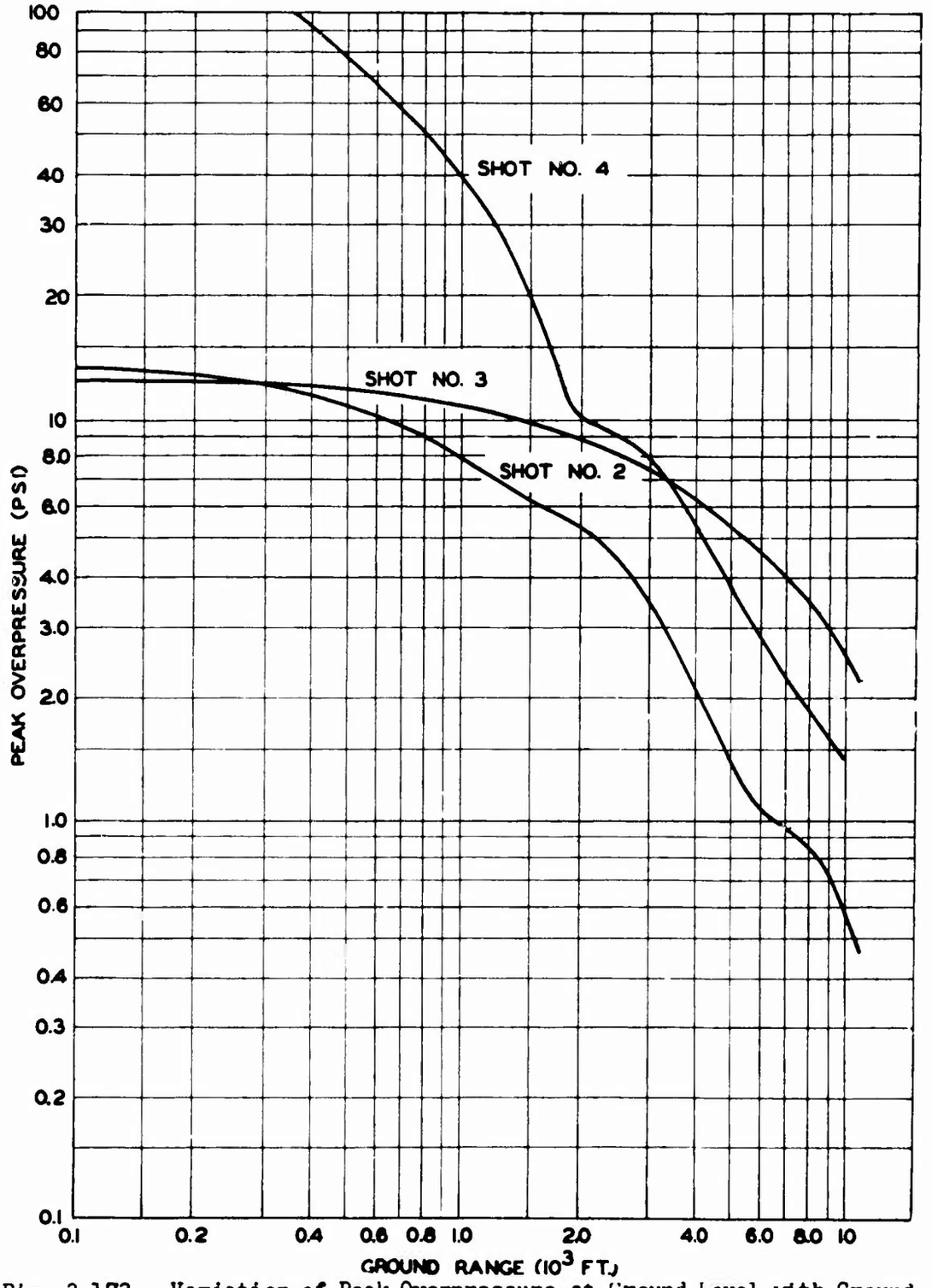

Fig. 3.173 Variation of Peak Overpressure at Ground Level with Ground Range for Shots 2, 3, and 4 (Composite Data)

[redacted]

[redacted]

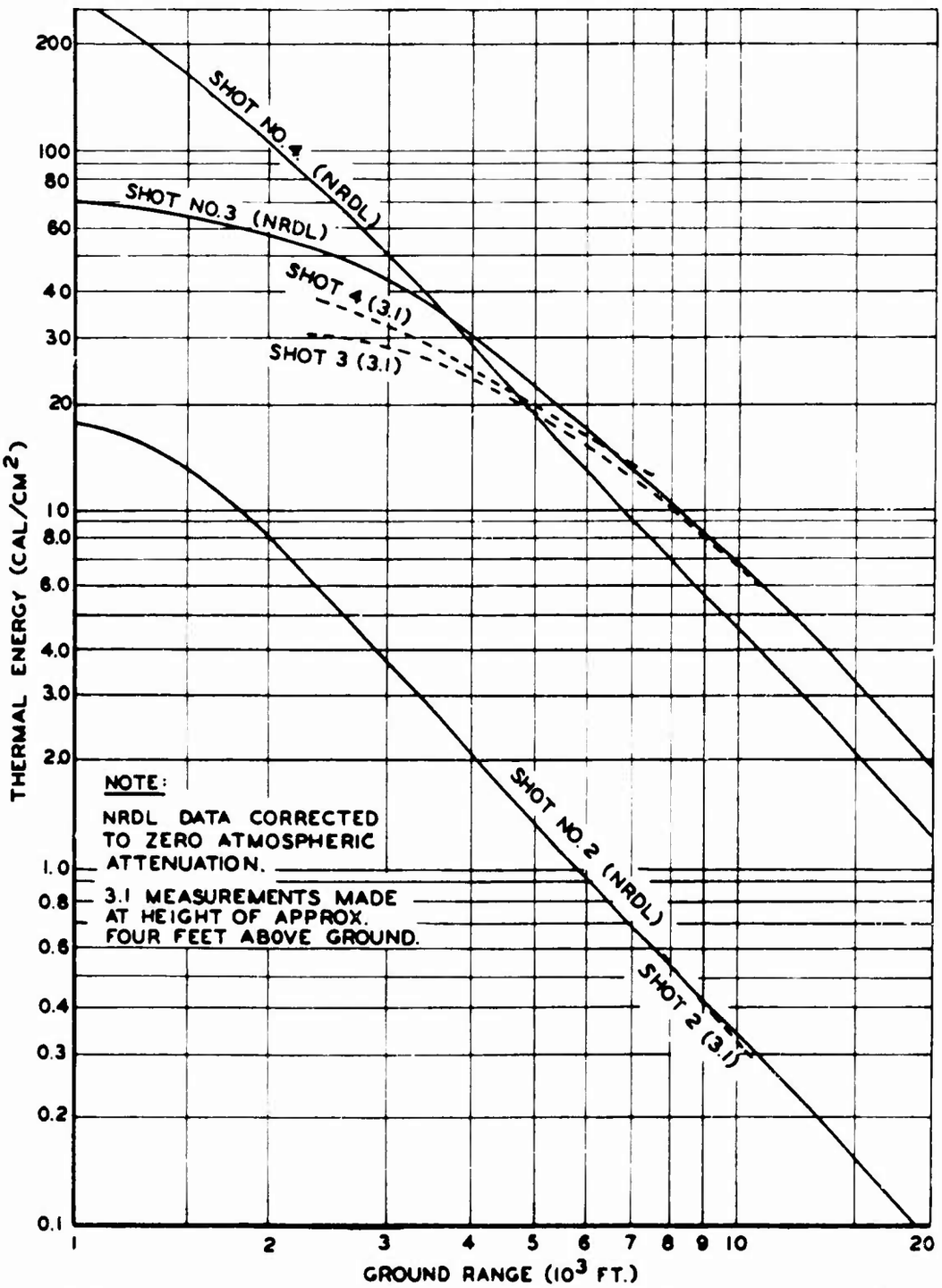

Fig. 3.174 Variation of Total Thermal Energy With Ground Range for Shots 2, 3, and 4. NRDL Data Corrected for Attenuation. Project 3.1 Data as Measured.

[redacted]

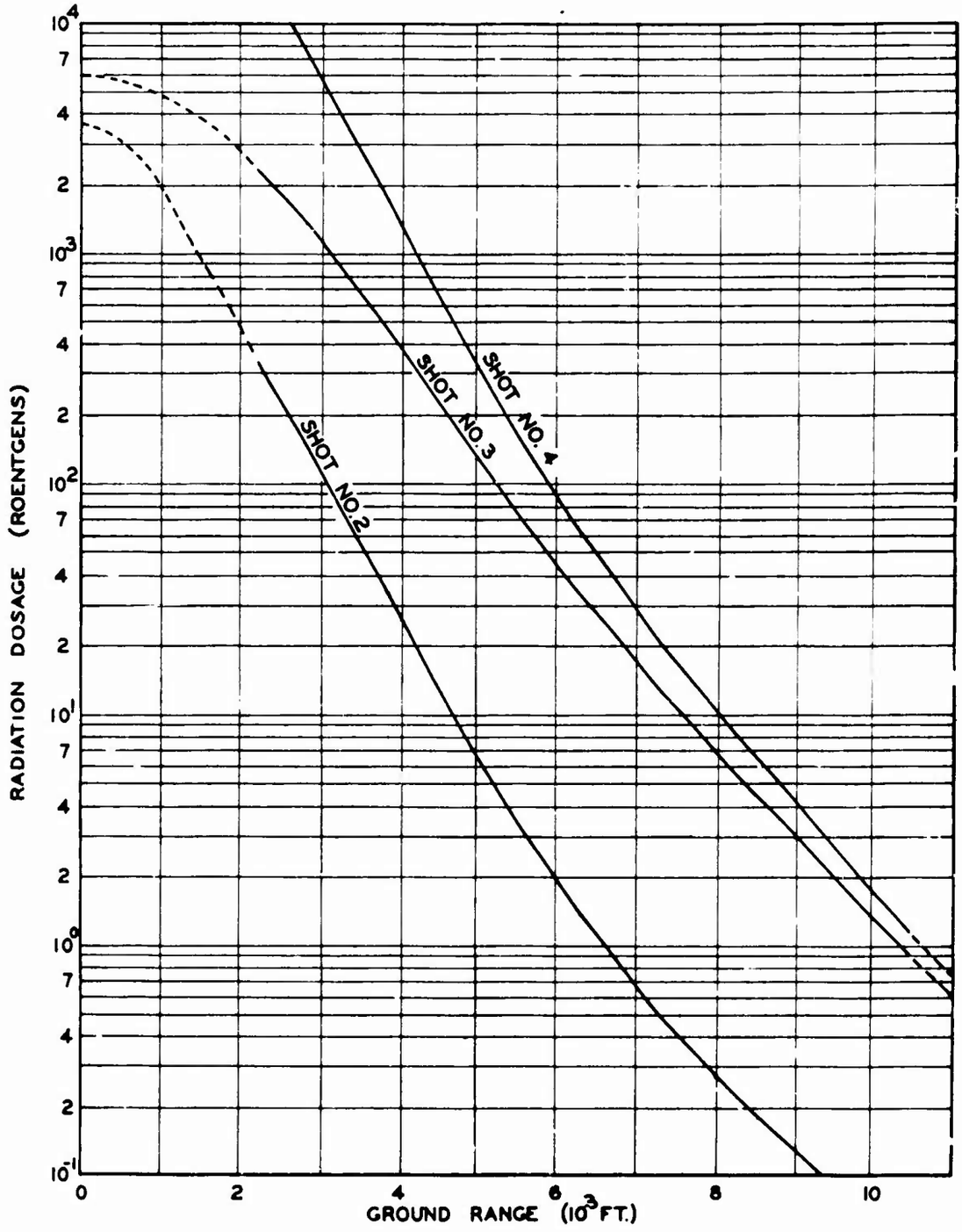

Fig. 3.175 Variation of Gamma Radiation With Ground Range for Shots 2, 3, and 4, Based on Film Badge Data

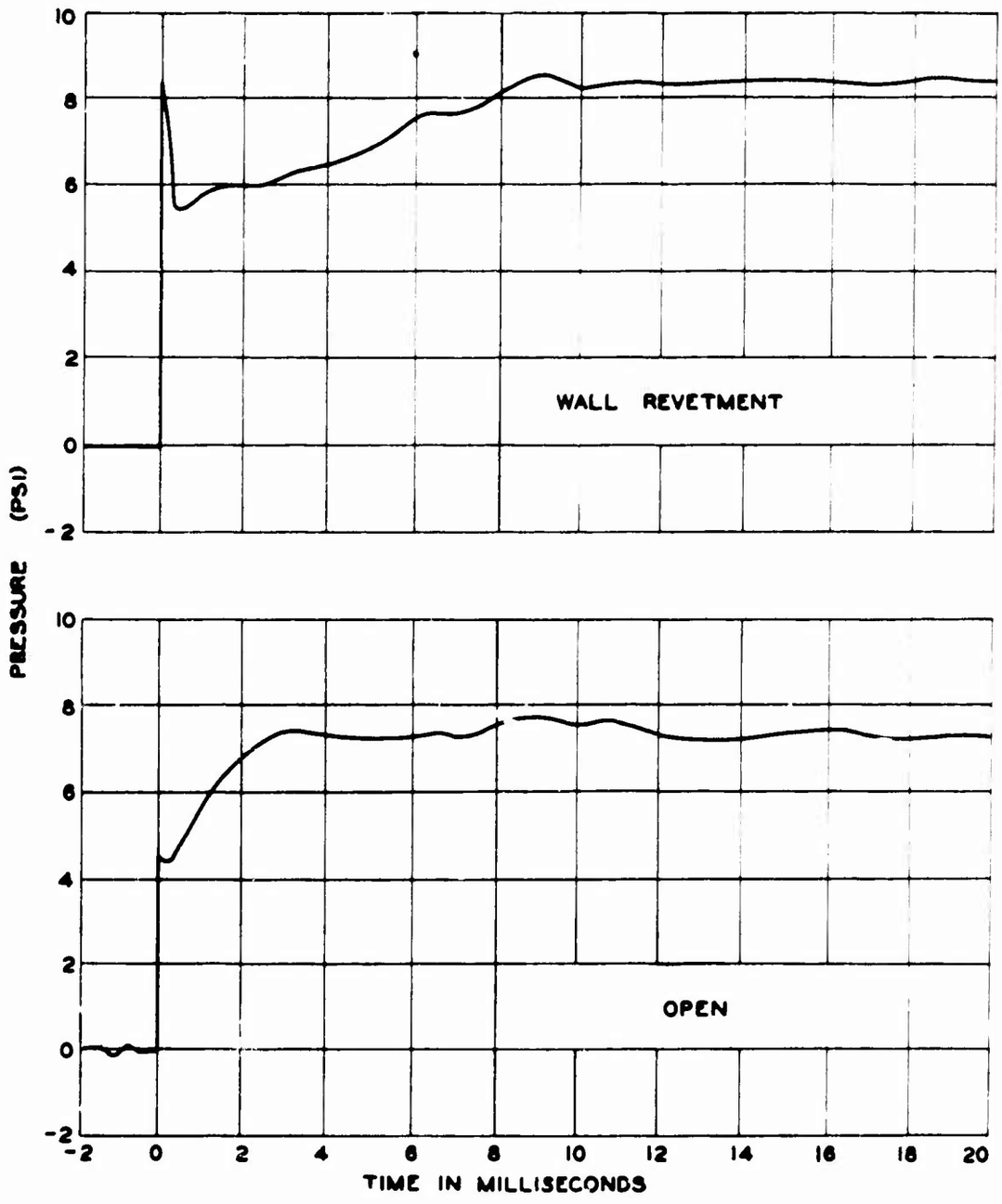

Fig. 3.176 Comparison of Overpressure-time Measurements Made Behind the Wall Revetment and in the Open at Station 4000, Shot 4 (Project 1.13 Data)

TABLE 3.1

TUMBLER-SNAPPER Test Conditions

Condition	Shot 1	Shot 2	Shot 3	Shot 4
Date	1 April	15 April	22 April	1 May
Time (PST)	0900:07.5	0929:57.05	0930:10.0	0929:58.63
Location (Area)	Frenchman Flat	T-7	T-7	T-7
Yield - Radio Chemical (KT)	1.05	1.15	30.0	19.6
Height of Burst (ft)	793	1109	3447	1040
Height of Burst (ft) (Scaled to 1 KT at sea level)	699	960	1000	361
Ground Zero - relative to aiming point (ft)	67-E 122-N	143-S 84-E	80-S 124-W	140-S 153-W
Ground Zero Atmosphere Pressure (mb)	914	878	873	877
Burst Height Atmosphere Pressure (mb)	888.5	842	770	845
Ground Zero Air Temperature (°F)	58.0	54.1	66.7	62.6
Burst Height Air Temperature (°F)	56.5	48.4	45.7	59
Ground Zero Relative Humidity (%)	28	30	30	47
Burst Height Relative Humidity (%)	30	30	47	50
Surface Wing Velocity (MPH)	2-E	5-NE	6-SSW	3-SSW
Atmospheric Transmission (%/mi)	96	96	95	95

TABLE 3.2

TUMBLER-SNAPPER Geometric Data

Shot	Date	Yield (KT)	Burst Altitude (Feet)	Circular Error (Feet)
2	15 Apr 1952	1.15	1109	166
3	22 Apr 1952	30.0	3447	148
4	1 May 1952	19.6	1040	208

Pre-shot Data		Shot 2		Shot 3		Shot 4	
Station	Station Elevation (Feet)	Ground Range(a) (Feet)	Slant Range(b) (Feet)	Ground Range(a) (Feet)	Slant Range(b) (Feet)	Ground Range(a) (Feet)	Slant Range(b) (Feet)
GZ	4193						
1000	4208(c)			1053	3590	1110	1511
1350	4212(c)					1456	1778
1384	4213(c)			1435	3715	1490	1806
1500	4215(c)					1605	1901
2200	4224	2361	2595	2249	4090	2302	2513
2500	4230(c)					2601	2788
3320	4242(c)					3419	3560
3450	4243(c)					3549	3685
4000	4118	3926	4101	3867	5231	3801	3961
4500	4200(d)	4345	4486	4445	5629		
5000	4106(c)					4799	4930
8000	4072	7966	8060	7855	8627	7792	7878
10500	4080	10468	10539	10354	10949		

(a) Measured from actual ground zero
(b) Measured from actual burst point
(c) Value interpolated between surveyed stations
(d) BUSTER-JANGLE station, approximate elevation

[redacted]

TABLE 3.3

TUMBLER-SNAPPER Preliminary Forcing Functions
Shots 2, 3, and 4

Station[a]	Ground Range[b] (Feet)	Total Thermal Energy (cal/cm^2) Corrected to Zero Attenuation	Peak Overpressure (psi)	Radiation Dosage (Roentgens)
Shot 2				
2200	2361	5.7	4.7	280
4000	3926	2.2	2.1	28
4500	4345	1.8	1.8	16
8000	7966	0.6	0.8	0.3
10500	10468	0.3	0.5	0.1
Shot 3				
1000	1053	70	10.6	4800
1384	1435	64	9.9	3900
2200	2249	53	8.4	2200
4000	3867	32	6.4	410
4500	4445	27	5.8	230
8000	7855	11	3.6	7.7
10500	10354	6.7	2.4	1.0
Shot 4				
1000	1110	235	36	> 10000
1350	1456	170	22	> 10000
1384	1490	164	21	> 10000
1500	1605	148	18	> 10000
2200	2302	83	9.4	> 10000
2500	2601	68	8.9	10000
3320	3419	41	6.9	3100
3450	3549	38	6.5	2600
4000	3801	33	5.8	1700
5000	4799	21	4.0	410
8000	7792	8.0	1.9	11.4

(a) Station numbers denote distances in feet to target ground zero.
(b) Ground ranges denote the distances to actual ground zero.

[redacted]

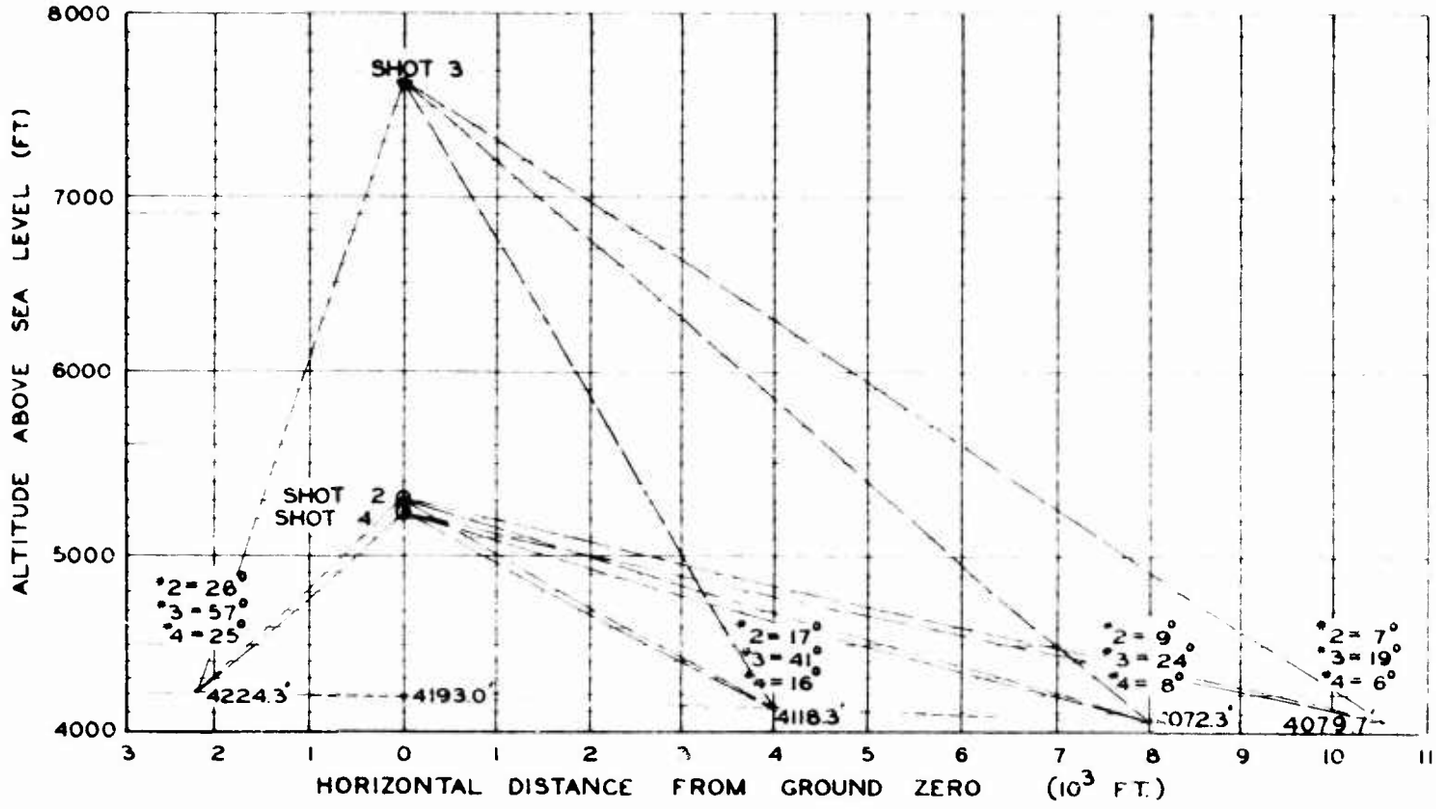

Fig. 3.177 Station Elevations and Horizontal Distances From Target Ground Zero Showing Bomb Burst Points. Numbers Designate Direct Ray Incidence Angles at Range Shown.

Fig. 3.178 B-17 (3722), Lef. Side-in, Station 8000 (11 cal/cm^2), Shot 3, Showing Condition of Aircraft During Thermal Phase Approximately One Second After Time Zero

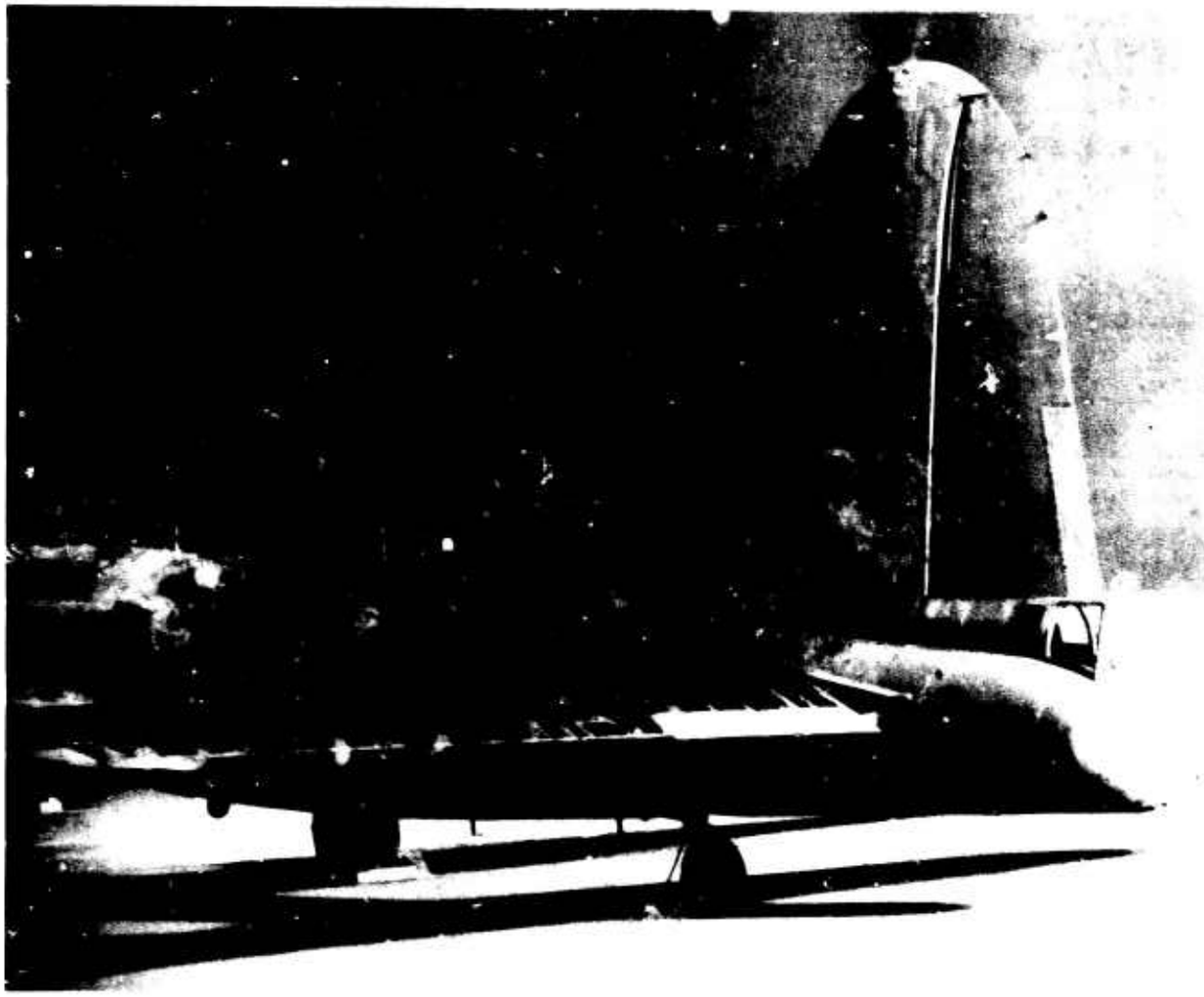

Fig. 3.179 B-17 (3730), Tail-in, Station 10,500 (6.7 cal/cm^2), Shot 3, Showing Condition of Aircraft During Thermal Phase Approximately One Second After Detonation

[redacted]

CHAPTER 4

DISCUSSION

4.1 GENERAL

Whereas this is primarily a data report, much of the data are based on visual observations and conclusions drawn therefrom. Therefore, a limited amount of discussion on various phases of the work is included. In general, the (Project 3.1) test was conducted to provide information that would assist in the prediction of effects of atomic bombs on parked aircraft. Various compromises were effected during all phases of the project, due to limitations of time, equipment, funds, and personnel, in an attempt to maintain a balanced program. The results of the test are specific for the weapons, burst heights, and aircraft types employed, as well as the terrain configuration and elevation. However, an effort has been made to extend the data by interpolation and extrapolation for the aircraft types tested. Additional analytical work is being done to extrapolate to foreign types and to modern USAF types as a separate problem but will not be included in this report.

The thermal and blast input functions, responsible for producing damage to parked aircraft, were measured at the aircraft parking stations and on the "blast line". Noticeable variation between measurements made at the different locations is apparent; however, it was felt that use of the composite data from the blast line measurement would be the most desirable at this time since future studies and predictions will probably be based on generalized curves developed from these data. Prognoses and results could be correlated with either pressure data. The accuracy of aircraft vulnerability predictions is probably less than the variations in overpressure measurements. Whereas the shock wave appears quite symmetrical in aerial photographs, local disturbances near the ground, introduced by terrain features, may be responsible for some of the observed pressure variations. Aerodynamic influences in the vicinity of the baffle and at the sensing element orifice or diaphragm may also influence the results.

Thermal inputs measured at the aircraft stations were in reasonable agreement with the measurements made on the blast line. Except for one point, the values were lower indicating greater attenuation as measured approximately 4 ft above the ground while the blast line data presently available for comparison was measured at 50 ft above the ground.

Damage sustained by parked aircraft exposed to atomic detonations

[redacted]

[redacted]

results from a complicated interplay of the thermal and overpressure forcing functions. The degree of damage inflicted depends upon the magnitude of the thermal and blast inputs as well as a variety of factors, such as aircraft heading and structural configuration, which greatly influence aircraft vulnerability. A comprehensive study of all factors affecting aircraft damage could not be made because of the prohibitive number of aircraft required to solve completely the problems introduced by the large number of variables involved. Hence, the tests were designed to facilitate evaluation of the forcing functions and the more influential variables in relation to their effect upon the damage sustained by parked aircraft. No attempt was made to isolate the separate effects of thermal and blast inputs and in general, damage was correlated with overpressure.

4.2 AIRCRAFT DAMAGE ANALYSIS

The data contained in this report consist primarily of information obtained from the exposure of F-47 and B-17 aircraft. Additional aircraft of the more modern types would have been desirable, but availability for destructive tests of this type was extremely limited. The F-47 and B-17 aircraft were used in sufficient numbers to permit determination of the effect of the orientation parameter and a reasonably complete knowledge of the inputs required to produce damage ranging from light to complete destruction of the aircraft.

The exposures of the B-29, B-45, F-90, and two F-86 aircraft were so planned that the results from these limited exposures could be readily compared with the more complete data from the F-47 and B-17 aircraft.

To facilitate analysis of the damage and to make possible a comparison with other aircraft types, the man-hours to repair damage was employed as the common denominator. This figure indicates the necessary labor, in man-hours, required to return the aircraft or particular component to pre-shot condition. The total damage was divided into four categories: wing, fuselage, empennage, and miscellaneous. The miscellaneous category includes such items as electronic equipment, canopies, doors, windows, landing gear, armament, tanks, etc. All data were grouped according to aircraft orientation, plotted as a function of peak overpressure, and the best curve correlating damage with overpressure drawn. Values for peak overpressure were taken from the set of curves (Fig. 3.173) presenting the composite results of Program 1 pressure measuring agencies. Because of the variety of factors that influence damage to parked aircraft, an exact correlation with one variable is not possible. For this reason the curves are necessarily approximate; however, it is felt they do adequately represent the influence of the orientation parameter and the effects of the overpressure forcing functions for ratios of energy partition of the same magnitude.

[redacted]

[redacted]

An artist's conception of the damage sustained by twenty-seven of the twenty-eight aircraft that participated in Shot 3 is shown in Fig. 4.1. This figure shows the range and orientation of each participating aircraft and the degree of damage sustained by the total aircraft, as well as the particular components damaged. Thermal and blast forcing functions are also given.

4.2.1 F-47 Aircraft

The summarized data obtained from the exposure of sixteen F-47 aircraft to three atomic detonations were segregated according to aircraft orientation and plotted as a function of peak overpressure. The three orientation parameters used were side-in, tail-in, and nose-in, shown in Figs. 4.2, 4.3, and 4.4, respectively. Damage is plotted as man-hours required to return aircraft to pre-shot condition. The value of 3000 man-hours damage is taken as the limit above which the aircraft would be considered beyond economical repair.

Comparison of the damage sustained by variously oriented F-47 aircraft at a given overpressure shows that the side-in orientation is the most vulnerable. Tail-in oriented aircraft are next most readily damaged with nose-in aircraft being the least susceptible to damage. This analysis is most correct in the overpressure range of 3 to 6 psi. At overpressures considerably above this range the orientation parameter becomes less influential. At these overpressures the aircraft will be damaged beyond repair regardless of orientation.

The miscellaneous damage curve (instruments, armament, electronic equipment, etc.) closely follows the curve for fuselage damage for all three orientations. The degree of fuselage damage, as with total damage, is a function of the orientation parameter, being greatest for side-in orientations, less for tail-in, and least affected when the aircraft is headed nose-in to the blast. Wing damage does not follow the above pattern but is found to be highest in the tail-in position, lower for aircraft parked side-in, and lowest for nose-in oriented aircraft. Wing damage includes damage sustained by flaps and ailerons which are susceptible to damage at relatively low overpressures. Damage to these components contributes significantly to wing damage when the aircraft is oriented tail-in, since this leaves the flaps and ailerons in a most vulnerable position. For close-in aircraft, blast incidence may play an important part in producing damage of this type. Conclusions regarding orientation parameter arrived at for total damage and fuselage damage, also apply for empennage damage.

Damage to F-47 aircraft begins at overpressures of 2 psi or slightly above. At overpressures of 6 psi, nose-in aircraft are still only lightly damaged; whereas, aircraft oriented side-in would be heavily damaged. In general, F-47 aircraft subjected to overpressures of 9 psi would be considered beyond economical repair regardless of

[redacted]

[redacted]

orientation; however, higher pressures would be required for complete destruction.

4.2.2 B-17 Aircraft

Seven B-17 aircraft were employed in Operation TUMBLER-SNAPPER. One of these was the B-17 previously damaged in Operation BUSTER-JANGLE. As with the F-47 aircraft, the results from exposing these aircraft to Shots 2, 3, and 4 were divided into three groups according to the orientations, side-in, tail-in, and nose-in, and plotted against peak overpressures. Since fewer B-17 aircraft were used, the data for B-17 aircraft vulnerability are somewhat less reliable than those obtained for F-47 aircraft. The total damage and damage sustained by the wings, fuselage, empennage, and miscellaneous items, is shown in Figs. 4.5, 4.6, and 4.7 for side-in, tail-in, and nose-in orientations, respectively.

In relation to the F-47 damage curves, the range of overpressures covered is quite small; however, from the standpoint of degree of damage, the coverage is similar. In contrast to the figure of 3000 man-hours damage given as the limit of economical repair of F-47 aircraft, B-17 aircraft may be considered damaged beyond economical repair when the damage exceeds 15,000 man-hours. It is recognized that this man-hour limit is somewhat arbitrary and, being dependent upon a variety of conditions, is subject to wide fluctuations.

In the 1 to 3 psi region B-17 aircraft are most vulnerable when parked side-in and least vulnerable when parked nose-in, with tail-in being the orientation of intermediate vulnerability. The general effect of the orientation parameter is the same for the two aircraft types (B-17 and F-47) discussed, but has the greater influence on fighter damage. In the side-in and nose-in orientations the fuselage suffers the greatest number of man-hours damage as shown in Figs. 4.5 and 4.7. The high fuselage damage for the nose-in orientation is a departure from observed fighter behavior. At the lower overpressures with the aircraft parked tail-in, the empennage suffers the greatest damage. This again is not as observed with fighter aircraft wherein empennage damage was quite light for the tail-in condition. The fabric covered control surfaces of the B-17 empennage are more susceptible to thermal damage in the tail-in position. This, and other obvious structural differences, notably control surface area and specific strength, tend to explain the observed reactions of the fighter and bomber empennages. Miscellaneous damage curves are lower in amplitude but follow the curves for fuselage damage quite closely. Window breakage and radome breakage represent a considerable portion of the miscellaneous damage which in turn represent a significant fraction of the total damage. Unlike F-47 aircraft, B-17 aircraft wing damage is not extraordinarily high in the tail-in position at overpressures below that required to damage the aircraft beyond economical repair. At

[redacted]

higher overpressures, however, wing damage increases rapidly to become the component sustaining heaviest damage. Figures 3.154 and 3.155 show the wing damage sustained by the tail-in B-17 aircraft parked at Station 4000 during Shot 4.

Bomber aircraft as represented by the B-17 configuration were designed to much lower load factors than the F-47 aircraft. Consequently, the range of overpressures covering from little or no damage to heavy damage is much lower for the relatively weaker B-17 aircraft. At overpressures of 3 to 4 psi the aircraft is heavily damaged. Overpressures in the neighborhood of 5 psi are required to damage the aircraft beyond salvaging of any major components.

It should be remembered, especially in the case of aircraft similar to the B-17, that even though an aircraft may sustain damage requiring several thousand man-hours for complete repair, in emergency situations the aircraft could possibly be patched up in far less time and used for tactical purposes though flight would be restricted and hazardous.

4.2.3 B-29 and B-45 Aircraft

Only one B-29 and one B-45 aircraft were made available for the parked aircraft vulnerability program. In the two exposures, Shots 3 and 4, where noticeable damage was sustained, both aircraft were oriented nose-in. The highest overpressures to which these aircraft were subjected produced only moderate damage. On the basis of these limited data and B-17 data by analogy, curves showing component damage as a function of overpressure were drawn up for nose-in B-29 and B-45 aircraft.

During Shot 4 the nose compartment and rear compartment of the B-29 fuselage were destroyed by fire. Fire fighting crews arriving on the scene as soon as possible after the detonation were successful in putting out the fire before it spread to the 4500 gal of 100 octane gasoline in the wing tanks, thus saving enough of the aircraft to permit a moderate evaluation of overpressure damage.

Damage versus peak overpressure for nose-in B-29 aircraft is presented in Fig. 4.8 which covers damage ranging from light to moderate. An outstanding feature is the exceptionally high empennage damage. From behavior of B-17 aircraft it would be expected that empennage damage would be light for the nose-in position. Since damage somewhere in the neighborhood of 25,000 man-hours is required to classify a B-29 aircraft as damaged beyond economical repair, it is seen that Fig. 4.8 represents only the very low damage region. It is apparent, however, that B-29 aircraft are considerably more resistant to damage than B-17 aircraft. The damage threshold for nose-in B-29 aircraft is somewhere in the neighborhood of 2 psi. It is expected that

B-29 aircraft would suffer heavy damage when exposed to overpressures in the 5 to 6 psi range. Complete destruction may be expected at overpressures of 7 psi or higher.

The vulnerability of B-45 aircraft, parked nose-in, as a function of overpressure is presented in Fig. 4.9 for the overpressure range up to 7 psi. At the maximum overpressure investigated, the B-45 aircraft was only moderately damaged. The thick skinned wings of the B-45 aircraft are very damage resistant. Even at overpressures of 6 psi, wing damage is negligible. Empennage damage is quite light and contributes little to the total damage in the range of overpressures covered. Fuselage and miscellaneous damage are of primary importance. Damage to bomb-bay doors, access doors and hatches, and plastic articles were among the more vulnerable components.

The over-all damage resistivity of the B-45 aircraft is better than both the B-17 and B-29 type aircraft. Damage commences at an overpressure of somewhere below 3 psi for nose-in orientation. Heavy damage should be expected at overpressures of 8 psi with approximately 9 psi or higher required for complete destruction.

4.2.4 F-86 and F-90 Aircraft

Two F-86 aircraft and an F-90 aircraft were included in the test as representative of modern fighter types. The F-90 suffered damage in all three tests, whereas the two F-86 aircraft were damaged only during Shots 3 and 4. Insufficient data were available from these limited exposures to allow presentation of the data in chart form, as a function of overpressure.

Both the F-86 and F-90 aircraft are more damage resistant than F-47 aircraft at the higher overpressures, regardless of aircraft orientation. For nose-in orientation, the F-47 appears to be less susceptible to damage than the F-86 and more vulnerable than the F-90 for overpressures up to 7 psi. The F-86 aircraft appear to be more damage resistant than F-47 aircraft for the tail-in orientation at all overpressures. Total damage of nose-in F-90 and F-47 aircraft just above the damage threshold is almost equivalent; however, at higher overpressures the F-90 is considerably more damage resistant.

An overpressure of 9 psi would be expected to inflict heavy damage on F-86 aircraft even though oriented nose-in. It is estimated that F-90 aircraft must be subjected to overpressures of 10 to 11 psi to produce equivalent damage. It is estimated that overpressures in the neighborhood of 12 to 15 psi would be required to destroy aircraft of the F-86 and F-90 type.

[redacted]

4.2.5 Equipment and Systems

Both jet and reciprocating type power plants and power plant accessories are very damage resistant. Under conditions which would damage the airframe beyond repair, power plants will in general remain operable. Unfilled or partially filled fuel and oil tanks are among the more vulnerable accessories. Dust and other foreign matter that collect in air-intake ducts represent a potential hazard to aircraft engines and introduce additional maintenance problems. Post-shot flight preparations must include thorough cleaning of engine air-intake ducts. Propellers are similar to the power plants in that they suffer no significant damage up to the point where the airframe is damaged beyond repair, unless accidental contact with the ground or flying debris is made. Power plants and propellers would not be expected to be the cause for grounding an aircraft exposed to a nuclear detonation and should in fact represent only a small fraction of the work required to return any aircraft to service.

An adequate analysis of effect of atomic detonations on armament equipment can not be made because of the limited amount of armament tested and the lack of modern equipment. Armament equipment, such as machine guns and cannons, would be unaffected by thermal and overpressure forcing functions which are not of sufficient severity to destroy the aircraft structure. It is expected that modern electronic sighting equipment installed in aircraft subjected to overpressures of 6 psi or greater would be damaged sufficiently to require replacement or readjustment. Armament equipment installed in aircraft exposed to overpressures of about 3 psi would probably need only check-out and minor maintenance. Most bombs, rockets, and ammunition probably would not be affected in the lower overpressure regions. Armament equipment would not be a primary cause for grounding of aircraft.

In general, electronic equipment was adequately protected against thermal and blast forcing functions by the aircraft fuselage. Failure of mounts contributed to electronic equipment damage. External elements such as radomes and antenna components were damaged by the thermal phase when accompanying overpressures were too low to cause noticeable damage. Radomes exposed to thermal energies of 15 cal/cm^2 would be charred to varying degrees, depending upon the surface coating. The charring may be expected to have a deleterious effect upon the transmission of certain radar frequencies. External radio antenna components subjected to thermal energies in the neighborhood of 15 cal/cm^2 would be damaged to varying degrees depending upon the type of surface.

Damage to aircraft electrical systems, mechanical systems, and instruments will be of a minor nature in comparison to total damage when the aircraft is not structurally damaged beyond repair. The electrical system and components received essentially no damage,

[redacted]

other than that sustained by external fittings such as wing navigation lights, except in instances of major structural damage. Except for occasional loosening of fittings hydraulic systems were not damaged. Fire detecting and extinguishing systems, cooling equipment, and pressurization equipment, other than door and canopy seals, are not vulnerable. Protection provided by the airframe is adequate to reduce the damage to these systems to a negligible quantity. Thermal radiation (50 cal/cm^2, unattenuated) caused charring of tires and produced a spongy layer no greater than one-sixteenth of an inch deep. Tires were considered serviceable although useful life was undoubtedly shortened. At the close-in stations, Shot 4, pieces of aircraft debris and sharp stones were found embedded in the tires. All tires not destroyed by fire retained their original air pressure. Landing gear struts and components, wheels and brakes, and mechanical actuators were found to be serviceable on all aircraft which did not sustain extreme damage.

Aircraft instrument damage does not contribute significantly to the total damage from a man-hour standpoint; however, many instruments of importance may suffer damage at relatively low overpressures. Aircraft instrument damage has been summarized and is given in Table 4.1. This table lists each instrument damaged and gives type, orientation, and blast pressure received by aircraft in which damaged instrument was installed. For purposes of continuity, any aircraft receiving instrument damage is included under all three tests whether or not previous or additional damage was sustained.

In the three tests a total of twenty-nine instruments were damaged. A breakdown of instrument damage according to fighter and bomber aircraft is given in the summary below.

	Fighter	Bomber
Number instruments damaged	16	13
Aircraft exposures[1]	45	20
Average overpressure[2]	6.6	3.7

If damaged instruments had been replaced before each test, the total number of instruments damaged probably would have been increased by three or four for both fighters and bombers.

It is seen that while the number of fighter exposures are over double that of bomber exposures, the total number of instruments damaged is only slightly greater. In addition the average overpressure of the aircraft receiving instrument damage is almost twice as high for fighter aircraft. Bombers, on the other hand, have a higher instruments-per-aircraft ratio. Taking all factors into consideration it

---

1/ Includes aircraft undergoing post-test instrument inspection only.

2/ Includes aircraft with instrument damage only.

appears that bomber aircraft are more vulnerable to instrument damage than are fighter aircraft. An analysis of the minimum overpressure required to damage air-speed indicators and altimeters in fighters and bombers substantiates the above conclusion.

The most vulnerable instrument is the air-speed indicator representing over 40 per cent of the instruments damaged. In fighter aircraft damage begins at an overpressure of about 5 psi with the aircraft facing directly toward or away from the blast. For fighter aircraft parked side-in damage appears to begin at an overpressure somewhere above 7 psi. The simple precaution of installing a pitot-static tube cover should protect the instrument at overpressures up to 10 psi as is shown by results on aircraft F-47 (9232), Shot 3 (see Table 4.1). In bombers the air-speed indicators appear to suffer damage at extremely low overpressures (1.8 psi).

Of the six altimeters damaged, one was installed in a fighter and five were installed in bombers. The fighter aircraft in which the damaged altimeter was installed received an overpressure of 6.8 psi. Bomber aircraft sustaining damage to altimeters were in all cases subjected to overpressures lower than 6.8 psi.

No consistency regarding directional gyro damage versus overpressures exists. Damage to this type instrument was confined to fighter aircraft. The above statements also apply to damage to rate-of-climb instruments. It is apparent that B-17 fuel pressure transmitters are extremely sensitive. Damage to the tachometer in the F-86 (9597), in Shot 4 was caused by flying debris.

4.2.6 General Observations

Thermal and blast inputs both contribute to structural damage of aircraft. The importance of one input versus the other depends to a great extent upon the structural configuration in question. To minimize thermal and overpressure damage an optimum longeron-frame ratio must be used. A fuselage consisting of a few heavy stringers and many frames will be more resistant to damage of primary structure; however, the vulnerability of the panels will be increased because of size. If panel size is decreased by using a greater number of relatively lighter stringers, panel vulnerability is decreased but the substructure damage may occur at a lower overpressure. Modern-integrally-stiffened structures should suffer somewhat less damage from the combined effects of heat and pressure than the conventional riveted and spot welded assemblies because of superior heat transfer. Better heat transfer will reduce the skin temperature and the temperature differential between skin and substructure. The advantage may be partially offset by the strength reduction in the integral stiffeners if the temperature rise is critical.

[redacted]

Thermal damage resulting from exposure to atomic detonations can be minimized by using only bare, bright metal surfaces. External marks and instructions should be light rather than dark in color. Protection of aircraft against thermal damage should not be too difficult and well may merit investigation, possibly in conjunction with camouflage technique. Efforts should be made to reduce the possibility of fires in crew compartments by minimizing the amount of combustible material and by introducing protective methods. If the entire aircraft is not protected, use of a highly reflective, fire proof covering for windows, windshields, canopies, etc. could be employed.

Considerable damage to aircraft at the close-in stations was effected by sandblasting and missiles. Damage would have been reduced had the area been hard-surfaced and free from debris.

The differences in aircraft attitude as represented by the tricycle landing gear of the F-86 aircraft and the conventional landing gear of the F-47 aircraft may be a factor influencing damage to parked aircraft. Cribbing of the tails of several F-47 aircraft prior to Shot 4 to simulate tricycle gear attitude did not yield conclusive results regarding the effect of this parameter. This investigation included only a narrow range of overpressures and may not have included more critical regions.

Examination of the type of damage sustained by many aircraft, especially fighter type in higher overpressure regions, indicates that adequate tie-downs may have reduced the damage considerably for nose-in orientations. The additional restraint imposed may result in greater stresses and therefore more severe damage for orientations, other than nose-in. Examination of the damage sustained by the nose-in F-86 aircraft parked at Station 2500 for Shot 4 plus analysis of the marks on the hardstand indicate the aircraft underwent severe gyrations during the blast phase. In being jostled about, considerable damage was caused by contact with the ground which may have been significantly reduced had the aircraft been restrained by adequate tie-downs.

Several F-47 aircraft caught fire at close-in stations. Fires probably resulted from a combination of thermal and blast effects. In this region, where overpressures are of sufficient severity to destroy major components of the aircraft, there is little advantage in shielding combustible material from thermal radiation. Under certain conditions, as with the B-29 on Shot 4, the thermal energy may be sufficient to initiate a destructive fire at ranges where overpressure damage would be moderate. This fire was apparently caused by the ignition of combustible material in the forward nose compartment and, following the collapse of the nose structure causing the aircraft to assume a tail-high attitude, the fire progressed through the crew tunnel to the aft crew compartment destroying the aft section of the fuselage. Covering of the windows with a highly reflective material would probably

[redacted]

have prevented this fire. Pressure doors on either end of the crew tunnel would have prevented the flu action of the tunnel and probably reduced the damage.

4.3 PASSIVE DEFENSE STRUCTURES

The value of revetments as a means of reducing damage to parked aircraft exposed to a nuclear detonation was investigated using F-47 aircraft. Three revetments, each a different type, were constructed at two different locations, Station 4000 and Station 8000. The structural configuration and dimension of these revetments are shown in Fig. 2.5. At Station 4000 a wall-type and a pit-type revetment were constructed, and a G-type revetment was constructed at Station 8000. The "G" revetment was large enough to accomodate three F-47 aircraft; however, only two aircraft were placed therein. The wall and pit revetments each accomodated one aircraft.

Three F-47 aircraft, oriented side-in, were parked at Station 4000 for Shot 3. Two of the aircraft were behind the revetments and the third directly exposed between these two. The overpressure was 6.4 psi with a thermal input of 32 cal/cm^2. These inputs caused heavy damage to all three aircraft. There was a slight damage differential, with the aircraft in the pit revetment sustaining the least damage. The aircraft behind the wall revetment sustained slightly more damage than the aircraft protected by the pit revetment, but sustained less damage than the unprotected aircraft. Passive defense structures of this type are apparently not a very efficient means of protecting aircraft from high-burst bombs, at least in the overpressure regions investigated. The limiting ray showing what portion of the aircraft was subjected to direct radiation and what portion was shielded by the revetments is shown in Fig. 4.10.

One aircraft was parked nose-in and another side-in in the "G" revetment for Shot 3. A plan view of the revetment including the aircraft is shown schematically in Fig. 2.3. A side view showing the limiting ray is presented in Fig. 4.10. The nose-in aircraft, F-47 (9719), parked in the entrance, sustained only minor damage; however, F-47 (0065), directly exposed, likewise suffered minor damage. At this low damage level the revetment appeared to afford no protection. The directly exposed side-in aircraft, F-47 (9785), was considerably more damaged than the side-in F-47 (9074) protected by the wall revetment.

No aircraft were parked in the "G" revetment for Shot 4. Two F-47 aircraft were protected by revetments at Station 4000; one was parked tail-in behind the wall revetment and the other, also tail-in, was placed in the pit revetment. For comparison purposes an aircraft, similarly oriented, was placed between the two revetments. With this lower angle shot, the revetments afforded considerably more protection than in Shot 3. The limiting rays of direct radiation are shown in

Fig. 4.10. The two aircraft protected by revetments were lightly damaged; whereas, the aircraft directly exposed sustained heavy damage.

It appears, therefore, that the effectiveness of revetments depends considerably upon the relationship between distance from ground zero and the burst height. Greater protection is afforded when used in connection with low bursts. Protection is the result of both thermal and blast shielding. Instrumentation indications are that peak overpressures are not greatly influenced by the revetments but that the time to maximum is greater behind the revetments. No results have been obtained on the effectiveness of revetments at overpressures greater than 6 psi.

4.4 THERMAL DAMAGE

Damage sustained by aircraft as exposed in this test resulted from a combination of thermal and blast energies, thus making it difficult to determine the specific effect and importance of thermal inputs in causing damage to various structures at different energy levels. The apparent thermal damage of aircraft surfaces was segregated into three categories according to degree of damage: little or no damage, moderate damage, and heavy damage. Little damage denotes light scorching, moderate damage denotes heavy scorching and burning with buckling prevalent, and heavy damage denotes severe thermal damage, including occasional holes in the skin surface. The damaged surfaces were then classified according to skin thicknesses and the total thermal energy normal to the skin surface required to produce the damage observed was computed (assumed absorptivity of 0.5, thermal inputs from Fig. 3.174). By assuming an ambient temperature of 110°F, the maximum temperature of the skin surfaces was also calculated. These results are presented in graphical form in Fig. B.3. This graph applies to 24ST aluminum only. Skin thickness of F-47 aircraft components is given in Figs. 4.11 and 4.12. Damage apparently begins in the 340°F to 390°F range. Heavy damage begins anywhere from 420°F to 535°F. Doped fabric skin surfaces may burn when subjected to incident thermal energies as low as 2 cal/cm^2. The data are very incomplete and no trend regarding damage threshold for particular skins as a function of peak temperature can be established. Part of this variation is caused by the influence of the overpressure damage variable, for which no correction was made.

4.5 INSTRUMENTATION RESULTS

A short discussion of specific aircraft responses as measured by oscillographic instrumentation is presented in this section. The detailed treatment of oscillographic instrumentation is given in Appendix A of this report.

[redacted]

4.5.1 Total Thermal Energy

Total thermal energy measurements were made during all shots and at all instrumented stations, except Station 2200 during Shot 2. The measurements were of two types: cockpit measurements (see A.4.1.2, Appendix A) which indicated the level of thermal energy in the cockpit of airplanes and site measurements (see A.4.1.1, Appendix A) which gave the general level of thermal energy at the various stations. The site measurements were made at heights varying from 2½ to 5 ft above the ground. Curves that present the blast line measurements and those of Project 3.1 for all instrumented stations and all shots are presented in Fig. 3.174. In general, Project 3.1 measurements were less than those which were made on the blast line. It is believed that Project 3.1's lower values are due to the attenuation of the smoke and dust near the ground. An attempt to correlate the attenuation due to dust and smoke as a function of ground range for each shot is shown in Fig. A.65. These curves are preliminary and additional data are required to draw even tentative conclusions; however, the data presented are considered accurate.

4.5.2 Overpressure

Ground level overpressure measurements were made by Project 3.1 and Project 1.13 (DTMB) at several aircraft parking stations. A comparison of the Project 3.1 and Project 1.13 peak overpressure data with the average of all peak overpressure measurements made along the blast line, presented in Fig. A.73, shows them to be higher than the composite blast line data. Of particular interest are pressure measurements at Station 10,500 during Shot 3, when both the Project 1.13 and Project 3.1 station overpressure measurements were about 25 per cent higher than the mean of all the overpressure measurements which were made along the blast line. This increase in overpressure may have been due to local terrain and surface conditions. A more detailed discussion of these data is given in A.4.2.1 of Appendix A.

4.5.3 Temperature Rise

Temperature rise measurements were made on the wings of F-86, F-47, and B-17 aircraft at the particular stations and for the specific shots mentioned in A.2.1.3 of Appendix A. For reasons of comparison, temperature rise measurements were made on polished and unpolished skin surfaces and on skin and adjacent stringer members. The polished and unpolished measurements were made on the right and left wing, respectively, of B-17 (5715), as described in A.2.1.3 in Appendix A. The temperature rise of the unpolished surface was of the order of two or three times that of the polished surface. The temperature rise of the skin and adjacent stringer on F-47 (0065) indicated that the temperature rise of the stringer was much slower, reaching a peak of 15°C above pre-shot temperature in 20 sec, whereas the skin

[redacted]

[redacted]

(0.040 in.) rose to a peak of 49°C above pre-shot temperature in only 6 sec.

4.5.4 Wing and Fin Bending Moment Measurements

The F-47 (0065) and the F-86 (9597) were chosen as representative configurations of old and new types of fighter aircraft for the purpose of comparing the response of the two types of wing structure. For Shots 2 and 3 these aircraft were parked in juxtaposition and oriented nose-in at Station 8000. They were positioned adjacently and oriented tail-in at Station 4000 during Shot 4. During Shot 3 at Station 8000, where the peak overpressure was 3.6 psi, the F-47 wing bending moment was equivalent to 48.6 per cent of ultimate, whereas the F-86 wing bending moment was negligible. A comparison of the bending moments of these two aircraft was not possible during Shots 2 and 4 because valid measurements of the F-86 wing bending moment were not obtained.

Thermal effects on the wing bending of B-17 (5715) at Station 4000 during Shot 4 were pronounced. The Shot 4 curve in Fig. A.49 indicated an initial bending moment of -700,000 in-lb before the shock wave arrived at the aircraft. The oscillograph record shows bending began immediately after the thermal ray struck the aircraft and increased uniformly until the shock front arrived. This bending probably occurred when the skin on the top surface of the wing, which was subjected to a tensile stress, expanded and allowed the wing to bend downward, thus causing a negative bending moment. This phenomenon occurred only during Shot 4, because more of the wing surface was exposed to the thermal rays due to the tail-in orientation of the aircraft and also because the thermal radiation was more intense.

The measurements of the fin bending moment on F-47 (9785) are presented in Fig. A.50. During Shots 3 and 4 the fin was subjected to bending moments far in excess of the static test ultimate of 54,700 in-lb and yet no failure other than permanent set occurred in the spars of the fin. This extremely high loading, which was equal to 475 per cent of ultimate, was applied over such a short period of time that failure of the spars did not occur. The stress was partly relieved when the aircraft shifted side-wise from its original position. This instrumentation was thoroughly checked for errors but no reason to believe the readings inaccurate was discovered. There was no unbalance due to temperature effects which would indicate a false bending moment, and the oscillograph record showed that there was no drift or overswing of the galvanometer.

4.5.5 Acceleration

Normal and lateral acceleration measurements of certain aircraft were made at the particular stations and on the specific shots

[redacted]

[redacted]

indicated in A.2.1.3, Appendix A. Inspection of the normal acceleration curves (see Fig. A.37) obtained from F-47 (8785) at Station 2200 on Shots 3 and 4 indicates that the acceleration design limit of the aircraft was exceeded on both shots. The various normal and lateral acceleration curves were integrated with respect to time in order to obtain the aircraft velocity curve. This velocity curve was in turn integrated to obtain the displacement of the aircraft. Although the velocity and displacement curves are not presented in this report they are discussed in detail in A.4.5 of Appendix A.

4.5.6 Measurement of Overpressure on Aircraft Wings

A comparison of the overpressure measurements on the wing surfaces of F-86 (9597) and F-47 (0065) during Shot 4 is presented in Fig. A.30, Appendix A. Both of these aircraft were placed side-by-side at Station 4000 and oriented tail-in. As shown in Fig. A.30, the peak overpressure measurement on the F-86 wing amounted to approximately 75 per cent of the F-47 wing overpressure. Inasmuch as the F-47 wing was more nearly parallel to the shock front, a greater overpressure was exerted on this wing; however, there did not seem to be any ratio relationship between the angles of the two wings with respect to the shock front and their respective peak overpressures.

[redacted]

[redacted]

SUMMARY OF DAMAGE TO PARKED AIR

OPERATION SNAPPER --- SHOT 3

AIRCRAFT DAMAGE KEY

COMPLETE AIRCRAFT	AREA AND COMPONENTS
LITTLE OR NO DAMAGE	LITTLE OR NO DAMAGE
LIGHT DAMAGE	MODERATE DAMAGE
MODERATE DAMAGE	HEAVY DAMAGE
HEAVY DAMAGE	BURNING FABRIC SURFACES
DAMAGE BEYOND REPAIR	NOTE: BOMB BAY DOORS DAMAGED AT ALL RANGES

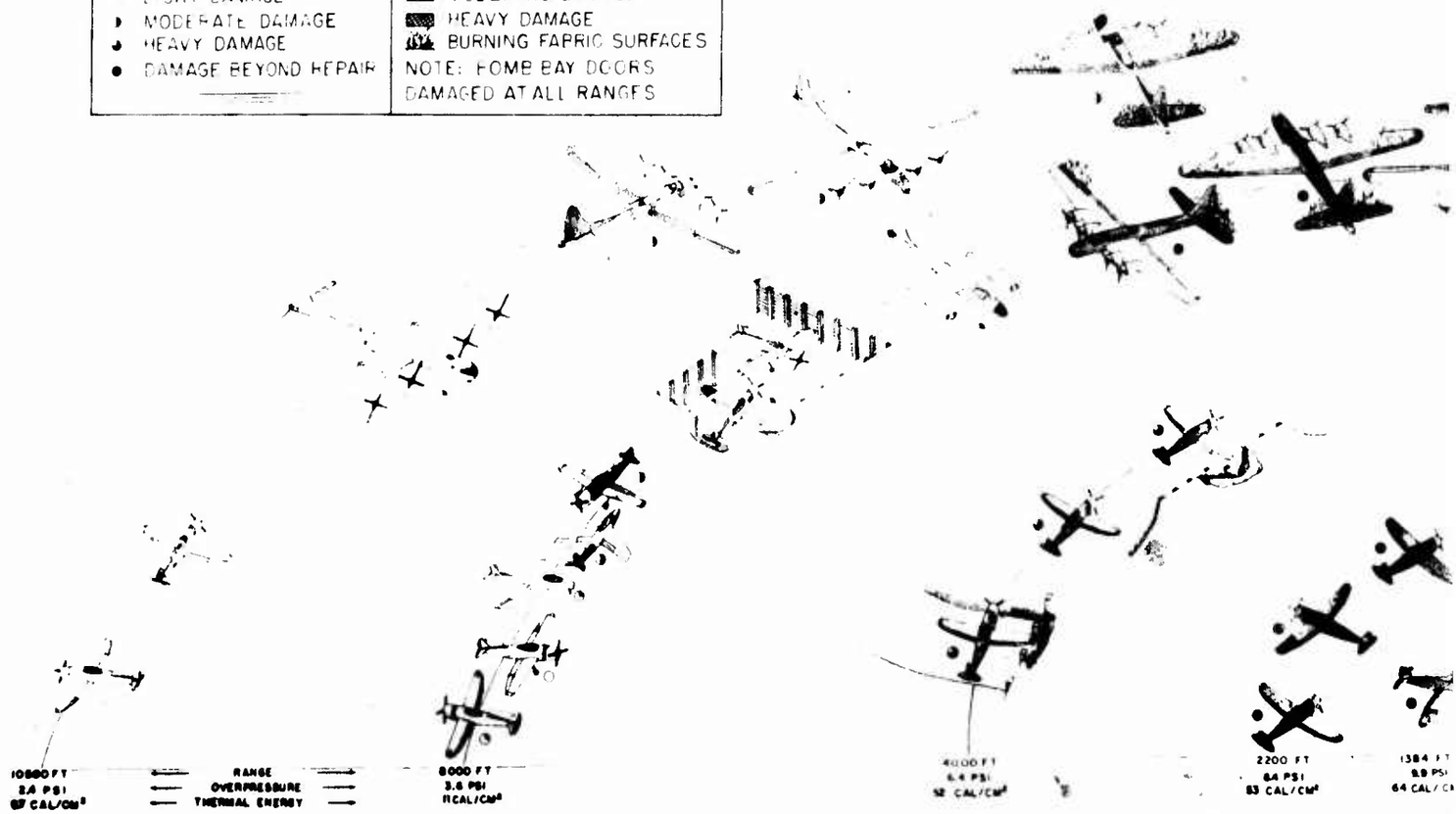

Fig. 4.1 Pictorial Representation of Aircraft Exposed During Shot 3, Showing Extent and

[redacted]

[redacted]

OF DAMAGE TO PARKED AIRCRAFT

OPERATION SNAPPER --- SHOT 3

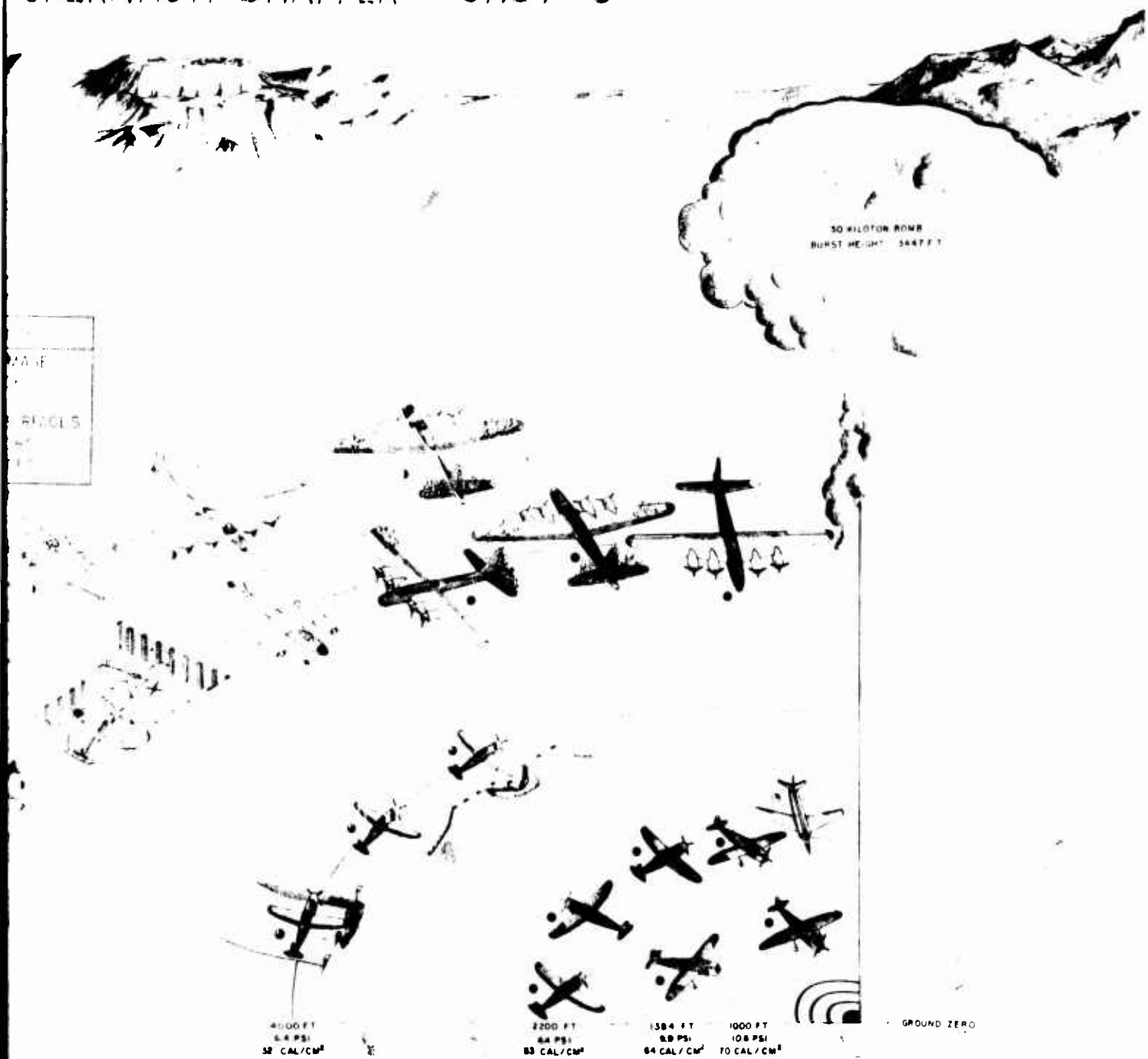

tion of Aircraft Exposed During Shot 3, Showing Extent and Severity of Damage

[redacted]

[redacted]

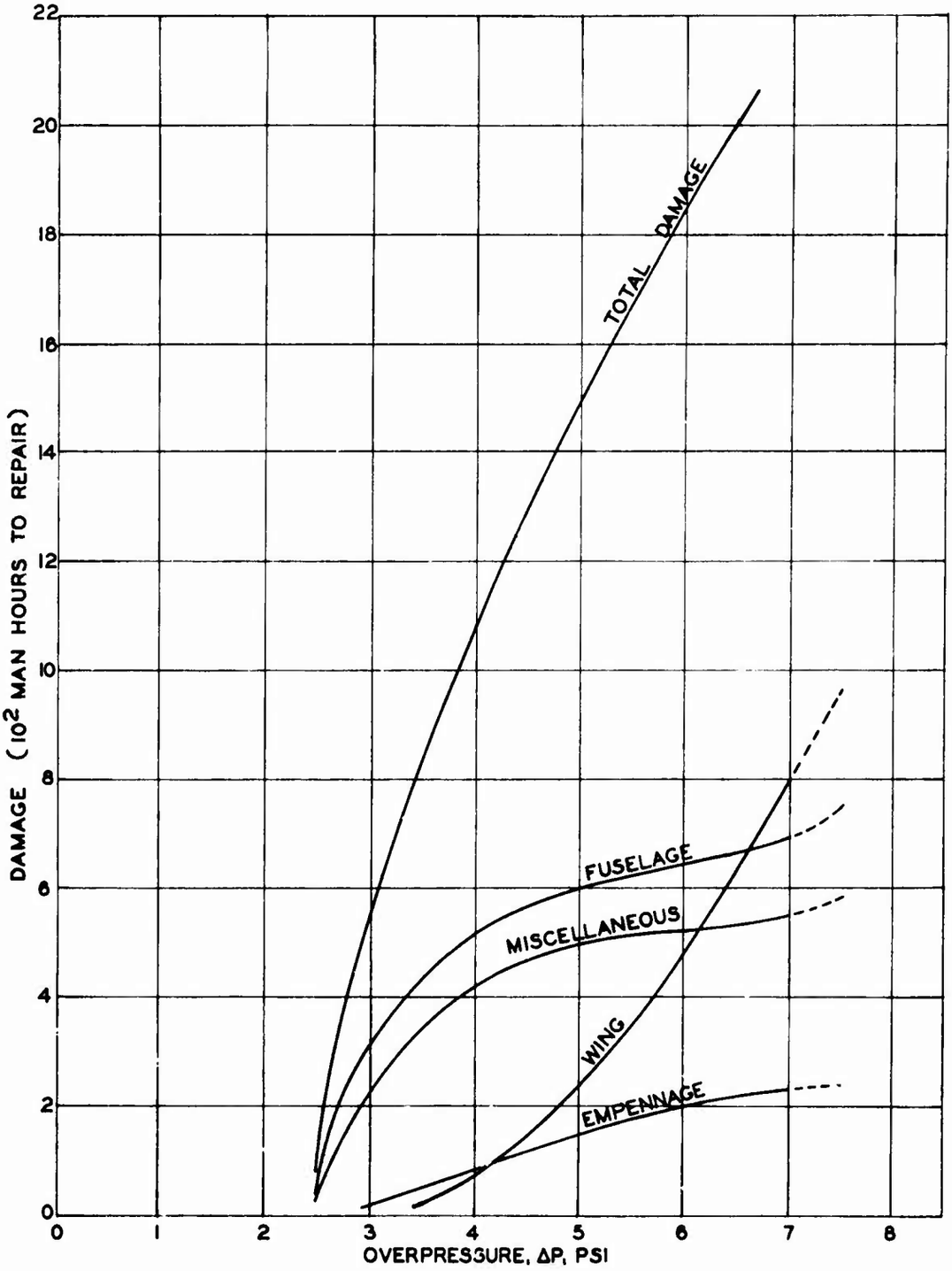

Fig. 4.2 Vulnerability of F-47 Aircraft Parked Side-in as a Function of Peak Overpressure

[redacted]

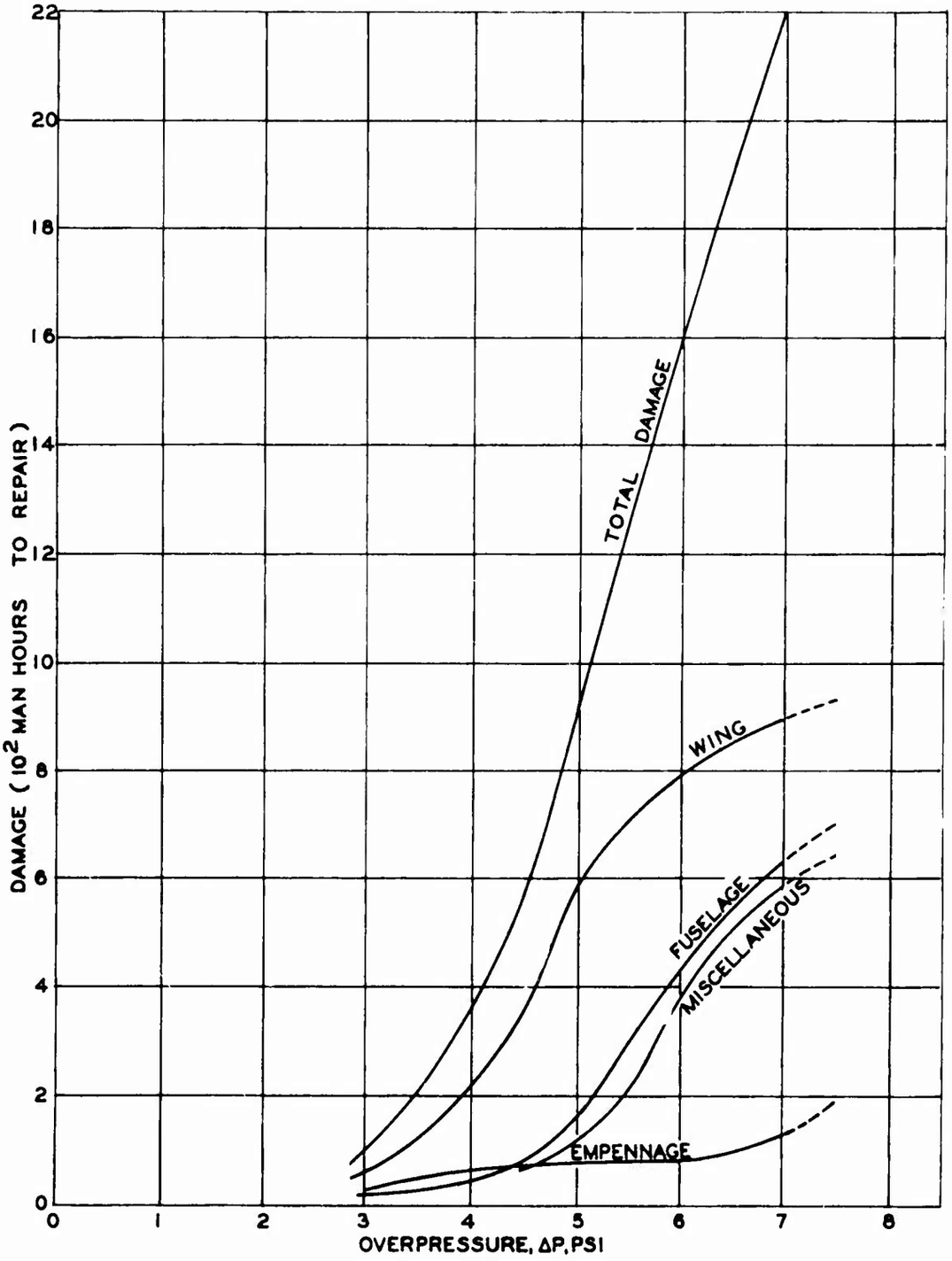

Fig. 4.3 Vulnerability of F-47 Aircraft Parked Tail-in as a Function of Peak Overpressure

[redacted]

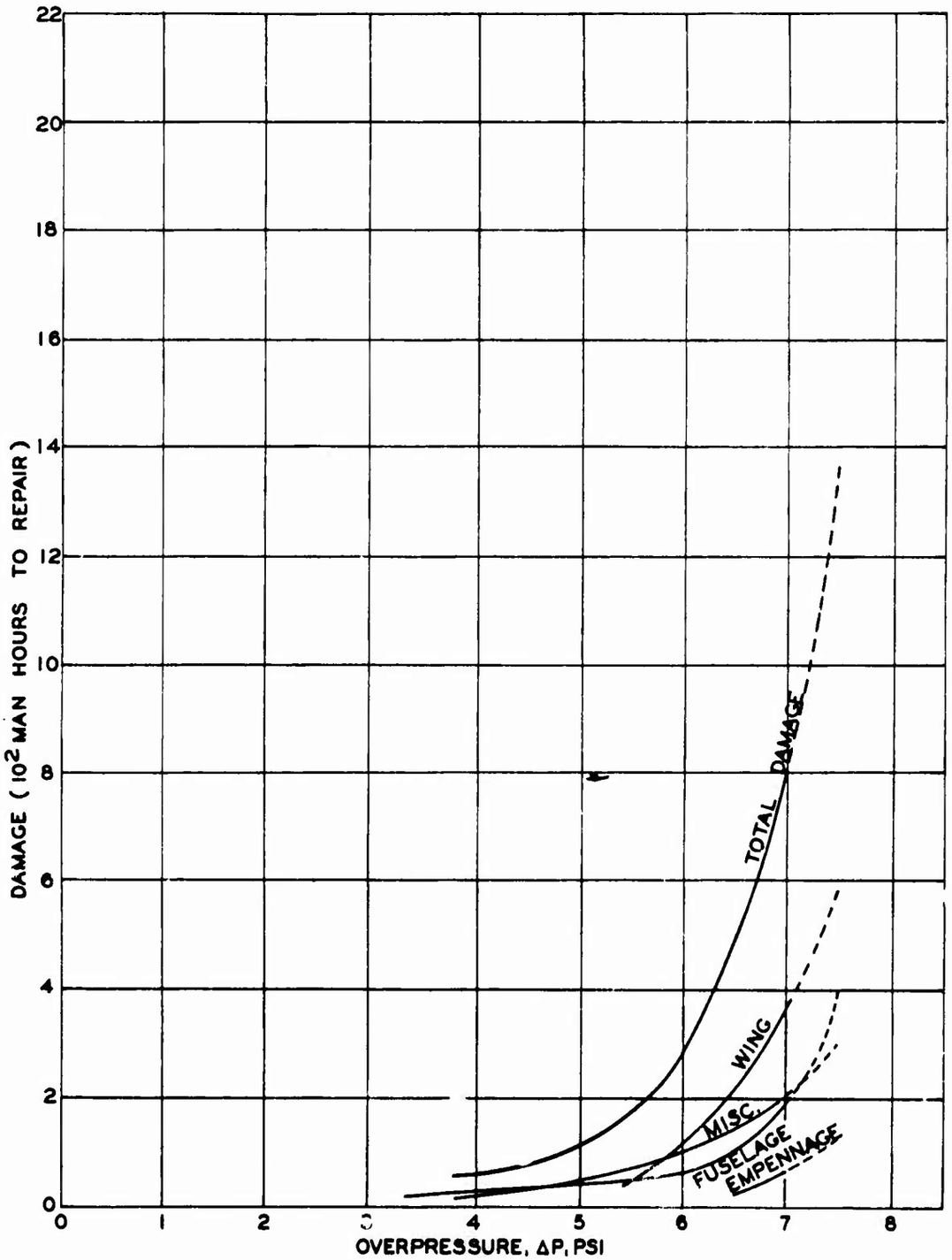

Fig. 4.4 Vulnerability of F-47 Aircraft Parked Nose-in as a Function of Peak Overpressure

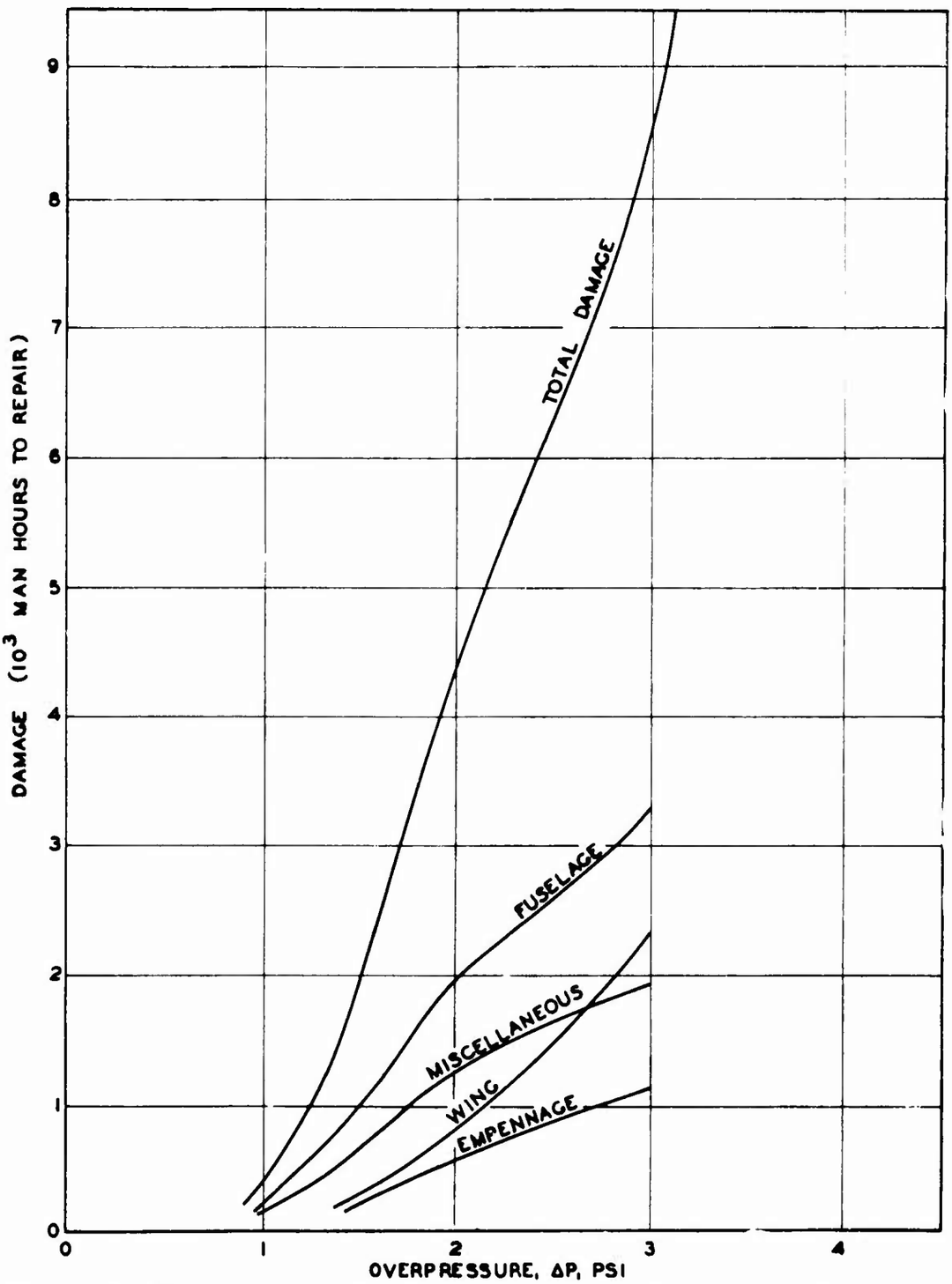

Fig. 4.5 Vulnerability of B-17 Aircraft Parked Side-in as a Function of Peak Overpressure

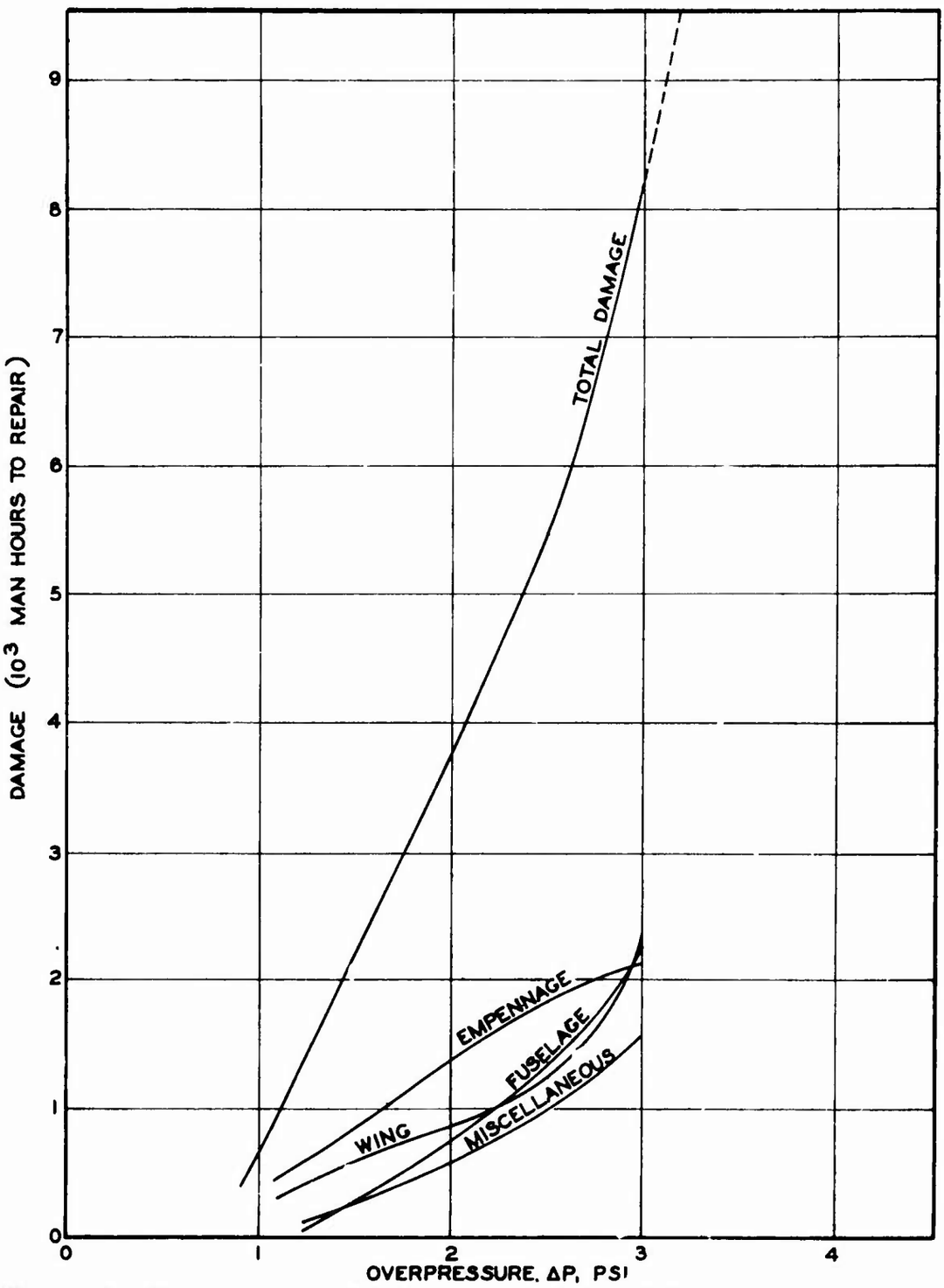

Fig. 4.6 Vulnerability of B-17 Aircraft Parked Tail-in as a Function of Peak Overpressure

[redacted]

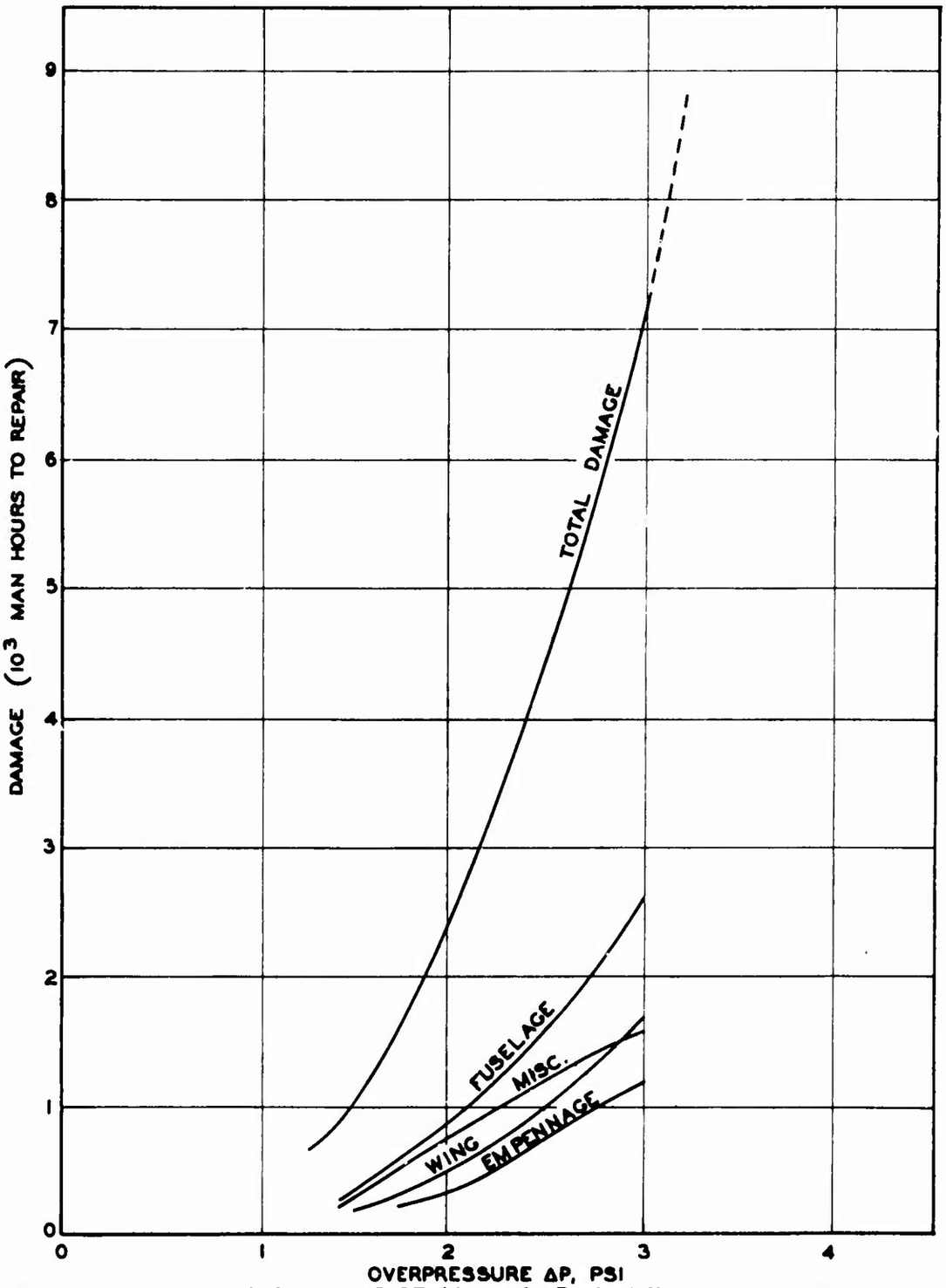

Fig. 4.7 Vulnerability of B-17 Aircraft Parked Nose-in as a Function of Peak Overpressure

[redacted]

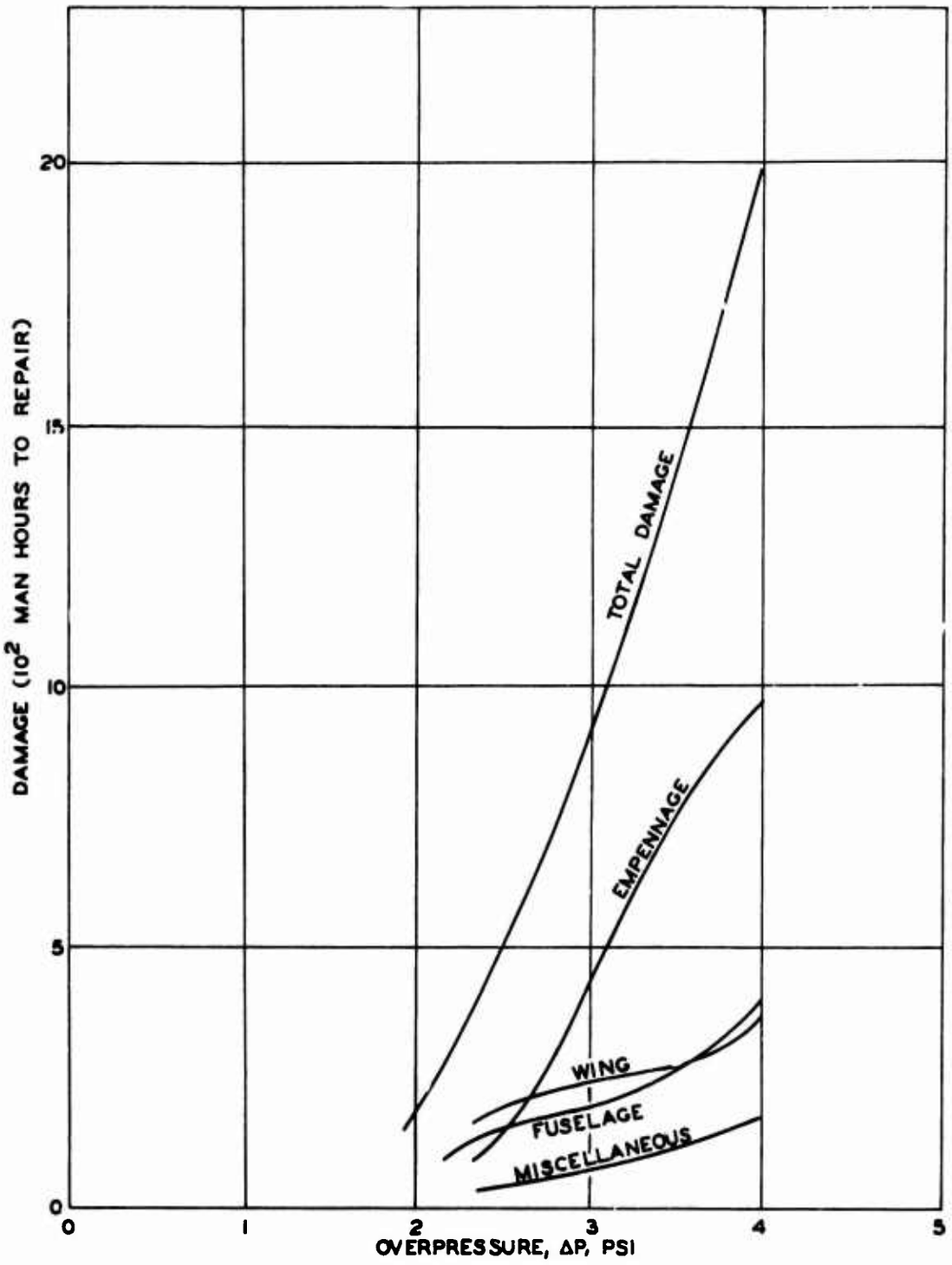

Fig. 4.8 Vulnerability of B-29 Aircraft Parked Nose-in as a Function of Peak Overpressure

[redacted]

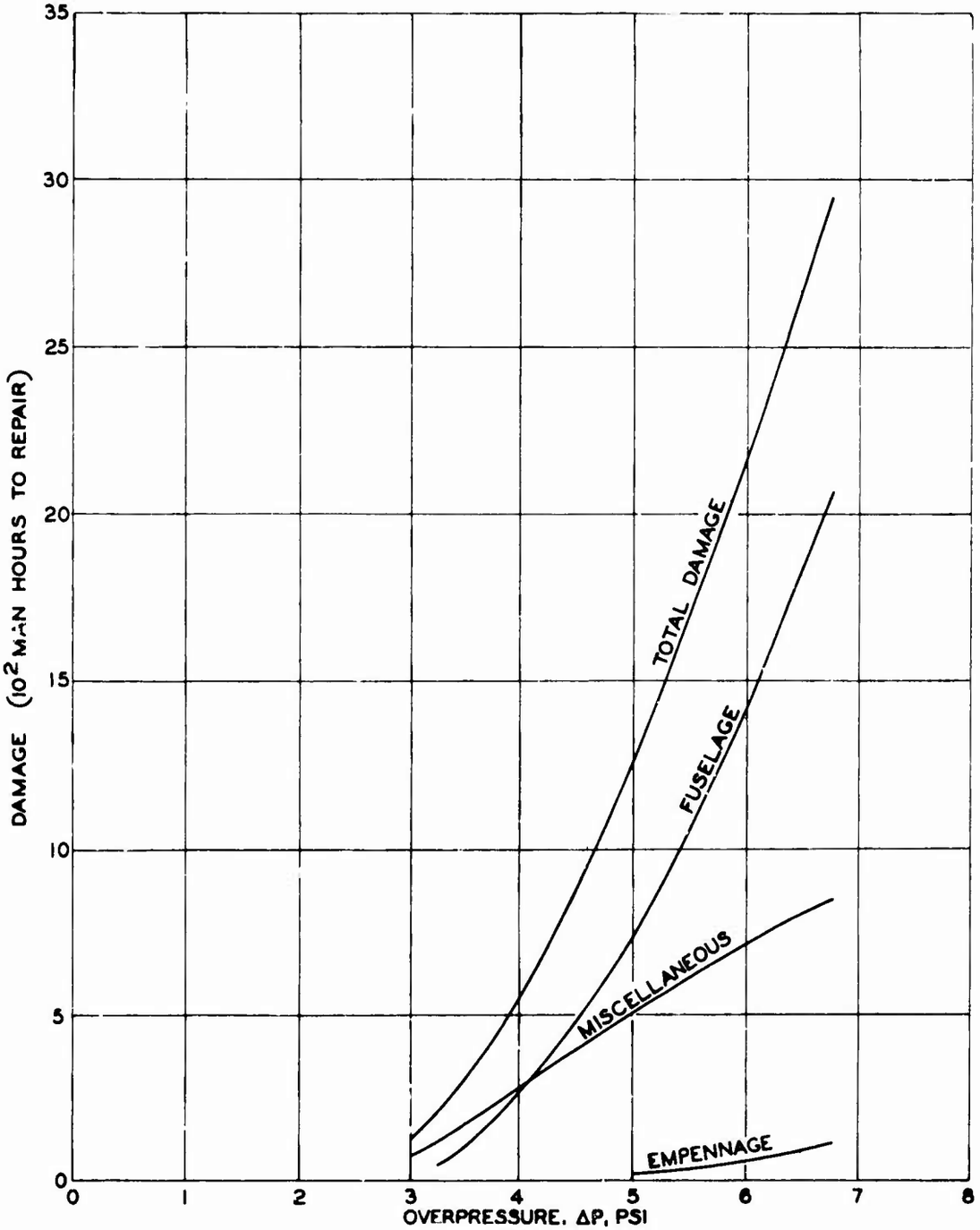

Fig. 4.9 Vulnerability of B-45 Aircraft Parked Nose-in as a Function of Peak Overpressure

[redacted]

TABLE 4.1

Aircraft Instrument Damage, Shots 2, 3, and 4

Aircraft		Shot 2			Shot 3			Shot 4		
Type	No.	Δp	Orient.	Inst. Damage	Δp	Orient.	Inst. Damage	Δp	Orient.	Inst. Damage
F-47	8785	5.0	N	A, B	8.5	N		9.5	N	X
	9232	5.0	S	D	10.0	N	Pitot covered	24.0	N	X
	9075	2.1	N	D	6.2	S				
	9931	0.5	N		8.5	N-45°	A	9.1	S	
	9082	0.5	S		8.5	S	A			
	9114	5.0	T		10.7	N	A, B	41.0	N	X
	9851	0.5	T		8.5	T	A, D	25.0	T	X
	9072	0.8	T		3.5	T		6.8	N	A, C
	3828	0.8	S		2.4	S		6.7	T	A, G
	9110	2.1	N*		6.2	S*		5.4	T*	A
F-86	9597	0.8	N		3.5	N		5.4	T	H
B-17	5715	0.8	N		3.5	N	F, OA, OC	5.4	T	PA
	3769	0.5	S		2.4	S	F, RC			
	3575	0.5	N		2.4	N	F, OA	1.8	S	PA
B-45	9481	0.8	S		3.5	N	OC	6.7	N	QC, PC, E

Prefix Code:
O-Bombardier
P-Pilot
Q-Cabin
R-Radio Op.

Instrument Code:
A-Airspeed
B-Rate-of-Climb
C-Altimeter
D-Directional Gyro
E-Gyro Horizon
F-Fuel Pres. Trans.
G-Fuel Quantity
H-Tachometer
X-No Inspection (Aircraft non-repairable)

Orientation Code:
N-Nose-in
S-Side-in
T-Tail-in
*-Revetment

Total Damaged by Type:

1.	Airspeed	12
2.	Altimeter	6
3.	Directional Gyro	3
4.	Fuel Pres. Trans.	3
5.	Rate-of-Climb	2
6.	Gyro Horizon	1
7.	Fuel Quantity	1
8.	Tachometer	1
	Total	29

[redacted]

G-TYPE REVETMENT SECTION, STATION-8000

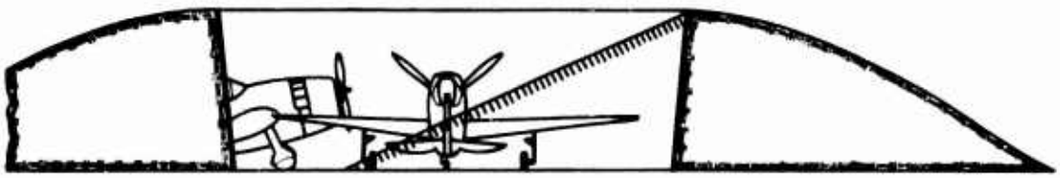

SHOT 3, 7,855' TO AGZ (ACTUAL GROUND ZERO) ⟶

PIT REVETMENT SECTIONS, STATION — 4000

SHOT 3, 3,867' TO AGZ ⟶ SHOT 4, 3,801' TO AGZ ⟶

WALL REVETMENT SECTIONS, STATION — 4000

SHOT 3, 3,867' TO AGZ ⟶ SHOT 4, 3,801' TO AGZ ⟶

Fig. 4.10 Section Views of the Aircraft Revetments Utilized During Shots 3 and 4, Showing the Areas Exposed to Direct Thermal Radiation

[redacted]

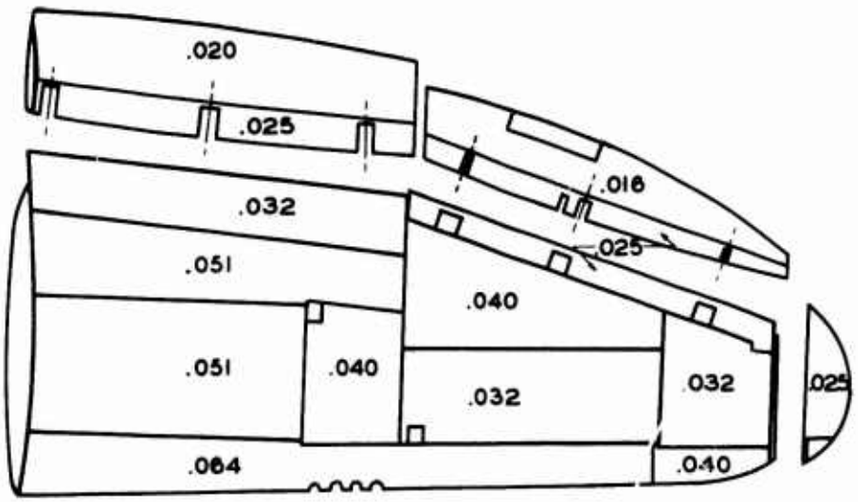

F-47 WING PANELS, TOP SURFACE

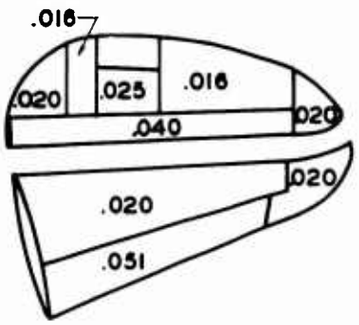

F-47 HORIZONTAL STABILIZER PANELS,
TOP SURFACE

Fig. 4.11 Skin Thicknesses (Inches) of F-47 Aircraft Wing and Horizontal Stabilizer, Top Surfaces

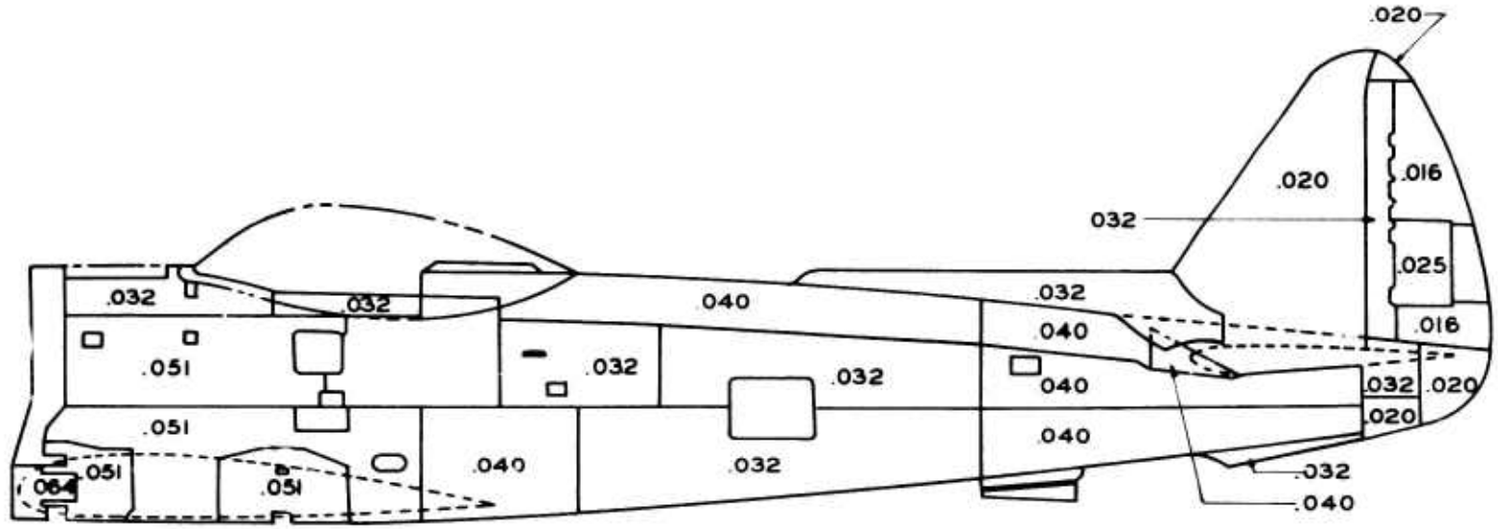

F-47 FUSELAGE AND VERTICAL TAIL PANELS

Fig. 4.12 Skin Thickness (Inches) of F-47 Aircraft Fuselage and Vertical Tail

[redacted]

CHAPTER 5

CONCLUSIONS AND RECOMMENDATIONS

5.1 CONCLUSIONS

Support for general conclusions relating to aircraft vulnerability is contained in the main body of the report. Details regarding time-history instrumentation may be found in Appendix A. For details of the peak skin temperature survey, refer to Appendix B.

It is concluded that:

1. Parked aircraft damage results from a combination of thermal and overpressure forcing functions. Over the range of yields and heights of burst investigated, aircraft damage can be correlated with peak overpressure.

2. Aircraft vulnerability is a function of aircraft heading relative to the burst point. Orientations in order of decreasing vulnerability are side-in, tail-in, and nose-in.

3. Unprotected fighter aircraft as represented by the F-47 configuration have a damage threshold of 2 to 3 psi. Overpressures of 9 psi will cause the aircraft to be damaged beyond repair regardless of orientation, but higher overpressures would be required to assure complete destruction.

4. Bomber aircraft, as represented by the B-17 type, are damaged beyond repair at overpressures of 3½ psi except for the nose-in orientation which may require overpressures in the neighborhood of 4 psi to produce an equivalent degree of damage.

5. The B-29 aircraft are more damage resistant than B-17 aircraft, probably requiring a peak overpressure in the neighborhood of 6 to 7 psi to damage the aircraft beyond economical repair.

6. The B-45 aircraft are more resistant than B-17 and B-29 aircraft, probably requiring peak overpressures on the order of 9 psi for destruction.

7. The F-86 aircraft are generally more damage resistant than F-47 aircraft, especially in the higher overpressure regions. It is expected that overpressures on the order of 10 to 12 psi would be required for destruction.

[redacted]

[redacted]

8. The F-90 aircraft are less vulnerable than both the F-47 and F-86 aircraft. It is estimated that overpressures of approximately 12 to 15 psi would be required for destruction.

9. Passive defense structures offer limited protection for high angle bursts and significant protection for low angle bursts in the range of overpressures investigated.

10. Overpressure measurements made at the aircraft parking stations were slightly higher, but were in general agreement with similar measurements made along the blast line.

11. Thermal energy levels at the aircraft parking stations were generally lower than on the blast line indicating greater thermal energy attenuation.

12. The attenuation of the thermal energy effected by the cockpit enclosures of F-47 and B-17 aircraft varied from 1.2 for the F-47 canopy (side-in Shot 4) to 3.2 for the B-17 enclosure (nose-in Shot 3). Personnel inside the B-17 would have sustained moderate burns on exposed skin; whereas, severe burns would have been sustained if in the F-47 cockpit.

13. Doped fabric skin surfaces on B-17 aircraft exposed to thermal radiation from atomic detonations may burn when subjected to incident thermal energies as low as 2 cal/cm^2.

14. For a given skin thickness, incident thermal energy, and angle of incidence, the temperature rise of an unpolished aluminum aircraft surface can be approximately three times as great as that of a polished surface. The thermal damage hazard can be reduced by polishing the exterior surface. Thick-skinned aircraft are less susceptible to thermal damage than thin-skinned aircraft.

15. Shielding of parked aircraft from the thermal phase of atomic detonations can be easily accomplished and could be incorporated in the methods of camouflaging these aircraft.

16. The 24ST aluminum skins on the parked aircraft sustained no apparent damage from thermal energies sufficient to produce skin temperatures up to the neighborhood of 350°F. This represents the approximate damage threshold temperature and may be induced in 0.016 in. thick skin, of 0.5 absorptivity, by an incident thermal energy of 7 cal/cm^2.

17. Oscillographs, properly shock mounted and adequately shielded from nuclear radiation, are suitable recording systems for tests of this nature.

[redacted]

18. Open instrument pits are not suitable enclosures for the recording equipment because they do not permit the continuance of work during adverse weather conditions, and because they do not adequately protect the equipment from dust and rain.

19. With further development, the use of temperature tapes employing eutectic alloys and/or pigmented papers will provide a very effective method for obtaining peak temperatures of aircraft skin surfaces.

5.2 RECOMMENDATIONS

It is recommended that:

1. The separate effects of thermal and blast inputs in the production of aircraft damage be investigated.

2. These data be supplemented to include additional data on damage response of modern fighter and bomber type aircraft.

3. The degree of protection afforded by passive defense structures, at overpressures from 9 psi (preferably about 12 to 15 psi) up to the maximum expected to result from a nuclear strike, be investigated.

4. A complete study of the protective efficiency of various revetment configurations be made.

5. The isolated effects and coupling effects of thermal and blast forcing functions be reduced to fundamental concepts applicable to aircraft damage prediction.

6. Future tests include a study of the effect of protecting parked aircraft against thermal radiation. The possibility of providing thermal shielding in conjunction with the camouflaging of friendly aircraft should be considered.

7. Criteria for the structural design of aircraft and missiles participating in atomic bomb missions, and for those likely to be exposed to an atomic explosion, should restrict the use of exposed materials that would be subject to burning, such as fabric covered control surfaces and other opaque heat sensitive materials, including those in crew compartments, which can be effectively replaced. In addition, the use of black or other non-reflecting markings on exterior surfaces should be minimized.

8. The information gained from TUMBLER-SNAPPER be applied to the problem of defending friendly aircraft against atomic attack.

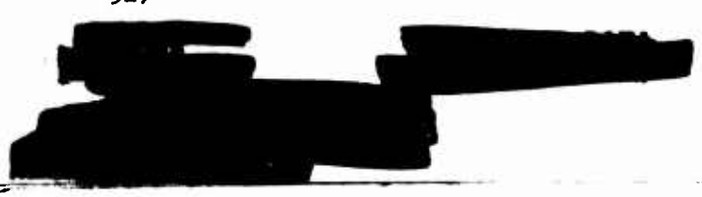

[redacted]

9. Angle-of-blast incidence be measured at heights from ground level to 50 ft. Also that measurements of the angle-of-blast incidence be made by measuring the differential pressure between two points which are separated by an arc of 90° on the surface of a cylinder, and which lie on the same cross-section.

10. The instrumentation program for future tests on parked aircraft include a complete acceleration measuring program for determination of aircraft displacement versus time, and also include measurements of the pressures exerted on aircraft surfaces so that the relation between overpressure and aircraft response can be better analyzed.

11. Galvanometers used in measuring acceleration of complete aircraft have a low frequency response very nearly equal to the frequency of vibration of the aircraft center of gravity in order to eliminate the superimposed higher frequencies.

12. The USAF utilize the skin temperature data presented herein to check current theories regarding response of aircraft surfaces to the thermal radiation accompanying nuclear detonations. Further, that an analysis of existing thermal energy data be made for the purpose of correlating thermal energy attenuation as a function of range and height above ground for a given atomic explosion.

13. The USAF utilize these thermal and overpressure data to determine loads imposed on wings of aircraft subjected to atomic explosions, and to perform a dynamic analysis on the wing structures of the instrumented aircraft in order to compare the theoretical results with the experimental bending moment and acceleration measurements.

14. Oscillographs be used as the recording medium for time-history instrumentation on future atomic tests unless another fully proven system which has been previously demonstrated in actual tests is shown to be more desirable. Further, that this instrumentation be housed in a totally enclosed, dust-free structure.

15. The development of temperature tapes using eutectic alloys and/or pigmented papers be continued.

[redacted]

[redacted]

APPENDIX A

OSCILLOGRAPHIC INSTRUMENTATION

A.1 INTRODUCTION

A.1.1 General

The main purpose of these tests was to obtain aircraft damage data as referred to in the basic report. However, as a support group, oscillographic instrumentation was employed to augment the aircraft damage assessments.

A.1.2 Objective

The chief objective of the instrumentation program was to obtain measurements of the aircraft response functions so that a more accurate knowledge of the method of structural failure could be obtained for extrapolation to other aircraft structures and configurations. An additional objective was to measure the various general input functions at all sites where the aircraft were located.

A.2 PROCEDURE

A.2.1 Selection of Instrumentation

A.2.1.1 General Input Measurements

The general input functions selected for measurement were total thermal energy, overpressure, and angle-of-blast incidence. Total thermal energy is a measure of the total thermal energy received per unit of area and is not to be confused with thermal flux or thermal intensity. Measurements of total thermal energy were selected for Stations 2200, 8000, and 10,500 on Shots 2 and 3 and Stations 2200, 4000, and 8000 on Shot 4. Overpressure is the additional pressure, above atmospheric, of the shock wave from the bomb. Overpressure measurements were selected for Stations 2200, 8000, and 10,500 on Shots 2 and 3 and for Stations 2200, 4000, and 8000 on Shot 4. Angle-of-blast incidence is the angle between the horizontal and the direction of flow of the advancing air mass behind the shock front. Angle-of-blast incidence was selected for measurement at Station 8000 on Shots 2 and 3 and Station 4000 on Shot 4.

The positions selected for measurement of the general input functions were well in front of all obstructions at the individual sites. Such a position was particularly necessary for the

[redacted]

[redacted]

overpressure and angle-of-blast incidence measurements in order to minimize aerodynamic interference. The location of the concrete bases on which the general input sensing instruments were mounted is shown on the following figures: Stations 2200 in Fig. A.1, 4000 in Fig. A.2, 8000 in Fig. A.3, and 10,500 in Fig. A.4.

In view of the limited time available for the preparation phase of this operation, standard recording oscillographs were chosen with the realization that considerable shock proofing, radiation protection, and protection from dust and moisture would be required. Two Consolidated Engineering Corporation 18-channel oscillographs were selected to record the bulk of the data and were located at Station 8000 on Shots 2 and 3 and Station 4000 on Shot 4. Two Heiland Research Corporation six-channel oscillographs were selected to record the remaining data. One of the latter was located at Station 2200 on Shots 2, 3, and 4, and the other was located at Station 10,500 on Shots 2 and 3 and Station 8000 on Shot 4.

The system that was used in the recording of data by oscillographs can be briefly explained as follows. The quantity to be measured was converted to an electrical signal by the sensing element. This signal, which may have required amplification or attenuation, was then fed to the galvanometer in the oscillograph. The galvanometer converted the electrical signal to a movement of a spot of light which in turn fell on moving photo sensitive paper. The result, after development of the paper, is a black trace on a white field. The displacement of this trace is a measure of the galvanometer deflection, which in turn is a function of the input signal from the sensing element.

It was determined that the transmitter selected for measurement of pressure would not develop a signal large enough to deflect the galvanometer sufficiently, so that some type of amplifying system was needed to increase the strength of the signal from this sensing instrument. In order to increase the strength of the signal, Consolidated Engineering Corporation's System D with carrier amplifiers was selected on the basis of availability and previous experience with this type of equipment. This system consists essentially of an oscillator and power supply, in addition to from one to eight carrier amplifiers, depending upon the number of channels requiring amplification. The purpose of the oscillator and power supply was to supply the 3000 cycle exciting voltage to the pressure transmitter and the high voltage and filament power to the carrier amplifiers. The transmitter output was fed into the carrier amplifier where the signal was amplified and demodulated. The output from the carrier amplifiers was then fed into the recording oscillograph. In view of the System D's power requirement, an inverter was used to convert the available 24 volts D.C. to 115 volts, 400 cycle A.C. The frequency response of the carrier amplifiers is flat from 0 to 500 cps.

[redacted]

The quantities that were measured with strain gages or strain gage type of instruments, such as angle-of-blast incidence, required a bridge balance unit. This unit provides a means of balancing the strain gage bridge; it also supplies the bridge voltage to the strain gages and incorporates a method of adjusting the output resistance of the strain gage bridge to a value that will provide critical damping for the galvanometer in the oscillograph. Balancing bridges were needed at Stations 2200 and 8000 on Shots 2 and 3, and Stations 2200 and 4000 on Shot 4.

The thermocouple output of the calorimeter for measurement of total thermal energy was capable of deflecting the galvanometer directly, so that no auxiliary equipment was required for measurement of this quantity.

A relay switching unit was required with each oscillograph to serve as a remote control. The timing signals distributed by Edgerton, Germeshausen, and Grier, Inc. (E.G.&G.) operated relays in this unit which activated the 3 kc system, the oscillograph, and auxiliary items before the shot, kept the equipment running during the shot, and turned it off after the shot. The University of Dayton designed and built five of these relay switching units, one for each of the four operating oscillographs and one spare.

A bank of five 24-volt wet batteries supplied the power for each site, and an inverter converted this 24-volt D.C. supply to 115-volt, 400 cycle, A.C. for use by the 3 kc equipment. A bulb type rectifier was used to charge the batteries until shortly before shot time. All of the equipment at each site was situated in an open concrete pit, which was covered and sandbagged during the shots. The location of these pits relative to the instrumented airplanes can be determined by referring to the following figures, Stations 2200 in Fig. A.1, 4000 in Fig. A.2, 8000 in Fig. A.3, and 10,500 in Fig. A.4. Figure A.5 shows the pit used at Stations 8000 and 4000 and Fig. A.6 shows the pit used at Stations 2200 and 10,500. All cables coming from the instrumented airplanes and general input sensing elements were buried in the ground. They were run into the instrument pits through conduits located below ground level. Where exposure to the effects of the bomb was unavoidable, they were covered with braided aluminum shielding.

An intensive search revealed that the only available meter for measurement of total thermal energy was the field calorimeter designed by the Naval Radiological Defense Laboratory (NRDL) which was used to measure total thermal energies on Operation GREENHOUSE. Arrangements were made to borrow 10 of the calorimeters for this operation. This calorimeter is essentially a sensing element consisting of a black circular disc of known emissivity, conductivity, and heat capacity with a thermocouple fastened to its rear surface.

[redacted]

Mounted behind the calibrated disc are two large solid copper blocks which form the cold-junction of the thermocouple. The disc, thermocouple, and cold-junction blocks are encased in a cadmium plated steel cylinder, as depicted in Fig. A.7. A protective window, which was chosen by NRDL after an intensive study of various materials, is constructed of fused quartz having a transmissibility factor of 92 per cent. The window and the aperture of its holder are designed to afford the instrument a 90° field of vision. The calorimeters were connected directly to the recording oscillograph, and were mounted on welded steel pipe support 2½ to 5 ft above the ground, as displayed in Fig. A.7.

The overpressure measurements were made with a flush mounting differential pressure transmitter having a bonded strain gage mounted on the under side of a thin metal diaphragm. These transmitters, manufactured by the Sierra Electronic Corporation, were used for a major part of the pressure measurements because the flush mounting prevents orifice pressure disturbances, because uniformity in amplifying equipment and mounting techniques was possible and because they were readily available. A more complete description of this transmitter is presented in Paragraph A.2.1.2. At Station 2200 after Shot 3, the two flush mounting transmitters were replaced by one Wiancko and one Statham pressure gage, because these gages were inherently less heat sensitive than the Sierra gages. The gage manufactured by the Statham Laboratories has a strain gage-type transducive element with a four-active arm Wheatstone bridge circuit which affords sufficient sensitivity so that no amplification is required, making possible the use of a simple d-c circuit. The gage manufactured by the Wiancko Engineering Company is a differential type pressure gage capable of measuring differential pressures up to 10 psi. The response to pressure is linear within plus or minus 3 per cent to 500 cps with a maximum rise time of 0.7 msec to 90 per cent of the full scale output. The pressure sensing element employs a variable-reluctance principle. Figures A.8 and A.9 depict the standard installation of the pressure cells, and Figs. A.2, A.3, and A.4 show the location of the pressure cells at each station.

A vane-operated angle-of-blast incidence indicator, manufactured by the Statham Laboratories, was chosen to measure the angle of attack of the air mass behind the shock front. This instrument utilized a split trangular vane mounted on a conical body, which contained the pivot point for the vane and the unbonded strain gage sensing element, as in Fig. A.10. This instrument, designed with a minimum mass for the vane, has been tested for accuracy and response under supersonic conditions and is capable of measuring variations in the air mass 14° on either side of its neutral position. These instruments were mounted 40 in. above the ground on probes which were 20 in. and 30 in. long, supported horizontally by welded steel pipe "A" frames. For Shots 2 and 3, the 30 in. probe, (Installation 11) which is

[redacted]

[redacted]

displayed in Fig. A.11, was located on the concrete slab 67 ft to the left of the survey control point at Station 8000. In preparation for Shot 4, the same installation was moved to Station 4000 and located similarly with respect to the survey control point there. The 20 in. probe (Installation 26) was located 81 ft to the right of the survey control point at Station 8000 for Shots 2 and 3. This installation was omitted during Shot 4 because it was damaged.

A.2.1.2 Specific Input Measurements

The specific input functions selected for measurement were samples of pressures on wings and vertical stabilizers, and total thermal energy directed at crew position in the airplanes. These measurements were taken at Station 8000 on Shots 2 and 3 and Station 4000 on Shot 4. The pressure on the wing and stabilizer surfaces may be considerably higher than the ambient peak overpressure, so that measurement of the pressure on these surfaces was selected for analysis of this effect.

The measurement of total thermal energy inside the cockpit determined the amount of energy transmitted through the windshield and other transparent parts of the cockpit. This information was selected to provide an indication of the level of thermal energy to which personnel inside the cockpit would be subjected under similar conditions of bomb yield, burst height, and ground range.

The oscillograph and related amplifier installation described in Paragraph A.2.1.1 was utilized for recording the specific input functions.

In order to ascertain the effects of thermal energy radiation on the pilot of an aircraft, a calorimeter of the type described in A.2.1.1 was located in the cockpit of B-17 (5715), at Station 8000. With the aid of NRDL personnel, this instrument was mounted on a galvanized pipe framework located on the center of the co-pilot's seat at a height and angle coincident with the thermal ray passing through the center of the co-pilot's window, as shown in Figs. A.12 and A.13a. This meter was connected directly to the recording oscillograph as in Fig. A.7. This installation was changed after Shot 3 when the meter was moved to the cockpit of F-47 (9785), Station 4000. The meter was located at the average height of the pilot's face, 9 in. from the surface of the canopy along the line of sight to the bomb burst.

Sierra pressure transmitters were installed on some of the aerodynamic surfaces of the aircraft that were instrumented. The purpose of this installation was to measure the pressures where the angle of the surface might increase or decrease the pressure of the incident blast wave. For the vertical stabilizer pressure measurement, F-47 (9785) was placed with its left side toward the blast, and the

[redacted]

[redacted]

gages were installed on the left side near the centroid of the vertical stabilizer as in Figs. A.14 and A.15a. On the other aircraft the pressure transmitters were located on the top surface of the wing at a point far enough away from the fuselage to minimize interaction between fuselage and wing. This surface on the wing also had to be rigid and as free from movement, due to local wing skin deflection, as possible. A flush mounted pressure transmitter should be used to properly measure these pressures. Statham Laboratories were making a transmitter of this description at the time procurement was being made. However, these transmitters were only in the development stage and could not be available in quantity until June 1952. No other d-c sensing elements were available at that time which would satisfy the needs of this project. As a compromise, a flush mounting transmitter that required amplification was purchased from Sierra Electronic Company. This was a differential type pressure transmitter having as transducive element a bonded Baldwin SR-4 strain gage with a resistance of 120 ohms. This gage was fastened to the under surface of the diaphragm, Fig. A.8. A reference pressure tube projecting from the transmitter body allowed the inner chamber of the transmitter to remain at a constant reference pressure. This reference pressure was equal to the ambient air pressure prior to the pressure disturbance. This pressure was maintained by connecting the transmitter to a tank with a volume that was large compared to the volume of the transmitter. The inside volume of the wing and fin was used as the tank to which the reference pressure tube was connected. These transmitters are designed to measure dynamic pressure from 1/5 to 500 cps. Due to their independence from orifices and connecting tubing, these transmitters yield data free from phase distortion. Figures A.8 and A.16 show the standard method of mounting these transmitters to the wing and fin surfaces. Since skin stresses are high in these thin-skinned sections, a mounting flange was used to install the pressure pickups. A hole slightly larger than the diameter of the transmitter was cut in the skin surfaces and the mounting flange was flush riveted to the under side of the skin. The pressure transmitter was screwed into the flange until the diaphragm was flush with the outside surface. One purpose of the mounting flange was to distribute the local skin stresses around the hole in order that the transmitter would be uneffected. To insure a pressure tight connection, a non-hardening caulking compound was spread on the threads of the mounting flange before the transmitter was screwed in.

A.2.1.3 Response Measurements

Airplane response functions selected for measurement were skin, stringer, and propeller cuff temperature rise, normal and lateral acceleration, and wing and vertical stabilizer bending moments. The temperature rise was measured on four distinct types of surfaces. The first was on a polished skin surface, the second on an ordinary unpolished skin surface, the third on a stringer inside a wing, and the fourth on a black surfaced propeller cuff. Two temperature

[redacted]

[redacted]

measurements on the unpolished skin of the left wing and one on an internal stringer of the same wing were selected for measurement of F-47 (0065), as shown in Fig. A.17c. Two different types of thermocouple installations, a copper insert type and a standard type, were chosen for the measurement of the temperature rise of the left wing skin of the F-86 (9597), as in Fig. A.18b. On the B-17 (5715) a polished surface on the right wing and an unpolished surface on the left wing were selected for measurement of the skin temperature rise. The three airplanes mentioned above were located at Station 8000 for Shots 2 and 3 and Station 4000 for Shot 4. The propeller cuff temperature rise was measured only on Shot 4 at Station 2200 on F-47 (8785), and this installation is shown in Figs. A.19a, A.19b, and A.20. The two types of acceleration selected for measurement were: normal acceleration, which was measured in a vertical direction; and lateral acceleration, which was measured in a horizontal direction. The airplanes chosen for normal acceleration measurements were the F-47 (0065), F-86 (9597), and B-17 (5715) at Station 8000 on Shots 2 and 3 and at Station 4000 on Shot 4, and the F-47 (8785) at Station 2200 on Shots 2, 3, and 4. Lateral acceleration was selected for measurement on F-47 (9785) at Station 8000 on Shots 2 and 3 and Station 4000 on Shot 4. Wing bending was selected for measurement at Station 8000 on Shots 2 and 3 and Station 4000 on Shot 4. Measurements were made on F-47 (0065), F-86 (9597), and B-17 (5715). Vertical stabilizer or fin bending was measured on the F-47 (9785) on Shots 2 and 3, Station 8000 and Shot 4, Station 4000.

The system used for recording the response measurements was that described in Paragraph A.2.1. The temperature measurements, since they were made with thermocouples, required no amplification, balancing, or attenuation and so were fed directly into the oscillograph. The only exception to this was the propeller cuff temperature which required attenuation in the form of a series resistor in the circuit. The acceleration and bending moment measurements utilized the equipment described in Paragraph A.2.1 with their outputs going through the bridge balance unit and into the oscillograph.

A time pulse to indicate the time of detonation of the bomb was recorded on each oscillograph for each shot. One channel in each of the oscillographs was used to monitor the bridge voltage for the strain gages, accelerometers, and blast incidence gage.

Temperature measurements were made on the wing of F-47 (0065), F-86 (9597), and B-17 (5715) for Shots 2 and 3 at Stations 8000 and 4000 on Shot 4. Also, on Shot 4, a temperature measurement was made of the propeller cuff on F-47 (8785). These measurements were made using copper-constantan thermocouples in two different types of installations. The standard type installation was made by pressing the two thermocouples wires through holes in the skin which were drilled approximately 1/32 in. on center. The wires were then peened solidly

[redacted]

in place from the under side of the surface. The thermocouple wires were then cut flush with the outer skin surface and polished smooth with emery cloth. For this installation No. 24 copper-constantan thermocouple wires were used, Fig. A.21. The other installation that was used, the copper insert type, can also be seen in Fig. A.21. This installation was used in an attempt to measure the temperature of the exposed skin surface, as distinct from the average temperature of the skin through its thickness. For this installation, No. 30 thermocouple wires were pressed through holes in the copper disc and soldered into place. The temperature control used for the cold-junction of these thermocouple installations was a standard one-pint thermos bottle, filled with ice and water mixture. The wires for the cold-junction were lead through the cork and extended about four inches into the thermos bottle. A schematic drawing of this installation appears in Fig. A.21. These thermos bottles were filled with crushed ice and water 20 hours prior to the test. It was possible to maintain a constant temperature in this manner from two to three days. From the cold-junction, the leads were connected directly to the recording oscillograph.

On F-47 (0065) thermocouples were installed at wing station 114 on the top surface of the left wing gun-bay door, Fig. A.17c. Two of the standard installations were made here to test the consistency of this installation. In addition, a standard type installation was made on an inner-stringer one-half inch aft of the leading edge of the gun-bay door, so that a comparison of skin temperature and stringer temperature could be made. The purpose of these temperature measuring installations on B-17 (5715) was to obtain a comparison of skin temperature on a highly polished wing surface with the skin temperature on a normally oxidized wing surface. The thermocouples were mounted, using the standard installation, on the oil cooler doors for No. 2 engine (left wing) and No. 3 engine (right wing). The access door for No. 3 engine was polished, so that its surface was almost equal to that of a mirror, and No. 2 access door was left unpolished. This installation was used for Shots 2 and 3; however, when the airplanes were moved to Station 4000 in preparation for Shot 4, the B-17 was positioned with its tail toward the blast. This required that the thermocouples be relocated because they were no longer exposed to the thermal ray. The new location was near the trailing edge of the wing, directly aft of the original installation. On the right wing an area 6 in. square, in which the thermocouple was centered, was polished to a mirror finish, and the installation on the left wing was left unpolished. Figure A.13b shows the detail of these two installations. To obtain skin temperature data at stations where there was extremely high thermal input, the propeller cuff of F-47 (8785) was instrumented with a standard thermocouple installation for Shot 4 only. The propeller cuff surface was black, and the thermocouple was installed at approximately the center of the cuff. The surface on which this thermocouple was mounted was almost normal to the thermal ray from the bomb.

[redacted]

Accelerometers used during the test were made by the Statham Laboratories. These linear accelerometers contained a balanced four-active arm bridge of the unbonded strain gage type. These accelerometers had an accuracy and linearity of 1 per cent of full scale and were damped by a silicon fluid from 60 to 70 per cent of critical damping at room temperature. Accelerations in normal and lateral directions were measured in the instrumented aircraft at Station 8000 and Station 2200. In measuring these accelerations, the motion of the airplane as a unit was desired and not the accelerations of components of the aircraft. This necessitated mounting the accelerometer on as heavy a structure as could be accessible near the center of gravity. After Shot 2, it was determined that the accelerations of the structure were being measured rather than the acceleration of the aircraft, so the accelerometers were mounted on lead blocks which were fixed rigidly to the structure. Normal accelerations were measured on F-86 (5957), F-47 (0065), and B-17 (5715) at Station 8000. The F-47 (8785) was instrumented for normal acceleration at Station 2200. The only lateral acceleration measured was F-47 (9785) at Station 8000. On all of the F-47's the accelerometers were mounted on the armor plate directly behind the instrument panel during Shot 2. On F-47 (0065) and F-47 (8785) the accelerometer was changed to the floor of the cockpit at the front edge of the seat on the center line of the aircraft, mounted on heavy lead blocks for Shots 3 and 4, as shown in Figs. A.17a, A.17b, A.19a, and A.19b. On the F-47 (9785), the lateral acceleration of which was being measured, the accelerometer's position was changed to the bottom spar cap on the main spar of the right wing and mounted inside the wheel well after Shot 2, Fig. A.15b. The Shot 2 accelerometer mount in the F-86 was on the radio platform just inside the radio access door. For Shots 3 and 4, however, a heavy block of lead was added between the accelerometer and the radio platform. There installations are shown in Figs. A.18b and A.18a. On the B-17, the accelerometer was mounted on the bottom chord of the truss running along the center line inside the bomb bay. After Shot 2, the accelerometer was moved to the top of the bomb bay catwalk and mounted on a lead block which was securely fastened to the catwalk. Both of these accelerometer positions are described in Fig. A.13a.

Strain gages were used to measure the wing bending moments on B-17 (5715), F-47 (0065), and F-86 (5957), and the bending moment of the vertical fin of F-47 (9785). The strain gages used were Baldwin-Southwark A-13 gages having a nominal resistance of 350 ohms. These gages were selected because previous experience showed they were very reliable. It was also known from previous desert tests that the climatic conditions at the Nevada Proving Grounds would have an adverse effect on strain gages not given a protective coating. Therefore, the gages were coated with glyptol which enabled them to withstand the conditions of high temperature, moisture, and dust without mal-functioning. The gages were applied with General Radio Cement. These bending channels were connected into four-active arm Wheatstone

[redacted]

[redacted]

bridge circuits with strain gages applied on the tension and compression surfaces of the main and rear spars of the wings and fin that were instrumented. Refer to Figs. A.23b, A.23a, A.25b, and A.25a for the schematic wiring diagrams of the bridge circuit to the recording oscillograph. Figures A.13b, A.17b, A.18b, and A.15a give the location of the strain gages used on the B-17, F-47, and F-86 wings and the F-47 fin, respectively. The gages were located as near as possible to the root station of the wings and fin, so that greater output could be measured. Due to the inaccessibility of these stations, the gages were mounted elsewhere, as shown on the figures mentioned above. These bending measurements were made at Station 8000 for Shots 2 and 3 and at Station 4000 for Shot 4.

A.2.2 Calibration

A.2.2.1 Introduction

In order to achieve the maximum accuracy from the various instrumented test components, calibration procedures were established and conducted to determine the specific response to a known function. Details of the calibration methods used for the different types of instrumentation are given in the following paragraphs.

A.2.2.2 General Procedure

The calibration of the circuits which included the bridge balancing unit were plotted as a function of applied load vs visual signal deflection, which was in terms of per cent of a known calibration scale. These circuits are for the wing and fin bending, acceleration, and blast incidence measurements, and are shown in Figs. A.22a, A.22b, A.22c, A.23a, A.23b, A.25a, and A.25b. This calibration scale was obtained by switching a given resistance across one arm of the Wheatstone bridge, thus giving a definite deflection. The percentage obtained from the ratio of the galvanometer deflection caused by a given applied load to the deflection caused by the unbalance of this calibrate signal was the percentage used on the calibration curve. This calibration signal was applied in both positive and negative directions, so that a deflection could be referred in terms of the positive calibration (cal+) or the negative calibration signal (cal-) according to its direction of deflection.

The calibration of sensing elements was conducted in the range where the output of that sensing element was linear. Thus the resulting calibration curve should be a straight line; and accordingly, all calibration curves were plotted as the best straight lines through the test points. The applied load required to produce a signal deflection equal to the deflection produced by one per cent of the calibration signal was designated as the calibration factor. For those sensing elements which did not employ the bridge balance unit, as

[redacted]

shown in Figs. A.22a, A.22b, A.23a, A.23b, A.24a, A.24b, A.25a, and A.25b, the calibration curve was drawn in terms of applied load vs actual galvanometer deflection in inches. As this also was a straight line relationship, the calibration factor was expressed as the ratio of the applied load to one inch of galvanometer deflection.

A.2.2.3 General and Specific Input Functions

The instruments measuring general input functions were calibrated as follows:

1. The total thermal energy calorimeter was basically a thermocouple instrument of the copper-constantan type. An unattenuated circuit consisting of the thermocouple, galvanometer, and connecting wires was used at all stations on Shot 2. The attenuated circuit used at all stations on Shots 3 and 4 consisted of the thermocouple, galvanometer, attenuating parallel and series resistors, and connecting wires. A separate calibration of the unattenuated and attenuated circuits was required for each calorimeter. Calibration was accomplished using a millivolt source of very low internal resistance and a poteniometer. The procedure was to impress known millivolt steps on the circuit and record the corresponding galvanometer deflection. By combining this millivolt vs galvanometer deflection data with the millivolt vs cal/cm^2 calibration factor supplied by NRDL, a curve of galvanometer deflection vs cal/cm^2 input was plotted.

2. The calibration of the differential pressure gages was made at the test site after the pressure transmitters were permanently installed. Since the circuit used for the pressure measurement did not include the bridge balance unit, the calibration was made in terms of inches of deflection and not in terms of per cent of a known calibrate signal. A type C-1 portable instrument testing unit modified for use in pressure calibration was used to apply both positive and negative pressures to the gages. Pressure was applied by placing a small bell-jar over the pressure transmitter installation and varying the pressure or vacuum. A mercury manometer was used to measure the pressure applied to the transmitter. Pressures were applied in two psi increments throughout the maximum and minimum ranges of the transmitter. While returning to zero differential pressure, these same points were checked. The output from the individual gages was sufficiently different that separate calibration curves had to be made for each gage. The calibration curve was plotted in terms of inches of galvanometer deflection vs the manometer reading converted to psi.

3. The calibration of the vane type angle-of-blast incidence indicators was accomplished by placing the vane at various angles on either side of its neutral position and by measuring these angles with an accurate inclinometer. Calibration points were recorded in 2° increments from minus 14° to plus 14°. The oscillograph record was then

[redacted]

compared with the inclinometer readings, and a graph was prepared in terms of deflection vs the vane angle.

A.2.2.4 Response Functions

The instruments for measuring response functions were calibrated as follows:

1. The thermocouples were calibrated in terms of galvanometer deflection vs an applied emf. A d-c millivolt source applied to the thermocouple circuit was measured by a slide-wire potentiometer. The calibration was made in increments varying from one-tenth of a millivolt to one-half millivolt, depending on the magnitude of the temperature to be measured by the thermocouple. The galvanometer deflections observed on the oscillograph record were plotted vs the temperature which was equivalent to the number of millivolts applied during the calibration. The temperature in degrees F per millivolt were obtained from standard thermocouple tables. Since the resulting calibration curve was not a straight line, results from the shot record were read directly from the curve and not computed by use of a calibration factor.

2. The instruments used for calibration of the accelerometers were of two types. One was a Consolidated Calibrator, 6-101 A, which was used to calibrate the accelerometers at the Aircraft Laboratory of the Wright-Patterson Air Force Base and the other was a LeBouef Portable Calibrator which was used at the Nevada Proving Grounds. The 6-101A consisted of a shake table which generated a sinusoidal motion having a single amplitude that could be varied from 0 to 1 in. and having a frequency that could be varied from 0 to 50 cps. The LeBouef portable calibrator was similar to the 6-101A, with the exception that it was smaller and had a fixed shake table amplitude. The calibration procedure was to mount the accelerometer to be calibrated on the table and shake it at various frequencies. The output of the accelerometer, which was channeled through the bridge balance unit, was fed to the oscillograph where a record was made for each frequency. Since the vibration amplitude of the shake table was known and its frequency could be determined from the oscillograph record, the acceleration could be computed. The calibration was completed by drawing a calibration curve of the computed accelerations as a function of deflection in per cent of cal+ and cal-.

3. The calibration of wing bending on B-17 (5715), F-47 (0065), and the fin bending on F-47 (9785) was performed in the Structures Test Bldg at the Wright-Patterson Air Force Base. The wing bending calibration for the F-86 (9597) was done at the test site.

For purposes of calibration, the B-17 was supported by a rectangular jig underneath the fuselage at the aircraft's center of gravity, the wheels did not touch the ground, and the tail was jacked up so

[redacted]

[redacted]

that the wing-root chord would be level. The load was applied to the wing spars by jacks placed 12 ft from the tip and by hoists which were placed 6 ft from the tip. These loads were applied to both wings to equalize the rolling moment.

A maximum positive moment equivalent to 52 per cent of the ultimate bending moment was applied in calibration steps of five equal increments. The maximum bending moment applied to the wing by an up-load was 6,375,000 in.-lbs, and the maximum bending moment for a down-load was 3,000,000 in.-lbs at the station where the strain gages were applied. These gages were located outboard of Station 3, as shown in Fig. A.13b. After the wing was flexed to take up the slippage of bolts and rivets, the calibrating loads were applied in increments of 20 per cent of the maximum load. These points were checked as the load was released. This loading procedure was repeated when there was any appreciable unbalance at the end of the calibration. This procedure was followed for both the positive and negative loadings, the positive load being in the upward direction.

The F-47 (0065) was supported at the wing attach-points on the front and rear spar by a structural steel jig; the landing gear was not retracted, but the wheels were free. The fuselage was supported such that the chord at the root of the wing was horizontal. The bending moments obtained at Station 50, where the strain gages were applied, were 1,963,000 in.-lbs for the up-load, and 1,251,000 in.-lbs for the down-load. These moments are equivalent to 53.2 and 51.5 per cent of the ultimate bending moment, respectively. The loads were applied by means of torque arms at Stations 88, 120, 145, and 175 so that failure in wing shear would not occur. As in the B-17 calibration, the loads were applied in 20 per cent increments of the maximum load until 100 per cent was reached. The 20 per cent increments were checked as the load was removed on both positive and negative bending moment calibrations. A check calibration was made to determine the effect of the landing gear reactions on the calibration results obtained from the "wheel free" condition. These effects were found to be negligible; therefore, the "wheel free" calibration was used to reduce the test data.

For the F-86 calibration a maximum load of 30 per cent of the ultimate root bending moment was applied at Station 120, where the strain gages were mounted. The loads, which were applied while the airplane was in a normal parked position, consisted of lead weights applied along the wing. Only negative bending moments were calibrated, due to the lack of suitable equipment for applying an up-loading (positive bending moment). The loads were applied in 800 pound increments until a total load of 3800 pounds was applied. To equalize the rolling moment caused by the application of these loads, equivalent weights were applied to the right wing, and weights were added to the nose to equalize the pitching moment.

[redacted]

[redacted]

For the F-47 fin bending calibration, the aircraft was supported at the tail so that its longitudinal axis was horizontal. Loads were applied at fin Stations 17½, 32, 47½, and 54, such that a maximum bending moment of 32,000 in.-lbs, 60 per cent of ultimate, was obtained at the station where the strain gages were mounted. This installation is shown in Fig. A.13a. To relieve the yawing moment caused by the load on the vertical fin, a restoring couple was formed by applying fore and aft loads on the two landing gears. The rolling moment was relieved by structural steel jigs which were located at approximately Station 74 on both wings. Calibration loads of 10, 20, 40, 60, 80, and 90 per cent of the limit load, which was 35,600 in.-lbs, were applied. The points were checked as the load was removed. After the bending moment calibrations were computed, the deflections on the oscillograph record were reduced to per cent of the calibrate signal and plotted versus the corresponding applied load.

One galvanometer in each Consolidated oscillograph was calibrated to monitor the bridge voltage supplied by the bridge balance unit.

A.2.3 Operations

This operation was similar to field operations by other instrument groups engaged in this project. The one procedure worthy of note, particularly because it may explain apparent gaps in the information obtained from each station for each shot, related to the transfer of the instrumentation from Station 8000 to Station 4000 between Shots 3 and 4 (spaced seven working days apart) necessitated the accomplishment of the following work:

1. New instrument pits and concrete bases for mounting of general input sensing elements, had to be built at Station 4000 before the equipment could be moved.

2. The cables to all of the sensing elements at Station 8000 had to be removed from the trenches in which they were buried, so that they could be used again at Station 4000. To facilitate this transfer, steel cables were originally buried with the instrumentation cables; and when it was desired to remove the instrumentation cables, the earth covering them was loosened by ripping the steel cables out of the ground.

3. The four instrumented airplanes at Station 8000 were towed to Station 4000 and placed in the same positions relative to the new instrument pits, but generally in new orientations.

4. At Station 10,500 the concrete base on which the pressure transmitters were mounted was dug out of the ground and moved to Station 8000.

[redacted]

[redacted]

5. All of the equipment in the instrumented pits, such as the oscillographs, 3 kc system, and auxiliary equipment, was mounted on wooden benches. When a move was made, this bench was transported as a unit from one station to the other, and upon arrival all of the circuits were reconnected and checked out. Five channels were omitted on Shot 4 due to the effect of Shot 3 on the sensing elements, the subsequent move, and prevailing weather conditions (intermittent rain for the two days preceding Shot 4).

A.3 TEST RESULTS

A.3.1 General

Each item of measured data from all oscillograph channels was considered separately for significant points, maximum values, frequency patterns, and spurious indications. Each item was then considered in relation to the other data, and multiple curves (cross-plots) showing comparison, combinations, averages and integrations were plotted. The curves and combinations of curves chosen for presentation were selected on a basis which would include at least one direct graph of all data considered to be accurate and those combinations of curves which appeared most significant. Various time scales, expressed in seconds or milliseconds, were chosen as the abscissas of these graphs. The expanded time scales were selected to present the more rapid oscillations of the oscillograph traces for use in engineering analysis. The less expanded scales were used to show frequency relationships, decreasing magnitudes through the end of the positive pressure phase, and other characteristics having significant changes over a longer period of time. Whenever more than one requirement governed the selection of time scales, graphs of each were drawn so that duplication of certain items of data is noticeable in the group of figures presented. The selection of time scales and the choice of combinations for each quantity measured are listed in Tables A.1, A.2, A.3, and A.4 to facilitate cross reference.

Time zero for the temperature and thermal data was chosen to coincide with the time of the bomb burst. For all other measurements, an arbitrary time zero was chosen as the time when the pressure transmitter, which measured site overpressure, first showed a measurable deflection. The difference in time between these two references was the length of time required for the blast front to traverse the distance from the point of detonation to the site where response functions were being measured. On Shot 4, Station 4000, the first deflection of the angle-of-blast incidence vane was used as zero time because the site pressure gage was inoperative.

Although the information presented here includes all items of data which were successfully measured and represents a completed report of the measurements themselves, the information is

[redacted]

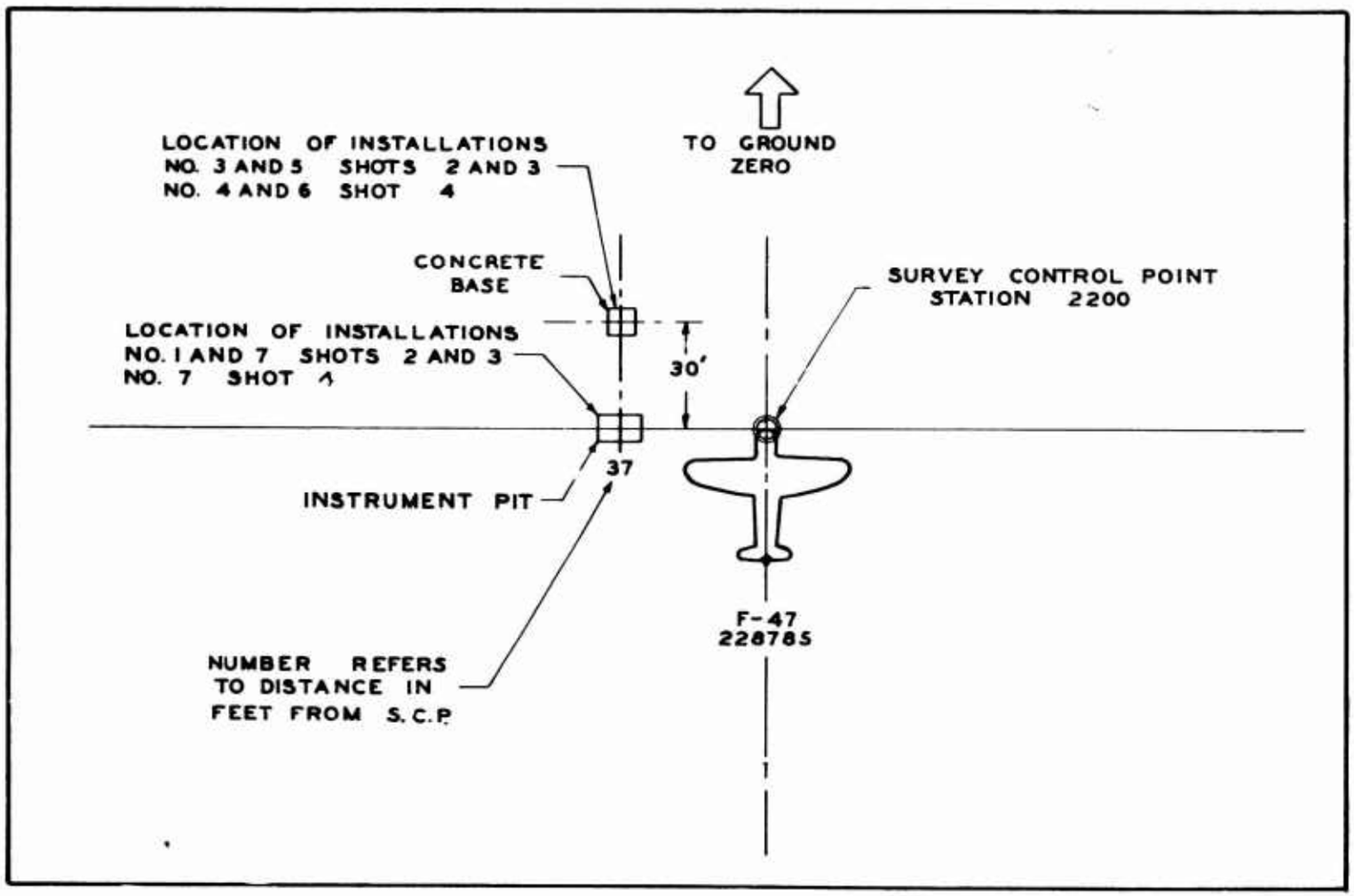

Fig. A.1 Location of the Instrumented Airplane, Instrument Pit, and Concrete Base with Respect to the Survey Control Point at Station 2200

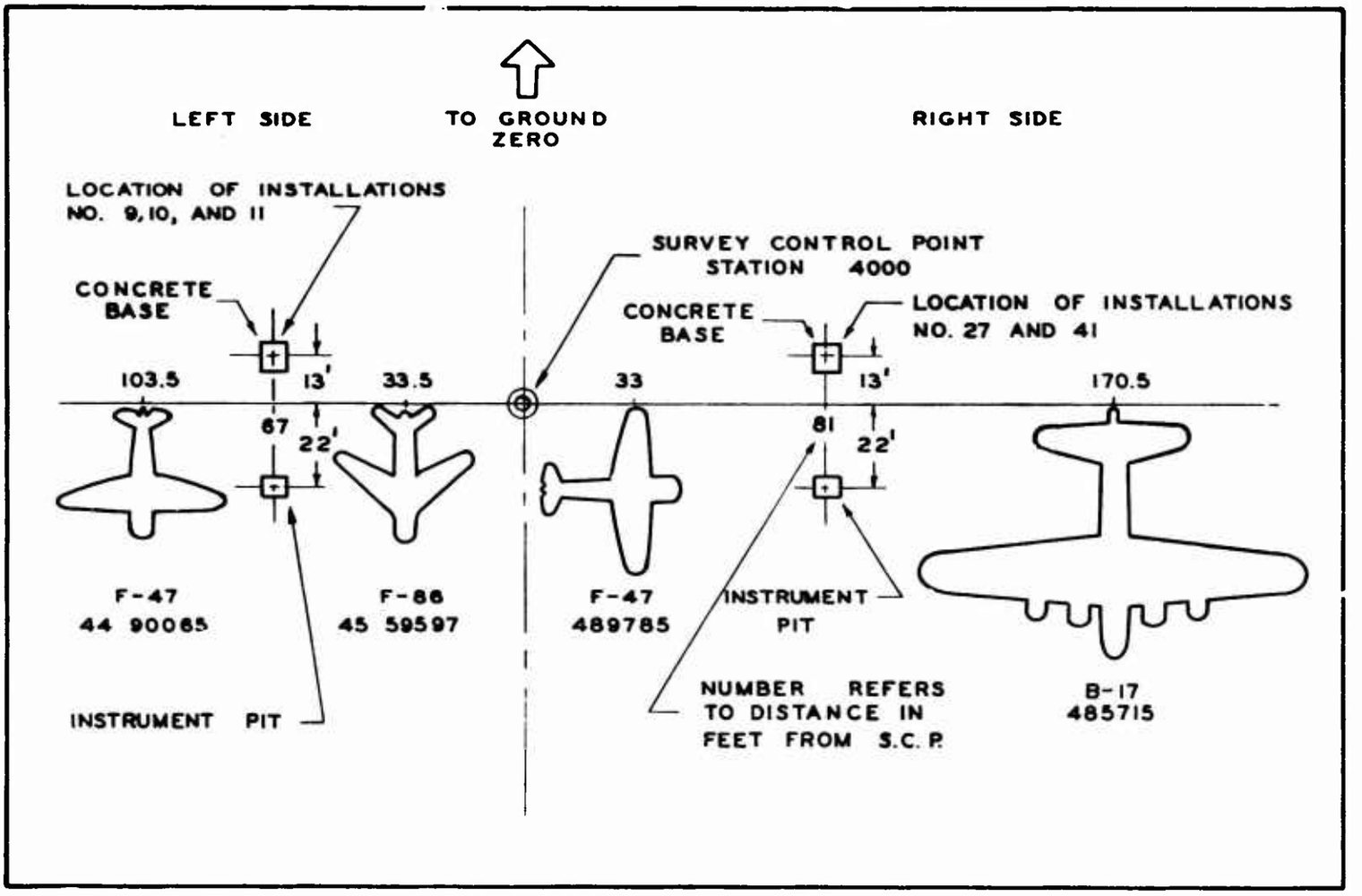

Fig. A.2 Location of the Instrumented Airplanes, Instrument Pits, and Concrete Bases With Respect to the Survey Control Point at Station 4000

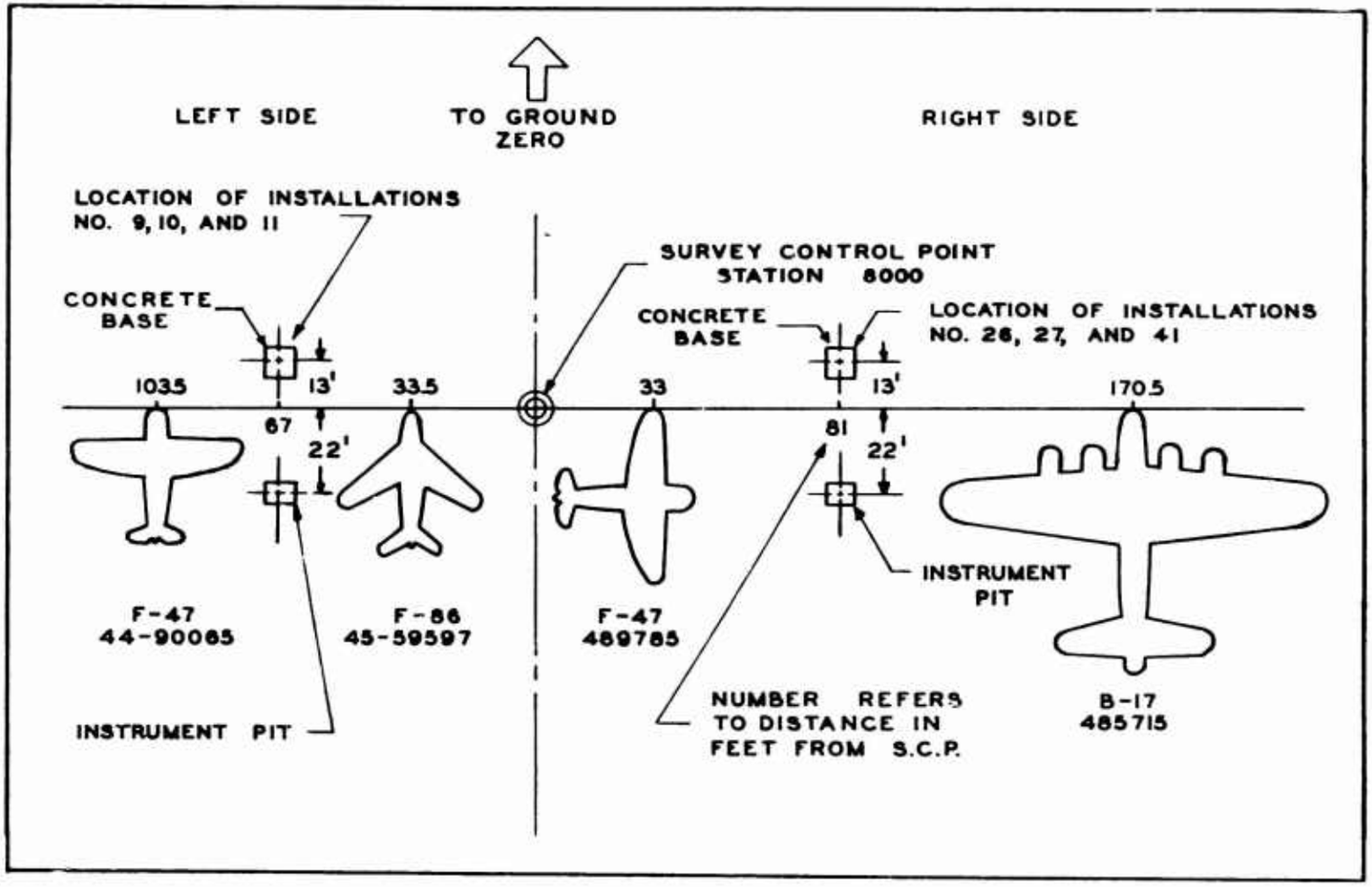

Fig. A.3 Location of the Instrumented Airplanes, Instrument Pits, and Concrete Bases With Respect to the Survey Control Point at Station 8000

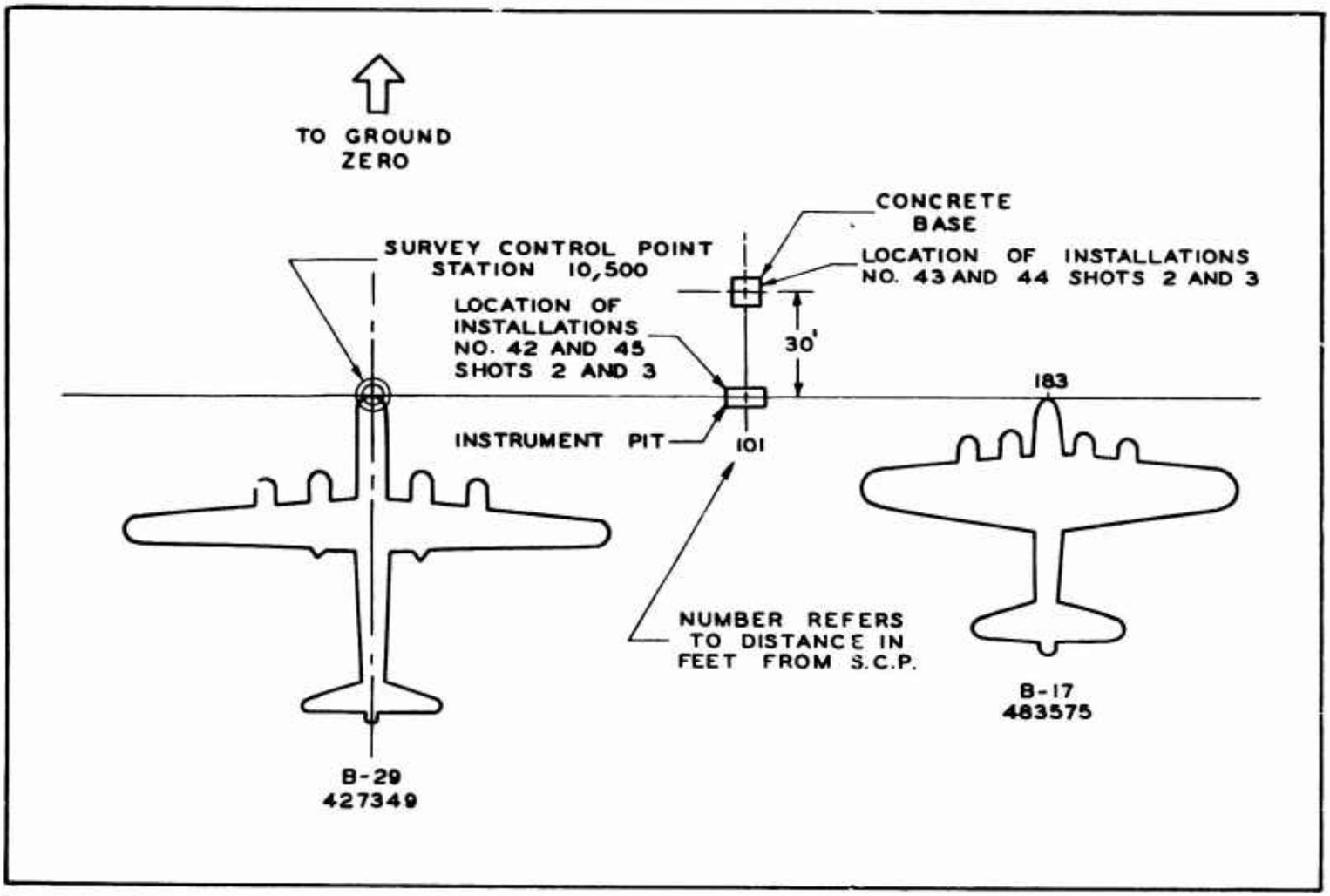

Fig. A.4 Location of the Instrumented Airplanes, Instrument Pits, and Concrete Base With Respect to the Survey Control Point at Station 10,500

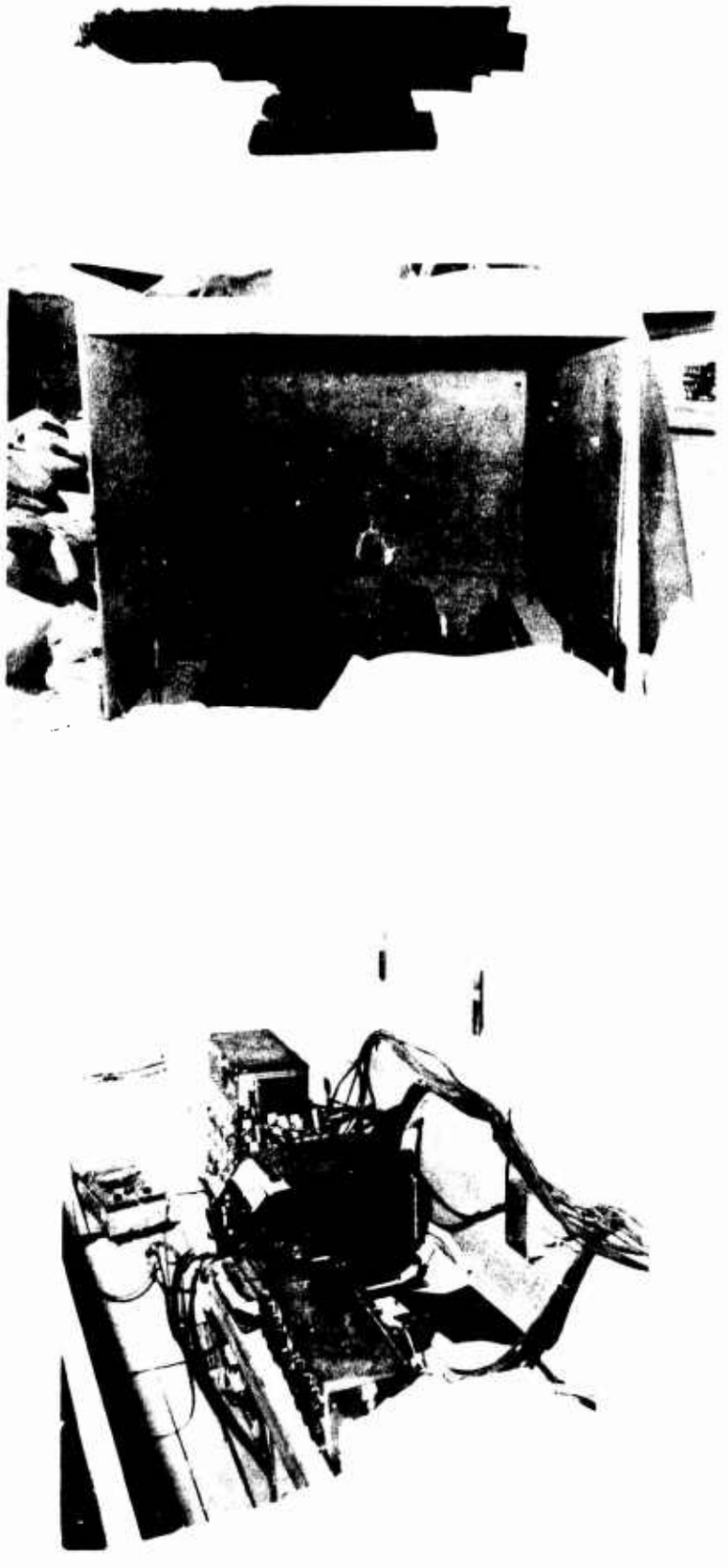

Fig. A.5 Typical Installation of the Recording and Amplifying Equipment in the Instrument Pits at Stations 4000 and 8000

Fig. A.6 Typical Installation of the Recording and Amplifying Equipment in the Instrument Pit at Station 2200. Note the Relative Positions of the Calorimeter Installations.

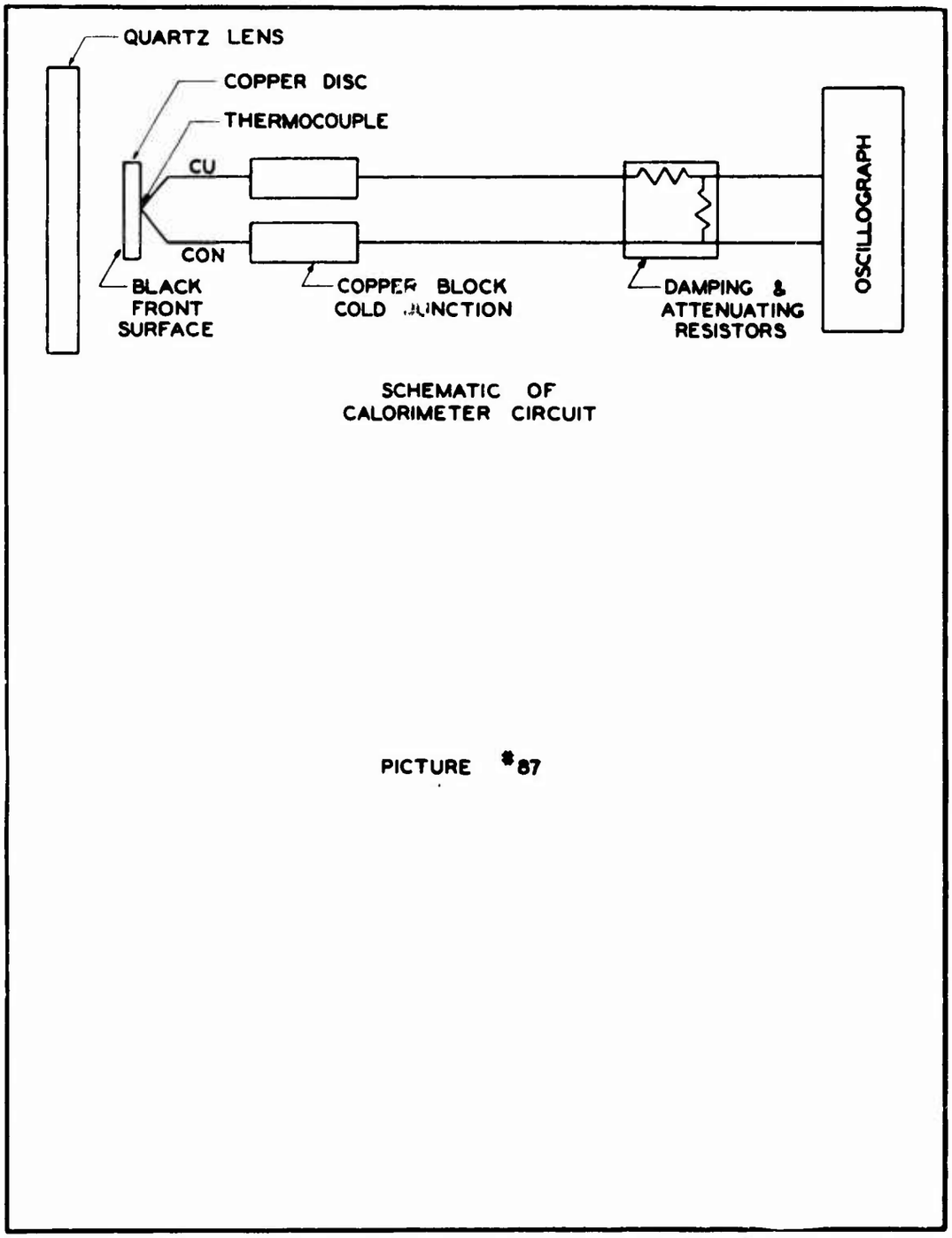

Fig. A.7 Schematic Wiring Diagram of Calorimeter Circuit and a Typical Mounting Installation of the Calorimeter

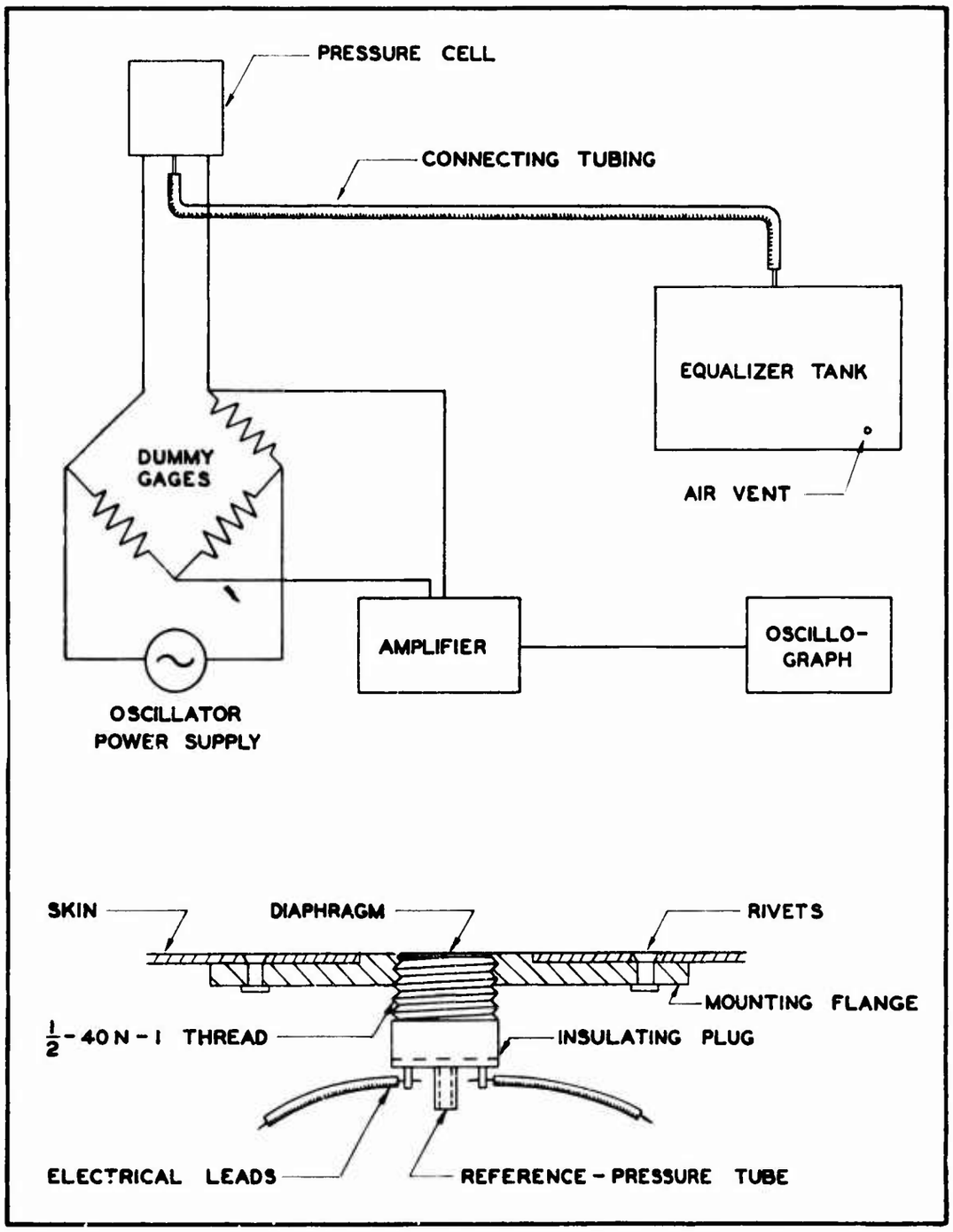

Fig. A.8 Schematic Wiring Diagram of Pressure Transmitter Circuit and a Typical Mounting Installation of the Pressure Transmitter

Fig. A.9 Typical Installation of Pressure Transmitter for Ground Overpressure Measurement

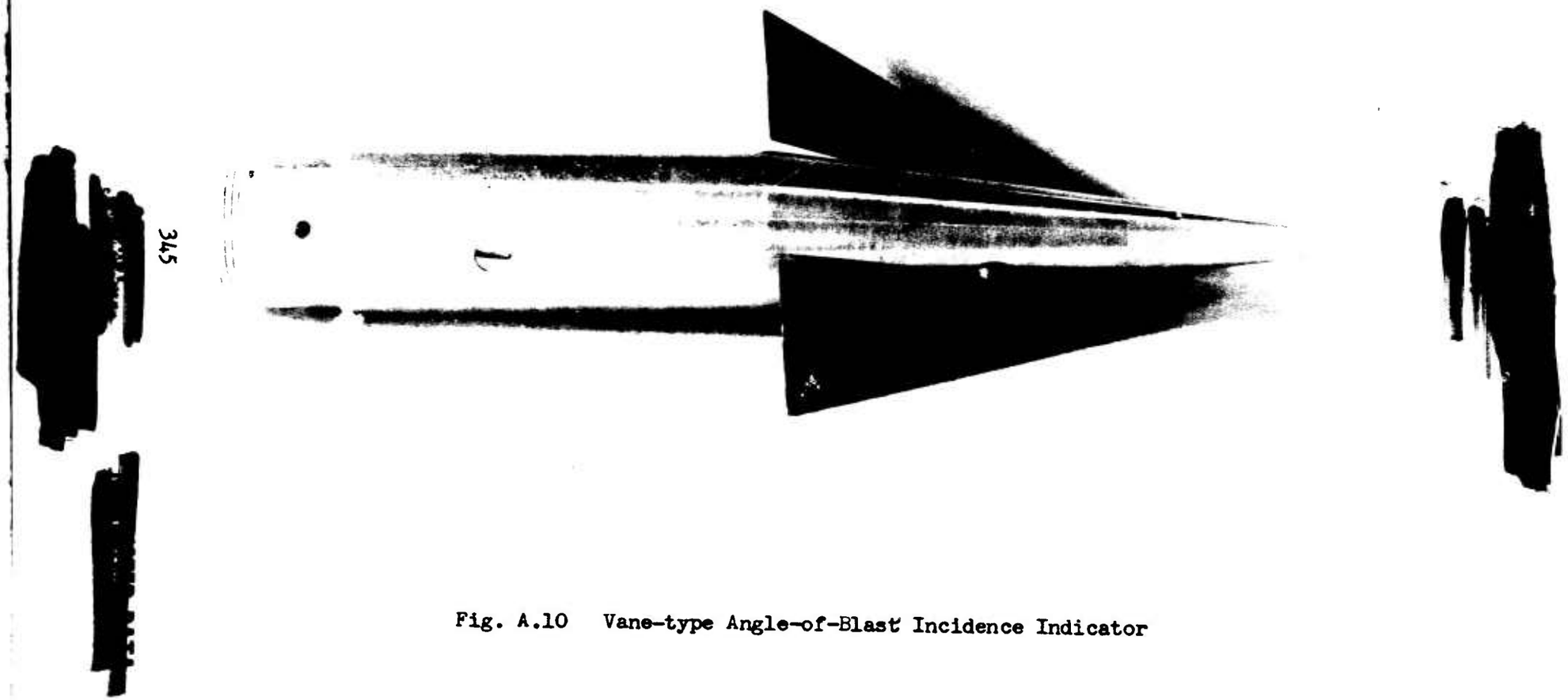

Fig. A.10 Vane-type Angle-of-Blast Incidence Indicator

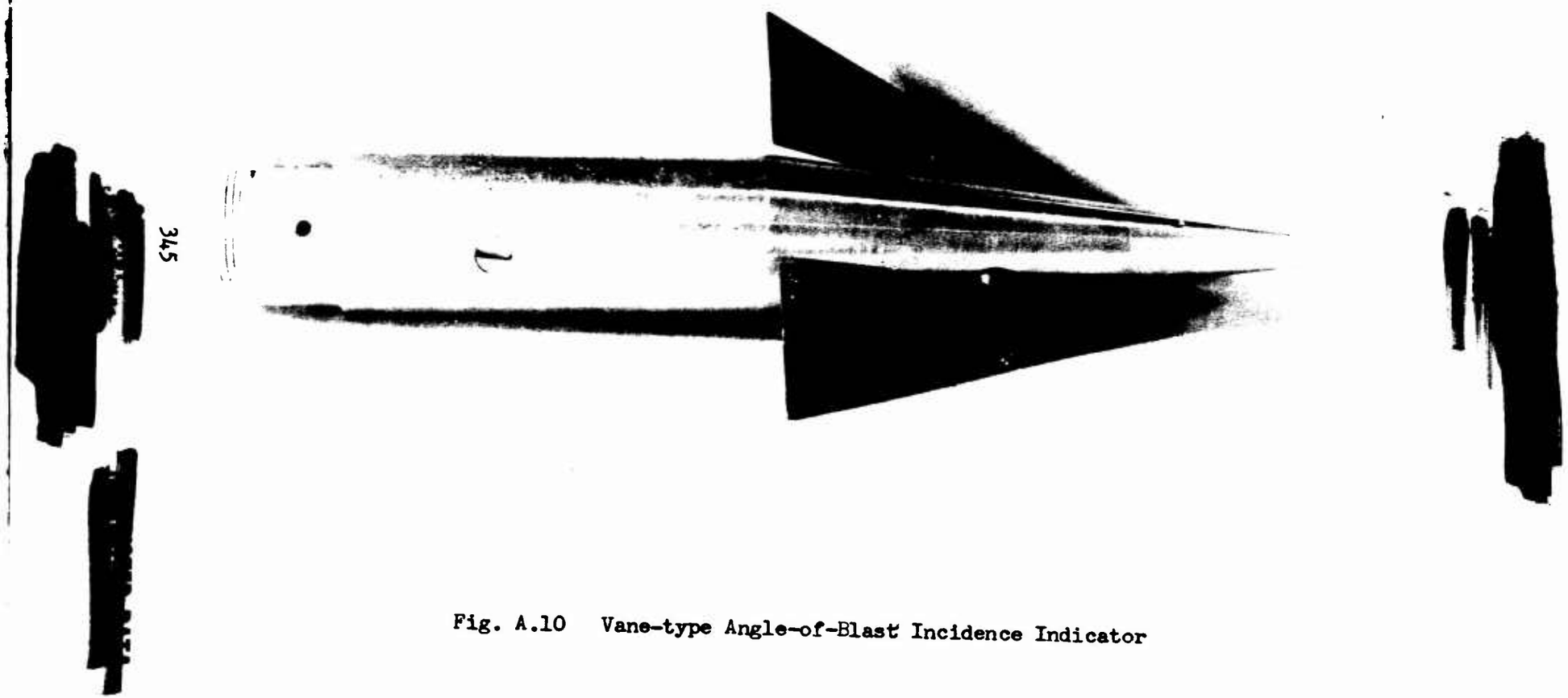

Fig. A.10 Vane-type Angle-of-Blast Incidence Indicator

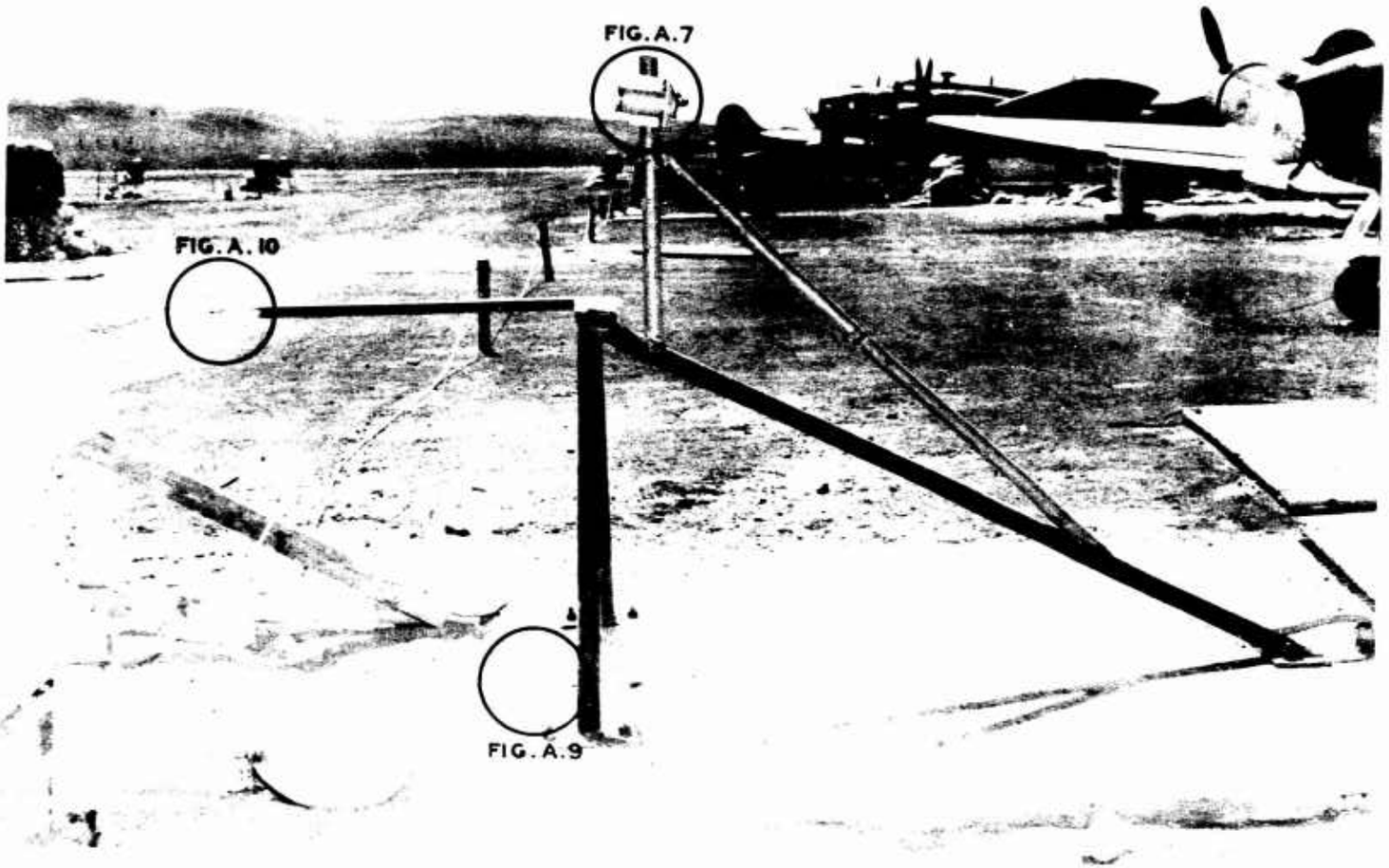

Fig. A.11 Typical Installation of Angle-of-Blast Incidence Indicator, Calorimeter and Site Pressure Transmitter

Fig. A.12 Installation of Calorimeter in the Co-pilot's Seat of B-17 (5715)

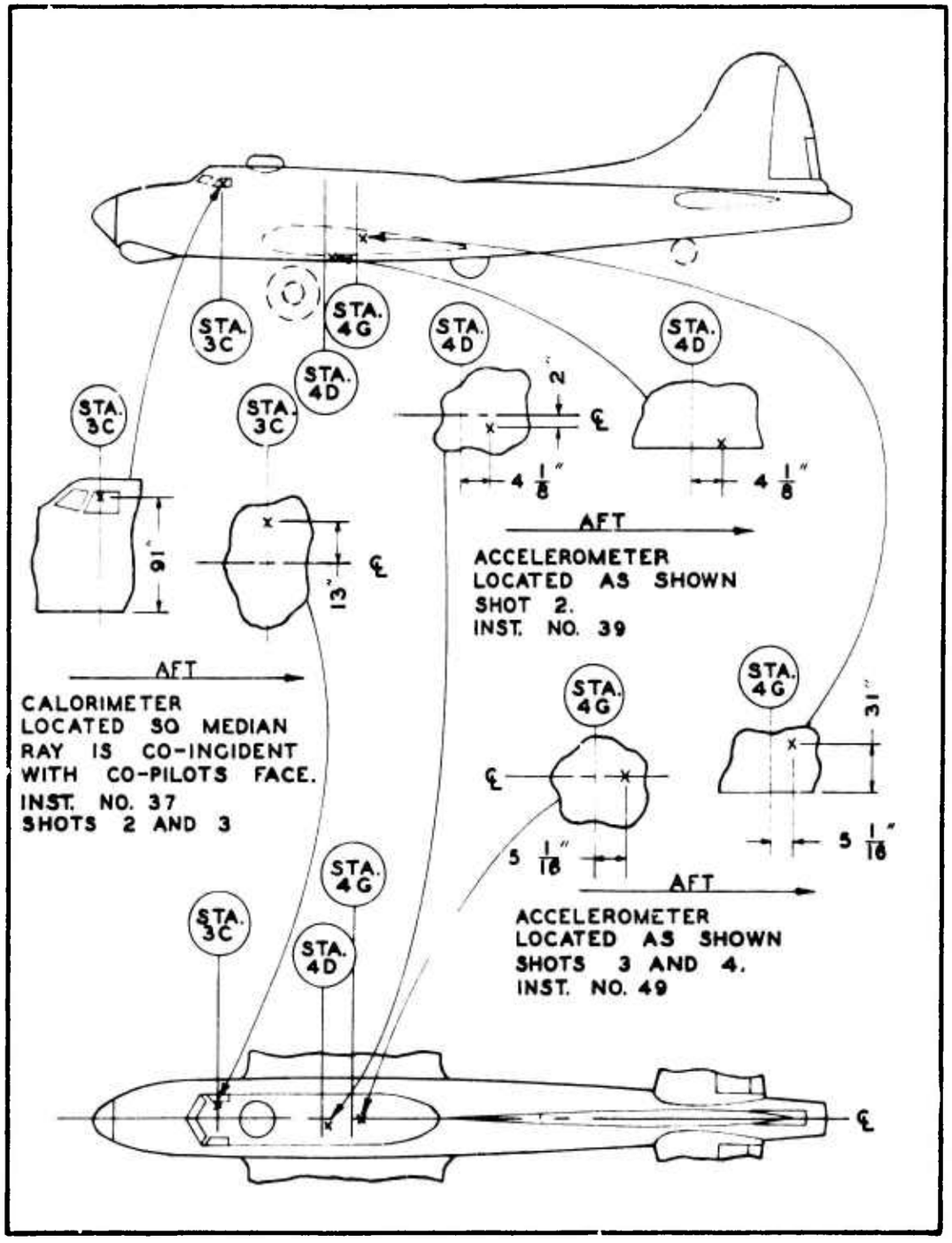

Fig. A.13a Location of Instrumentation Inside the Fuselage of B-17 (5715)

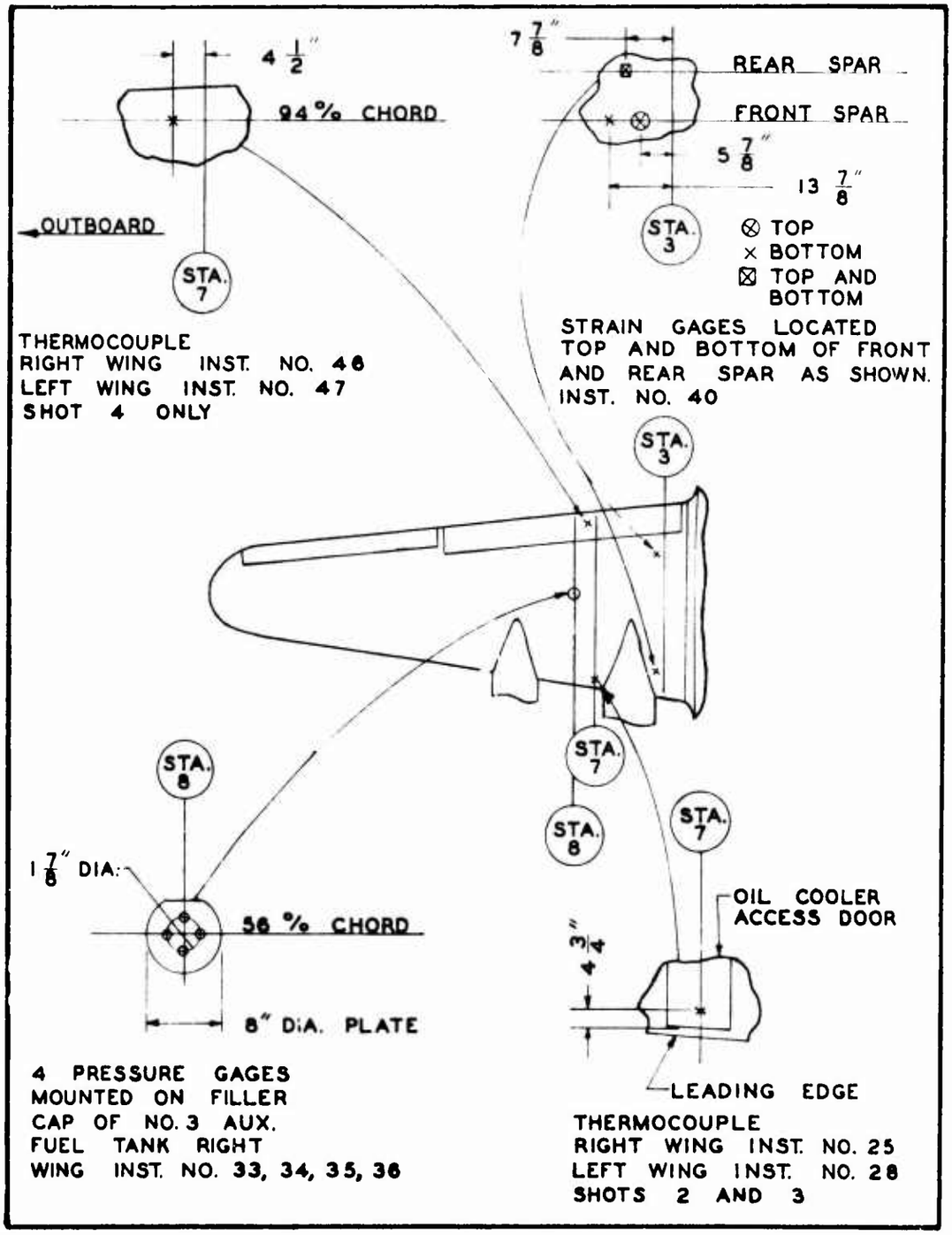

Fig. A.13b Location of Instrumentation on the Wing of B-17 (5715)

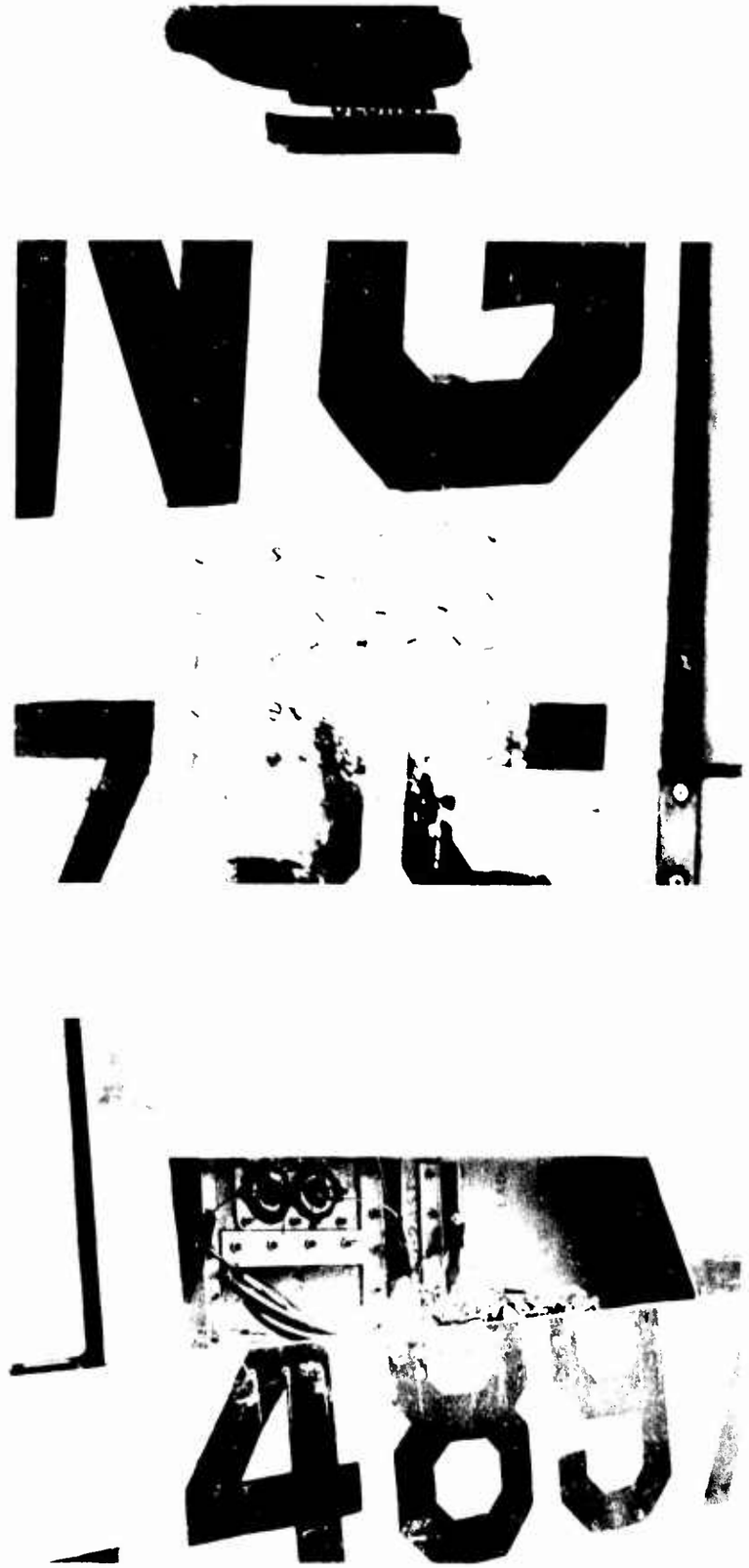

Fig. A.14 Installation of the Pressure Transmitters on the Vertical Stabilizer of F-47 (9785)

RESTRICTED DATA

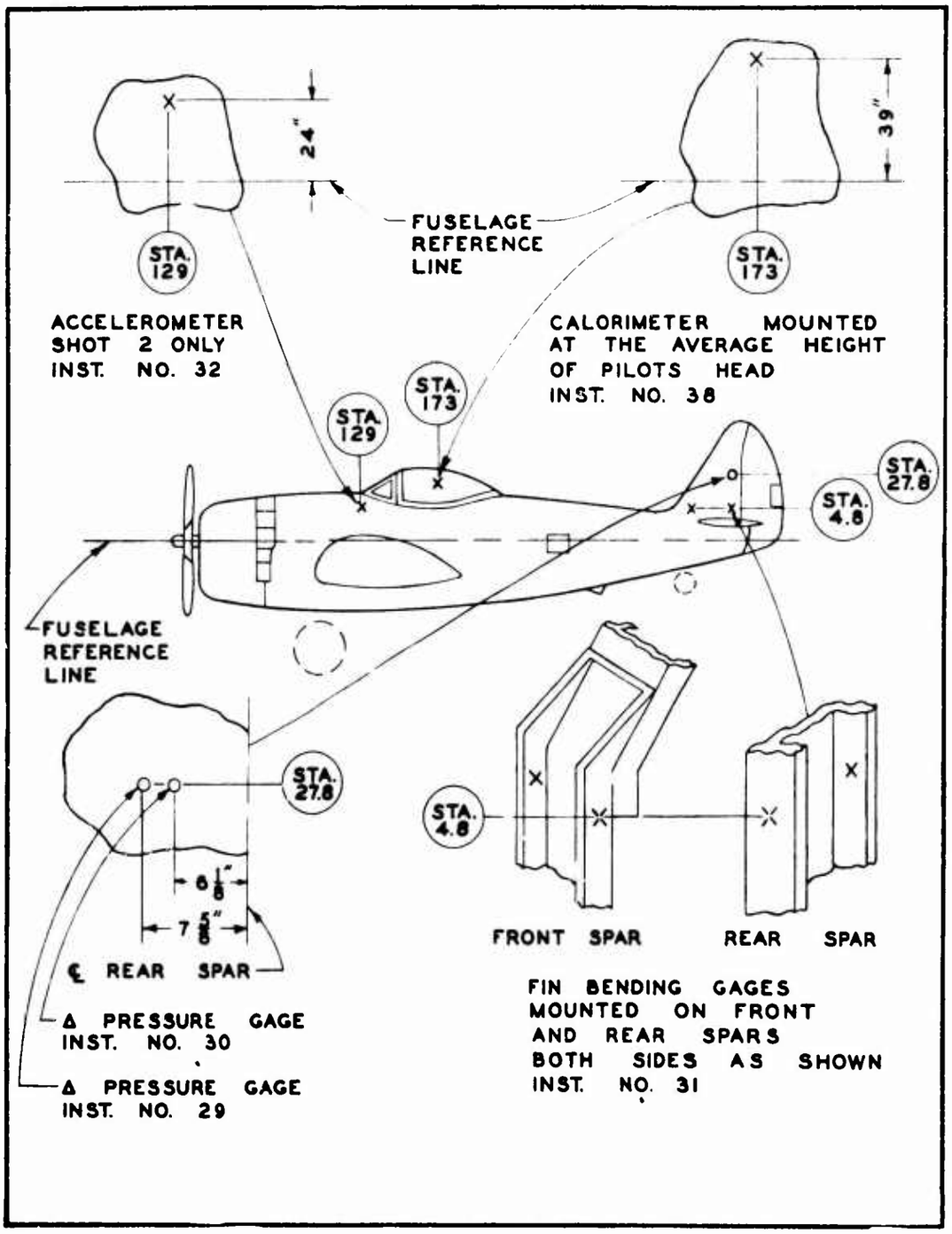

Fig. A.15a Location of Instrumentation on F-47 (9785)

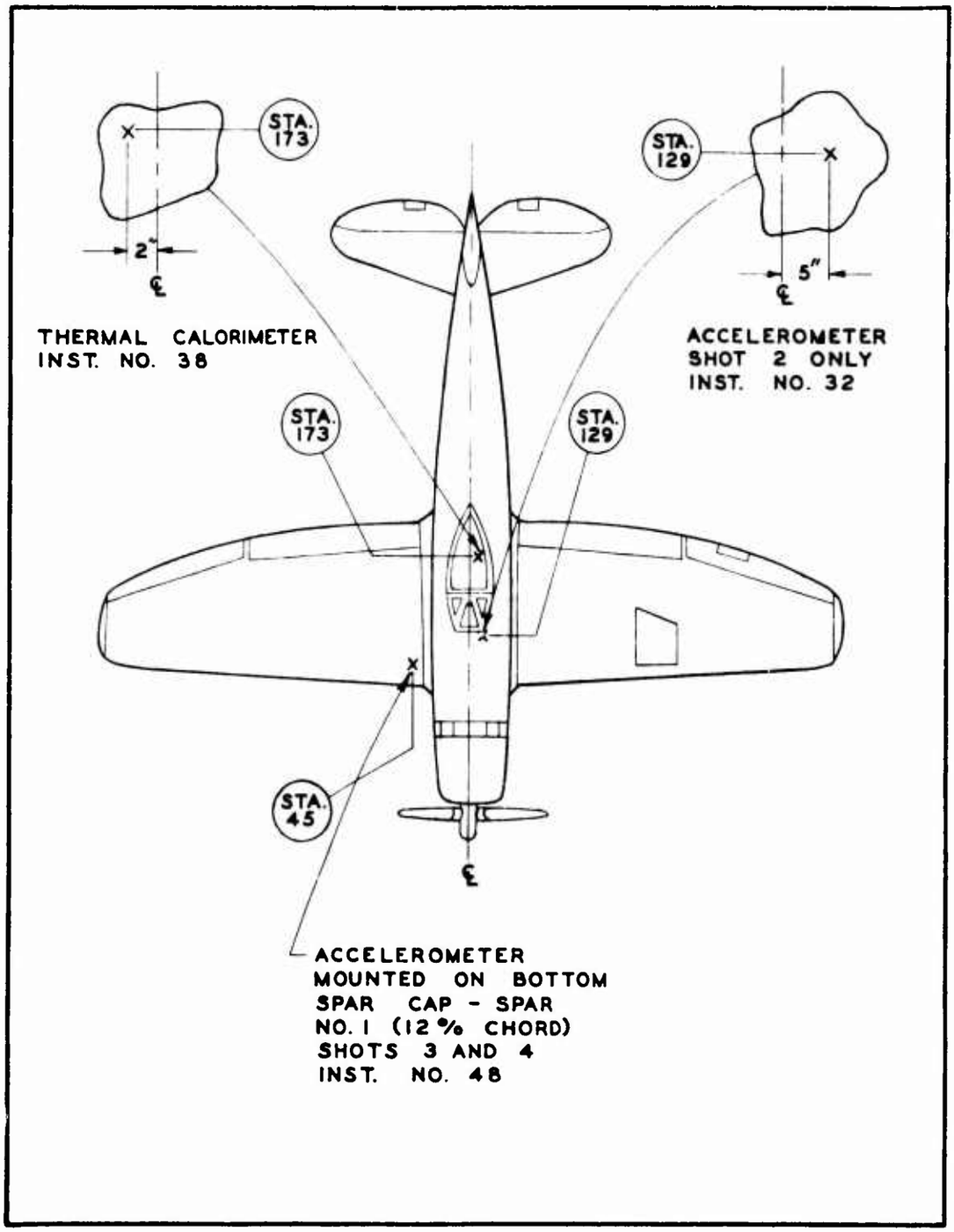

Fig. A.15b Location of Instrumentation on F-47 (9785)

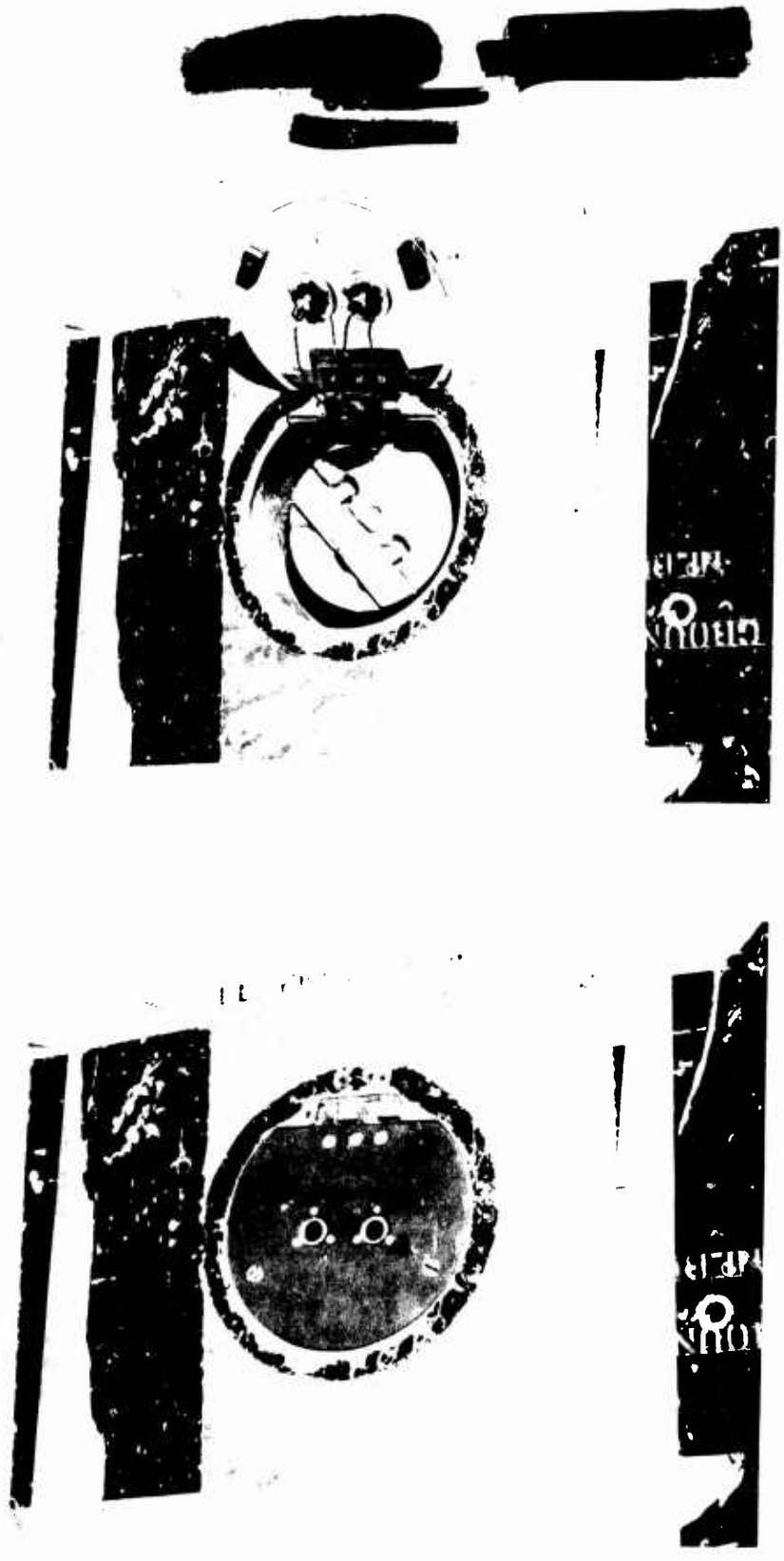

Fig. A.16 Installation of the Pressure Transmitters on the Wing of F-86 (9597)

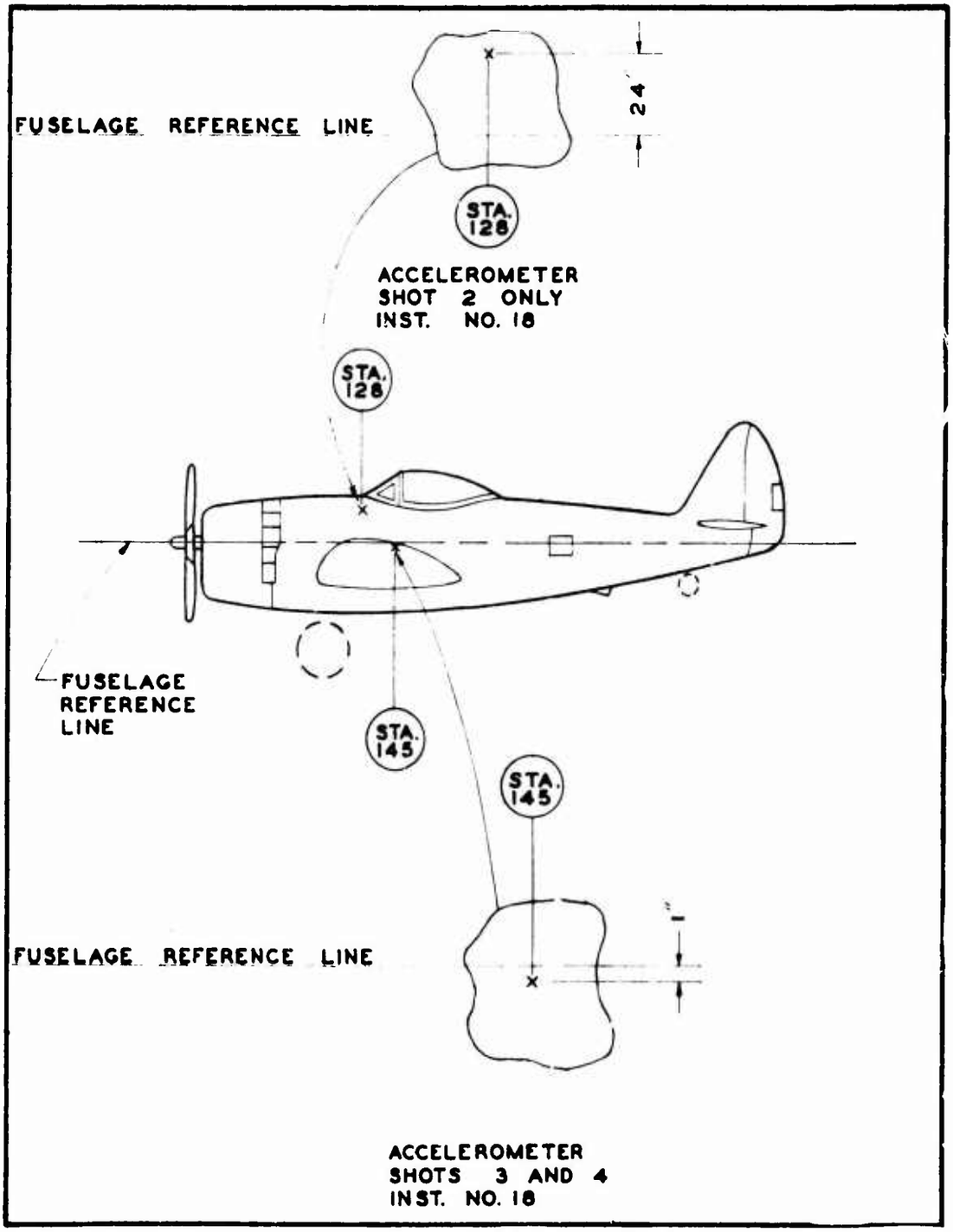

Fig. A.17a Location of Instrumentation Inside the Fuselage of F-47 (0065)

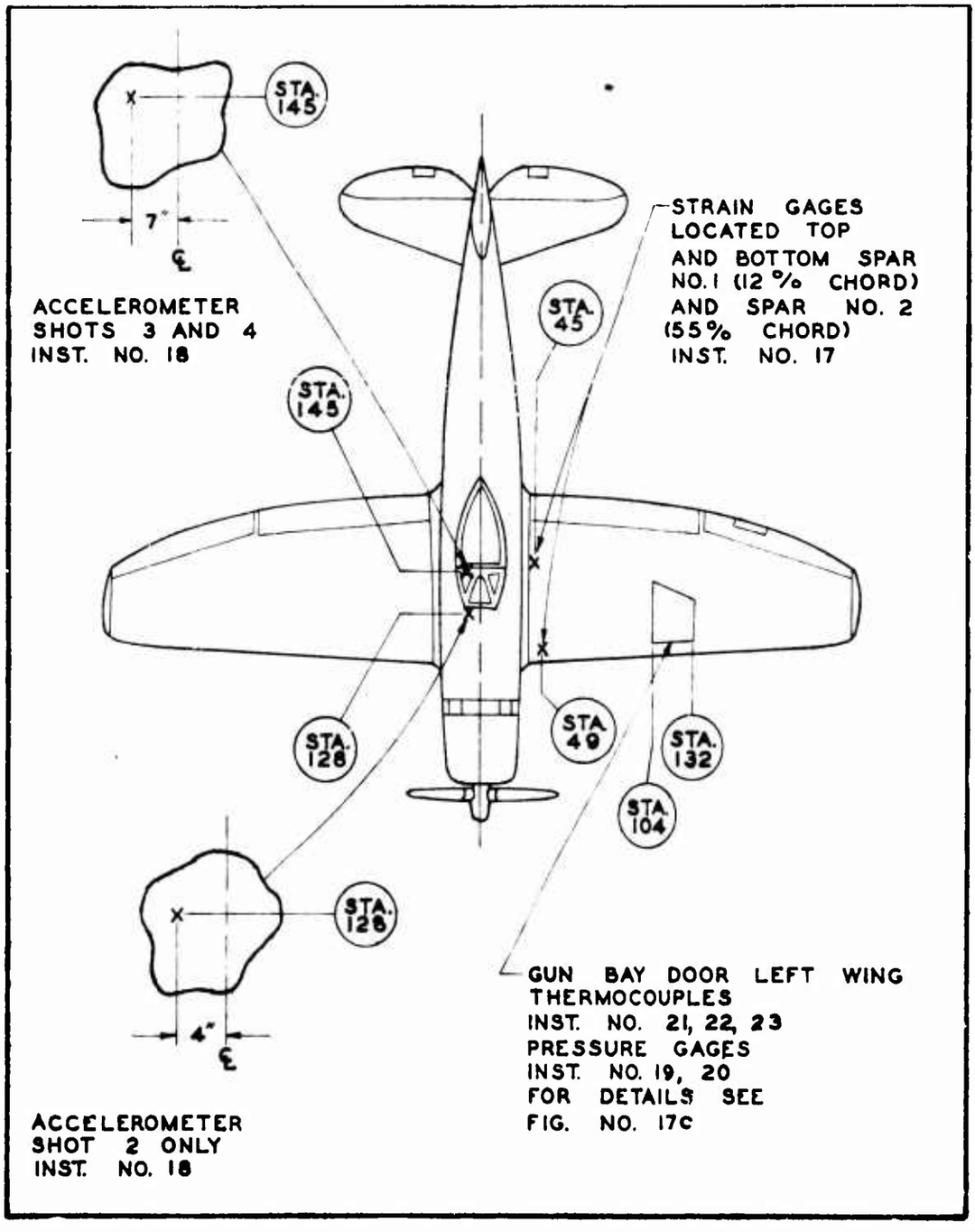

Fig. A.17b Location of Instrumentation on F-47 (0065)

[redacted]

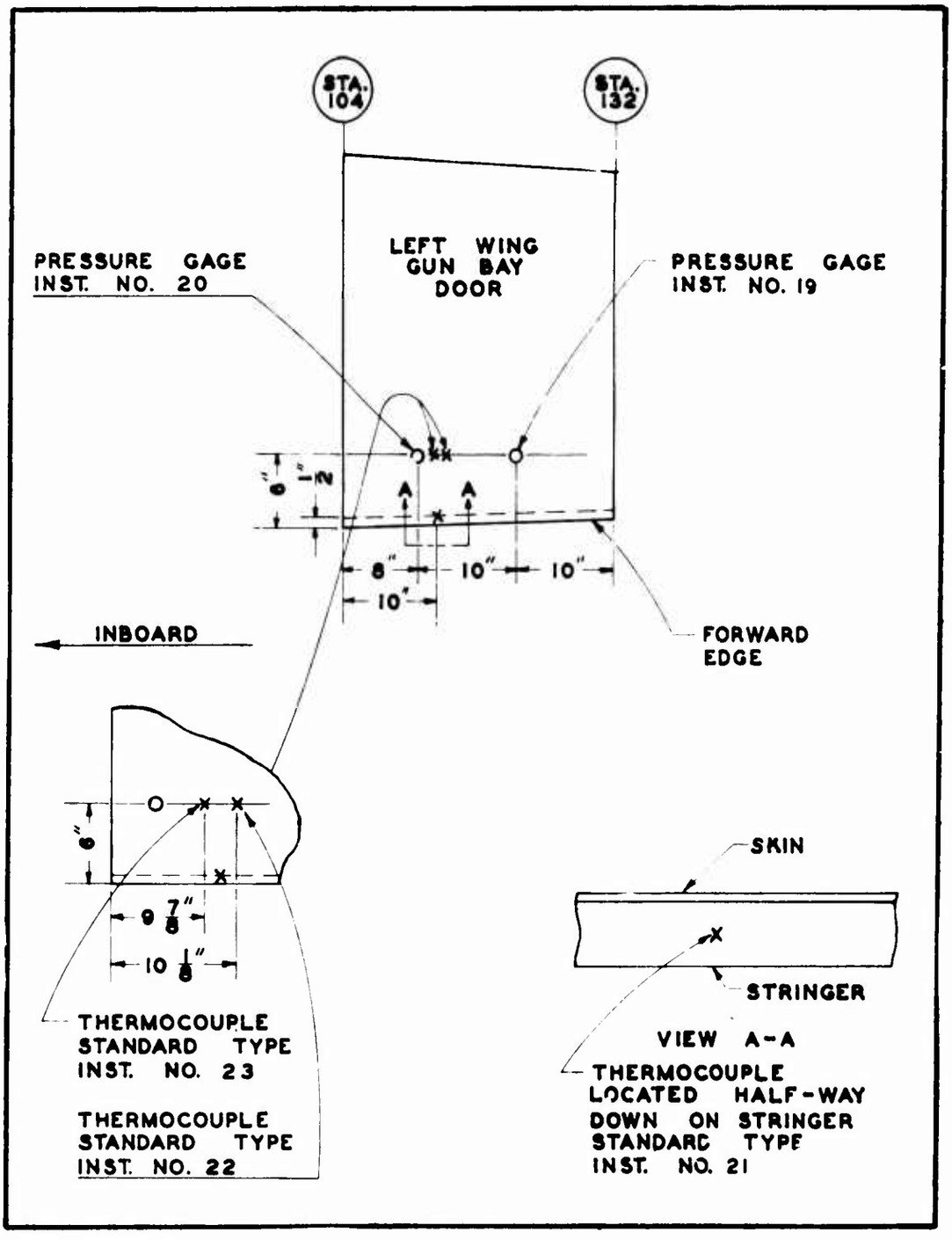

Fig. A.17c Location of Instrumentation on Left Wing Gun-bay Door on F-47 (0065)

[redacted]

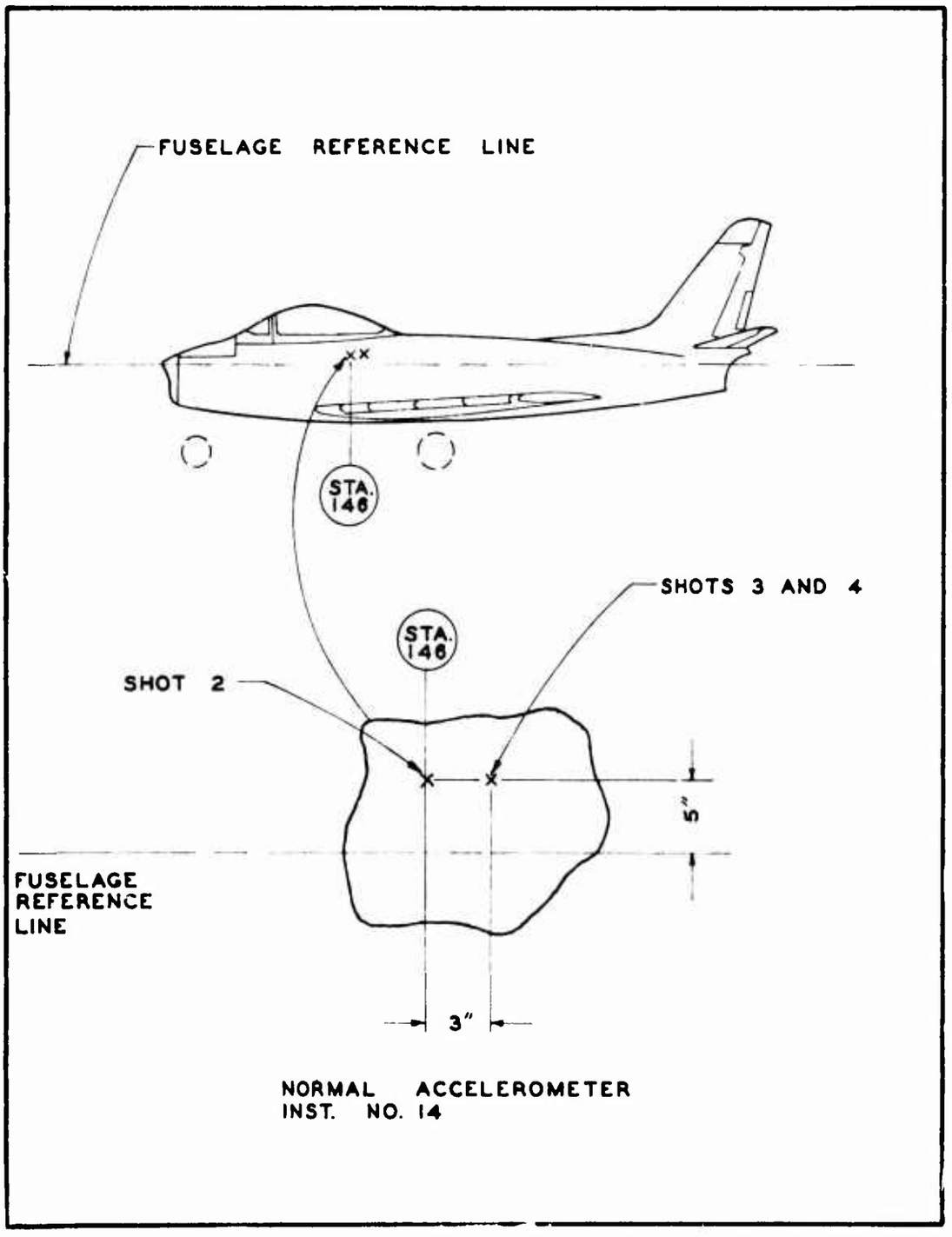

Fig. A.18a Location of Instrumentation Inside Fuselage of F-86 (9597)

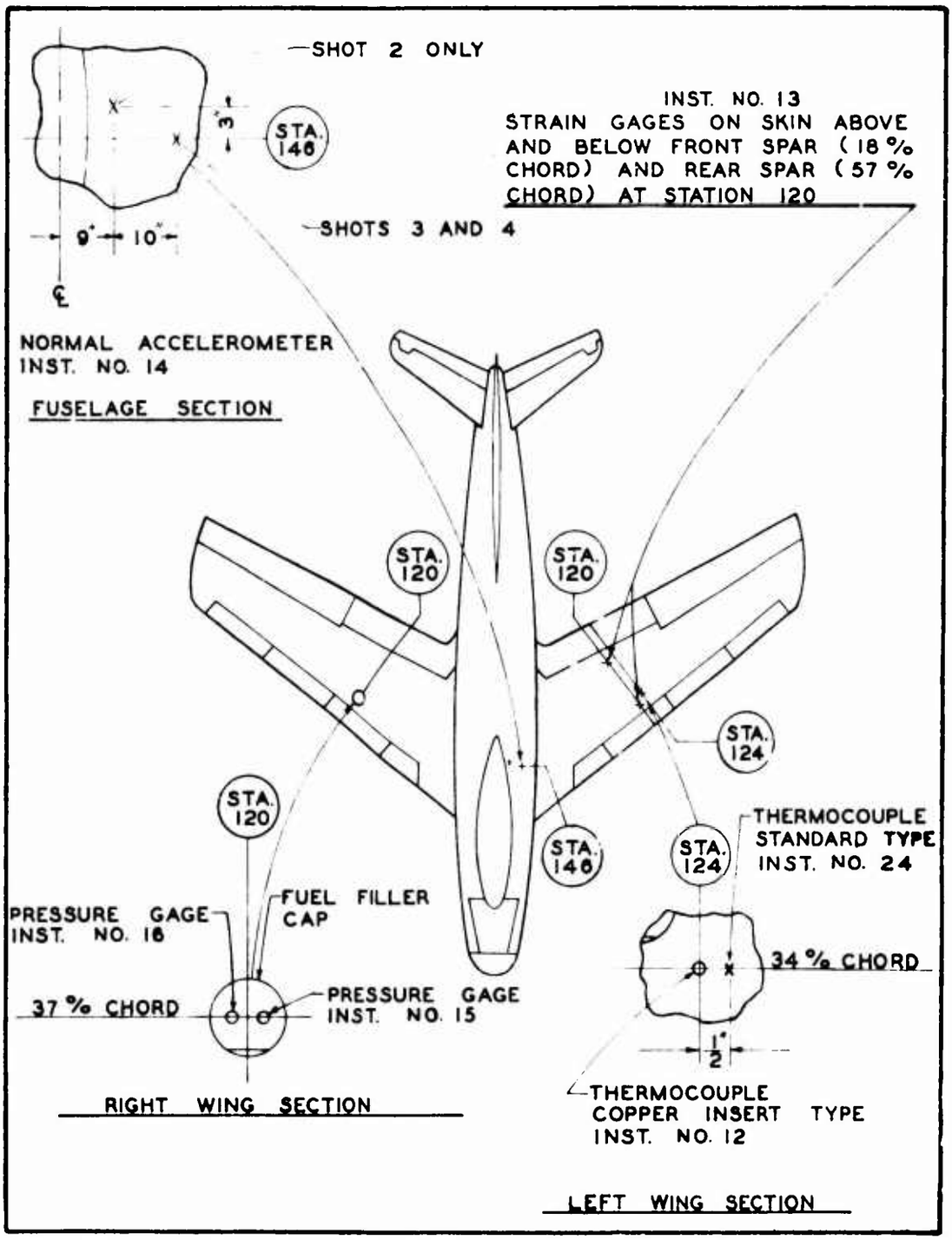

Fig. A.18b Location of Instrumentation on F-86 (9597)

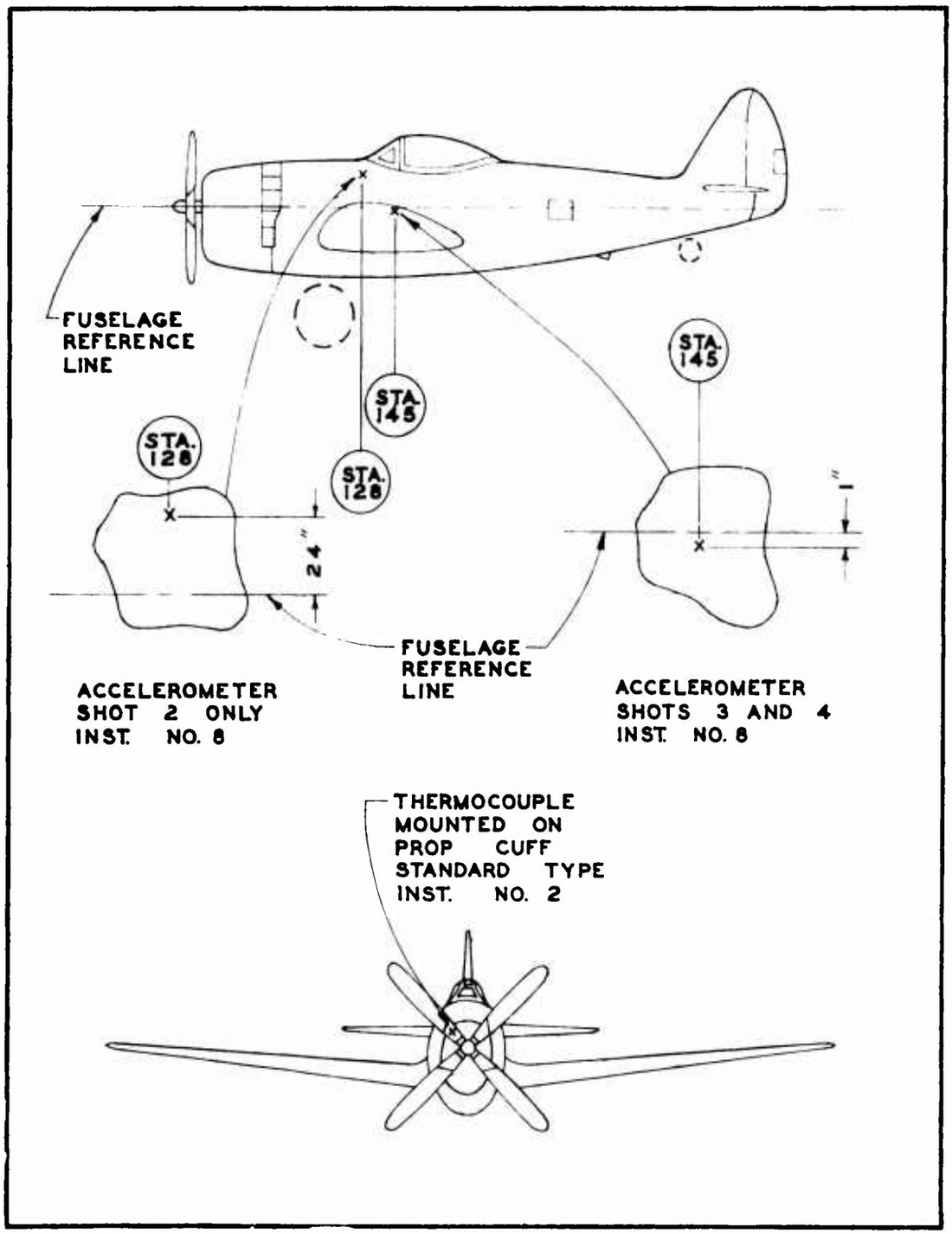

Fig. A.19a Location of Instrumentation on F-47 (8785)

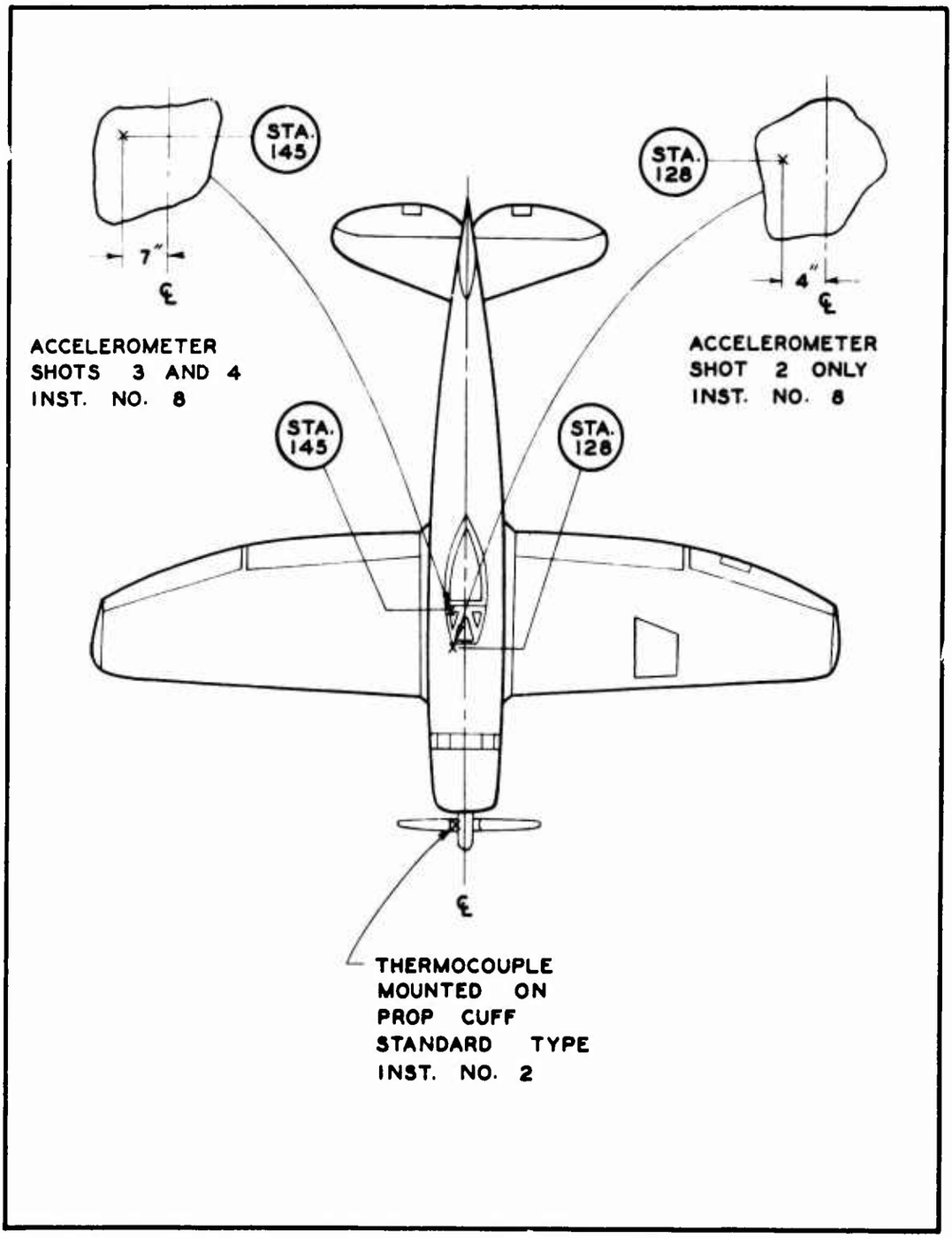

Fig. A.19b Location of Instrumentation on F-47 (8785)

Fig. A.20 Installation of the Thermocouple on the Propeller Cuff of F-47 (8785)

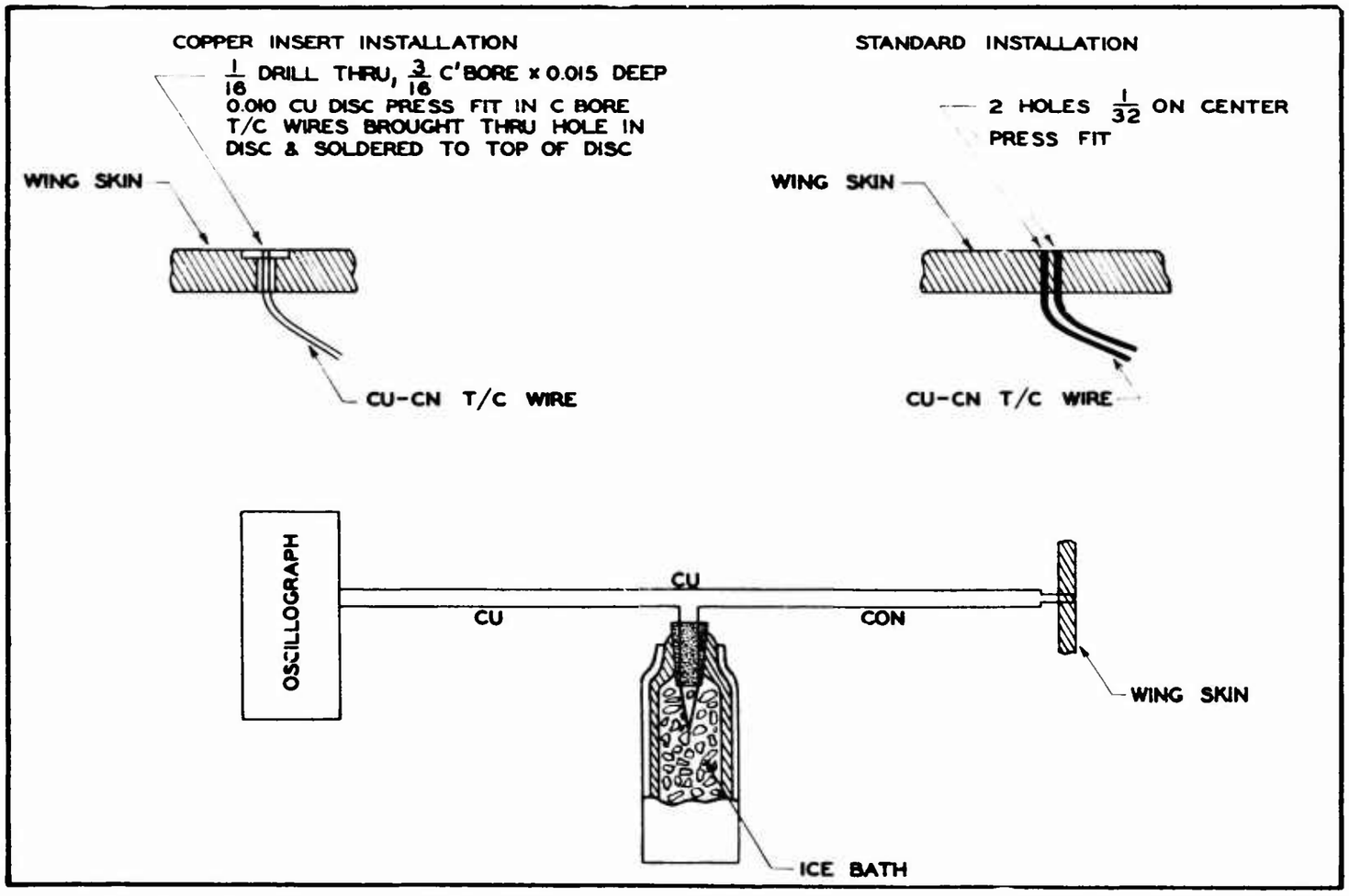

Fig. A.21 Standard and Copper Insert Type Thermocouple Installations and Schematic Wiring Diagram of the Thermocouple Circuit

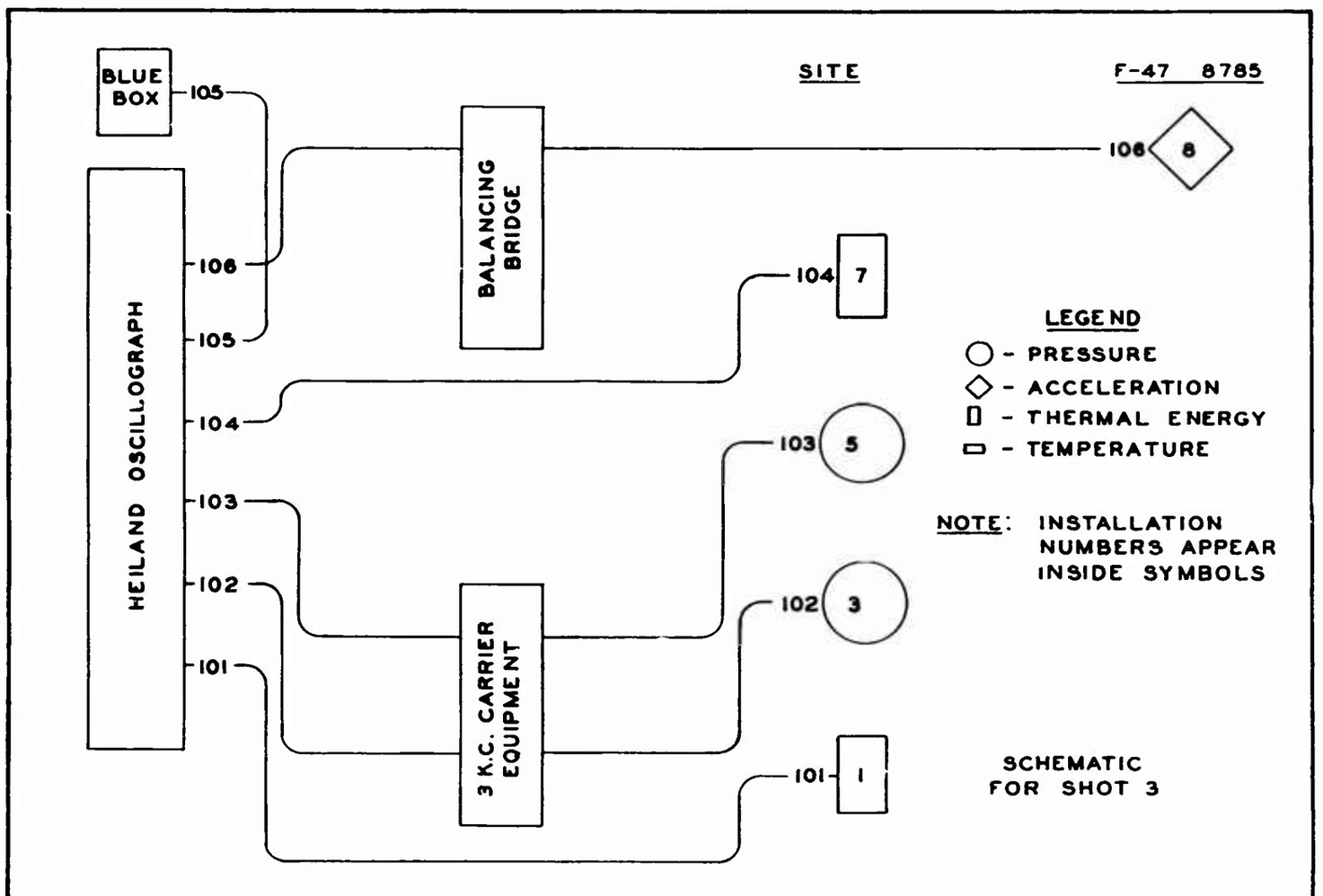

Fig. A.22a Instrumentation Schematic for Station 2200, Shot 3

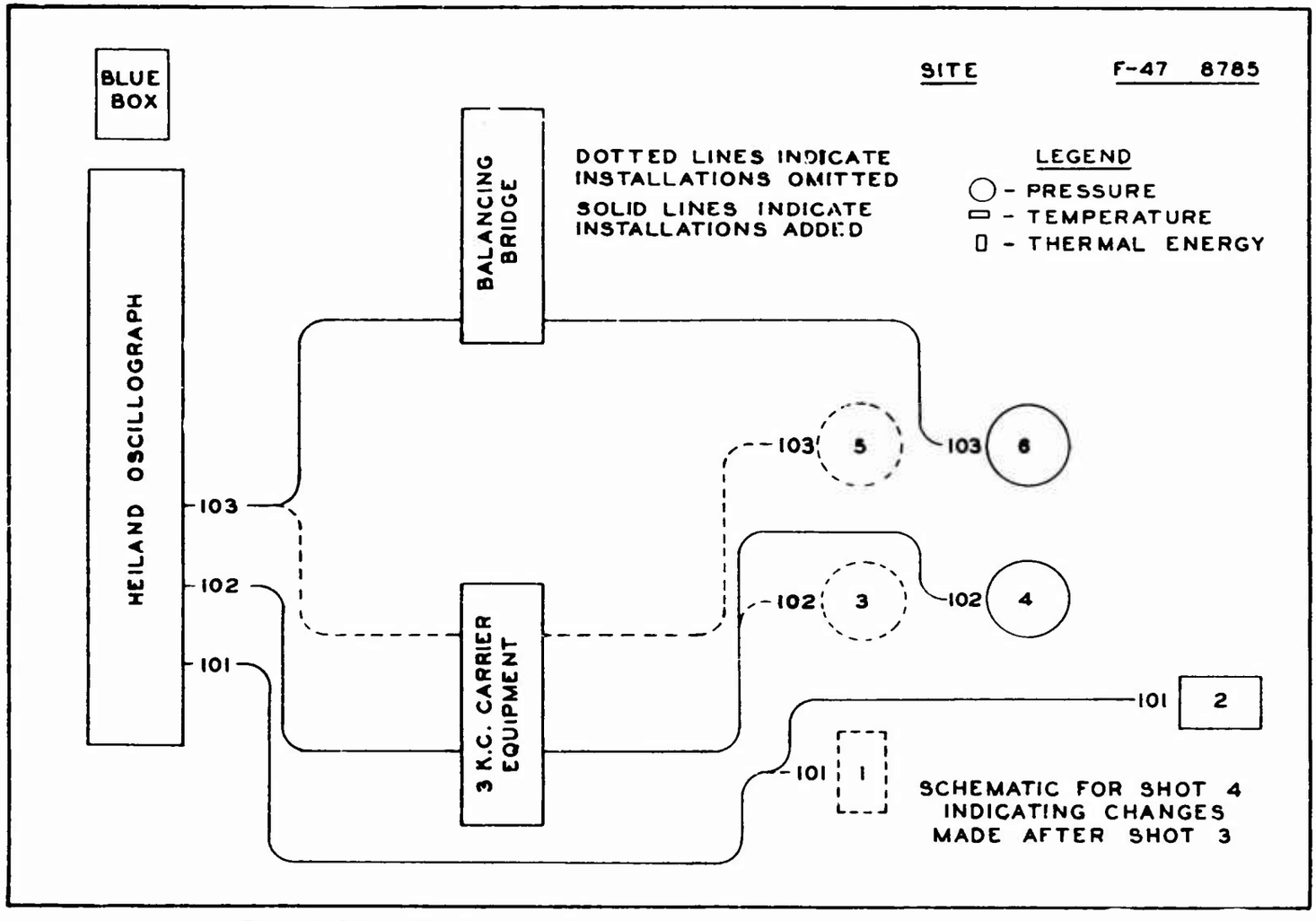

Fig. A.22b Instrumentation Schematic for Station 2200, Shot 4

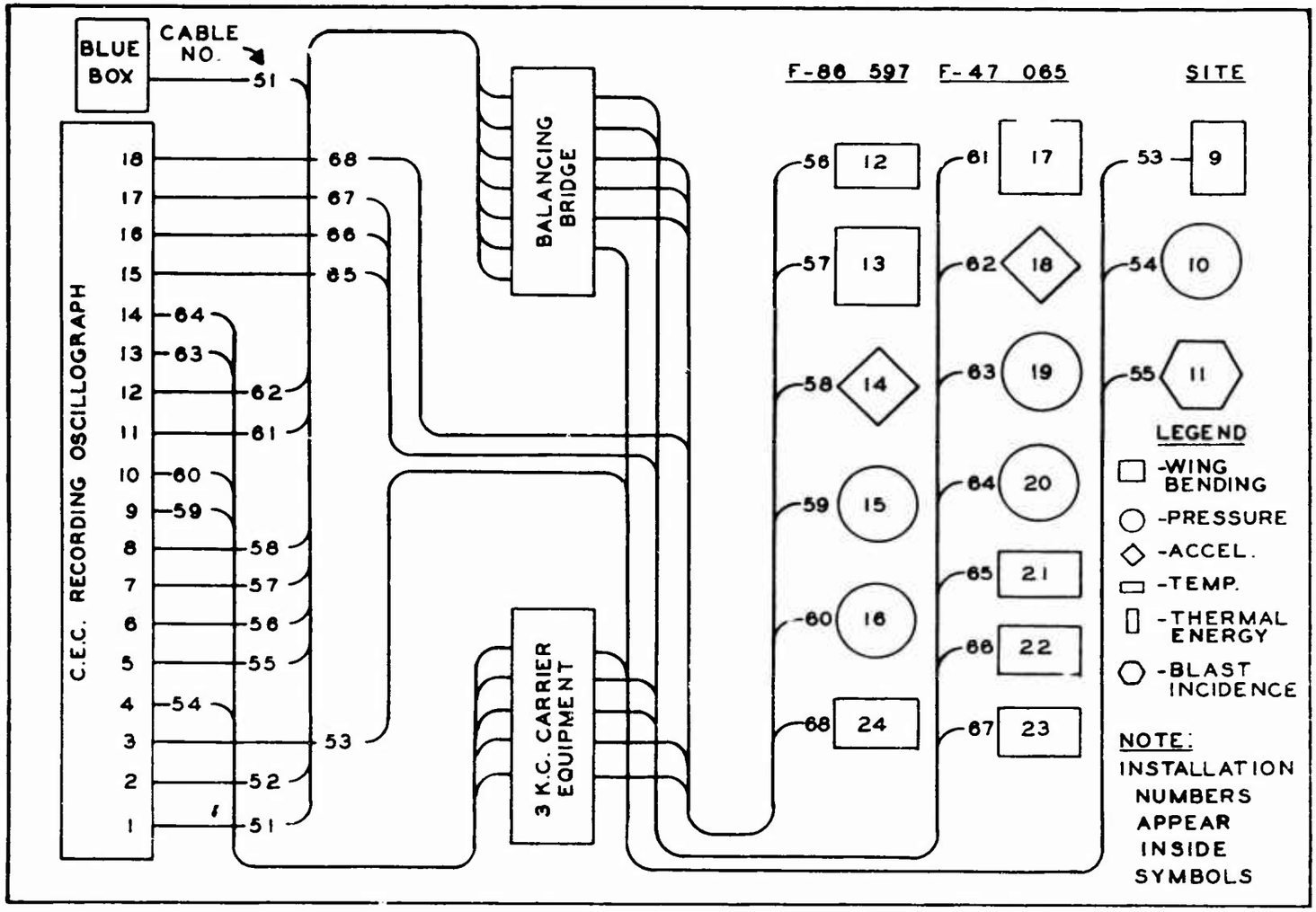

Fig. A.23a Instrumentation Schematic for Station 8000, Left Side, Shots 2 and 3

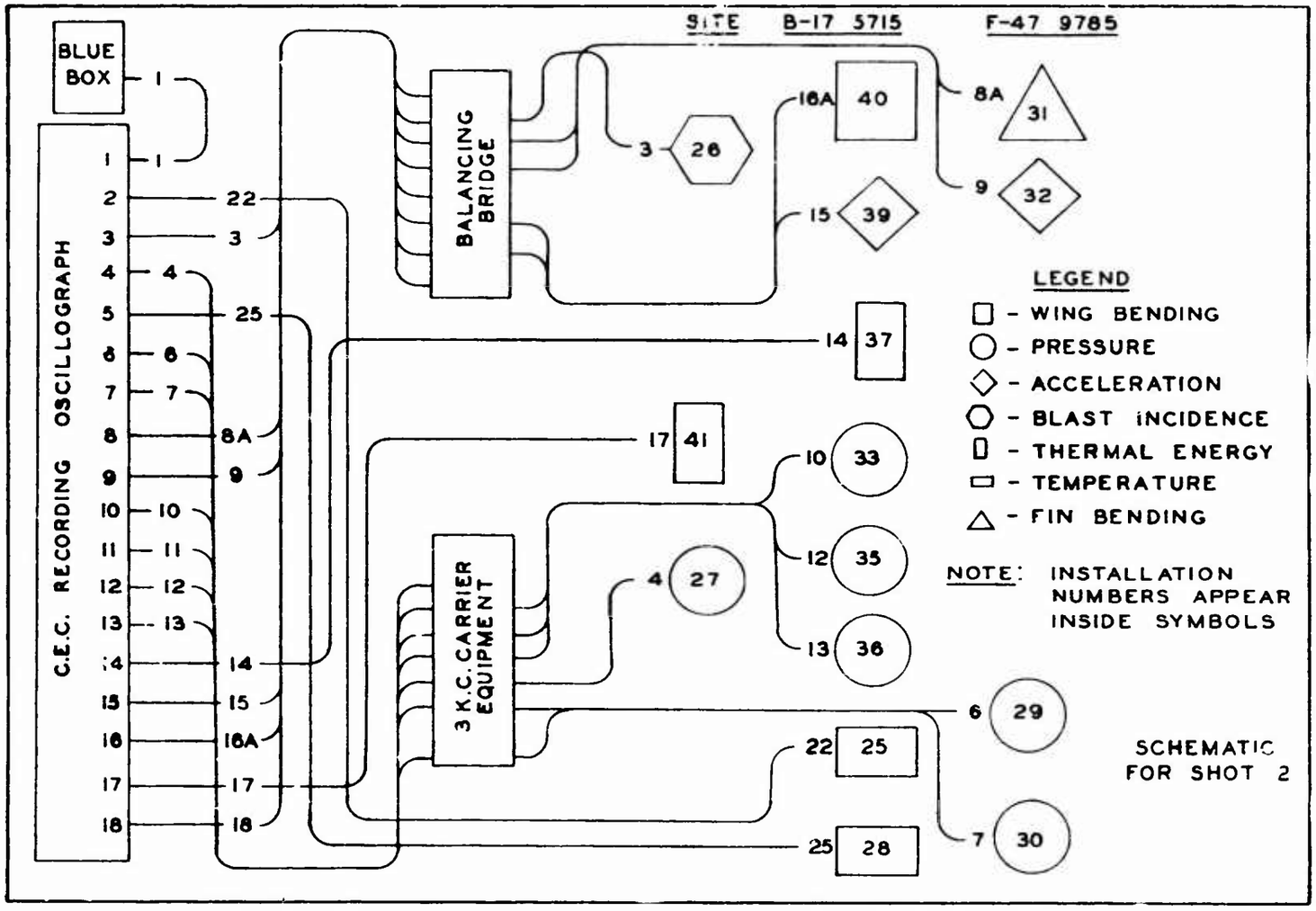

Fig. A.23b Instrumentation Schematic for Station 8000, Right Side, Shot 2

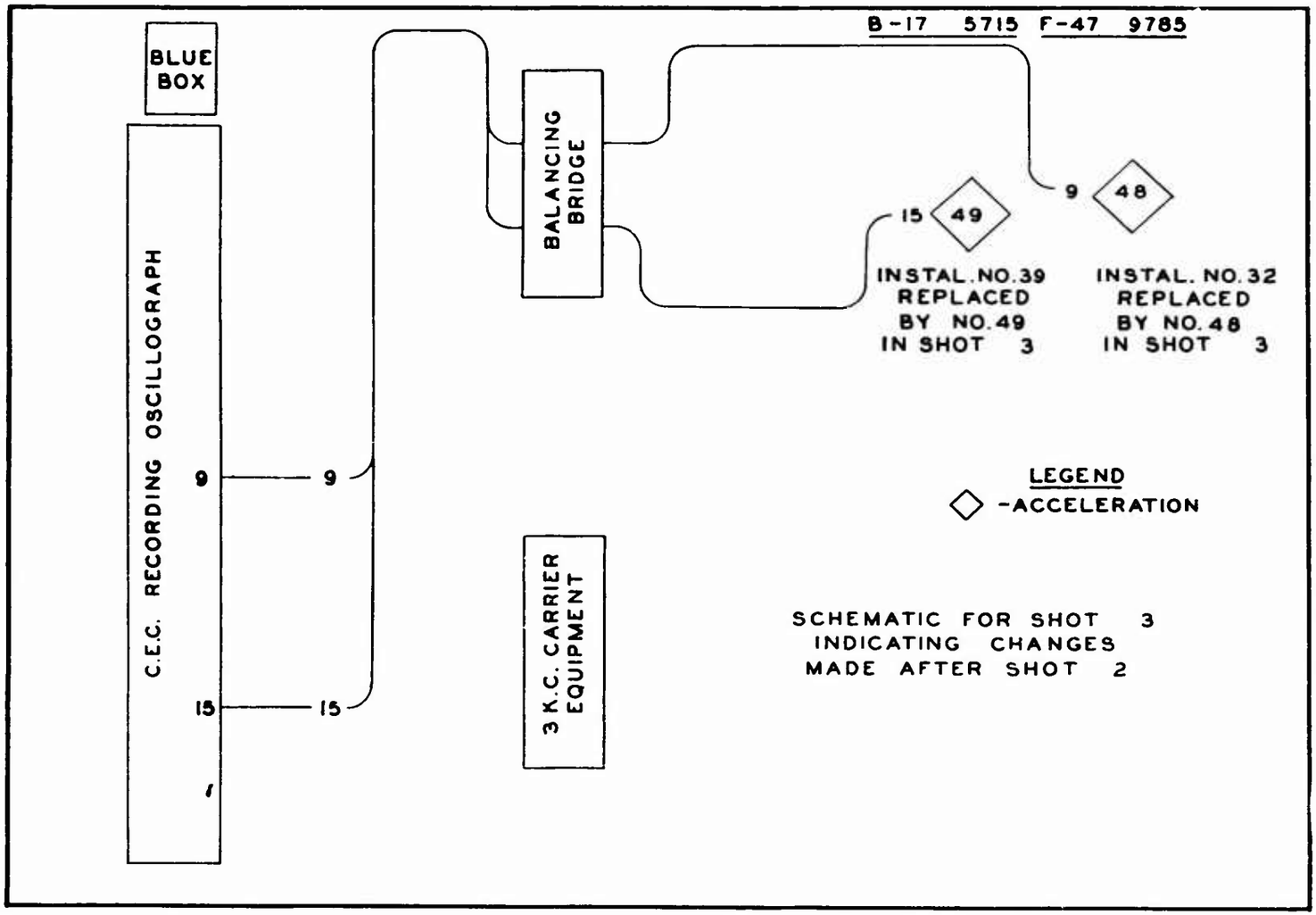

Fig. A.23c Instrumentation Schematic for Station 8000, Right Side, Shot 3

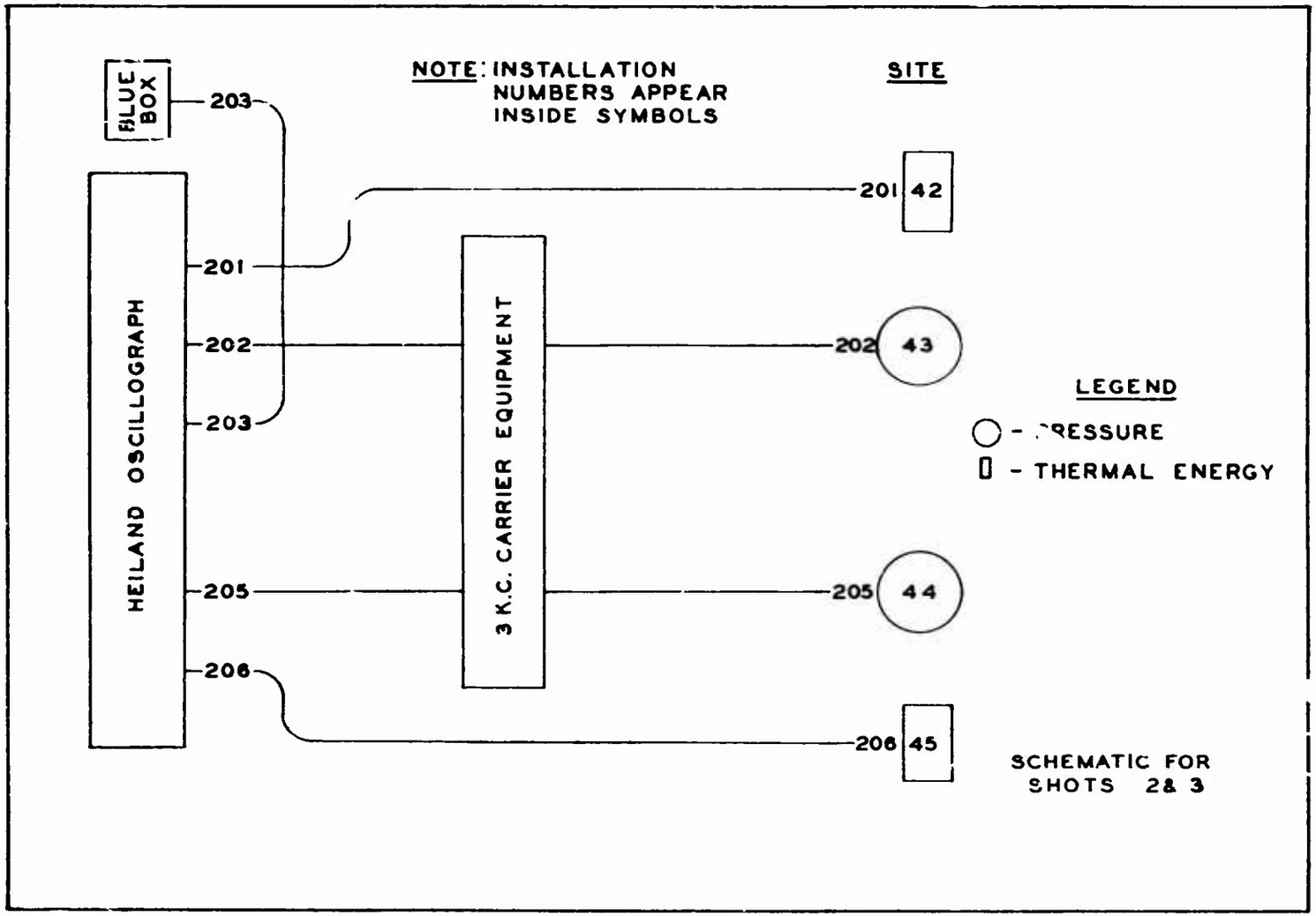

Fig. A.24a Instrumentation Schematic for Station 10,500, Shots 2 and 3

Fig. A.24b Instrumentation Schematic for Station 8000, Shot 4

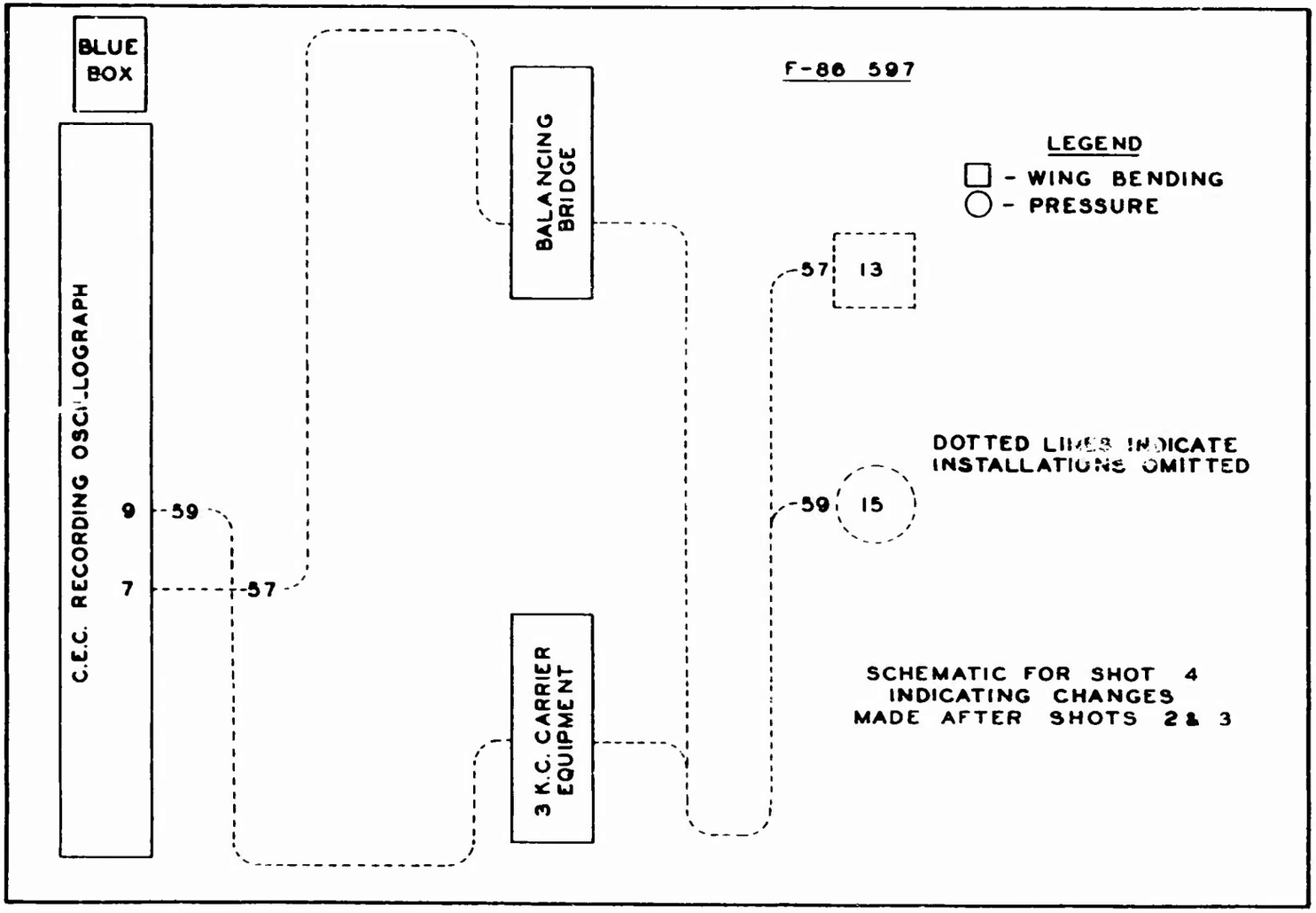

Fig. A.25a Instrumentation Schematic for Station 4000, Left Side, Shot 4

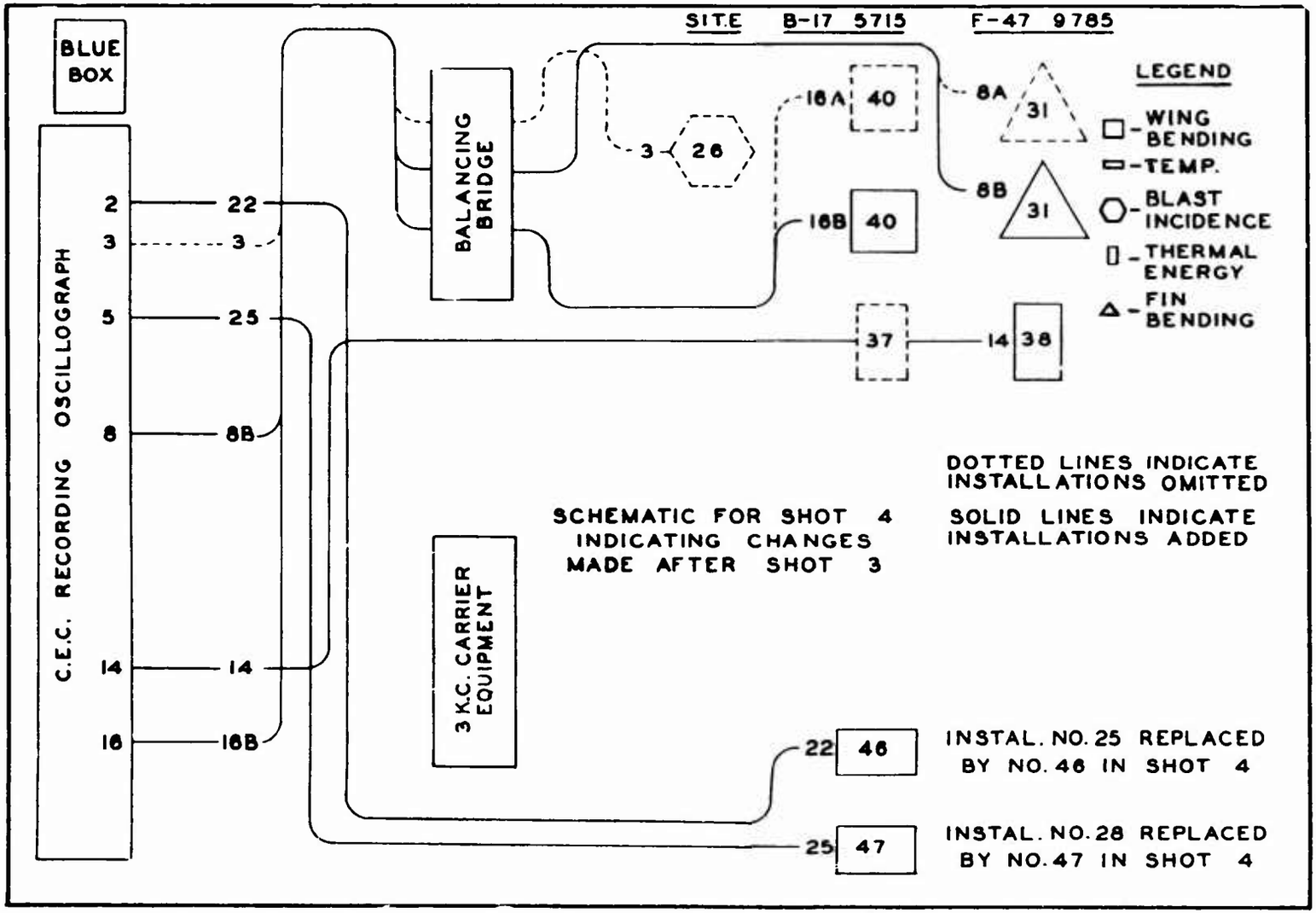

Fig. A.25b Instrumentation Schematic for Station 4000, Right Side, Shot 4

[redacted]

preliminary in the sense that full evaluation of its significance and conformity with theoretical concepts has not been completed. This evaluation will follow the completion of theoretical studies of the forcing functions based upon thermal and overpressure data. These theoretical studies will be compared with the reported test results for the observances of similarities and discrepancies, the exact form and distribution of this final evaluation being unknown at the present time.

Of the 133 channels of intelligence recorded during this series of three shots, 84 items, (63 per cent) may be reported as valid data. The best percentage obtained for a single shot was during Shot 4, for which 71 per cent of the channels were reportable. Total thermal energy and temperature measurements, which represented 32 per cent of the total installations, yielded good data in 90 per cent and 100 per cent of their installations, respectively. Due to the paper jamming in the oscillograph at Station 2200, Shot 2, two thermal measurements were lost. This was the only instance in which good thermal data were not obtained.

Thirty-two per cent of the instrumentation program consisted of overpressure measurements; however, only 21 per cent of the 42 pressure channels yielded reportable data. The reason for this low percentage is that the pressure transmitters were not capable of withstanding the temperature changes which occurred.

Accelerations were the only other type of measurement for which less than 50 per cent of the possible data were obtained. Only 40 per cent of the 15 accelerometer installations were considered accurate. The difficulty encountered was that the frequency response of the galvanometers used was too high. This allowed the true acceleration curve to be obscured by high frequency oscillations.

Of the other measurements, 60 per cent of the angle-of-blast incidence, and 82 per cent of the bending moment channels were considered to be accurate. Table A.5 is presented to give a complete picture of the results obtained from each shot. Installation numbers for each measurement are given to facilitate cross-reference during the presentation of test results and the discussion.

A.3.2 Presentation of Shot 2 Data

A.3.2.1 Station 2200

No general input data were obtained because the paper jammed in the oscillograph.

A.3.2.2 Station 4000

No measurements were attempted.

[redacted]

[redacted]

A.3.2.3 Station 8000

The general input function measurements were as follows:

1. Total thermal energy was measured by installations 9 and 41 at this station. Their location at the site, relative to the instrumented aircraft, is shown in Fig. A.3. Curves showing total thermal energy as a function of time for both installations are presented in Fig. A.26. Two types of corrections were incorporated in each curve. One correction was obtained by applying to the period preceding the maximum point on the curve the rate of heat dissipation obtained from the curve in the interval following this maximum point. The second correction was applied to compensate for the attenuation of the quartz window, which amounted to an increase of 8 per cent for each point on the curve.

The corrected curve obtained from installation 9, which was located 5 ft above the ground on the left side at Station 8000, reached a peak of 0.60 cal/cm^2 3 sec after time zero. This curve is presented in Fig. A.26. The corrected curve obtained from installation 41, which was located 5 ft above the ground on the right side at Station 8000, reached a peak of 0.55 cal/cm^2 4 sec after time zero.

2. Overpressure was measured at Station 8000 on Shot 2 by installations 10 and 27. Their location at the site relative to the instrumented aircraft is shown in Fig. A.3. Curves of overpressure as a function of time for installations 10 and 27 are shown in Fig. A.27. The peak reached on both curves is 1.05 psi with an apparent rise time of 3 msec. The positive phase lasted 0.225 sec on installation 10 and 0.275 sec on installation 27.

The specific input function measurements were as follows:

1. Total thermal energy inside the cockpit of B-17 (5715), installation 37, was selected for measurement to determine the level of thermal energy to which personnel in the cockpit would be subjected under similar conditions. This measurement was made 13 ft above the ground behind the co-pilot's windshield, which was 2.15 in. thick and of laminated construction. Figure A.28 shows the corrected curve (see the first part of this paragraph, A.3.2.2, for the explanation of total thermal energy corrections) of the total thermal energy inside the cockpit as a function of time. A peak of 0.28 cal/cm^2 was attained 1.75 sec after time zero.

2. The pressure transmitter, installation 19, mounted on the wing of F-47 (0065) produced a peak value of 2.25 psi. Figure A.29 shows an apparent rise time of 3 msec and a positive phase of 43 msec.

[redacted]

The time, 28 msec, between zero and the rise of the pressure in Fig. A.30 on the wing of F-47 (0065) is the time required for the shock wave to travel the 30 ft from the site pressure transmitter to the F-47 wing pressure transmitter. Installation 19 is actually the mean of two curves (see A.4.7 for explanation).

The response function measurements were as follows:

1. Only three aircraft at Station 8000, namely B-17 (5715), F-47 (0065), and F-86 (9597), were instrumented to measure skin temperature rise. The locations of the thermocouples are shown in Figs. A.13b, A.17b, A.17c, and A.18b. Due to low output of the thermocouples for Shot 2, the skin and flange temperature measurements on F-47 (0065), the skin temperature measurements on the F-86, and the measurement of skin temperature on the polished right wing surface of the B-17 were too small to be measurable. A small skin temperature rise of 5°F was measured on the unpolished surface (left wing) of the B-17. This peak was reached 1.2 sec after zero time as shown in Fig. A.31. This wing surface absorbed more heat than the others because it was a darker color, due to oxidation, and because its angle of incidence was smaller than that of the other surfaces. The angle of incidence is defined as the acute angle between the normal to the surface and the incident thermal ray.

2. The measurement of normal acceleration on B-17 (5715) was the only valid acceleration data obtained during Shot 2. This acceleration curve, presented in Fig. A.32, has a relatively uniform 4 cps vibration with peak accelerations of plus 0.16 G's and minus 0.22 G's. The initial interval of 0.3 sec of this measurement has been omitted because transient high frequency oscillations, caused by the vibration of various structural components, obscured the regular pattern of this trace. These vibrations were the factor which made the other acceleration measurements invalid.

3. Wing bending was measured on B-17 (5715), F-47 (0065), and F-86 (9597) at Station 8000, Shot 2. Due to insufficient loading on the F-47 and the F-86 wings, no appreciable data were recorded. There was an observed response for the F-47 installation; however, the magnitude of its bending moment was too small to be accurately measured. Thus this graphical presentation has not been included, and specific indication of peak bending moments has been omitted. The deflections were sufficiently large, however, to indicate that the first mode frequency was 10.5 cps. Good results were obtained from the B-17 wing bending measurement. This bending moment, shown in Fig. A.32, indicates superposition of the first and second bending modes. The maximum positive and negative peaks were 470,000 in-lbs and 600,000 in-lbs, respectively, equivalent to 3.8 per cent of ultimate for the positive and 4.9 per cent of ultimate for the negative loads.

[redacted]

4. The measurement of fin bending moment on F-47 (9785) yielded very good data. As shown in Fig. A.33, the maximum positive peak occurred at 45 msec and is equal to 27,000 in-lbs, which may be expressed as 76 per cent of the ultimate root bending moment. The average bending frequency is 27.3 cps. Figure A.33 shows that the bending moment is predominately positive for the first 0.7 sec. No permanent set in the fin was discovered after this shot.

A.3.2.4 Station 10,500

The general input function measurements were as follows:

1. Total thermal energy was measured with two installations located 8 ft apart at either end of the instrument pit as shown in Fig. A.6. The total galvanometer deflection was quite small for both of these measurements, for which 0.01 in. deflection was equivalent to 14 per cent of the maximum deflection. Both measurements plotted vs time are presented in Fig. A.34 with the preliminary NRDL data, which was corrected to zero atmospheric attenuation. These curves have been corrected for the attenuation due to the quartz window and for the loss in thermal energy due to the heat dissipation from the calorimeter. The methods used for these corrections were described in A.3.2.3. A peak measurement of 0.31 cal/cm^2 occurring after a rise time of 2 sec was obtained from the calorimeter on the right side, installation 42; and a peak measurement of 0.30 cal/cm^2 occurring after a rise time of 1.8 sec was obtained on the left side, installation 45.

2. Two overpressure sensing installations were placed 8 in. apart on a concrete slab well forward of the instrument pit installation, as shown in Fig. A.4. The graphical results of these measurements are presented in Fig. A.35. The curve representing the measurement made by installation 43 rose to a peak of 0.68 psi in 4 msec. The maximum peak reached during the negative phase was equal to 0.23 psi, which was equivalent to 34 per cent of the maximum positive peak overpressure. The other curve, installation 44, reached its peak of 0.76 psi in 3 msec. The negative phase began at 0.25 sec, and the peak negative pressure was 0.31 psi, which was 41 per cent of the maximum positive peak.

A.3.3 Presentation of Shot 3 Data

A.3.3.1 Station 2200

The general input function measurements were as follows:

1. Total thermal energy at this station was measured by two installations, 1 and 7, in which the instruments were mounted 50 in.

[redacted]

TABLE A.1

Presentation, Comparison, and Composite Curves for Corrected Total Thermal Energy

Shot Number	Installation Number	Station	Comparison of Total Thermal Energy and NRDL Curve at One Station for One Shot	Comparison of Total Thermal Energy at Site with Total Thermal Energy Measured in Airplane and NRDL Curve	Total Thermal Energy vs Time for Each Shot All Stations	Total Thermal Energy vs Time for One Station All Shots	Peak Total Thermal Energy Measurements vs Slant Range All Shots	Peak Total Thermal Energy Measurements vs Ground Range All Shots	Comparison of Total Thermal Energy Delivered and Corresponding Temperature Rise	Particle Attenuation Factor vs Ground Range
2	9	8000	A.26		A.66	A.70	A.72	A.71		A.65
2	37	8000		A.28						
2	41	8000	A.26	A.28	A.66	A.70	A.72	A.71	A.31	A.65
2	42	10500	A.34		A.66		A.72	A.71		A.65
2	45	10500	A.34		A.66		A.72	A.71		A.65
3	1	2200	A.36		A.67	A.69	A.72	A.71		A.65
3	7	2200	A.36		A.67	A.69	A.72	A.71		A.65
3	9	8000	A.38		A.67	A.70	A.72	A.71	A.41 A.43	A.65
3	37	8000		A.40						
3	41	8000	A.38	A.40	A.67	A.70	A.72	A.71	A.44	A.65
3	42	10500	A.52		A.67		A.72	A.71		A.65
3	45	10500	A.52		A.67		A.72	A.71		A.65
4	7	2200			A.68	A.69	A.72	A.71	A.5[illegible]	A.65
4	9	4000	A.55		A.68		A.72	A.71	A.59 A.75	A.65
4	38	4000		A.57						
4	41	4000	A.55	A.57	A.68		A.72	A.71	A.61	A.65
4	42	8000	A.63		A.68	A.70	A.72	A.71		A.65
4	45	8000	A.63		A.68	A.70	A.72	A.71		A.65

TABLE A.2

Presentation, Comparison, and Composite Curves for Temperature Rise

Shot Number	Installation Number	Station	Comparison of Temperature Rise for Similar Installations Same Station and Shot	Comparison of Temperature Rise of Polished and Unpolished Surface	Comparison of Temperature Rise of Skin and Stringer	Comparison of Total Thermal Energy Delivered and Corresponding Temperature Rise	Tensile Strength of Propeller Cuff vs Time	Comparison of Temperature Rise of Copper Insert and Standard Thermocouple Installations
2	28	8000				A.31		
3	12	8000				A.41		A.41
3	21	8000			A.43	A.43		
3	22	8000	A.42		A.43	A.43		
3	23	8000	A.42		A.43	A.43		
3	24	8000				A.41		A.41
3	25	8000		A.44		A.44		
3	28	8000		A.44		A.44		
4	2	2200				A.54	A.76	
4	12	4000				A.59		A.59
4	21	4000			A.75	A.75		
4	22	4000	A.60		A.75	A.75		
4	23	4000	A.60		A.75	A.75		
4	24	4000				A.59		A.59
4	46	4000		A.61		A.61		
4	47	4000		A.61		A.61		

TABLE A.3

Presentation, Comparison, and Composite Curves for Overpressure and Angle-of-Blast Incidence

Shot Number	Installation Number	Station	Measured Quantity	Comparison of Two or More Instruments Measuring the Same Quantity at the Same Station for the Same Shot	Comparison of Measurements for Each Airplane or Station for All Shots	Comparison of Site Overpressure with Airplane Overpressure for Same Shot	Comparison of Site Overpressure with Wing or Fin Bending Moment at the Same Station for Same Shot	Peak Measurement vs Ground Range All Shots	Measurement vs Time	Comparison of Measurement vs Time
2	10	8000	Site Overpressure	A.27	A.64	A.29	A.33	A.73		A.30
2	19	8000	Wing Overpressure							
2	27	8000	Site Overpressure	A.27	A.64	A.29	A.33	A.73		
2	43	10500	Site Overpressure	A.35	A.53			A.73		
2	44	10500	Site Overpressure	A.35	A.53			A.73		
3	43	10500	Site Overpressure		A.53			A.73		
4	16	4000	Wing Overpressure						A.58	A.30
4	19	4000	Wing Overpressure							A.30
4	43	8000	Site Overpressure		A.64			A.73	A.74	
3	11	8000	Angle-of-Blast Incidence	A.39						A.56
3	26	8000	Angle-of-Blast Incidence	A.39						
4	11	4000	Angle-of-Blast Incidence							A.56

TABLE A.4

Presentation, Comparison, and Composite Curves for Bending Moment and Acceleration

Shot Number	Installation Number	Station	Measured Quantity	Comparison of Measurements vs Time for Each Airplane All Shots	Comparison of Site Overpressure with Wing or Fin Bending Moment for Same Station and Shot	Comparison of Wing or Fin Bending Moment with Corresponding Acceleration for that Airplane	Measurement vs Time
[illegible]	31	8000	Fin Bending Moment	A.50	A.33		
2	40	8000	Wing Bending Moment	A.49	A.33	A.32	
3	17	8000	Wing Bending Moment	A.47			
3	31	8000	Fin Bending Moment	A.50		A.51	
3	40	8000	Wing Bending Moment	A.49		A.46	A.48
4	17	4000	Wing Bending Moment	A.47			
4	31	4000	Fin Bending Moment	A.50		A.62	
4	40	4000	Wing Bending Moment	A.49			
2	39	8000	Normal Acceleration			A.32	
3	8	2200	Normal Acceleration	A.37			
3	48	8000	Lateral Acceleration	A.45		A.51	
3	49	8000	Normal Acceleration			A.46	
4	8	2200	Normal Acceleration	A.37			
4	48	4000	Lateral Acceleration	A.45		A.62	

TABLE A.5

Measured Quantity vs Quality of Data Obtained

Quantity	Installation Number	Shot 2			Shot 3			Shot 4		
		Station	G*	B*	Station	G*	B*	Station	G*	B*
Total Thermal Energy, Site	1	2200		X	2200	X				
Propeller Cuff Temp. F-47 (8785)	2							2200	X	
Overpressure, Site	3	2200		X	2200		X			
Overpressure, Site	4							2200		X
Overpressure, Site	5	2200		X	2200		X			
Overpressure, Site	6							2200		X
Total Thermal Energy, Site	7	2200		X	2200	X		2200	X	
Normal Acceleration F-47 (8785)	8	2200		X	2200	X		2200	X	
Total Thermal Energy, Site	9	8000	X		8000	X		4000	X	
Overpressure, Site	10	8000	X		8000		X	4000		X
Blast Incidence, Site	11	8000		X	8000	X		4000	X	
Skin Temperature F-86 (9597) (INBD)	12	8000	X		8000	X		4000	X	
Wing Bending F-86 (9597)	13	8000		X	8000		X			
Normal Acceleration F-86 (9597)	14	8000		X	8000		X	4000		X
Overpressure, Wing F-86 (9597) (INBD)	15	8000		X	8000		X			
Overpressure, Wing F-86 (9597) (OUTBD)	16	8000		X	8000		X	4000	X	
Wing Bending F-47 (0065)	17	8000	X		8000	X		4000	X	
Normal Acceleration F-47 (0065)	18	8000		X	8000		X	4000		X
Overpressure, Wing F-47 (0065) (OUTBD)	19	8000	X		8000		X	4000	X	
Overpressure, Wing F-47 (0065) (INBD)	20	8000		X	8000		X			
Stringer Temperature F-47 (0065)	21	8000	X		8000	X		4000	X	
Skin Temperature F-47 (0065) (OUTBD)	22	8000	X		8000	X		4000	X	
Skin Temperature F-47 (0065) (INBD)	23	8000	X		8000	X		4000	X	
Skin Temperature F-86 (9597)	24	8000	X		8000	X		4000	X	
Right Wing Temperature B-17 (5715)	25	8000	X		8000	X				
Right Wing Temperature B-17 (5715)	46							4000	X	
Blast Incidence, Site	26	8000	X		8000	X				

TABLE A.5 (Continued)

Measured Quantity vs Quality of Data Obtained

Quantity	Installation Number	Shot 2			Shot 3			Shot 4		
		Station	G*	B*	Station	G*	B*	Station	G*	B*
Overpressure, Site	27	8000	X		8000		X	4000		X
Left Wing Temperature B-17 (5715)	28	8000	X		8000	X				
Left Wing Temperature B-17 (5715)	47							4000	X	
Overpressure F-47 (9785)	29	8000		X	8000		X	4000		X
Overpressure F-47 (9785)	30	8000		X	8000		X	4000		X
Fin Bending F-47 (9785)	31	8000	X		8000	X		4000	X	
Lateral Acceleration F-47 (9785)	32	8000		X						
Lateral Acceleration F-47 (9785)	48				8000	X		4000	X	
Overpressure, B-17 (5715)	33	8000		X	8000		X	4000		X
Overpressure, B-17 (5715)	35	8000		X	8000		X	4000		X
Overpressure, B-17 (5715)	36	8000		X	8000		X	4000		X
Total Thermal Energy, B-17 (5715)	37	8000	X		8000	X				
Total Thermal Energy, F-47 (9785)	38							4000	X	
Normal Acceleration B-17 (5715)	39	8000	X							
Normal Acceleration, B-17 (5715)	49				8000	X		4000		X
Wing Bending B-17 (5715)	40	8000	X		8000	X		4000	X	
Total Thermal Energy, Site	41	8000	X		8000	X		4000	X	
Total Thermal Energy, Site	42	10500	X		10500	X		8000	X	
Overpressure, Site	43	10500	X		10500	X		8000	X	
Overpressure, Site	44	10500	X		10500		X			
Total Thermal Energy	45	10500	X		10500	X		8000	X	

*G - Good
B - Bad

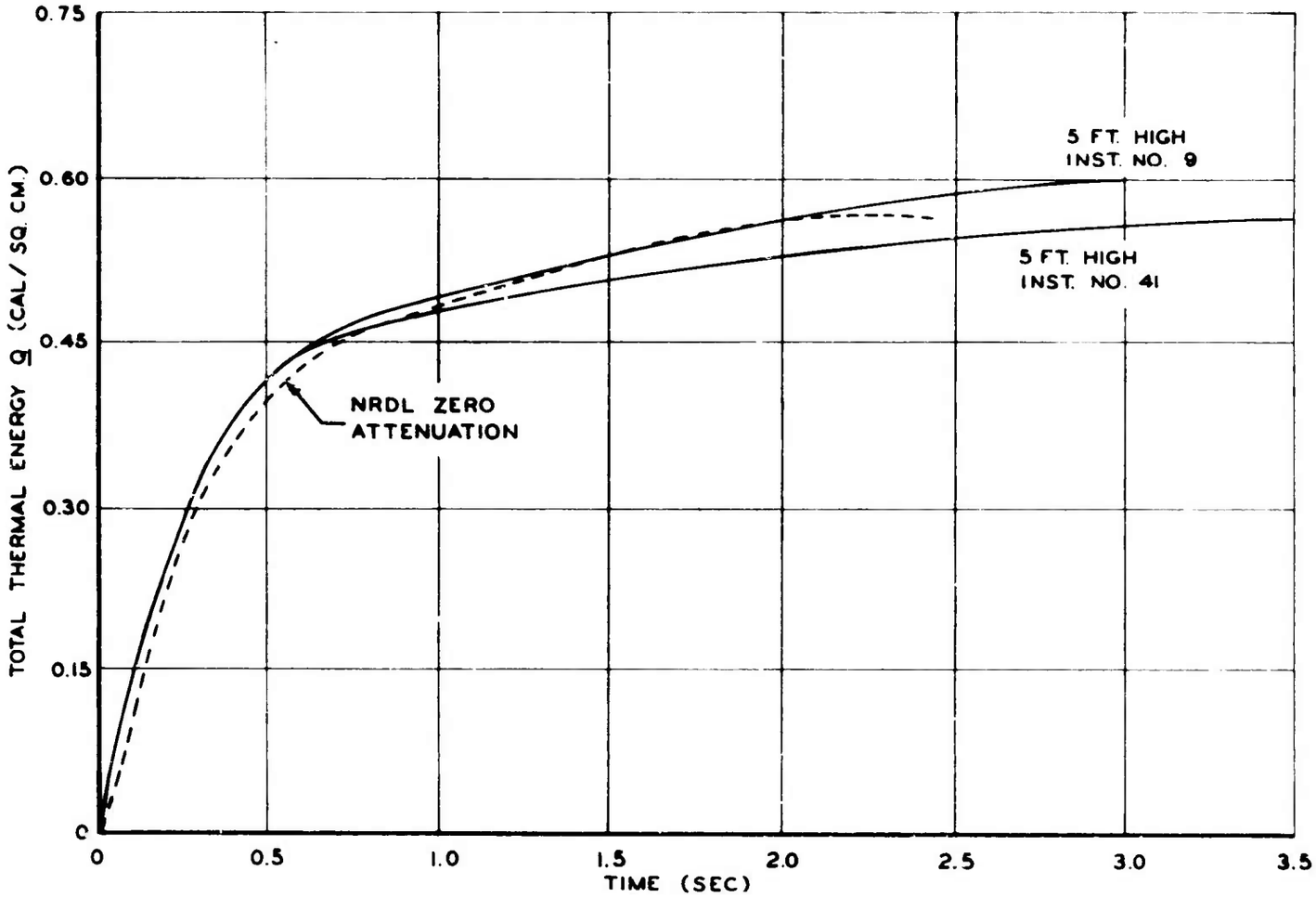

Fig. A.26 Comparison of the Variation of Corrected Total Thermal Energy With Time at Various Heights, Station 8000, Shot 2. Installations 9 and 41 Were 148 Ft Apart.

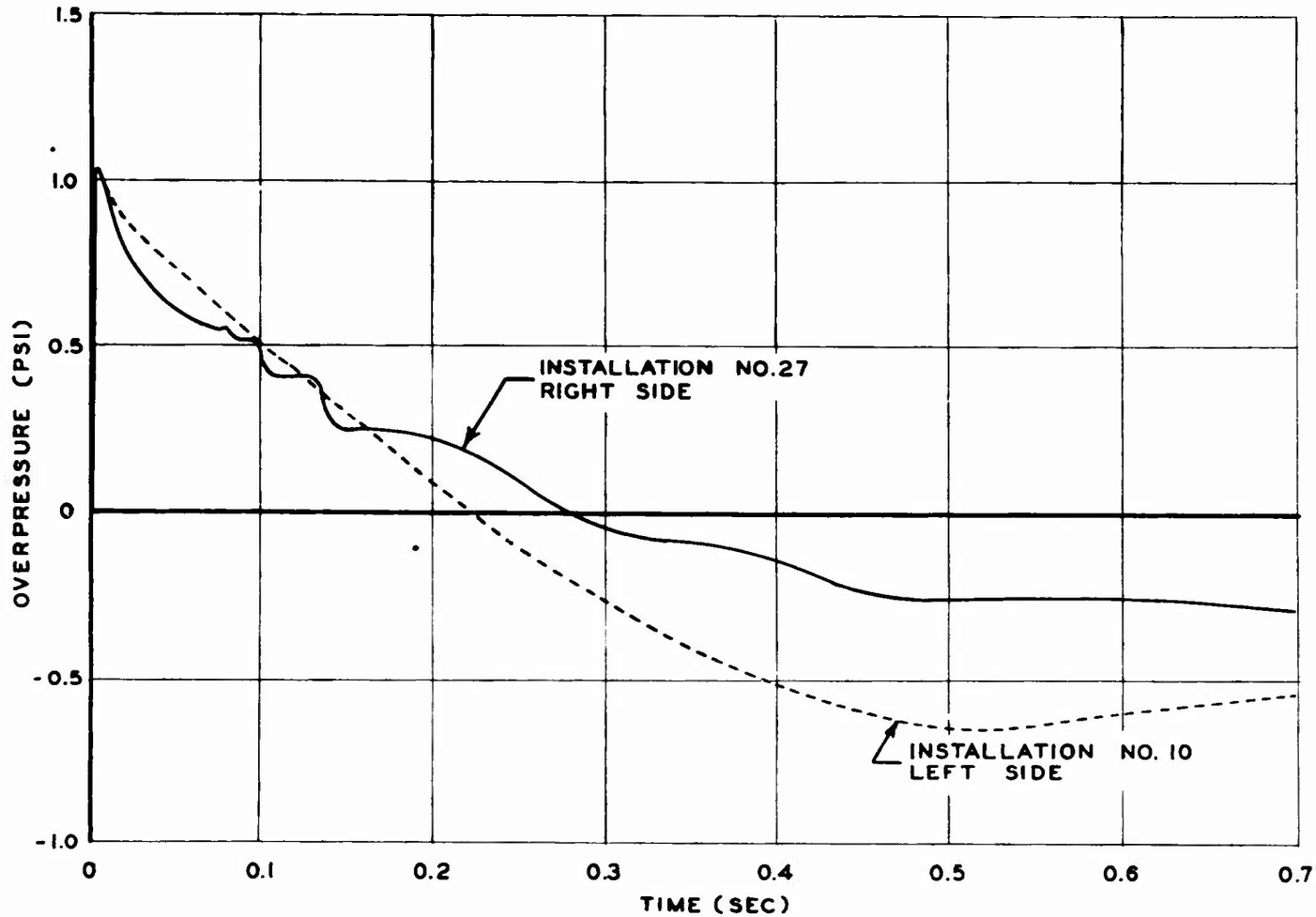

Fig. A.27 Comparison of the Variation of Overpressure With Time at Two Points on the Ground 148 Ft Apart, Station 8000, Shot 2

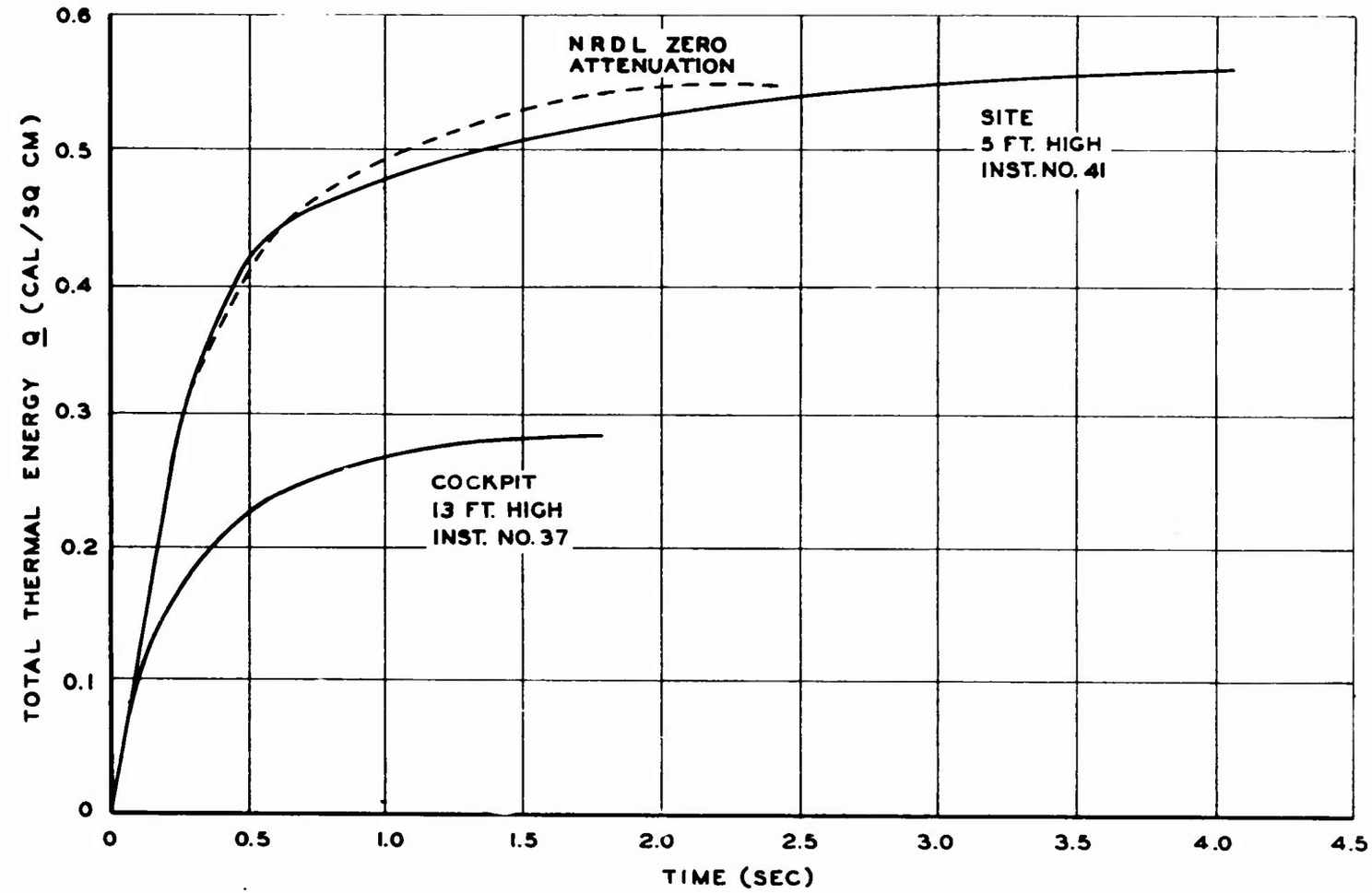

Fig. A.28 Comparison of the Variation of Corrected Total Thermal Energy With Time at Various Heights, Station 8000, Shot 2. One Measurement Was Made in the Cockpit of B-17 (5715).

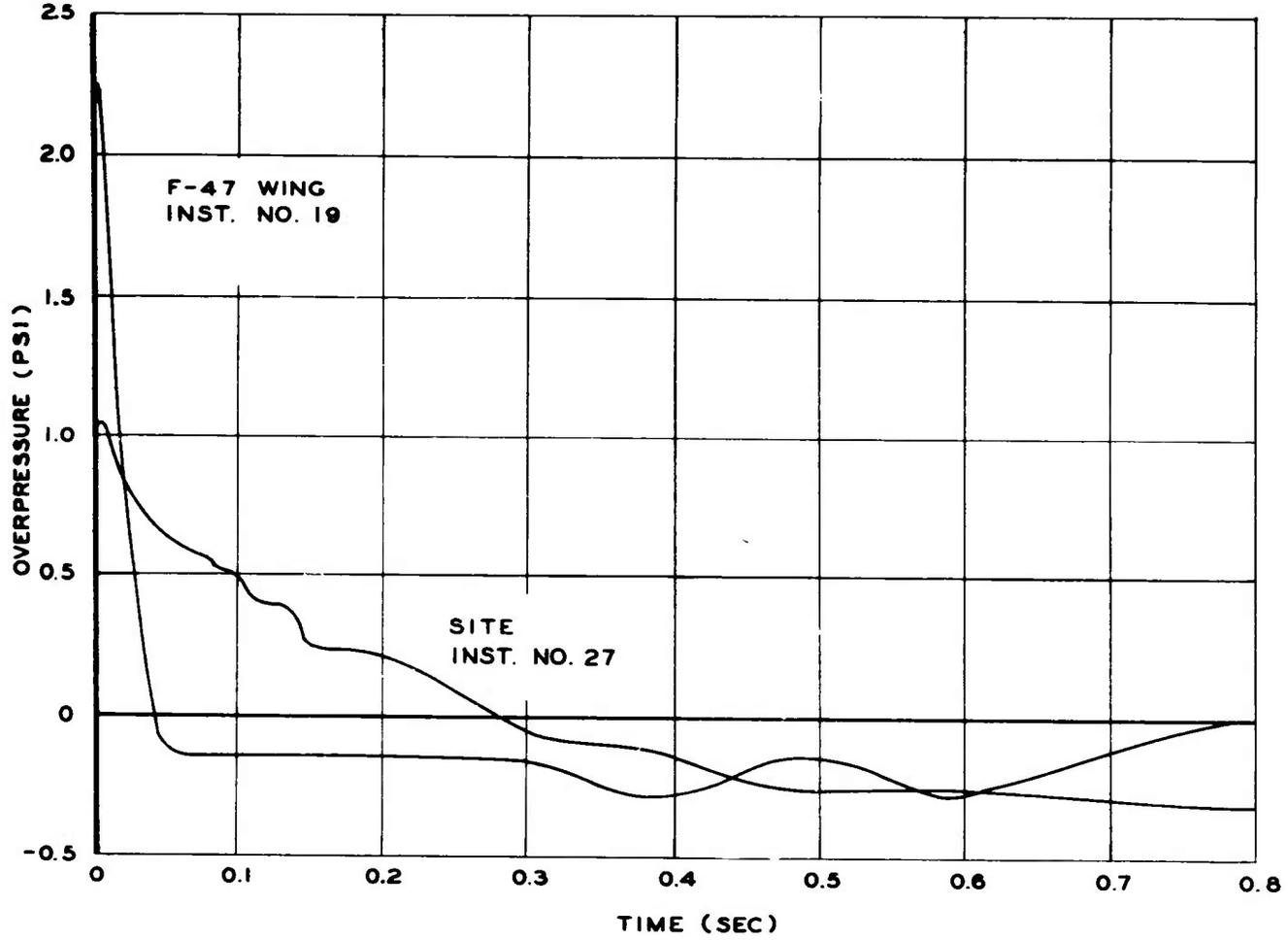

Fig. A.29 Comparison of the Variation of Overpressure With Time on the Wing of F-47 (0065) and a Point on the Ground, Station 8000, Shot 2

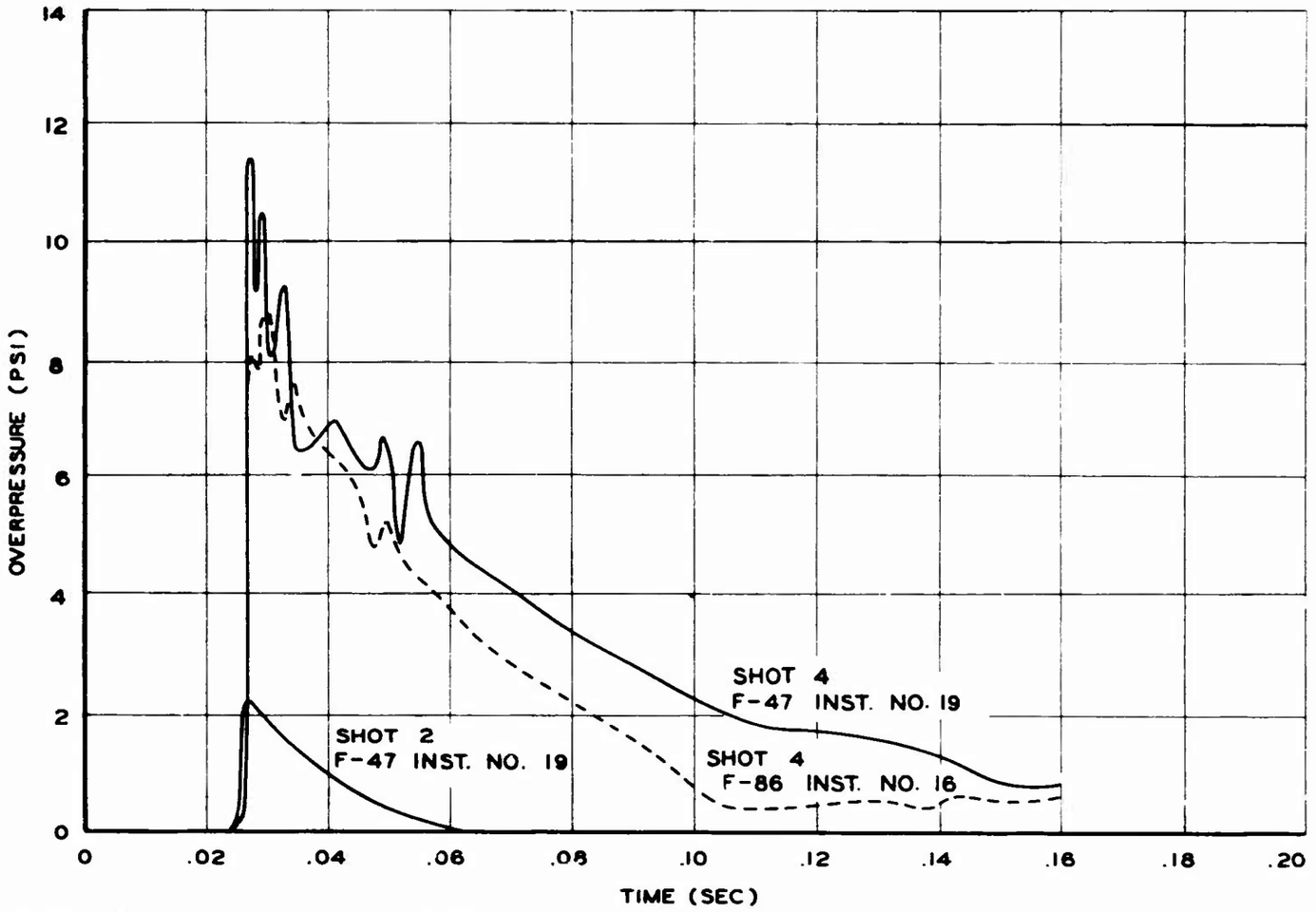

Fig. A.30 Comparison of the Variation of Overpressure With Time on Wings of F-47 (0065) and F-86 (9597). Shots 2 and 4 Were at Stations 8000 and 4000, Respectively.

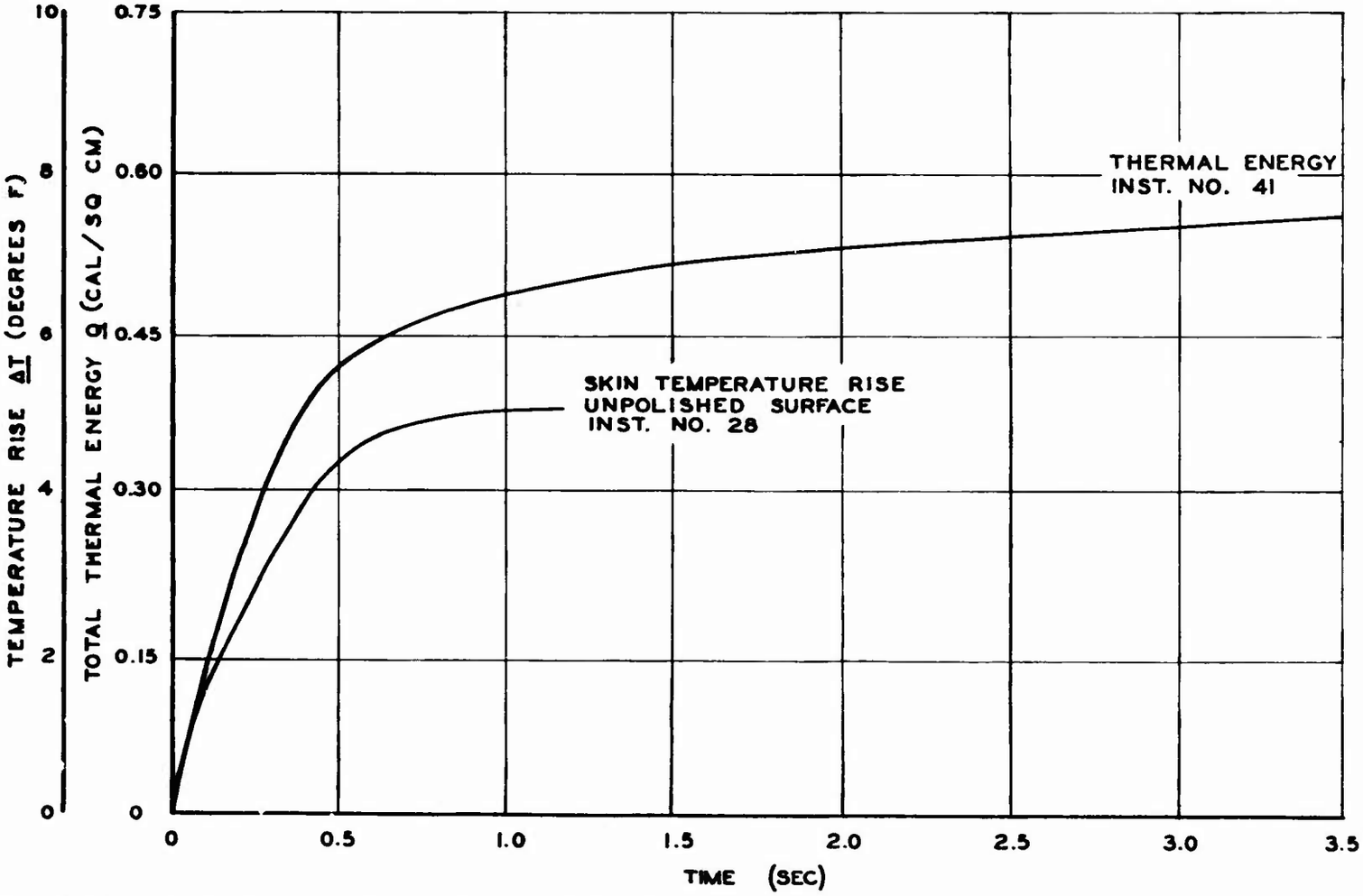

Fig. A.31 Comparison of the Variation of Total Thermal Energy 5 Ft Above Ground With B-17 (5715) Wing Temperature Rise, Angle of Incidence 57°, Station 8000, Shot 2. The Skin Temperature Just Before Time Zero Was 82°F.

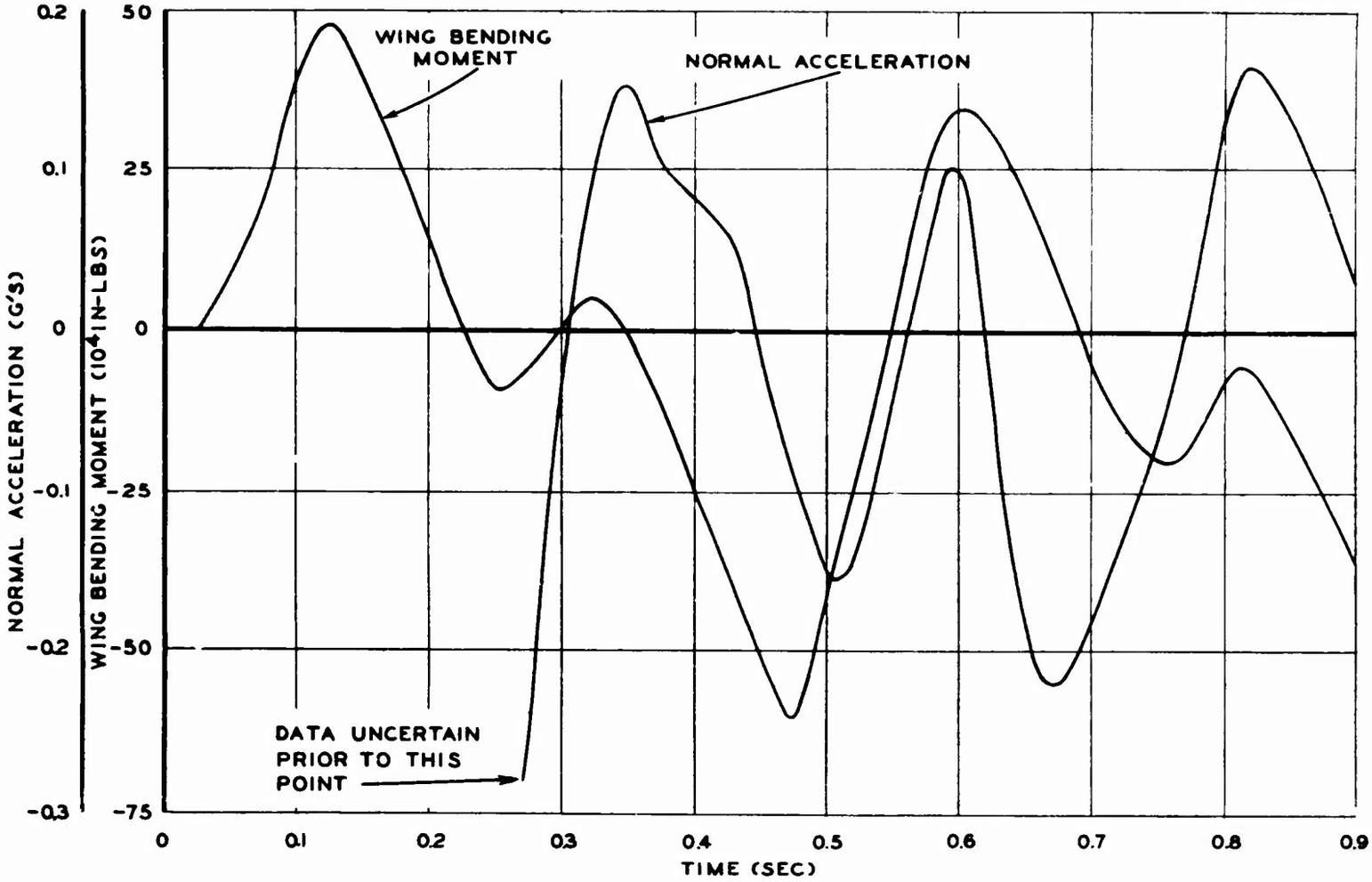

Fig. A.32 Comparison of the Variation of Normal Acceleration and Wing Bending Moment With Time, Station 8000, Shot 2, B-17 (5715)

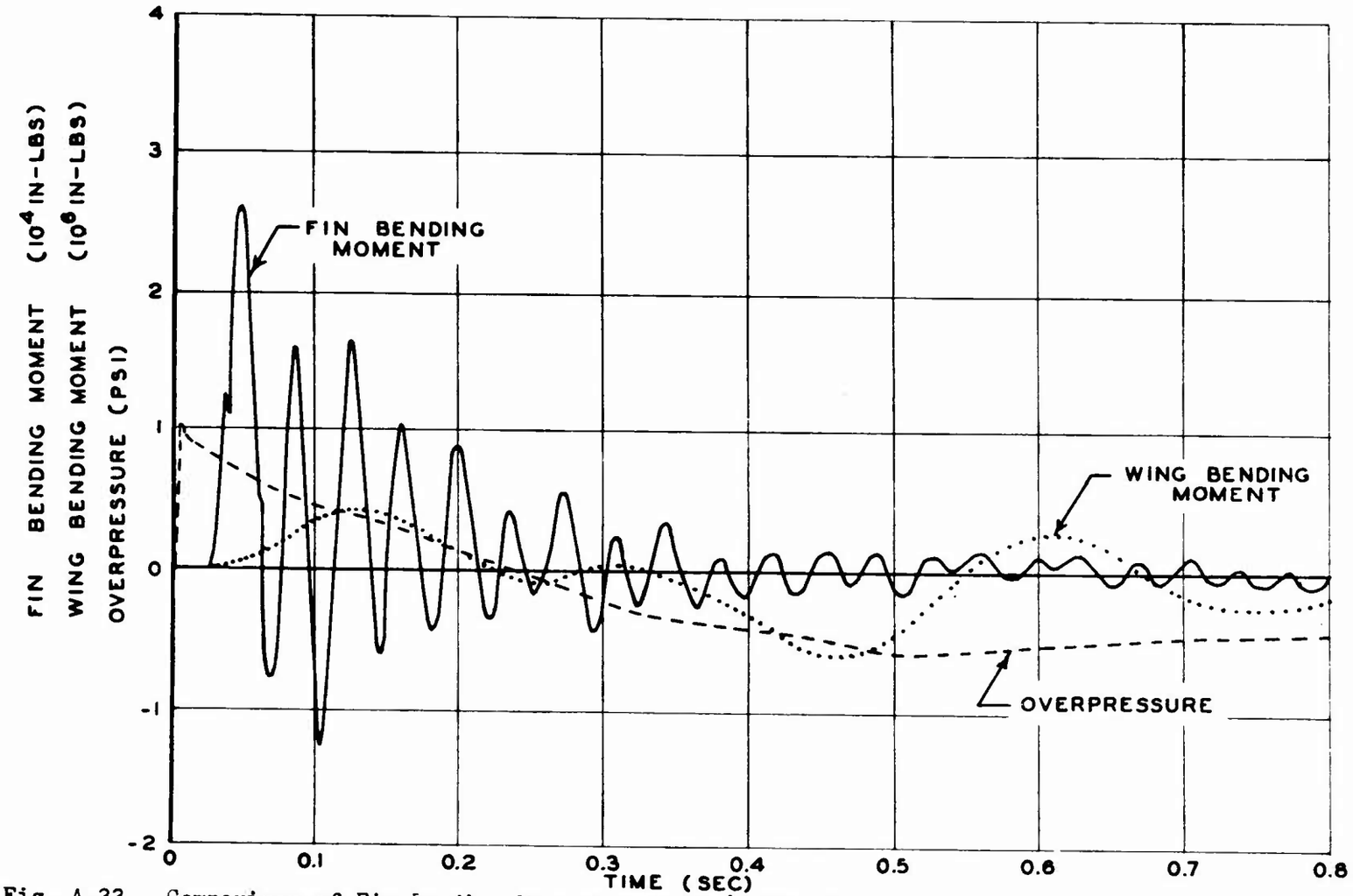

Fig. A.33 Comparison of Fin Bending Moment on F-47 (9785), Wing Bending Moment on B-17 (5715), and Overpressure at a Point on the Ground, Station 8000, Shot 2

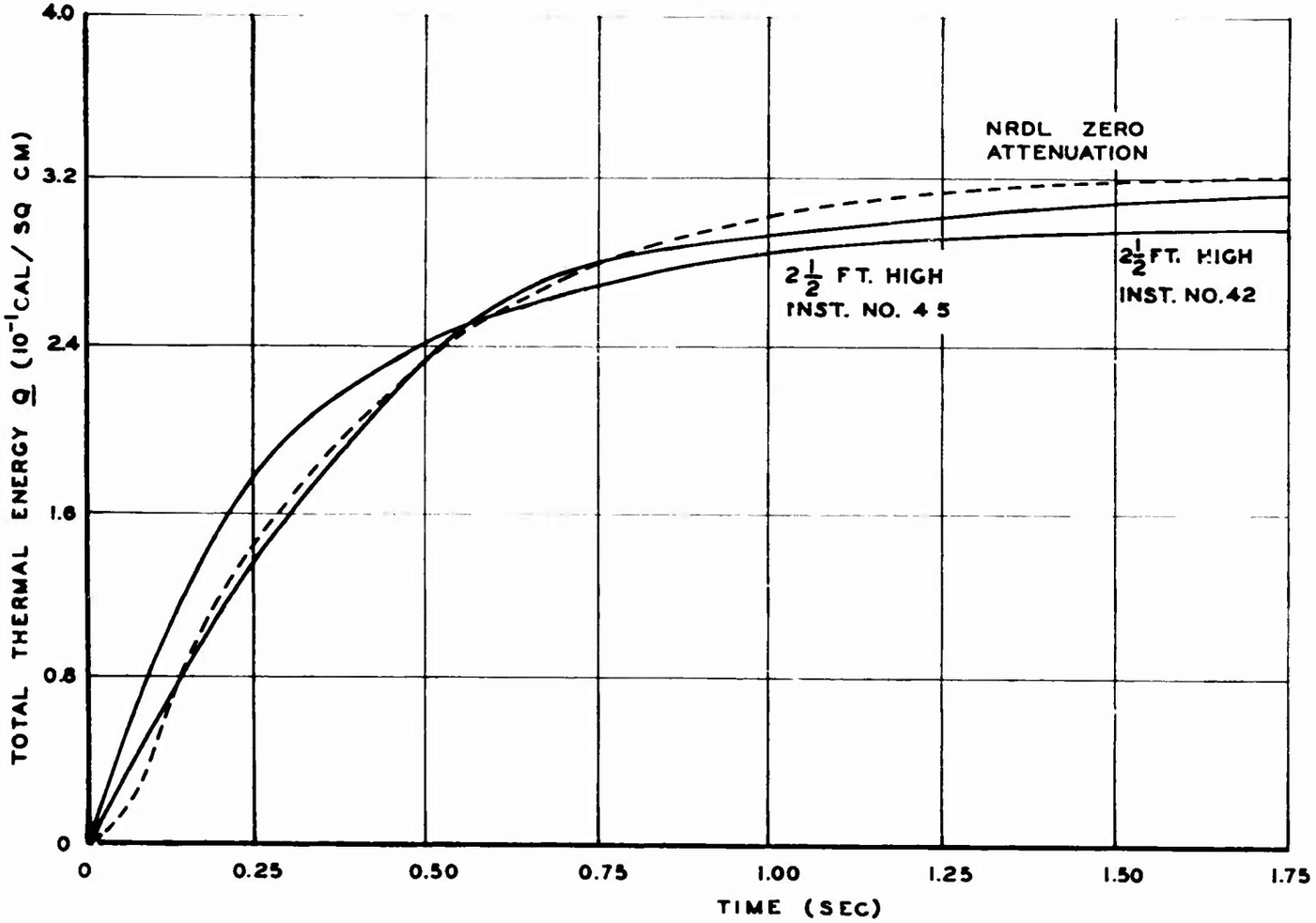

Fig. A.34 Comparison of the Variation of Corrected Total Thermal Energy With Time at Various Heights, Station 10,500, Shot 2

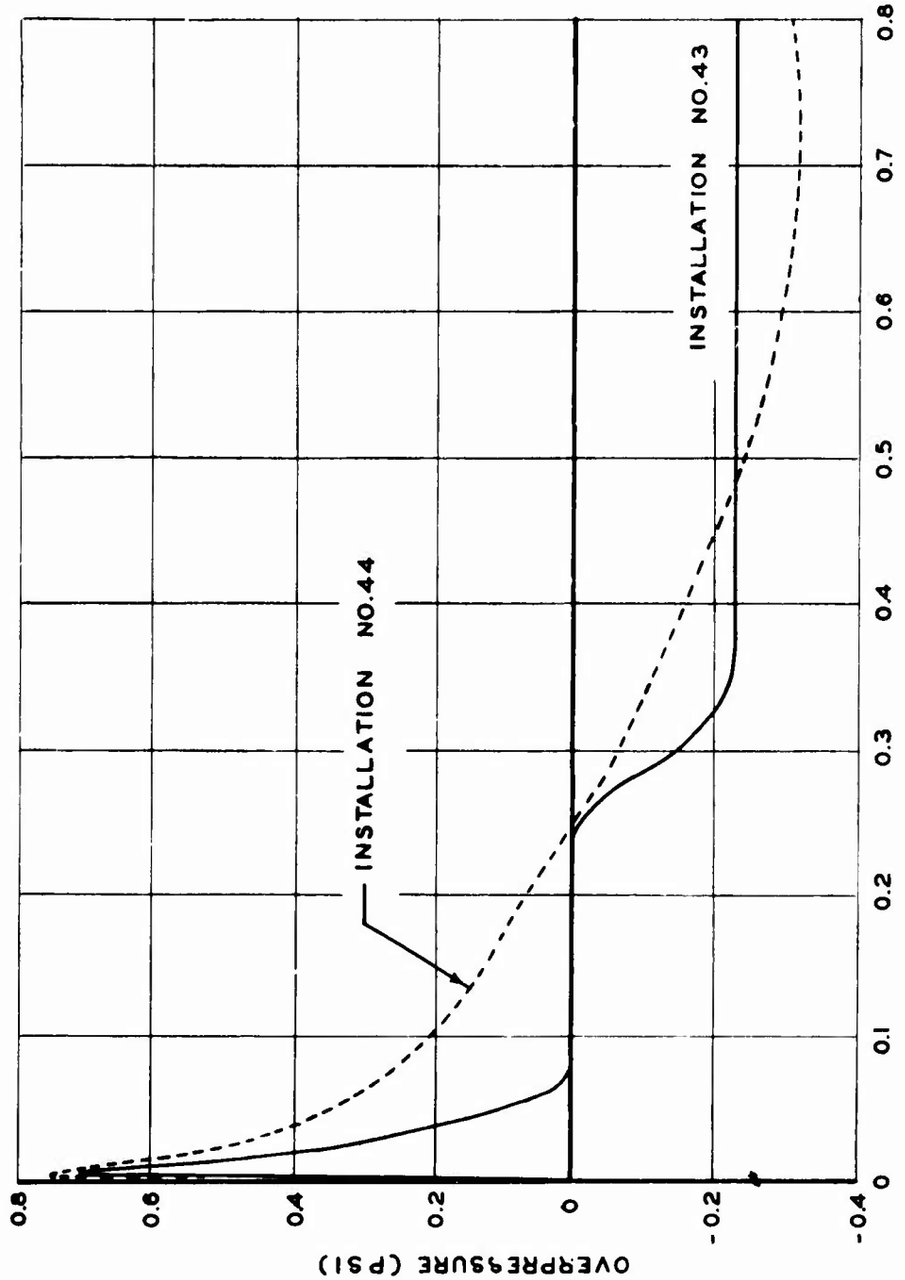

Fig. A.35 Comparison of the Variation of Overpressure With Time at a Point on the Ground, Station 10,500, Shot 2. The Two Installations Were Located 8 In. Apart.

[redacted]

above ground and 8 ft apart. Figure A.36 presents the data corrected for heat dissipation and the attenuation due to the quartz window, as previously explained in A.3.2.3. No irregular tendencies are noticeable in the two curves. The curve for installation 1 reached its peak of 29.5 cal/cm^2 in 3.2 sec, whereas the curve for installation 7 rose to a peak of 33 cal/cm^2 in 2 sec.

2. Neither of the overpressure installations yielded valid data, because the pressure transmitters were damaged by the thermal radiation.

3. One response function, the normal acceleration of F-47 (8785), was measured at Station 2200 by installation 8. This data is presented in Fig. A.37. The curve drops abruptly from zero to a minimum of -6.4 G's in 3 msec, then rises sharply to a maximum of +10.3 G's. An irregular, damped oscillation follows which ends at a relatively constant value of -1 G between 0.4 and 0.8 sec. Integration of the acceleration curve twice with respect to time in order to yield displacement showed a 30 in. vertical movement of the airplane.

A.3.3.2 Station 4000

No measurements were attempted.

A.3.3.3 Station 8000

The general input function measurements were as follows:

1. The installations used in measuring total thermal energy were identical to those used during Shot 2, as described in A.3.2.2. Peak values of 10.9 and 10.7 cal/cm^2 were recorded on the left and right sides, respectively. These two curves are presented in Fig. A.38 together with the data obtained by NRDL.

2. There were no valid overpressure measurements obtained at this station during Shot 3.

3. Two measurements of the angle of incidence of the air behind the blast front were made. The instruments used were described in A.2.2.1, and they were located at a height of 3½ ft above concrete slabs as shown in Fig. A.11. The curve for installation 11, Fig. A.39 indicates that the vane was at a 3.4° angle prior to the arrival to the shock front. A positive angle is attained when the nose of the vane is up. When the shock front arrived, the vane dropped toward zero, attaining a zero angle of incidence in 15 msec, and thereafter, the vane oscillated between 0° and plus 2° at an irregular frequency of approximately 17.5 cps. At approximately 1.9 sec the vane was driven to its maximum positive position during the negative pressure phase. There was no clear cut transition from the positive to the negative phase,

[redacted]

and thus it is not possible to determine accurately the positive phase duration from this measurement. The vane on the right side of the survey control point, installation 26, showed a zero angle before the shock front arrived. From zero to 0.6 sec, the oscillations of the vane were predominately negative, the vane oscillating between 0° and -3.4°. The end of the positive phase and the advent of the negative is quite evident as the vane was abruptly driven to a 13.6° angle at 1.4 sec.

The only specific input function obtained during this shot at Station 8000 was the measurement of total thermal energy in the B-17 cockpit. This measurement is plotted vs time and presented in Fig. A.40. A peak of 4 cal/cm^2 was measured after a rise time of 4 sec.

The response functions were measured as follows:

1. The temperature rise of the skin of the F-86 (9597) was measured by two types of thermocouple installations, namely the copper insert type and the standard type, both of which are described in Paragraph A.2.1.3. The installations were mounted on the unpolished surface of an F-86 wing. The location of the two installations is shown in Fig. A.18b. Installation 12, the copper insert type, was at a temperature of 102°F at shot time. The angle of incidence of the skin surface at the thermocouple location was 70°, and the thickness of the skin at that point was 0.081 in. A temperature rise of 50°F with a rise time of 0.4 sec was recorded and is graphically presented in Fig. A.41. Installation 24, the standard type, was at a temperature of 107°F at shot time. The angle of incidence at this installation was 69°, and the thickness of the skin at that point was 0.081 in. A peak temperature rise of 21°F with a rise time of 6 sec was recorded and is presented graphically in Fig. A.41.

2. Temperature rise was measured on the skin of the wing of F-47 (0065) by installations 22 and 23 and on a stringer inside the wing of the F-47 (0065) by installation 21. The location of the three installations on the gun-bay door of the left wing of this aircraft is shown in Fig. A.17c. The condition of the surface was that of a normal unpolished wing of an F-47. Installations 22 and 23 were at a temperature of 132°F at shot time. The angle of incidence at the thermocouple installations was 75° and the skin thickness was 0.040 in. Figure A.42 shows a curve of skin temperature rise as a function of time for installations 22 and 23. It took 6 sec for these curves to rise to a peak value of 49°F. Installation 23 was located ¼ in. inboard of installation 22 as shown in Fig. A.17c. Installation 21, the stringer temperature installation, was located on the forward edge of the left wing gun-bay door on F-47 (0065). The temperature of the stringer at shot time was 122°F. A curve of stringer temperature rise as a function of time is shown in Fig. A.43. The curve reaches a peak of 15°F, 20 sec after the detonation of the bomb, and remains at this peak for

[redacted]

at least 12 sec. The shock wave arrived at F-47 (0065), on Shot 3, 6.07 sec after detonation of the bomb which is the approximate time of the unevenness of the curve.

3. Two skin temperature measurements were made on B-17 (5715). The surface of installation 25 was polished and was located on the right wing of B-17 (5715). The angle of incidence of the installation was 42°, the temperature at shot time was 104°F, and the skin was 0.040 in. thick at installation 25. A peak of 47°F was reached 6.5 sec after detonation of the bomb. A graph of temperature rise as a function of time is presented in Fig. A.44. This graph shows a spike on the curve at time 5.9 sec which is 5°F in magnitude and about 0.1 sec in duration. This spike occurred at the time the shock wave reached the aircraft. Installation 28 was located on an unpolished surface of the left wing of B-17 (5715). The angle of the incidence 42°, and the temperature at shot time was 127°F, and the skin was 0.040 in. thick at installation 28. The curve of temperature rise as a function of time is shown in Fig. A.44. A peak of 145°F was reached 5.8 sec after detonation. This curve shows a spike at time 5.9 sec which is 15°F in magnitude and 0.10 sec in duration. This spike occurred at the time the shock wave arrived at the airplane.

4. Lateral acceleration, installation 48, was measured on F-47 (9785) at Station 8000. The location of the accelerometer on the airplane is shown in Fig. A.15b. A graphical presentation of the lateral acceleration of F-47 (9785) as a function of time is shown in Fig. A.45. A peak acceleration of 13.5 "G's" was reached at 33 msec, and the approximate frequency of the oscillations was 76 cps. The positive direction of acceleration as shown by the graph indicates a lateral acceleration in the direction of movement of the air mass from the blast of the bomb. The airplane was tied down with a rope from each wing and one from the tail. Integration of the acceleration curve twice with respect to time, in order to yield displacement, showed the maximum lateral movement of the airplane was 21 in.

5. Normal acceleration of B-17 (5715), installation 49, was measured at Station 8000 on Shot 3. The location of the accelerometer in the airplane is shown in Fig. A.13a. Figure A.46 is a graphical presentation of the data obtained. The curve presented is a faired one, that is, the relatively high frequency oscillations have been removed. It starts abruptly at 0.11 sec because the high frequency oscillations were unreadable before this time. The peak acceleration was probably reached during the time interval not presented; consequently, no peak value is reported. The frequency of the airplane, computed from the acceleration curve is 3.5 cps. Positive acceleration on the graph indicates an upward movement of the airplane.

6. Maximum positive and negative bending movements equivalent to 375,000 and 155,000 in-lb, respectively, were obtained from the F-47

[redacted]

(0065), wing bending measurement as presented in Fig. A.47, the positive peak being equivalent to 10.7 per cent of the ultimate bending moment. Another point of interest is the build-up of the positive bending moment beginning at 0.44 sec. This vibration is discussed more completely in A.4.5.

7. The curve showing B-17 wing bending moment vs time is presented in Fig. A.48 and Fig. A.49. The expanded curve is of interest as it resembles the stress-strain curve for steel quite closely. This indicates the structural yield due to rivet slippage and the maximum bending moment of 2,550,000 in-lb at 0.15 sec. The curve plotted on the compressed time scale shows the first mode frequency of 3.9 cps. It is interesting to note that the trace of the mid-points of the oscillations is very similar to the positive phase of the site overpressure curve.

8. Figure A.50 presents the F-47 (9785) fin bending moment measurement. A maximum bending moment of at least 110,000 in-lb was measured before the oscillograph trace left the record. This load is equivalent to 201 per cent of the ultimate root bending moment which is 54,700 in-lb. This ultimate value was exceeded on the two succeeding oscillations as well. The time required for the rise to the first peak was 8 msec, which is an indication of the short time period during which the load was applied and relieved. Although the fin did not break, there was failure in the sense that permanent set in the fin occurred, and replacement of the structure would be required. This was evident during inspection of the aircraft after the shot and is upheld by the curve not returning to zero (Fig. A.51). This permanent set is equivalent to the amount of strain caused by a load of 9400 in-lb, which is 17 per cent of the ultimate bending moment. On the rise to the first peak there was a slight yield probably due to rivet slippage which occurred at a load of 85,000 in-lb. Although this is greater than the ultimate moment, structural yield probably did not occur because of the extremely short time of load application. A uniform frequency of 22.6 cps was attained until 0.22 sec, at which time the vibration broke down to a non-uniform, small amplitude oscillation. This was probably the point where the structure yielded and where a decrease in vertical stabilizer area occurred when the bottom rudder hinge broke loose from the fuselage, allowing the rudder to deflect.

A.3.3.4 Station 10,500

The general input function measurements were as follows:

1. Total thermal energy at this station was obtained by two similar installations, namely 42 and 45, and the instruments were located as described in A.3.2.4. The data, corrected for dissipation and quartz window attenuation, are presented in Fig. A.52. The curves for

[redacted]

the two installations are practically identical. Maximum values of 6 cal/cm^2 were reached in 3 to 4 sec.

2. The overpressure measurement at Station 10,500 was obtained by installation 43, and the data are presented in Fig. A.53. The peak pressure was 3.1 psi with a rise time of 3 msec. The positive pressure phase ended at 0.74 sec.

A.3.4 Presentation of Shot 4 Data

A.3.4.1 Station 2200

The general input function measurements were as follows:

1. Total thermal energy at this station was measured using an installation which was similar to that described in A.3.3.1. The data obtained, corrected for heat dissipation and quartz window attenuation (see A.3.2.3), are presented in Fig. A.54. A maximum of 39.4 cal/cm^2 was reached at 1 sec.

2. The two overpressure installations did not yield any measurable data.

The response function measurements were as follows:

1. Installation 8 measured the normal acceleration of F-47 (8785) and this measurement plotted vs time is shown in Fig. A.37. A maximum of 11.5 G's was reached at 0.142 sec followed by a sharp drop to -2.6 G's at 0.153 sec. A second positive peak of 8.4 G's was reached at 0.227 sec. The acceleration curve was integrated twice with respect to time to obtain the vertical displacement of the airplane. This integration showed that the airplane was 33 in. off of the ground when the instrumentation cable broke.

2. The temperature rise of a propeller cuff of F-47 (8785) was measured by installation 2. The curve is shown in Fig. A.54. The actual peak temperature rise of the propeller cuff was not recorded because the cuff was destroyed by blast. However, a maximum temperature rise of 800°F was recorded at 1.04 sec before the blast hit the aircraft. Figure A.54 shows that the temperature was still rising sharply when the cut-off occurred.

A.3.4.2 Station 4000

The general input function measurements were as follows:

[redacted]

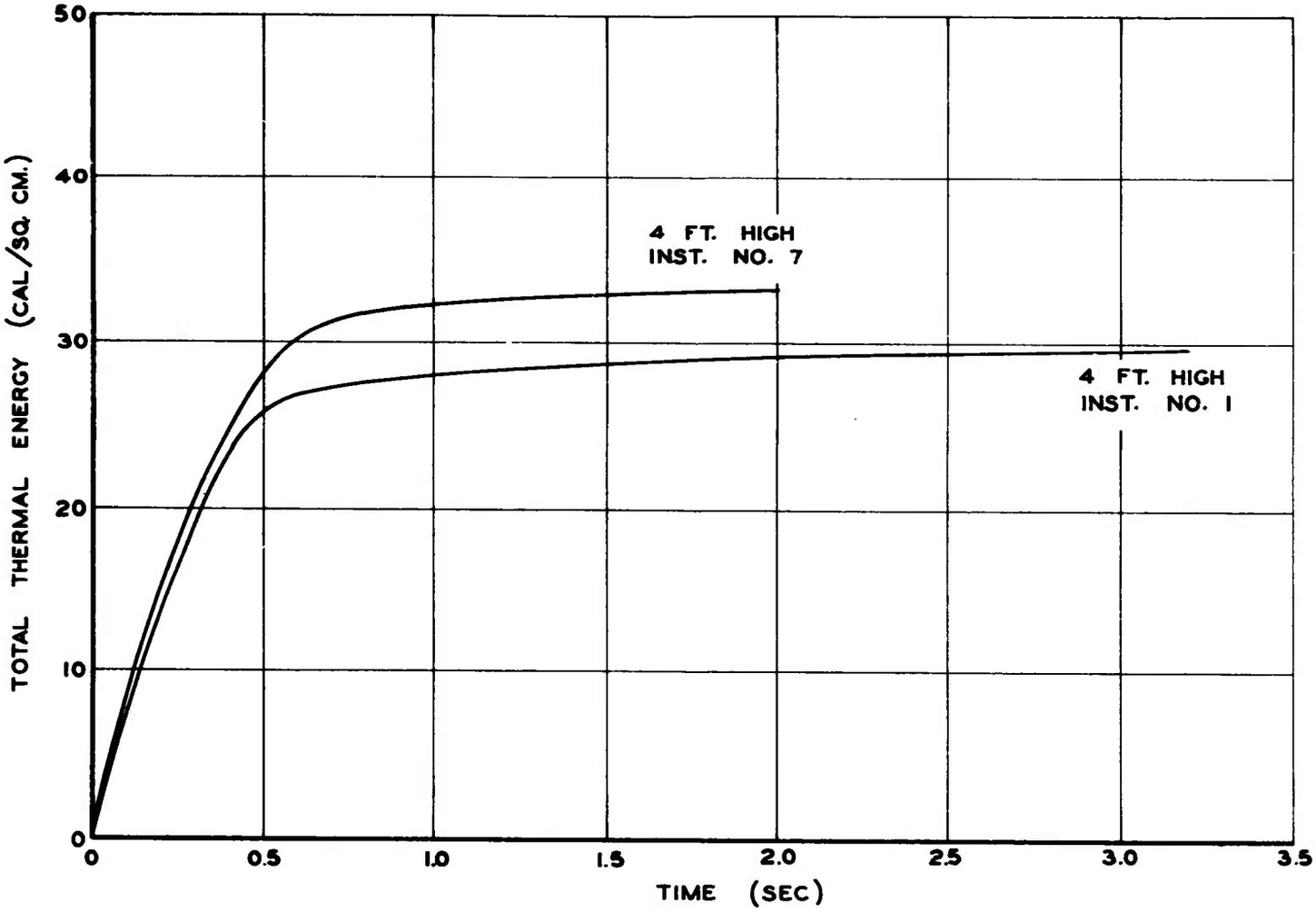

Fig. A.36 Comparison of the Variation of Corrected Total Thermal Energy With Time at Various Heights, Station 2200, Shot 3. Installations 1 and 7 Were 8 Ft Apart.

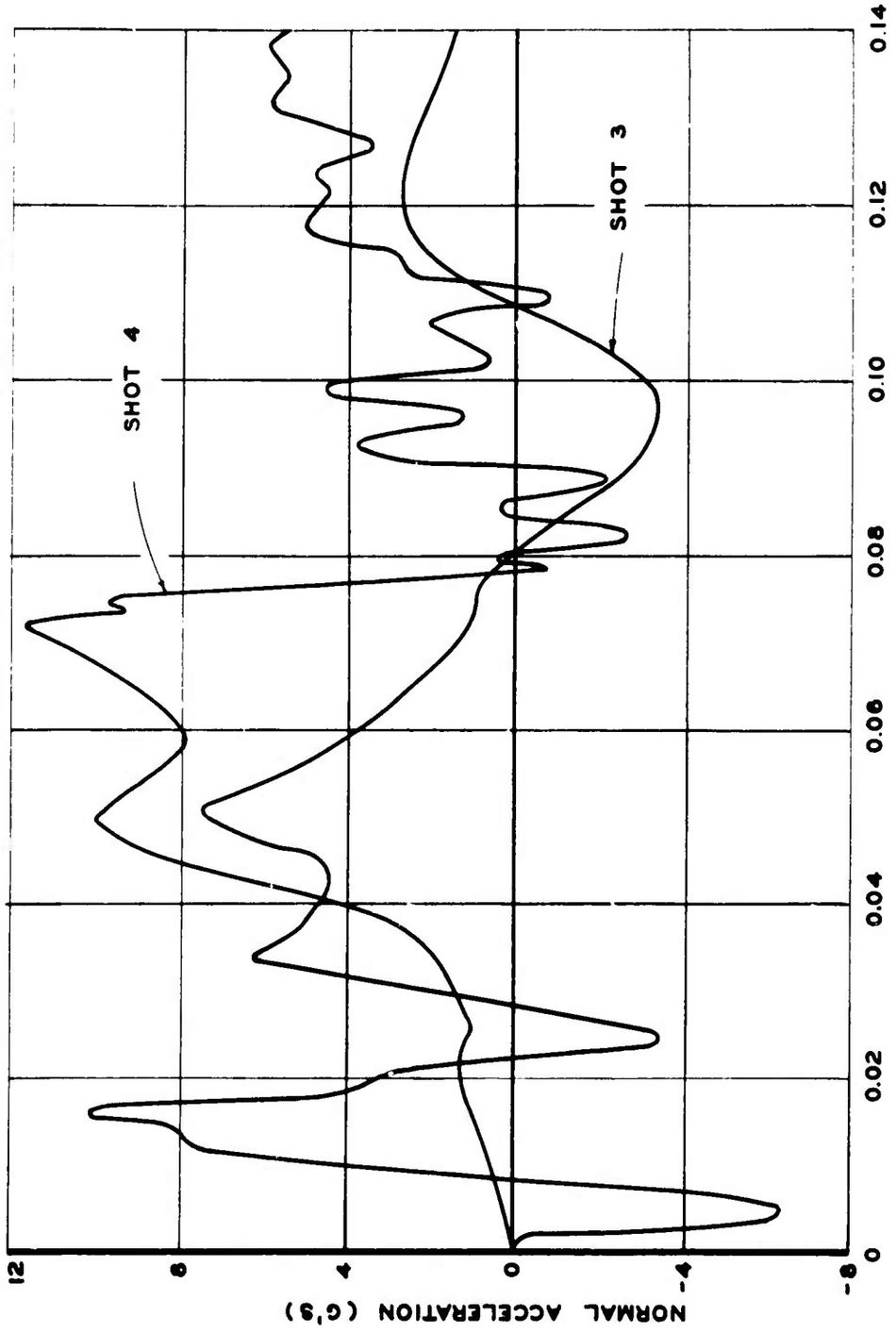

Fig. A.37 Comparison of the Variation of Normal Acceleration With Time on F-47 (8785) During Shots 3 and 4, Station 2200

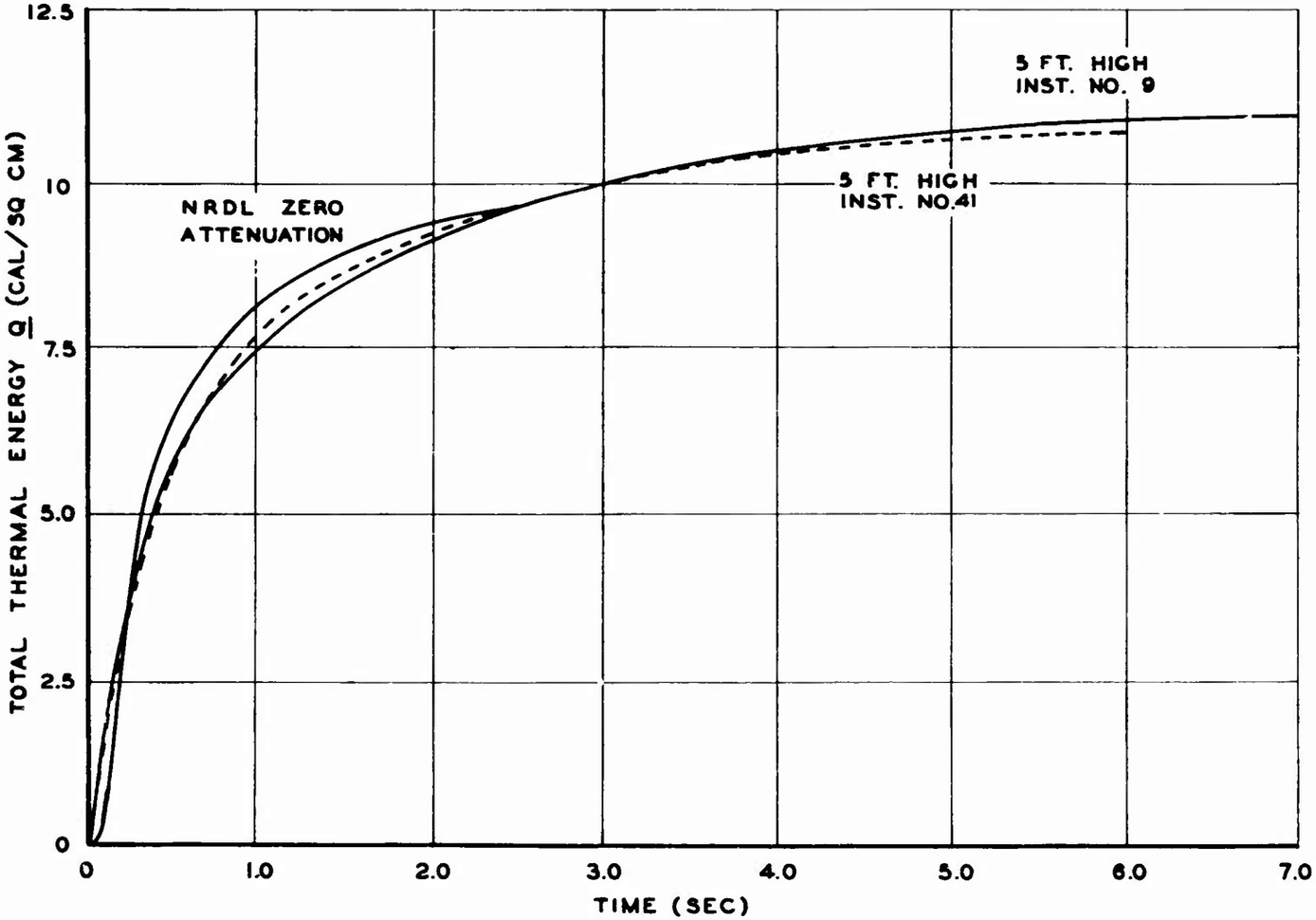

Fig. A.38 Comparison of the Variation of Corrected Total Thermal Energy With Time at Various Heights, Station 8000, Shot 3. Installations 9 and 41 Were 148 Ft Apart.

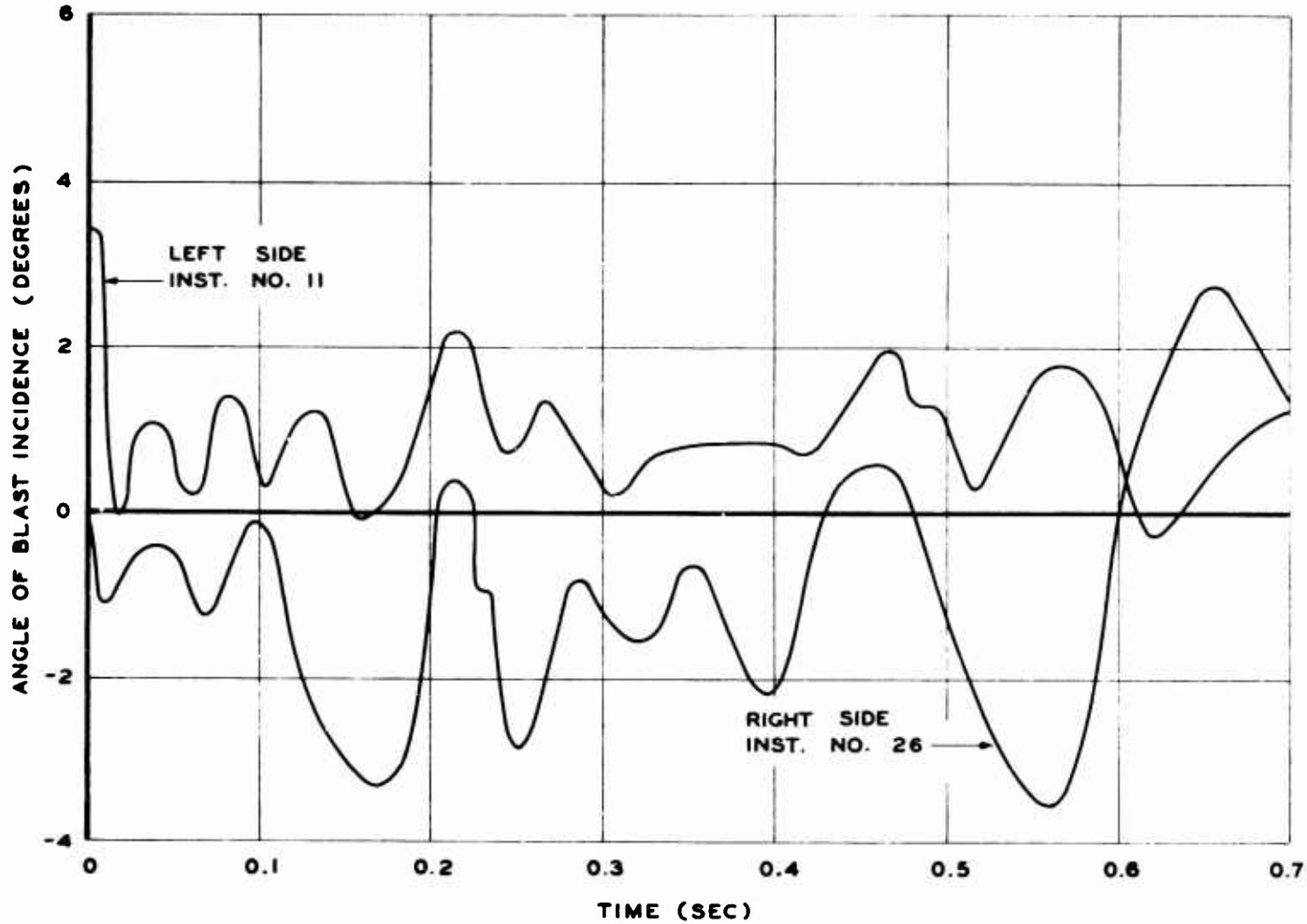

Fig. A.39 Comparison of the Variation of Angle-of-blast Incidence With Time, 3½ Ft Above Ground, Station 8000, Shot 3. The Two Installations Were Located 148 Ft Apart.

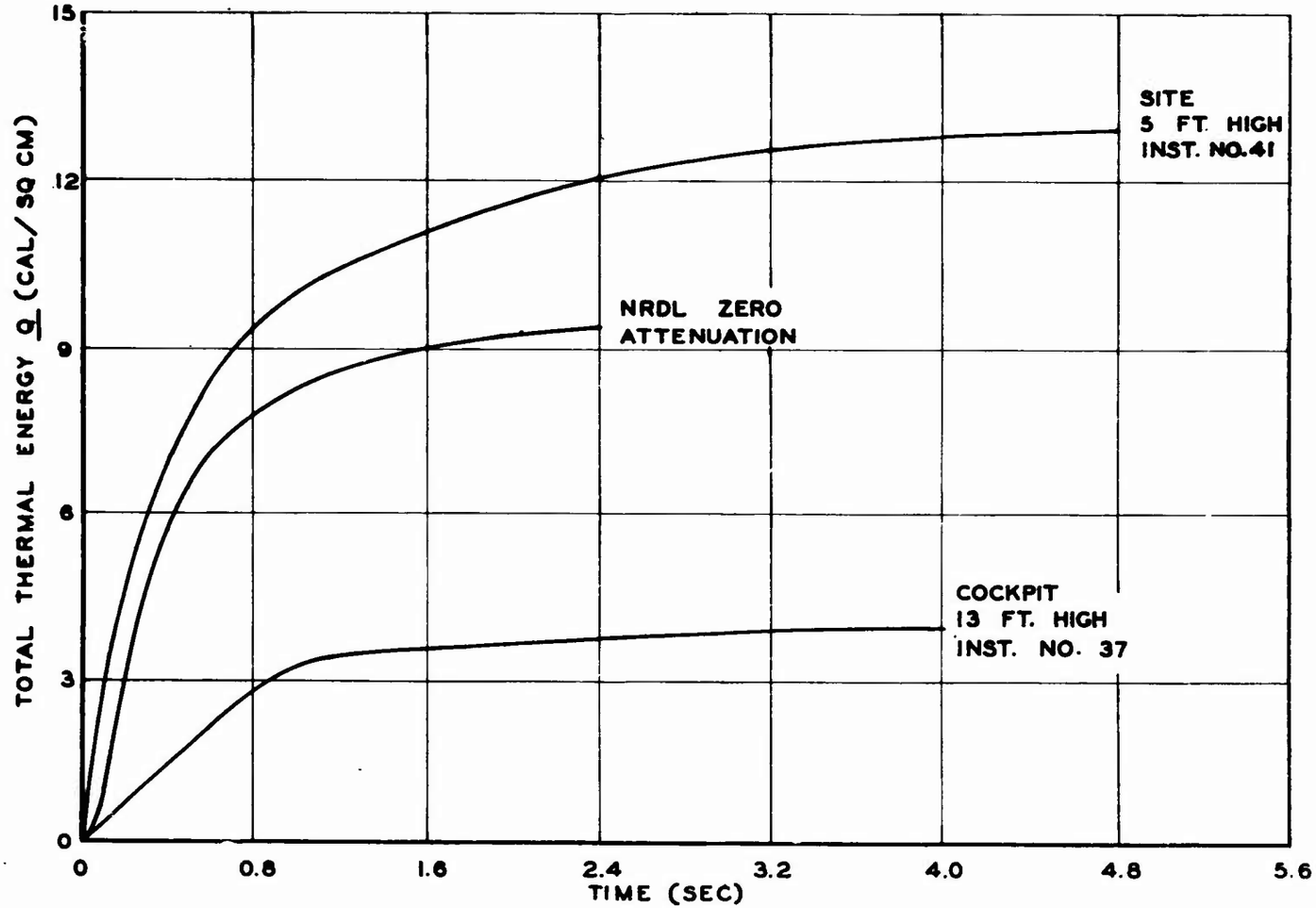

Fig. A.40 Comparison of the Variation of Corrected Total Thermal Energy With Time at Various Heights, Station 8000, Shot 3. One Measurement Was Made in the Cockpit of B-17 (5715).

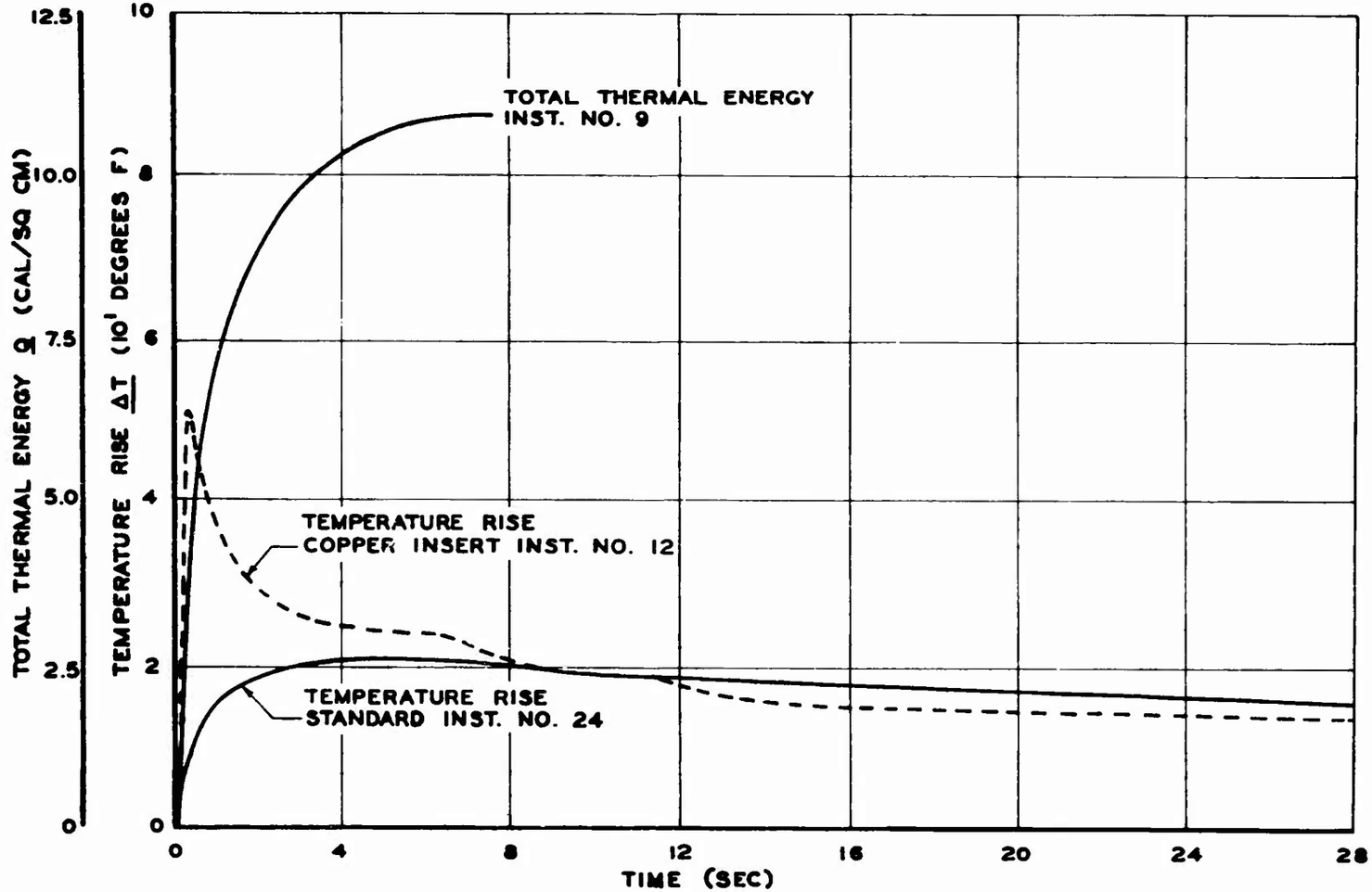

Fig. A.41 Comparison of the Total Thermal Energy 5 Ft Above Ground With F-86 (9597) Wing Temperature Rise, Angle of Incidence 70°, Station 8000, Shot 3. The Skin Temperature Just Before Time Zero Was 105°F.

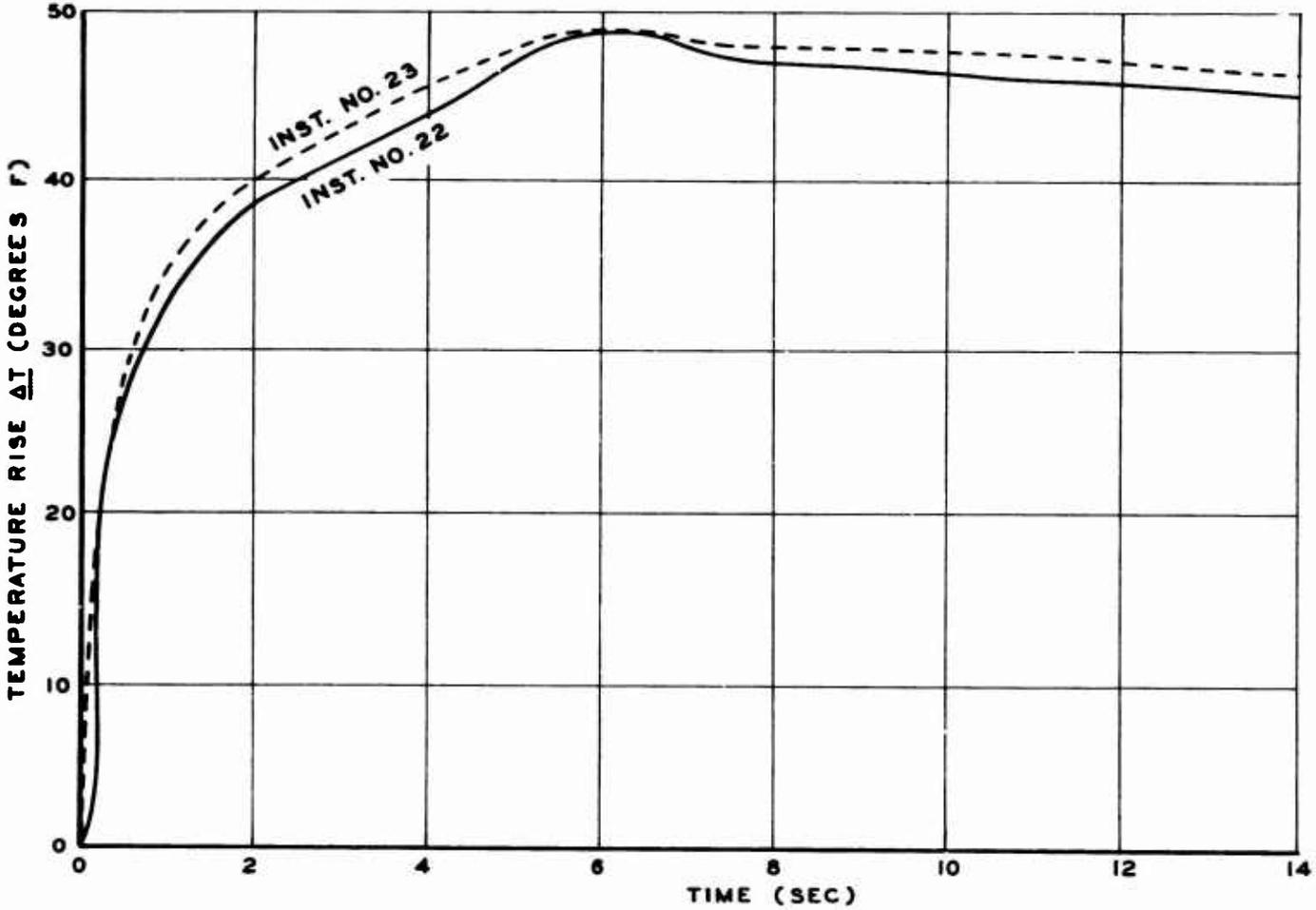

Fig. A.42 Comparison of the Variation of Temperature Rise With Time on Wing of F-47 (0065), Angle of Incidence 75°, Station 8000, Shot 3. The Skin Temperature of Both Installations Was 132°F Just Before Time Zero.

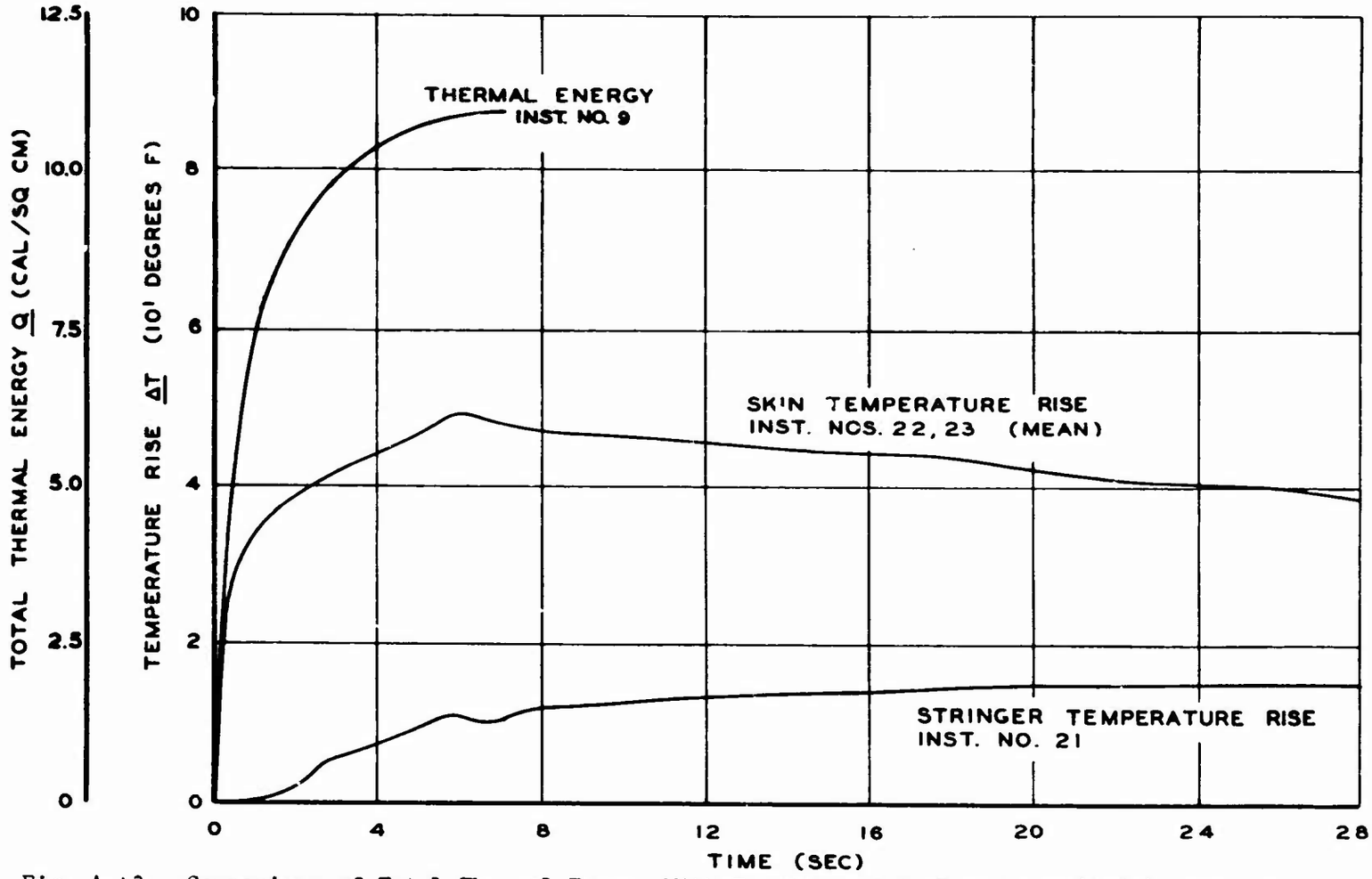

Fig. A.43 Comparison of Total Thermal Energy With Temperature Rise of F-47 (0065) Wing, Angle of Incidence 75°, Station 8000, Shot 3. The Temperatures of the Stringer and Skin Just Before Time Zero Were 122°F and 132°F, Respectively.

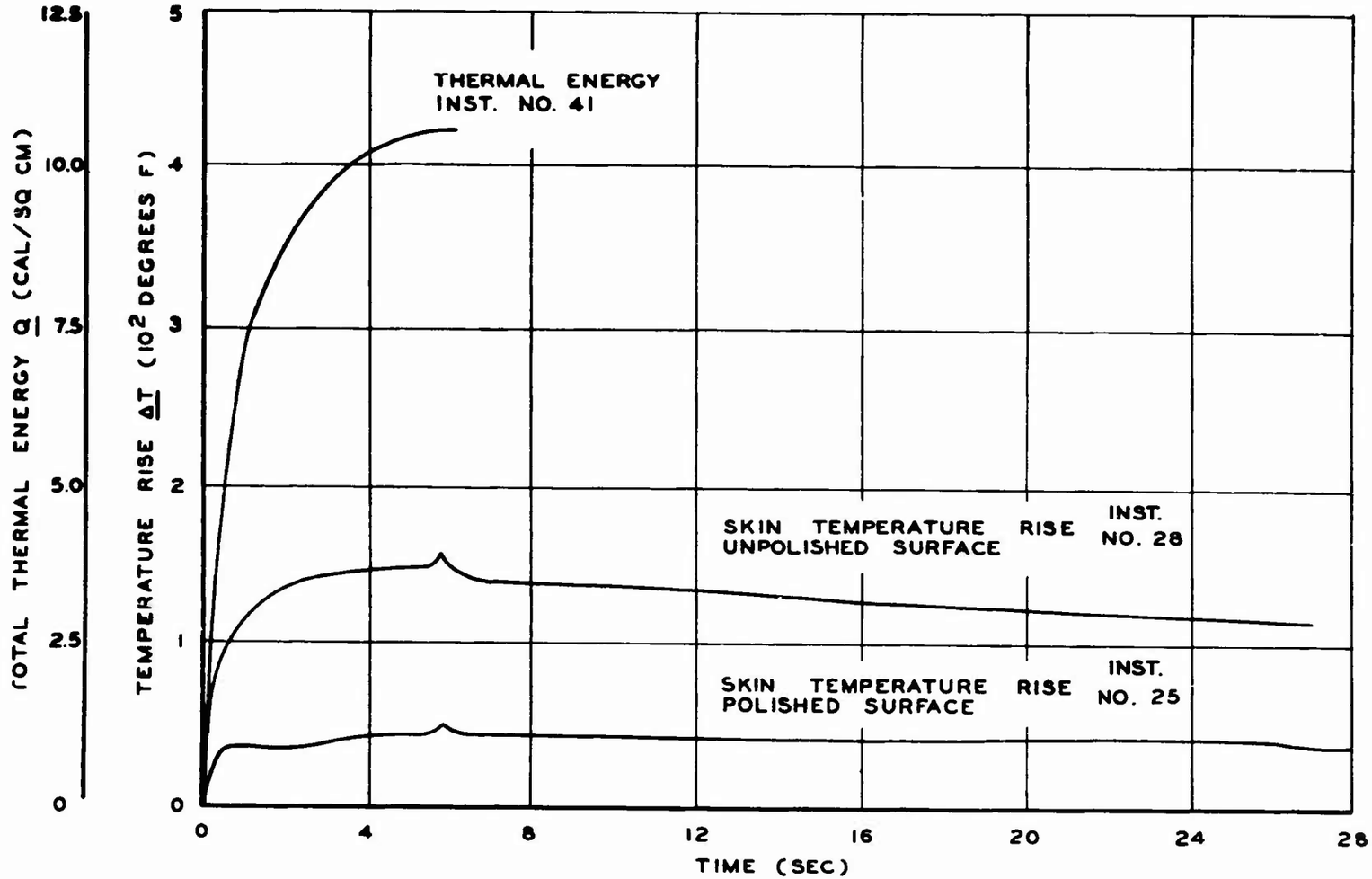

Fig. A.44 Comparison of the Total Thermal Energy 5 Ft Above Ground, and Temperature Rise on Wing of B-17 (5715), Angle of Incidence 42°, Temperature Just Before Time Zero of Polished Surface 104°F, Unpolished Surface 127°F, Station 8000, Shot 3

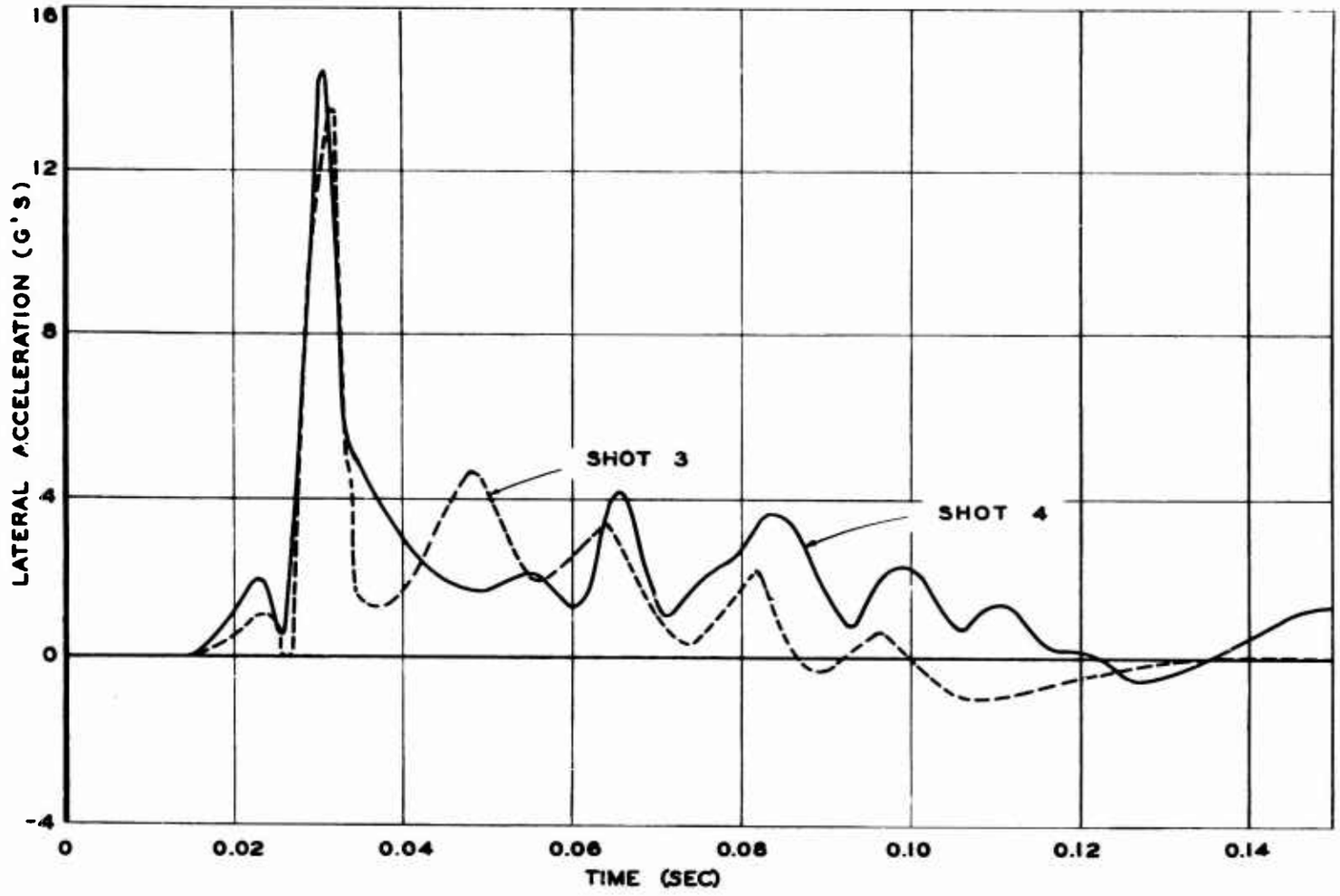

Fig. A.45 Comparison of the Variation of Lateral Acceleration With Time on F-47 (9785), Station 8000, Shot 3, and Station 4000, Shot 4

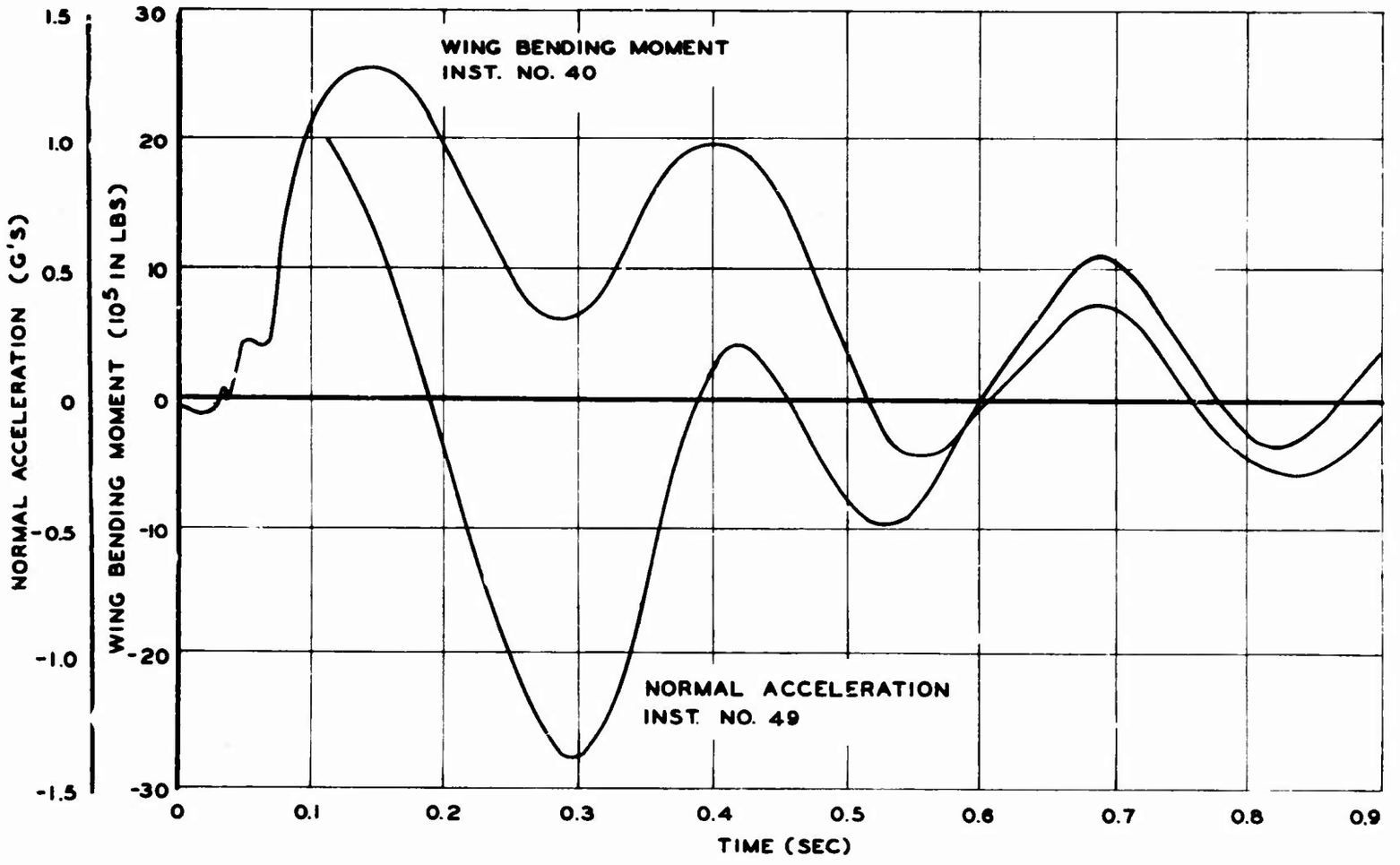

Fig. A.46 Comparison of the Variation of Wing Bending Moment and Normal Acceleration With Time on B-17 (5715), Station 8000, Shot 3

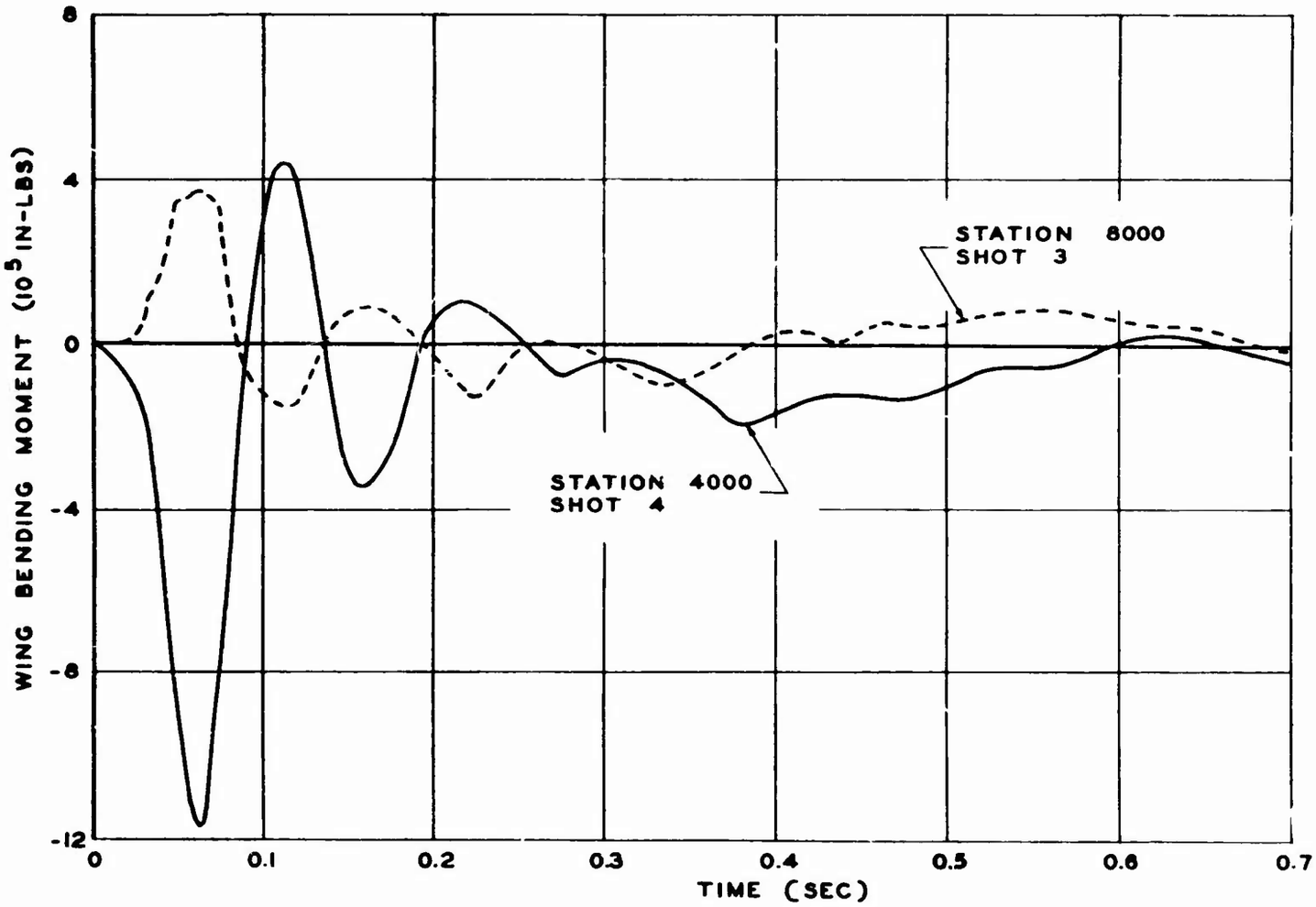

Fig. A.47 Comparison of the Variation of Wing Bending Moment With Time on F-47 (0065) at Different Stations and Shots

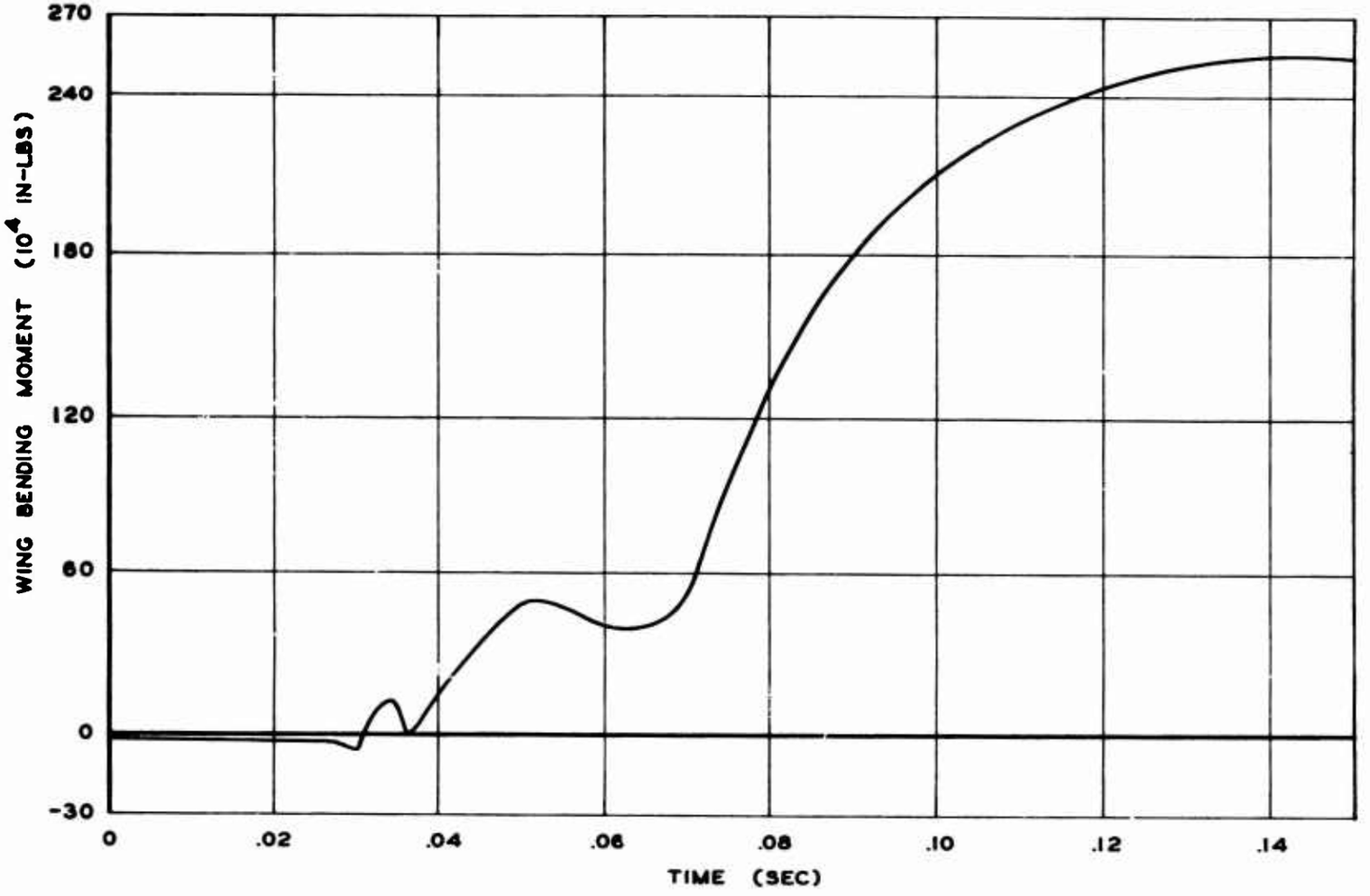

Fig. A.48 Variation of Wing Bending Moment With Time at Station 8000, Shot 3, B-17 (5715)

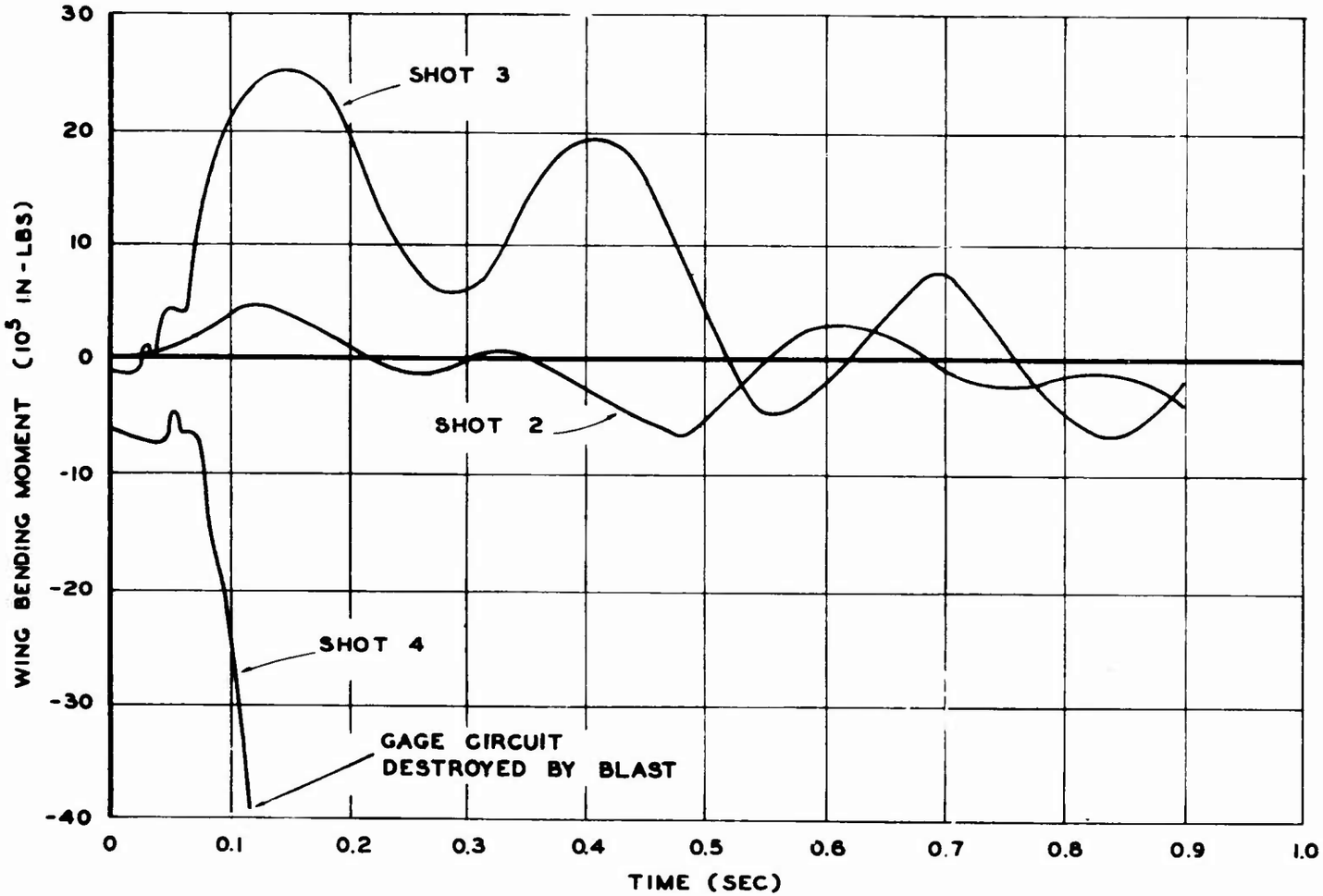

Fig. A.49 Comparison of the Variation of Wing Bending Moment With Time on B-17 (5715) at Station 8000, Shots 2 and 3, and Station 4000, Shot 4

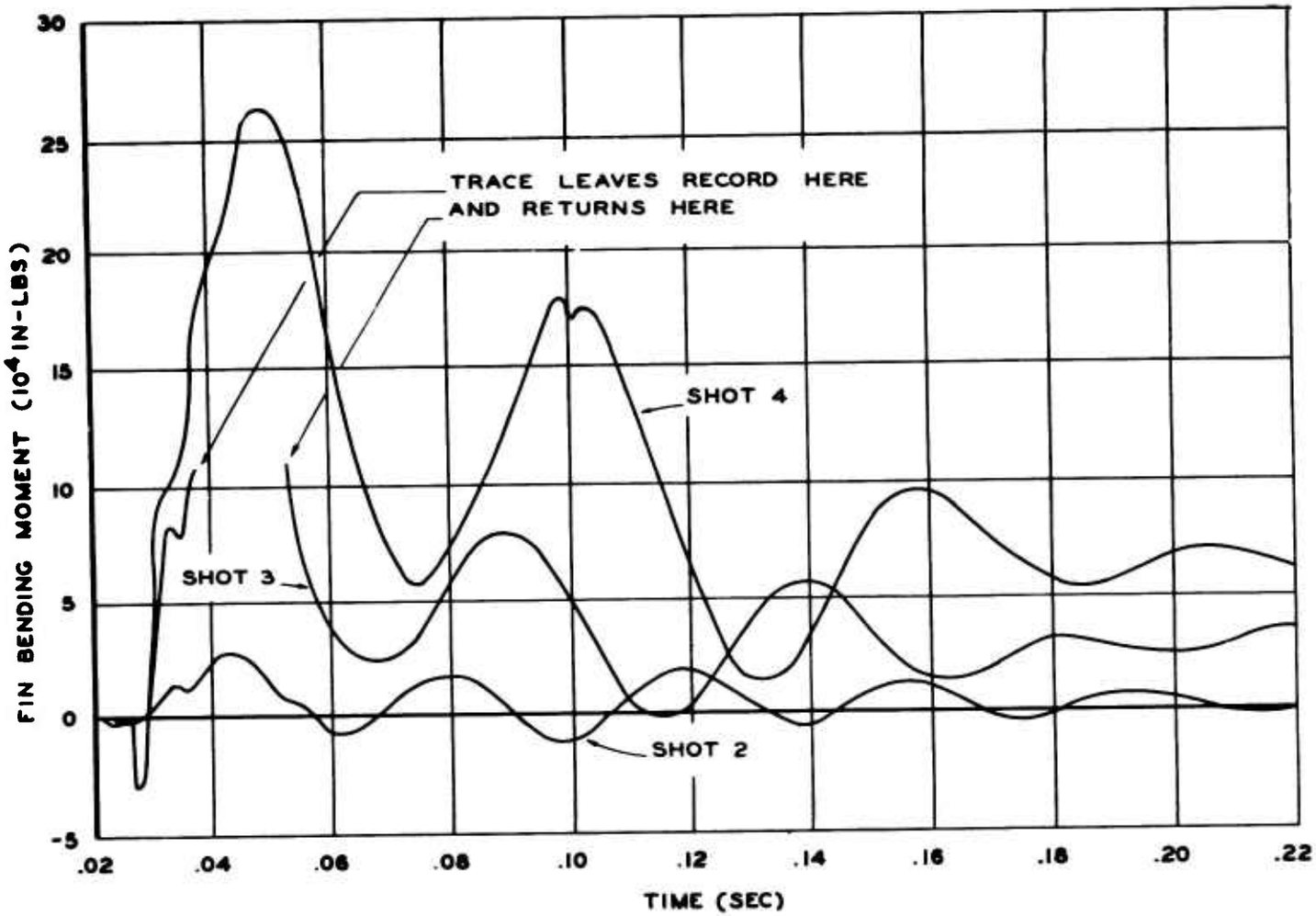

Fig. A.50 Comparison of the Variation of Fin Bending Moment With Time on F-47 (9785) at Station 8000, Shots 2 and 3, and Station 4000, Shot 4

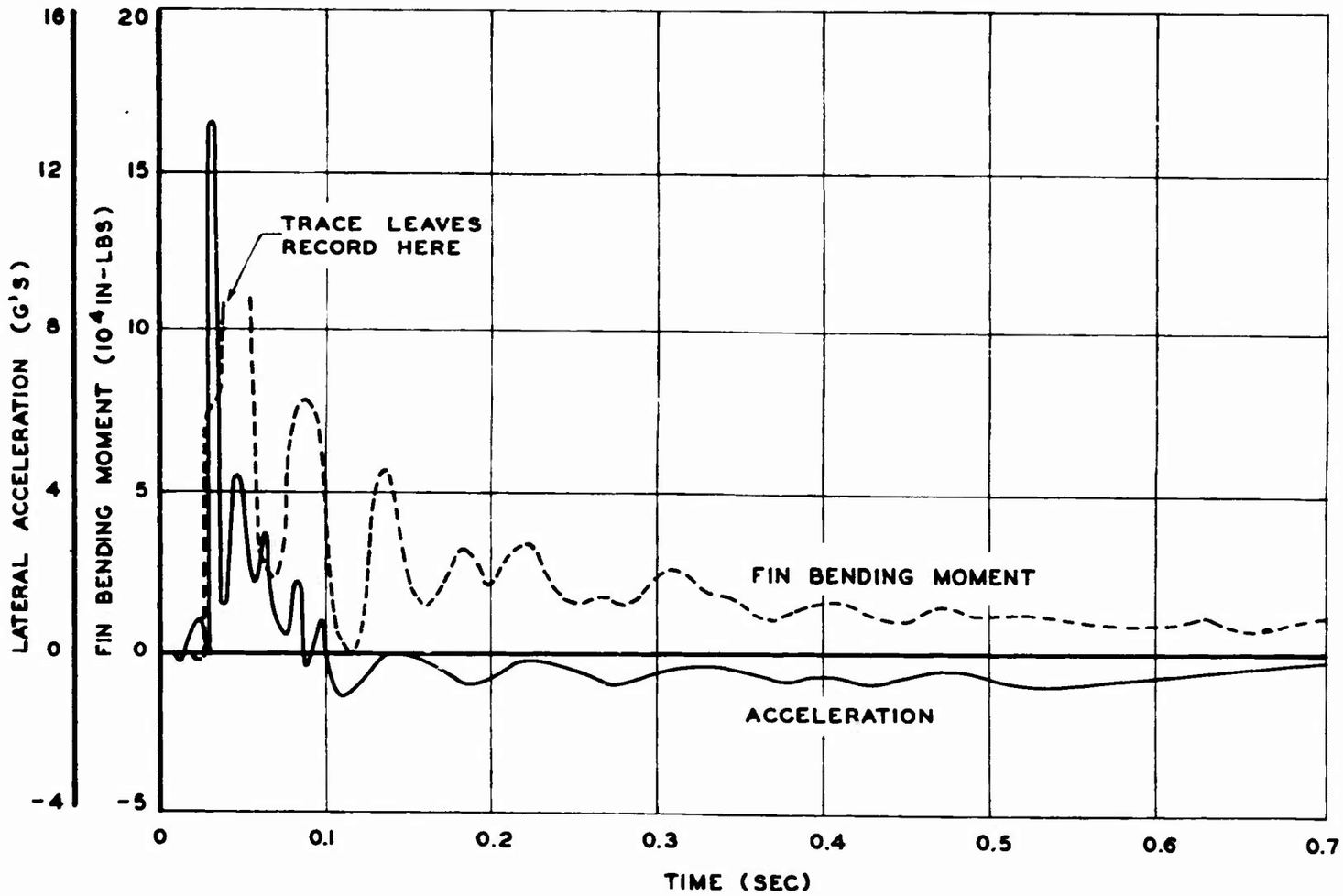

Fig. A.51 Comparison of the Variation of Lateral Acceleration and Fin Bending Moment With Time on F-47 (9785) at Station 8000, Shot 3

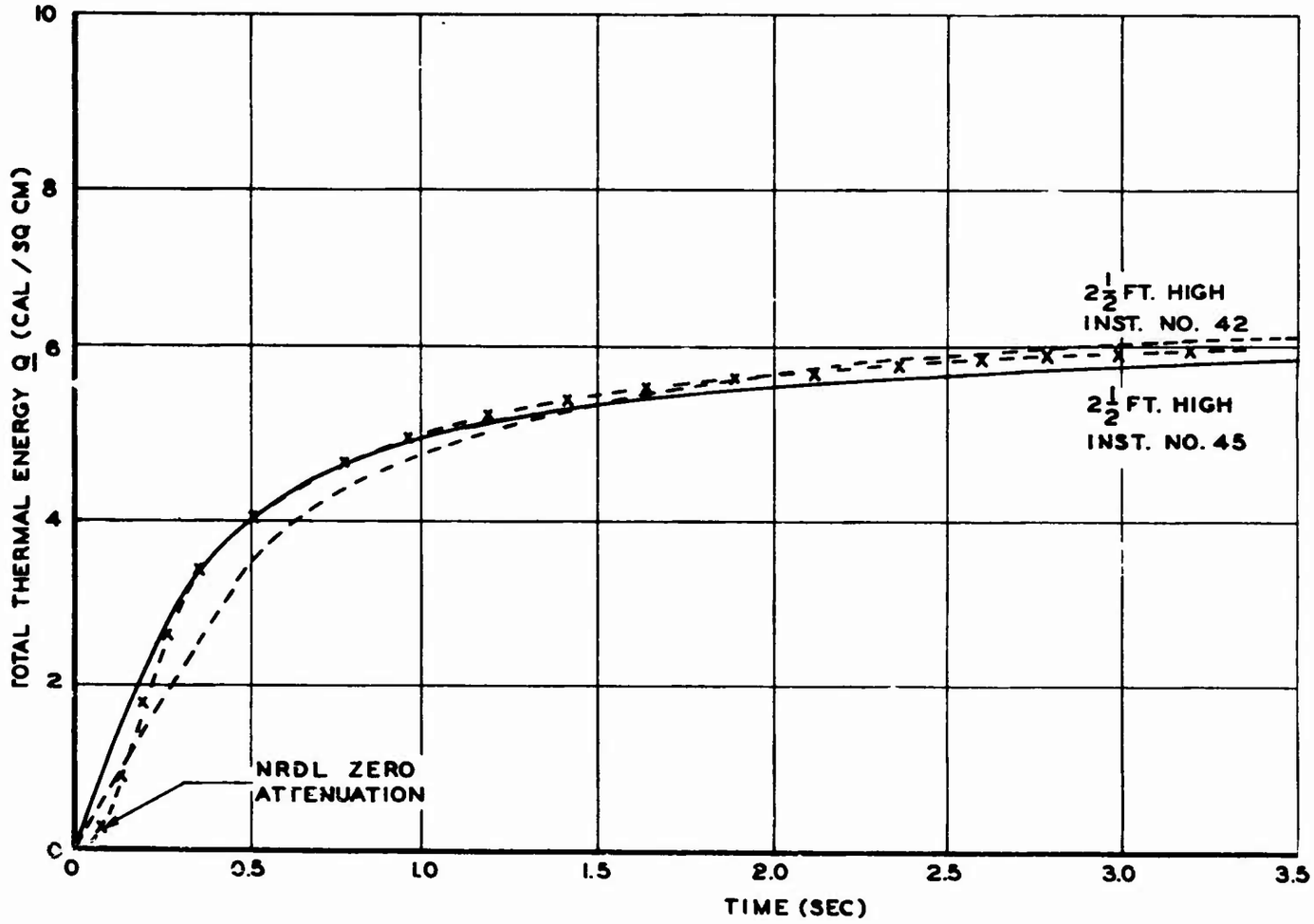

Fig. A.52 Comparison of the Variation of Corrected Total Thermal Energy With Time at Various Heights, Station 10,500, Shot 3

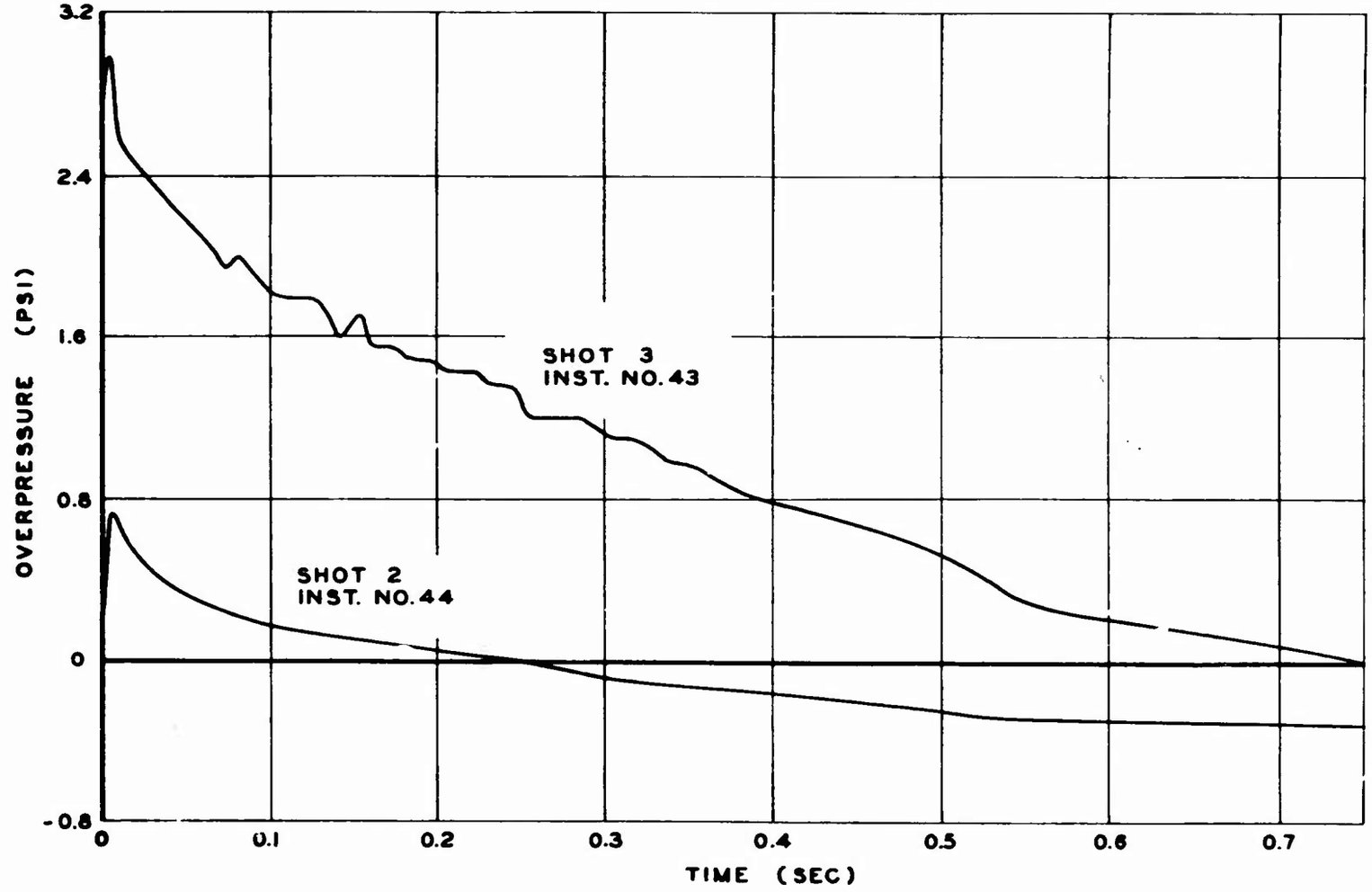

Fig. A.53 Comparison of the Variation of Ground Overpressure Measurements at Station 10,500, Shots 2 and 3

[redacted]

1. The total thermal energy measurements vs time are plotted in Fig. A.55. The instruments were located 5 ft above the ground well ahead of the aircraft. Installation 41, located on the right side of the survey control point, showed a more rapid rise to its peak of 27 cal/cm^2 than did the curve for installation 9, which reached a peak of 26.8 cal/cm^2.

2. Neither of the two overpressure measurements were valid because the transmitters were damaged by the thermal radiation.

3. The measured variation of the angle-of-blast incidence with time at this station is presented in Fig. A.56. This figure indicates initial fluctuations of the vane ranging from +4° to -6°. The frequency of these oscillations was about 39 cps for the first 0.3 sec, after which time a very unstable oscillation occurred ranging from +9° to -11°. These oscillations do not show any particular sense, i.e., positive or negative, for the angle of flow behind the shock front.

The specific input function measurements were as follows:

1. The measurement of the total thermal energy delivered to the cockpit of F-47 (9785) is presented in Fig. A.57. A peak of 22.7 cal/cm^2 was measured 2.4 sec after the blast occurred. The position of this installation is shown in Fig. A.15a and Fig. A.15b was described in A.2.1.2.

2. Two pressure measurements, one on the wing of F-86 (9597) and the other on the wing of F-47 (0065), yielded reliable data. These are plotted on two time scales and presented in Figs. A.30 and A.58. The pressure on the F-86 wing, installation 16, rises sharply to a peak of 8.8 psi in 4 msec and decays rapidly. A second major peak equal to 1.6 psi occurs at 0.38 sec. A negative overpressure equal to 0.6 psi was measured after 3 sec had elapsed.

The peak pressure measured on the F-47 wing, installation 19, was 11.5 psi. This pressure rose extremely rapidly (1 msec) and decayed very similarly to the F-86 wing pressure curve. A minimum pressure of 0.3 psi was measured at 0.8 sec.

The response function measurements were as follows:

1. Two types of thermocouple installations, the copper insert type and the standard type (see Paragraph A.2.1.3), were used to measure the temperature rise on F-86 (9597). The locations of the two installations on the left wing of the airplane are shown in Fig. A.18b. The finish of the surface was that of a normal unpolished F-86 wing. Installation 12, the copper insert type, had an angle of incidence of

[redacted]

[redacted]

72° and was at a temperature of 106°F at shot time. The skin was 0.081 in. thick. A graphical presentation of temperature rise as a function of time for installation 12 is shown in Fig. A.59. This curve peaks at a value of 112°F after a rise time of 0.30 sec. Installation 24, the standard type thermocouple, had an angle of incidence of 73° and the skin was at a temperature of 103°F at shot time. The skin thickness at this installation was 0.081 in. A graphical presentation, Fig. A.59, of the temperature rise as a function of time for installation 24 shows a peak of 50°F was reached 2.40 sec after detonation of the bomb.

2. The temperature rise of the skin on F-47 (0065) was measured by two standard type installations. The location of the two installations, 22 and 23, is shown in Fig. A.17b and Fig. A.17c. The condition of the surface for both installations was that of a normal unpolished wing of an F-47 and the temperature at shot time was 130°F. The angle of incidence for both installations was 67° and the skin thickness was 0.040 in. Installation 22, the outboard thermocouple, reached a peak temperature rise of 180°F 8 sec after detonation of the bomb. Fig. A.60 shows the curve of temperature rise as a function of time for installation 22. The shock wave from the bomb reached the airplane 2.30 sec after detonation. The inverted spike, shown at 2.9 sec on the curve, was undoubtably caused by some phenomena of the shock wave. Installation 23, the inboard thermocouple, reached a peak temperature rise of 180°F 7.5 sec after detonation of the bomb. Figure A.60 shows the temperature rise of installation 23 as a function of time. The shock wave from the bomb took 2.30 sec to reach F-47 (0065), which is precisely the time that the spike occurred on the curve of installation 23. The spike reaches a temperature of 177°F then drops off to 172°F at 2.8 sec.

3. The temperature rise of B-17 (5715) was measured by two installations one consisting of a polished surface on the right wing, installation 46, and the other of a normal unpolished surface on the left wing, installation 47. The location of the two installations on the airplane are shown in Fig. A.13b. The temperature of installation 46 at shot time was 104°F, the angle of incidence of this installation was 58°, and the skin was 0.025 in. thick. Figure A.61 shows a curve of temperature rise as a function of time for the polished surface of installation 46. A maximum temperature rise of 280°F was reached before the installation ceased to operate due to the effects of the shock wave on the wing. This temperature rise was accomplished in 2.2 sec. At shot time, installation 47, the unpolished surface, was at a temperature of 127°F, the angle of incidence was 58°, and the skin thickness was 0.025 in. The curve for installation 47, showing temperature rise as a function of time, is presented in Fig. A.61. A maximum temperature rise of 215°F was recorded before the trace went off the record. The rise of the temperature at the time the trace left the paper was very fast, the slope being 1280°F per sec at that time.

[redacted]

[redacted]

4. Lateral acceleration of F-47 (9785), installation 48, was measured at Station 4000 on Shot 4. Figure A.15b shows the location of the accelerometer on the airplane, and Fig. A.2 indicates the orientation and location of the airplane relative to ground zero. A presentation of lateral acceleration as a function of time for installation 48 is shown in Fig. A.45 and Fig. A.62. A peak of 14.5 G's was reached in 45 msec. The approximate frequency indicated by the accelerometer from 0.03 to 0.12 sec was 55 cps. The airplane was orientated with its left side toward ground zero before the detonation of the bomb and was observed to be facing approximately head on toward ground zero after the shot. The blast of the bomb thus caused a 90° counterclockwise rotation of the whole airplane. The airplane pivoted around the right landing gear, and the accelerometer was mounted very close to this gear so the angular acceleration experienced by the accelerometer should be relatively small. No attempt, however, was made to separate the lateral acceleration from the angular acceleration in the analysis of the data.

5. The F-47 (0065) was placed so that its tail was toward ground zero during Shot 4. Therefore, the first bending moment peak was expected to be negative. As shown in Fig. A.47, the first peak indicates a bending moment of -1,180,000 in-lb. This value was attained only 90 msec after the shock front arrived, and it represents a bending moment equivalent to 48.6 per cent of the ultimate bending moment. A maximum positive peak of 440,000 in-lb, equivalent to 11.9 per cent of ultimate, was recorded. The deflection was predominately negative for the portion of the curve shown, and the wing vibrated at a frequency of 8 cps. There was little or no deflection in the period 1 sec after the shock front arrived.

6. The B-17 (5715) was also placed with its tail into the blast. As was expected, its primary wing bending moment was negative. Figure A.49 shows this measurement plotted vs time. The curve is abruptly discontinued without reaching a peak because the strain gage leads were torn loose when the blast ripped off the entire wing surface aft of the rear spar. This wing failure occurred 115 msec after the shock front hit the aircraft. The maximum bending moment obtained was -3,900,000 in-lb or 31.6 per cent of ultimate. It should be noted that at zero time (zero time being the time when the site pressure gage deflects) there was a negative bending moment equal to -557,000 in-lb even though the shock front was well ahead of the aircraft. This will be explained in A.4.5.

7. As a result of Shot 4, the vertical stabilizer of F-47 (9785) was severely damaged. Figures A.50 and A.62 show the measurements of fin bending vs time, and show that damage in the form of 47,700 in-lb of permanent set did occur. This permanent set is equivalent to 87 per cent of the ultimate bending moment. The maximum positive peak was reached in 19 msec and indicates a bending moment of 260,000 in-lb,

[redacted]

[redacted]

equivalent to 476 per cent of the ultimate bending moment. The only negative bending moment was immediately prior to the first positive peak and was equal to -30,000 in-lb. A stress relief and build-up was noted at the second positive peak.

A.3.4.3 Station 8000

The general input function measurements were as follows:

1. The total thermal energy data are shown in Fig. A.63. The curves, corrected for dissipation and quartz window attenuation (see A.3.2.3) are quite similar, reaching a maximum of 10.5 cal/cm^2 in 3 to 4 sec.

2. The overpressure vs time curve, Fig. A.64, showed a maximum overpressure of 2.0 psi at 7 msec and the duration of the positive pressure phase was 0.97 sec.

A.3.4.4 Station 10,500

No measurements were attempted on this shot.

A.4 DISCUSSION

A.4.1 Total Thermal Energy Measurements

Total thermal energy measurements were made at the stations mentioned in Paragraphs A.2.1.1 and A.2.1.2 of this report. In general, two installations were used to measure the total thermal energy at each station on each shot. The only exception to this was at Station 2200 on Shot 4, where only one installation was used. The correlation between two similar installations at the same station on the same shot was very good, the difference generally being less than 10 per cent at the maximum points. Graphical illustrations of this correlation are shown in Figs. A.26 and A.34 for Shot 2, Figs. A.36, A.38, and A.52 for Shot 3, and Figs. A.55 and A.63 for Shot 4.

A.4.1.1 Particle Attenuation

Particle attenuation includes all of the non-predictable attenuation of the thermal radiation. The particle attenuation factor is defined as the quotient of an NRDL value of thermal energy divided by a corresponding value obtained by Project 3.1. The values of total thermal energy chosen were not necessarily the peak values for either the NRDL or Project 3.1 data but were chosen as close to the peak as possible, consistent with the requirement that the time after detonation be the same for both. The NRDL curves have been corrected to zero atmospheric attenuation; however, this correction is

[redacted]

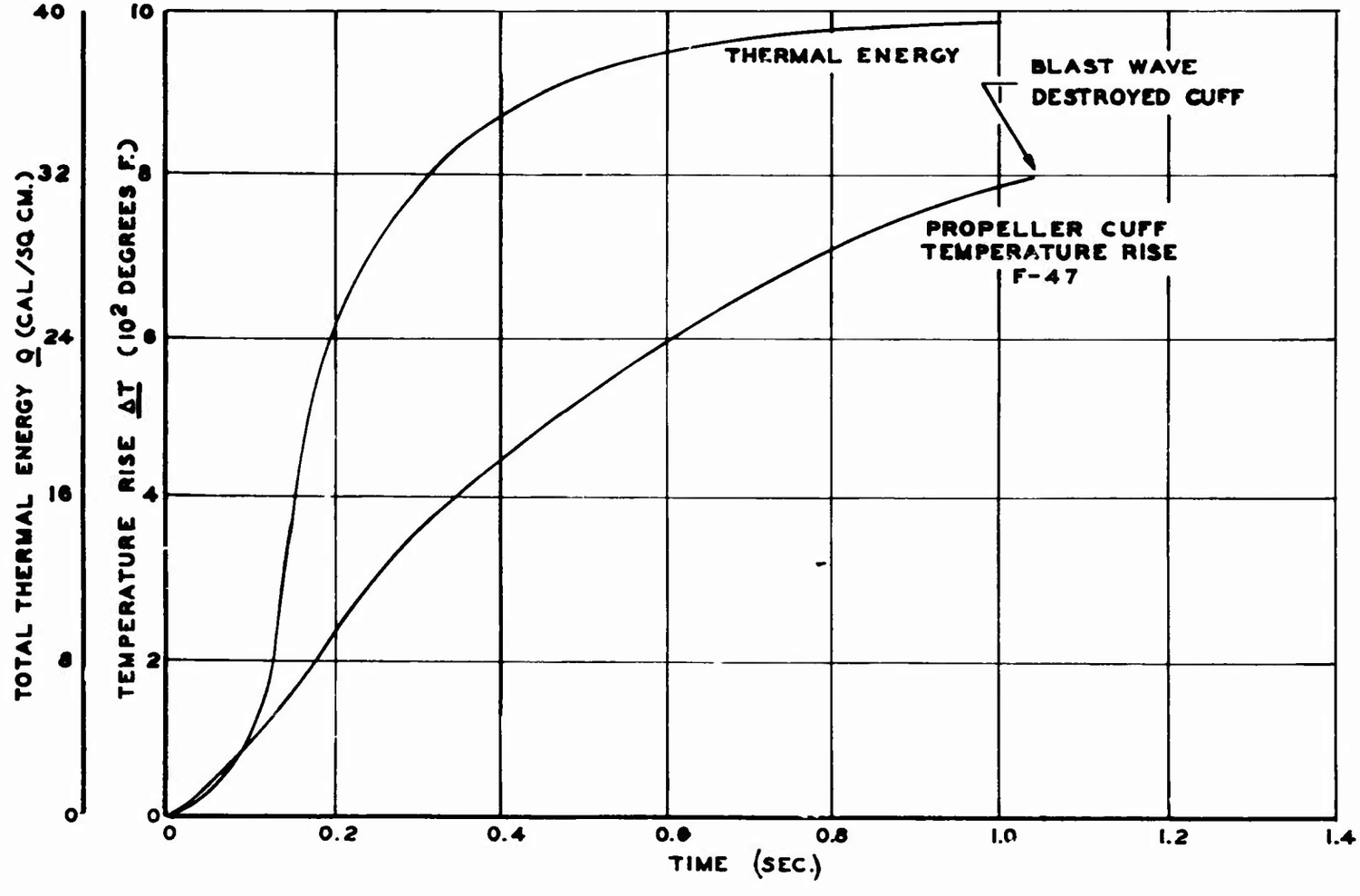

Fig. A.54 Comparison of the Corrected Total Thermal Energy 4 Ft above Ground and Temperature Rise on Propeller Cuff of F-47 (8785), Station 2200, Shot 4

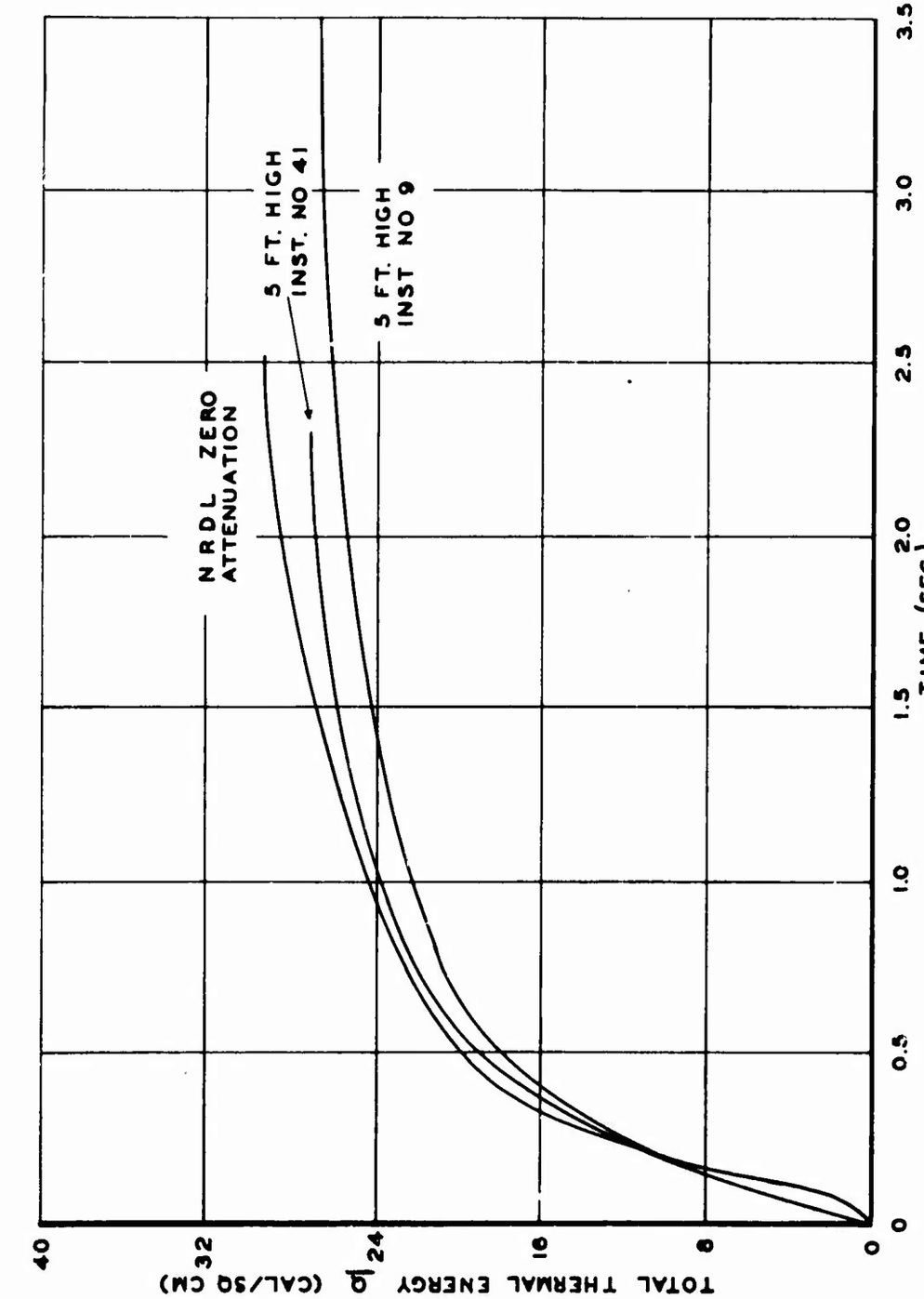

Fig. A.55 Comparison of the Variation of Corrected Total Thermal Energy With Time at Various Heights, Station 4000, Shot 4

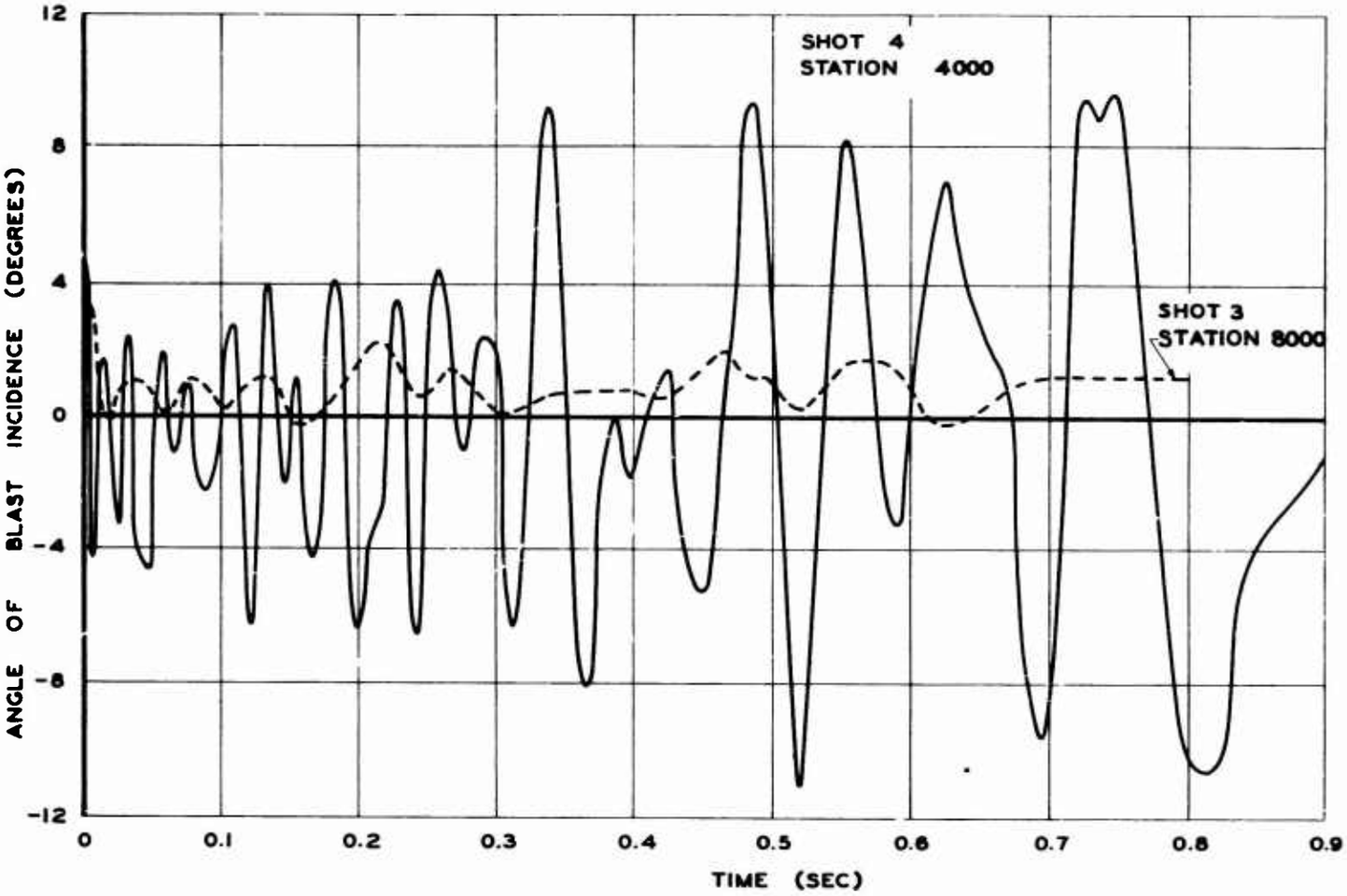

Fig. A.56 Comparison of the Variation of the Angle of Blast Incidence With Time, 3½ Ft Above Ground, at Different Stations and Shots

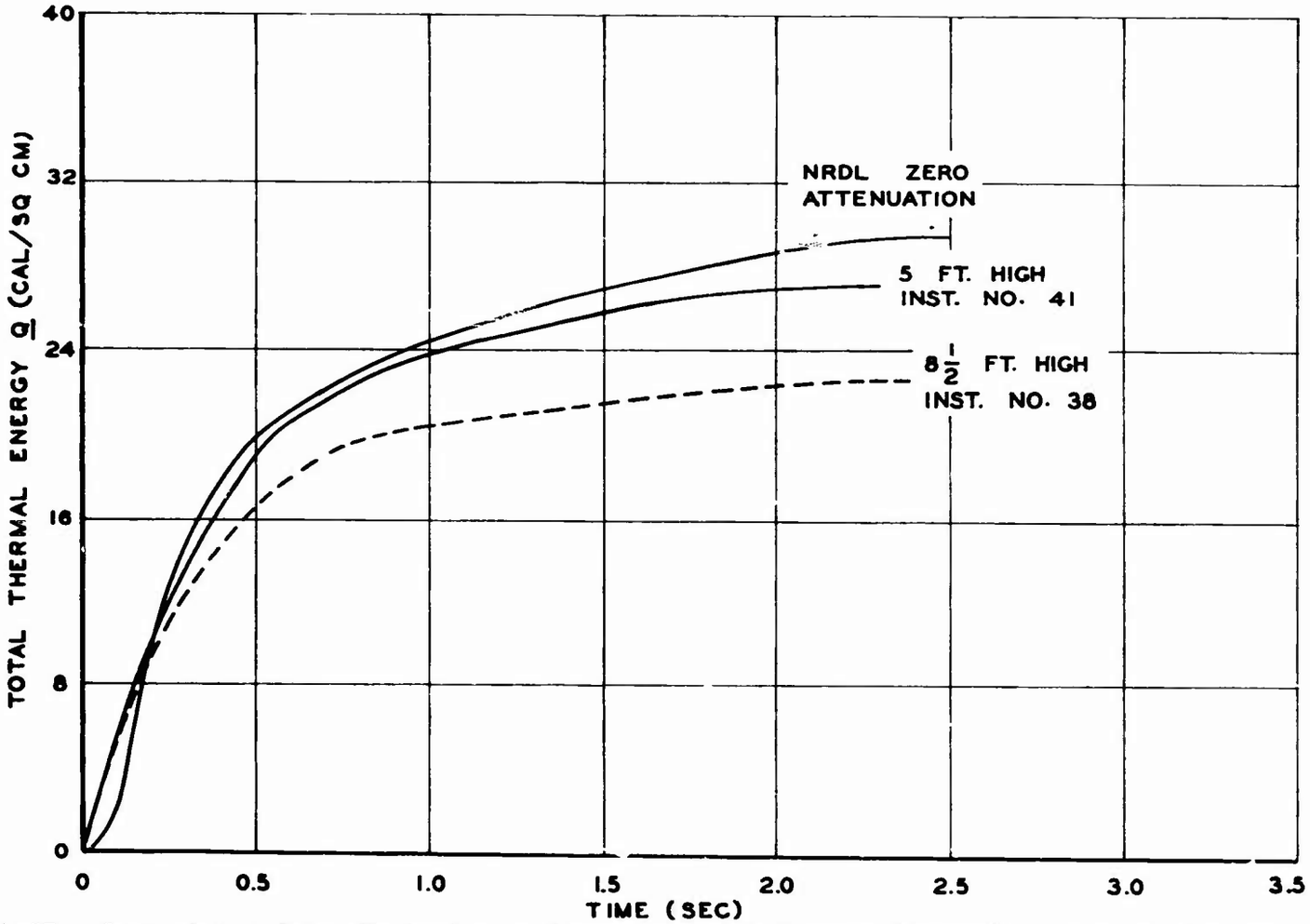

Fig. A.57 Comparison of the Variation of Corrected Total Thermal Energy With Time at Various Heights, Station 4000, Shot 4. One Measurement, Installation 38, Was Made at the Average Height of the Pilot's Head in the F-47 (9785).

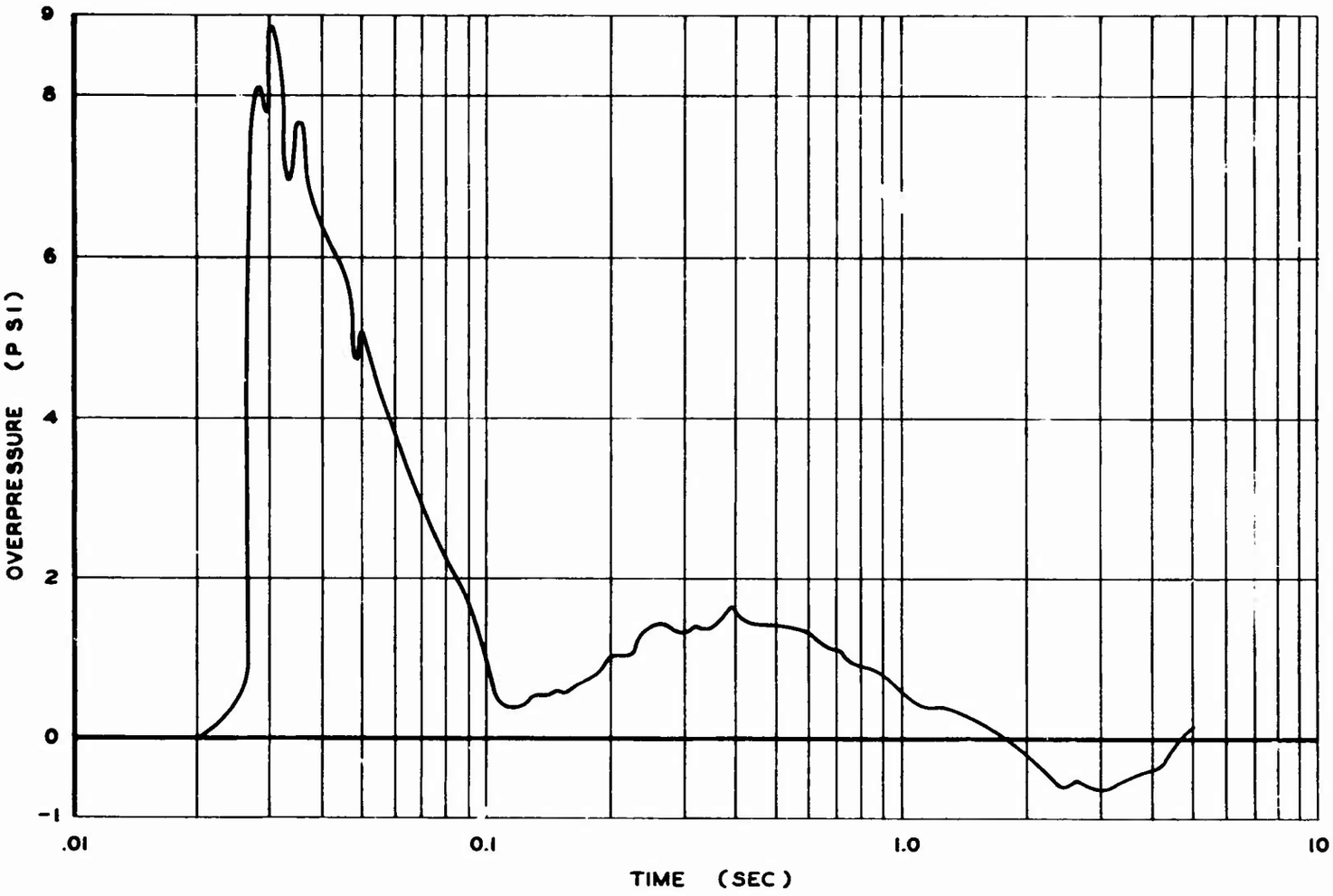

Fig. A.58 Variation of Overpressure With Time at Station 4000, Shot 4, on Wing of F-86 (9597)

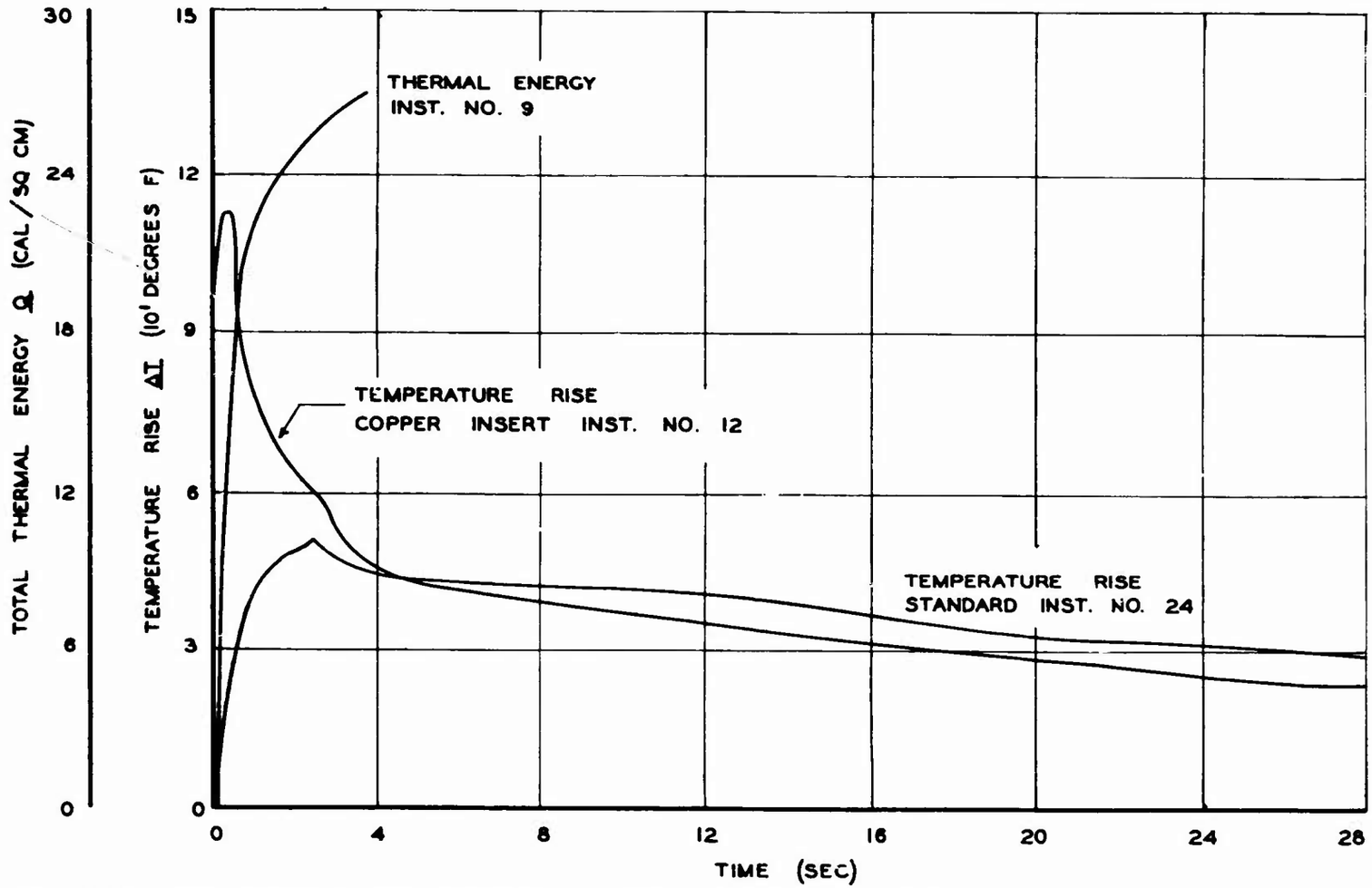

Fig. A.59 Comparison of the Variation of Corrected Total Thermal Energy 5 Ft Above Ground and Temperature Rise on F-86 (9597) With Time, Station 4000, Shot 4, Angle of Incidence 73°. Skin Temperature Just Before Time Zero Was 104°F.

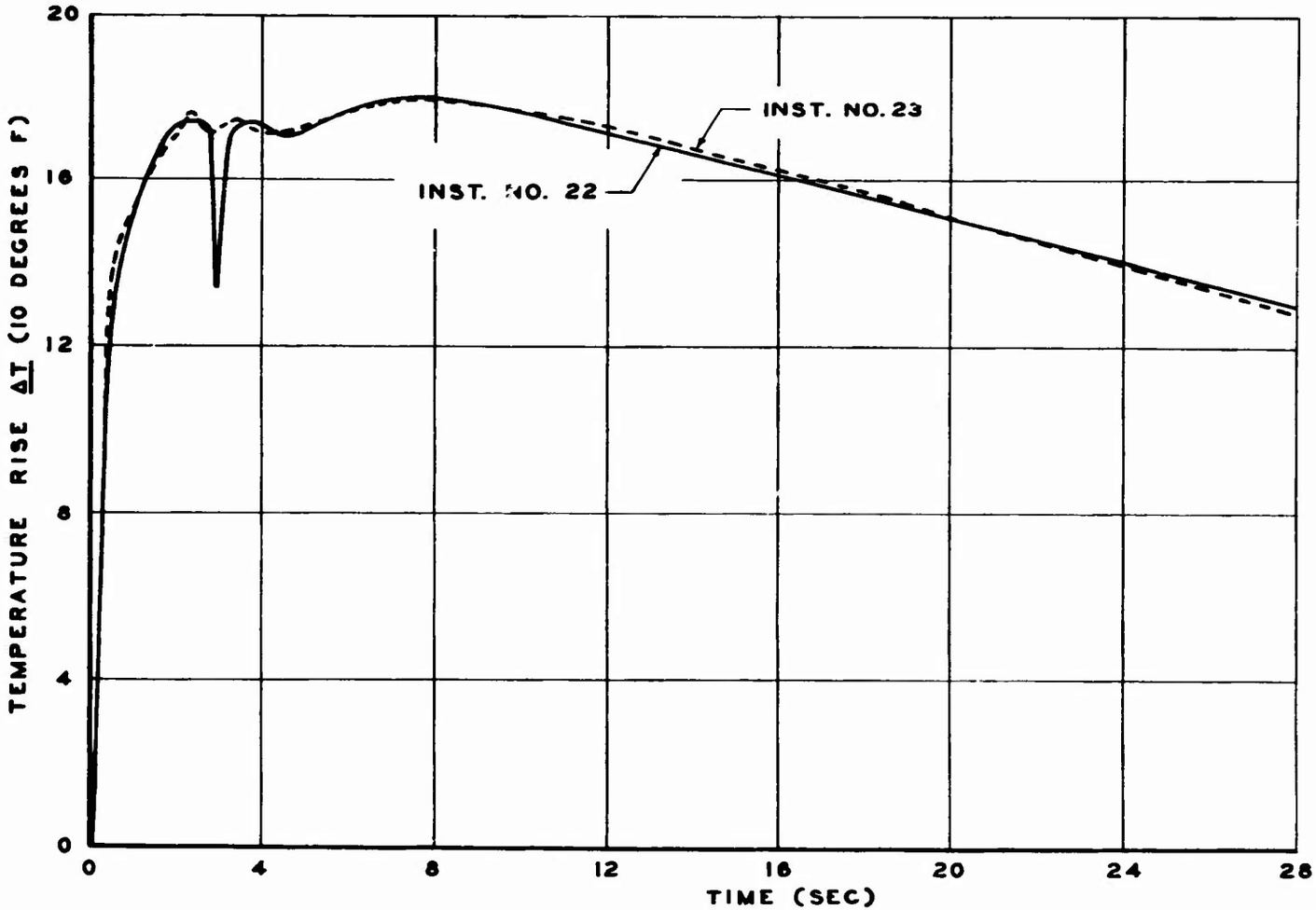

Fig. A.60 Comparison of the Variation of Wing Temperature Rise With Time on F-47 (0065), Angle of Incidence 67°, Station 4000, Shot 4. The Skin Temperature Just Before Time Zero Was 130°F.

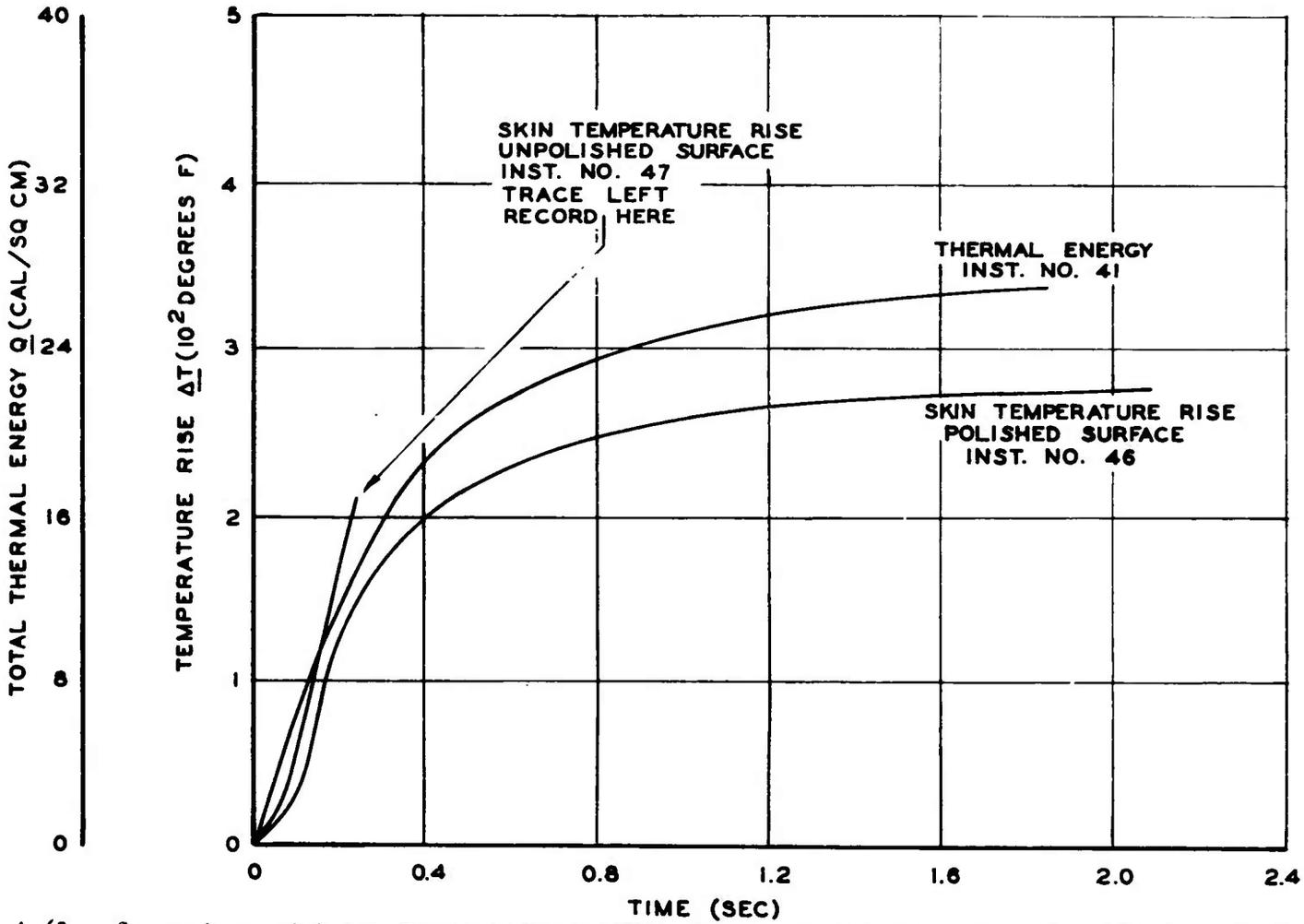

Fig. A.61 Comparison of Total Thermal Energy With Temperature Rise of B-17 (5715) Wing, Angle of Incidence, 58°, Station 4000, Shot 4. The Temperatures of Installations 46 and 47 Just Before Time Zero Were 104°F and 127°F, Respectively.

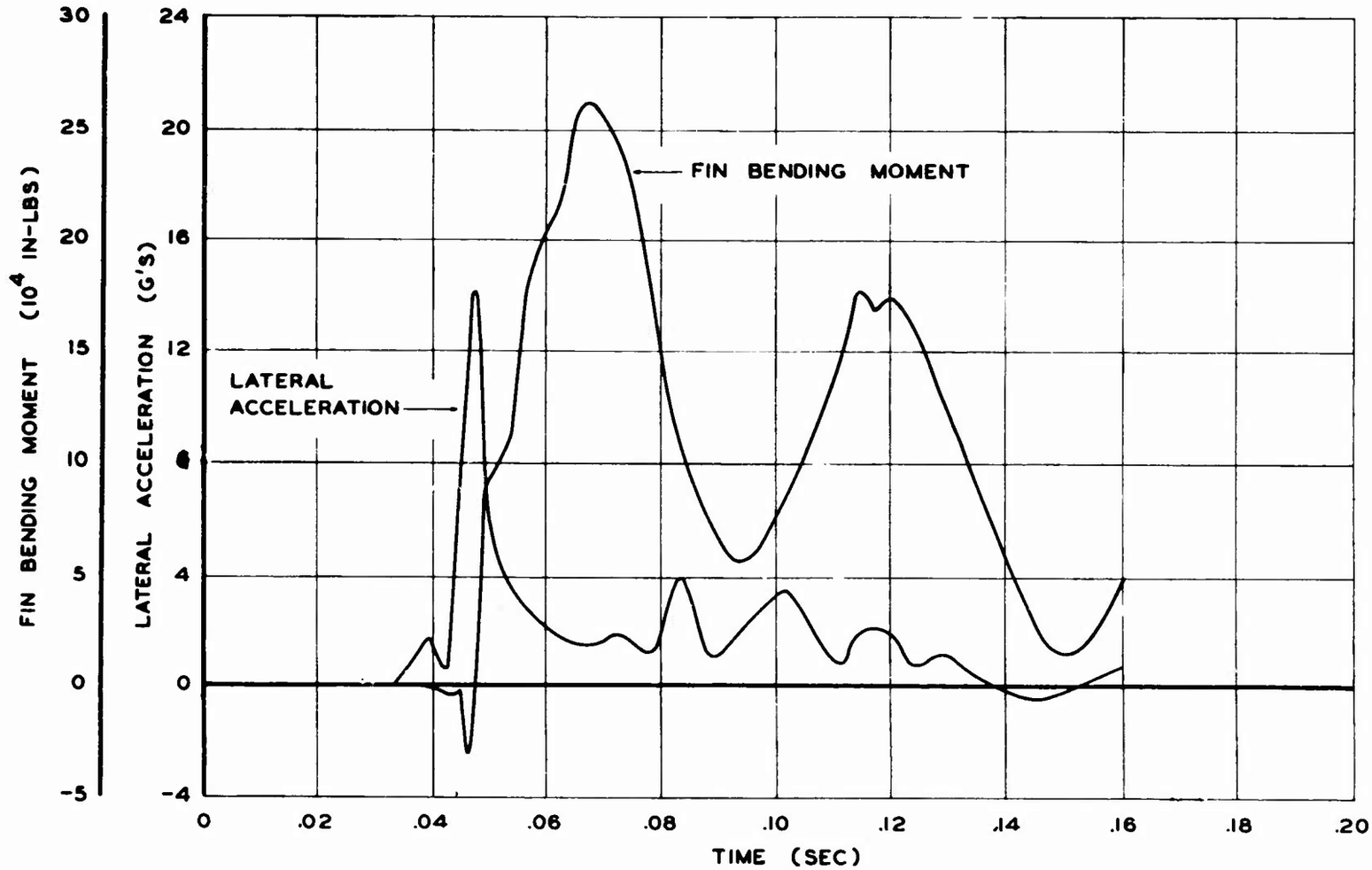

Fig. A.62 Comparison of the Variation of Lateral Acceleration and Fin Bending Moment With Time on F-47 (9785), Station 4000, Shot 4

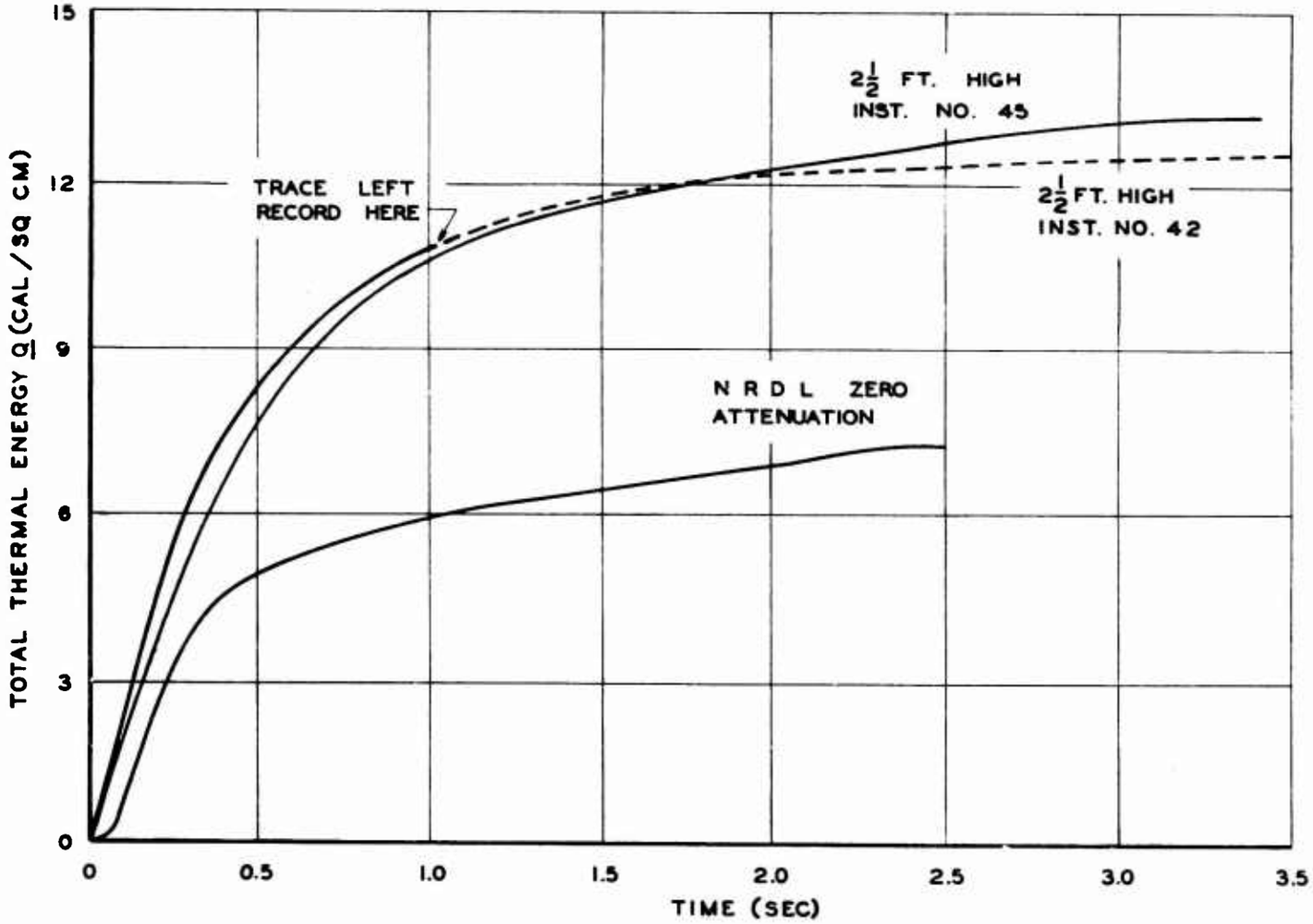

Fig. A.63 Comparison of the Variation of Corrected Total Thermal Energy With Time at Various Heights, Station 8000, Shot 4

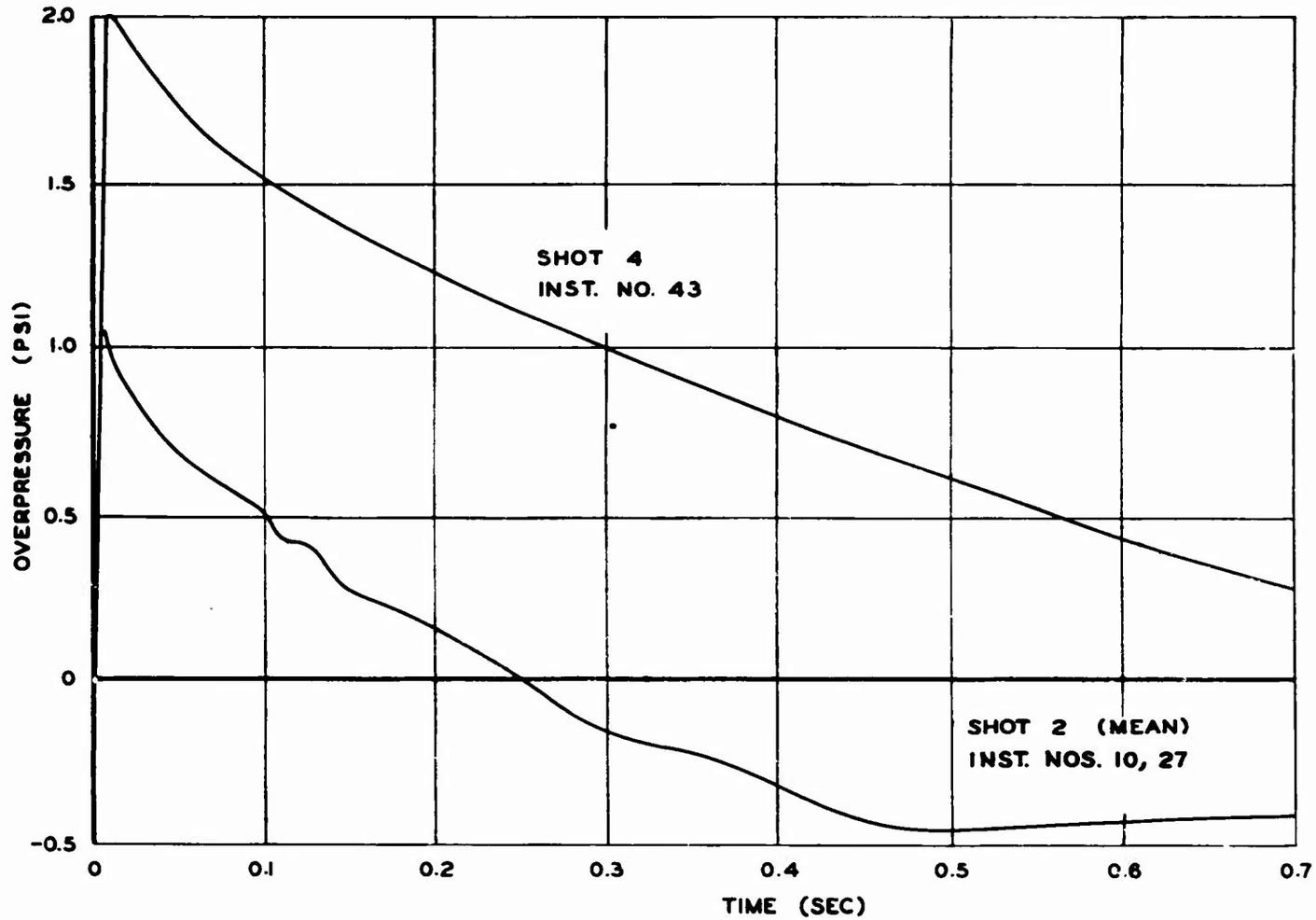

Fig. A.64 Comparison of the Variation of Overpressure With Time at a Point on the Ground, Station 8000, Shots 2 and 4

[redacted]

very small and can be considered negligible for slant ranges under 11,000 ft. Consequently, the difference between the NRDL and 3.1 data is due to particle attenuation.

Figure A.65 shows the particle attenuation plotted as a function of ground range for each shot. A particle attenuation factor of greater than one indicates an attenuation, whereas a factor less than one indicates an amplification. An actual amplification was measured on Shot 4 at ground range 7792 (Station 8000). Two installations at that range indicated a higher value of total thermal energy at 2½ ft above the ground than was measured by NRDL on the blast line at this range.

Two alternative possibilities exist for explanation of this measurement, i.e., the possibility of physical phenomena causing amplifications, or the possibility of error in instrumentation. The following facts support the hypothesis of increase in total thermal energy by reflection either from the ground, or from the upper surface of the dust or smoke cloud formed ahead of the station.

1. The angle of the incident ray with the horizontal from the bomb at Station 8000 on Shot 4 was approximately 7 degrees.

2. The calorimeter was pointed at the burst point of the bomb and included a field of 90°. In other words any thermal radiation included within an angle of 45° in any direction from the line connecting the burst point with the calorimeter could have been measured.

3. The area on which the calorimeter was mounted was black topped for a distance of approximately 100 yards in front of the installation, however from that point to ground zero the color of the ground was light grey.

The possibility of instrumentation error requires the coincidence of omission of circuit resistances on each of the two circuits, which would have produced, according to calculations, results consistant with NRDL thermal data.

Particle attenuation is probably caused by the dust and smoke that accompany atomic detonations. The major factors affecting the particle attenuation are height of burst, yield, ground range, and height above ground of the surface receiving the thermal radiation. Since the particle attenuation is probably caused by the dust and smoke, anything affecting these, such as type of terrain and amount of fissionable material present will also affect the particle attenuation.

[redacted]

[redacted]

A.4.1.2 Specific Attenuation

Specific attenuation refers to the predictable attenuation of the thermal radiation. Atmospheric attenuation and that due to glass, quartz, or plastics fall into the category of specific attenuation. The B-17 windshield attenuation, defined as the total thermal energy at the site divided by the total thermal energy measured inside the cockpit, was computed from Fig. A.28 on Shot 2 and Fig. A.40 on Shot 3. The attenuation on Shot 2 was 1.85 and on Shot 3, 3.2. The windshield was of laminated construction, 2.15 in. thick. B-17 (5715) was orientated the same for both shots, but the calorimeter inside the cockpit was reorientated due to the difference in burst height. The fact that little correlation exists between the windshield attenuation of Shots 2 and 3 can be accounted for by considering the following variable factors.

1. The largest portion of the attenuation of glass is due to reflection. The reflection of the B-17 windshield could have been affected by the dust that settled on it and, also, by the difference in the angle of the incidence rays from the two shots.

2. The plexiglas panel above the co-pilot's seat of B-17 (5715) was destroyed by burning on Shot 3, as shown in Figs. 3.70 and 3.71. The smoke that accompanied this burning could have attenuated the thermal radiation.

3. Another factor which affects the attenuation is that the cockpit measurement was made at a height of 13 ft above the ground, whereas the site measurement was made at 5 ft. The 8 ft difference in height will cause a change in the particle attenuation; and consequently, the attenuations as computed can not be wholly attributed to the cockpit glass.

4. The fourth factor is the low thermal input measured on Shot 2 which was of the order of 0.5 cal/cm^2. This low measurement could contain considerable error, since the calorimeter was designed to measure higher value of thermal energy.

A calorimeter was mounted inside the cockpit of F-47 (9785) on Shot 4 to measure the total thermal energy level. The canopy was 0.225 in. thick and made of plexiglas. The attenuation was 1.22, as computed from the site and cockpit measurements shown in Fig. A.57. The cockpit measurement was made at a height of 8 ft, whereas the site measurement was made at 5 ft. No comparison was made between the B-17 windshield attenuation and F-47 canopy attenuation because of the great difference in thickness.

The level of the total thermal energy in the cockpit of the B-17 on Shot 3 was 4 cal/cm^2. Table 6.50, page 201, in

[redacted]

"The Effects of Atomic Weapons", indicates that personnel inside the B-17 cockpit would have received moderate burns on Shot 3. The thermal energy level in the F-47 cockpit on Shot 4 was 22.7 cal/cm^2, which indicates that very bad burns would have been sustained by personnel in the cockpit.

A.4.1.3 Variation in Rise Time

The measurements made by Project 3.1 show a variety of rise time for the thermal energy at the various stations on the various shots. Two factors, ground range and height of the bomb burst, affect the rise time because of their effect on particle attenuation (see A.4.1.1), which probably is the primary cause of the difference in rise time. Ground range affects particle attenuation because the dust and smoke at stations closer to ground zero is more dense and rises faster than at stations farther from ground zero, thus reducing the transmission of thermal energy sooner and to a greater extent at the nearer stations. Figures A.66, A.67, and A.68 for Shots 2, 3, and 4, respectively, present a comparison of the thermal energies at various ranges, which may be studied for observation of these effects. Figure A.68 in particular is a very good example of longer rise times with increasing ground range.

Comparisons of total thermal energies vs time for different shots are presented in Figs. A.69 and A.70, respectively. Total thermal energy as a function of ground and slant range are presented in Figs. A.71 and A.72, respectively.

A.4.2 Blast Phenomena

A.4.2.1 Overpressure Measurements

Figure A.73 shows the relationship between the peak pressure data obtained by Project 3.1 and the curves representing the average of data obtained by other projects. The lack of pressure measurements at ranges nearer to ground zero than 8000 ft is a result of the thermal damage to the pressure transmitters at the nearer positions. The greatest discrepancy, percentage-wise, occurred during Shot 2 at Station 10,500, where the Project 3.1 data was 48 per cent higher than the composite results. The large discrepancy between these (Project 3.1) data and the composite data was due to the extremely low galvanometer deflection which was a result of the low overpressure at this station, and the discrepancy was actually smaller than the minimum error which was introduced during the record reduction procedure. The two points at Station 8000 were well within the limits of data scatter through which the composite curves were drawn.

A comparison of data obtained by David Taylor Model Basin (DTMB) capacitance gages with data obtained by Project 3.1

[redacted]

is also made in Fig. A.73. These DTMB data, which are plotted as triangles were the only other pressure measurements which were made in the same general locations as the Project 3.1 aircraft. The most interesting data comparison between the measurements of these two organizations occurred during Shot 3, Station 10,500 where both the DTMB and the Project 3.1 overpressure measurements were approximately 25 per cent higher than the composite data. Although only one Project 3.1 installation was used to measure this overpressure thus preventing a check on the accuracy by a duplication of measurements, there was no reason to believe that the instrumentation was in error or the data reduction was incorrect. Because this anomaly occurred at only one point, it can not be used as a basis for a theory demonstrating asymmetrical pressure distribution of the bomb burst; however, these data are presented in hopes that they may aid in future investigations. A possible explanation for these measurements being high is that the increase may have been due to a ground reflection which locally increased the overpressure peaks.

To facilitate comparisons of the relative peak overpressure and positive phase durations, the overpressures at Station 10,500 for Shots 2 and 3 and at Station 8000 for 2 and 4 are plotted in Figs. A.53 and A.64, respectively.

A.4.2.2 Angle-of-Blast Incidence Measurements

Two comparisons of the angle-of-blast incidence data were made as shown in Figs. A.39 and A.56. Figure A.39 presents data from two similar installations at Station 8000, demonstrating that the air behind the shock front, at a height 3½ ft above the ground, does not have the same angle of flow at two points 148 ft apart. The only similarity in the flow was the coincidence of some of the peaks, but no actual angle of airflow could be determined from these curves. Figure A.56 compares the angle-of-blast incidence at Station 8000, Shot 3, with the same measurement at Station 4000, Shot 4. There were no trends that coincided, and whereas there was a positive trend in the angle of airflow at Station 8000, there was no definite trend in the airflow direction at Station 4000. This same method of obtaining the angle-of-blast incidence was used on Operation GREENHOUSE, and the same high frequencies and irregular patterns prevailed at that time. These measurements indicate that the air near the ground is very turbulent and that the use of this instrument in measuring angle-of-blast incidence is still unproven.

A.4.3 Temperature Rise Measurements

Temperature rise measurements were made at the stations and on the airplanes mentioned in Paragraph A.2.1.3. In general, two installations were used to measure the temperature rise on each airplane. The correlation between similar installations at the same

[redacted]

[redacted]

station for the same shot was very good. The similar installations, numbers 22 and 23, on F-47 (0065) were generally within 3 per cent of each other on Shot 3 (see Fig. A.42) and within 1 per cent of each other on Shot 4 (see Fig. A.60), except during the period of the blast wave effect (see A.4.3.5).

A.4.3.1 Comparison of Polished and Unpolished Surfaces

The temperature rise of a polished and unpolished surface was measured on B-17 (5715) on all shots. The installations are described in detail in Paragraph A.2.1.3. A comparison of the temperature rise of the polished and unpolished surfaces, Figs. A.44 and A.61, indicates that for the unpolished surface on Shot 3 the rise was approximately three times as great as that of the polished surface. Calculation of the absorptivities of the two surfaces shows that the unpolished surface had an absorptivity of approximately 80 per cent, whereas the polished surface had an absorptivity of 30 per cent. Since light colored and polished surfaces reflect heat and thereby reduce the temperature rise of the surface, structural weakening due to the thermal effects may be considerably reduced by keeping the aircraft reasonably clean and by restricting the use of dark colored paints.

A.4.3.2 Comparison of Skin and Stringer Temperature Rise

Skin and stringer temperature rise measurements were made on F-47 (0065). The thermocouples were located on the left wing gun-bay door as shown in Fig. A.17c and as described in detail in Paragraph A.2.1.3. Figures A.43 and A.75 show a comparison of the temperature rise of the wing skin and wing stringer on F-47 (0065) for Shots 3 and 4 respectively. During Shot 3, at the time the skin temperature attained it maximum value (6 sec after time zero), it was found that the stringer temperature was only ½ as great as the skin temperature, however, during Shot 4 at the time of maximum value (8 sec after time zero) for the skin temperature the stringer temperature was only 1/8 as great. After the skin temperature had attained its maximum value the stringer temperature continued to rise and did not reach its peak value until the elapse of approximately 24 sec after time zero on both shots. The fact that the stringer does not reach as high a temperature as the skin coupled with the fact that the stringer temperature peaks occur as late as they do, indicates that basic structures will fail from thermal input as a result of the deterioration of the stressed skin as a load carrying member.

A.4.3.3 Propeller Cuff Failure

The installation measuring the temperature rise of the propeller cuff on F-47 (9785) (see Fig. A.54) is described in Paragraph A.2.1.3. The absorptivity of the black propeller cuff was not computed because no peak temperature was recorded. The blast

[redacted]

[redacted]

destroyed the cuff at approximately 1.05 sec after time zero. Figure A.76 shows a graph of the tensile strength of the propeller cuff as a function of time after time zero. This graph was obtained by combining the curve of temperature vs time of the propeller cuff with a curve of the tensile strength of 24ST aluminum as a function of temperature. The data, used in plotting the curve of tensile strength as a function of temperature for aluminum, were for aluminum maintained at a constant temperature and not for the rapid heating caused by the thermal radiation from an atomic explosion. Another example of the combined effects of the thermal radiation and overpressure is shown in Fig. A.77. This is a picture of a damaged propeller cuff which was on an F-47 at Station 2200 on Shot 3. Only the portion of the cuff which received the most direct thermal radiation was weakened sufficiently to be destroyed by the shock wave.

A.4.3.4 Copper Insert vs Standard Thermocouple Installation

The copper insert and standard type thermocouple installations located on F-86 (9597) are described in detail in A.2.1.3. Figure A.21 shows sketches of the two types of installation and also the method of connecting the thermocouples to the oscillograph. Figures A.41 and A.59 show a comparison of the two installations for Shots 3 and 4, respectively. The outstanding feature of this comparison is the quickness of response of the copper insert type of installation. On Shot 3 the copper insert installation reached a peak temperature at approximately 0.40 sec after time zero, whereas the standard installation peaked at approximately 5.0 sec. Similarly on Shot 4, the copper insert installation peaked at 0.3 sec, whereas the standard installation reached a peak at approximately 2.4 sec after time zero. The exceptionally fast response of the copper insert type installation can be attributed to the relatively thin section of copper with its low specific heat. Since the F-86 skin was considerably thicker and of a lower specific heat than the copper insert installation, it is felt that the copper insert installation did not give an indication of the true temperature of the skin. The standard installation with its slower rise was a much better measure of the actual skin temperature rise.

A.4.3.5 Effects of Shock Wave

The roughness of the temperature curves in the vicinity of the arrival time of the shock wave can be attributed to the shock wave in the following two ways.

1. The sharp spikes that are shown on some of the temperature curves generally occur at the time when the shock wave arrived at the installation. These spikes may be explained by consideration of the transfer of heat from the compressed shock wave to the aircraft surfaces. Examples of these spikes are shown in Figs. A.40 and A.60. The

[redacted]

[redacted]

inverted spike in the curve of installation 22, Fig. A.60, occurred after the time the shock wave arrived and was probably caused by an unknown malfunction in the thermocouple circuit.

2. The decrease in temperature immediately following the shock wave can be attributed to local cooling of the surface. This effect might be caused by the air mass from the blast passing over and cooling the surface upon which the thermocouple is mounted. Examples of local cooling are shown in Figs. A.42, A.43, A.44, A.59, A.60, and A.75.

A.4.3.6 Computed Absorptivities

Table A.6 shows absorptivities computed for the various surfaces upon which the temperature rise was measured. The absorptivities were measured in the following manner. Considering the temperature rise of a surface the corresponding thermal energy that has fallen on the surface, the angle of incidence of the incident ray, and the thickness of the surface an absorptivity for that surface can be computed. The formula used in computation of the absorptivities was as follows:

$$A = \frac{155\ T \Delta t}{\cos \alpha Q_t} \qquad \text{where} \qquad (A.1)$$

A = Absorptivity in per cent

Δt = Temperature rise of surface in degrees C

α = Angle between the incident ray and the normal to the surface

Q_t = Total thermal energy incident upon the surface in cal/cm^2

T = Thickness of surface in inches

The constant, 155 includes the density and specific heat of aluminum, and the conversion factors which make the units consistant.

The temperature rise and total thermal energy were obtained from Project 3.1 data. It is important to use values for these quantities that were taken the same time after time zero and also values that are close to the peak of both quantities. If values are chosen too soon before the peaks are reached, the steep slopes of the curves coupled with the time lag between an input of thermal energy and the corresponding temperature rise introduce considerable error into the calculations of the absorptivities. For the reasons mentioned above the calculation of absorptivities was omitted for surfaces which

[redacted]

have incomplete temperature curves that don't peak such as the propeller cuff temperature curve in Fig. A.54.

The variation in the values of absorptivity (see Table A.6) for the polished surface on B-17 (5715) may be accounted for by considering the following. Installation 25 had a polished surface 18 in. square in the center of which the thermocouple was located. The computed absorptivity of this surface was 23 per cent. Installation 46, on the other hand had only a 6 inch square polished surface with the thermocouple located in its center. Its computed absorptivity was 41 per cent. The maximum temperature rise of installation 46 could have been increased because of the relative closeness of the unpolished surface and the accompanying heat flow into the polished area. Considering the above facts the 23 per cent absorptivity is considered the more accurate value, for the absorptivity of a polished airplane surface.

TABLE A.6

Computed Absorptivities

Shot No.	Curves Compared: Temperature Rise Inst. No.	Curves Compared: Temperature Rise Airplane	Curves Compared: Total Thermal Energy Inst. No.	Comparison Time In Sec	Absorptivity In Per Cent
3	28	B-17 (5715)	41	5.7	65
4	47	(Unpolished)	41	0.2	66
3	25	B-17 (5715)	41	5.7	23
4	46	(Polished)	41	2.0	41
3	24	F-86 (9597)	9	4.0	39
4	24		9	2.3	51
3	23	F-47 (0065)	9	4.0	58
3	22		9	4.0	56
4	22		9	2.6	64

A.4.4 Wing Bending Moment Measurements

A.4.4.1 World War II Bomber

The primary wing structure of the B-17 (5715) was not damaged by the blast under any combination of station, orientation, or shot intensity established in this series of tests. The maximum recorded bending moment of this aircraft's wing occurred during Shot 4 at Station 4000 because the peak overpressure experienced by the aircraft was higher than on previous shots, and because the airplane was oriented such that more wing surface was exposed to the shock front than on Shots 2 and 3. The wing bending moment vs time curves for this

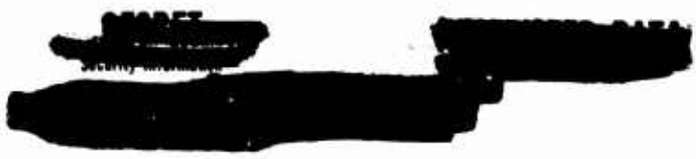

[redacted]

airplane are presented in Fig. A.49. Peak overpressures of 0.85, 3.6, and 5.8 psi caused peak bending moments of 4.0, 20.8, and 31.6 per cent of the design ultimate during Shots 2, 3, and 4, respectively. The ratios of the peak bending moments for Shots 2, 3, and 4 are nearly equal to the ratios of their respective overpressures, but due to the different orientation of the aircraft during Shot 4, a scaling factor can not be assigned. The Shot 4 curve (Fig. A.49) indicates an initial negative bending moment at zero time. This bending moment was not caused by the shock front because it had not yet reached the aircraft. (The actual wing bending due to the shock front began 70 msec later.) It is probable that the thermal radiation on the top wing surface, which was in tension, caused the skin to expand and allowed the wing to bend under its own weight. This bending began at the time the thermal radiation arrived and increased until the shock front struck the aircraft. The bending moment due to thermal effects was -700,000 in-lb, approximately 6 per cent of ultimate.

A.4.4.2 World War II Fighter

Figure A.47 presents the wing bending moment of F-47 (0065) plotted as a function of time during Shots 3 and 4. The Shot 4 curve, although it is initially negative due to the tail-in orientation of the airplane, has essentially the same peculiar characteristics as does the curve for Shot 3. Of particular interest is the build-up of the bending moment (0.55 sec during Shot 3 and 0.40 sec during Shot 4) which is of a much lower frequency than that of the first mode of wing vibration. This portion of each curve represents the natural wing bending moment due to its bending as a cantilever beam superimposed on the bending moment induced at the strain gage location by the movement of the airplane fuselage. The latter movement was similar to that of a mass supported by a simple beam, the end points of which were the landing gear strut attachments. The frequency of the pure wing bending for both shots was approximately 11 cps and the frequency of the mass supported by a simple beam was about 1.6 cps.

A.4.4.3 World War II Fighter vs Modern Fighter

The F-47 (0065) and the F-86 (9597) were chosen as representative configurations of old and new types of fighter aircraft for the purpose of comparing wing structural response to atomic blasts. For Shots 2 and 3 these aircraft were parked in juxtaposition and oriented nose-in at Station 8000, whereas they were oriented tail-in at Station 4000 during Shot 4. During Shot 3 at Station 8000 where the peak overpressure was 3.6 psi, the F-47 wing bending moment was equivalent to 49 per cent of ultimate whereas the F-86 wing bending moment was negligible. Such factors as the low angle-of-attack and the extreme wing stiffness contributed to the low bending moment output of the F-86 wing. A comparison of the bending moments of these two aircraft was not possible during Shots 2 and 4 because valid measurements

[redacted]

of the F-86 wing bending moment were not obtained. Inasmuch as no measurements were obtained from the F-86 bending moment installation, no graphical presentation of the foregoing comparison could be made.

A.4.4.4 Fin Bending on World War II Fighter

The measurements of fin bending moment on F-47 (9785) for Shots 2, 3, and 4 are presented in Fig. A.50. The three curves have been shifted along their time axis so that the initial positive deflections occur at the same time. The most important information shown on this graph is the measurement of bending moments which were far in excess of the static test ultimate of 54,700 in-lb. This extremely high loading, which was equal to 475 per cent of ultimate on Shot 4, did cause a considerable amount of permanent set in the vertical stabilizer but did not cause failure of the primary structure because the loads were applied over such a short period of time; i.e., during Shots 3 and 4, the first four positive peaks occurred in 0.15 and 0.19 sec, respectively. In addition, the movement of the airplane in response to the blast was such that pressure relief was effected.

Another interesting feature of the three curves plotted in Fig. A.50 is an apparent yield point which occurs at 30 msec. This yield was apparently due to slippage of rivets and bolts and could not have been caused by structural yield because this slippage occurred well below the yield point on Shot 2 and occurs at the same time on all the other curves, although it is less pronounced on the Shot 4 curve.

The affect of the permanent set on the dynamic response of the vertical stabilizer is also depicted in Fig. A.50. As the series of shots progressed, there was a decrease in the frequency of vibration from approximately 27 cps on Shot 2 to 19 cps on Shot 4.

At the time of arrival, the shock front on all of the F-47 fin bending moment curves and on two of the B-17 wing bending moment measurements, there is a deflection in the direction opposite to that of the primary bending moment. This deflection is a very rapid one which has a frequency much higher than the first or second mode vibration of either the wing or the fin. Two possible explanations for this negative bending moment are offered. An explanation based on mathematical analysis of similar structures indicates that third mode vibrations may exist with initial root deflections toward the blast. Superposition of the first cycle of this deflection upon the comparatively small deflections of the first and second mode vibrations at this time indicates initial root bending in the direction opposite to the disturbing force. Alternatively, the reverse bending may occur as the skin on the blast side of the fin or the under side of the wing is buckled inward at the initial impact of the shock front. (Since the skin has very little mass, it is reasonable to assume that

it can follow the high frequency input of the shock wave.) The buckling creates a stress which may cause the structure to bend initially toward the buckled surface. Then, as flow around the structure is established, the lift force and the drag force on the wing and vertical stabilizer, respectively, will cause these structures to bend in the direction of the lift or the drag.

A.4.5 Acceleration Measurements

A.4.5.1 Normal Acceleration Measurements

The normal acceleration curve for Shot 3 of F-47 (8785) at Station 2200 was integrated with respect to time to obtain the velocity curve which was in turn integrated to obtain the displacement of the airplane. The velocity and displacement curves are not presented in this report, however, significant values of the two quantities will be discussed. A very small downward velocity was attained during the 5 msec immediately following the arrival of the shock wave at F-47 (8785), however, this velocity was very shortly reversed and the airplane attained a maximum upward velocity of 8.5 ft/sec at 0.15 sec. This velocity gradually diminished due to the acceleration of gravity until it was zero at 0.50 sec at which time the displacement was at a maximum of approximately 30 in. The airplane then began to fall and hit the ground at approximately 1.085 sec.

The F-47 (8785) was demolished on Shot 4 as shown in Figs. 3.107 through 3.110. Integration of the acceleration curve for F-47 (8785) on Shot 4 indicated that at 0.285 sec when the accelerometer cable broke, the airplane had an upward component of 26 ft/sec. Integration of the velocity curve indicated that the airplane was 33 in. off of the ground when the cable broke.

Figures A.32 and A.46 show comparisons of normal acceleration and wing bending moment on B-17 (5715) for Shots 3 and 4, respectively. Figure A.37 shows a comparison of the acceleration curves on F-47 (8785) for Shots 3 and 4. Inspection of the graph indicates that very little if any correlation exists. The shot 3 acceleration curve shows an initial negative peak of -6 "G's" which may be explained by the fact that Shot 3 was a relatively high burst, the angle with the horizontal of the line from the burst point to Station 2200 being 57°. The blast from the bomb would thus hit the airplane from this 57° angle causing it to accelerate toward the ground. The blast reflected from the ground, coupled with the recoil of the landing gear probably caused the positive 10.3 G acceleration peak ich appeared at time 15 msec on the graph. The acceleration curve on Shot 4 does not have the initial negative peak because of the low burst height.

The F-47 airplane was designed to withstand an acceleration of +7.33 and -3.0 G's. On Shot 3 at Station 2200 at a

[redacted]

peak overpressure of 8.4 psi the design limit was exceeded three times in the positive and three times in the negative direction on F-47 (8785). The first negative peak measured was -6 G's or 200 per cent of the design limit, and the first positive peak measured was 10.3 G's, about 150 per cent of the design limit. At an overpressure of 9.4 psi, on Shot 4 at Station 2200, the design limit was exceeded in the positive direction with peaks of 10 and 11.6 G's being recorded. The acceleration curve indicates that the design limit of +7.33 G's was exceeded for a period of 30 msec. F-47 (8785) was demolished on this shot.

A.4.5.2 Lateral Acceleration Measurements

Lateral acceleration of F-47 (9785) was measured on Shot 3 and the data obtained is presented in Fig. A.51. Integration of the acceleration curve yielded a maximum velocity of lateral movement away from ground zero of 6.6 ft/sec at 0.10 sec which dropped to zero at 0.52 sec. The maximum displacement of the airplane away from ground zero was 21 in. at 0.52 sec.

On Shot 4 a lateral acceleration measurement was obtained on F-47 (9785) at Station 4000, where the overpressure was 5.8 psi. The airplane was rotated approximately 90° by the blast on this shot as described in A.3.4.2. Integration of the Shot 4 lateral acceleration with respect to time indicated that a maximum velocity of 9.0 ft/sec was attained at 0.19 sec. This velocity dropped to zero at 0.53 sec. The displacement at this point obtained by integrating the velocity curve, reached a maximum of 33 in. In the calculations made above the effects of angular acceleration due to the rotation of the airplane was considered negligible, although it is noted that the direction of the acceleration being measured changed 90° with the rotation of the airplane, and the velocities and distances were approximately those of the C.G. of the airplane moving on a curved path.

Figures A.51 and A.62 show comparison of lateral acceleration and fin bending moment on Shots 3 and 4, respectively. The lateral acceleration curves for Shots 3 and 4 are compared in Fig. A.45. The curve for Shot 4 has been shifted on the time axis so that the points of initial deflection are superimposed. The curves are similar in shape, the one significant difference being that the first peak after the maximum is very much smaller on Shot 4 as compared to Shot 3. This could be due to the rotation of the airplane on Shot 4.

A.4.6 Overpressure Measurements on Aircraft Surfaces

Many of the aircraft-surface pressure installations did not yield reliable data due to high thermal inputs which ruined the transmitters and due also to the extremely rapid oscillations of their galvanometer traces. In addition, although the reliable measurements indicated the actual overpressure at the point of installation, they

[redacted]

did not in most cases indicate the maximum value of pressure build-up which probably occurred. On the wings this maximum build-up was probably on the under side.

A.4.6.1 F-47 Wing

A comparison of the overpressure at a point on the ground measured on the wing of F-47 (0065) during Shot 2 is presented in Fig. A.29. The airplane was oriented with its nose into the blast and was resting in a normal, parked position. The difference in time which occurred between the initial deflections of the two curves occurred because the point at which the site overpressure was measured was at least 20 ft ahead of the aircraft pressure installation. A comparison of the peak pressures of the two curves indicates that the wing pressure was slightly larger than twice the site overpressure. The rapid drop-off of the wing overpressure indicates an equalization of the pressure on the outside of the wing surface. Inasmuch as the pressure transmitter was vented to the inside wing surface and the wing was full of openings which permitted the air to pass in and out quite easily, an accurate analysis of this pressure measurement after 68 msec, when the pressure returned to zero, could not be made. These features of this installation were responsible for the rapid equalization of the differential pressure.

A.4.6.2 F-47 Wing vs F-86 Wing

A comparison of the overpressures which were measured on the wings of F-86 (9597) and F-47 (0065) during Shot 4 is presented in Fig. A.30. Both aircraft were located at Station 4000 with their tails pointed toward ground zero. As would be expected, the F-47 experienced a greater wing overpressure because its conventional landing gear produced a greater angle of incidence between the blast and the upper wing surface. Peak overpressures of 8.8 and 11.5 psi, equivalent to 152 and 198 per cent of the 5.8 psi station overpressure, were recorded on the wings of the F-86 and F-47, respectively. The pressure transmitters on the F-86 and the F-47 wings were mounted on surfaces which made an angle with the horizontal of 3° and 15°, respectively. Variations in the airflow passing over the wing surfaces were probably the cause of the fluctuations which occurred as the pressure decayed. This rate of equalization appears to be quite similar for both of the aircraft configurations and seems to be identical for Shots 2 and 4 on the F-47. Two similar pressure installations located 10 in. apart were used to measure the F-47 (0065) wing pressure. When these two measurements were recorded during Shot 4, they were identically superimposed. Therefore, the curve which is presented in Fig. A.30 represents not one, but two independent measurements.

[redacted]

A.4.6.3 Wing Surface With Obtuse Angle of Incidence

One anomaly which presents itself in the comparison of site overpressure and the wing overpressure occurred during Shot 2 in the F-47 (0065) pressure measurements. The reported wing pressure was approximately twice that of the site overpressure, yet this measurement was made on a surface which had a 105° angle of incidence with respect to the shock front. This measurement was made at Station 8000, which was well beyond the formation of the Mach stem for such a low, weak shot as Shot 2. Therefore, the movement of the shock front was reasonably parallel to the ground and could not have caused a pressure build-up such as that which occurs when a blast wave strikes the front surface of a structure. An aerodynamic pressure does not seem possible; therefore, this data is presented only for possible correlation with future measurements or theoretical explanation.

[redacted]

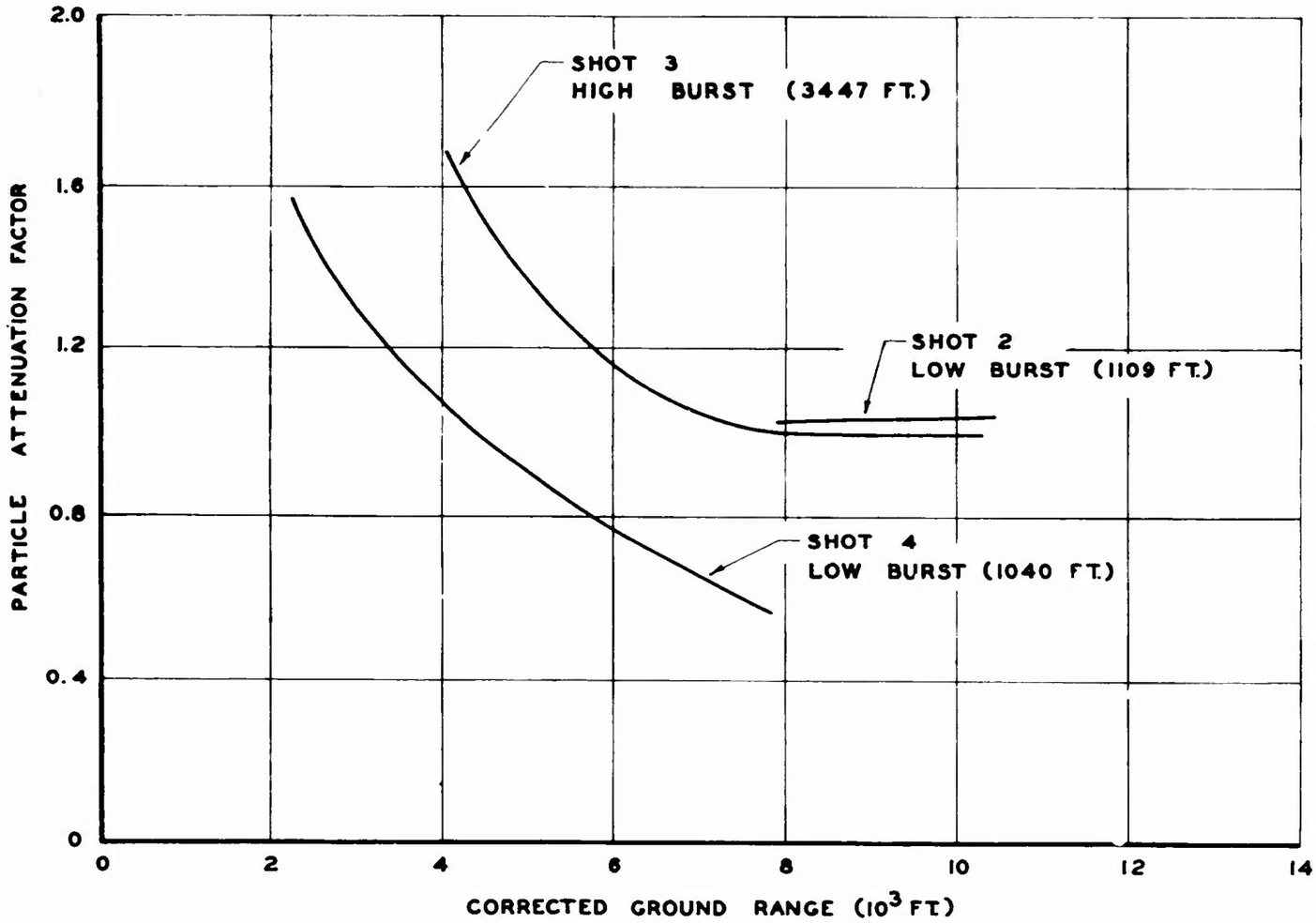

Fig. A.65 Comparison of the Variation of the Particle Attenuation Factor With Corrected Ground Range for Different Shots and Burst Altitudes

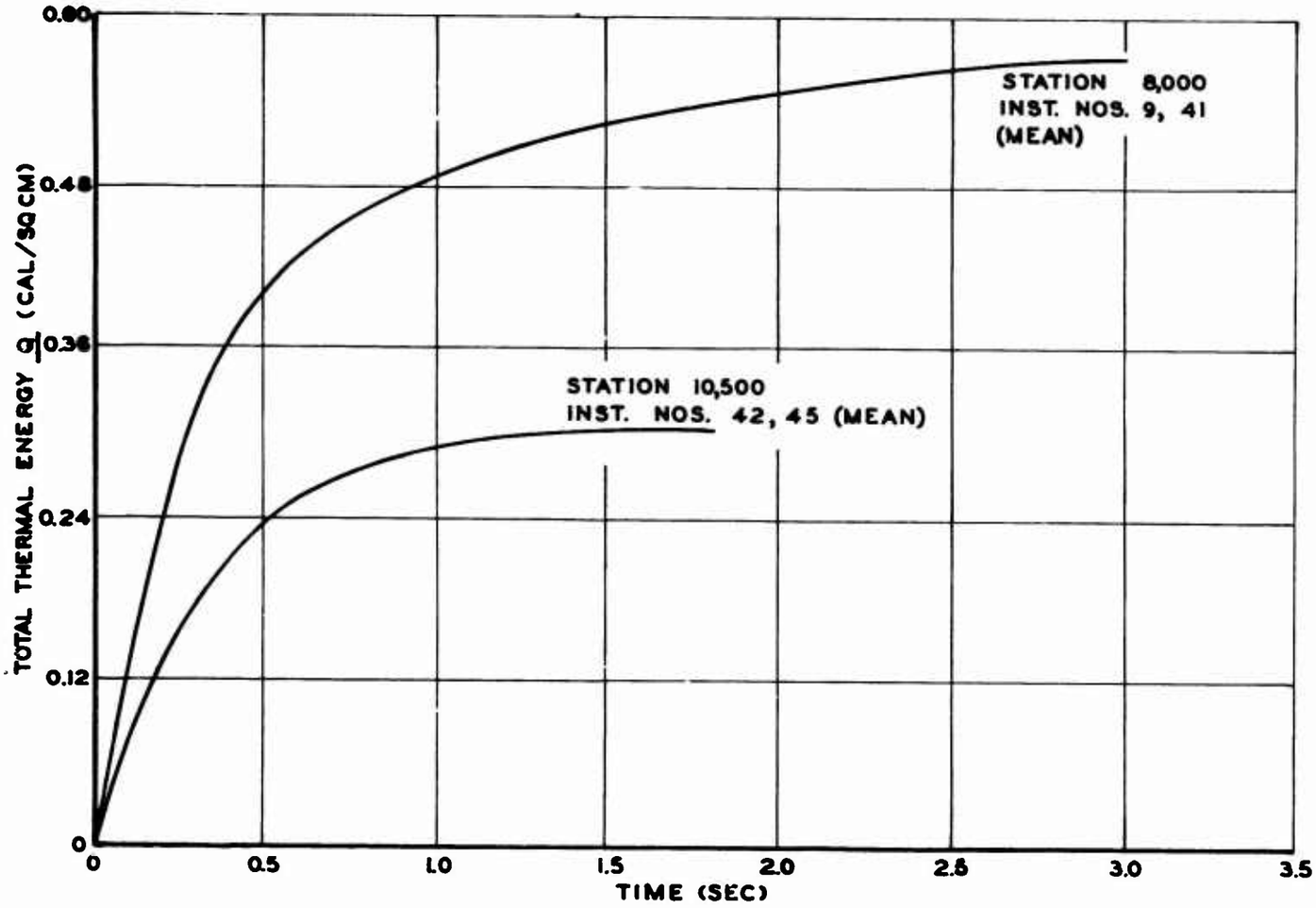

Fig. A.66 Comparison of the Variation of Corrected Total Thermal Energy With Time at Different Stations, Shot 2

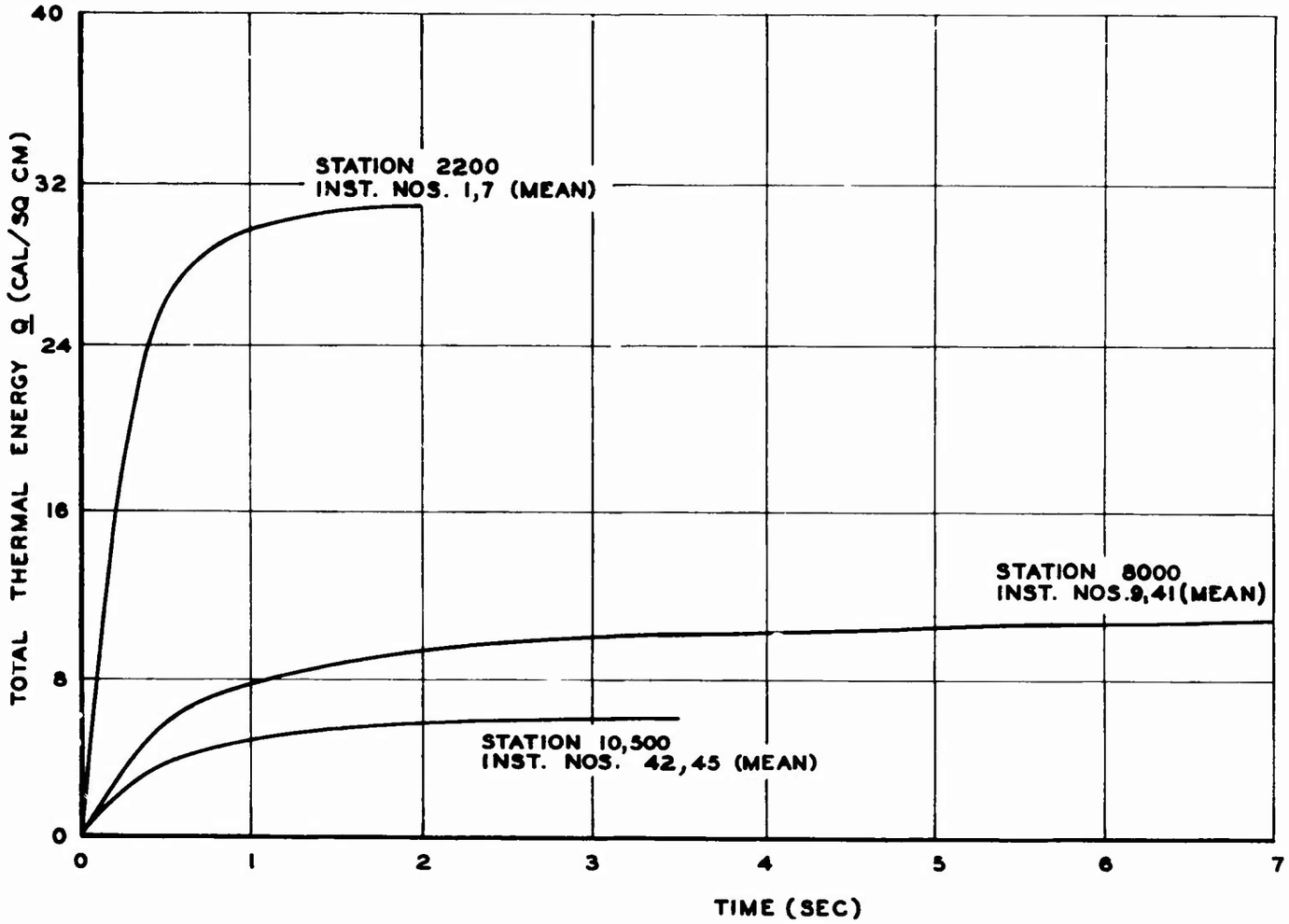

Fig. A.67 Comparison of the Variation of Corrected Total Thermal Energy With Time at Different Stations, Shot 3

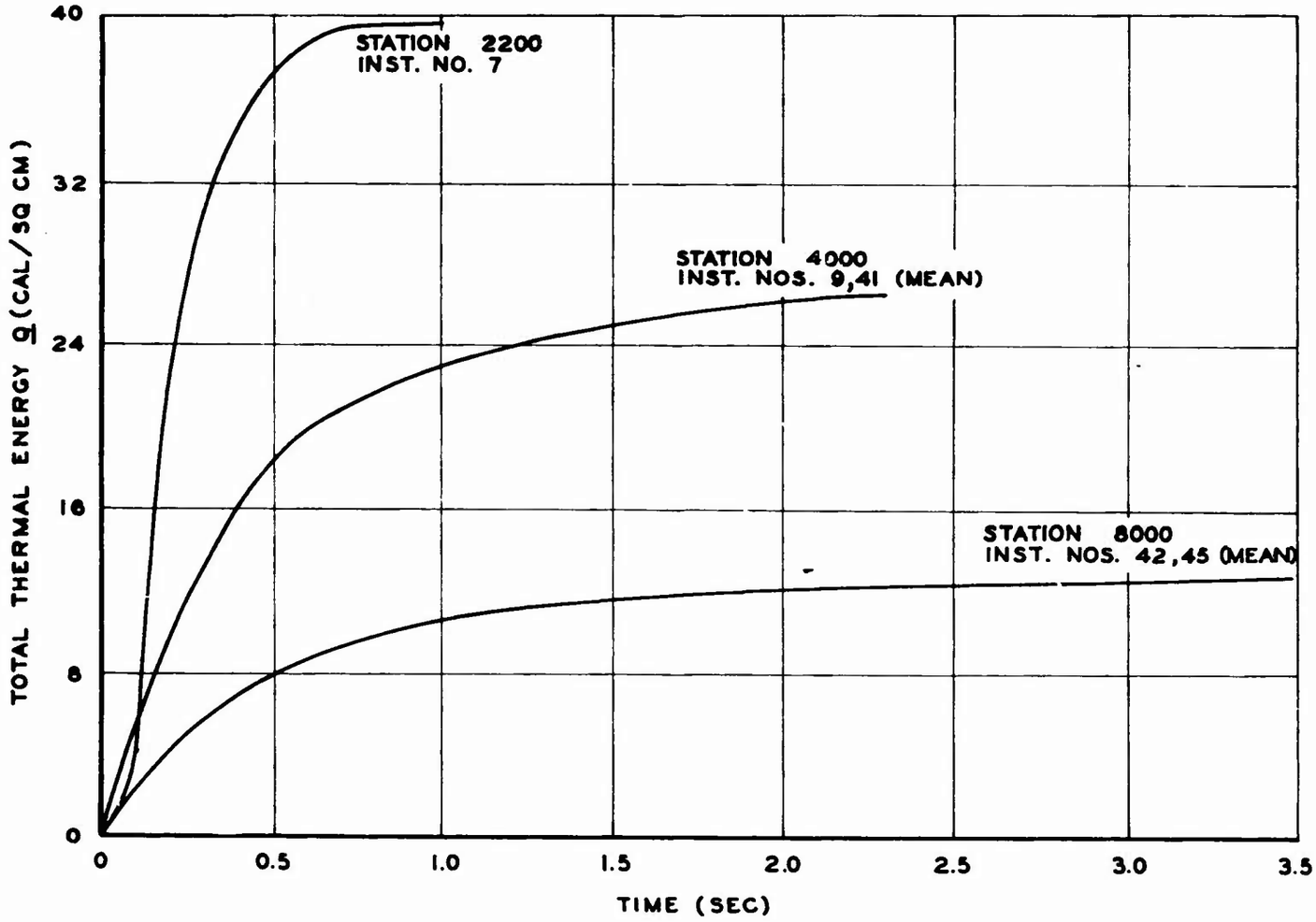

Fig. A.68 Comparison of the Variation of Corrected Total Thermal Energy With Time for Different Stations, Shot 4.

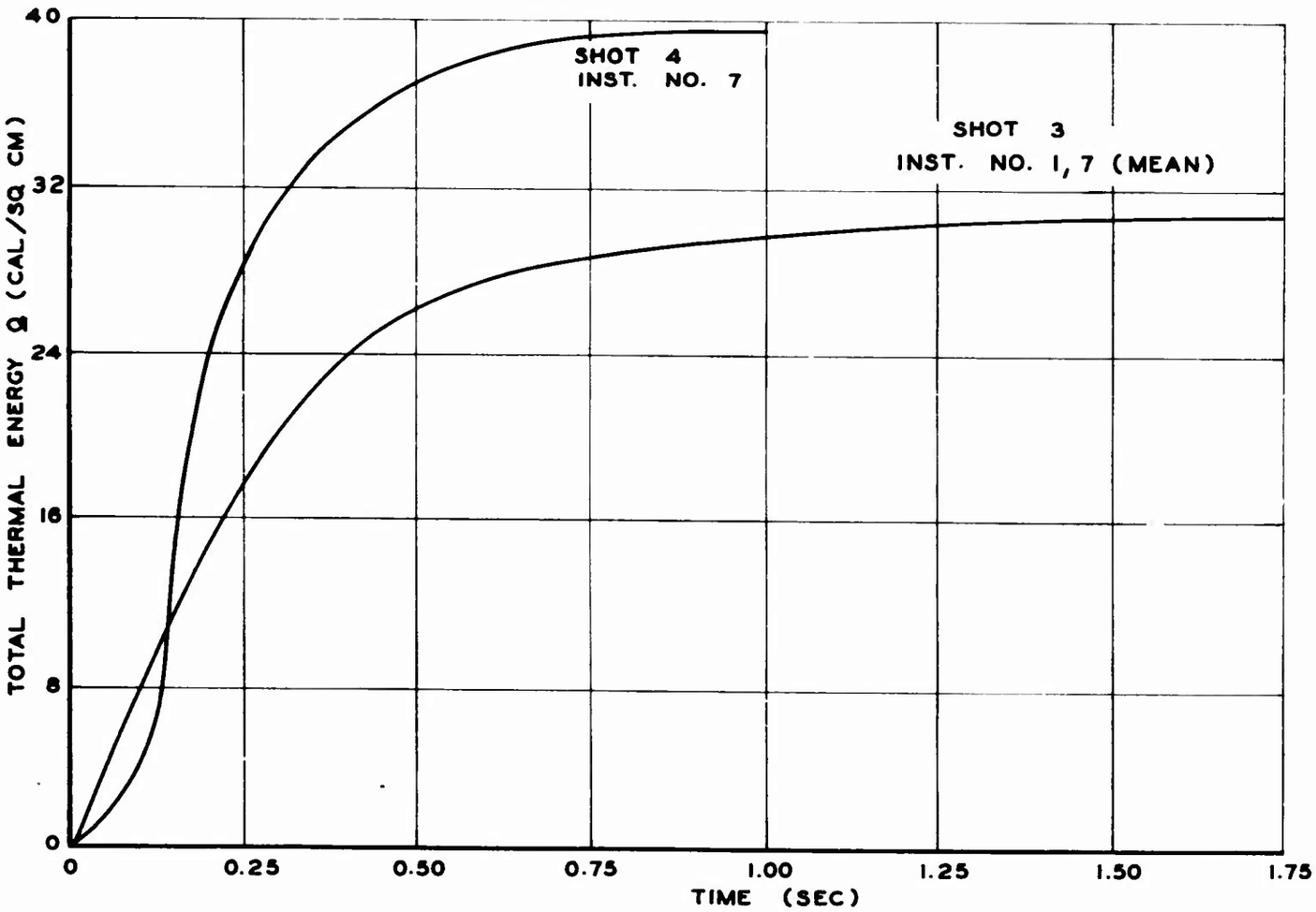

Fig. A.69 Comparison of the Variation of Corrected Total Thermal Energy With Time at Station 2200, Shots 3 and 4

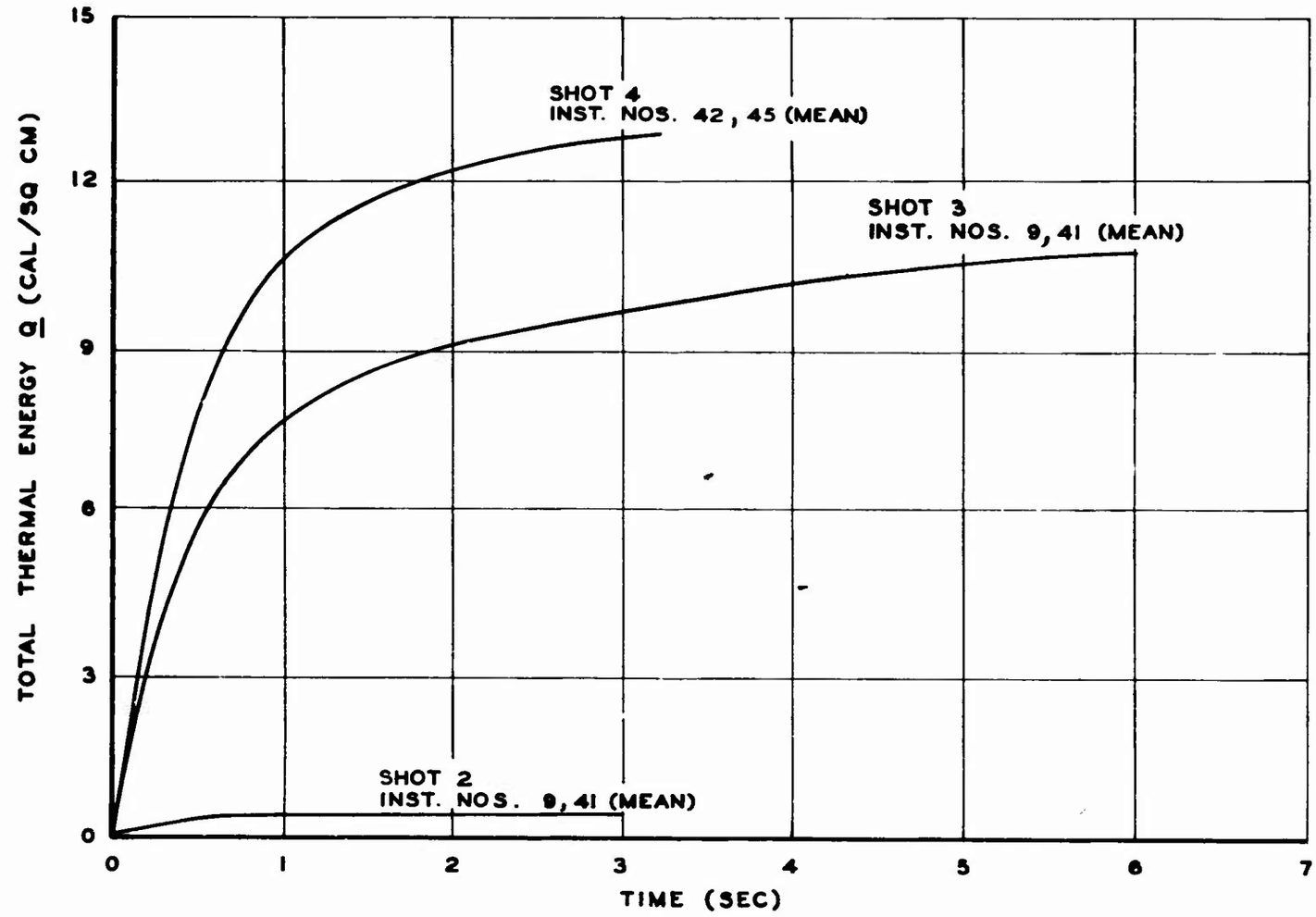

Fig. A.70 Comparison of the Variation of Corrected Total Thermal Energy With Time for Different Shots, Station 8000

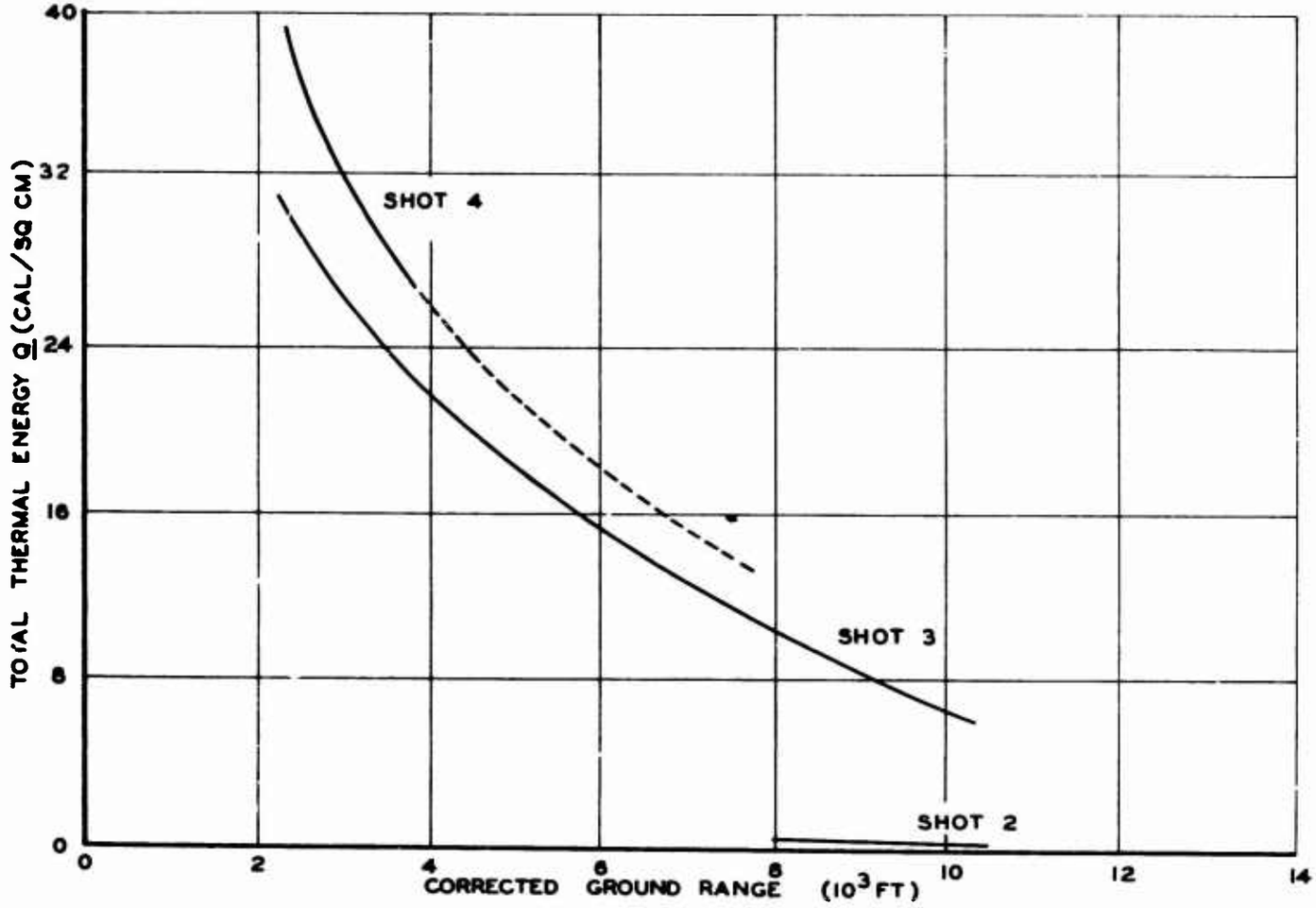

Fig. A.71 Comparison of the Variation of Peak Total Thermal Energy With Corrected Ground Range, at Different Shots

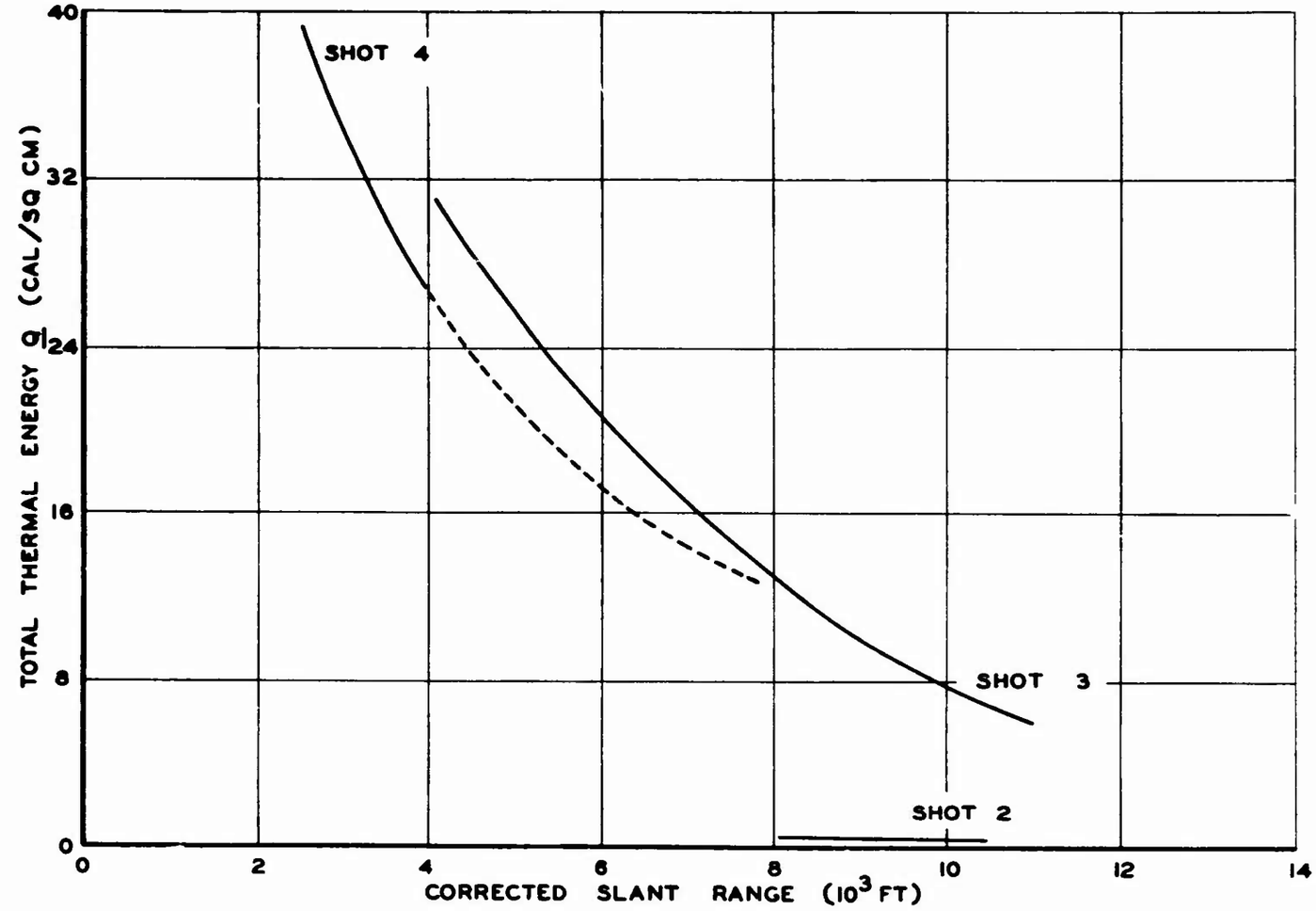

Fig. A.72 Comparison of the Variation of Peak Total Thermal Energy With Corrected Slant Range, at Different Shots

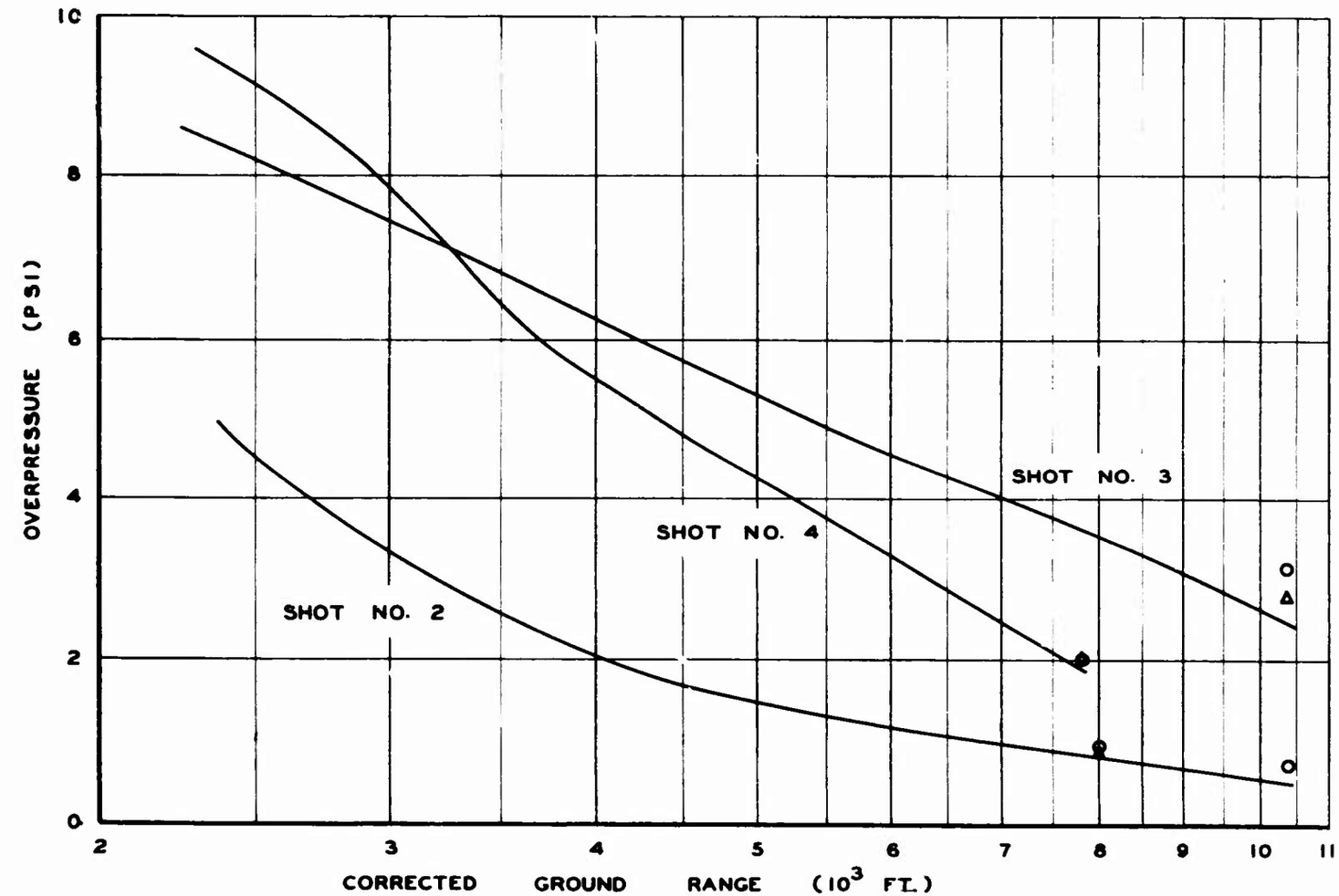

Fig. A.73 Comparison of the Variation of Peak Overpressure With Corrected Ground Range for Different Shots

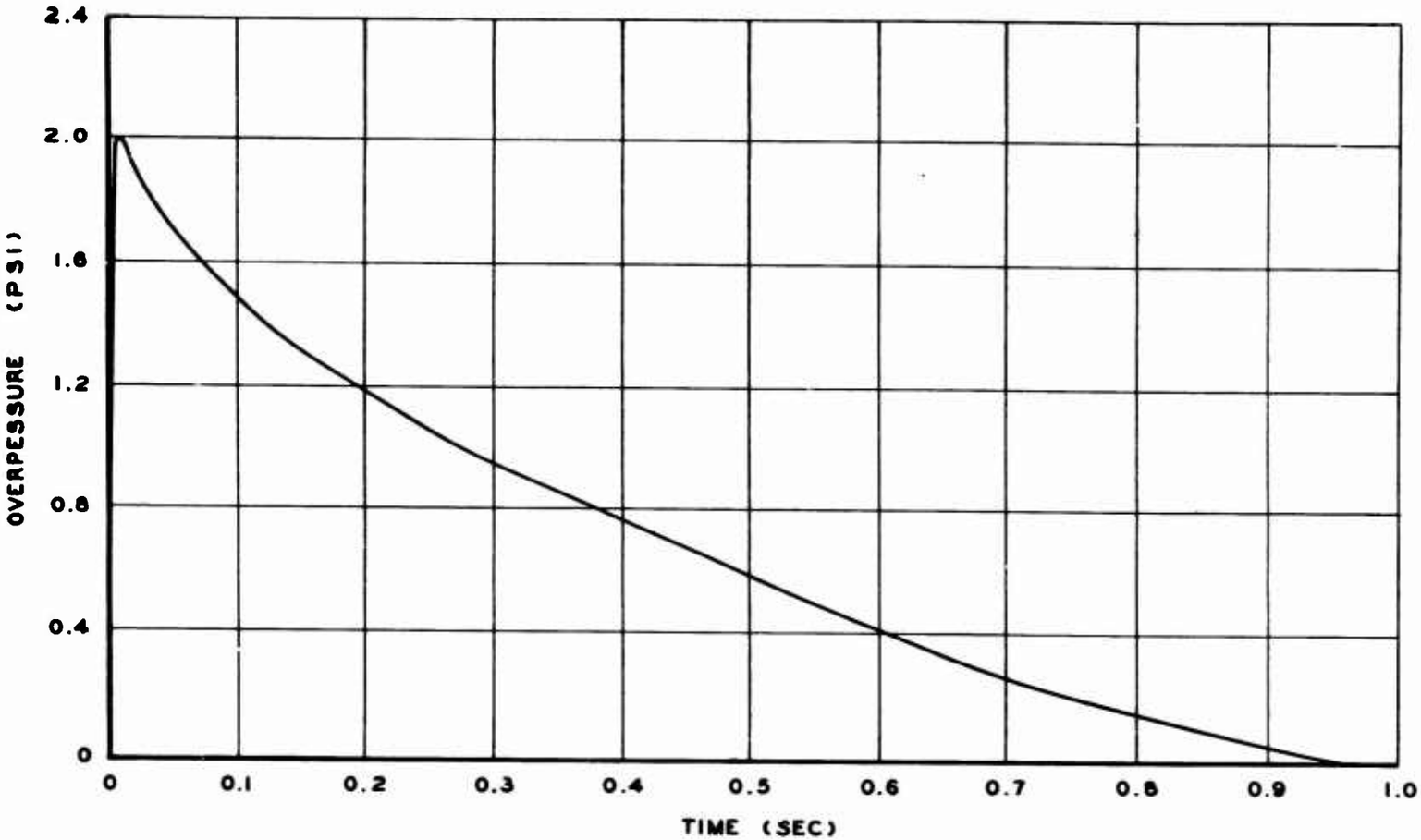

Fig. A.74 Variation of Overpressure With Time at a Point on the Ground, Station 8000, Shot 4

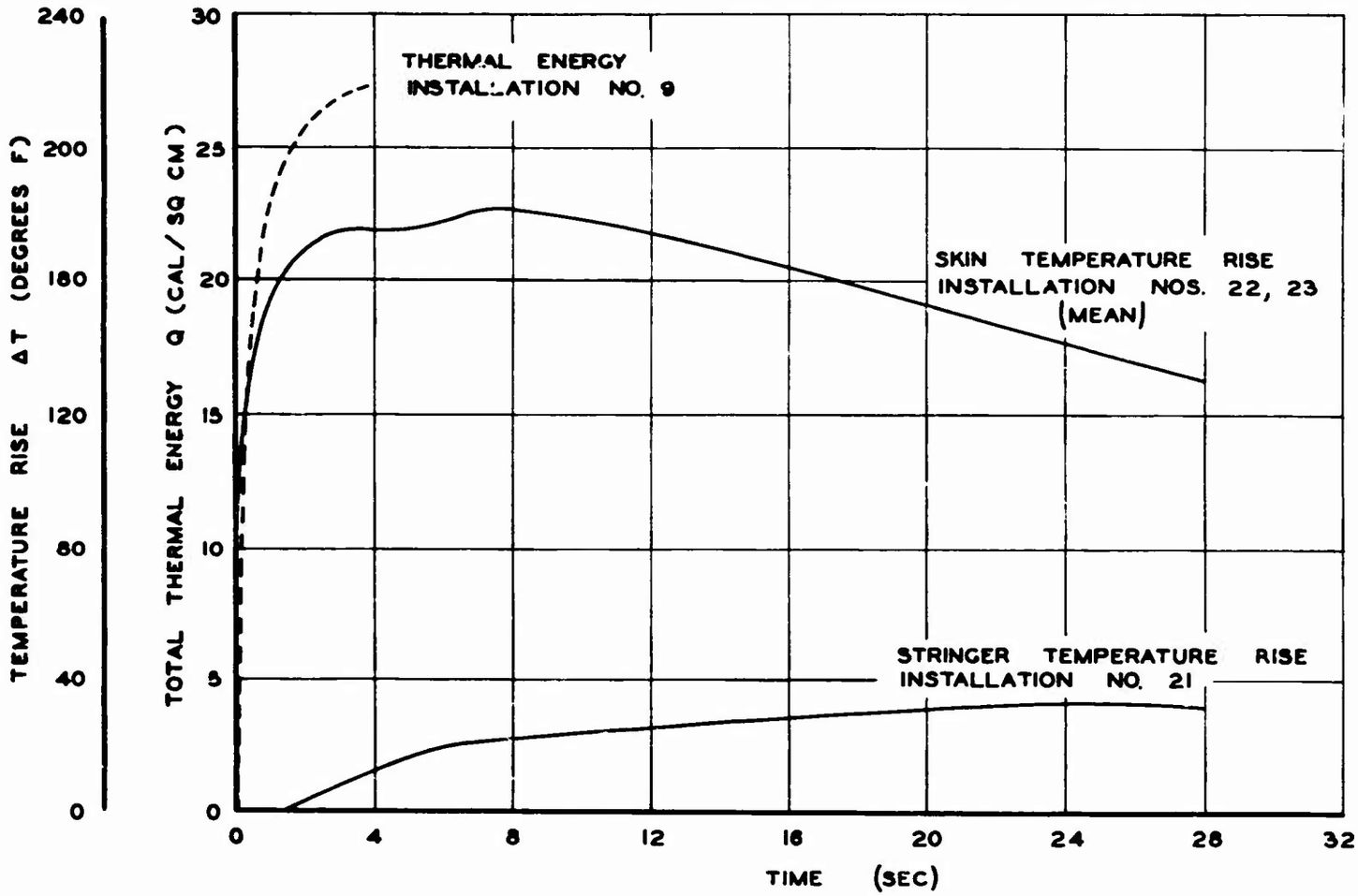

Fig. A.75 Comparison of the Variation of the Corrected Total Thermal Energy With Wing Temperature Rise of F-47 (0065), Angle of Incidence 67°, Station 4000, Shot 4. The Temperatures of the Stringer and Skin Just Before Zero Time Were 115°F and 130°F, Respectively.

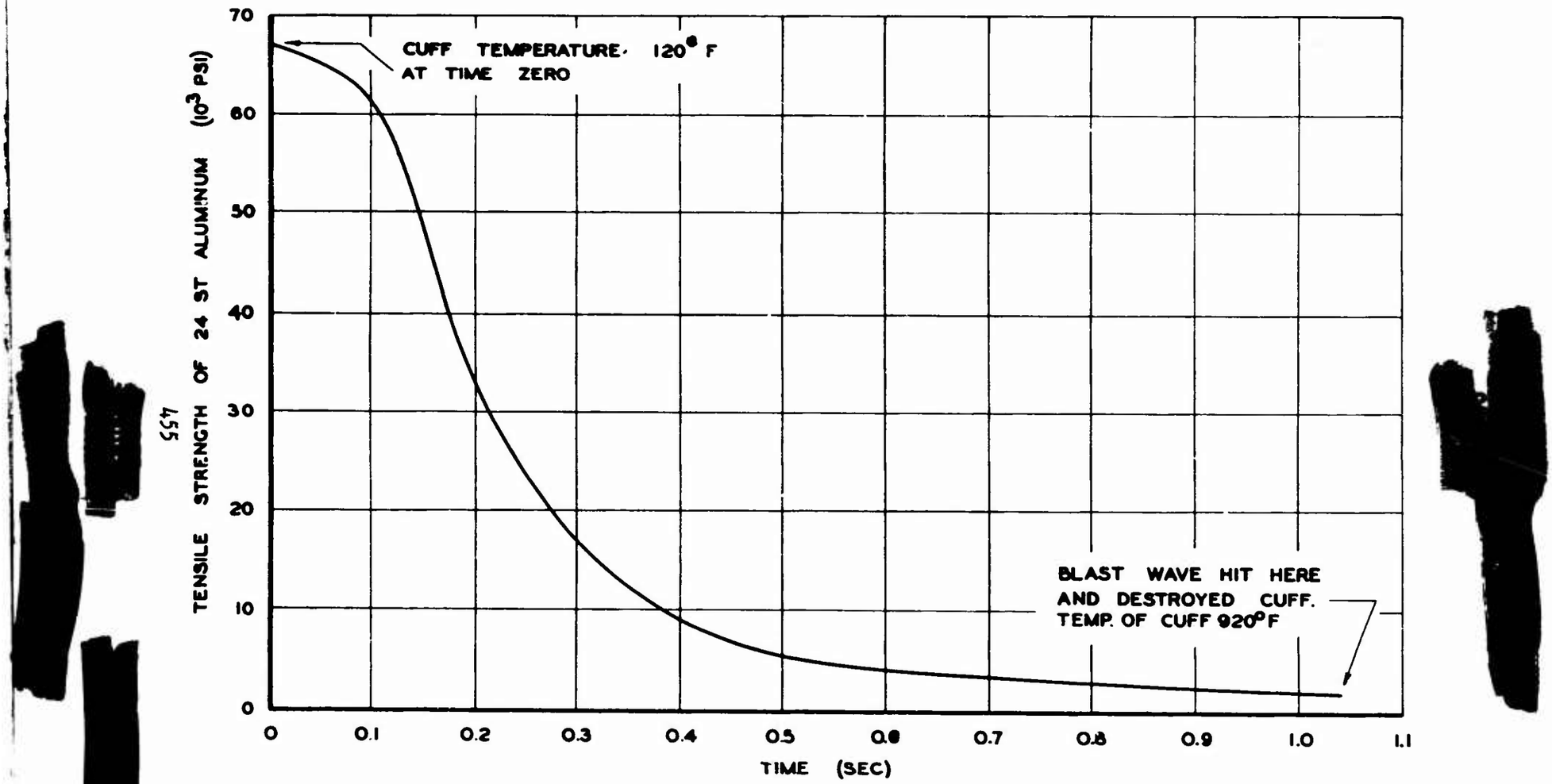

Fig. A.76 Variation of the Tensile Strength of an F-47 Prop Cuff With Time, Station 2200, Shot 4

Fig. A.77 F-47 Prop Cuff Showing Damage Caused by Thermal Radiation and Blast, Station 2200, Shot 3

[redacted]

APPENDIX B

SURVEY OF MAXIMUM SKIN TEMPERATURES

B.1 GENERAL

The investigation of maximum skin temperatures was a separate phase of the instrumentation program of Project 3.1. The objective of this investigation was to determine the maximum skin temperatures induced on parked aircraft exposed to various thermal energies from atomic detonations. The instrumentation for this phase consisted mainly of maximum temperature indicating tapes developed for Operation GREENHOUSE. The results and conclusions presented in this appendix constitute first approximations only.

B.2 TEMP TAPE INSTRUMENTATION

B.2.1 Temp Tape Configuration

Temp Tapes[1/] for Operation SNAPPER were manufactured, calibrated, and read by the University of Dayton. Their original design was modified for this operation. Each Temp Tape consisted of 14 temperature indicating patches mounted on the adhesive side of a 2 in. x 5-3/4 in. strip of temperature resistant adhesive tape. Each patch was assembled by first placing a 1/4 in. square of fish paper on the tape. Next, a 1/4 in. square, .004 in. to .007 in. thick, foil of a eutectic alloy was laid on the fish paper. Finally, a 1/2 in. square of commercial aluminum foil was placed over the alloy to hold it in position.

B.2.2 Mounting Procedure

The difference between the maximum temperatures on the inside and outside surfaces of thin skin aluminum has been found to be small. Therefore, all Temp Tapes could be placed on the inside skin surfaces of the test aircraft and effectively measure the maximum skin temperature. As these were the surfaces away from the thermal radiation, the tapes measured maximum skin temperatures only. The Temp Tapes were mounted adhesive side down on the skin surfaces. To insure

---

1/ J. C. Wayne, J. C. Lehmkuhl, "Blast Effects on Aircraft in Flight", Annex No. 8.1 to Scientific Director's Report as in GREENHOUSE Report No. 99, Operation GREENHOUSE; and Alphonso Ambrosio, Bertram Bussell, Calibration of a Temperature Measuring Device (Los Angeles 24, California: University of California, Department of Engineering, Under Air Force Contract AF 33(038)-14381, April 1951).

[redacted]

that the temperature sensitive patches had good thermal contact with the skin surfaces, these surfaces were thoroughly cleaned of all paint, oil and dirt, and the tapes were carefully smoothed down in place. The eutectic alloys in these patches had melting points ranging from 115°F to 554°F. Thus, each patch was sensitive to a different band of temperatures. When an instrumented surface was subjected to the thermal flux from a bomb, it experienced a rapid rise to a peak temperature and then slowly cooled to ambient temperature. The eutectic foils in the temperature sensitive patches melted successively as their respective melting points were reached and solidified during the cooling phase. By examining the temperature patches, it was possible to determine which of the eutectic foils had melted and their degree of melt, thereby establishing the maximum temperature experienced by the surface.

B.2.3 Organic Pigment Tapes

A report from the US Army Quartermaster described a new method of measuring maximum temperatures[2/]. The sensing elements used were black porous papers sprayed with white organic pigments. Each pigment had a specific melting point and upon melting was absorbed into the porous paper. This action appeared to change the color of the paper from white to black. It was believed that, once developed, temperature tapes using this type of sensing element would prove cheaper and easier to fabricate, easier to read, and, in view of the large number of organic pigments from which to choose, would provide better coverage of temperatures applicable to this investigation (150°F to 650°F).

It was decided to construct temperature tapes using pigmented papers. The assembly of these tapes was similar to that of the Temp Tapes. Fifteen, 1/4 in. square, pigmented papers were mounted, pigment side up, directly on the adhesive side of a 2 in. x 3-1/4 in. strip of temperature resistant tape. Since the time for fabrication was extremely limited, strips of commercial aluminum foil were substituted for the individual cover patches used in the Temp Tapes. The pigment tapes were mounted on the skin surfaces of the aircraft in the same manner as the Temp Tapes. The method of reading the pigment tapes was similar to that used for the Temp Tapes; but, instead of determining the degree of melting as on eutectic alloy foils, the degree of apparent color change of the papers was determined. In order to obtain the best comparison between the pigment tapes and the Temp Tapes, a large number of duplicate installations were made.

2/ Joseph D. Loconti, Stanley L. Knesback, E. D. Weil, "Temperature Indicator Papers", Research Service Test Report No. GC-30 (Philadelphia, Pennsylvania: Quartermaster Research and Development Laboratories, Pioneer Research Laboratories, October 1951).

B.3 CALIBRATION

Both the Temp Tapes and the pigment tapes were calibrated in the same manner. A one-foot square, 0.040 in. thick aluminum plate blackened on one side, was heated by an array of 750 watt photo flood bulbs. The temperature of this plate was measured with calibrated iron-constantan thermocouples and recorded by a high speed recording potentiometer. The temperature tapes were mounted on the side of this plate facing away from the radiation source. The plate was heated to various temperatures, and the maximum temperatures recorded by the tapes were compared with those recorded from the thermocouples. The Temp Tapes covered a temperature range of 122°F to 601°F in 70 gradations. The pigment tapes covered a range of 135°F to 530°F in 30 gradations. It was possible to determine five degrees of melting for each eutectic alloy (zero, 1/4, 1/2, 3/4, and complete). These alloys did not have sharp melting points because of the thermal lag introduced by the aluminum foil covers, and the effective air gap between the temperature patches and the instrumented skin. The results of the pigment tape calibration showed repeatability only for partial melt and complete melt conditions. These two degrees of melt differed as a rule by 40°F and were as much as 177°F apart. This wide variation was attributed to the use of aluminum cover strips instead of the separate aluminum cover patches used for the Temp Tapes.

B.3.1 Accuracy of Maximum Temperature Indicator Tapes

B.3.1.1 Eutectic Alloy Tapes

The accuracy of the Temp Tapes was a function of many variables. An outline of these variables is presented below:

Construction
1. Oxidation of metals during fabrication of the eutectic alloy foils.
2. Variation in the thickness of both the eutectic and the aluminum foils.
3. Variation in the assembly of the different temperature indicating patches.

Calibration
1. The slow rise time to maximum temperature during calibration as compared to the actual test conditions.
2. Normal reading error.

Installation
1. Variation in thermal contact between the skin and the temperature sensitive patches caused by:
   a. Variation in the surface conditions of the instrumented skins (scratches, oil, dirt).
   b. Variations in the applications of the tapes to the skin surfaces.

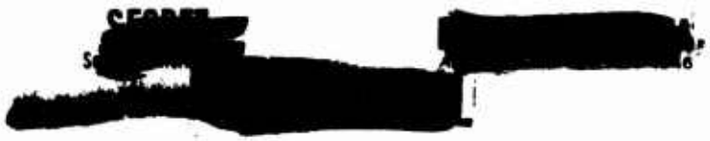

[redacted]

Operation During Test

1. Softening of adhesive.
2. Bulging of the center of the tapes at temperatures over 400°F caused by volatile chemicals in the adhesive.

Reading and Recording

1. Normal reading and recording errors.

The over-all accuracy of the Temp Tapes was considered to be ±10°F. This accuracy was determined from an examination of the calibration data and does not include the error introduced by the rapid rise time during the test. This rapid-rise time caused the Temp Tapes to indicate peak temperatures approximately 10 per cent to 15 per cent below those believed to have been experienced by the aircraft skin surfaces (Figs. B.1 and B.2).

B.3.1.2 Organic Pigment Tapes

An actual value of the accuracy of the pigment tapes is not given. These tapes had a greater thermal lag than the Temp Tapes, due to the use of the aluminum cover strips previously mentioned. The only maximum temperature readings reported from the pigment tapes were those between 369°F and 421°F. The Temp Tape readings did not cover this range; as a result, any value reported in this range should be considered approximate.

B.4 CORRELATING MEASUREMENTS

In order to correlate the maximum skin temperatures indicated by the Temp Tapes, data on the properties of the instrumented aircraft skin panels were needed. These data consisted of designation of type of material, skin thickness, angle of incidence to the blast, and absorptivity.

B.4.1 Skin Material

All instrumented surfaces were constructed of either 24ST or 75ST aluminum. The differences in density and specific heat of these two alloys were negligible. The following values were used: density 2.7 g/cm^3, and specific heat 0.23 g-cal/g °C.

B.4.2 Skin Thickness

A number of representative skin thicknesses were measured with a micrometer. These measurements together with the aircraft drawings were used to determine the skin thicknesses for all the instrumented surfaces. The standard error for these thicknesses was ±0.0025 in.

[redacted]

[redacted]

B.4.3 Incidence Angles at Surfaces

The incidence angle at a point on a surface was defined as the angle between the outward normal to that surface at the point and the line of sight from that point to the burst point. The angle between the tangent plane of the surface and the horizontal plane, the location of the surface on the aircraft, and the orientation and range of the aircraft were recorded. Using this information and the location of the actual burst point, the angle of incidence was computed. These computed angles were accurate to ±5°.

B.4.4 Absorptivities of Skin Surfaces

The absorptivities of the skin surfaces were approximated by photographic methods. A grey scale was made at the test site and photographed adjacent to various representative skin surfaces. This grey scale was composed of an aluminum sheet with nine painted strips ranging from white, absorptivity 0.30, to black, absorptivity 0.95, and one strip of bare aluminum, approximate absorptivity 0.35. The painted surfaces reflected diffused light; hence, they could be calibrated in a MacBeth illuminometer. The absorptivity of the aluminum surface was approximated, as no means were at hand to calibrate specular surfaces. Densitometer readings were taken on the photographic negatives, and comparisons between the grey scale readings and those of the skin surfaces were made. From these densitometer readings, photographs, and on site notes, an approximate absorptivity was determined for each instrumented skin surface. While these absorptivities were only approximate, they were believed fairly accurate for the zinc chromated surfaces with absorptivities over 0.7. These surfaces reflected diffused light, hence were sufficiently similar in reflective properties to the painted strips on the grey scale for valid comparison.

B.5 RESULTS

B.5.1 Maximum Skin Temperatures

Table B.1 contains over 300 maximum skin temperatures measured on Shots 2, 3, and 4. All the Temp-tape readings are recorded, but only pigment tape readings between 369°F and 421°F are recorded. This table also lists the location, skin thickness, incidence angle, absorptivity and maximum thermal energy for each instrumented skin surface. The accuracies of all values are indicated in the applicable column headings.

B.5.2 Thermal Input Comparisons

Figures B.1 and B.2 compare the thermal energies computed from the data in Table B.1 with those measured by NRDL and Project 3.1 (Appendix A).

[redacted]

[redacted]

B.5.3 Critical Thermal Energies for Various Aircraft Skin Surfaces

Figure B.3 presents a trend of critical incident thermal energies for various skin surfaces of parked aircraft and an estimate of the skin temperatures induced by these thermal energies. It is noted that doped fabric surfaces may burn when exposed to incident thermal energies as low as 2 cal/cm^2; and that .016 in. gage skin may sustain moderate damage at approximately 7 cal/cm^2. All aluminum skin surfaces sustained heavy damage when exposed to thermal energies sufficient to raise the surface temperatures to approximately 515^{o}F. The skin damage sustained was caused by both thermal and blast inputs. Since it was not possible to isolate completely thermal damage from blast damage, the actual thermal inputs required to produce a given degree of damage would be somewhat higher than indicated in Fig. B.3.

B.6 DISCUSSION

B.6.1 Correlation of Data

The problem of correlating the data presented in Table B.1 was complicated by a number of variables. First, the values in this table contained certain inaccuracies discussed in the section under instrumentation, the most important of which being those incurred in the determination of skin surface absorptivity. These errors could have caused variations in the correlated data as high as 20 per cent. Second, the incidence angle of the skin surface was calculated for time zero only, without compensation for the large diameter of the fireball nor for its vertical ascent. Therefore, the instrumented skin surfaces actually had varying, instead of fixed, angles of incidence. Third, the rise times to maximum temperature during the tests were of from 3 to 6 seconds duration and hence were much shorter than those obtained during calibration (approximately one minute). As a result, the Temp Tapes did not reach the same degree of melt per maximum temperature during the test as they did during calibration; this caused the Temp Tapes to indicate maximum temperatures approximately 10 per cent to 15 per cent below those experienced by the skin surfaces. Fourth, due to their complex structure, various sections of the aircraft had different thermal capacities; and thus, it was possible to have two or more surfaces on the same aircraft with the same skin thicknesses, incidence angles, and absorptivities and still have different maximum temperatures. Finally, the presence of the dust and water vapor raised by the bomb created local atmospheric attenuations of varying degrees and unknown magnitudes. As a result, the test aircraft were exposed to thermal energies somewhat different from those measured by NRDL and by Project 3.1 (Appendix A).

[redacted]

[redacted]

B.6.2 Discarded Data

There were approximately 100 points presented in Table B.1 which were not considered for correlation for the following reasons. First, the data from F-90 (6688) and F-47 (8785), Shot 2, 2200 ft, indicated maximum temperatures considerably above those expected at this range for aircraft with absorptivities approximating .45. These temperatures were attributed to those induced by solar radiation. The other two aircraft at this range had zinc chromated skin surfaces and, it was believed, had sufficiently high absorptivities to render usable data. Second, no data from surfaces with double thicknesses of skin were considered, as the heat transfer properties from one layer to the other were unknown. Third, data from the surfaces of the following aircraft were also not considered:

4 points	right wing	F-47 (9074)	Shot 3,	Station 8000
8 points	right and left wings	F-47 (9186)	Shot 4,	Station 4000
11 points	right and left fuselage and wings	F-47 (9110)	Shot 4,	Station 4000

From a study of the geometric configurations of the revetments and the burst heights of the bombs and from a comparison of the maximum skin temperature readings, it was concluded that these surfaces were shielded from the direct radiation of the bombs by the forward walls of their respective revetments. Finally, those data with incidence angles equal to 90 degrees or more were not correlated, as the correction for this angle could not be made. The remaining 218 points were considered for correlation.

B.6.3 Computed Incident Thermal Energies

The correlation which was selected entailed the computation of the theoretical thermal energies necessary to produce the indicated maximum skin temperatures reported in Table B.1. The formula used was

$$Q = \frac{M\ Cp\ \Delta T\ V}{A \cos \alpha} \qquad \text{where} \qquad \text{(B.1)}$$

Q =	Total thermal energy	cal/cm^2
M =	Density	$2.7\ g/cm^3$
ΔT =	Change in temperature	^oF
V =	Volume per unit area of skin	cm^3/cm^2
Cp =	Specific heat of aluminum	$.13\ cal/g\ ^oF$
A =	Absorptivity	(no units)
α =	Incidence angle	degrees

In order to compute ΔT, values of ambient skin temperature were assumed for each aircraft, and these values were subtracted from the indicated

[redacted]

[redacted]

maximum temperatures. The ambient skin temperatures were approximated by studying those reported in Appendix A and comparing the absorptivities of surfaces on which those temperatures were measured with the absorptivities of the surfaces instrumented with temperature tapes. The ambient skin temperatures assumed were:

Shot 2:

All ambient skin temperatures 90°F

Shots 3 and 4:

F-47 (8785) 115°F	F-47 (9785) 115°F
F-47 (9072) 125°F	F-47 (9931) 115°F
F-47 (9074) 125°F	F-47 (0065) 115°F
F-47 (9075) 125°F	F-86 (8209) 105°F
F-47 (9082) 125°F	F-86 (9597) 105°F
F-47 (9110) 115°F	F-90 (6688) 105°F
F-47 (9114) 125°F	B-17 (3575) 115°F
F-47 (9186) 115°F	B-17 (3722) 115°F
F-47 (9232) 125°F	B-17 (3769) 115°F
F-47 (9719) 115°F	

Of the 218 values considered 177 were correlated and 41 were discarded as bad data. The correlations consisted in determining the arithmetic mean of the computed thermal energies at each station. These means and the ranges of values correlated at each station were compared with the thermal energy data obtained by NRDL and Project 3.1 (Figs. B.1 and B.2). The fraction at each Temp-tape station represents the ratio of correlated points to the number of points considered. It is noted that the computed data points generally fell below the NRDL curve and the 3.1 curve. This result was attributed to the long response time of the Temp Tapes plus the atmospheric attenuation due to dust and vapors near the ground.

B.6.4 Critical Thermal Energies

Figure B.3 shows the trend of critical thermal energies for various aircraft skin surfaces and the approximate temperatures induced in the skin surfaces by these thermal energies. The data for this figure were obtained from an examination of all the post-shot photographs and all the aircraft damage reports submitted to this project. All data on damage to aluminum skins were divided into three groups: little or no damage, moderate damage, and heavy damage. All data on damage to doped fabric surfaces were also divided into three groups: unburned, charred, and burned. The incident thermal energy (corrected for angle of incidence) was computed for each skin surface. The data for each type and/or thickness of skin surface was then arranged in order of extent of damage, and a trend of critical thermal energies was

[redacted]

observed. The approximate temperatures of the aluminum surfaces induced by these thermal energies were computed by assuming an absorptivity of .5 and an ambient skin temperature of 110°F for each surface. It must be pointed out that it was not possible to separate the damage done to the skin surfaces by the thermal phase from that done by the blast phase. Hence, the data presented in Fig. B.3 are meant to indicate only the trend of critical thermal energies for 24ST aluminum skin and doped fabric surfaces.

B.6.5 Residual Effect on Material Properties

Test specimens were cut from the leading edge of F-47 (9114) after Shot 3 and examined to determine their structural properties. This examination indicated a reduction of approximately 25 per cent in the yield strength of the material and a reduction of approximately 20 per cent in the ultimate strength. The estimated maximum temperature experienced by this surface was 775°F.

B.6.6 Calibration

The calibration of the temperature tapes used for this project was accomplished after the test. As a result of this calibration and further experimentation, it was found that the thermal lags of both the eutectic foils and the pigmented papers could be considerably reduced by the removal of the commercial aluminum patches and strips and that the bulging of the Temp Tapes at high temperatures due to the volatile chemicals in the adhesive could be eliminated by perforating the tapes. Although there were many factors present during the test to cause inaccuracies in the data presented in Table B.1, the values correlated in Figs. B.1 and B.2 were sufficiently accurate for an investigation of the structural integrity of the instrumented skin surfaces.

B.6.7 Passive Defense

All test aircraft could have been effectively shielded from the thermal phases of the atomic detonations. This shielding could have been accomplished by a number of methods from carefully fitted asbestos covers to inexpensive fabrics draped over the aircraft. However, if the practice of parking aircraft under camouflage netting during wartime is expected to continue, this netting could very easily be designed to protect an aircraft from thermal radiation; it could also be designed to withstand certain overpressures and to include only fireproof or at least fire resistant materials. If this type of thermal protection were utilized, there would be little or no effect on the aircraft skin surfaces by the thermal phase of atomic bombs; this would probably result in reducing the damage done to these surfaces by the shock wave.

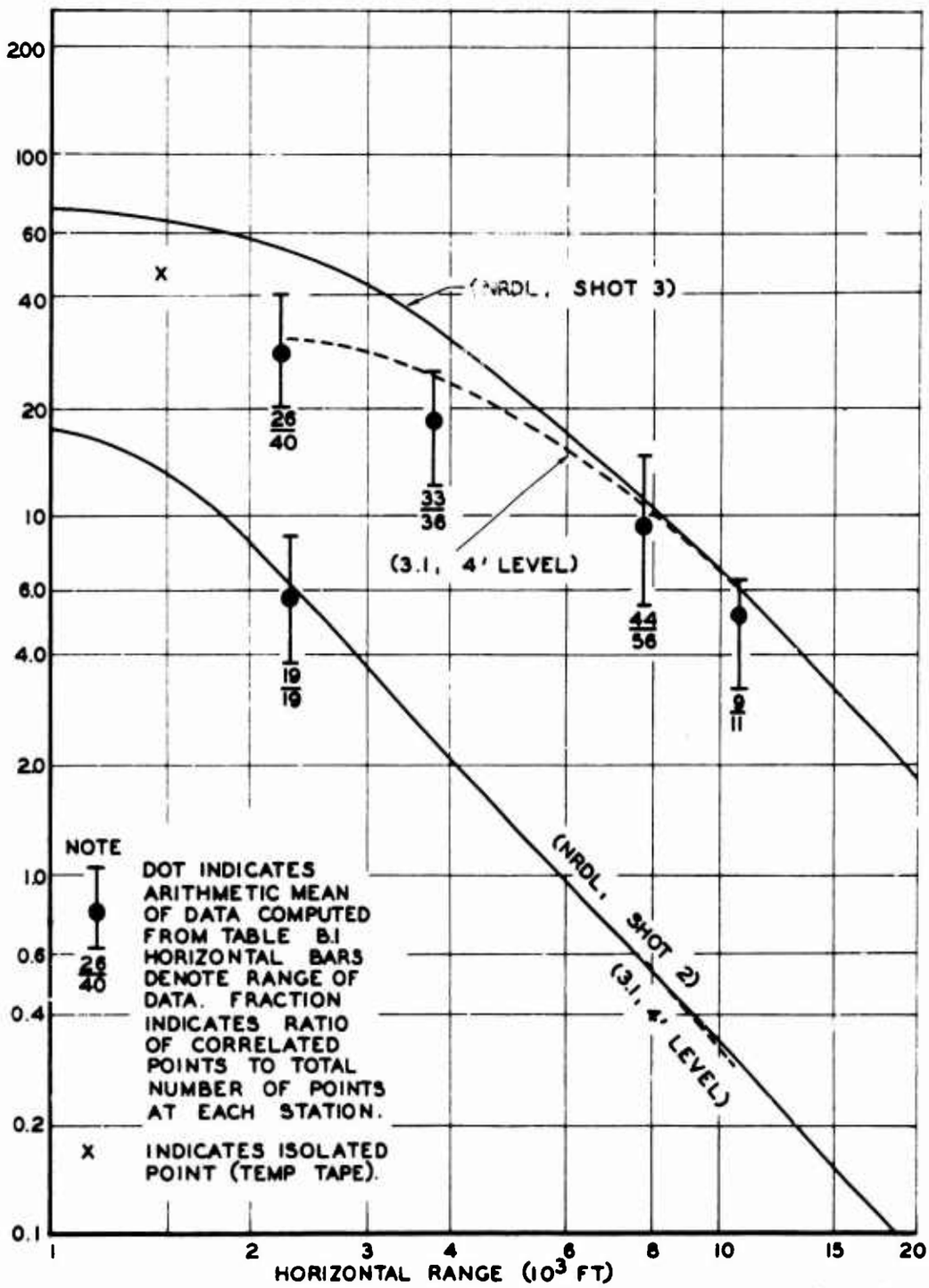

Fig. B.1 Comparison of Computed Thermal Energies From Temp Tape Data With Oscillographic Measurements by NRDL and by Project 3.1 for Shots 2 and 3. (NRDL Data Corrected to Zero Atmospheric Attenuation).

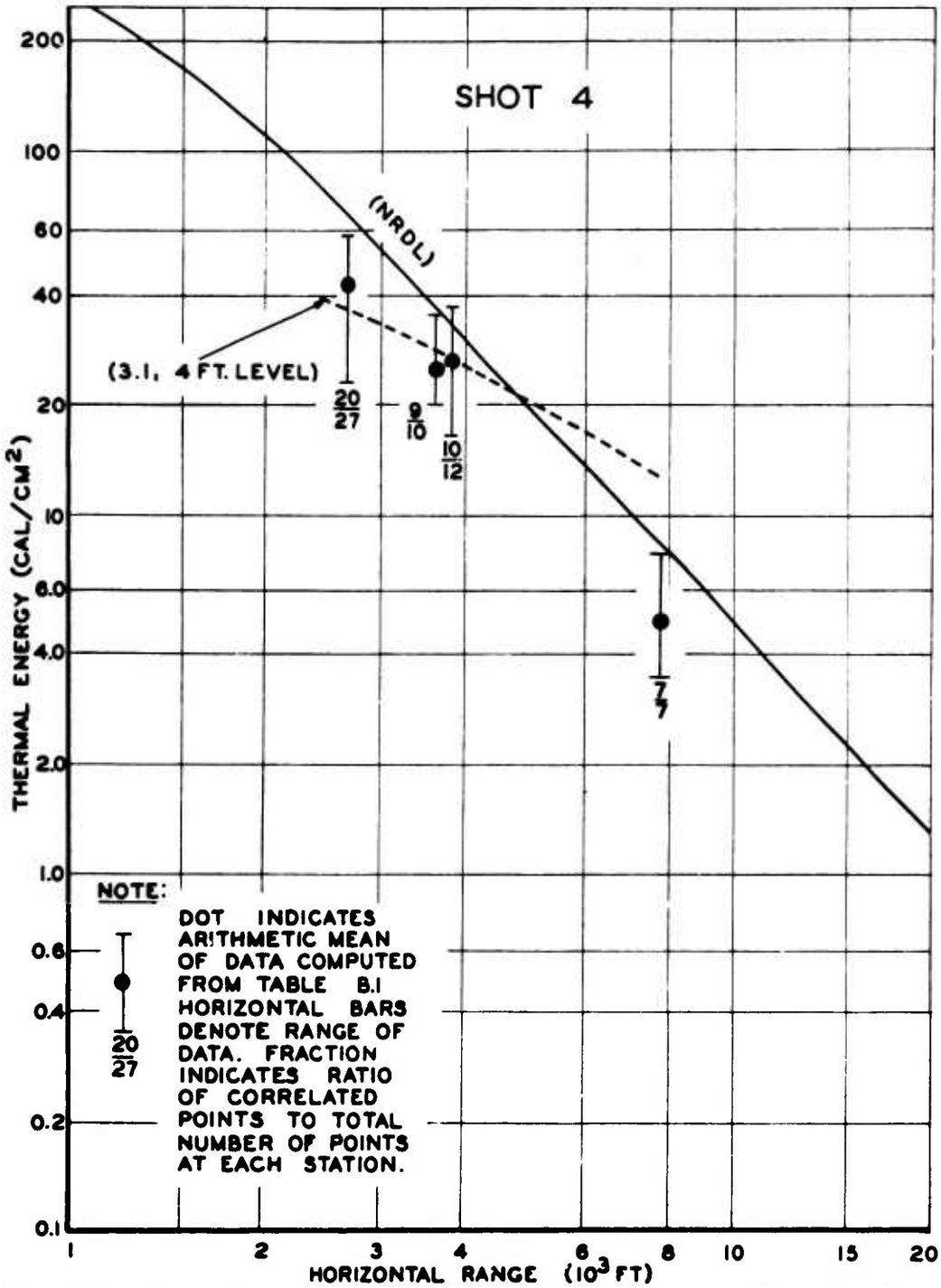

Fig. B.2 Comparison of Computed Thermal Energies From Temp Tape Data With Oscillographic Measurements by NRDL and by Project 3.1 for Shot 4. (NRDL Data Corrected to Zero Atmospheric Attenuation.)

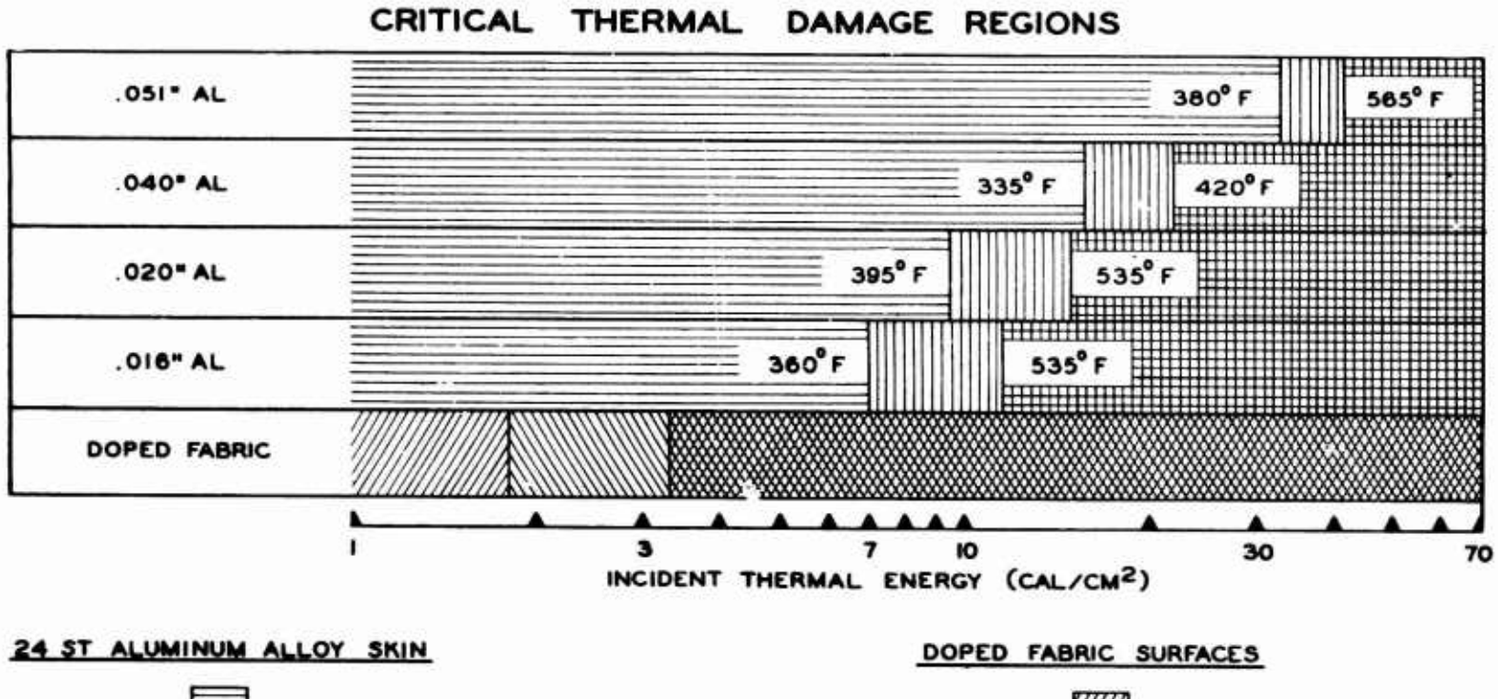

Fig. B.3 Trend of Critical Incident Thermal Energies for Various Skin Surfaces of Parked Aircraft Exposed to Atomic Detonations. Estimated Skin Temperatures at Critical Points Are Shown (Absorptivity .5 and Ambient Skin Temperature 110°F Assumed).

TABLE B.1

Maximum Skin Temperatures

Shot	Station	Total Thermal Energy (cal/cm^2) (a)	Aircraft & Orient.	Temp Tape Location (b)	Incidence Angle (c) $\pm 5^\circ$	Absorptivity (Approx.)	Skin Thickness $\pm$.0025 in.	Maximum Skin Temp. $\pm 10^\circ F$ (d)
B.1.1								
2	2200	5.7	F-90 (6688) Nose-in	RW	70	.43	.040	146
				RF	64	.43	.081	142
				RF	66	.43	.040(e)	154
				RF	66	.43	.040(e)	142
				RF	67	.43	.067	140
				RF	68	.43	.051	151
				RF	70	.43	.051	<122
				RF	72	.43	.051	153
				TF	66	.43	.032	157
				LF	69	.43	.051	187
				LF	68	.43	.067	150
				LF	66	.43	.040(e)	140
				LF	66	.43	.040(e)	140
				LF	65	.43	.081	156
				LF	69	.43	.051	136
				LF	71	.43	.051	147
				LW	69	.43	.040	140
			F-47 (8785) Nose-in	RW	78	.45	.040	146
				RW	78	.45	.040	140
				RW	80	.45	.040	141
				RW	80	.45	.040	144
				RF	79	.60	.040	152
				RF	72	.94	.040	152

TABLE B.1 (Continued)

Maximum Skin Temperatures

Shot	Station	Total Thermal Energy (cal/cm^2) (a)	Aircraft & Orient.	Temp Tape Location (b)	Incidence Angle (c) $\pm 5^o$	Absorptivity (Approx.)	Skin Thickness $\pm$.0025 in.	Maximum Skin Temp. $\pm 10^oF$ (d)
B.1.1 (Cont.)								
2	2200	5.7	F-47 (8785) Nose-in (Cont.)	RF	86	.60	.040	147
				RF	75	.60	.040	145
				LF	70	.94	.040	149
				LW	78	.45	.040	144
				LW	78	.45	.040	152
				LW	80	.45	.040	154
				LW	80	.45	.040	150
			F-47 (9232) Left Side-in	RW	65	.79	.040	143(f)
				RW	65	.79	.040	140(f)
				RW	65	.79	.040	136(f)
				LF	22	.79	.040	186(f)
				LF	10	.79	.040	200(f)
				LF	23	.50	.051(e)	188
				LF	13	.79	.040	201(f)
				LF	25	.79	.051	164(f)
				LW	66	.79	.040	143(f)
				LW	67	.79	.040	137(f)
			F-47 (9114) Tail-in	RW	51	.45	.040	151(f)
				RW	51	.79	.040	152(f)
				RW	50	.45	.032(e)	139
				RW	50	.45	.032(e)	148

TABLE B.1 (Continued)

Maximum Skin Temperatures

Shot	Station	Total Thermal Energy (cal/cm^2) (a)	Aircraft & Orient.	Temp Tape Location (b)	Incidence Angle (c) $\pm 5^o$	Absorptivity (Approx.)	Skin Thickness $\pm$.0025 in.	Maximum Skin Temp. $\pm 10^oF$ (d)
B.1.1 (Cont.)								
2	2200	5.7	F-47 (9114) Tail-in (cont.)	RF	68	.79	.040	151(f)
				RF	74	.79	.040	144(f)
				LF	64	.79	.040	149(f)
				LF	70	.79	.040	151(f)
				LW	50	.79	.040	152(f)
				LW	50	.79	.040	160(f)
				LW	47	.79	.040	149(f)
				LW	47	.79	.040	149(f)
B.1.2								
3	1000	70.0	F-47 (9114) Nose-in	RW	29	.79	.040	316
				RW	29	.79	.040	331
				RF	10	.79	.040	308
				RF	32	.79	.040	380
				RF	41	.79	.040	327
				LF	18	.79	.040	314
				LW	33	.79	.040	422
				LW	33	.79	.040	296
				LW	30	.79	.040	332
				LW	30	.79	.040	321

TABLE B.1 (Continued)

Maximum Skin Temperatures

Shot	Station	Total Thermal Energy (cal/cm^2) (a)	Aircraft & Orient.	Temp Tape Location (b)	Incidence Angle (c) $\pm 5^o$	Absorptivity (Approx.)	Skin Thickness $\pm .0025$ in.	Maximum Skin Temp. $\pm 10^oF$ (d)
B.1.3								
3	1384	64.0	F-47 (9232) Nose-in	RW	36	.79	.040	374
				RW	34	.79	.040	314
				RW	31	.79	.040	304
				RW	31	.79	.040	307
				RW	4	.79	.051	374
				RW	4	.79	.051	418
				LF	48	.79	.051	322
				LF	93	.79	.051(e)	318
				LF	79	.79	.040	325(f)
				LF	55	.79	.040	280
				LW	35	.79	.040	308
				LW	32	.79	.040	318
				LW	4	.79	.051	358
				LW	0	.79	.051	443
B.1.4								
3	2200	53.0	F-90 (6688) Nose-in	RW	37	.43	.040	316(f)
				RF	57	.43	.051	306(f)
				RF	36	.43	.040(e)	342
				RF	36	.43	.040(e)	321
				RF	35	.43	.081	308(f)
				RF	33	.43	.067	325(f)
				RF	37	.43	.051	306(f)

TABLE B.1 (Continued)

Maximum Skin Temperatures

Shot	Station	Total Thermal Energy (cal/cm^2) (a)	Aircraft & Orient.	Temp Tape Location (b)	Incidence Angle (c) ±5°	Absorptivity (Approx.)	Skin Thickness ±.0025 in.	Maximum Skin Temp. ±10°F (d)
B.1.4 (Cont.)								
3	2200	53.0	F-90 (6688) Nose-in (Cont.)	TF	33	.43	.032	363(f)
				TF	33	.43	.032	374(f)
				LF	40	.43	.040(e)	303
				LF	40	.43	.040(e)	342
				LF	40	.43	.067	317(f)
				LF	57	.43	.051	363
				LF	57	.43	.051	374
				LF	65	.43	.051	264(f)
				LF	42	.43	.051	313(f)
				LF	41	.43	.081	341
				LW	37	.43	.040	335(f)
			F-47 (8785) Nose-in	RW	50	.45	.040	374(f)
				RW	48	.45	.040	364(f)
				RW	48	.45	.040	379(f)
				RW	46	.45	.040	440(f)
				RW	46	.45	.040	435(f)
				RW	41	.45	.040	374(f)
				RW	41	.45	.040	374(f)
				RF	38	.94	.040	374
				RF	38	.94	.040	328
				RF	75	.60	.040	224(f)
				RF	64	.60	.040	317(f)

TABLE B.1 (Continued)

Maximum Skin Temperatures

Shot	Station	Total Thermal Energy (cal/cm^2) (a)	Aircraft & Orient.	Temp Tape Location (b)	Incidence Angle (c) $\pm 5^o$	Absorptivity (Approx.)	Skin Thickness $\pm .0025$ in.	Maximum Skin Temp. $\pm 10^oF$ (d)
B.1.4 (Cont.)								
3	2200	53.0	F-47 (8785) Nose-in (Cont.)	RF	46	.94	.040	440
				LW	42	.45	.040	374(f)
				LW	46	.45	.040	431(f)
				LW	46	.45	.040	441(f)
				LW	48	.45	.040	425(f)
				LW	46	.45	.040	274
			F-47 (9082) Right Side-in	RF	53	.55	.040	313(f)
				RF	8	.80	.040	395
				RF	12	.80	.040	357
				RF	53	.80	.040	425(f)
				RF	78	.88	.040	374
				RF	0	.87	.040	425
				RF	0	.87	.040	374
				RF	24	.80	.051	263
				RF	41	.80	.040	316
B.1.5								
3	4000	32.0	F-47 (9186) Right Side-in Wall Revetment	RW	49	.59	.040	324(f)
				RW	49	.59	.040	323(f)
				RW	50	.60	.040	325(f)
				RW	50	.60	.040	320(f)
				RF	7	.59	.040	332(f)

TABLE B.1 (Continued)

Maximum Skin Temperatures

Shot	Station	Total Thermal Energy (cal/cm²) (a)	Aircraft & Orient.	Temp Tape Location (b)	Incidence Angle (c) ±5°	Absorptivity (Approx.)	Skin Thickness ±.0025 in.	Maximum Skin Temp. ±10°F (d)
B.1.5 (Cont.)								
3	4000	32.0	F-47 (9186) Right Side-in Wall Revetment (Cont.)	LF	86	.59	.051	148
				LW	48	.60	.040	337(f)
				LW	48	.60	.040	356(f)
				LW	49	.60	.040	332(f)
				LW	49	.60	.040	328(f)
			F-47 (9075) Right Side-in	RW	49	.60	.040	374(f)
				RW	50	.60	.040	330(f)
				RW	50	.60	.040	330(f)
				RW	50	.60	.040	316(f)
				RW	50	.60	.040	317(f)
				RF	11	.60	.040	323(f)
				LF	89	.59	.040	148
				LW	48	.60	.040	373(f)
				LW	48	.60	.040	374(f)
				LW	48	.60	.040	362(f)
				LW	48	.60	.040	343(f)
				LW	49	.60	.040	362(f)
				LW	49	.60	.040	331(f)
			F-47 (9110) Right Side-in Pit Revetment	RW	50	.60	.040	246(f)
				RW	50	.60	.040	307(f)
				RW	50	.60	.040	285(f)

TABLE B.1 (Continued)

Maximum Skin Temperatures

Shot	Station	Total Thermal Energy (cal/cm^2) (a)	Aircraft & Orient.	Temp Tape Location (b)	Incidence Angle (c) $\pm 5^o$	Absorptivity (Approx.)	Skin Thickness $\pm$.0025 in.	Maximum Skin Temp. $\pm 10^oF$ (d)
B.1.5 (Cont.)								
3	4000	32.0	F-47 (9110) Right Side-in Pit Revetment (Cont.)	RW	50	.60	.040	300(f)
				RF	10	.59	.040	328(f)
				RF	22	.59	.040	173
				LF	87	.59	.040	177
				LF	78	.60	.040	158(f)
				LW	48	.60	.040	395(f)
				LW	48	.60	.040	379(f)
				LW	48	.60	.040	380(f)
				LW	48	.60	.040	348(f)
B.1.6								
3	8000	11.0	F-47 (9719) Nose-in G Type Revetment	RW	77	.45	.040	150(f)
				RW	77	.45	.040	157(f)
				RW	79	.45	.040	168
				RW	79	.45	.040	169
				RF	72	.95	.040	183(f)
				LF	71	.59	.040	142
				LW	76	.45	.040	150(f)
				LW	76	.45	.040	159(f)
				LW	78	.45	.040	147(f)
				LW	78	.45	.040	146(f)

TABLE B.1 (Continued)

Maximum Skin Temperatures

Shot	Station	Total Thermal Energy (cal/cm^2) (a)	Aircraft & Orient.	Temp Tape Location (b)	Incidence Angle (c) $\pm 5^o$	Absorptivity (Approx.)	Skin Thickness $\pm$.0025 in.	Maximum Skin Temp. $\pm 10^oF$ (d)
B.1.6 (Cont.)								
3	8000	11.0	F-47 (9074) Right Side-in G Type Revetment	RW	67	.73	.040	151
				RW	67	.73	.040	150
				RW	68	.73	.040	153
				RW	68	.73	.040	148
				RF	22	.59	.040	214(f)
				LF	109	.59	.040	173
				LW	66	.73	.040	194(f)
				LW	66	.73	.040	184(f)
				LW	66	.73	.040	186(f)
				LW	66	.73	.040	193(f)
			F-86 (8209) Right Side-in	RF	44	.43	.032	200(f)
				RF	31	.43	.032	216(f)
				RF	88	.43	.032	< 122
				RF	66	.43	.032	131
				RF	66	.43	.032	< 122
			F-47 (9072) Tail-in	RW	52	.60	.040	187(f)
				RW	52	.60	.040	185(f)
				RW	50	.60	.040	202(f)
				RW	50	.60	.040	208(f)
				RF	72	.59	.040	148
				LF	74	.59	.040	204

TABLE B.1 (Continued)

Maximum Skin Temperatures

Shot	Station	Total Thermal Energy (cal/cm^2) (a)	Aircraft & Orient.	Temp Tape Location (b)	Incidence Angle (c) $\pm 5°$	Absorptivity (Approx.)	Skin Thickness $\pm$.0025 in.	Maximum Skin Temp. $\pm 10°F$ (d)
B.1.6 (Cont.)								
3	8000	11.0	F-47 (9072) Tail-in (Cont.)	LW	53	.60	.040	216(f)
				LW	53	.60	.040	215(f)
				LW	51	.60	.040	251(f)
				LW	51	.60	.040	234(f)
			F-47 (0065) Nose-in	RW	77	.45	.040	175
				RW	80	.45	.040	176
				RW	80	.45	.040	170
			F-86 (9597) Nose-in	RW	55	.43	.062	179
				RW	55	.43	.062	170(f)
				RF	67	.43	.032	176(f)
				RF	69	.43	.032	150(f)
				LF	66	.43	.032	180(f)
				LF	68	.43	.032	149(f)
			F-47 (9785) Left Side-in	LF	26	.95	.040	331(f)
				LF	43	.95	.040	303(f)
				LF	25	.60	.040	252(f)
				LF	9	.60	.040	264(f)
				LW	67	.45	.040	175(f)
				LW	67	.45	.040	159(f)

TABLE B.1 (Continued)

Maximum Skin Temperatures

Shot	Station	Total Thermal Energy (cal/cm^2) (a)	Aircraft & Orient.	Temp Tape Location (b)	Incidence Angle (c) ±5°	Absorptivity (Approx.)	Skin Thickness ±.0025 in.	Maximum Skin Temp. ±10°F (d)
B.1.6 (Cont.)								
3	8000	11.0	F-47 (9785) (Cont.)	LW	67	.45	.040	154(f)
				LW	67	.45	.040	161(f)
			B-17 (3722) Left Side-in	LF	31	.55	.051	252(f)
				LF	31	.55	.051	241(f)
				LF	12	.94	.051	271(f)
				LF	6	.94	.051	268(f)
				LF	11	.94	.051	306(f)
				LF	48	.55	.051	183(f)
				LF	78	.55	.051	129(f)
				LF	24	.55	.051	206(f)
				LF	6	.55	.051	205(f)
B.1.7								
3	10500	6.7	B-17 (3769) Right Side-in	RF	36	.55	.051	176(f)
				RF	36	.55	.051	179(f)
				RF	29	.55	.051	182(f)
				RF	17	.55	.051	170(f)
				RF	12	.55	.051	180(f)
				RF	8	.55	.051	155(f)
				RF	3	.55	.051	148
				RF	4	.55	.051	170(f)

479

TABLE B.1 (Continued)

Maximum Skin Temperatures

Shot	Station	Total Thermal Energy (cal/cm^2) (a)	Aircraft & Orient.	Temp Tape Location (b)	Incidence Angle (c) $\pm 5^\circ$	Absorptivity (Approx.)	Skin Thickness $\pm$.0025 in.	Maximum Skin Temp. $\pm 10^\circ$F (d)
B.1.7 (Cont.)								
3	10500	6.7	B-17 (3769) Right Side-in (Cont.)	RF	9	.94	.051	302
				RF	43	.55	.051	148(f)
				RF	47	.55	.051	161(f)
B.1.8								
4	2200	83.0	F-47 (8785) Nose-in	RW	69	.45	.040	237
				RW	69	.45	.040	215
				RW	69	.45	.040	220
				RW	69	.45	.040	192
				RF	69	.94	.040	205
				RF	82	.60	.040	189
				RF	68	.94	.040	216
				LF	74	.94	.040	295
				LW	84	.45	.040	212
				LW	84	.45	.040	212
				LW	82	.45	.040	250
B.1.9								
4	2500	68.0	F-47 (9931) Left Side-in	LW	71	.45	.040	226(f)
				LW	72	.45	.040	208(f)

TABLE B.1 (Continued)

Maximum Skin Temperatures

Shot	Station	Total Thermal Energy (cal/cm^2) (a)	Aircraft & Orient.	Temp Tape Location (b)	Incidence Angle (c) $\pm 5^\circ$	Absorptivity (Approx.)	Skin Thickness $\pm$.0025 in.	Maximum Skin Temp. $\pm 10^\circ F$ (d)
B.1.9 (Cont.)								
4	2500	68.0		RW	67	.43	.040	279(f)
				RW	67	.43	.051	138
				RW	67	.43	.051	138
				RF	90	.43	.081	137
				RF	91	.43	.040(e)	135
				RF	91	.43	.040(e)	135
				RF	86	.43	.067	128
				RF	87	.43	.051	136
			F-90 (6688)	RF	129	.43	.051	374
			Left Side-in	TF	69	.43	.032	322(f)
				LF	46	.43	.051	438
				LF	50	.43	.067	362(f)
				LF	44	.43	.040(e)	288
				LF	44	.43	.040(e)	262
				LF	42	.43	.081	316(f)
				LF	42	.43	.081	374(f)
				LW	71	.43	.1875	188
				LW	71	.43	.1875	194
				LW	71	.43	.040	321(f)
			F-47 (9719)	RW	75	.45	.040	246(f)
			Nose-in	RW	75	.45	.040	270(f)
				RW	77	.45	.040	210(f)

TABLE B.1 (Continued)

Maximum Skin Temperatures

Shot	Station	Total Thermal Energy (cal/cm^2) (a)	Aircraft & Orient.	Temp Tape Location (b)	Incidence Angle (c) $\pm 5^o$	Absorptivity (Approx.)	Skin Thickness $\pm .0025$ in.	Maximum Skin Temp. $\pm 10^oF$ (d)
B.1.9 (Cont.)								
4	2500	68.0	F-47 (9719) Nose-in (Cont.)	RW	77	.45	.040	194(f)
				RF	71	.95	.040	161
				LF	76	.59	.040	302(f)
				LW	76	.45	.040	260(f)
				LW	76	.45	.040	228(f)
				LW	74	.45	.040	257(f)
				LW	74	.45	.040	280(f)
			F-86 (8209) Nose-in	RF	69	.43	.032	257(f)
				RF	71	.43	.032	214(f)
				RF	106	.43	.032	176
				RF	99	.43	.032	214
				RF	99	.43	.032	190
B.1.10								
4	3320	41.0	F-47 (9072) Nose-in	RW	81	.60	.040	179(f)
				RW	81	.60	.040	210(f)
				RW	84	.60	.040	164(f)
				RW	84	.45	.040	168(f)
				RF	76	.59	.040	148
				LF	79	.59	.040	239(f)
				LW	82	.60	.040	183(f)

TABLE B.1 (Continued)

Maximum Skin Temperatures

Shot	Station	Total Thermal Energy (cal/cm²) (a)	Aircraft & Orient.	Temp Tape Location (b)	Incidence Angle (c) ±5°	Absorptivity (Approx.)	Skin Thickness ±.0025 in.	Maximum Skin Temp. ±10°F (d)
B.1.10 (Cont.)								
4	3320	41.0	F-47 (9072) Nose-in (Cont.)	LW	82	.60	.040	176(f)
				LW	80	.60	.040	202(f)
				LW	80	.60	.040	194(f)
B.1.11								
4	4000	33.0	F-47 (0065) Tail-in	RW	63	.45	.040	268(f)
				RW	59	.45	.040	322(f)
				RW	59	.45	.040	301(f)
			F-86 (9597) Tail-in	RW	83	.43	.062	137(f)
				RW	83	.43	.062	145
				RF	76	.43	.032	167(f)
				RF	74	.43	.032	182(f)
				LF	74	.43	.032	263(f)
				LF	75	.60	.032	248(f)
			F-47 (9186) Tail-in Wall Revetment	RW	58	.60	.040	172
				RW	58	.60	.040	147
				RW	63	.59	.040	165
				RW	63	.59	.040	153
				RF	78	.59	.040	187(f)
				LF	79	.59	.051	251

TABLE B.1 (Continued)

Maximum Skin Temperatures

Shot	Station	Total Thermal Energy (cal/cm^2) (a)	Aircraft & Orient.	Temp Tape Location (b)	Incidence Angle (c) ±5°	Absorptivity (Approx.)	Skin Thickness ±.0025 in.	Maximum Skin Temp. ±10°F (d)
B.1.11 (Cont.)								
4	4000	33.0	F-47 (9186) Tail-in Wall Revetment (Cont.)	LW	58	.60	.040	143
				LW	58	.60	.040	167
				LW	60	.60	.040	189
				LW	60	.60	.040	173
			F-47 (9110) Tail-in Pit Revetment	RW	61	.60	.040	149
				RW	61	.60	.040	145
				RW	60	.60	.040	146
				RW	60	.60	.040	146
				RF	77	.59	.040	137
				RF	79	.59	.040	138
				LF	79	.59	.040	218(f)
				LF	72	.60	.040	144
				LW	60	.60	.040	141
				LW	60	.60	.040	143
				LW	62	.60	.040	142
				LW	62	.60	.040	144
B.1.12								
4	8000	8.0	B-17 (3575) Left Side-in	LF	17	.95	.051	239(f)
				LF	32	.55	.051	195(f)

TABLE B.1 (Continued)

Maximum Skin Temperatures

Shot	Station	Total Thermal Energy (cal/cm^2) (a)	Aircraft & Orient.	Temp Tape Location (b)	Incidence Angle (c) ±5°	Absorptivity (Approx.)	Skin Thickness ±.0025 in.	Maximum Skin Temp. ±10°F (d)
B.1.12 (Cont.) 4	8000	8.0	B-17 (3575) Left Side-in (Cont.)	LF	37	.55	.051	150(f)
				LF	14	.30	.051	152(f)
				LF	12	.76	.051	175(f)
				LF	45	.55	.051	150(f)
				LF	16	.55	.051	170(f)

(a) Zero atmospheric attenuation.
(b) RW - Right wing; RF - Right side of fuselage; TF - Top of fuselage; LF - Left side of fuselage; LW - Left wing.
(c) The incidence angle of a surface is defined as the angle in degrees between the outward normal to a point on that surface and the line of sight from that point to the burst point.
(d) All temperatures are approximately 10% to 15% below those believed to have been experienced by the skin surfaces.
(e) Two layers of skin. Value represents the thickness of each layer.
(f) Value correlated in Figure B.1.

PRECEDING PAGE BLANK-NOT FILMED

CONFIDENTIAL

DISTRIBUTION

	Copy No.
ARMY ACTIVITIES	
Asst. Chief of Staff, G-2, D/A, Washington 25, D. C.	1
Asst. Chief of Staff, G-3, D/A, Washington 25, D. C. ATTN: DCofS, G-3, (RR&SW)	2
Asst. Chief of Staff, G-4, D/A, Washington 25, D. C.	3
Chief of Ordnance, D/A, Washington 25, D. C. ATTN: ORDTX-AR	4
Chief Signal Officer, D/A, P&O Division, Washington 25, D. C. ATTN: SIGOP	5- 7
The Surgeon General, D/A, Washington 25, D. C. ATTN: Chairman, Medical Research and Development Board	8
Chief Chemical Officer, D/A, Washington 25, D. C.	9- 10
Chief of Engineers, D/A, Military Construction Division, Protective Construction Branch, Washington 25, D. C. ATTN: ENGEB	11
Chief of Engineers, D/A, Civil Works Division, Washington 25, D. C. ATTN: Engineering Division, Structural Branch	12
The Quartermaster General, CER, Liaison Office, Research and Development Division, D/A, Washington 25, D. C.	13
Office, Chief of Transportation, Military Planning and Intelligence Division, Bldg. T-7, Washington 25, D. C.	14
Chief, Army Field Forces, Ft. Monroe, Va.	15- 21
Army Field Forces Board #1, Ft. Bragg, N. C.	22
Army Field Forces Board #2, Ft. Knox, Ky.	23
Army Field Forces Board #4, Ft. Bliss, Tex.	24
Commanding General, First Army, Governor's Island, New York 4, N. Y. ATTN: G-1	25
Commanding General, First Army, Governor's Island, New York 4, N. Y. ATTN: G-2	26
Commanding General, First Army, Governor's Island, New York 4, N. Y. ATTN: G-3	27
Commanding General, First Army, Governor's Island, New York 4, N. Y. ATTN: G-4	28- 29
Commanding General, Second Army, Ft. George G. Meade, Md. ATTN: AIABB	30
Commanding General, Second Army, Ft. George G. Meade, Md. ATTN: AIABD	31- 38

CONFIDENTIAL

[redacted]

DISTRIBUTION (Continued) Copy No.

Commanding General, Third Army, Ft. McPherson, Ga. ATTN: ACofS, G-3	39- 40
Commanding General, Fourth Army, Ft. Sam Houston, Tex. ATTN: G-3 Section	41
Commanding General, Fifth Army, 1660 E. Hyde Park Blvd., Chicago 15, Ill. ATTN: ALFEN	42
Commanding General, Fifth Army, 1660 E. Hyde Park Blvd., Chicago 15, Ill. ATTN: ALFOR	43
Commanding General, Fifth Army, 1660 E. Hyde Park Blvd., Chicago 15, Ill. ATTN: ALFMD-O	44- 47
Commanding General, Fifth Army, 1660 E. Hyde Park Blvd., Chicago 15, Ill. ATTN: ALFHQ	48
Commanding General, Sixth Army, Presidio of San Francisco, Calif. ATTN: AMGCT-4	49
Commander-in-Chief, European Command, APO 403, c/o PM, New York, N. Y.	50
Commander-in-Chief, Far East Command, APO 500, c/o PM, San Francisco, Calif. ATTN: ACofS, G-3	51- 55
Commanding General, U. S. Army Europe, APO 403, c/o PM, New York, N. Y. ATTN: OPOT Division, Combat Dev. Branch	56- 57
Commanding General, U. S. Forces Austria, APO 168, c/o PM, New York, N. Y. ATTN: ACofS, G-3	58
Commanding General, U. S. Army Alaska, APO 942, c/o PM, Seattle, Wash.	59
Commanding General, U. S. Army Caribbean, APO 834, c/o PM, New Orleans, La. ATTN: CG, USARCARIB	60
Commanding General, U. S. Army Caribbean, APO 834, c/o PM, New Orleans, La. ATTN: CG, USARFANT	61
Commanding General, U. S. Army Caribbean, APO 834, c/o PM, New Orleans, La. ATTN: Chemical Officer, USARCARIB	62
Commanding General, U. S. Army Caribbean, APO 834, c/o PM, New Orleans, La. ATTN: Surgeon, USARCARIB	63
Commanding General, U. S. Army Pacific, APO 958, c/o PM, San Francisco, Calif. ATTN: Chemical Officer	64- 65
Commanding General, Trieste, U. S. Troops, APO 209, c/o PM, New York, N. Y. ATTN: ACofS, G-3	66
Commandant, Command and General Staff College, Ft. Leavenworth, Kan. ATTN: ALLIS(AS)	67
Commandant, The Infantry School, Ft. Benning, Ga. ATTN: C.D.S.	68- 69
Commandant, The Artillery School, Ft. Sill, Okla.	70
Commandant, The AA&GM Branch, The Artillery School, Ft. Bliss, Tex.	71
Commandant, The Armored School, Ft. Knox, Ky. ATTN: Classified Documents Section, Evaluation and Research Division	72- 73

[redacted]

[redacted]

DISTRIBUTION (Continued) Copy No.

Commanding General, Medical Field Service School, Brooke Army Medical Center, Ft. Sam Houston, Tex. 74
The Superintendent, U. S. Military Academy, West Point, N. Y. ATTN: Professor of Ordnance 75
Commandant, Chemical Corps School, Chemical Corps Training Command, Ft. McClellan, Ala. 76
Commanding General, Research and Engineering Command, Army Chemical Center, Md. ATTN: Special Projects Officer 77
RD Control Officer, Aberdeen Proving Ground, Md. ATTN: Director, Ballistics Research Laboratory 78- 79
Commanding General, The Engineer Center, Ft. Belvoir, Va. ATTN: Asst. Commandant, The Engineer School 80- 82
Commanding General, The Transportation Center and Ft. Eustis, Ft. Eustis, Va. ATTN: Asst. Commandant, Military Sciences and Tactics 83
Chief of Research and Development, D/A, Washington 25, D. C. 84
Commanding Officer, Transportation Research and Development Station, Ft. Eustis, Va. 85
Commanding Officer, Engineer Research and Development Laboratory, Ft. Belvoir, Va. ATTN: Chief, Technical Intelligence Branch 86
Commanding Officer, Picatinny Arsenal, Dover, N. J. ATTN: ORDBB-TK 87
Commanding Officer, Frankford Arsenal, Philadelphia 37, Pa. ATTN: RD Control Officer 88
Commanding Officer, Chemical Corps Chemical and Radiological Laboratory, Army Chemical Center, Md. ATTN: Technical Library 89- 90
Asst. Chief, Military Plans Division, Rm 516, Bldg. 7, Army Map Service, 6500 Brooke Lane, Washington 25, D. C. ATTN: Operations Plans Branch 91
Director, Technical Documents Center, Evans Signal Laboratory, Belmar, N. J. 92
Director, Waterways Experiment Station, PO Box 631, Vicksburg, Miss. ATTN: Library 93
Director, Operations Research Office, Johns Hopkins University, 6410 Connecticut Ave., Chevy Chase, Md. ATTN: Library 94

NAVY ACTIVITIES

Chief of Naval Operations, D/N, Washington 25, D. C. ATTN: OP-36 95- 96
Chief of Naval Operations, D/N, Washington 25, D. C. ATTN: OP-51 97

[redacted]

[redacted]

DISTRIBUTION (Continued) Copy No.

Chief of Naval Operations, D/N, Washington 25, D. C. ATTN: OP-53	98
Chief of Naval Operations, D/N, Washington 25, D. C. ATTN: OP-374 (OEG)	99
Chief, Bureau of Medicine and Surgery, D/N, Washington 25, D. C. ATTN: Special Weapons Defense Division	100-101
Chief, Bureau of Ordnance, D/N, Washington 25, D. C.	102
Chief, Bureau of Personnel, D/N, Washington 25, D. C. ATTN: Pers C	103
Chief, Bureau of Personnel, D/N, Washington 25, D. C. ATTN: Pers 112	104
Chief, Bureau of Ships, D/N, Washington 25, D. C. ATTN: Code 348	105
Chief, Bureau of Supplies and Accounts, D/N, Washington 25, D. C.	106
Chief, Bureau of Yards and Docks, D/N, Washington 25, D. C. ATTN: P-312	107
Chief, Bureau of Aeronautics, D/N, Washington 25, D. C.	108-109
Office of Naval Research, Code 219, Rm 1807, Bldg. T-3, Washington 25, D. C. ATTN: RD Control Officer	110
Commander-in-Chief, U. S. Atlantic Fleet, Fleet Post Office, New York, N. Y.	111
Commander-in-Chief, U. S. Pacific Fleet, Fleet Post Office, San Francisco, Calif.	112
Commander, Operational Development Force, U. S. Atlantic Fleet, USN Base, Norfolk 11, Va. ATTN: Tactical Development Group	113
Commandant, U. S. Marine Corps, Headquarters, USMC, Washington 25, D. C. ATTN: Code A03H	114-117
President, U. S. Naval War College, Newport, R. I.	118
Superintendent, USN Postgraduate School, Monterey, Calif.	119
Commanding Officer, USN Schools Command, Naval Station, Treasure Island, San Francisco, Calif.	120-121
Director, USMC Development Center, USMC Schools, Quantico, Va. ATTN: Marine Corps, Tactics Board	122
Director, USMC Development Center, USMC Schools, Quantico, Va. ATTN: Marine Corps, Equipment Board	123
Commanding Officer, Fleet Training Center, Naval Base, Norfolk 11, Va. ATTN: Special Weapons School	124
Commanding Officer, Fleet Training Center, (SPWP School), Naval Station, San Diego 36, Calif.	125-126
Commander, Air Force, U. S. Pacific Fleet, Naval Air Station, San Diego, Calif.	127
Commander, Training Command, U. S. Pacific Fleet, c/o Fleet Sonar School, San Diego 47, Calif.	128
Commanding Officer, Naval Damage Control Training Center, USN Base, Philadelphia 12, Pa. ATTN: ABC Defense Course	129

[redacted]

[redacted]

[redacted]

DISTRIBUTION (Continued) Copy No.

Commanding Officer, Naval Unit, Chemical Corps School, Ft. McClellan, Ala. 130
Joint Landing Force Board, Marine Barracks, Camp Lejeune, N. C. 131
Commander, USN Ordnance Laboratory, Silver Spring 19, Md. ATTN: EE 132
Commander, USN Ordnance Laboratory, Silver Spring 19, Md. ATTN: Alias 133
Commander, USN Ordnance Laboratory, Silver Spring 19, Md. ATTN: Alisx 134
Commander, USN Ordnance Test Station, Inyokern, China Lake, Calif. 135
Officer-in-Charge, USN Civil Engineering Research and Evaluation Laboratory, Construction Battalion Center, Port Hueneme, Calif. ATTN: Code 753 136-137
Director, USN Research Laboratory, Washington 25, D. C. 138
Commanding Officer and Director, USN Engineering Experiment Station, Annapolis, Md. ATTN: Code 155 139
Commanding Officer, USN Radiological Defense Laboratory, San Francisco, Calif. ATTN: Technical Information Division 140-141
Commanding Officer and Director, David W. Taylor Model Basin, Washington 7, D. C. ATTN: Library 142
Commander, Naval Air Development Center, Johnsville, Pa. 143
Commanding Officer, Office of Naval Research Branch Office, 1000 Geary St., San Francisco, Calif. 144-145

AIR FORCE ACTIVITIES

Surplus in TISOR for AFSWP 146
Asst. for Atomic Energy, Headquarters, USAF, Washington 25, D. C. ATTN: DCS/O 147
Asst. for Development Planning, Headquarters, USAF, Washington 25, D. C. 148-149
Director of Operations, Headquarters, USAF, Washington 25, D. C. 150-151
Director of Plans, Headquarters, USAF, Washington 25, D. C. ATTN: War Plans Division 152
Directorate of Requirements, Headquarters, USAF, Washington 25, D. C. ATTN: AFDRQ-SA/M 153
Directorate of Research and Development, Armament Division, DCS/D, Headquarters, USAF, Washington 25, D. C. 154
Directorate of Intelligence, Headquarters, USAF, Washington 25, D. C. 155-156
The Surgeon General, Headquarters, USAF, Washington 25, D. C. 157-158

[redacted]

[redacted]

DISTRIBUTION (Continued) Copy No.

Commanding General, USAF--Europe, APO 633, c/o PM, New York, N. Y. 159
Commanding General, Far East Air Forces, APO 925, c/o PM, San Francisco, Calif. 160
Commanding General, Alaskan Air Command, APO 942, c/o PM, Seattle, Wash. ATTN: AAOTN 161-162
Commanding General, Northeast Air Command, APO 862, c/o PM, New York, N. Y. 163
Commanding General, Strategic Air Command, Offutt AFB, Neb. ATTN: Chief, Operations Analysis 164
Commanding General, Tactical Air Command, Langley AFB, Va. ATTN: Documents Security Branch 165-167
Commanding General, Air Defense Command, Ent AFB, Colo. 168-169
Commanding General, Air Materiel Command, Wright-Patterson AFB, Dayton, Ohio 170-172
Commanding General, Air Training Command, Scott AFB, Belleville, Ill. 173-174
Commanding General, Air Research and Development Command, PO Box 1395, Baltimore 3, Md. ATTN: RDDN 175-177
Commanding General, Air Proving Ground Command, Eglin AFB, Fla. ATTN: AG/TRB 178
Commanding General, Air University, Maxwell AFB, Ala. 179-183
Commandant, Air Command and Staff School, Maxwell AFB, Ala. 184-185
Commandant, Air Force School of Aviation Medicine, Randolph AFB, Tex. 186-187
Commanding General, Wright Air Development Center, Wright-Patterson AFB, Dayton, Ohio. ATTN: WCOESP 188-193
Commanding General, AF Cambridge Research Center, 230 Albany St., Cambridge 39. Mass. ATTN: Atomic Warfare Directorate 194
Commanding General, Air Force Special Weapons Center, Kirtland AFB, N. Mex. ATTN: Chief, Technical Library Branch 195-197
Commandant, USAF Institute of Technology, Wright-Patterson AFB, Dayton, Ohio. ATTN: Resident College 198
Commanding General, Lowry AFB, Denver, Colo. ATTN: Department of Armament Training 199-200
Commanding General, 1009th Special Weapons Squadron, Tempo "T", 14th & Constitution Sts., NW, Washington 25, D.C. 201-203
The RAND Corporation, 1700 Main St., Santa Monica, Calif. ATTN: Nuclear Energy Division 204-205

OTHER DEPTS. OF DEFENSE ACTIVITIES

Executive Secretary, Joint Chiefs of Staff, Washington 25, D. C. 206

[redacted]

DISTRIBUTION (Continued) Copy No.

Director, Weapons Systems Evaluation Group, OSD, Rm 2E1006, Pentagon, Washington 25, D. C.	207
Asst. for Civil Defense, OSD, Washington 25, D. C.	208
Chairman, Armed Services Explosives Safety Board, D/D, Rm 2403, Barton Hall, Washington 25, D. C.	209
Chairman, Research and Development Board, D/D, Washington 25, D. C. ATTN: Technical Library	210
Executive Secretary, Committee on Atomic Energy, Research and Development Board, Rm 3E1075, Pentagon, Washington 25, D. C.	211-212
Executive Secretary, Military Liaison Committee, PO Box 1814, Washington 25, D. C.	213
Commandant, Armed Forces Staff College, Norfolk 11, Va. ATTN: Secretary	214
Commanding General, Field Command, AFSWP, PO Box 5100, Albuquerque, N. Mex.	215-220
Chief, AFSWP, PO Box 2610, Washington 13, D. C.	221-229

ATOMIC ENERGY COMMISSION ACTIVITIES

U. S. Atomic Energy Commission, Classified Document Room, 1901 Constitution Ave., Washington 25, D. C. ATTN: Mrs. J. M. O'Leary (for DMA)	230-232
University of California Radiation Laboratory, PO Box 808, Livermore, Calif. ATTN: Margaret Folden	233
Los Alamos Scientific Laboratory, Report Library, PO Box 1663, Los Alamos, N. Mex. ATTN: Helen Redman	234-236
Sandia Corporation, Classified Document Division, Sandia Base, Albuquerque, N. Mex. ATTN: Wynne K. Cox	237-256
Weapon Test Reports Group, TIS	257
Surplus in TISOR for AFSWP	258-282

ADDITIONAL DISTRIBUTION

Director, Special Weapons Developments, OCAFF, Fort Bliss, Texas	283

AEC, Oak Ridge, Tenn., A31899